Elastography

A Practical Approach

Richard G. Barr

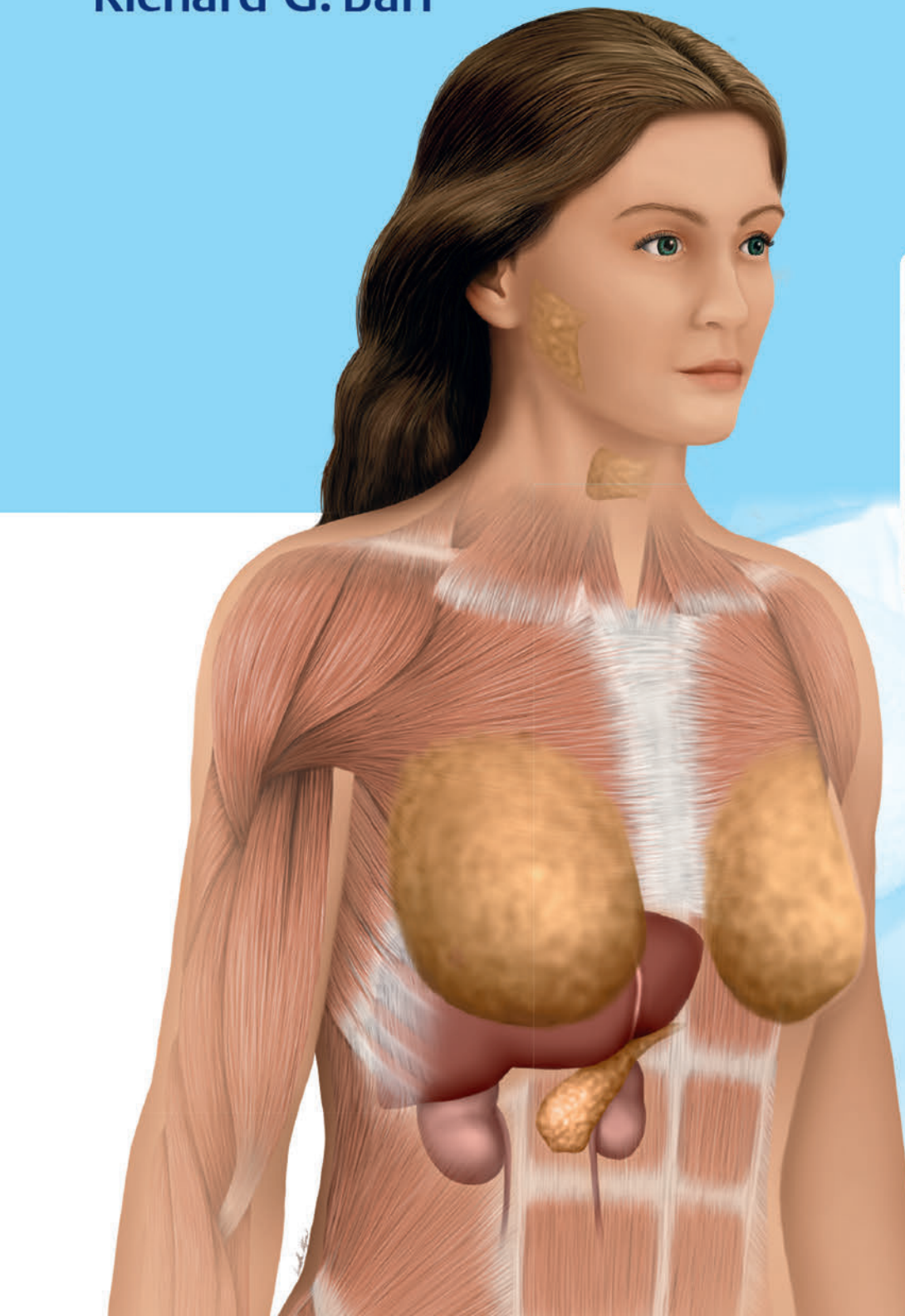

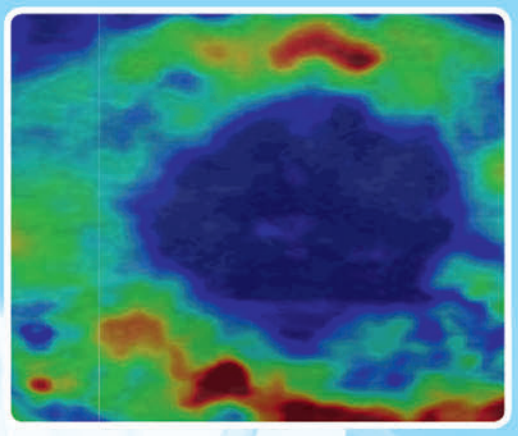

Thieme

Elastography

A Practical Approach

Richard G. Barr, MD, PhD, FACR, FSRU
Professor
Department of Radiology
Northeast Ohio Medical University
Rootstown, Ohio
Southwoods Imaging
Youngstown, Ohio

Thieme
New York • Stuttgart • Delhi • Rio de Janeiro

Thieme Medical Publishers, Inc.
333 Seventh Avenue
New York, New York 10001

Executive Editor: William Lamsback
Managing Editor: J. Owen Zurhellen IV
Editorial Assistant: Mary B. Wilson
Director, Editorial Services: Mary Jo Casey
Production Editor: Sean Woznicki
International Production Director: Andreas Schabert
Vice President, Editorial and E-Product Development: Vera Spillner
International Marketing Director: Fiona Henderson
International Sales Director: Louisa Turrell
Director of Sales, North America: Mike Roseman
Senior Vice President and Chief Operating Officer: Sarah Vanderbilt
President: Brian D. Scanlan
Printer: Asia Pacific Offset

Library of Congress Cataloging-in-Publication Data
Names: Barr, Richard G., author, editor.
Title: Elastography : a practical approach / Richard G. Barr.
Description: First edition. | New York : Thieme, [2017] | Includes bibliographical references and index.
Identifiers: LCCN 2016011911 (print) | LCCN 2016012562 (ebook) | ISBN 9781626232716 | ISBN 9781626232723
Subjects: | MESH: Elasticity Imaging Techniques–methods
Classification: LCC RC804.E59 (print) | LCC RC804.E59 (ebook) | NLM WN 208 |
DDC 616.07/543–dc23
LC record available at http://lccn.loc.gov/2016011911

Thieme Publishers New York
333 Seventh Avenue, New York, NY 10001 USA
+1 800 782 3488, customerservice@thieme.com

Thieme Publishers Stuttgart
Rüdigerstrasse 14, 70469 Stuttgart, Germany
+49 [0]711 8931 421, customerservice@thieme.de

Thieme Publishers Delhi
A-12, Second Floor, Sector-2, Noida-201301
Uttar Pradesh, India
+91 120 45 566 00, customerservice@thieme.in

Thieme Publishers Rio de Janeiro, Thieme Publicações Ltda.
EdifícioRodolpho de Paoli, 25º andar
Av. NiloPeçanha, 50 – Sala 2508,
Rio de Janeiro 20020-906 Brasil
+55 21 3172-2297 / +55 21 3172-1896

Typesetting by Thomson Digital, India

ISBN 978-1-62623-271-6

Also available as an ebook:
eISBN 978-1-62623-272-3

To my family, friends, and co-workers

Contents

Foreword

This second book from Richard G. Barr on elastography expands on the rapidly increasing practice of ultrasound elastography in a variety of clinical applications. Elastography is an imaging modality that maps the elastic properties of soft tissue. The main concept behind elastography is that tissue stiffness or softness will give diagnostic information about the manifestation or status of disease. Elastography is being used to investigate many disease conditions in various organs. It provides additional diagnostic information beyond what can be learned from an anatomical 2D image.

Elastography use has expanded in recent years. It now encompasses multiple organs and the vast majority of ultrasound manufacturers have at least one version on their systems. This has led to the need for a comprehensive text that covers all aspects of elastography: clinical use on a variety of organs; the how, why and where during practice; and the pitfalls, tips and tricks for a successful and relevant examination. There are few physicians world wide with the experience and knowledge required. Dr. Barr has included many of them in this very comprehensive text, bringing their clinical and practical knowledge together in one place.

This comprehensive book covers the principles and techniques used in elastography. Each chapter expands on the different types of elastography; the tips and tricks in obtaining a diagnostic elastogram; methods for interpretation of the information; and understanding artifacts and limitations that are encountered and being able to tell if they are related to one's technique or actual diagnostic information.

Beyond just covering techniques, Dr. Barr includes information on the use of elastography in a variety of organs. Chronic liver disease is a substantial worldwide problem, with the major consequence of increasing deposition of fibrous tissue within the liver leading to the development of cirrhosis. Dr. Barr exquisitely covers technique for imaging diffuse liver disease, including how to perform the procedure and limitations and pointers for clinical assessment of liver disease and focal liver diseases. Ultrasound has been used to evaluate the breast in both diagnostic and screening studies. Breast elastography is a fairly new ultrasound method that can provide supplementary diagnostic information in evaluation of pathology. Ultrasound is accurate and precise in the detection of thyroid nodules, but has a relatively low diagnostic performance for the differentiation between benign and malignant nodules. Elastography is a valid and useful tool in thyroid evaluation. Even with adequate training and suitable parameters, proper equipment and clinical appropriateness of examination are essential. Other clinical applications for elastography that are presented in this book include imaging of prostate, lymph nodes, spleen, pancreas, kidney, MSK, salivary glands and testes, all of which make this book enormously helpful in understanding the practices of elastography in any given department.

Elastography: A Practical Approach is written to encompass a wide variety of clinical elastography applications for one's daily practice. The clinical images, diagrams, and technical tips and tricks on how to obtain a quality elastogram are excellent. I believe that this book will be extremely useful to all ultrasound departments.

Cynthia L. Rapp, RDMS, FAUM, FSDMS
Senior Clinical Marketing Manager
Toshiba Ultrasound
Tustin, California

Preface

This book, a comprehensive review of the current clinical applications of elastography, is designed for sonographers and physicians performing elastography in routine clinical practice. The techniques to optimize each type of elastography for each organ system are discussed in detail with pitfalls clearly explained. A review of all artifacts and how to avoid them is included. If artifacts provide clinical information, their clinical significance is highlighted. This book is designed to be useful both for beginner and experienced imagers. The uses of elastography for each organ system are explored so that the reader can determine which of these applications would be of value in his or her department or clinical practice.

This book is a compilation of the experience of world experts on elastography. An attempt has been made to include all of the available techniques for each organ and to compare and contrast these techniques. Enough information is included for each technique so that those with access to only one technique will be able to optimize the clinical utility of their system. For those readers with multiple techniques available on different equipment, the discussion of the various techniques will help them determine which patients are best suited for each technique.

Clinical cases have been selected to demonstrate a wide range of pathology. Within a given disease state, cases have been selected to demonstrate the range of elastographic findings for that pathology. Cases where elastography can give false-positive or false-negative results are pointed out and discussed in detail, with tips on how to recognize findings that may be inaccurate and should not be used for clinical diagnosis.

The basic science principles of ultrasound elastography are covered in Chapter 2. The basic science presented in this book is not meant to be exhaustive but to give an overview highlighting the information needed when obtaining clinical images. In Chapters 3 through 12 the clinical use of elastography in specific organ systems is discussed, highlighting practical approaches to incorporating elastography into clinical practice. The clinical chapters give detailed tips and tricks to obtain high quality elastograms. The differences in SE and SWE for each organ system are discussed. Magnetic resonance elastography is discussed in Chapter 12, following the chapters on clinical uses of ultrasound-based elastography.

Elastography has been extensively validated for improved clinical diagnosis in diffuse liver disease and diseases of the breast and thyroid gland. Guidelines for the use of elastography for these organs have been published. The clinical applications of elastography for these organs are discussed in detail, highlighting in particular the use of elastography as an aid in clinical diagnosis.

There has been widespread evaluation of other organs with the approval of clinical use of elastography. In these organ systems, well-defined clinical applications have not been validated; however, many appear promising. Initial research on prostate elastography has excellent results in detection and characterization of prostate cancer in the peripheral zone. In many other organs, there appears to be overlap between stiffness values of benign and malignant lesions limiting the specificity and sensitivity of elastography in detection and characterization of disease states. Chapters on focal liver disease, prostate, lymph nodes, other abdominal organs, and the musculoskeletal system present the current state of development of techniques for these organs, systems and disease states. In the final chapter of this book newer applications that are in development are discussed.

Acknowledgments

Many people are associated with and support the research and clinical studies of elastography that have made this book possible, and I thank them. A special thanks to the chapter authors, who are all experts in their field and have shared their expert advice and opinion.

The number of our vendor collaborators, both engineers and clinical applications specialists, is too large to list individually. All deserve acknowledgement for working with the authors, advising on the application of elastography to their many fields of interest.

I thank the staff at Southwoods Imaging for their hard work, which has made significant contributions to my research efforts. Finally, I thank the thousands of patients who have volunteered for my research studies, which has allowed the progress we have made.

Contributors

Anupam Bam, MBBS
Thane Ultrasound Center
Thane, India

Richard G. Barr, MD, PhD, FACR, FSRU
Professor
Department of Radiology
Northeastern Ohio Medical University
Rootstown, Ohio
Southwoods Imaging
Youngstown, Ohio

Chandra Bortolotto, MD
Department of Radiology
Policlinico San Matteo
Università degli Studi
Pavia, Italy

Costanza Bruno, MD
Department of Radiology
Policinico, "GB Rossi"
University of Verona
Verona, Italy

Fabrizio Calliada, MD
Department of Radiology
Policlinico San Matteo
Università degli Studi
Pavia, Italy

Vito Cantisani, MD, PhD
Department of Radiological Sciences
Oncology and Pathology
Policlinico Umberto I
University Sapienza
Rome, Italy

Carlo Catalano, MD
Department of Radiology
Anatomo-pathology and Oncology
University of Rome
Rome, Italy

Nitin Chaubal, MD, DMRD, FICR, FAIUM, FICMU, FSRU
Thane Ultrasound Center
Thane, India

Valentina Ciaravino, MD
Department of Radiology
University of Verona
Verona, Italy

Jean-Michel Correas, MD, PhD
Vice Chairman of the Adult Radiology Department
Paris-Descartes University & Necker University Hospital
Batiment Hamburger
Paris, France

David O. Cosgrove, MD
Imperial and King's Colleges
London, United Kingdom

Stefano Crosara, MD
Department of Radiology
University of Verona
Verona, Italy

Ferdinando D'Ambrosio, MD
Department of Radiology
Anatomo-pathology and Oncology
University of Rome
Rome, Italy

Emanuele David, MD
Department of Radiological Sciences
Oncology and Pathology
Policlinico Umberto I
University Sapienza
Rome, Italy

Riccardo De Robertis, MD
Department of Radiology
Casa di Cura Pederzoli
Peschiera del Garda
Italy

Nicola Di Leo, MD
Department of Radiology
Anatomo-pathology and Oncology
University of Rome
Rome, Italy
Department of Biomedical Sciences and
Morphological and Functional Imaging
University of Messina
Messina, Italy

Mattia DiSegni, MD
Department of Radiology
Anatomo-pathology and Oncology
University of Rome
Rome, Italy

Mirko D'Onofrio, MD
Associate Professor
Department of Radiology
GB Rossi University Hospital
University of Verona
Verona, Italy

Bogdan Dzyubak, PhD
Department of Radiology
Mayo Clinic
Rochester, Minnesota

Giovanna Ferraioli, MD
Department of Infectious Disease
Fondazione IRCCS
Policlinico San Matteo
University of Pavia
Pavia, Italy

Carlo Filice, MD
Department of Infectious Disease
Fondazione IRCCS
Policlinico San Matteo
University of Pavia
Pavia, Italy

Antonio Giulio Gennari, MD
Department of Radiology
University of Trieste
Trieste, Italy

Hektor Grazhdani, MD
Department of Biomedical Sciences
and Morphological and Functional Imaging
University of Messina
Messina, Italy

Nelson A. Hager, MD
Franciscan Orthopedic Associates
Tacoma, Washington

Olivier Hélénon, MD
Department of Radiology
Necker Hospital
Paris, France

Andrea Isidori, MD
Department of Radiological Sciences
Oncology and Pathology
Policlinico Umberto I
University Sapienza
Rome, Italy

Ketki Khadtare, MBBS, MD
Thane Ultrasound Center
Thane, India

Amy M. Lex, MS, RT(R), RDMS
National Strategic Business and Luminary Manager
for General Imaging and Women's Healthcare
Philips Ultrasound
Bothell, Washington

Raffaella Lissandrin, MD
Department of Infectious Disease
Fondazione IRCCS
Policlinico San Matteo
University of Pavia
Pavia, Italy

Antonio Masciotra, MD
Department of Medical Imaging
Casa di Cura Villa Maria
Campobasso, Italy

Roberto Pozzi Mucelli, MD
Department of Radiology
University of Verona
Verona, Italy

Michele Pontello, MD
Department of Radiology
Cattinara Hospital
University of Trieste
Trieste, Italy

Emilio Quaia, MD
Department of Radiology
Cattinara Hospital
University of Trieste
Trieste, Italy

Giuseppe Schillizzi, MD
Department of Radiological Sciences
Oncology and Pathology
Sapienza University of Rome
Rome, Italy

Stephanie R. Wilson, MD
Clinical Professor of Radiology
Clinical Professor of Medicine
Division of Gastroenterology
University of Calgary
Calgary, Alberta, Canada

Mabel Zicchetti, MD
Department of Infectious Disease
Fondazione IRCCS
Policlinico San Matteo
University of Pavia
Pavia, Italy

Abbreviations/Terminology

ARFI	acoustic radiation force impulse
E/B ratio	the length of a breast lesion measured on strain imaging compared to the length of the lesion on B-mode imaging
ECI	elasticity contrast index
EI	elasticity index
Elasticity score	a scoring system to characterize lesions on strain elastography; also known as the 5-point color scale, Tsukuba score, or strain pattern
5-point color scale	a scoring system to characterize lesions on strain elastography; also known as Tsukuba score, elasticity score, or strain pattern
FLR	fat to lesion ratio, a method of semi-quantitating strain results; it determines the relative stiffness of a lesion compared to the stiffness of fat
FNA	fine needle aspiration
FNAB	fine needle aspiration biopsy
FNAC	fine needle aspiration cytology
FOV	field of view
Length ratio	the length of the lesion measured on strain imaging compared to the length of the lesion on B-mode imaging, also known as E/B ratio or width ratio
Manual displacement method	the use of the transducer or patient breathing and/or heartbeat to generate the compression–release force needed to generate a strain elastogram
3D-MRE	three-dimensional magnetic resonance elastography
MRI	magnetic resonance imaging
RTSE	real-time strain elastography, Hitachi's strain imaging
ROI	region of interest
SE	strain elastography, generic term for all strain elastography
SR	strain ratio, the ratio of the stiffness of a lesion to that of a reference standard (e.g., fat in breast elastography); a semiquantitative (relative) measure of strain
SSI	supersonic shear wave imaging; SuperSonic Imagine's shear wave imaging
Strain ratio	lesion to fat ratio, the ratio of the stiffness of a lesion to a reference standard (e.g., fat in breast elastography)
SWE	shear wave elastography, generic term for shear wave imaging
p-SWE	point shear wave elastography, a shear wave technique where the SWS is calculated in a small ROI
2D-SWE	two-dimensional shear wave elastography, shear wave techniques where the SWS is calculated over a wide field of view with the SWS color-coded on the image; one or more ROIs can then be placed within the FOV to obtain stiffness measurements
3D-SWE	three-dimensional shear wave imaging, a shear wave technique where the SWS is calculated over a 3D volume with the SWSs color-coded on the image; one or more ROIs can then be placed within the FOV to obtain stiffness measurements
SWS	shear wave speed in meters per second (m/s); also called SWV, shear wave velocity
SWV	shear wave velocity in meters per second (m/s); also called SWS, shear wave speed
Strain pattern	a scoring system to characterize lesions on strain elastography; also known as the 5-point color scale, Tsukuba score, or elasticity score

TSI	thyroid stiffness index
Tsukuba score	a scoring system to characterize lesions on strain elastography; also known as 5-point color scale, elasticity score, or strain pattern
VTI	Virtual Touch Imaging (Siemens strain imaging using ARFI)
VTQ	Virtual Touch Quantification (Siemens shear wave point quantification), a p-SWE technique
US	ultrasound
Width ratio	comparison of the size of a lesion measured on strain imaging compared to the size measured on B-mode imaging
Young's modulus	a mechanical property of linear elastic solid materials; it defines the relationship between stress (force per unit area) and strain (proportional deformation) in a material; it is a measure of stiffness expressed in kPa.

1 Introduction to Elastography

Richard G. Barr

The evaluation of tissue stiffness has been used for thousands of years to diagnosis diseases.[1] Many disease states lead to changes in lesion stiffness, most notably cancers. These changes have been assessed by clinical palpation in the past and have provided one of the primary assessments when performing a physical exam.[2,3,4] For superficial organs such as the breasts this is quite easy; however, for deeper organs this is problematic. Elastography is a new imaging technique that can produce an image based on tissue stiffness.[5] It provides additional clinical information that B-mode ultrasound, which evaluates acoustic properties, and Doppler, which assesses vascular flow, do not (▶ Table 1.1).

Ultrasound elastography (commonly just called *elastography*) has been used in research settings for many years. Since the advent of the first clinically approved system in 2003, there has been great interest and much research into the use of this technology in clinical diagnosis for many disease states. Since its initial clinical introduction, there has been the rapid and continual development of several variations of elastography. Initially, *strain elastography (SE)* was developed and used clinically. This technique assesses tissue changes when an external force is applied (either with a transducer or via patient respiration or heartbeat). Stiff tissues do not deform while softer tissues do when a force is applied. With all the strain-based techniques, the amount of force applied is not known and therefore the exact quantitative stiffness of the tissues cannot be measured. Thus, these techniques are qualitative.[5] However, the relative stiffness of tissues in the field of view can be assessed. Semi-quantitative approaches have been developed where the stiffness of the tissue of interest is compared to the stiffness of a standard tissue in the field of view. From this, a ratio can be determined representing the relative stiffness of the tissue of interest.[6] For example the stiffness of a thyroid lesion can be compared to that of normal thyroid tissue, which is relatively similar in stiffness across patients. A cutoff value comparing the relative stiffness to the reference standard can be determined, through which one can differentiate a benign lesion from one suspicious for malignancy.

There is a learning curve for obtaining accurate strain elastograms. There is significant variability in the technique for performing SE depending on the system used. To obtain optimal elastograms and accurate results, it is important to find the “sweet spot” for the compression-release and frequency techniques for each vendor’s system.

There are several methods to display the results. Various color or grayscale strain maps can be displayed. In addition, these maps can be superimposed over a grayscale B-mode image. Care must be taken when interpreting color elastograms to know which of several available color keys are being used to display the map results. For some, stiff (or hard) tissues are red and for others, stiff tissues are blue. However, if a grayscale strain map is used to display the elastographic data, the background B-mode image should be turned off to prevent confusion that would arise in reading information from the two overlapping grayscale images. ▶ Fig. 1.1 shows the various ways in which the results can be displayed.

Table 1.1 Comparison of different modes of medical ultrasonography

Mode	What is measured:	What is displayed:
B-mode	Acoustic impedance	Anatomy
Doppler	Motion	Vascular flow
Elastography	Mechanical properties	Tissue stiffness

Vendors are developing methods for real-time feedback for the user on the quality of elastograms to help in learning the appropriate technique for obtaining optimal images. One important principal in performing SE is to apply uniform stress throughout the field of view of the image. One vendor provides a real-time “motion map” that uses color to indicate the amount of displacement throughout the image (▶ Fig. 1.2). For accurate SE results, the same displacement should be present throughout the image. This is especially true when you are obtaining a strain ratio.

Other vendors provide a real-time display of the amount of stress applied (globally over the whole image). The display depicts the region of optimal compression–release, which aids in performing the examination. Some vendors also provide a bar that allows the user to visualize in real-time when the optimal compression–release and frequency of the push pulses are obtained (▶ Fig. 1.3). Systems are being developed that can automatically detect a lesion’s borders for more consistent region of interest placement as well as identify the "best" area to use as the reference tissue to calculate the strain ratio. The addition of these new capabilities will allow for more accurate and reproducible SE results.

The second major elastographic technique developed was *shear wave elastography (SWE).* In this technique, either a mechanical force or an acoustic radiation force impulse (ARFI) is used to generate shear waves within the tissues being examined. Shear waves propagate perpendicular to the applied force, similar to the ripples in water when a stone is dropped into a pond. The ripples correspond to the shear waves and the stone to the applied force. Shear wave speed (SWS) can be estimated by observing the tissue motion in response to the shear waves using B-mode ultrasound. SWS is dependent on tissue stiffness: it is slower in softer tissues and faster in stiffer tissues. This technique when performed with mechanical pushes and when no ultrasound image is acquired is called *transient elastography* (*TE*). There are several techniques using ARFI pulses to generate shear waves and where a B-mode image is obtained to determine where the SWS measurement is being obtained. In one, a single small region of interest (ROI) can be placed in the tissue of interest and ARFI pulses used to generate shear waves. The resultant SWS is then calculated and displayed; it usually represents the mean value of the shear wave speeds within the ROI. This technique is called *point shear wave elastography (p-SWE).* In another technique, multiple ARFI pulses can be applied over a larger field of view (FOV) to estimate the SWS over a larger area of tissue. With this technique, color-coding of the pixels in the display map is used to visualize the variation of the SWS in the FOV. This technique is called *two-dimensional shear wave elastography (2D-SWE).* Some vendors provide 2D-SWE for a

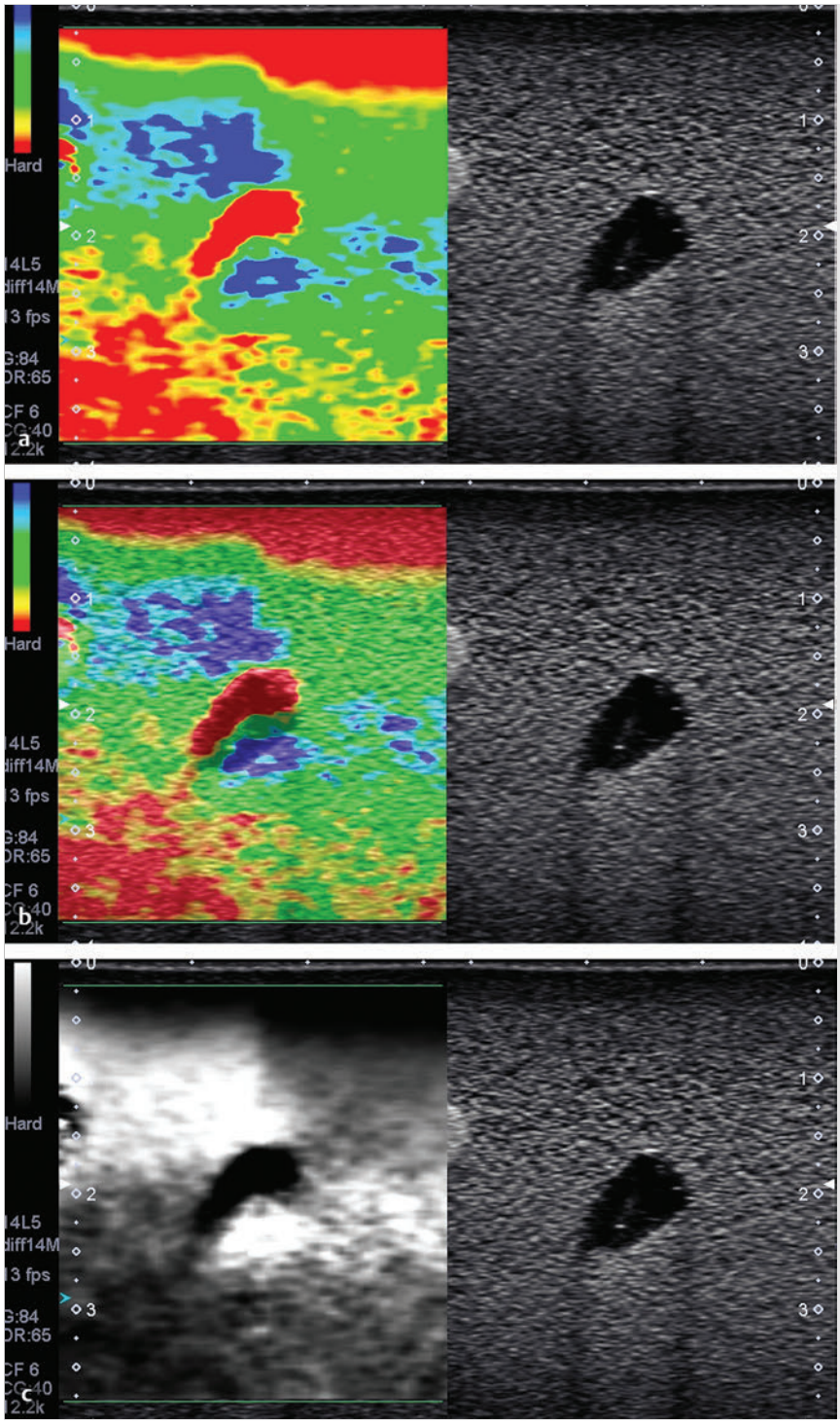

Fig. 1.1 Examples of strain elastography images from a cystic lesion in a phantom using different display maps. In (**a**), red represents stiff, blue represents soft, and there is no overlay on the B-mode image; in (**b**), red represents stiff, blue represents soft, and there is overlay on the grayscale B-mode image; in (**c**), in the grayscale map, black represents stiff, white represents soft, and there is no overlay on the B-mode image. It is important to not display the B-mode overlay when using the grayscale strain map, as two grayscale images overlaid on each other are not interpretable.

single moment in time, while other vendors provide ongoing 2D-SWE in real-time.

With SWE, a convention of color-coding stiff as red and soft as blue has been adopted. However in SE various color and grayscale maps with different color-coding are usually available. For some vendors, their default display color-codes stiff as blue, while for others, their default display color-codes stiff as red. For this reason, it is important to always display the color-coding map used when evaluating SE images. The color map in 2D-SWE can be adjusted to reflect the appropriate SWS from the tissues of interest. Changing the scale can be used to help visualize differences in the stiffness of the tissue being evaluated.

With both SE and SWE, it is important for the transducer to remain in one location during data collection and to limit motion in the field of view. Motion either caused by transducer movement or from patient sources can lead to poor-quality data.

One critical factor in performing elastography is precompression. Precompression is the amount of force applied to the tissues when acquiring images. As tissues are compressed, they

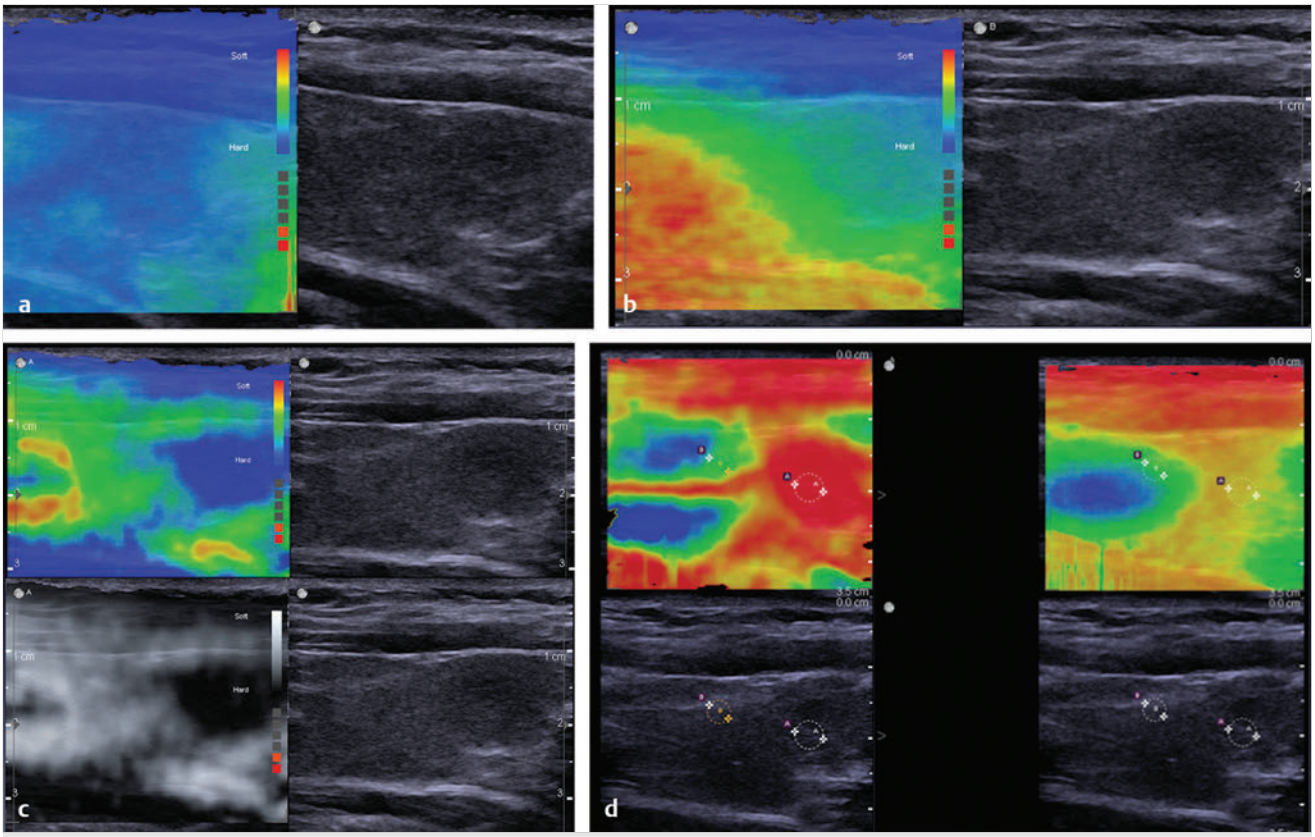

Fig. 1.2 A real-time "motion map" developed by one vendor displays the displacement caused by the applied stress when obtaining the elastogram. The amount of tissue displacement in the image is displayed using a color map. For an optimal strain elastogram, the stress should be uniformly applied across the image. In (**a**), optimal stress is applied. Note that at similar depth, the color in the image is similar. In (**b**), the transducer was heeled, applying more stress to the left side of the image (red). Therefore, the stiffness calculated for a lesion on the right of the image would appear different than that of a similar lesion on the left side of the image. In (**c**), the effect of carotid artery pulsation can be identified in this thyroid strain elastogram. The motion maps are displayed on the left with the upper image showing a color map and the lower image showing a grayscale map. The two images on the upper and lower right are the grayscale elastograms corresponding to the motion maps. Note the red ring (upper left image) corresponds to the white area (lower left image) in the motion map; these indicate increased stress (increased pressure [strain] applied) due to the pulsating carotid artery. In (**d**), the upper images are the motion maps and the lower images are the B-mode images. The motion maps are selected from a cine clip of the same tissue. Significant stress was applied when obtaining this clip (red in motion map). In the two sets of images, the strain ratio was obtained in the same location. The strain ratio obtained from the frame on the left was 7.4, while that on the right was 5.2. The reason for the difference is the disparity in stress applied from the location of the two ROIs (lesion, dotted circle A, and reference tissue, dotted circle B), which is clearly identified using the motion maps.

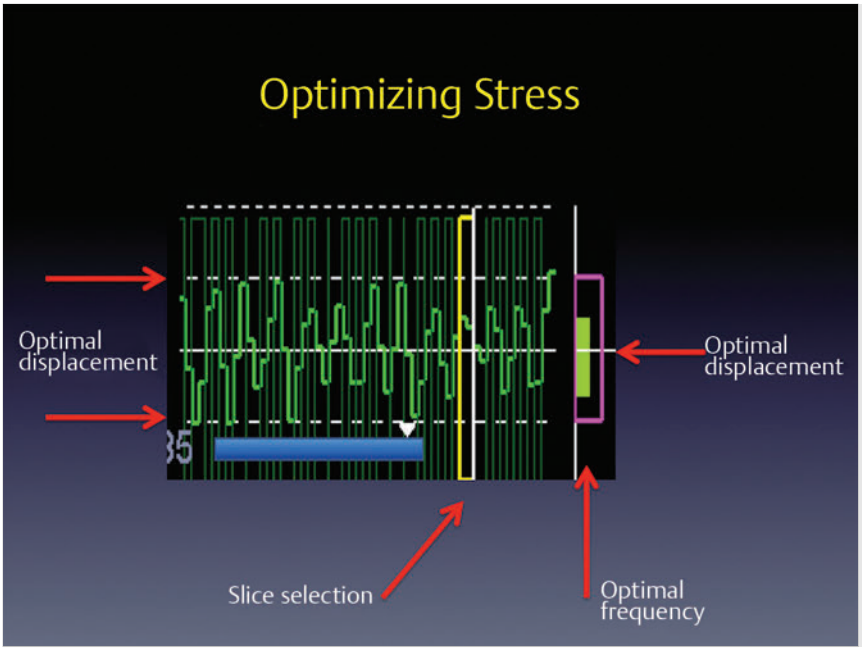

Fig. 1.3 Many vendors have a real-time scale on the image that depicts the stress being applied. In this example of a scale, the optimal displacement is when the stress applied (green line) is between the two dashed lines highlighted with the red arrows. The purple box on the right is used to optimize both the frequency of compression and the optimal displacement. When optimal, the yellow rectangle in the purple box just fills the purple box.

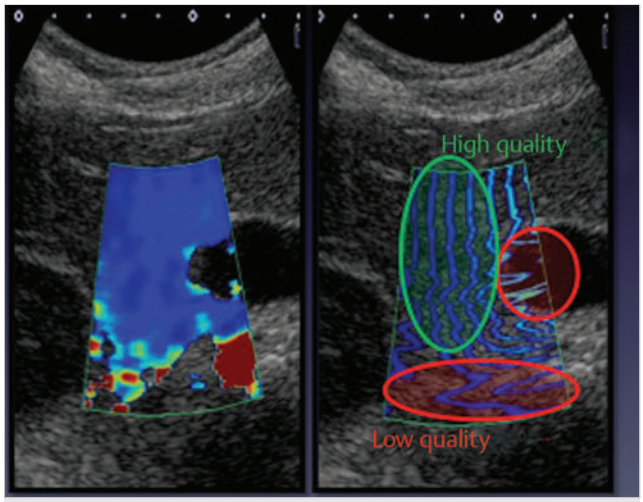

Fig. 1.4 An example of how vendors provide real-time feedback on the quality of shear wave generation. The 2D-SWE image is on the left and the "quality image" is on the right. With 2D-SWE, when the shear wave propagation lines are parallel, the image quality is high, and when the propagation lines are not parallel, the quality is poor. The propagation lines within the green circle are parallel, confirming high-quality shear wave generation. In the two red circles the propagation lines are not parallel, representing poor-quality shear wave propagation, which results in poor accuracy in estimating the shear wave speed.

become stiffer. In general, softer tissues increase in stiffness faster than stiffer tissues when compression is applied. It is possible to make benign tissues as stiff as malignant tissues by applying compression. Elastography images, both SE and SWE, should be obtained using a "light touch." This is more critical in superficial organs such as the breasts, where it is easy to increase tissue stiffness by compressing the breast tissue between the transducer and the ribs. In deeper organs, especially those deep to the ribs, this effect is less problematic. A method for consistently applying minimal precompression has been reported.[7]

Poor-quality shear waves may be generated during both p-SWE and 2D-SWE imaging. All vendors have rejection algorithms that evaluate the quality of the shear waves generated. These algorithms are continuously being improved to allow the user to better determine if the results obtained are accurate. One vendor displays a pictorial image of the shear wave propagation. When the shear wave propagation lines are moving in parallel, the quality of the shear waves is high; when they are not, the quality of the shear waves is poor (▶ Fig. 1.4).

In p-SWE most vendors do not provide a shear wave speed (SWS) if the quality of the shear waves is poor. They may display "x.xx" or "0.00" as the value. In 2D-SWE if the quality of the shear waves is poor, no color is displayed in the image.

A third major type of elastography, *magnetic resonance elastography (MRE)*, is becoming more common and preliminary work with it is being performed on many organ systems.[8] Its use in liver evaluation for diffuse disease is growing rapidly.

Elastography has been extensively validated for improved clinical diagnosis in liver for diffuse liver disease, breast, and thyroid gland diagnoses. Guidelines for the use of elastography for these organs have been published.[9,10,11,12]

Breast elastography has very unique features.[5] Breast cancers appear larger on strain elastograms than on the corresponding B-mode images, while benign lesions appear smaller. For SE, this unique feature allows a very sensitive and specific method for characterizing breast lesions even though SE is qualitative. This change in the size of lesion on elastography appears unique to lesions of the breast. The cause of this feature is not completely understood.

There has been extensive research on the use of both mechanical- and ARFI-generated SWE and on the use of MRE in the evaluation of diffuse liver disease.[11] There are many causes of diffuse liver disease all of which lead to liver fibrosis and ultimately to cirrhosis and its complications. The liver stiffness can be measured using these SWE techniques with high accuracy. In many cases, this technology is replacing random liver biopsy for staging and monitoring diffuse liver disease.

With the advent of B-mode ultrasound a large number of thyroid nodules were able to be identified. Fine needle aspiration is the method of choice for diagnosis of these nodules. Both SE and SWE have been shown to improve selection of thyroid nodules for biopsy.[13,14,15,16] Further work is needed to determine if elastographic data will be able to predict which thyroid cancers are more likely to metastasize.

There has been widespread elastographic evaluation of other organs with approved clinical use of elastography.[10] In these organs, well-defined clinical applications have not been validated; however, many appear promising. Initial research on prostate elastography has yielded excellent results in detection and characterization of prostate cancer in the peripheral zone.[17,18] In many other organs, there appears to be an overlap of stiffness values for benign and malignant lesions, limiting the specificity and sensitivity of elastography in detection and characterization of disease states in those organs.[19] Although studies have confirmed that, in general, malignant focal liver lesions are stiffer than benign focal liver lesions, there is significant overlap of stiffness values. For an individual case, elastography has not been demonstrated to be useful in characterization of a focal liver lesion as benign or malignant. Further work is in progress to determine if the stiffness value can be used for other clinical indications, such as evaluating the efficacy of chemotherapy or radiofrequency ablation.

Initial studies on SWE of the prostate suggest that it has a high sensitivity and specificity in detecting clinically significant prostate cancers in the peripheral zone. Preliminary studies suggest that the stiffness value of a prostate cancer may correlate with the Gleason score.[17] Because the transitional zone is often stiff without a malignancy, elastography has been less accurate in detecting cancers in the transitional zone. Further work is needed to determine if elastography can be helpful in characterization of lesions in the transitional zone. Studies are just being performed to compare multiparametric magnetic resonance imaging (mpMRI) and prostate elastography to determine if they could be complimentary techniques. Further studies are needed to determine if prostate SWE can be used to follow patients on active surveillance for prostate cancer.

The evaluation of lymph nodes is often problematic. Although increased lymph node size and loss of the normal hilar fat are indicative of tumor invasion, they are not specific especially for small foci of metastatic disease. Elastography may be able to detect small foci of metastatic disease due to the

increased stiffness of these foci. Elastography can also be used to guide biopsies in these small foci, which may not be identified on B-mode imaging.[20,21,22,23]

Elastographic evaluation of other abdominal organs is only now being evaluated. Studies are being performed to determine if elastography can be useful in chronic renal failure and in characterizing renal masses, pancreatic masses, and bowel pathology.[24,25,26]

Elastography could also be very valuable in the musculoskeletal system. As opposed to tumors that are stiffer than normal tissue, tendons are one of the stiffest organs in the body, and, when diseased, they become softer. As these tendons heal, they regain their stiffness. Healing can be monitored with ultrasound elastography, which is low cost and does nor involve the use of radiation. The elastographic findings may provide a method of individually tailoring physical therapy.

Newer techniques are being developed that may help overcome some of the limitations of the present elastographic technology. It is clear that elastography will become a standard of care for the detection and characterization of many disease states.

References

[1] Tanter M, Bercoff J, Athanasiou A et al. Quantitative assessment of breast lesion viscoelasticity: initial clinical results using supersonic shear imaging. Ultrasound Med Biol 2008; 34(9):1373–1386

[2] Ophir J, Céspedes I, Ponnekanti H, Yazdi Y, Li X. Elastography: a quantitative method for imaging the elasticity of biological tissues. Ultrason Imaging 1991; 13(2):111–134

[3] Samani A, Zubovits J, Plewes D. Elastic moduli of normal and pathological human breast tissues: an inversion-technique-based investigation of 169 samples. Phys Med Biol 2007; 52(6):1565–1576

[4] Frey H. [Real-time elastography. A new ultrasound procedure for the reconstruction of tissue elasticity][in French] Radiologe 2003; 43(10):850–855

[5] Barr RG. Sonographic breast elastography: a primer. J Ultrasound Med 2012; 31(5):773–783

[6] Shiina T, Nightingale KR, Palmeri ML et al. WFUMB guidelines and recommendations for clinical use of ultrasound elastography: Part 1: basic principles and terminology. Ultrasound Med Biol 2015; 41(5):1126–1147

[7] Barr RG, Zhang Z. Effects of precompression on elasticity imaging of the breast: development of a clinically useful semiquantitative method of precompression assessment. J Ultrasound Med 2012; 31(6):895–902

[8] Mariappan YK, Glaser KJ, Ehman RL. Magnetic resonance elastography: a review. Clin Anat 2010; 23(5):497–511

[9] Barr RG, Nakashima K, Amy D et al. WFUMB guidelines and recommendations for clinical use of ultrasound elastography: Part 2: breast. Ultrasound Med Biol 2015; 41(5):1148–1160

[10] Cosgrove D, Piscaglia F, Bamber J et al. EFSUMB guidelines and recommendations on the clinical use of ultrasound elastography. Part 2: Clinical applications. Ultraschall Med 2013; 34(3):238–253

[11] Ferraioli G, Filice C, Castera L et al. WFUMB guidelines and recommendations for clinical use of ultrasound elastography: part 3: liver. Ultrasound Med Biol 2015; 41(5):1161–1179

[12] Barr RG, Ferraioli G, Palmeri ML et al. Elastography assessment of liver fibrosis: Society of Radiologists in Ultrasound consensus conference statement. Radiology 2015; 276(3):845–861

[13] Bhatia KS, Tong CS, Cho CC, Yuen EH, Lee YY, Ahuja AT. Shear wave elastography of thyroid nodules in routine clinical practice: preliminary observations and utility for detecting malignancy. Eur Radiol 2012; 22(11):2397–2406

[14] Bojunga J, Herrmann E, Meyer G, Weber S, Zeuzem S, Friedrich-Rust M. Real-time elastography for the differentiation of benign and malignant thyroid nodules: a meta-analysis. Thyroid 2010; 20(10):1145–1150

[15] Luo S, Kim EH, Dighe M, Kim Y. Thyroid nodule classification using ultrasound elastography via linear discriminant analysis. Ultrasonics 2011; 51(4): 425–431

[16] Luo S, Lim DJ, Kim Y. Objective ultrasound elastography scoring of thyroid nodules using spatiotemporal strain information. Med Phys 2012; 39(3): 1182–1189

[17] Correas JM, Tissier AM, Khairoune A et al. Prostate cancer: diagnostic performance of real-time shear-wave elastography. Radiology 2015; 275(1): 280–289

[18] Barr RG, Memo R, Schaub CR. Shear wave ultrasound elastography of the prostate: initial results. Ultrasound Q 2012; 28(1):13–20

[19] Yu H, Wilson SR. Differentiation of benign from malignant liver masses with acoustic radiation force impulse technique. Ultrasound Q 2011; 27(4):217–223

[20] Bhatia KS, Cho CC, Yuen YH, Rasalkar DD, King AD, Ahuja AT. Real-time qualitative ultrasound elastography of cervical lymph nodes in routine clinical practice: interobserver agreement and correlation with malignancy. Ultrasound Med Biol 2010; 36(12):1990–1997

[21] Choi JJ, Kang BJ, Kim SH et al. Role of sonographic elastography in the differential diagnosis of axillary lymph nodes in breast cancer. J Ultrasound Med 2011; 30(4):429–436

[22] Tourasse C, Dénier JF, Awada A, Gratadour AC, Nessah-Bousquet K, Gay J. Elastography in the assessment of sentinel lymph nodes prior to dissection. Eur J Radiol 2012; 81(11):3154–3159

[23] Ying L, Hou Y, Zheng HM, Lin X, Xie ZL, Hu YP. Real-time elastography for the differentiation of benign and malignant superficial lymph nodes: a meta-analysis. Eur J Radiol 2012; 81(10):2576–2584

[24] D'Onofrio M, Gallotti A, Salvia R, Capelli P, Mucelli RP. Acoustic radiation force impulse (ARFI) ultrasound imaging of pancreatic cystic lesions. Eur J Radiol 2011; 80(2):241–244

[25] Goya C, Hamidi C, Hattapoglu S et al. Use of acoustic radiation force impulse elastography to diagnose acute pancreatiitis at hospital admission: comparison with sonography and computed tomography. J Ultrasound Med 2014; 33 (8):1453–1460

[26] Mei M, Ni J, Liu D, Jin P, Sun L. EUS elastography for diagnosis of solid pancreatic masses: a meta-analysis. Gastrointest Endosc 2013; 77(4):578–589

2 Principles of Elastography

Richard G. Barr

2.1 Introduction

Elastography, or elasticity imaging, is a newer ultrasound imaging modality that can provide clinically useful information about tissue stiffness (rather than anatomy), which was previously unavailable. Palpation has been used to assess stiffness to evaluate for malignancies for at least a thousand years.[1] Ultrasound elastography can be considered the imaging equivalent of clinical palpation as it can quantify the stiffness of a lesion, which was previously judged only subjectively by physical examination. With the addition of elastography, we now have three ultrasound modes: B-mode which evaluates acoustic impedance and provides anatomical information; Doppler which evaluates motion and provides vascular flow information; and elastography which evaluates mechanical properties and provides tissue stiffness information.

There are two major types of ultrasound elastography, strain elastography (SE) and shear wave elastography (SWE).[2] SE produces an image based on how tissues respond to a displacement force from an external transducer, an acoustic radiation force impulse (ARFI), or from a patient source (breathing or heartbeat). This allows for a qualitative assessment of how stiff the lesion is compared to surrounding tissues in the field of view (FOV). With SE, the exact stiffness is not known, only how stiff one tissue is compared to other types of tissue in the field of view (FOV). SWE utilizes acoustic radiation force impulse (ARFI), often called a "push pulse," as the compressive force. The natural sequel to this push pulse is the production of shear waves. Shear wave speeds are measured using conventional B-mode imaging to identify the tissue displacement caused by the shear waves. The shear wave speed (SWS) varies with tissue stiffness, with slow SWSs in softer tissue and higher SWSs in stiffer tissue. Therefore, the SWS allows for quantification of tissue stiffness.

Most vendors offer multiple elastographic choices depending on the transducer. A detailed list of each vendor and what they offer can be found in the World Federation for Ultrasound in Medicine and Biology (WFUMB) guidelines.

Here we present a brief discussion of the principles of ultrasound elastography. The goal of this chapter is to provide a very clinically oriented overview, and not a rigorous discussion, of the physics of ultrasound elastography. A detailed discussion of the principles of elastography can be found in other publications.[3,4] Here we present a brief review of the basic principles behind approved ultrasound elastography techniques that are used for performing clinical exams.

2.2 Strain Elastography

SE determines the relative strain on, or elasticity of, tissue within an FOV.[2] The more an object deforms when a force is applied, the higher the strain and the softer the object; the less an object deforms when a force is applied, the lower the strain and the stiffer the object. To determine the strain on a tissue or lesion, an external force is applied and how the tissue changes shape is monitored. This force can vary from minimal, such as patient breathing or his/her heart beating, to moderate rhythmic force generated by transducer movement. For example, if we had an almond within some gelatin (▶ Fig. 2.1) and pushed down on the gelatin, the gelatin would deform significantly indicating it has high strain and is therefore soft. However, the almond would not deform indicating it has low strain and is therefore stiff.

SE is performed on standard ultrasound equipment using specific software that evaluates the frame-to-frame differences in deformation in tissue when a force (stress) is applied. The force can be from patient movement (such as breathing or heartbeat) or from external compression due to rhythmic motion of the ultrasound transducer or ARFI pulses.[2] In SE the value of the absolute strain modulus (Young's modulus)—a numerical value quantifying the stiffness—cannot be calculated because the amount of the force cannot be accurately determined. The real-time SE image is displayed with a scale based on the relative strain (or stiffness) of the tissues within the FOV. Therefore, if the types of tissue in the FOV differ from one display map to the next, a different dynamic range of stiffness values will be used in the display map leading to a different "color" for the same tissue.

2.2.1 Application of Stress

The technique required to obtain the optimal SE images varies with the algorithm used by the manufacturer of the system.[2] For SE, the amount of external displacement needed varies depending on the algorithm used; presently, approved systems require from a 0.1 to 3.0% displacement for optimal

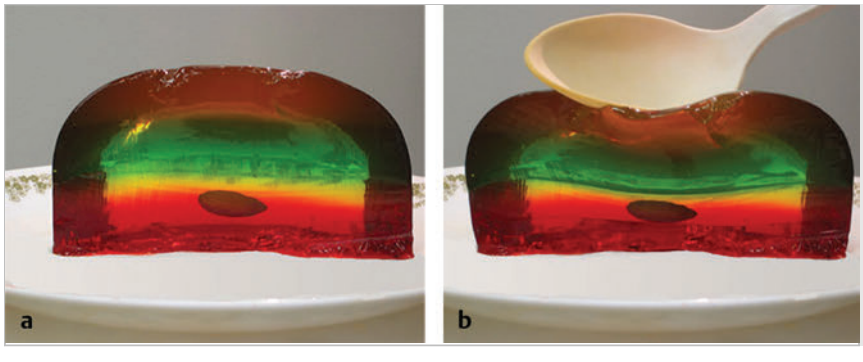

Fig. 2.1 A simplified model of the principle of strain elastography. (**a**) Consider an almond in gelatin. (**b**) If we apply a stress, such as compressing the gelatin with a spoon, the gelatin changes shape because it is soft (more strain), while the almond does not change shape because it is stiff (less strain). The ultrasound strain system compares the frame-to-frame changes of tissue when the tissue is compressed and released. Tissues that deform the most are considered soft, while those that deform the least are considered stiff.

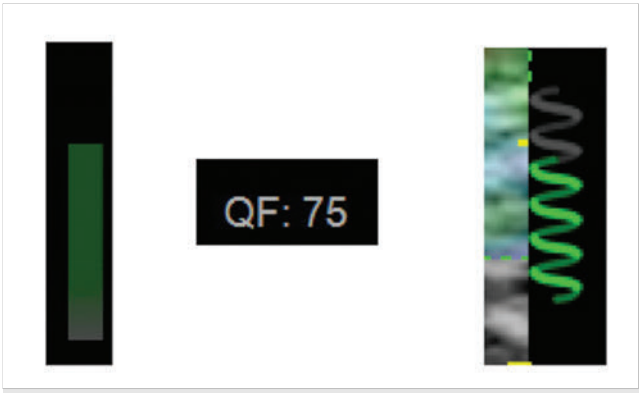

Fig. 2.2 Several of the numerical or visual scales used to display the amount of compression–release being applied. When the appropriate amount of compression–release is applied, the scales are maximized. If the compression–release is either too great or not sufficient, the scale will be smaller. For some systems, maximizing the green bar height confirms adequate compression-release, while in others increasing the number confirms adequate compression-release.

elastograms. With some systems very little if any manual compression–release is needed, while with others a rhythmic compression-release cycle is required. With experience and practice the compression-release technique for a specific system to obtain optimal image quality can be learned. Applying too much compression–release will result in image noise, while not applying enough compression-release will result in no image being obtained. Learning the "sweet spot" for the equipment being used is critical for optimal images. The amount of displacement and the frequency of displacement significantly affect the quality of the elastogram.

Some vendors have a visual scale that helps to confirm that the optimal compression-release and frequency are applied. This could be displayed via a quality measure, usually a number from 0, very poor, to 100, optimal. The information can also be displayed as a bar that changes size with the image quality, with a small bar as suboptimal and a large bar as optimal (▶ Fig. 2.2). Some systems provide a display that plots the displacement and frequency of the applied force and has optimal displacement and frequency displayed. The user can then monitor the displacement and frequency applied and try to optimize the stress for that system (▶ Fig. 2.3).

When learning how to perform SE with the manual displacement method, it is helpful to practice varying the amount of displacement and the frequency of displacement while watching the display bar, quality measure, confidence bar, or displacement plots. You can identify the appropriate technique required by experimenting with your displacement technique and using the color bar or number to identify the optimal technique for the system you are using. When the appropriate technique is used, the elastogram should be similar on all frames. Other factors are important in obtaining optimal images so a high quality factor does not guarantee optimal images. The lesion should appear similar on all frames of the SE clip. If not, there is non-uniform displacement of the lesion during scanning or unacceptable precompression is being applied.

The algorithm used in SE requires the strain changes be measured in a lesion that remains within the imaging plane. Thus, the same location in the lesion needs to remain in the imaging plane during the entire compression-release cycle (▶ Fig. 2.4). Monitoring of the B-mode image to confirm that the lesion is only displaced in depth (not in- and out-of-plane) during scanning and only moving axially in the FOV will allow for optimal images. Positioning of the patient so that breathing or other motion, such as that from the heartbeat, is parallel to the transducer will help. With the SE techniques that involve displacement surveying an organ cannot be performed, as scanning must be done in one stationary position.

Also the displacement needs to be applied uniformly to the tissues in the field of view. If the transducer is heel-toed, the stress applied will be different throughout the image and inaccurate results will be obtained. Examples of properly and improperly applied displacement are shown in ▶ Fig. 2.5. The

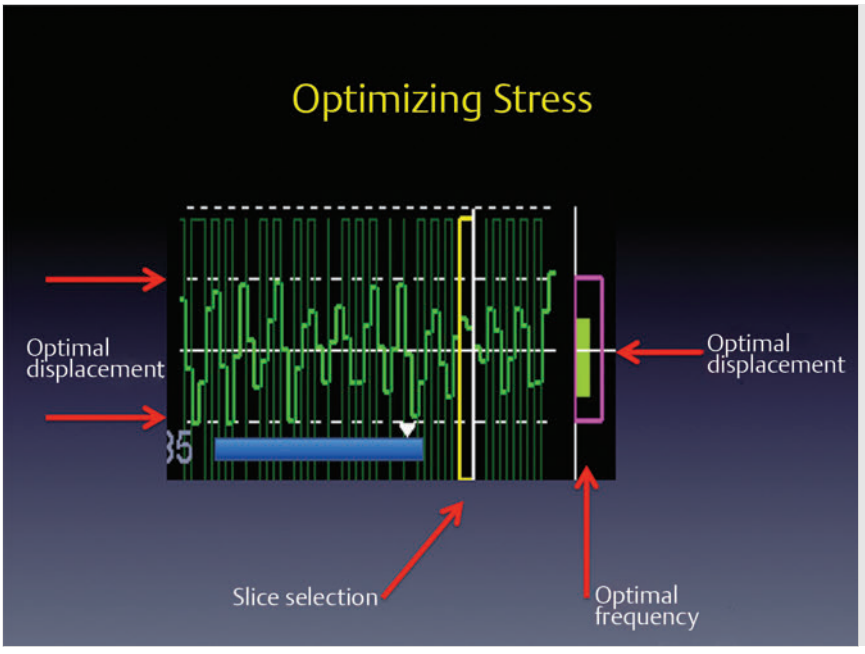

Fig. 2.3 Monitor display of the compression–release in real-time, available on some systems. In this example, the two central dotted lines are the optimal degree of displacement. The purple box on the right displays the displacement and frequency of the applied stress in yellow. The optimum displacement and frequency occur when the yellow just fills the purple box. This real-time feedback allows the sonologist the ability to optimize the elastogram while scanning.

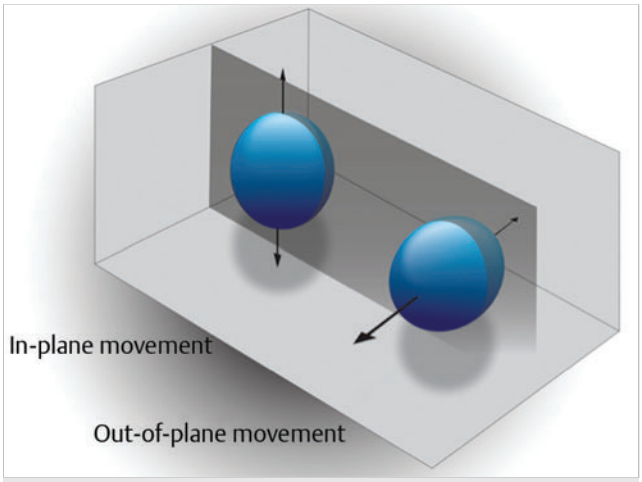

Fig. 2.4 When performing strain elastography, it is important that the same image plane through a lesion be maintained during data acquisition. The dark gray plane corresponds to the ultrasound beam. An optimal elastogram is obtained with only in-plane movement of the lesion. Out-of-plane movement may result in inaccurate elastography results.

degree of displacement can be displayed in a "motion map" using a color scale to indicate the amount of stress applied to the tissue. This technique is not yet clinically available but would be an excellent training tool. In the ideal case, the color of the motion map would be uniform throughout (▶ Fig. 2.5a). However, usually horizontal zones of color are displayed because the displacement often varies with tissue depth. Ideally when comparing tissues (such as in strain ratios discussed below), the same displacement should be applied to the tissues being compared to ensure accurate measurements.

SE images are generated from the raw data of the B-mode images. Therefore it is important to obtain quality B-mode images before activating the SE mode. Find a scanning window that allows for stable positioning of the transducer during the compression-release cycle. If there are areas of shadowing they degrade the accuracy of the elastogram. Placing the palm of your hand on the patient helps stabilize the transducer and allows for more sensitive movements (▶ Fig. 2.6).

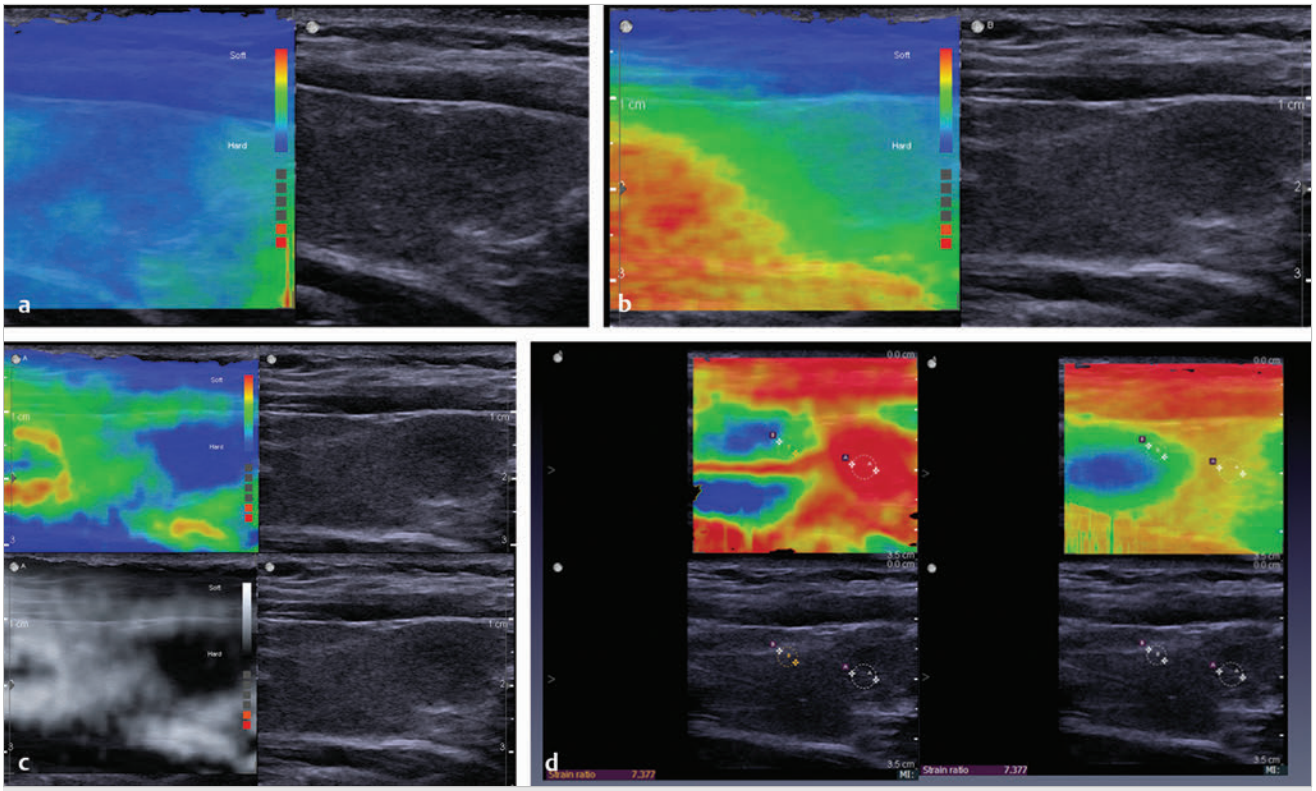

Fig. 2.5 A display of the distribution of stress in real-time, which has been developed but is not yet clinically available. In this display, the amount of stress in each region of the FOV is color-coded based on the amount of tissue displacement. A uniform blue display would be the optimal application of stress. Usually the stress varies with tissue depth (vertically) (**a**) but should be uniform at the same tissue depth (horizontally) in the image. When obtaining strain ratios, measurements should be taken at the same tissue depth; that is, within the same color. If the transducer is heel-toed, the stress applied is not uniform (**b**), with the stress being higher at one side of the image compared to the other. The map also allows one to visualize stress that may be coming from a different source, such as the carotid artery pulsations. The red and yellow ring in the left side of the image (**c**) is caused by carotid artery pulsations in this SE image of the thyroid. If too much stress is applied, the motion map will display a significant amount of red in the image (**d**). This real-time technique can be used as a training method for learning how to apply the stress to obtain the optimal images.

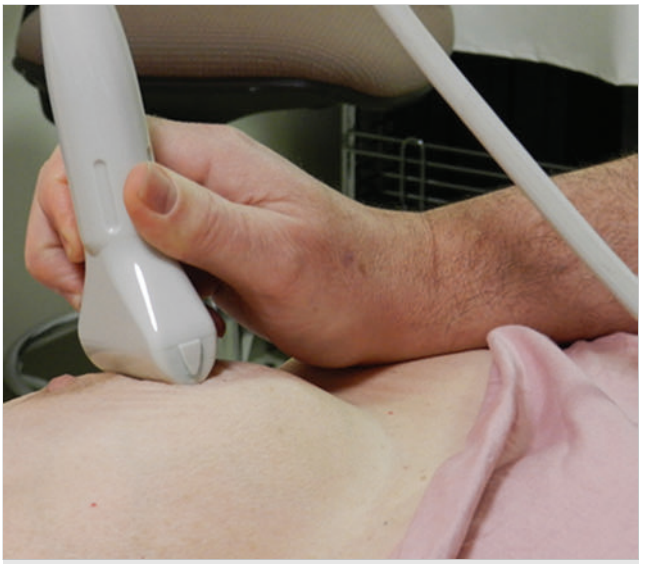

Fig. 2.6 Patient and transducer positioning for obtaining optimal elastograms. The patient should be positioned so that the imaging plane is the same as plane of patient's respiration movements. Placing the palm of the scanning hand on the patient will help stabilize the transducer and improve the ability to execute fine movements.

2.2.2 Display of SE Results

▶ Fig. 2.7 demonstrates a simplified explanation of how the mapping of SE data is performed on most systems. The boxes on the left represent tissue identified on B–mode imaging before the application of any compressive force. The boxes in the middle represent the deformation of the same tissue on B-mode imaging after the application of compressive force. The tissues that do not change shape are very stiff, while those that are soft change size based on their relative stiffness. The strain elastography algorithm evaluates the relative changes in size of the tissues and assigns a color (or shade of gray) based on the distribution of the size changes in the image. In our example in ▶ Fig. 2.7a, the tissue that does not change shape at all is color-coded black as it is the stiffest of all the tissue being evaluated. The lower box changes the most and is therefore the softest and is color-coded white. The tissue in between these extremes is given a shade of gray corresponding to the amount of change in the tissue; darker gray if stiffer and lighter gray if softer. However, if we did not include the stiffest tissue in field of view (FOV) of ▶ Fig. 2.7a, different color-coding of the other tissues will result, as in ▶ Fig. 2.7b. Note that the coloring of the first three tissues has changed because the second tissue is now the stiffest and is therefore coded black. Thus, the range of stiffness values is dynamic; it changes depending on the tissues present in the FOV. Thus, the "color" of a tissue will vary depending on the FOV.

Therefore, if the same variety of tissues are included in each image acquired, a more relatively constant color display will be obtained for each tissue. For example, in breast SE, if a portion of the pectoralis muscle, glandular tissue, and some fat are included in the FOV each time, a more consistent color (or grayscale) depiction of these tissues will be obtained across images. The fat will be the softest tissue coding white and the pectoralis muscle will be the stiffest tissue (if a cancer is not present) coding black. The color scale (or dynamic range of stiffness values) will be fairly constant as the stiffness of fat and pectoralis muscle are very constant between patients and within a patient. However, if a breast cancer, which is stiffer than pectoralis muscle, is present within the FOV, it will be the stiffest tissue and will be black, with most other tissues being displayed as white or light gray.

Results can be displayed in grayscale or with various color displays; which is preferred is often determined by the user's exposure to elastography and preference in interpretation. The choice of display map is a postprocessing function, and, on most equipment, the map can be changed when the image is frozen. The default on many systems has the elastogram displayed over the grayscale B-mode image. Most systems display in a dual mode, with a separate B-mode image also displayed. This helps in determining the location of the elastographic findings. However, if a grayscale map is chosen, the background B-mode image in the elastogram should be turned off, as the two superimposed grayscale images are difficult to interpret. Because color display scales can code red as stiff and blue as soft or vice versa, it is important to always include the color display scale in the image for accurate interpretation.

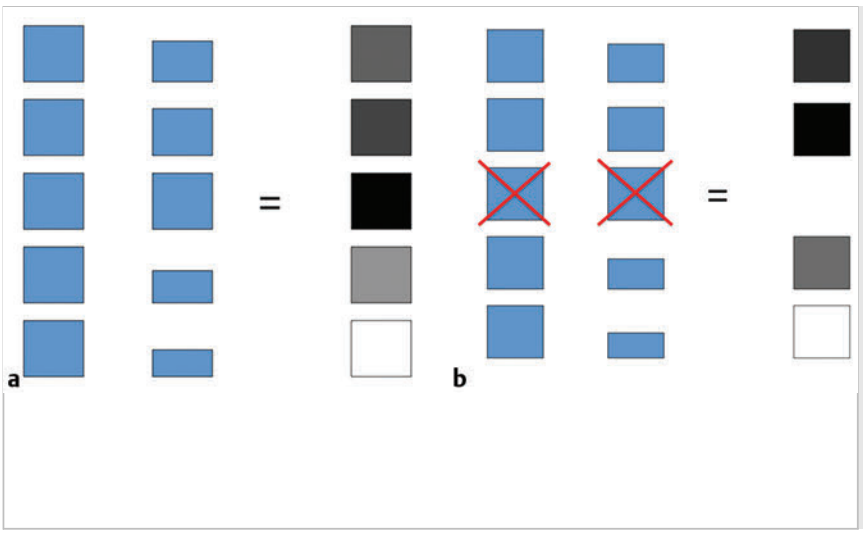

Fig. 2.7 Changes that occur in the color-coding of the pixels in the elastogram based on changes in the field of view (FOV). In these diagrams, the boxes on the left depict different tissues within the field of view. When compression is applied, the boxes change shape based on the stiffness of the tissue (center column). The box that changes shape the most is color-coded white, while the box that changes the least is color-coded black (right column). The boxes whose changes are between these two extremes are color-coded in shades of gray based on the amount of change they experience (**a**). If the FOV is changed (**b**) and the stiffest tissue in (**a**) is not included, the color mapping changes, with the second box now the stiffest and therefore being color-coded black. The dynamic range of the color-coding changes and the first and fourth tissues are now color-coded with darker shades of gray.

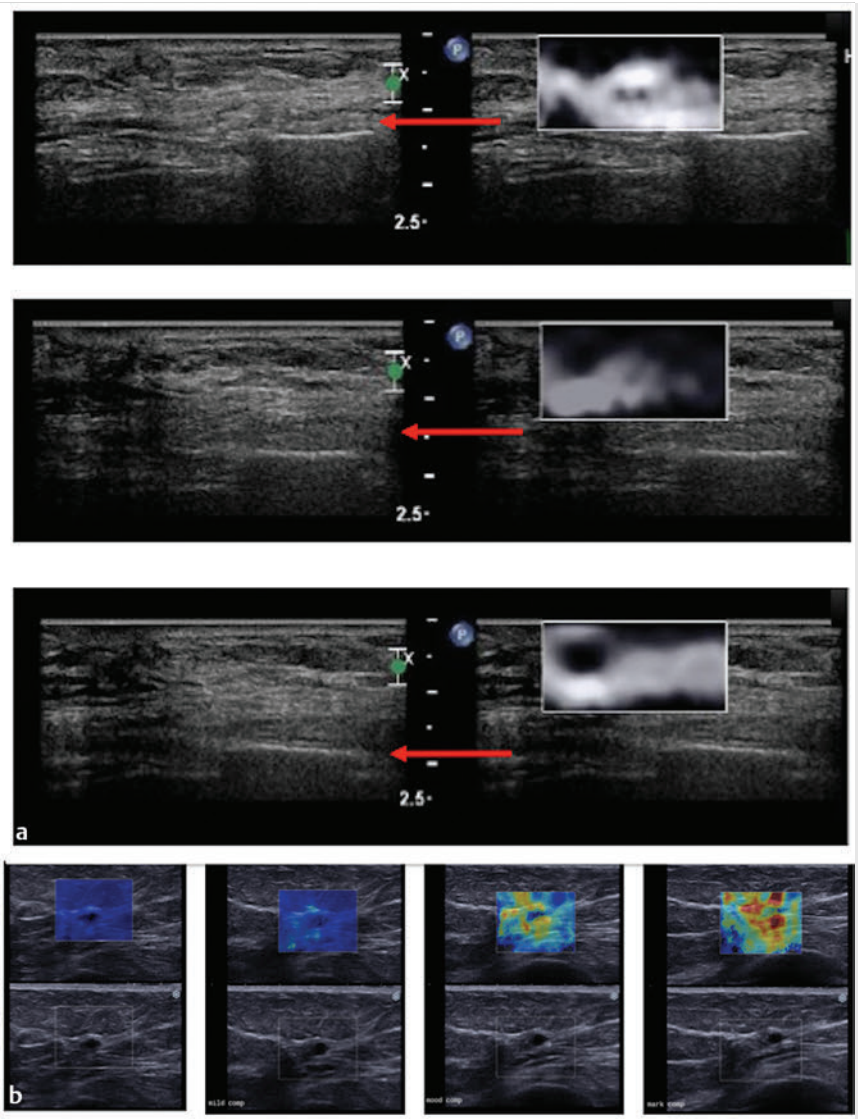

Fig. 2.8 When precompression is applied with the transducer, it can significantly affect both SE and SWE results. In (**a**), SE images of an epidermoid cyst are presented. The red arrows point to a rib. The upper image has significant precompression, the middle moderate precompression, and the bottom minimal precompression. Note as precompression is released, the rib moves deeper in the image. When minimal compression is applied (bottom image), optimal elastograms are obtained. In this case, the elastograms will be consistent during a cine clip. When moderate precompression is applied, the frames obtained on the release phase are often good; however, those on the compression phase are of poor quality (middle image). When a significant amount of precompression is applied, the elastogram is only noise and is not interpretable (upper image). Similar effects are seen with SWE (**b**). In this figure, the SWE of a simple cyst is presented with increasing amounts of precompression. The SWSs increase as precompression is applied. Note that rib in the far field is located closer to the transducer as precompression is added. With moderate precompression, a benign lesion can have shear wave speeds (V_s) suggestive of a malignancy.

It is important to remember that when using color-coded SE, only a relative stiffness value is obtained, which should not be confused with SWE where an absolute stiffness value is obtained and color-coded on a per pixel basis. On SWE, in the color display a lesion will have the same color (assuming the same color scale is used for each image obtained) regardless of the other tissues present in the FOV. On SE the lesion may appear a different color if the other tissues in the FOV are different.

2.2.3 Precompression

A critical factor in generating a diagnostic elastogram is the amount of pressure you apply with the probe to the patient when scanning.[5] This is called precompression, or preload. This is different than the amount of displacement (compression–release) used in generating the elastogram. Scanning with a "heavy hand" compresses the tissues and changes their elastic properties. For example if you have a balloon filled with air and lightly touch the balloon you create a moderate displacement of the balloon. However, if you compress the balloon between two heavy books and then lightly touch the balloon, you will create a much smaller displacement because the compression caused by the books increases the air pressure in the balloon.

This precompression markedly changes the image quality and can significantly affect results (▶ Fig. 2.8).[5] This is confirmed with SWE where the SWS can change by a factor of 10 with precompression. As precompression increases, the differences in SWS between tissues decreases, leading to less conspicuity between tissues on the strain elastogram. If enough precompression is applied, all tissues will have similar stiffness and the SE elastogram will be mostly noise while the SWE will have high shear wave speeds thoughout the image.

▶ Fig. 2.9 summarizes the SWS of the different tissue types in the breast at the various amounts of precompression. The amount of precompression is classified into 4 zones: zone A, minimal precompression, 0 to 10%; zone B, mild precompression, 10 to 25%; zone C, moderate precompression, 25 to 40%; and zone D, marked precompression, > 40%.

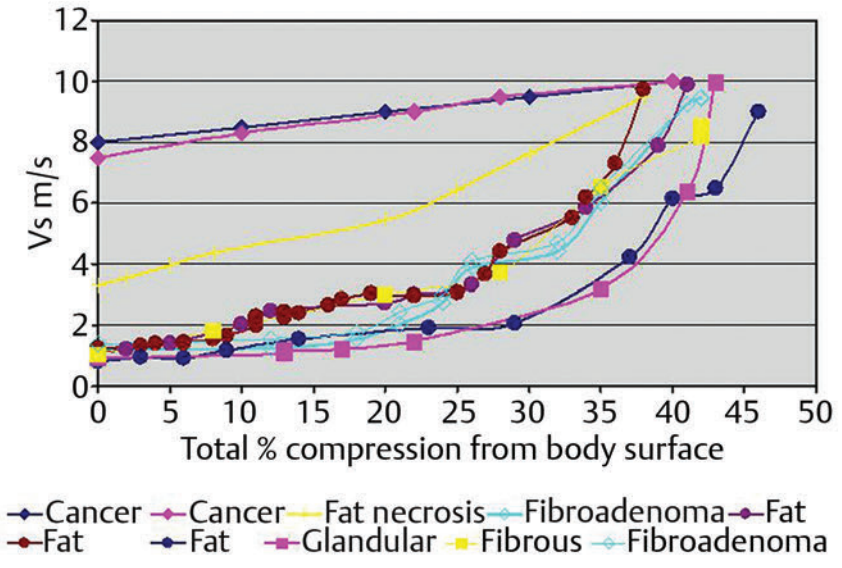

Fig. 2.9 Average changes in the Vs in tissue types that occur in the breast. We identified 4 regions of precompression that explain clinical elastographic results. In zone A (0%–10% precompression using the technique for measuring precompression), clinical results using both strain and shear wave elastography are not affected. In zone B (10%–25% precompression), strain images with only benign pathologic characteristics begin to degrade, whereas shear wave elastographic measurements increase but in general will not change from a Vs suggestive of a benign lesion to a value suggestive of a malignant lesion. In zones C (25%–40% precompression) and D (>40% precompression), strain images with benign pathologic characteristics show only noise as the elastic properties of all of the tissues become too similar to distinguish. If a malignant lesion is present, strain imaging will be accurate in zones A, B, and C as the elastic properties of normal breast tissues remain different enough from the malignancy to provide accurate results. Benign lesions in zones C and D on shear wave will have Vs and kPa values suggestive of a malignant lesion. It is recommended that all clinical images be obtained in zone A. (Reproduced with permission from Barr RG, Zhang Z. Effects of precompression on elasticity imaging of the breast. J Ultrasound Med 2012; 31:895–902.)

How Can Precompression Affect Strain Elastography Images?

In SE, images are based on the relative stiffness of the lesions within the FOV of an image. It is qualitative (how stiff relative to other tissues in the field of view) but not quantitative (an absolute value). The imaging scale used is relative and based on tissues within the image plane. Using breast as an example, in the case where both soft tissues (fat, fibroglandular tissue) and a very stiff lesion (malignancy) are present in zones A, B, and C, the difference in elasticity (SWS measured in meters per second [m/s]) between the soft tissues and the malignant tissues are adequate to generate an accurate elastogram. However, in zone D the elasticity of both the soft tissues and malignancies are similar; hence, the elastogram is not diagnostic and only represents noise.

However, in a case where the area of interest contains only soft tissues (fat, fibroglandular tissue, soft fibroadenoma, or fibrocystic change) the results are different. In zone A, the elasticity differences between the tissues allows for a diagnostic elastogram. In zone B, the elastogram is borderline for diagnostic value with some frames of good diagnostic quality and some of poor diagnostic value. This is due to precompression, which has made the difference of stiffness between tissues smaller. Based on the author's experience, this appears to depend on if the frame was taken in a compression or release phase of the cycle. This may be due to the increased precompression on the compression phase of the cycle. In zones C and D, the elasticity properties of the soft tissues are very similar due to the precompression and the elastogram is mostly noise and nondiagnostic.

In one technique to apply a minimal amount of precompression reproducibly,[5] a structure in the far field is identified, such as a rib or Cooper's ligament. The transducer is lifted slowly while watching the structure. As the probe is lifted, the structure will move deeper in the image. While keeping the structure as deep in the image as possible and having adequate probe contact, the elastogram is obtained. The use of ample coupling gel is helpful. This technique has been shown to be highly reproducible both intraoperator and interoperator.[5]

Another technique that can be used to apply a minimal amount of precompression is to make a standoff pad with coupling gel, making sure some coupling gel is present between the transducer and the patient when obtaining the elastogram.

The quality factor or compression bar used by some vendors does not assess the amount of precompression being applied, just the displacement of tissues during the compression–release cycle. Even when significant precompression is applied leading to a poor elastogram, the quality factor or compression bar can suggest a good elastogram was obtained.

Usually a small amount of precompression (10–20%) is used to obtain B-mode images as it improves B-mode image quality.

2.2.4 Strain Elastography Using ARFI

An ultrasound pulse can be reflected or absorbed (attenuated), or it can transfer its momentum (it can push). This transfer of energy causes tissue to move. Increased energy in the ultrasound beam creates increased force and hence movement. The movement of the tissue has two consequences for elastography: (1) it can be measured directly in strain elastography; or (2) it can generate a lateral transverse (shear) wave through the tissue, the speed of which can be measured in shear wave elastography.

Acoustic radiation force impulse (ARFI),[6,7,8] a low-frequency ultrasound pulse which is tailored to optimize the momentum transfer to tissue, can also be used to create the displacement of tissue. The ARFI pulse replaces the patient or probe movement to generate the stress on the tissue. By analyzing the tissue

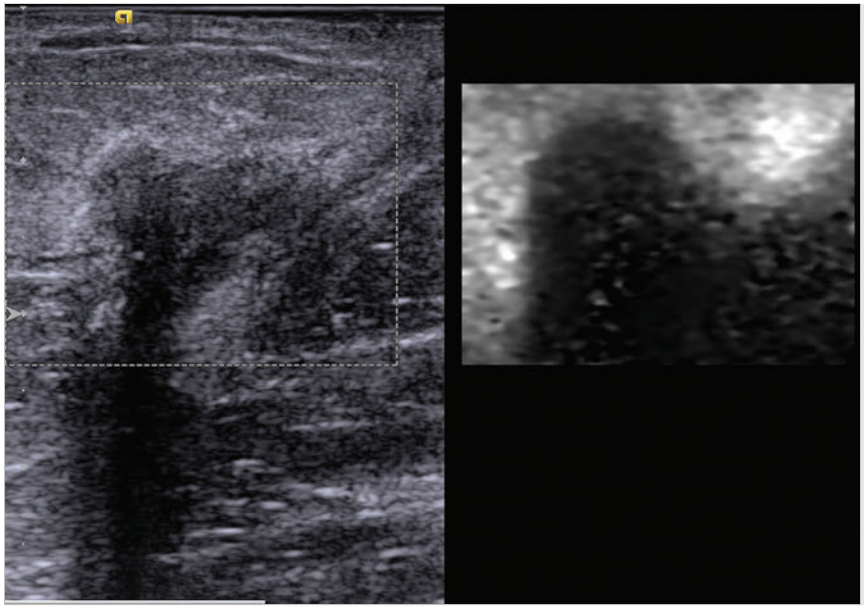

Fig. 2.10 An ARFI pulse creates two types of tissue motion, the displacement of the tissue and the generation of shear waves. When the displacement is tracked, a strain elastogram is obtained. This is an example of an SE elastogram (so only relative stiffness values are displaced) of invasive ductal cancer using Virtual Touch imaging (VTI, Siemens Ultrasound, Mountain View, CA). As opposed to SE using the manual compression technique, the FOV has a maximum allowable size and is placed to include the lesion. Using a very light touch with the transducer on the breast, the patient is asked to remain still and not talk while the update button is pressed to activate the ARFI pulse. The system will freeze for a few seconds and then the VTi image will be displayed. The grayscale map is used here with black as stiff and white as soft. The lesion is significantly stiffer than the surrounding breast tissue.

displacement (not the shear waves generated), a SE image can be generated. This technique may be less user dependent than the manual compression technique.

Note that this SE technique is different than SWE technique where the speed of shear waves generated from the ARFI pulse are measured. The SE technique is qualitative (it provides a relative measure of the tissue stiffness in the field of view) while the SWE technique is quantitative (it provides a numerical value of the tissue stiffness). The power of ARFI push pulse is limited by guidelines on the amount of energy that can be put into the body, thus limiting the depth of tissue displacement and therefore the tissue depth of the SE elastogram. This is usually not a problem. When the tissue of interest is too deep, manual displacement technique can be used as it can be adjusted to have appropriate displacement at any tissue depth.

If an ARFI push pulse is used to generate the tissue displacement, no manual displacement (transducer compression-release) should be used. This technique is implemented on one vendor's system, Virtual Touch Imaging (VTI, Siemens Ultrasound, Mountain View, CA). The probe should be held steady and the patient should refrain from talking, suspend their respiration, and remain motionless during the image acquisition. An ROI box is placed over the area of interest. Because of the power of the ARFI pulse, the system will freeze for a few seconds for transducer cooling. During this period, the system will not respond to knob activation. The color-mapping algorithm is slightly different than that used in the manual compression technique and some differences in the appearance of the elastogram between the two techniques can be seen. In general the ARFI push pulse is limited in producing tissue displacement deeper than 4 to 5 cm with most small-parts (e.g., breast, thyroid, testicles, salivary glands) imaging transducers and 8 cm with abdominal transducers. The ARFI pulse is only generated within the ROI box; therefore only the ROI box has strain data within it on the elastogram (▶ Fig. 2.10).

2.2.5 Interpretation

Three methods of interpreting SE have been proposed: evaluating the size change between the B-mode image and the elastogram (E/B ratio), various color scale scores, and the strain ratio (ratio of the lesion stiffness to that of a reference tissue). The relative stiffness (i.e., is the lesion stiff or soft) can also be helpful clinically in interpreting images.

E/B Ratio

Breast tissue has a very unique elastographic feature. Different than cancers of other organs, breast cancers appear larger on elastograms and benign lesions appear smaller as compared to their corresponding B-mode images. This unique feature is not fully understood but has been shown to be highly sensitive and specific for characterizing breast lesions.[9,10,11]

The location where the elastogram is taken within the lesion does not affect the results.[2] Either the lesion length ratio or a lesion area ratio can be used for computing this ratio. The lesion is measured in the same position on both the elastogram and B-mode image. The use of a copy, shadow, or mirror function in the measurement technique is helpful. These software keys allow one to measure the lesion on either the B-mode image or elastogram image in a dual mode display and have the length measurement depicted on the opposite image in the exact same position (▶ Fig. 2.11). This allows for one to determine if the ratio is greater or less than 1 visually. One can then correct the copied or mirrored image measurement to obtain the ratio. This method of interpretation requires that the lesion be visualized well enough to get an accurate measurement on both the B-mode image and the elastogram image. Difficulty can occur when measuring the lesion size on the elastogram when a fibroadenoma or fibrocystic lesion is present in dense breast tissue. The strain properties of the fibroadenoma or the fibrocystic lesion are similar to the background dense breast tissue. Therefore, one may visualize the combination of the lesion and normal dense breast tissue as one lesion, creating a false positive.[2] This problem can be avoided by comparing the stiffness of the lesion to surrounding tissue; if it is similar to fibroglandular tissue it is most likely benign (discussed in detail below).[12]

Previous studies[7] have demonstrated that the sensitivity of this technique is quite high (> 98%). In a large multicenter trial,

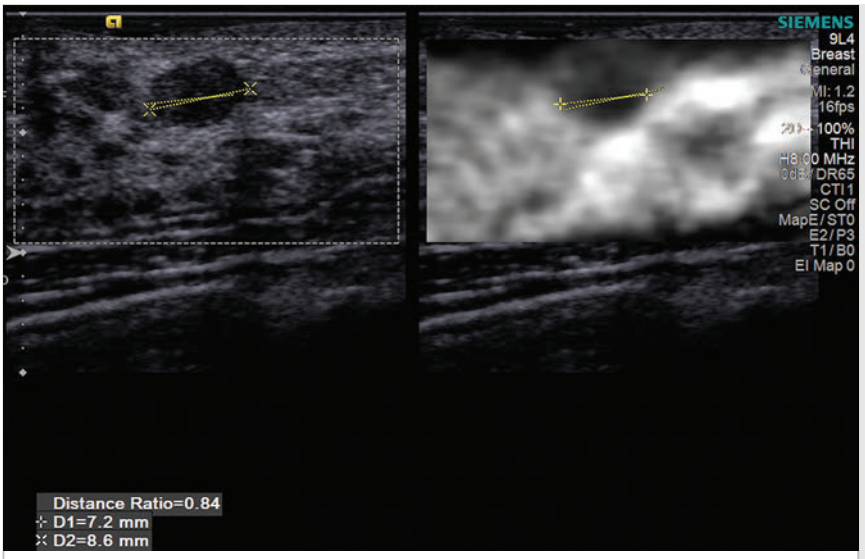

Fig. 2.11 Strain elastogram of a fibroadenoma. The image on the left of the dual display is the conventional B-mode image, and the image on the right is the elastogram. A black and white color scale is used for the image with black corresponding to stiffest tissue. In this example, the lesion measures 8.6 mm on the B-mode image and 7.2 mm on the elastogram, resulting in an E/B ratio of 0.8 suggestive of a benign lesion. A copy or shadow function is used to "duplicate" the measurement on the B-mode image to the same location on the elastogram (*yellow lines*). This function is helpful in confirming the location of a lesion in the elastogram or in the B-mode image. The use of a copy or shadow function can help in confirming the location of a lesion noted on one image but not easily seen on the other. This function allows you to measure a lesion and have the measurement placed in the identical position in the other image. In this example, the dotted yellow line with the x's is the actual measurements of the lesion. The dotted yellow line without the x's is the copied measurement from the other image.

there were 3 cancers out of 222 that had a ratio of less than 1 (see Chapter 5 Elastography of the Breast). One difficulty that occurs is in measuring the lesion size on the elastogram when a fibroadenoma or fibrocystic lesion is present in dense breast tissue. The strain properties of the fibrocystic lesion or fibroadenoma are similar to the background dense breast tissue. Therefore one may visualize the combination of the lesion and normal dense breast tissue as one lesion, therefore concluding that the lesion is larger and therefore malignant. Another confounding factor is the presence of two lesions adjacent to each other. These may appear as one lesion on the B-mode image. Close inspection of the elastogram can distinguish the two lesions. In these cases, care must be taken in performing measurements. If different results are obtained when the lesion is positioned differently in the image, the possibility of the lesion being two adjacent lesions should be considered. Always use the results of the larger E/B ratio. If such a lesion is biopsied, always try to biopsy the portion of the lesion that has the largest E/B ratio. The E/B ratio has been shown to correlate with breast tumor grade.[13]

Various Color Scale Scores

Various 4- or 5-point color scales have been proposed to evaluate elastograms. These vary by the organ being evaluated. In these scales, the color-coded appearance of the lesion is evaluated usually with a score of 1 for very soft lesions and higher scores for lesions of increasing stiffness. The scales used for the various applications are discussed in the appropriate clinical chapters in this book. It is important when using these color scales that the same color display map for the image is used; that is, if the scale designates stiff as blue and soft as red, then the color display map for the image being evaluated must do the same. Studies then evaluate the probability of malignancy for each of the color-coded scores.

As an example, a 5-point color scale (Tsukuba score) has been proposed to classify breast lesions using SE (▶ Fig. 2.12).[14,15] This scale combines the ratio changes and degree of stiffness of the lesion. In this diagnostic approach, a score from 1 to 5 is assigned based on the color (balance of green and blue, with the scale set to blue as stiff) inside the target lesion and surrounding area on the elastogram, with a higher score indicating a higher diagnostic confidence of malignancy. When a lesion is hard and the same size on the elastogram as in the B-mode image, the lesion is given a score of 4. If the lesion is hard and larger on the elastogram than on the B-mode image, the lesion is classified as 5. It is recommended that lesions that are hard and equal in size to B-mode or larger on the elastogram than B-mode are biopsied. If the lesion is soft, it is classified as a score of 1. If the lesion has a mixed hard and soft pattern, it is classified as a 2. If the lesion is hard but smaller on the elastogram, it is given a score a score of 3. Scores of 1 to 3 are classified as benign. This technique has been shown to have moderate to substantial interobserver agreement and substantial to perfect intraobserver agreement.[16] There was no significant difference in interobserver and intraobserver agreements according to lesion size. If another color scale is used with this technique (such as red is stiff), the appropriate changes to the colors in the scale need to be made. When making a diagnosis using this method it is important to choose an FOV that includes various other tissue types (depending on tissue being evaluated) and the lesion should account for no more than 1/4 to 1/2 of the FOV.

Strain Ratio

Taking the *strain ratio*, the ratio of lesion stiffness to that of another tissue that has fairly constant stiffness, is a semiquantitative method of evaulating strain. This ratio is based on the knowledge that the properties of certain reference tissues (e.g., fat in breast evaluation) are fairly constant, whereas the properties of other surrounding tissues and lesions are variable. This diagnostic approach was advocated by Ueno et al[17] as a semiquantitative method of evaluating stiffness. For breast imaging,

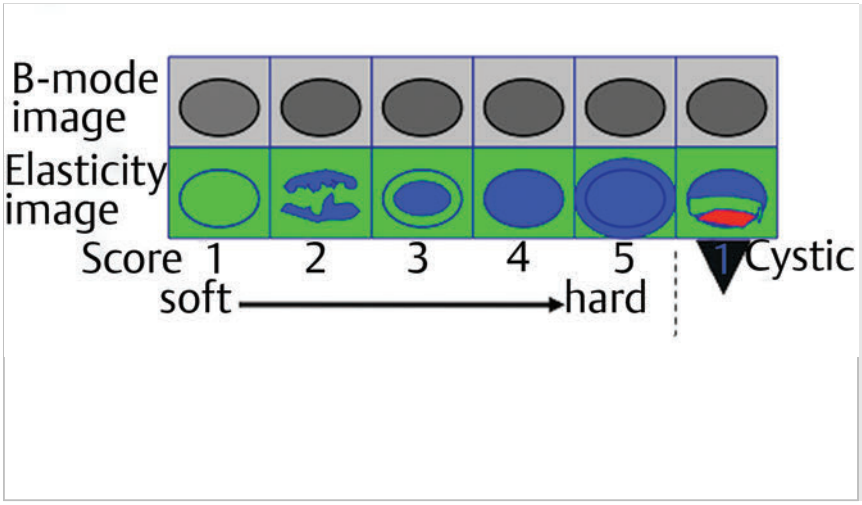

Fig. 2.12 A 5-point color scale that has been proposed as a method of characterizing breast masses as benign or malignant. In this example of the scale, stiff lesions are coded blue and soft lesions are coded green and red. If a lesion is entirely soft, it is given a score of 1. If the lesion has both soft and stiff components, it is given a score of 2. If the lesion is stiff but smaller than the lesion on B-mode imaging, it is scored as 3. If the lesion is stiff and the same size as on the B-mode image, it is given a score of 4 and, if stiff and larger than on the B-mode image, it is given a score of 5. A score of 1, 2, or 3 is suggestive of a benign lesion, while a score of 4 or 5 is suggestive of a malignant lesion.[14] Other color scales are used and discussed in the clinical chapters, Chapters 3 to 11. For some systems a three color pattern, blue, green, red (BGR) is seen with cysts.

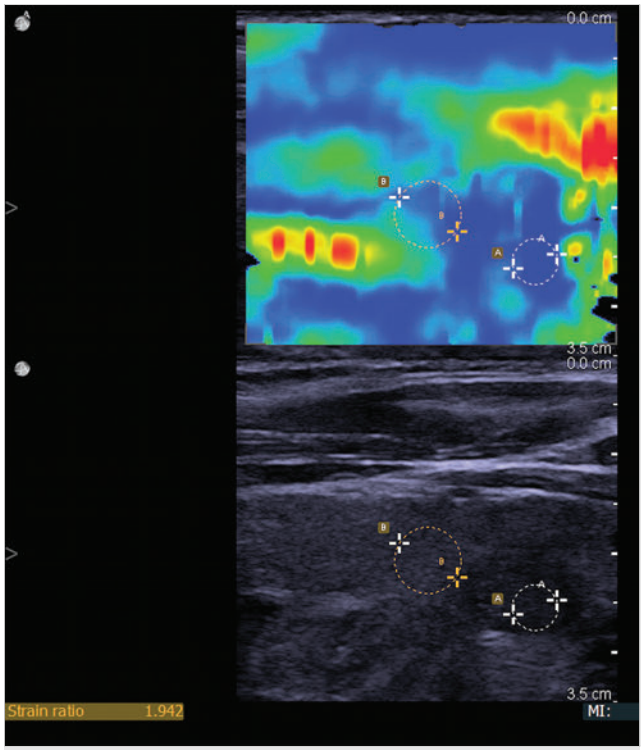

Fig. 2.13 One method of obtaining semiquantitative measurements in SE imaging is to compare the strain (stiffness) of the lesion to that of a reference tissue. In this example, the white "A" ROI is placed on a thyroid lesion and the yellow "B" ROI is placed in normal thyroid tissue. The color scale used has blue as stiff and red as soft. The system then calculates a strain ratio, in this case 1.9, meaning the lesion has 1.9 times the strain of the normal thyroid tissue. Cutoff values for this technique are discussed in the clinical chapters, Chapters 3 to 11.

the strain ratio is the ratio of the strain in a mass to the strain in subcutaneous fat, and it can be thought of as a semiquantitative method for numerically evaluating how many times stiffer the mass is as compared to subcutaneous fat.

The ROIs should be taken at the same depth from the skin surface if possible to limit errors from differing compression at differing tissue depths, especially if one is using a system that requires more displacement to obtain the elastogram. When applying the compression–release cycle, tissues at different depths experience different amounts of compression that change the stiffness of the tissue. Care should also be taken not to use the very soft signal sometimes seen adjacent to lesions because this is an artifact and will artificially elevate the strain ratio. ▶ Fig. 2.13 is an example of a strain ratio measurement.

It is possible to evaluate the stiffness of one specific part of a mass or of a nonmass abnormality by placing the target ROI where desired. The stiffness of the area of interest is an approximation. It is easy to perform, and the results of clinical studies using this diagnostic approach have already been reported and are discussed in Chapters 3 to 11.

Care must be taken with these measurements as precompression can significantly change the strain value of the reference tissue.[5] As precompression is applied, the stiffness of all tissues increases. However, the stiffness of some tissues will change more rapidly than others. For example, the of fat changes more rapidly than that of other tissues. Therefore, with precompression, the strain ratio of lesion to fat will decrease. Care must also be taken that the FOV for the reference tissue measurement contains only uniform reference tissue.

In addition to performing a single measurement comparing the lesion strain to that of a reference tissue, one vendor offers parametric imaging. In this technique, an ROI is placed in an area of the reference tissue and the entire FOV is color-coded based on the ratio of each pixel's stiffness to the stiffness of the reference tissue (▶ Fig. 2.14). A color-coded semiquantitative image is obtained over a large FOV. The area with the highest strain ratio can then be identified visually and a point measurement obtained.

The cutoff value to distinguish probably benign from probably malignant lesions for this technique can vary greatly between studies. The result can vary between vendors, as the stiffness may be calculated differently by different systems. When using this technique, the appropriate cutoff in your lab should be determined with your technique and equipment.

Lesion Relative Stiffness

In addition to using the methods previously discussed to determine if a lesion is benign or malignant, information about

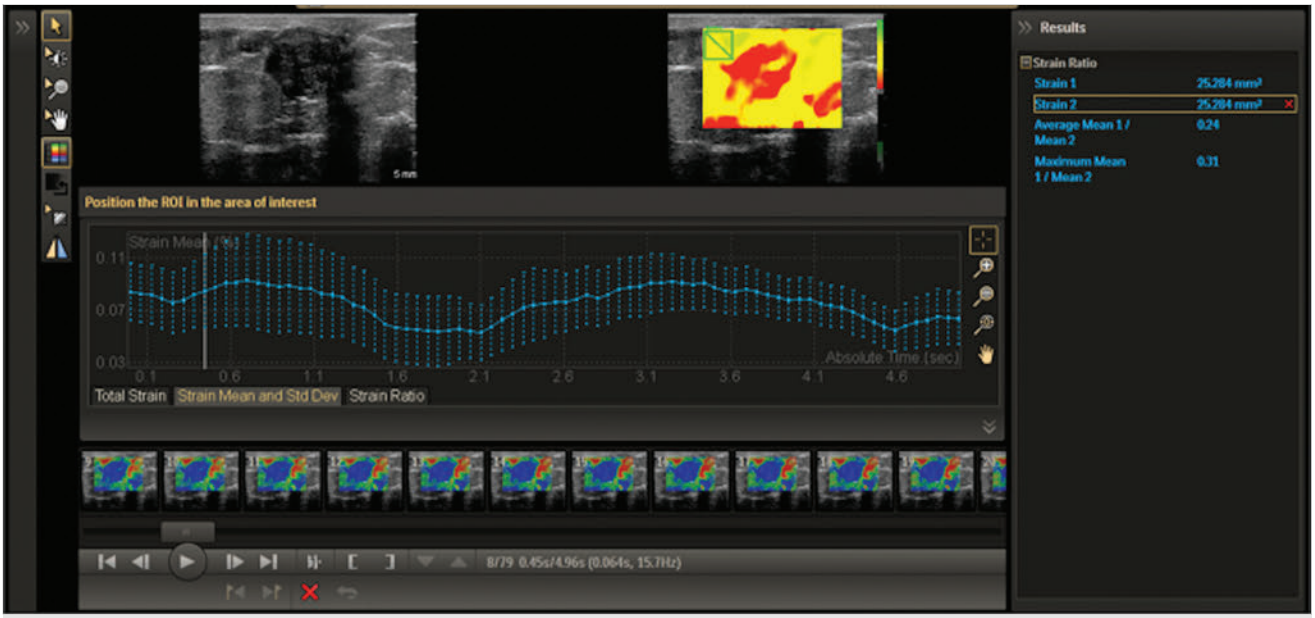

Fig. 2.14 In addition to performing a single measurement of the ratio of lesion stiffness to fat stiffness (strain ratio or lesion to fat ratio), parametric imaging can be performed. An ROI is placed to demarcate fat, the reference tissue, and the entire image is color-coded to indicate the strain ratios, with red indicating higher strain ratios. In this example, the green box is the ROI placed on fat.

whether a lesion is soft, hard or visible on elastography imaging is clinically helpful in some situations.

If a lesion has the same stiffness as fat in the image, the lesion should be considered to be a lipoma. Comparison to other tissues in the FOV can also be helpful. If a hypoechoic breast lesion has a similar stiffness to glandular tissue, it is most likely benign (for example, a fibroadenoma or fibrocystic change); malignant lesions are much stiffer than glandular tissue.

2.2.6 Limitations

There is a learning curve to routinely apply the appropriate stress in the manual displacement SE technique. Accuracy of readings can differ between shallow tissue sites and deep tissue sites due to problems associated with variable displacement of tissues at different depths. Further improvement of applications and adjustments to imaging methods are needed to overcome these problems.

2.2.7 Artifacts

There are several artifacts that can be encountered with SE, some of which result from suboptimal technique, while others contain diagnostic information.

Bull's Eye Artifact

A unique artifact, the *bull's eye artifact*, is found in images of cystic lesions in some systems (▶ Fig. 2.15). This artifact has been described in detail.[18] It is characterized by a white central signal within a black outer signal and a bright spot posterior to the lesion.[18] It is caused because fluid is moving in the cysts; therefore there is decorrelation of pixels in adjacent images. This artifact has a high predictive value for the lesion being a benign simple or complicated cyst. If there is a solid component in the cyst, it will appear as a solid lesion within the pattern (▶ Fig. 2.16).

Blue-Green-Red Artifact

Some systems have a *blue-green-red (BGR) artifact* that occurs in elastograms of cysts (▶ Fig. 2.17).[2,14,15] A detailed study evaluating the sensitivity and specificity of this artifact has not been performed.

Sliding Artifact

A white ring or group of circular wavelike artifacts around a lesion on the elastogram indicate the lesion was moving in and out of the imaging plane while the elastogram was being obtained (▶ Fig. 2.18). This has been named the *sliding artifact*.[2] Having the lesion remain within the imaging plane during the image acquisition can eliminate the artifact. Repositioning the patient, using less compression, or having the patient hold their breath may help keep the lesion in the scanning plane.

Worm Pattern

If there is very little variability in the elastic properties of the tissues within the FOV or when significant precompression is applied, a varying signal pattern is noted representing noise (▶ Fig. 2.19). This has been named the *worm pattern*.[2] There is

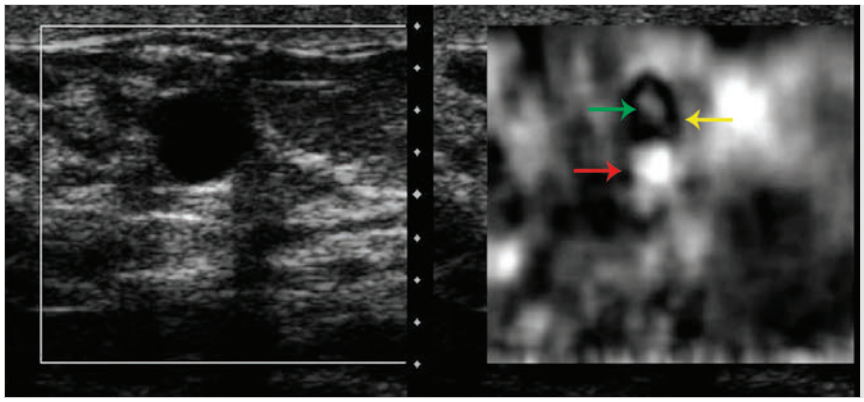

Fig. 2.15 On some systems an artifact, the bull's eye artifact, is identified with benign simple and complicated cysts. This artifact is characterized with the cyst black (*yellow arrows*) with a bright central spot (*green arrow*) and a bright spot behind the cyst (*red arrow*). This artifact has been shown to have a very high sensitivity and specificity for characterization of benign cystic lesions. (Reproduced with permission from Barr RG, Lackey AE. The utility of the "bull's-eye" artifact on breast elasticity imaging in reducing breast lesion biopsy rate. Ultrasound Q 2011; 27(3):151–155.)

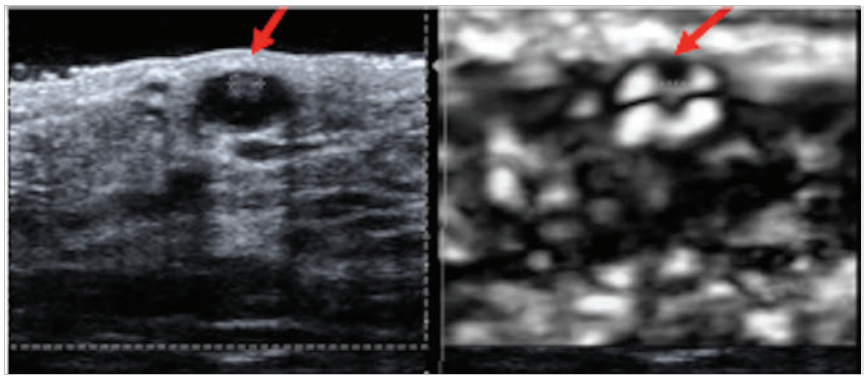

Fig. 2.16 If a cystic lesion has a solid component (i.e., a complex cystic mass), the solid component will appear as a stiff defect in the bull's eye artifact. In this example of a benign papillary lesion, the solid component (*red arrow*) appears as a stiff defect in the bull's eye artifact. (Courtesy of Carmel Smith, Brisbane, Australia.)

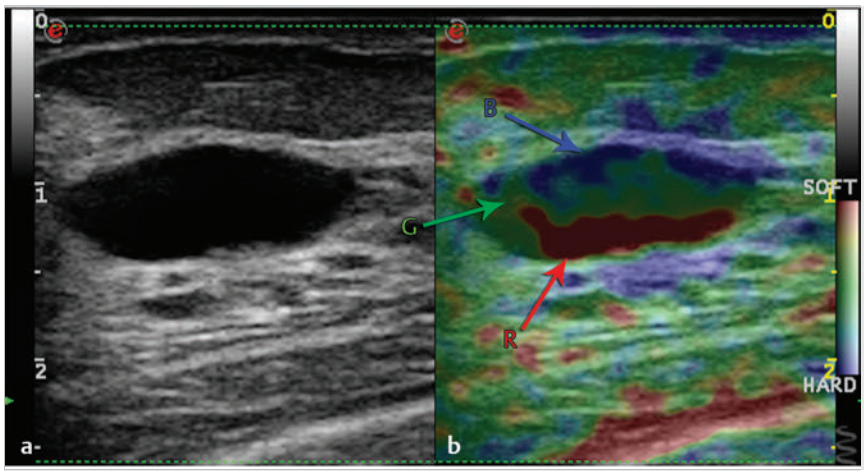

Fig. 2.17 In some systems, the bull's eye artifact is not observed for cystic lesions, but instead a blue-green-red (BGR) artifact is observed. This is an example of this artifact in a simple cyst using a grayscale map (**a**) and using the color map with blue as stiff (**b**).

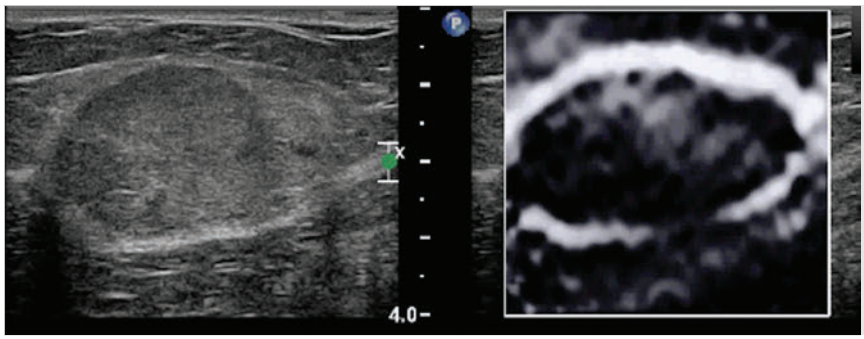

Fig. 2.18 When a lesion is moving in and out of the imaging plane during the elastogram acquisition, a sliding artifact occurs.[2] The artifact is characterized by a white ring or series of rings surrounding the lesion on the elastogram. This example of a sliding artifact is a lipoma. The artifact signifies the lesion is not attached to adjacent tissue and is therefore unlikely to be a malignancy.

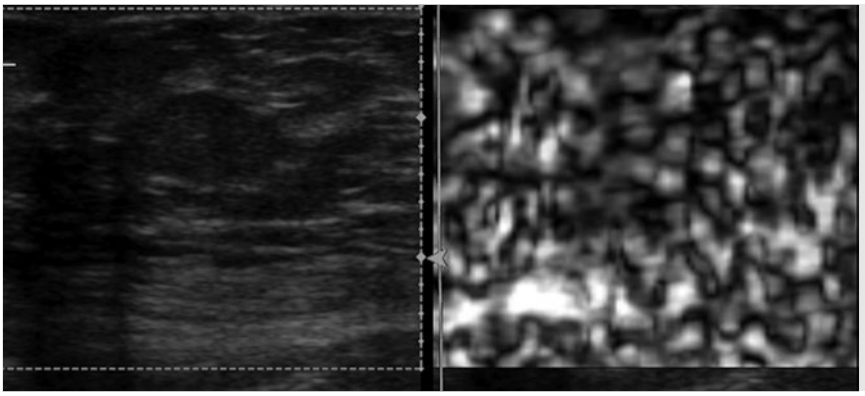

Fig. 2.19 When there is very little variability of tissues stiffness within the strain elastogram field of view, only noise is obtained. As in this example, the pattern seen is one of varying white and black areas within the entire field of view. This artifact can be seen when significant precompression is used.

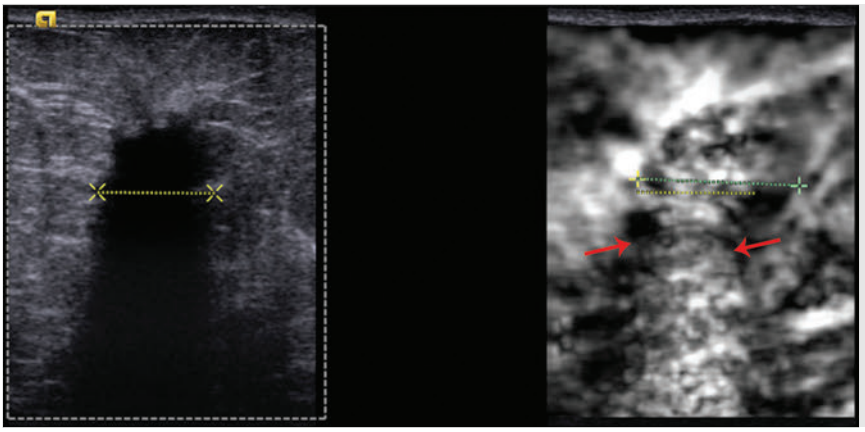

Fig. 2.20 In this image of an invasive ductal carcinoma, there is significant shadowing. If the shadowing is marked, the elastogram will demonstrate a white-black artifact pattern in the area of the shadowing, and the posterior border of the lesion will not be identified (*red arrows*).

no clinical information in these images. This artifact can be eliminated by the use of minimal precompression and by including a range of tissues of varying stiffness within the field of view.

Shadowing Artifact

The degree of tissue deformation used to calculate the strain is based on the frame to frame changes in the returning B-mode signal. In cases where there is B-mode shadowing, the returning signal amplitude is decreased in the areas of shadowing. If the shadowing is not severe, a strain elastogram is obtained in the areas of shadowing. However, if the shadowing is severe and little or no signal is returned, an accurate strain value is not obtained and a pattern of white and black blotches occurs, the *shadowing artifact* (▶ Fig. 2.20). This artifact can also occur in areas of marked refractive shadowing.

2.2.8 Tips and Tricks

- Keep the FOV large enough to include tissues with varying stiffnesses. This will maintain a more constant color map (and a consistent dynamic range of strain values) between images.
- Maintain a FOV where the lesion of interest is less than 50% of the FOV.
- Use the B-mode image to determine the amount of tissue displacement being applied.
- Maintain the transducer perpendicular to the lesion and in the plane of motion.
- Use the appropriate technique for your system.
- Use the B-mode image to confirm that the scan plane through the lesion remains constant.
- Position the patient so the displacement motion is in the plane of the transducer.
- Do not apply precompression with the transducer.
- Compare the lesion stiffness to that of the other tissues (i.e., in the breast, fat and normal breast tissue).
- Have the patient hold still and maintain uniform shallow breathing. No talking during data acquisition.
- Turn off the background B-mode image on the elastography image if a grayscale map is used for the elastogram.
- Remain in a stationary plane when acquiring data (do not survey).
- Acquire static and cine clips.

2.3 Shear Wave Elastography

The second technique to determine the elastic properties of a tissue is shear wave speed (SWS) measurement.[6,7,8,19,20,21,22,23] In this technique, an initial ultrasound pulse (push pulse), or ARFI pulse, is applied to the tissue that induces a shear wave perpendicular to the ultrasound beam. This is similar to dropping a stone (the push pulse) into a lake: the ripples generated correspond to the shear waves. Conventional B-mode ultrasound sampling techniques are used to calculate the velocity of the shear wave generated through the tissues by monitoring the tissue displacement caused by the shear waves. This is diagrammed in ▶ Fig. 2.21. From the shear wave speed (SWS) through the tissues the strain modulus (called Young's modulus)

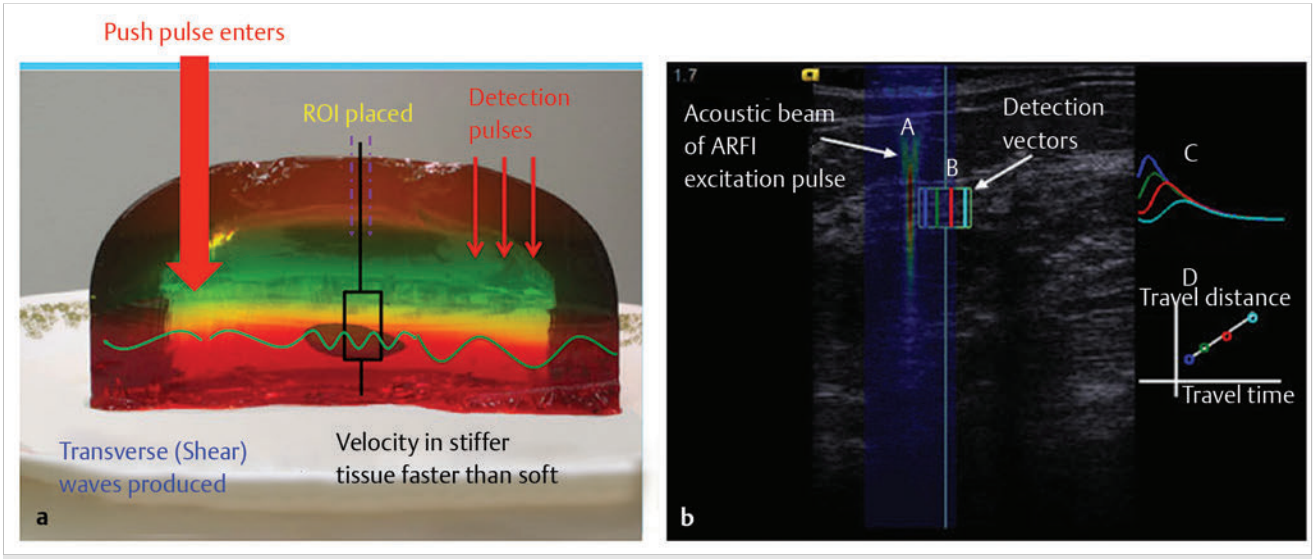

Fig. 2.21 (**a**) A simplified model of shear wave imaging using the almond in gelatin example (**Fig. 2.1**) is presented. The ARFI push pulse (*wide red arrow*) is applied generating shear waves (green waves). The shear waves travel through the tissues and change speed depending on the stiffness of the tissue. Conventional B-mode pulses are used to identify the shear waves and calculate their speed. (**b**) The shear wave speed is calculated using B-mode scanning to monitor the shear wave movement through the tissue. This diagram depicts the process. (*A*) is the ARFI pulse which generates the shear wave. (*B*) is the area that is monitored by B-mode imaging for the tissue movement caused by the shear wave. (*C*) displays the curves that are identified by plotting the tissue displacement at a given location over time. The slope of the line obtained by plotting the time of the maximum tissue displacement at the different locations due to the ARFI pulse is the shear wave speed (*D*).

can be estimated by making several assumptions. The SWS is directly correlated with tissue stiffness, with higher SWS representing greater stiffness and vice versa. The stiffness of a lesion can be displayed as the SWS (in meters per second [m/s]) or, by making some assumptions, as Young's modulus, (in kilopascals [kPa]). The strain modulus is calculated by making the assumptions that the density of tissue is 1.0 g/cm^3 and that Poisson's ratio is 0.5 for the tissue and using the following equation,

$$\text{Young's modulus (kPa)} = 3C_s^2$$

where C_s is the SWS in meters per second.

▶ Table 2.1 lists the conversion of the two scales, Young's modulus and SWS, at various measurements. Most systems allow the user to select which scale they prefer to use.

Table 2.1 Conversion of Young's modulus to shear wave velocity

Young's modulus (kPa)	Shear wave velocity (m/s)
180	7.7
150	7.1
125	6.5
100	5.8
90	5.5
80	5.2
70	4.8
60	4.5
50	4.1
40	3.7
30	3.2
25	2.9
20	2.6
15	2.2
10	1.8

With SWE, a quantitative measure of the lesion stiffness is obtained either in point of interest (point shear wave elastography, p-SWE) or in a larger field of view with pixel-by-pixel color-coding of the SWS (two-dimensional shear wave imaging, 2D-SWE).

Several vendors now offer SWE on several transducers. There are two types of SWE: point shear wave elastography (p-SWE) and two-dimensional shear wave elastography (2D-SWE). The development of three-dimensional shear wave elastography (3D-SWE) is now also becoming available. In p-SWE a small (approximately 1 cm^3) ROI is placed at the site of interest and a single measurement of the shear wave velocity is obtained from that location. For 2D-SWE multiple measurements are obtained in a larger FOV and displayed using a color-coded map. An ROI can then be placed within the FOV to obtain the shear wave velocity at that location.

2.3.1 Point Shear Wave Elastography

The principles of scanning techniques using SE also pertain to SWE. Maintaining the same location of the lesion with no movement is important to obtain accurate results. After the ARFI pulse is applied, data acquisition occurs for a short period of time. During the data acquisition period, the movement of the shear wave is monitored by B-mode imaging. If the tissue moves due to movement of the transducer or the patient, the system will interpret this nonshear wave movement in the calculation of SWS. Having the patient hold still and hold their breath (stop breathing) and then waiting to 2 to 3 seconds before acquiring the data for the structure of interest (to allow it to stop moving) will lead to more accurate measurements. Depending on the transducer and the system there is a limit to the tissue depth at which accurate measures of SWS can be

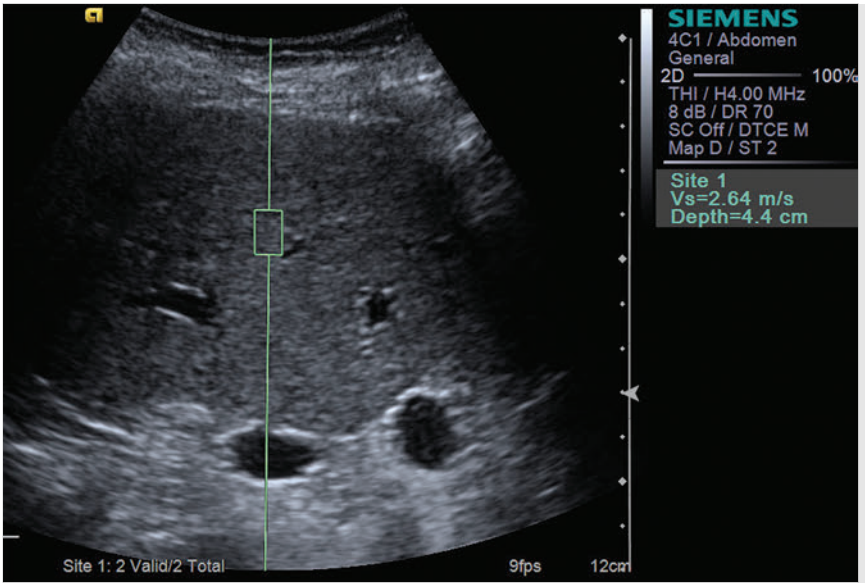

Fig. 2.22 In this example of a p-SWE of the liver, the ROI box (*green box*) is placed at the site of interest. Following the appropriate technique (discussed in Chapter 3), the p-SWE button is activated. The system then provides the SWS and the tissue depth of the measurement, in this case, 2.64 m/s at 4.4 cm. After activating the p-SWE button, the system will freeze and not allow additional imaging until a cooling-off period is over. The cooling-off period varies with vendor and application.

obtained. Most systems will not allow measurements below a certain tissue depth depending on the transducer. One important factor in obtaining accurate measurements is the strength of the ARFI pulse. Like all other ultrasound pulses, the ARFI pulse can be attenuated, refracted, and reflected, weakening the strength of the pulse. The strength of the ARFI pulse is directly related to the degree of displacement of the tissues by the shear wave. A weaker ARFI pulse will result in a decrease in the signal to noise of the measurements of the shear wave and an increase in error in the shear wave measurement. The techniques for optimizing the ARFI pulse for the various organs are discussed in Chapters 3 to 11.

The ROI box,which is usually a fixed size, is placed at the area of interest. After the activation of the p-SWE application, the results are displayed, following a cooling-off period due to the heat energy generated by the ARFI pulse. This period varies from vendor to vendor, being imperceptible with some vendors.

With p-SWE, a quantitative measure of the lesion stiffness is obtained in a small fixed ROI. The ROI in p-SWE is a fixed size and usually cannot be changed. The ROI box is placed at the site where the stiffness value is desired. In some tissues where the lesion may be of heterogeneous stiffness, multiple p-SWE measurements at various locations are needed to fully assess the lesion stiffness. This varies with the tissue being evaluated and is discussed in Chapters 3 to 11.

Display of p-SWE Results

The p-SWE results are displayed on the monitor either as SWS in meters per second (m/s) or as Young's modulus in kilopascals (kPa). An example of a p-SWE in the liver is presented in ▶ Fig. 2.22. Some systems provide a quality measure of the measurement. This quality measure is determined by the amount of tissue displacement and the signal to noise of the tracking pulses. For most organs the recommendation is to obtain multiple measurements and use the mean value for diagnosis. For example the recommendation is to obtain 10 measurements when determining liver stiffness and use the mean value. With 10 measurements, the interquartile range (IQR) can also be calculated and used to determine the quality of the measurements. Most vendors have a reporting package that will record and track the serial measurements and provide the mean, standard deviation, and/or the IQR. A sample report is presented in ▶ Fig. 2.23.

If a shear wave is not generated or is of very poor quality, then a value will not be obtained and the displayed measurement will be "0.00" or "x.xx". This could be caused by patient or sonographer movement or patient factors that do not allow for an accurate measurement (e.g., high body mass index [BMI], deep lesion).

2.3.2 Two-Dimensional Shear Wave Elastography

The principles of scanning techniques using SE and p-SWE also pertain to 2D-SWE. Maintaining the same location of the lesion with no movement is important to obtain accurate results. With 2D-SWE a larger FOV (usually greater than 1 cm x 1 cm but limited in size by the system) is placed over the area of interest. The FOV can be placed to include both the lesion of concern as well as adjacent tissues. Similar to p-SWE the patient must hold still during the measurement. Results are color-coded and displayed over a B-mode image and can be displayed as either shear wave velocity in meters per second or Young's modulus in kilopascals. An example of a 2D-SWE is presented in ▶ Fig. 2.24.

There are systems that provide a "one-shot" 2D-SWE, where after activating the measurement, a single image is displayed. In these systems there is a delay up to a few seconds before the system can be used again. Some 2D-SWE systems, however, allow measurements to be performed in real-time; to obtain optimal images, remaining in the same plane for several seconds is required for adequate measurements. A video clip can be saved and the appropriate image identified and measurements obtained. On the image to be used for measurements, one or more ROIs can be placed to obtain the stiffness value including the maximum, mean, and standard deviation of the measurements in the ROI. Most systems allow the ROI size to be changed as desired. The color-coded image allows determination of the stiffness values over a larger area. The area of maximum stiffness and stiffness heterogeneity can be quickly

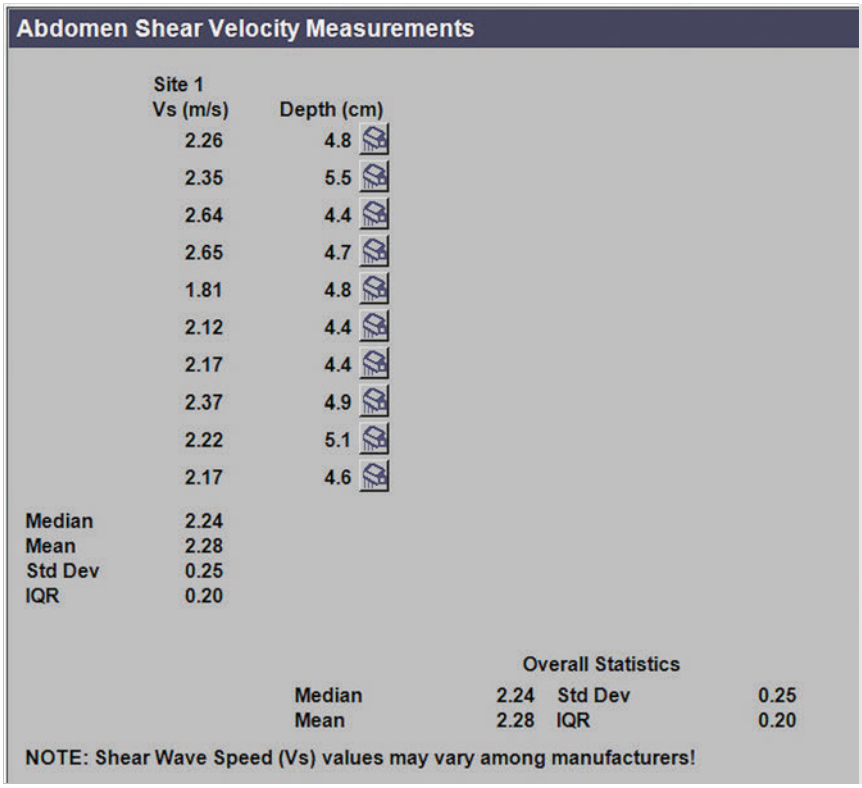

Fig. 2.23 For most applications of p-SWE, it is recommended that several measurements be taken and the mean used for diagnosis. This is an example of a report page where 10 measurements were obtained. The median, mean, standard deviation, and interquartial (IQR) measurements are displayed. Many vendors allow multiple measurements to be taken for each of several sites.

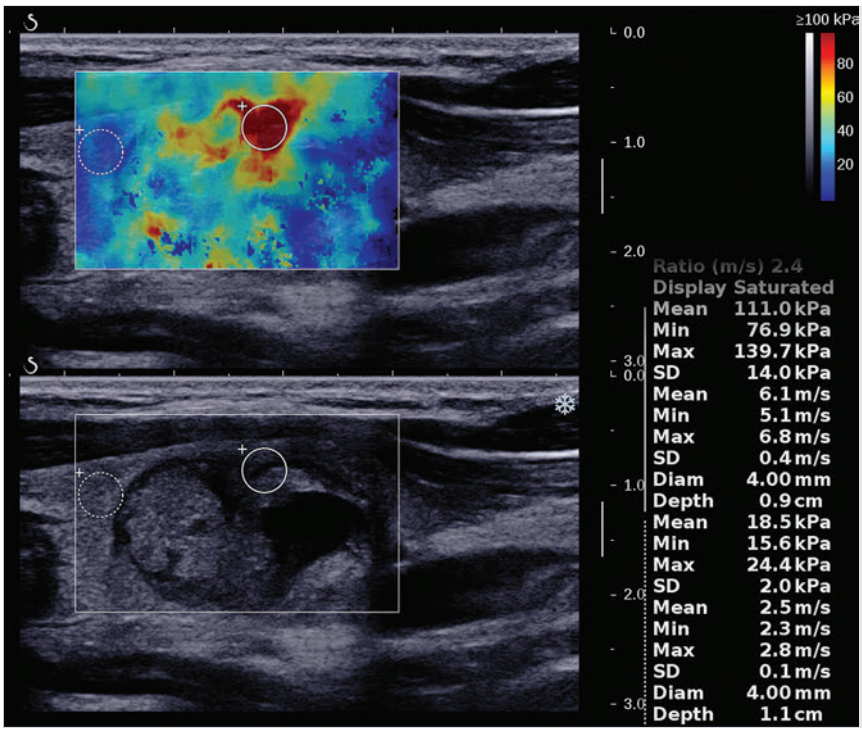

Fig. 2.24 This is an example of 2D-SWE taken in the thyroid gland. The FOV box (*white box*) is placed over the site of interest. Usually the box is placed to include both the abnormality and surrounding tissue. After activating the 2D-SWE button, a color-coded SWS map is obtained (upper image). The map is also presented in the image, in this case in the upper right corner of the image. Here, the map was set to have a maximum display of 100 kPa. To obtain the stiffness values for a specific location, ROIs (*white circles*) are placed in the areas of concern. In this case one ROI was placed within the solid portion of the lesion with the highest SWS, as determined by the color-coded map. A second ROI was placed in the normal thyroid tissue. The measurements are displayed on the right. The mean, minimum, and maximum values, and the standard deviation of the pixels in each ROI, are displayed. Here we selected to display the SWS in both meters per second and kilopascals. The system also calculated a stiffness ratio of the lesion to normal thyroid that is 2.4 using the meter per second measurements.

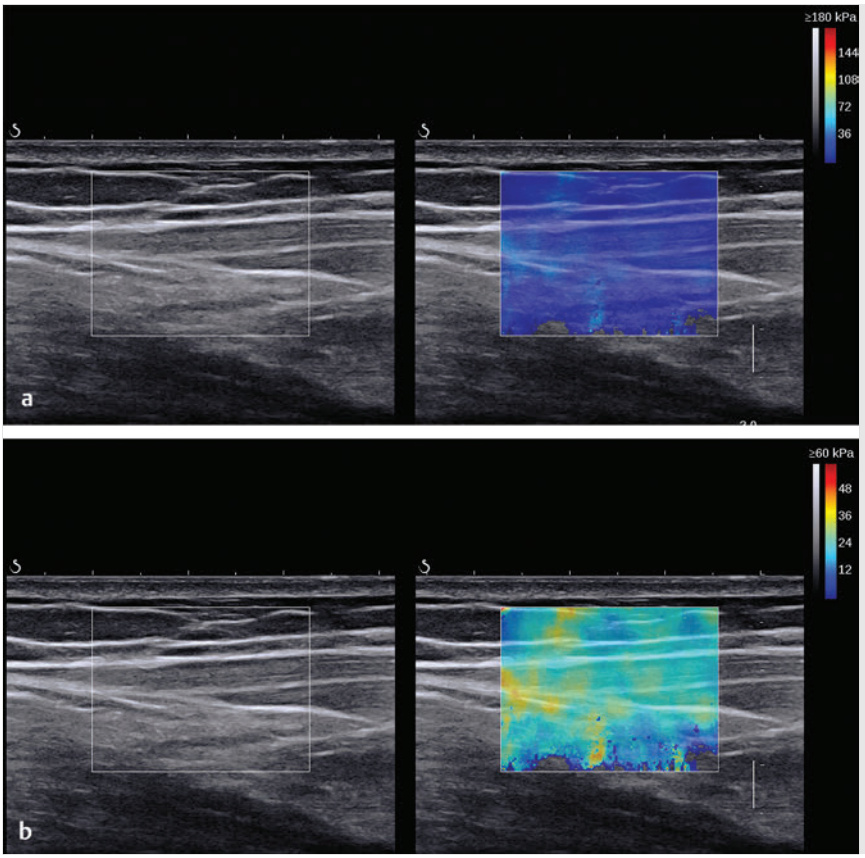

Fig. 2.25 The color-coded velocity map can be adjusted to highlight differences in the tissue stiffness. In this image, normal muscle (**a**) is displayed with a maximum of 180 kPa. In (**b**) the same image is displayed with a maximum scale of 60 kPa. Note that the differences in stiffness of the muscle are better visualized in (**b**) since the scale has been adjusted.

identified. A strain ratio can be calculated if both the lesion and reference tissue are present in the FOV.

Display of 2D-SWE Results

The display of 2D-SWE varies by vendor. Some have a single image where the FOV can be placed and the results are displayed, while others have a dual display where the B-mode image is displayed as one image and the 2D-SWE color-coded results are presented in the other (and overlaid on the B-mode image).

With shear wave imaging, the color scale can be changed. Red always codes for stiff tissues and blue for soft tissues. However, the stiffness at which the color changes occur can be changed. For breast tissues, a scale with a maximum of 7.7 m/s (180 kPa) is usually the default. With this scale, lesions coded green, yellow, and red are stiff within the range of malignancies. When evaluating only benign tissue, decreasing the maximum value of the color scale (e.g., to a maximum of 3.7 m/s or 40 kPa) will allow for a greater color differentiation of the stiffness of the benign tissues. However, red will no longer code for a stiffness value suggestive of a malignancy (▶ Fig. 2.25).

Shear wave generation is depth limited and depends on tissue density. If a lesion is deeper than 4 to 5 cm, a result may not be obtained. Repositioning of the patient to bring the region of interest (ROI) closer to the transducer may help. If there is no shear wave generation, no color-coding in this area will occur.

2.3.3 Precompression

The principles of scanning using SE discussed in the previous section also pertain to SWE. Precompression can change results and the same technique discussed earlier is recommended to limit it (▶ Fig. 2.8b). In some tissues such as breast, the addition of precompression is hard to avoid. Since the breast is relatively soft and is superficial to the ribs, it is very easy to compress the breast. However, with other organs that are deep to the ribs such as the liver, it is difficult to compress the liver through an intercostal approach.

2.3.4 Interpretation

Point Shear Wave Elastography

With p-SWE, a tissue stiffness value is obtained for the ROI. For most applications, several measurements from the location are suggested to confirm an accurate stiffness value. The suggested number of measurements to be taken varies with the clinical application and are discussed in the clinical chapters (Chapters 3 to 11). The stiffness value can be used to characterize the tissue and/or lesion. Usually a cutoff value is used to determine if the lesion is benign or malignant. The cutoff values vary with the tissue being evaluated and are discussed in the clinical chapters. Unlike 2D-SWE where a large FOV of stiffness values are displayed and the maximum stiffness and stiffness heterogeneity of a lesion is evident, with p-SWE it is difficult to determine where to obtain the optimal stiffness value. This limits the procedure's usefulness in heterogeneous tissues and/or lesions but in more uniform tissues, such as liver, stiffness measurements from p-SWE can be very accurate.

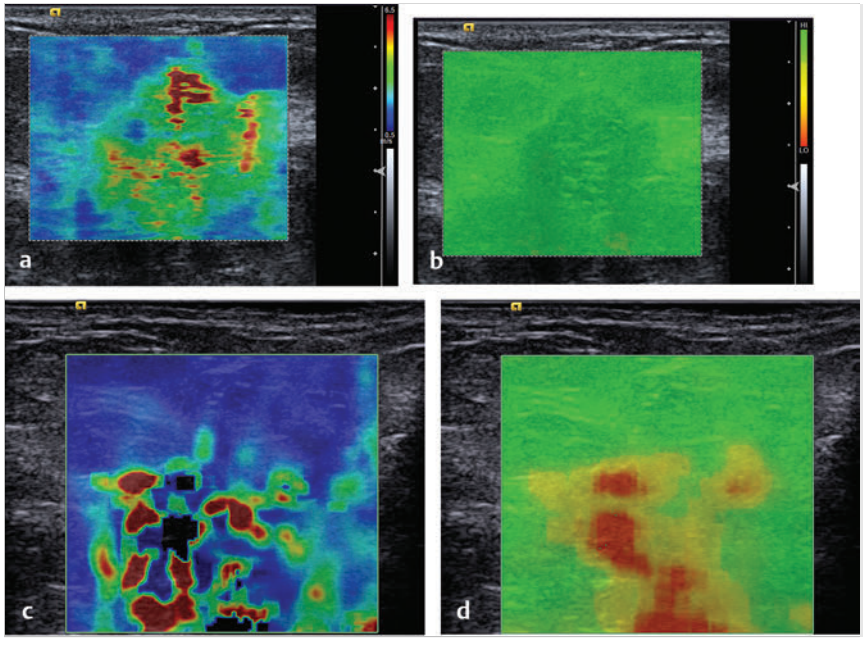

Fig. 2.26 One method of improving the accuracy of the color-coding is to provide a quality map that assesses the quality of the shear waves. This map uses a "stop-light" pattern: green (go) for high-quality shear waves, yellow (caution) and red (stop) if the shear wave quality is not adequate for accurate measurement. The SWS map of a SWE image from an invasive ductal cancer is presented in (**a**). The high SWS are suggestive of a malignant lesion. The quality map for the same image is presented in (**b**). The area of the tumor is color-coded green, documenting the SWSs as accurate. In (**c**), a similar color pattern for the area of concern in (**a**) is obtained. However, in this case, the quality map (**d**) shows the areas of high SWS color-coded in yellow and red, documenting the SWSs as not accurate and not to be used in diagnosis.

Two-Dimensional Shear Wave Elastography

With 2D-SWE, the stiffness values over a large FOV are displayed in a color-coded map. An ROI can be placed over the area of interest and the stiffness value in either meters per second or kilopascals will be displayed. Since the ROI will contain multiple pixels, the results are usually displayed as the maximum stiffness value, the minimum stiffness value, the mean stiffness value, and the standard deviation for all the pixels in the ROI. Most studies have used the maximum stiffness value as the criteria to determine if a lesion is benign or malignant. By visual inspection of the color map, the area of maximum stiffness is usually easily identified. The ROI can then be placed in this area. Measurement of the adjacent tissue can also be obtained.

One system (Siemens Ultrasound, Mountain View, CA) provides in addition to a color-coded velocity map, a quality measure map, a time map, and a displacement map. The quality map is discussed in the section Quality Map, which follows. The time map displays the time to maximum displacement, which is another method of displaying the SWS data. The displacement map displays the amount of tissue displacement caused by the ARFI pulse. The time map and displacement map are useful for research purposes but are not required to interpret the results in a clinical setting. The velocity map and quality map are used in routine clinical practice to interpret the results.

Quality Map

All systems have a rejection algorithm that determines if the data is adequate to calculate an accurate SWS. In the cases where the data is inadequate to calculate an accurate SWS, those pixels are not color-coded. However, the present rejection algorithms may not be adequately robust to reject all inaccurate measurements. In some lesions including some breast cancers, the shear waves may not propagate in an orderly fashion and an erroneously low shear wave speed may be displayed. Often in these cases there will be a ring of higher shear wave velocities that allow accurate diagnosis. To overcome this problem, one vendor (Siemens Ultrasound, Mountain View, CA) has developed a quality map that is more rigorous in evaluating the raw data to determine if an accurate SWS can be calculated. This quality map uses a stoplight color map to code the quality of the measurement with green as high quality, yellow as poor quality, and red as inaccurate (▶ Fig. 2.26). The quality map can be used with the color-coded map that displays the SWS to determine which stiffness values are suitable for clinical use. Some vendors have recently added a numerical quality factor of the calculated stiffness value.

In a recent study[24] the addition of a quality measure (QM) in shear wave imaging of the breast limited false negative findings (sensitivity without QM 22/46 [48%, 95% confidence index: 33–63%];sensitivity with QM 42/46 [91%, 95% confidence index: 79-98%, $p < 0.0001$]).

2.3.5 Limitations

Shear waves will not propagate through simple cysts and so they will not be color-coded (▶ Fig. 2.26). Shear waves will propagate in complicated cysts, and these will be color-coded as soft lesions. The shear wave is detected by conventional B-mode ultrasound. Therefore, when areas in the B-mode image show extremely low signal (anechoic), the echo signal is too low for successful shear wave detection. These areas will not be color-coded. This will occur in areas with marked shadowing, such as with ribs, tumors with significant shadowing, and areas with macrocalcification.[2]

2.3.6 Artifacts

There are several artifacts that you may encounter. Some of these indicate that your technique is suboptimal, and several contain diagnostic information.

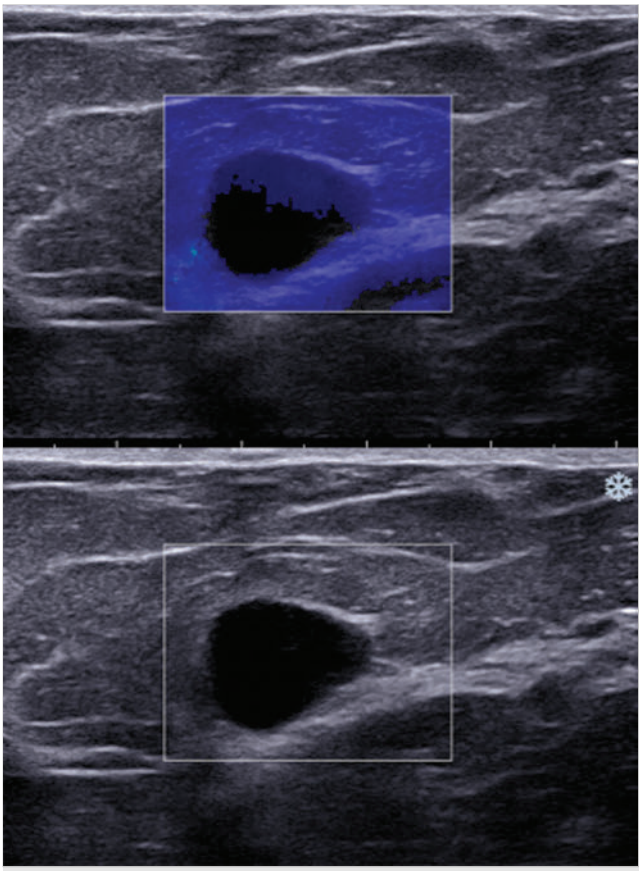

Fig. 2.27 Shear waves do not propagate in simple fluid such as that in a simple cyst. In these cases, the cyst will not be color-coded. Occasionally there is some bleeding of color into the proximal portion of the cyst. If the cyst is complex, it can support shear wave propagation and the cyst will be color-coded.

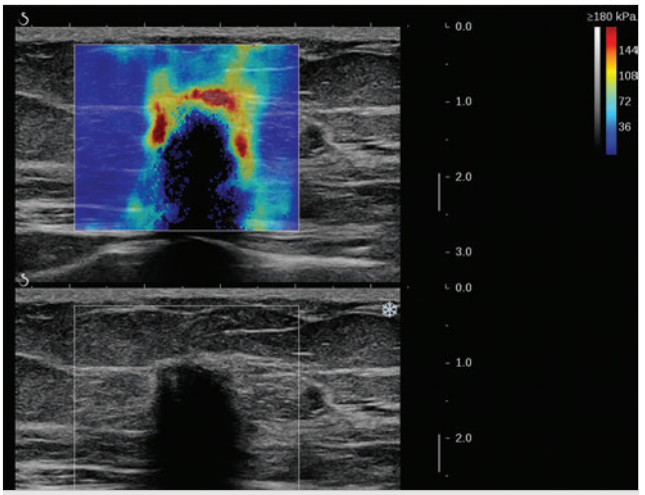

Fig. 2.28 If the shear wave speed cannot be determined at a location, then the pixel is not color-coded (black central area). This can occur (1) if the lesion is too deep and the ARFI pulse is attenuated and no longer strong enough to generate a measureable shear wave; (2) if the tissue does not support generation of shear waves (e.g., simple cyst); or (3) if there is significant noise in the displacement results and an accurate shear wave speed cannot be calculated. A unique feature of breast cancers is that some do not allow for adequate shear waves necessary for accurate measurement. In these cases, the tumor will not be coded, but, as in this figure, a ring of high SWSs are identified around the lesion.

No Color-Coding (Lack of Shear Wave Signal)

Shear waves will not propagate through simple cysts, and so they will not be color-coded (▶ Fig. 2.27).

The shear wave is detected by ultrasonic echo signal. Therefore when areas in B-mode image show extremely low signal (anechoic), the echo signal will be too low for successful detection. These areas also will not be color-coded. This will occur in areas with marked shadowing, such as ribs, tumors with significant shadowing, and areas with calcification,[2] in areas deeper than where the shear wave is generated, and in very stiff and heterogeneous structures where the shear wave contains significant noise.

In very stiff lesions, such as invasive cancers, the shear wave may not propagate. Therefore no results would be obtained and so the area would not be color-coded (▶ Fig. 2.28). This is discussed in the Chapter 5.

Bang Artifact

If one uses precompression, there will be a pattern of red in the near field (▶ Fig. 2.29).[2,5] This can be corrected by using minimal pressure from the transducer on the patient.

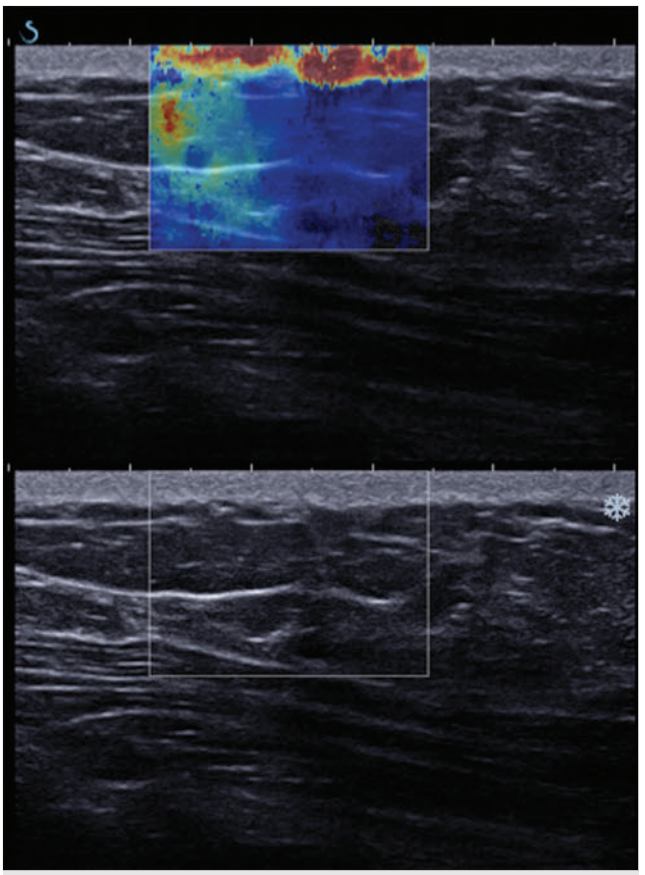

Fig. 2.29 If too much pressure is applied with the transducer (precompression), the near field in SWE will appear stiff (red), as in this case. This can be corrected by decreasing the pressure being applied by the transducer.

2.3.7 Tips and Tricks

- Keep the FOV slightly larger than the lesion to evaluate the surrounding tissue.
- Maintain the transducer perpendicular to skin.
- Hold the transducer still and ask the patient to hold his or her breath (stop breathing) during measurements.
- Wait 2 to 3 s after asking patient to stop breathing before acquiring the data to allow the structure to stop moving.
- Do not apply precompression with the transducer.
- When using real-time shear wave imaging, allow several seconds for the image to stabilize before taking a measurement.

2.4 Conclusion

There are two major types of ultrasound elastography, SE and SWE. Both have their advantages and disadvantages. Both have been used to evaluate tissues from a number of organ systems. The advantages and disadvantages of these techniques for each organ system are detailed in the clinical chapters, Chapters 3 to 11. But generally, SE can be performed at any tissue depth as long as an adequate B-mode image and the appropriate compression–release can be applied, while SWE is limited in tissue depth due to the attenuation of the ARFI pulse. Both SE and SWE are severely affected by precompression. SWE is quantitative while SE is not. There are artifacts present in results from some SE systems that are highly accurate in identifying a lesion as a benign simple or complicated cyst, which is not possible with SWE.

There has been rapid growth of elastography since its implementation on approved clinical systems. Guidelines have been developed for its use in several clinical applications. Improved algorithms, quality assessment, and hardware are becoming available, which will improve the accuracy of these techniques.

References

[1] Emerson K. Diseases of the breast. In: Wintrobe MM, Thorn GW, Adams RD, et al, eds. Harrison's Principals of Internal Medicine.7th ed. New York, NY: McGraw-Hill; 582–587

[2] Barr RG. Sonographic breast elastography: a primer. J Ultrasound Med 2012; 31(5):773–783

[3] Bamber J, Cosgrove D, Dietrich CF et al. EFSUMB guidelines and recommendations on the clinical use of ultrasound elastography. Part 1: Basic principles and technology. Ultraschall Med 2013; 34(2):169–184

[4] Shiina T, Nightingale KR, Palmeri ML et al. WFUMB guidelines and recommendations for clinical use of ultrasound elastography: Part 1: basic principles and terminology. Ultrasound Med Biol 2015; 41(5):1126–1147

[5] Barr RG, Zhang Z. Effects of precompression on elasticity imaging of the breast: development of a clinically useful semiquantitative method of precompression assessment. J Ultrasound Med 2012; 31(6):895–902

[6] Nightingale K, Soo MS, Nightingale R, Trahey G. Acoustic radiation force impulse imaging: in vivo demonstration of clinical feasibility. Ultrasound Med Biol 2002; 28(2):227–235

[7] Fahey BJ, Nightingale KR, Nelson RC, Palmeri ML, Trahey GE. Acoustic radiation force impulse imaging of the abdomen: demonstration of feasibility and utility. Ultrasound Med Biol 2005; 31(9):1185–1198

[8] Rouze NC, Wang MH, Palmeri ML, Nightingale KR. Robust estimation of time-of-flight shear wave speed using a radon sum transformation. IEEE Trans Ultrason Ferroelectr Freq Control 2010; 57(12):2662–2670

[9] Hall TJ, Zhu Y, Spalding CS. In vivo real-time freehand palpation imaging. Ultrasound Med Biol 2003; 29(3):427–435

[10] Barr RG. Real-time ultrasound elasticity of the breast: initial clinical results. Ultrasound Q 2010; 26(2):61–66

[11] Destounis S, Arieno A, Morgan R et al. Clinical experience with elasticity imaging in a community-based breast center. J Ultrasound Med 2013; 32(2): 297–302

[12] Barr RG, Destounis S, Lackey LB, II, Svensson WE, Balleyguier C, Smith C. Evaluation of breast lesions using sonographic elasticity imaging: a multicenter trial. J Ultrasound Med 2012; 31(2):281–287

[13] Grajo JR, Barr RG. Strain elastography for prediction of breast cancer tumor grades. J Ultrasound Med 2014; 33(1):129–134

[14] Ueno EIA. Diagnosis of breast cancer by elasticity imaging. Eizo Joho Medical 2004; 36:2–6

[15] Itoh A, Ueno E, Tohno E et al. Breast disease: clinical application of US elastography for diagnosis. Radiology 2006; 239(2):341–350

[16] Park JSM. Inter- and intraobserver agreement in the interpretation of ultrasound elastography of breast lesions. Paper presented at the 93rd Scientific Assembly and Annual Meeting of the Radiological Society of North America. November 25–30, 2007; Chicago, IL

[17] Ueno E, Bando H, Tohno E, Waki K, Matsumura T. New quantitative method in breast elastography: fat lesion ratio (FLR). Paper presented at the 93rd Scientific Assembly and Annual Meeting of the Radiological Society of North America; November 25–30, 2007; Chicago, IL

[18] Barr RG, Lackey AE. The utility of the "bull's-eye" artifact on breast elasticity imaging in reducing breast lesion biopsy rate. Ultrasound Q 2011; 27(3):151–155

[19] Sarvazyan AP, Rudenko OV, Swanson SD, Fowlkes JB, Emelianov SY. Shear wave elasticity imaging: a new ultrasonic technology of medical diagnostics. Ultrasound Med Biol 1998; 24(9):1419–1435

[20] Bercoff J, Tanter M, Fink M. Supersonic shear imaging: a new technique for soft tissue elasticity mapping. IEEE Trans Ultrason Ferroelectr Freq Control 2004; 51(4):396–409

[21] Nightingale K, McAleavey S, Trahey G. Shear-wave generation using acoustic radiation force: in vivo and ex vivo results. Ultrasound Med Biol 2003; 29 (12):1715–1723

[22] Tanter M, Bercoff J, Athanasiou A et al. Quantitative assessment of breast lesion viscoelasticity: initial clinical results using supersonic shear imaging. Ultrasound Med Biol 2008; 34(9):1373–1386

[23] Parker KJ, Lerner RM. Sonoelasticity of organs: shear waves ring a bell. J Ultrasound Med 1992; 11(8):387–392

[24] Barr RG, Zhang Z. Shear-wave elastography of the breast: value of a quality measure and comparison with strain elastography. Radiology 2015; 275(1): 45–53

3 Elastography for Diffuse Liver Disease

Giovanna Ferraioli, Mabel Zicchetti, Raffaella Lissandrin, and Carlo Filice

3.1 Introduction

Liver fibrosis is an excessive accumulation of extracellular matrix material produced by fibroblastlike cells, including stellate cells, due to the chronic activation of the wound-healing reaction as a result of one of several agents. It changes the normal architecture of the liver and ultimately leads to liver cirrhosis, hepatic decompensation, portal hypertension and its complications, hepatocellular carcinoma (HCC), and eventually death. The major causes of hepatocellular damage are hepatitis viruses and liver inflammation due to steatosis or alcohol abuse.

The hepatitis C virus (HCV) and the hepatitis B virus (HBV) are leading causes of chronic liver disease. An estimated 130 to 150 million people have chronic hepatitis C infection worldwide. A significant number of those who are chronically infected will develop liver cirrhosis or liver cancer, and 350,000 to 500,000 die annually from HCV-related liver diseases.[1] In high endemic areas, where 3/4 of the world's population live, 70 to 90% of the population becomes HBV-infected and 8 to 20% of those are HBV-carriers. About 1 million people die each year due to chronic forms of the disease.[2]

Nonalcoholic fatty liver disease (NAFLD) is a common clinical condition characterized by significant deposition of lipid droplets in the hepatocytes of individuals without a history of alcohol abuse. It is emerging as the most common chronic liver disease in adults and children, with the increased incidence of obesity and diabetes in Western countries. NAFLD is a benign and reversible condition that, however, may progress to nonalcoholic steatohepatitis (NASH) with an increased risk for cirrhosis, liver failure, HCC, and death. The worldwide prevalence of NAFLD is estimated to range from to 6 to 33% with a median of 20% in the general population.[3] The prevalence of NASH is estimated to range from 3 to 5% of patients with NAFLD, and 5 to 8% of patients with NASH will develop cirrhosis within 5 years. The prevalence of NAFLD in pediatric patients is 3 to 10%, increasing to 40 to 70% in obese children.[4]

The presence and extent of liver fibrosis are associated with disease progression and complications; thus, early detection of fibrosis is crucial for the prognosis and management of patients. In chronic viral hepatitis the assessment of the severity of liver fibrosis is necessary for determining when to begin the antiviral treatment. The guidelines on the management of chronic hepatitis B and C have indicated that in the presence of significant fibrosis antiviral therapy is required, because maintenance of hepatitis B viral suppression or hepatitis C viral eradication can decrease liver-related complications.[5,6] Liver biopsy is considered the reference standard for assessing liver fibrosis. The histological evaluation of liver biopsy specimens is carried out using scoring systems that give values for various categories of inflammation (grades) and of fibrosis (stages). There are several scoring systems, but essentially they categorize similar features. In the assessment of chronic viral hepatitis, the most reproducible scoring system is the METAVIR. On the METAVIR scoring system, liver fibrosis is evaluated semiquantitatively and staged on a 5-point scale from 0 to 4 (F0, absent; F1, enlarged fibrotic portal tract; F2, periportal or initial portal-portal septa but intact architecture; F3, architectural distortion but no obvious cirrhosis; and F4, cirrhosis).[7]

Liver biopsy is a painful, expensive, and invasive procedure with some morbidity and mortality risks; moreover, the results can be impaired by sampling errors, and intraobserver and interobserver variability in a specimen's readings. The liver biopsy yields only a small sample of the liver and a sampling bias can occur especially when fibrosis is heterogeneously distributed, as happens in the mild stage. It should be underlined that fibrosis has a continuous spectrum, but the histology reading gives a semiquantitative staging of fibrosis in a categorical scale. Due to these limitations, sequential liver biopsy to decide when to start or to monitor the response to treatment is not feasible. In patients with chronic hepatitis B or C, there are two important end points: the assessment of significant fibrosis, which indicates that an antiviral treatment should be started, and the assessment of liver cirrhosis, which indicates that the surveillance program for HCC and for complications related to portal hypertension should be initiated. In patients with NAFLD, the high prevalence of the disease and its frequently benign course make it difficult to decide the timing for performing liver biopsy in a low-risk population.

For all these reasons, the development of reliable noninvasive imaging modalities that indirectly assess liver fibrosis by measuring liver stiffness has generated great clinical interest. The accuracy of the elastographic methods in the evaluation of liver fibrosis has been assessed by comparing the results to those from liver histology.

The European Federation of Societies for Ultrasound in Medicine and Biology (EFSUMB) and the World Federation for Ultrasound in Medicine and Biology (WFUMB) have issued guidelines for the use of elastography for evaluation of liver stiffness.[8,9] Recently, the Society of Radiologists in Ultrasound (SRU) convened a panel of specialists for a consensus regarding the use of elastography in the assessment of liver fibrosis. The recommendations were established on the basis of analysis of current literature and common practice approaches.[10] The SRU consensus panel recommends interpreting liver stiffness results in patients with chronic viral hepatitis by using two cutoff values: < 7 kPa (1.5 m/s) and > 15 kPa (2.2 m/s). The first is for selecting patients who are at low risk for significant fibrosis, and the second is for selecting patients who are at high risk for advanced fibrosis or cirrhosis and who require different management and need to be treated. Those between these values may have mild or moderate fibrosis and follow-up should be based on clinical presentation and other laboratory tests.

3.2 Elastography Techniques

The elastography techniques are either shear wave–based (SWE) or strain-based (SE). Their technical aspects are discussed in depth in Chapter 2.

Briefly, vibration-controlled transient elastography (VCTE, Echosens, Paris, France) and acoustic radiation force impulse (ARFI)-based elastography measure shear wave speed. VCTE is performed with the FibroScan device, which is provided with

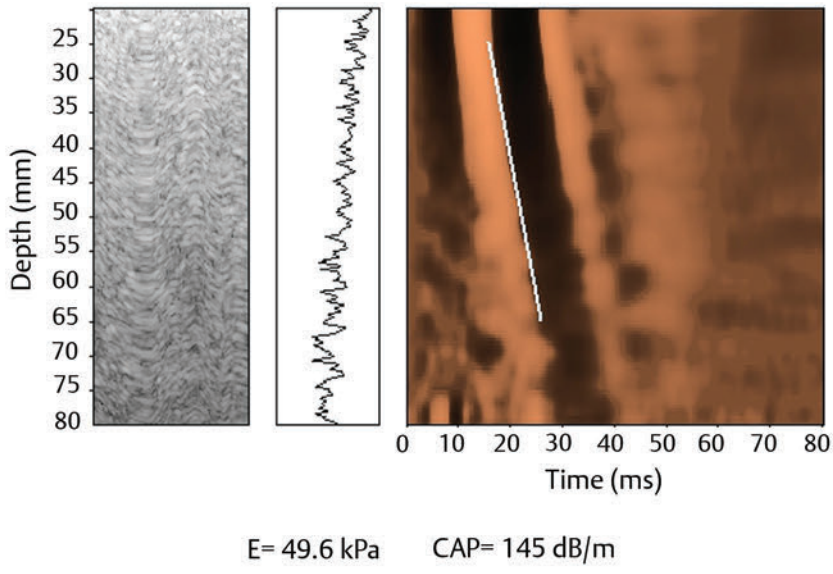

Fig. 3.1 A 71-year-old male with liver cirrhosis. Assessment of liver stiffness with the FibroScan device (Echosens, Paris, France). Time-motion–mode (*left*), A-mode (*middle*), and elastogram (*right*) images. The elastogram is the representation of the shear wave as a function of time. The slope of the white line becomes steeper with the increase of liver stiffness. The controlled attenuation parameter (CAP) is a measure in decibels per meter (dB/m) of the attenuation of the ultrasound waves as they propagate through the liver. The median value of stiffness is 49.6 kPa, consistent with liver cirrhosis. The median value of CAP is 145 dB/m, which is within the normal range.

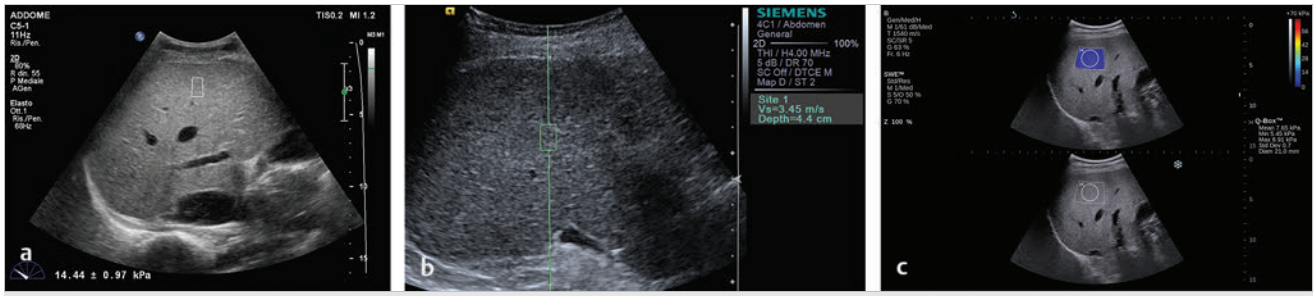

Fig. 3.2 **(a)** A 65-year-old male with chronic hepatitis C. Assessment of liver stiffness with a p-SWE technique (ElastPQ, Philips Medical Systems, Bothell, WA). The sample box has a fixed size and can be moved by the operator. The values of liver stiffness are expressed either in kilopascals (kPa), as in this image, or in meters per second (m/s). The mean value of the single measurement along with its standard deviation is shown in the image. The liver stiffness is also semiquantitatively displayed using the scale in the bottom left corner of the image. The median stiffness value is 14.44 kPa, which indicates the presence of liver cirrhosis. The diagnosis was confirmed by liver histology. (**b**) A 75-year-old female with alcoholic liver cirrhosis. Assessment of liver stiffness with a p-SWE technique (VTQ, Siemens Healthcare, Erlangen, Germany). The sample box has a fixed size and can be moved by the operator. Measurement of liver stiffness is given in meters per second (m/s). The mean value and the depth of the sample box are displayed. The mean value is 3.45 m/s, consistent with liver cirrhosis. (**c**) A 42-year-old male with chronic hepatitis C. Assessment of liver stiffness with a 2D-SWE technique (Aixplorer's ShearWave, Supersonic Imagine, Aix-en-Provence, France). The size and the location of the quantification box is adjustable by the operator. The shear wave measurements are color-coded and displayed in the quantification box. The measurement is taken in the white circle (ROI) inside the quantification box. Measurement of liver stiffness is given in kilopascals (kPa), as in the image, or in meters per second (m/s). The mean value and the standard deviation, the minimum and maximum values, and the size of the region of interest (ROI) are displayed. Liver stiffness is 7.65 kPa, consistent with significant fibrosis and confirmed by liver histology (METAVIR F2).

an ultrasound transducer mounted on the axis of a vibrator. Vibrations of mild amplitude and low frequency (50 Hz) are transmitted by the tip of the transducer through the liver, inducing an elastic shear wave that propagates through the underlying tissue. The FibroScan is not a real-time ultrasound device; however A-mode ultrasound is used to locate the area of liver parenchyma in which to perform the measurement and to monitor the velocity of propagation of the shear wave. The velocity of the wave is directly related to tissue stiffness (▶ Fig. 3.1).

Unlike FibroScan, ARFI technology is integrated in standard ultrasonographic systems and requires no external vibration to generate the shear wave. Indeed, ARFI is based on the generation of shear waves by the displacement of tissues induced by the force of a focused ultrasound beam deep within tissue. The shear waves propagate perpendicular to the direction of the ultrasound beam and travel at speed between 1 and 10 m/s depending on the tissue stiffness. In stiffer tissues, the shear waves propagate faster.[11]

The speed of the shear wave can be measured in a small region of interest—the technique is termed *point shear wave elastography (p-SWE)*—or in several small regions of interest inside a sample box. In this latter case, an image, a color-coded map of the shear waves speeds in the sample box, is built. This technique is called *two-dimensional shear wave elastography (2D-SWE)*.[12] ▶ Fig. 3.2 shows the p-SWE and 2D-SWE techniques that have been validated so far. ▶ Fig. 3.3 shows the p-SWE and 2D-SWE techniques that are commercially available today but for which there are no clinical studies on reproducibility or accuracy published yet in the literature.

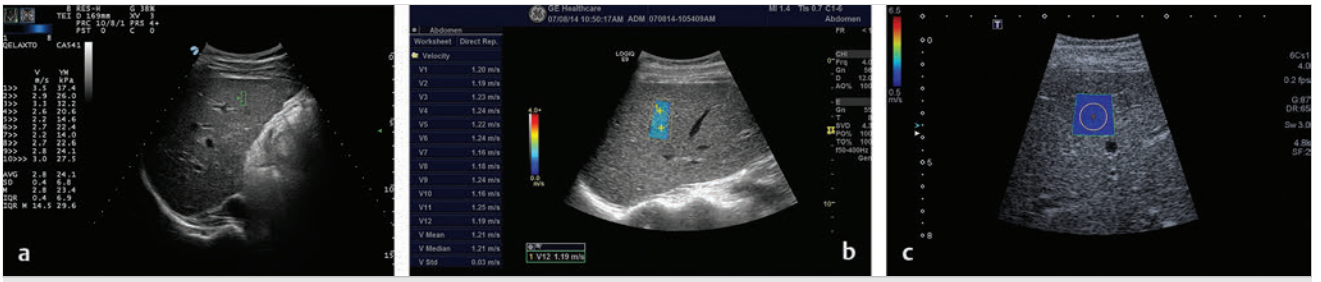

Fig. 3.3 **(a)** Assessment of liver stiffness with a p-SWE technique (QElaXto, Esaote, Genoa, Italy). The sample box has a fixed size and can be moved by the operator. The green solid square indicates the site where the shear wave is generated. Measurement of liver stiffness is given in kilopascals (kPa), as in the image, or in meters per second (m/s). Mean value and standard deviation, median value and interquartile range, and interquartile range/median ratio are shown. (**b**) Assessment of liver stiffness with a 2D-SWE technique (GE Healthcare, Milwaukee, WI). The size and the location of the sample box is adjustable by the operator. (**c**) Assessment of liver stiffness with a 2D-SWE technique (Toshiba Medical Systems, Tokyo, Japan). The size and the location of the sample box is adjustable by the operator. The shear wave measurements are color-coded and the stiffness value is taken in the region of interest (ROI) inside the sample box. Measurement of liver stiffness is given in meters per second (m/s), as in the image, or in kilopascals (kPa). The mean stiffness value along with the standard deviation is displayed.

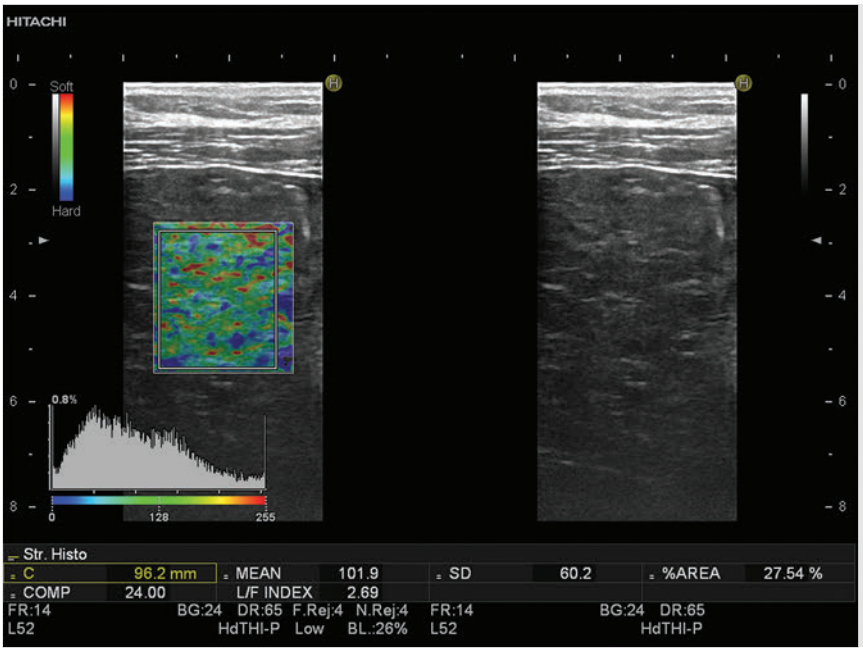

Fig. 3.4 A 64-year-old female with liver cirrhosis due to chronic hepatitis C. Assessment of liver stiffness with a real-time strain elastography technique (Hi-RTE, Hitachi Medical Systems, Tokyo, Japan). The color-coded elastography region of interest (ROI) is overlaid on a conventional B-mode image. The strain histogram, which displays the color dispersion in the ROI, and the liver fibrosis index (LF index) are displayed. The LF index, obtained by using nine image features that are extracted from each image, is 2.69, which is consistent with liver cirrhosis.

Real-time strain elastography (RTSE) measures the ratio of longitudinal tissue displacement after an applied stress that could be either an active external stress, such as the compression with the ultrasound transducer, or passive internal and physiologically induced stress (▶ Fig. 3.4).[12]

3.2.1 Procedure

With all the techniques, measurements are performed by positioning the patient in the dorsal decubitus position, with the right arm elevated above the head for optimal intercostal access. With shear wave elastography, in cases of patients difficult to scan, a slight (30 degree) left lateral decubitus position is helpful.[10] Fasting for at least 3 hours is recommended. The operator should search for the best acoustic window while the patient is breathing normally, then measurements should be performed while the patient holds his or her breath in a neutral position.

Shear Wave Elastography

Vibration-Controlled Transient Elastography

The software is set to take measurements at a depth depending on the frequency of the probe: between 25 and 65 mm below the skin surface with the 3.5 MHz probe, between 35 and 75 mm with the 2.5 MHz probe, and between 15 and 50 mm with the 5.0 MHz probe. The operator locates a portion of liver parenchyma at least 6 cm thick and free of large vascular structures using the A-mode ultrasound on the system. The software determines whether each measurement is successful or not. The entire procedure is considered to have failed when no value is obtained after 10 attempts. Recently, new reliability criteria have been proposed: a minimum of 10 valid measurements performed in the same area of the right lobe of the liver, an interquartile range (IQR)/median ≤ 30% only if the stiffness value is > 7.1 kilopascals (kPa). Measurements are defined as *very reliable* when the ratio IQR/median is less than 0.10; *reliable*

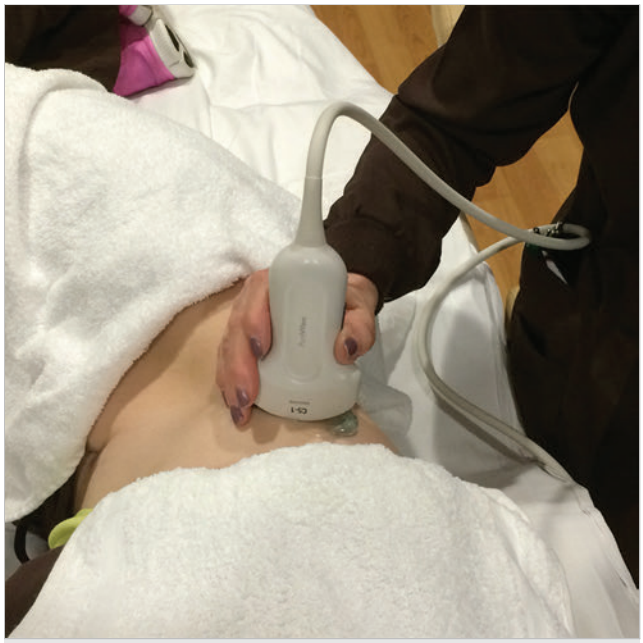

Fig. 3.5 When imaged, the patient is in a supine or slight (30-degree) left lateral decubitus position (as in this case) and the probe is positioned parallel to the rib space, perpendicular to the liver capsule.

when the ratio IQR/median is between 0.10 and 0.30 or when the ratio IQR/median is greater than 0.30 and the median liver stiffness < 7.1 kPa; and *poorly reliable* when the ratio IQR/median is greater than 0.30 and the median liver stiffness is greater than 7.1 kPa.[13] Actually these are the same criteria recommended by the manufacturer.

Ultrasound Shear Wave Elastography

The probe is placed in the intercostal space perpendicular to the liver surface. ▶ Fig. 3.5 shows how the probe should be positioned to obtain a reliable measurement of liver stiffness; ▶ Fig. 3.6 shows the correct positions of the probe. Measurement is taken in the resting respiratory position (breath-hold without deep inspiration). The sample box is positioned in an area of liver parenchyma free of large vessels and is placed at least 1.5 to 2.0 cm beneath Glisson's capsule to avoid reverberation artifacts. The B-mode image should be optimized for the "best acoustic window" to provide the best results. The amount of displacement of the liver is optimized when the ARFI pulse is perpendicular to the liver capsule, which limits refraction of the pulse (▶ Fig. 3.7, ▶ Fig. 3.8).[10] The median value of multiple measurements is reported. The WFUMB guidelines suggest considering the median value of 10 valid measurements with p-SWE, and the mean value of 4 measurements with 2D-SWE.[9] The SRU consensus conference statement on liver elastography suggests that the IQR should be used to assess quality of the data. An IQR/median < 0.30 suggests a data set is good. This can be used to monitor sonographer quality as well as laboratory quality.[10]

Tips and Tricks

The following are tips and tricks for liver stiffness measurements:

- Fasting for 4 to 6 hours is recommended.
- Scan with patient in decubitus or 30 degree oblique position with right arm above head.
- Scan between ribs.
- Optimize the B-mode image for the "best acoustic window" to provide the best results.
- Take into consideration acoustic window and depth: measurements that are taken at 4 to 5 cm depth usually have less variability.
- Ask the patient to breathe normally while looking for the best acoustic window; then perform the measurement while the patient holds his or her breath in a neutral position.
- Have the ARFI pulse perpendicular to the liver capsule to limit refraction of the pulse.
- Place the region of interest (ROI) 1.5 to 2.0 cm beneath Glisson's capsule to avoid reverberation artifacts.
- Do not include liver vessels in the ROI.
- Make multiple measurements in the same location.

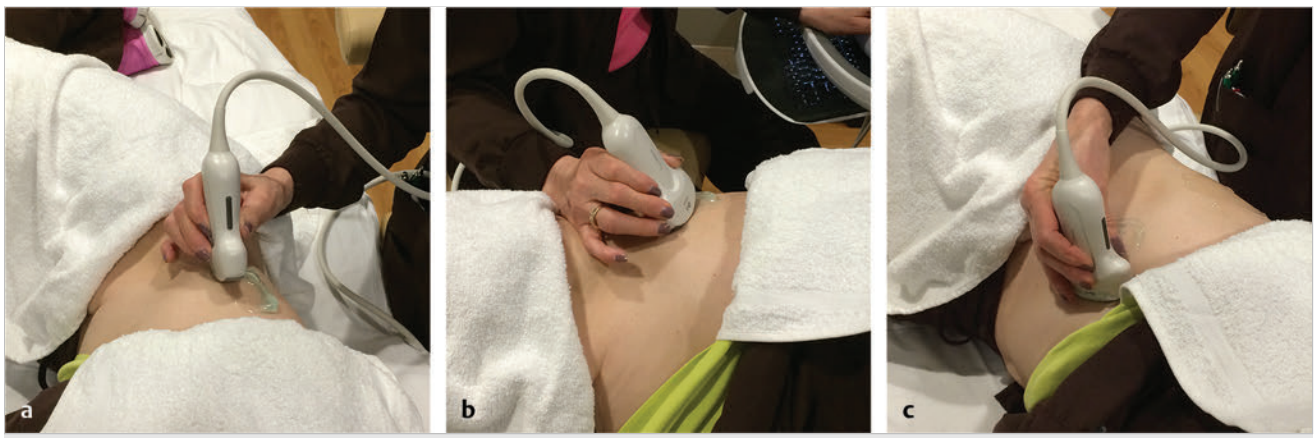

Fig. 3.6 Positions of the probe that should be avoided when imaging: (**a**) placing the probe across ribs; (**b**) angling of the probe to liver capsule; (**c**) substernal scanning.

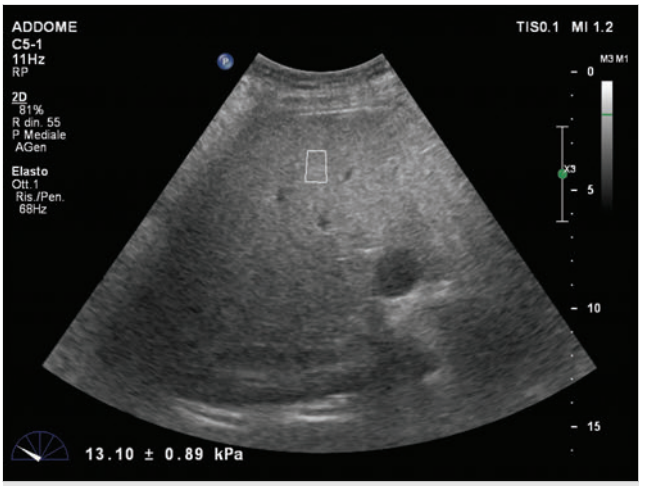

Fig. 3.7 Correct positioning of the sample box for imaging.

Artifacts

With all of the shear wave imaging techniques, a quality assessment is made on the data. If the data is of poor quality and an accurate shear wave speed cannot be calculated, the system does not provide a measurement, listing "0" or "x.xx" as the result, or in 2D-SWE it does not color-code that area.

Real-Time Strain Elastography

The B-mode images should be clear and free from artifacts. The transducer is placed on the skin in the right intercostal space without moving it and is pointed toward the heart. The manufacturer recommends that the ROI be placed deep to the liver capsule and to select a homogeneous region. The patient is asked to hold his or her breath while the RTSE images are displayed. To avoid large blood vessels, a 2.5 × 2.5 cm ROI is recommended. For the analysis, frames with strain generated in the depth direction with no artifacts should be selected. Good images may be obtained at the end of diastole with electrocardiographic gating or at the largest downward wave on a strain graph.[9] Few methods have been proposed for analyzing the strain information displayed inside the ROI. Basically, they are all strain ratios and give a semiquantitative assessment of liver stiffness. The liver fibrosis index (LF index) is the standard analytic method recommended by the manufacturer and is based on nine features extracted from each image. The results obtained with strain elastography in the assessment of liver fibrosis are reported in a separate section below.

3.3 Liver Stiffness Measurements

3.3.1 Reproducibility

The reproducibility of liver stiffness measurements has been assessed by means of the intraclass correlation coefficient (ICC) or the concordance correlation coefficient (CCC). With both coefficients, the agreement between measurements ranges in value from 0 to 1 and is classified as poor (0.00–0.20), fair (0.21–0.40), moderate (0.41–0.60), good (0.61–0.80), and excellent (0.81–1.00).

Measurements performed with VCTE shows an excellent interobserver agreement with an overall ICC of 0.98 (95% confidence interval [CI], 0.977–0.987). Reproducibility is not influenced by gender, patient age, or the degree of liver fibrosis, but it is negatively affected by a higher body mass index (BMI), by the presence of significant hepatic steatosis, and in cases of mild fibrosis (F0-F1).[14]

p-SWE methods are highly reproducible, with an agreement ranging from 0.81 to 0.93.[15,16] The interobserver reproducibility seems to decrease for BMI > 25 kg/m^2 and for low stages of liver fibrosis.[16] The interobserver agreement of measurements performed with 2D-SWE is excellent (ICC 0.88). However, the method is subject to the same limitations encountered with

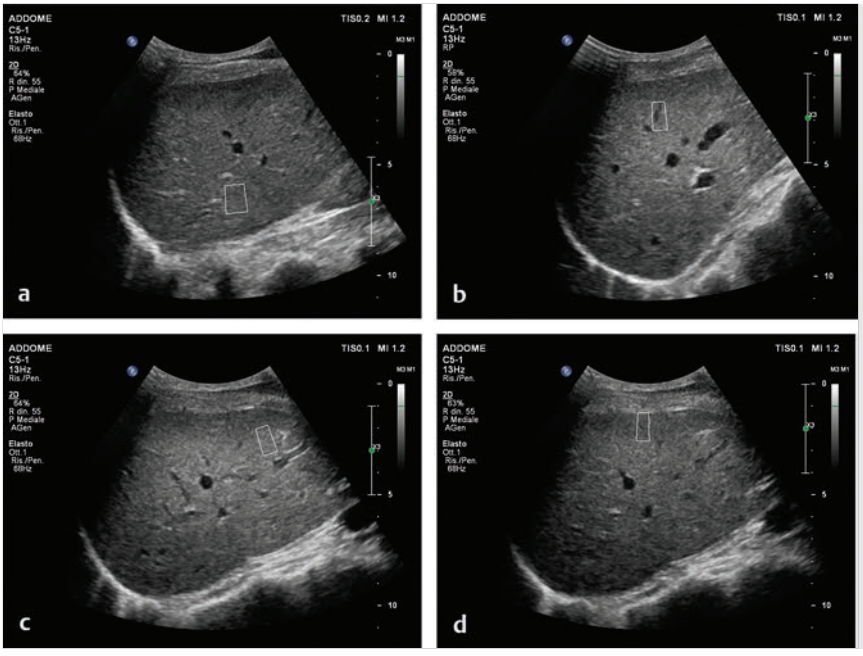

Fig. 3.8 Tips for positioning of the sample box for imaging: (**a**) avoid imaging at depth; (**b**) avoid imaging at vessels; (**c**) avoid imaging at angles; (**d**) avoid imaging < 1.5 cm deep to liver capsule.

conventional ultrasound imaging modes, such as the expertise of the operator and the patient body habitus; thus, it is recommended that at least 50 supervised scans and measurements should be performed by a novice operator in order to obtain consistent measurements.[17]

For all methods, there is a learning curve that could affect the reproducibility. VCTE is not a difficult procedure to learn; it requires the training of performing about 100 examinations. However, in a study, the failure rate in the measurements decreased from 8.3 to 3.5% when the operator had performed more than 500 VCTE examinations.[18] The experience of the operator is an important factor with all the techniques, thus training is required and the recommendations of the manufacturers should be followed.

3.3.2 Limitations and Confounding Factors

Fat attenuates ultrasound and elastic wave propagation; thus the measurement of liver stiffness in obese individuals is more challenging. The FibroScan device is equipped with the XL probe that reduces failure rates in obese patients. Fibrosis thresholds of VCTE are lower with the XL probe than the M probe, which is designed for normal weight patients, but further validation in larger cohorts of chronic liver disease patients is required. Since the shear wave originates at the skin level when using VCTE, VCTE cannot be used in individuals with ascites because the shear wave does not propagate into fluid. With all the techniques, measurements can be difficult in individuals with narrow intercostal spaces.

Liver stiffness is a physical parameter largely related to fibrosis, but it can also be influenced by other factors that modify liver elasticity. An increase in liver stiffness from postprandial blood flow has been reported, thus fasting for 4 to 6 hours before measurement is recommended.[10] Deep inspiration may falsely increase the stiffness. Liver stiffness values may be 1.3 to 3 times higher in cases of acute inflammation and/or moderate alanine aminotransferase (ALT) elevation. It has been reported that ALT levels greater than 80 international units per liter (IU/L), which is twofold the upper limit of normal, resulted in false positive results of liver stiffness in patients with chronic hepatitis C.[19] A significant and progressive reduction of liver stiffness values was observed in the follow-up of patients with acute hepatitis B in parallel with the reduction of ALT levels.[20]

It has been reported that liver stiffness values were some 10% higher in men than women and that individuals with a BMI > 30 kg/m^2 had higher liver stiffness values. After adjusting for gender and BMI, liver stiffness values were also higher in subjects with metabolic syndrome.[21] Congestive heart failure and extrahepatic cholestasis also result in higher liver stiffness values and this information needs to be taken into account when considering the liver stiffness results obtained.

The assessment of diagnostic accuracy, positive predictive value, and negative predictive value are affected by disease prevalence in the studied population.[10] The clinical interpretation of the results of liver stiffness measurements should always be based on information regarding patient demographics, disease etiology, and laboratory parameters.

Unlike liver biopsy, elastographic methods can neither determine the etiology of liver disease nor evaluate the presence and severity of the fatty infiltration. Even though these methods cannot replace biopsy in all settings, they will likely substitute for it when only the assessment of liver fibrosis is needed. The limitations and confounding factors are summarized in ▶ Table 3.1.

Table 3.1 Limitations and confounding factors

Limitations	Obesity. (Fat attenuates ultrasound and elastic wave propagation, and thus the measurement of liver stiffness in obese individuals is more challenging.)
	Vibration-controlled transient elastography (VCTE) cannot be used in individuals with ascites because shear waves do not propagate into fluid.
	Measurements can be difficult in individuals with narrow intercostal spaces.
	The learning curve could affect the reproducibility.
Confounding factors	Postprandial state.
	Acute hepatitis.
	Flares of transaminases.
	Deep inspiration.
	Congestive heart failure.
	Extrahepatic cholestasis.
	Several studies have reported liver stiffness values are about 10% higher in men than in women.

3.4 Accuracy of Elastography for the Assessment of Liver Fibrosis

3.4.1 Viral Hepatitis

The first available technique has been VCTE and validation studies were performed in chronic hepatitis C. The first published study was by Sandrin et al in 2003, and it showed that VCTE was 99% effective in detecting cirrhosis.[22] In 2005, the articles of Castera et al and Ziol et al confirmed the reliability of the method in the staging of liver fibrosis.[23,24] Since then a number of studies have validated the method in patients with chronic hepatitis C.[24,25,26,27,28,29,30,31,32,33,34,35] A meta-analysis that included 50 studies showed area under the receiver operating characteristics curves (AUROCs) of 0.84, 0.89, and 0.94 for significant fibrosis (F ≥ 2), advanced fibrosis (F ≥ 3), and cirrhosis, respectively.[25] The results of this meta-analysis show that VCTE is a good test for screening cirrhosis, with a 90% disease probability following a positive measurement. The findings of the published studies indicate that VCTE could be used to detect severe fibrosis and cirrhosis (METAVIR F3 or F4) and to exclude significant fibrosis (METAVIR F ≥ 2).

All the published studies indicate that the performance in scoring liver fibrosis of p-SWE or 2D-SWE is equivalent to VCTE, with some studies suggesting that the two ARFI-based methods perform better.[36,37,38,39,40,41,42,43,44,45,46,47,48,49,50,51,52,53] The obvious advantage of p-SWE or 2D-SWE is that they are integrated into a conventional diagnostic ultrasound system, and therefore, the real-time B-mode imaging for the assessment of

morphologic changes or detection of focal liver lesions (e.g., HCC) can also be performed. Different from VCTE, ARFI-based methods allow sampling from different areas of the liver parenchyma, thus they are more representative of the heterogeneous distribution of liver fibrosis. Moreover the use of the B-mode image for the guidance of shear wave acquisitions could diminish the variability in stiffness measurements and the noninvasive evaluation of liver stiffness can be achieved even in patients with a significant amount of ascites. In a study in which 139 patients with chronic hepatitis C were enrolled, it has been observed that p-SWE had a significantly higher performance than VCTE for intermediate stages of fibrosis.[36] A later meta-analysis that included 13 studies indicates that the diagnostic odds ratio of p-SWE and VCTE did not differ significantly for the detection of significant fibrosis ($F \geq 2$) and cirrhosis.[38]

The diagnostic accuracy of 2D-SWE and VCTE in estimating liver fibrosis was compared against histology in patients with chronic hepatitis C. 2D-SWE performed significantly better than VCTE in the identification of significant fibrosis.[53] A recent study has compared the diagnostic performance of VCTE, p-SWE and 2D-SWE. For the diagnosis of significant fibrosis ($F \geq 2$) 2D-SWE had a significantly better diagnostic performance than p-SWE, and for the diagnosis of severe fibrosis ($F \geq 3$) 2D-SWE had significantly better diagnostic performances than VCTE. For the diagnosis of cirrhosis ($F = 4$), no significant difference was observed between the performances of VCTE, p-SWE, and 2D-SWE.[52]

The diagnostic performance of the elastographic techniques is comparable between patients with chronic hepatitis C and those with chronic hepatitis B.[54,55] In a study that compared the diagnostic performance of p-SWE and VCTE in patients with chronic hepatitis B, no significant difference was found between the two techniques for the diagnosis of liver fibrosis in both the "per protocol" and the "intention to diagnose" analysis.[56] With all techniques, serum levels of aminotransferases should always be taken into account in interpreting the results in patients with hepatitis B.[57,58] In a large series of patients with chronic hepatitis B, the diagnostic performance of 2D-SWE was determined in an index cohort and then confirmed in a validation cohort. The areas under the receiver operating characteristics (ROC) curves for significant fibrosis, severe fibrosis, and cirrhosis were all greater than 0.90 and did not differ significantly between the index and validation cohorts.[59] 2D-SWE seems to provide more accurate correlation of liver elasticity with liver fibrosis stage compared with VCTE, especially in identification of stage F2 or greater.[60]

In a recent meta-analysis in which only patients with chronic hepatitis B were included, thus eliminating potential bias due to different viral etiologies, the diagnostic performance of VCTE was comparable to those from previous meta-analyses of studies conducted in patients with chronic hepatitis C but the cutoffs for fibrosis stages were slightly lower.[61] Patients with chronic hepatitis B have a complex natural history with necroinflammatory flares accompanied by fluctuating aminotransferase levels. In addition, histological specimens show fibrous septa that might be thinner than in those seen in patients with chronic hepatitis C with the same histological stage. Lastly, chronic hepatitis B may progress to cirrhosis with larger nodules than chronic hepatitis C, thus the amount of liver parenchyma between fibrotic septa is larger.[61]

3.4.2 Nonalcoholic Fatty Liver Disease

The value of the elastographic techniques in patients with NAFLD has been investigated in a limited number of studies with small sample sizes. Liver stiffness measurements in patients with NAFLD or NASH need to be interpreted cautiously because disease-related factors may modify the accuracy. Regarding the influence of severe steatosis on stiffness measurements, the results are controversial: some studies suggest a negative effect whereas others do not.[62,63,64]

Obesity is one of the main reasons for unreliable results with VCTE and individuals with NAFLD are usually overweight or obese. It should be noted that the M probe of the FibroScan device has been used in a majority of the published studies in patients with NAFLD, thus the rate of unreliable results could have been overestimated. The availability of the XL probe, which has been designed for obese subjects, can increase the applicability of the method. On the other hand, the number of successful acquisitions and their success rate has no influence on the diagnostic accuracy of VCTE.

3.5 Liver Elastography in Clinical Practice

3.5.1 Shear Wave Elastography

Before Treatment for Fibrosis Staging

With the availability of the interferon-free antiviral agents for the treatment of chronic hepatitis C (that are safe and effective with a potential efficacy over 90% and typically with a short duration of up to 12 weeks), noninvasive methods for staging liver fibrosis are accepted and preferred to liver biopsy. The guidelines for the management of patients with chronic hepatitis C issued by the European Association for the Study of the Liver (EASL) indicate that elastography can be used for the assessment of liver fibrosis before treatment, reserving liver biopsy for cases where there is uncertainty or potential additional etiologies.[5] Likewise, the consensus guidelines of the Canadian Association for the Study of the Liver recommends that all patients with HCV should undergo an assessment for the severity of liver fibrosis, and elastography is included among the acceptable methods to assess this.[65]

In the United Kingdom, the National Institute for Health and Care Excellence (NICE) recommends offering antiviral treatment without a liver biopsy to adults with a VCTE score ≥ 11 kPa; not offering liver biopsy to adults with a VCTE < 6 kPa who have normal ALT and HBV DNA less than 2000 IU/mL, as they are unlikely to have advanced liver disease or need antiviral treatment; and offering an annual reassessment of liver disease using VCTE to adults who are not taking antiviral treatment.[66]

Follow-Up of Chronic Liver Disease

Noninvasive assessment of liver stiffness is helpful in the follow-up of patients, whether they have been treated or not.[67,68,69] Pretreatment liver stiffness values may be useful for predicting a sustained virologic response after therapy in patients with hepatitis C.[70] The EASL guidelines advise that untreated patients or those who do not respond to treatment should have

regular follow-up, and indicate that noninvasive methods for staging fibrosis can be used for follow-up assessment at intervals.[5] Especially in patients with chronic hepatitis B, a decrease in liver stiffness could result from a decrease in inflammatory activity rather than fibrosis.[71] Repeated stiffness measurements indicate that inactive carriers of HBV do not show significant variation in liver stiffness values over time.[72]

Liver Fibrosis: Prognosis and Complications of Liver Cirrhosis

Liver stiffness correlates with fibrosis severity, thus stiffness values could be predictors of survival. The risk of developing HCC increases with the increase of liver stiffness values, and patients with already established cirrhosis could be grouped in different classes of risk based on stiffness values.[73,74] By following up with patients with chronic viral hepatitis who were assessed with elastography, it has been shown that the outcomes worsened as liver stiffness values increased.[75,76] In a meta-analysis of cohort studies, the degree of liver stiffness was associated with risk of decompensated cirrhosis, HCC, and death in patients with chronic liver disease.[77] In patients with chronic HBV infection who achieved complete virological response, the incidence of liver-related events increased significantly in association with higher liver stiffness values. Thus, tailored surveillance strategies might be established based upon the stiffness value observed at complete virological response.[78]

VCTE has been available for more than a decade; therefore, it has been used in several studies. A recent study reported that the diagnostic accuracy of p-SWE is comparable to VCTE for the detection of complications in patients with cirrhosis.[79]

Liver stiffness seems to correlate with the presence of large esophageal varices; however, elastography is not accurate enough to assess the severity of portal hypertension.[80] Recently, it has been suggested that the assessment of spleen stiffness might identify patients with esophageal varices and different degrees of portal hypertension.[81,82] However, results from use of this method do not meet expectations in the case of a small spleen, and spleen stiffness measurements are less reproducible than those of the liver and are highly dependent on operator expertise.[83,84] Further studies are required to understand the validity of the spleen stiffness assessment before introducing it in the clinical practice.

3.5.2 Strain Elastography

Staging of Liver Fibrosis

The literature regarding the assessment of liver fibrosis with real-time strain elastography (RTSE) is limited. The method is used mainly in Japan. The promising results obtained in that country were not confirmed in the European series.[85,86]

Various analysis methods are currently available, and they all show a clear correlation with liver fibrosis. However, a comparative study is needed to ascertain which is the most suitable one.[9]

Using the elastic ratio, the interobserver agreement between operators that had already performed at least 100 liver stiffness evaluations ranged from 88.6 to 97.1%.[87] In a validation study of the liver fibrosis index (LF index) in patients with cirrhosis and chronic hepatitis B and C, significant differences between advanced fibrosis and cirrhosis, but not between other consecutive stages of liver fibrosis, were observed.[88] The overall accuracy of RTSE for the staging of liver fibrosis has been investigated in a recent meta-analysis that systematically reviewed 15 studies.[89] The conclusion of this study was that RTSE is not highly accurate for any cutoff stage of fibrosis. Compared with the findings of meta-analyses on VCTE and p-SWE, the overall accuracy of RSTE seems to be most similar to that of the other two for the evaluation of significant liver fibrosis, but less accurate for the evaluation of cirrhosis. The authors point out that the estimated accuracy of the method may be overestimated due to publication bias.

Conversely, another meta-analysis has shown that the elastic ratio of the liver for the intrahepatic vein has excellent precision in differentiating each stage of hepatic fibrosis.[90] These conflicting results emphasize the need to standardize the methodology of measurement.

RTSE examination strongly relies on the expertise of the examiners and the method has a long learning curve. In a study conducted to assess the accuracy of the LF index in a large series of patients with chronic hepatitis B, 10.6% of the total cases were excluded because of unreliable examinations due to examiners' lack of skill and experience.[91] In another study 15% of subjects were excluded because more than three stable RTSE images could not be acquired. Most of the reasons for exclusion were related to the RTSE skill of the clinicians, which improved significantly with more experience.[92] In patients with NAFLD, a significant correlation between the elasticity ratio and liver fibrosis was found, and RTSE reliably identified the early stage of liver fibrosis.[93]

Liver Steatosis: The Controlled Attenuation Parameter

NAFLD has become the leading cause of chronic liver disease worldwide. The term comprises a range of conditions, from simple steatosis to NASH. This latter may evolve to cirrhosis and its complications. In patients with chronic hepatitis C the presence of steatosis could accelerate the progression of the disease and decrease the probability of sustained virological response. In patients undergoing liver resection, steatosis is an independent risk factor for complications and death.[94] Controlling weight and lifestyle adjustments are of utmost importance in the management of liver steatosis. Liver steatosis can be evaluated using noninvasive techniques, such as computed tomography, magnetic resonance imaging, or ultrasound. Magnetic resonance imaging shows high accuracy for quantification of liver steatosis, but it has high costs and is too complex to be used to monitor the disease. Computed tomography has the limitation of patient exposure to ionizing radiation. Ultrasound is a low-cost imaging modality but it lacks sensitivity for detection of mild steatosis. Moreover, the method is operator- and machine-dependent.

Recently, the controlled attenuation parameter (CAP) has been developed for the assessment and quantification of liver steatosis. CAP is based on the properties of the ultrasound signal acquired by the FibroScan device, using the postulate that fat affects ultrasound propagation. The CAP is evaluated using the same radiofrequency data and the same region of interest

used to assess liver stiffness measurements. The device estimates the loss of energy of ultrasound during the propagation through a medium. The attenuation is related to the ultrasound frequency and the properties of the medium, and it is exponentially related to tissue depth. The attenuation is measured in decibels per meter (dB/m) at the central frequency of the VCTE 3.5 MHz probe (▶ Fig. 3.1). The CAP and the liver stiffness are measured simultaneously in the same region of interest, thus no CAP measurement is obtained if the liver stiffness value is rejected by the machine.

In 2010 Sasso et al validated CAP as an estimate of the ultrasonic attenuation using phantoms, and the reproducibility was evaluated in a cohort of 115 patients affected by liver disease of different etiologies.[95] Since then, several studies have assessed the reliability of CAP in the estimation of liver steatosis by comparing the results to those obtained with liver biopsy as the reference standard.[98,99] At liver histology, steatosis is expressed as a percentage of fat in the hepatocytes and is usually graded according to the method of Kleiner et al or Brunt et al.[96,97] Kleiner et al classify steatosis as follows: S0, steatosis in less than 5% of hepatocytes; S1, in 5 to 33% of hepatocytes; S2, in 34 to 66% of hepatocytes; and S3, in more than 66% of hepatocytes. In the Brunt classification, S0 is the absence of liver steatosis, whereas the other grades are the same as Kleiner et al. The results of the published studies indicate that CAP is a reliable method in differentiating nonconsecutive grades of liver steatosis whereas the performance of the method in separating consecutive grades is still low.

Compared to serum biomarkers of liver steatosis, such as the hepatic steatosis index, SteatoTest, and the fatty liver index, the CAP shows a higher diagnostic accuracy.[98,99] These studies confirmed that CAP is an excellent tool for discriminating between S0 and S3 and S0 and S2, but it is not good for discriminating the difference of only one grade.

We have prospectively evaluated the accuracy of CAP in a series of 115 consecutive patients undergoing liver biopsy for chronic viral hepatitis. In our cohort, CAP demonstrated excellent negative predictive value for assessing and grading steatosis. The cutoff for the detection of steatosis was 219 dB/m, similar to that obtained by Sasso et al in a series of patients with chronic hepatitis C and by de Lédinghen et al in a series of patients with chronic hepatitis of mixed etiologies.[99,100,101] A significant correlation of CAP with the degree of liver steatosis as assessed by histology and with BMI after correction for confounding variables was observed. Several studies indicate that there is a strong correlation between CAP values, BMI, and steatosis grades.[98,100,101,102,103]

Our group has recently shown that CAP is a reproducible method for noninvasive assessment of liver steatosis.[104] The interobserver agreement was only fair for values that were lower than 240 dB/m and good for higher values. In our opinion, factors related to both the patient and the method could explain the lower agreement of CAP measurements in these cases. In fact, CAP measures the attenuation of the ultrasound waves, which refers to the loss of their energy while they travel into tissues and is directly linked to liver steatosis. When steatosis is likely absent, other tissue scatterers, such as small heterogeneities due to tiny blood vessels, may become predominant in determining the loss of amplitude of the ultrasound waves.

A recent study, which has assessed the usefulness of CAP in clinical practice by analyzing the results of 5,323 examinations, has shown that factors independently associated with elevated CAP were BMI, metabolic syndrome, consumption of more than 14 drinks per week of alcohol and liver stiffness higher than 6 kPa.[102] Factors independently associated with CAP measurement failure were female gender, BMI, and metabolic syndrome.[101]

The clinical value of CAP has also been assessed by comparing the method to other imaging techniques such as ultrasound, magnetic resonance, or dual-energy X-ray absorptiometry (DXA). In a study performed to assess the diagnostic accuracy of CAP for detection and quantification of steatosis in general population, CAP was significantly correlated with liver steatosis evaluated by ultrasound.[105] We have recently assessed the clinical relevance of CAP by analyzing the correlations between CAP and indirect indices of liver steatosis in obese or overweight patients. CAP showed a correlation with other indirect markers of central obesity and a good correlation with magnetic resonance evaluation of steatosis.[106]

In summary, CAP is a promising tool for the quantification of liver steatosis, but the number of studies that have investigated the diagnostic accuracy of the method is still limited.

3.6 Conclusion

Elastography is an accurate method for the noninvasive evaluation of diffuse liver disease, and it is accepted by clinicians for patient management. The use of the elastographic techniques in chronic hepatitis C is approved by clinical guidelines and allows for reduction of the number of liver biopsies, thus decreasing costs and risks. Moreover, the availability of these methods has allowed clinicians to monitor disease progression and response to treatment noninvasively. Further work should be aimed at improving the standardization of the techniques, which may decrease the need for 10 measurements.

References

[1] World Health Organization. Hepatitis C. Fact sheet No. 164, updated April 2014. http://www.who.int/mediacentre/factsheets/fs164/en/. Accessed on March 4, 2015.

[2] World Health Organization. Hepatitis B. http://www.who.int/csr/disease/hepatitis/HepatitisB_whocdscsrlyo2002_2.pdf. Accessed on March 4, 2015.

[3] Vernon G, Baranova A, Younossi ZM. Systematic review: the epidemiology and natural history of non-alcoholic fatty liver disease and non-alcoholic steatohepatitis in adults. Aliment Pharmacol Ther 2011; 34(3):274–285

[4] Milić S, Stimac D. Nonalcoholic fatty liver disease/steatohepatitis: epidemiology, pathogenesis, clinical presentation and treatment. Dig Dis 2012; 30 (2):158–162

[5] European Association for the Study of the Liver. EASL clinical practice guidelines: management of hepatitis C virus infection. J Hepatol 2014; 60(2):392–420 Erratum in: J Hepatol. 2014;61:183–184

[6] European Association for the Study of the Liver. EASL clinical practice guidelines: management of chronic hepatitis B virus infection. J Hepatol 2012; 57 (1):167–185

[7] Bedossa P, Poynard T; The METAVIR Cooperative Study Group. An algorithm for the grading of activity in chronic hepatitis C. Hepatology 1996; 24(2): 289–293

[8] Cosgrove D, Piscaglia F, Bamber J et al. EFSUMB. EFSUMB guidelines and recommendations on the clinical use of ultrasound elastography: part 2: Clinical applications. Ultraschall Med 2013; 34(3):238–253

[9] Ferraioli G, Filice C, Castera L et al. WFUMB guidelines and recommendations for clinical use of ultrasound elastography: part 3: liver. Ultrasound Med Biol 2015; 41(5):1161–1179
[10] Barr RG, Ferraioli G, Palmeri ML et al. Elastography assessment of liver fibrosis: society of radiologists in ultrasound consensus conference statement. Radiology 2015; 276(3):845–861
[11] Ferraioli G, Parekh P, Levitov AB, Filice C. Shear wave elastography for evaluation of liver fibrosis. J Ultrasound Med 2014; 33(2):197–203
[12] Bamber J, Cosgrove D, Dietrich CF et al. EFSUMB guidelines and recommendations on the clinical use of ultrasound elastography. Part 1: Basic principles and technology. Ultraschall Med 2013; 34(2):169–184
[13] Boursier J, Zarski JP, de Ledinghen V et al. Multicentric group from ANRS/HC/EP23 FIBROSTAR studies. Determination of reliability criteria for liver stiffness evaluation by transient elastography. Hepatology 2013; 57(3):1182–1191
[14] Fraquelli M, Rigamonti C, Casazza G et al. Reproducibility of transient elastography in the evaluation of liver fibrosis in patients with chronic liver disease. Gut 2007; 56(7):968–973
[15] Ferraioli G, Tinelli C, Lissandrin R et al. Point shear wave elastography method for assessing liver stiffness. World J Gastroenterol 2014; 20(16): 4787–4796
[16] Bota S, Sporea I, Sirli R, Popescu A, Danila M, Costachescu D. Intra- and interoperator reproducibility of acoustic radiation force impulse (ARFI) elastography—preliminary results. Ultrasound Med Biol 2012; 38(7):1103–1108
[17] Ferraioli G, Tinelli C, Zicchetti M et al. Reproducibility of real-time shear wave elastography in the evaluation of liver elasticity. Eur J Radiol 2012; 81 (11):3102–3106
[18] Castéra L, Foucher J, Bernard PH et al. Pitfalls of liver stiffness measurement: a 5-year prospective study of 13,369 examinations. Hepatology 2010; 51(3): 828–835
[19] Tapper EB, Cohen EB, Patel K et al. Levels of alanine aminotransferase confound use of transient elastography to diagnose fibrosis in patients with chronic hepatitis C virus infection. Clin Gastroenterol Hepatol 2012; 10(8): 932–937.e1
[20] Arena U, Vizzutti F, Corti G et al. Acute viral hepatitis increases liver stiffness values measured by transient elastography. Hepatology 2008; 47(2):380–384
[21] Roulot D, Czernichow S, Le Clésiau H, Costes JL, Vergnaud AC, Beaugrand M. Liver stiffness values in apparently healthy subjects: influence of gender and metabolic syndrome. J Hepatol 2008; 48(4):606–613
[22] Sandrin L, Fourquet B, Hasquenoph JM et al. Transient elastography: a new noninvasive method for assessment of hepatic fibrosis. Ultrasound Med Biol 2003; 29(12):1705–1713
[23] Castéra L, Vergniol J, Foucher J et al. Prospective comparison of transient elastography, Fibrotest, APRI, and liver biopsy for the assessment of fibrosis in chronic hepatitis C. Gastroenterology 2005; 128(2):343–350
[24] Ziol M, Handra-Luca A, Kettaneh A et al. Noninvasive assessment of liver fibrosis by measurement of stiffness in patients with chronic hepatitis C. Hepatology 2005; 41(1):48–54
[25] Tsochatzis EA, Gurusamy KS, Ntaoula S, Cholongitas E, Davidson BR, Burroughs AK. Elastography for the diagnosis of severity of fibrosis in chronic liver disease: a meta-analysis of diagnostic accuracy. J Hepatol 2011; 54(4): 650–659
[26] Degos F, Perez P, Roche B et al; FIBROSTIC study group. Diagnostic accuracy of FibroScan and comparison to liver fibrosis biomarkers in chronic viral hepatitis: a multicenter prospective study (the FIBROSTIC study). J Hepatol 2010; 53(6):1013–1021
[27] Friedrich-Rust M, Ong MF, Martens S et al. Performance of transient elastography for the staging of liver fibrosis: a meta-analysis. Gastroenterology 2008; 134(4):960–974
[28] Castera L, Forns X, Alberti A. Non-invasive evaluation of liver fibrosis using transient elastography. J Hepatol 2008; 48(5):835–847
[29] Stebbing J, Farouk L, Panos G et al. A meta-analysis of transient elastography for the detection of hepatic fibrosis. J Clin Gastroenterol 2010; 44(3):214–219
[30] Ferraioli G, Tinelli C, Dal Bello B et al. Performance of liver stiffness measurements by transient elastography in chronic hepatitis. World J Gastroenterol 2013; 19(1):49–56
[31] Pinzani M, Vizzutti F, Arena U, Marra F. Technology Insight: noninvasive assessment of liver fibrosis by biochemical scores and elastography. Nat Clin Pract Gastroenterol Hepatol 2008; 5(2):95–106
[32] Foucher J, Chanteloup E, Vergniol J et al. Diagnosis of cirrhosis by transient elastography (FibroScan): a prospective study. Gut 2006; 55(3):403–408
[33] de Lédinghen V, Douvin C, Kettaneh A et al. Diagnosis of hepatic fibrosis and cirrhosis by transient elastography in HIV/hepatitis C virus–coinfected patients. J Acquir Immune Defic Syndr 2006; 41(2):175–179
[34] Arena U, Vizzutti F, Abraldes JG et al. Reliability of transient elastography for the diagnosis of advanced fibrosis in chronic hepatitis C. Gut 2008; 57(9): 1288–1293
[35] Fraquelli M, Rigamonti C, Casazza G et al. Etiology-related determinants of liver stiffness values in chronic viral hepatitis B or C. J Hepatol 2011; 54(4): 621–628
[36] Rizzo L, Calvaruso V, Cacopardo B et al. Comparison of transient elastography and acoustic radiation force impulse for non-invasive staging of liver fibrosis in patients with chronic hepatitis C. Am J Gastroenterol 2011; 106 (12):2112–2120
[37] Frulio N, Trillaud H, Perez P et al. Acoustic radiation force impulse (ARFI) and transient elastography (TE) for evaluation of liver fibrosis in HIV-HCV coinfected patients. BMC Infect Dis 2014; 14:405
[38] Bota S, Herkner H, Sporea I et al. Meta-analysis: ARFI elastography versus transient elastography for the evaluation of liver fibrosis. Liver Int 2013; 33 (8):1138–1147
[39] Yap WW, Kirke R, Yoshida EM, Owen D, Harris AC. Non-invasive assessment of liver fibrosis using ARFI with pathological correlation, a prospective study. Ann Hepatol 2013; 12(4):608–615
[40] Nierhoff J, Chávez Ortiz AA, Herrmann E, Zeuzem S, Friedrich-Rust M. The efficiency of acoustic radiation force impulse imaging for the staging of liver fibrosis: a meta-analysis. Eur Radiol 2013; 23(11):3040–3053
[41] Cassinotto C, Lapuyade B, Aït-Ali A et al. Liver fibrosis: noninvasive assessment with acoustic radiation force impulse elastography—comparison with FibroScan M and XL probes and FibroTest in patients with chronic liver disease. Radiology 2013; 269(1):283–292
[42] Bota S, Sporea I, Peck-Radosavljevic M, et al. The influence of aminotransferase levels on liver stiffness assessed by Acoustic Radiation Force Impulse Elastography: a retrospective multicentre study. Dig Liver Dis. 2013; 45: 762-8.
[43] Sporea I, Bota S, Peck-Radosavljevic M et al. Acoustic radiation force impulse elastography for fibrosis evaluation in patients with chronic hepatitis C: an international multicenter study. Eur J Radiol 2012; 81(12):4112–4118
[44] Crespo G, Fernández-Varo G, Mariño Z et al. ARFI, FibroScan, ELF, and their combinations in the assessment of liver fibrosis: a prospective study. J Hepatol 2012; 57(2):281–287
[45] Yoon KT, Lim SM, Park JY et al. Liver stiffness measurement using acoustic radiation force impulse (ARFI) elastography and effect of necroinflammation. Dig Dis Sci 2012; 57(6):1682–1691
[46] Friedrich-Rust M, Nierhoff J, Lupsor M et al. Performance of acoustic radiation force impulse imaging for the staging of liver fibrosis: a pooled meta-analysis. J Viral Hepat 2012; 19(2):e212–e219
[47] Colombo S, Buonocore M, Del Poggio A et al. Head-to-head comparison of transient elastography (TE), real-time tissue elastography (RTE), and acoustic radiation force impulse (ARFI) imaging in the diagnosis of liver fibrosis. J Gastroenterol 2012; 47(4):461–469
[48] Haque M, Robinson C, Owen D, Yoshida EM, Harris A. Comparison of acoustic radiation force impulse imaging (ARFI) to liver biopsy histologic scores in the evaluation of chronic liver disease: a pilot study. Ann Hepatol 2010; 9 (3):289–293
[49] Takahashi H, Ono N, Eguchi Y et al. Evaluation of acoustic radiation force impulse elastography for fibrosis staging of chronic liver disease: a pilot study. Liver Int 2010; 30(4):538–545
[50] Lupsor M, Badea R, Stefanescu H et al. Performance of a new elastographic method (ARFI technology) compared to unidimensional transient elastography in the noninvasive assessment of chronic hepatitis C. Preliminary results. J Gastrointestin Liver Dis 2009; 18(3):303–310
[51] Friedrich-Rust M, Wunder K, Kriener S et al. Liver fibrosis in viral hepatitis: noninvasive assessment with acoustic radiation force impulse imaging versus transient elastography. Radiology 2009; 252(2):595–604
[52] Cassinotto C, Lapuyade B, Mouries A et al. Non-invasive assessment of liver fibrosis with impulse elastography: comparison of Supersonic Shear Imaging with ARFI and FibroScan®. J Hepatol 2014; 61(3):550–557
[53] Ferraioli G, Tinelli C, Dal Bello B, Zicchetti M, Filice G, Filice C Liver Fibrosis Study Group. Accuracy of real-time shear wave elastography for assessing liver fibrosis in chronic hepatitis C: a pilot study. Hepatology 2012; 56(6): 2125–2133
[54] Sporea I, Sirli R, Deleanu A et al. Liver stiffness measurements in patients with HBV vs HCV chronic hepatitis: a comparative study. World J Gastroenterol 2010; 16(38):4832–4837

[55] Cardoso AC, Carvalho-Filho RJ, Stern C et al. Direct comparison of diagnostic performance of transient elastography in patients with chronic hepatitis B and chronic hepatitis C. Liver Int 2012; 32(4):612–621
[56] Friedrich-Rust M, Buggisch P, de Knegt RJ et al. Acoustic radiation force impulse imaging for non-invasive assessment of liver fibrosis in chronic hepatitis B. J Viral Hepat 2013; 20(4):240–247
[57] Zhang D, Chen M, Wang R et al. Comparison of acoustic radiation force impulse imaging and transient elastography for non-invasive assessment of liver fibrosis in patients with chronic hepatitis B. Ultrasound Med Biol 2015; 41(1):7–14
[58] Ma JJ, Ding H, Mao F, Sun HC, Xu C, Wang WP. Assessment of liver fibrosis with elastography point quantification technique in chronic hepatitis B virus patients: a comparison with liver pathological results. J Gastroenterol Hepatol 2014; 29(4):814–819
[59] Zeng J, Liu GJ, Huang ZP et al. Diagnostic accuracy of two-dimensional shear wave elastography for the non-invasive staging of hepatic fibrosis in chronic hepatitis B: a cohort study with internal validation. Eur Radiol 2014; 24(10): 2572–2581
[60] Leung VY, Shen J, Wong VW et al. Quantitative elastography of liver fibrosis and spleen stiffness in chronic hepatitis B carriers: comparison of shear-wave elastography and transient elastography with liver biopsy correlation. Radiology 2013; 269(3):910–918
[61] Chon YE, Choi EH, Song KJ et al. Performance of transient elastography for the staging of liver fibrosis in patients with chronic hepatitis B: a meta-analysis. PLoS ONE 2012; 7(9):e44930
[62] Gaia S, Carenzi S, Barilli AL et al. Reliability of transient elastography for the detection of fibrosis in non-alcoholic fatty liver disease and chronic viral hepatitis. J Hepatol 2011; 54(1):64–71
[63] Yoneda M, Yoneda M, Mawatari H et al. Noninvasive assessment of liver fibrosis by measurement of stiffness in patients with nonalcoholic fatty liver disease (NAFLD). Dig Liver Dis 2008; 40(5):371–378
[64] Palmeri ML, Wang MH, Rouze NC et al. Noninvasive evaluation of hepatic fibrosis using acoustic radiation force–based shear stiffness in patients with nonalcoholic fatty liver disease. J Hepatol 2011; 55(3):666–672
[65] Myers RP, Ramji A, Bilodeau M, Wong S, Feld JJ. An update on the management of hepatitis C: consensus guidelines from the Canadian Association for the Study of the Liver. Can J Gastroenterol 2012; 26(6):359–375
[66] Sarri G, Westby M, Bermingham S, Hill-Cawthorne G, Thomas H Guideline Development Group. Diagnosis and management of chronic hepatitis B in children, young people, and adults: summary of NICE guidance. BMJ 2013; 346:f3893
[67] Goertz RS, Sturm J, Zopf S, Wildner D, Neurath MF, Strobel D. Outcome analysis of liver stiffness by ARFI (acoustic radiation force impulse) elastometry in patients with chronic viral hepatitis B and C. Clin Radiol 2014; 69(3):275–279
[68] Forestier N, Gaus A, Herrmann E et al. Acoustic radiation force impulse imaging for evaluation of antiviral treatment response in chronic hepatitis C. J Gastrointestin Liver Dis 2012; 21(4):367–373
[69] Martinez SM, Foucher J, Combis JM et al. Longitudinal liver stiffness assessment in patients with chronic hepatitis C undergoing antiviral therapy. PLoS ONE 2012; 7(10):e47715
[70] Stasi C, Piluso A, Arena U et al. Evaluation of the prognostic value of liver stiffness in patients with hepatitis C virus treated with triple or dual antiviral therapy: a prospective pilot study. World J Gastroenterol 2015; 21(10): 3013–3019
[71] Fung J, Lai CL, Wong DK, Seto WK, Hung I, Yuen MF. Significant changes in liver stiffness measurements in patients with chronic hepatitis B: 3-year follow-up study. J Viral Hepat 2011; 18(7):e200–e205
[72] Castéra L, Bernard PH, Le Bail B et al. Transient elastography and biomarkers for liver fibrosis assessment and follow-up of inactive hepatitis B carriers. Aliment Pharmacol Ther 2011; 33(4):455–465
[73] Masuzaki R, Tateishi R, Yoshida H et al. Prospective risk assessment for hepatocellular carcinoma development in patients with chronic hepatitis C by transient elastography. Hepatology 2009; 49(6):1954–1961
[74] Jung KS, Kim SU, Ahn SH et al. Risk assessment of hepatitis B virus-related hepatocellular carcinoma development using liver stiffness measurement (FibroScan). Hepatology 2011; 53(3):885–894
[75] Vergniol J, Foucher J, Terrebonne E et al. Noninvasive tests for fibrosis and liver stiffness predict 5-year outcomes of patients with chronic hepatitis C. Gastroenterology 2011; 140(7):1970–1979, 1979.e1–1979.e3
[76] Vergniol J, Boursier J, Coutzac C et al. Evolution of noninvasive tests of liver fibrosis is associated with prognosis in patients with chronic hepatitis C. Hepatology 2014; 60(1):65–76
[77] Singh S, Fujii LL, Murad MH et al. Liver stiffness is associated with risk of decompensation, liver cancer, and death in patients with chronic liver diseases: a systematic review and meta-analysis. Clin Gastroenterol Hepatol 2013; 11(12):1573–1584. e1-e2, quiz e88–e89
[78] Lee HW, Yoo EJ, Kim BK et al. Prediction of development of liver-related events by transient elastography in hepatitis B patients with complete virological response on antiviral therapy. Am J Gastroenterol 2014; 109(8): 1241–1249
[79] Vermehren J, Polta A, Zimmermann O et al. Comparison of acoustic radiation force impulse imaging with transient elastography for the detection of complications in patients with cirrhosis. Liver Int 2012; 32(5):852–858
[80] Vizzutti F, Arena U, Romanelli RG et al. Liver stiffness measurement predicts severe portal hypertension in patients with HCV-related cirrhosis. Hepatology 2007; 45(5):1290–1297
[81] Colecchia A, Montrone L, Scaioli E et al. Measurement of spleen stiffness to evaluate portal hypertension and the presence of esophageal varices in patients with HCV-related cirrhosis. Gastroenterology 2012; 143(3):646–654
[82] Bota S, Sporea I, Sirli R et al. Can ARFI elastography predict the presence of significant esophageal varices in newly diagnosed cirrhotic patients? Ann Hepatol 2012; 11(4):519–525
[83] Procopet B, Berzigotti A, Abraldes JG et al. Real-time shear-wave elastography: applicability, reliability and accuracy for clinically significant portal hypertension. J Hepatol 2015; 62(5):1068–1075
[84] Ferraioli G, Tinelli C, Lissandrin R et al. Elastography Study Group. Ultrasound point shear wave elastography assessment of liver and spleen stiffness: effect of training on repeatability of measurements. Eur Radiol 2014; 24(6):1283–1289
[85] Friedrich-Rust M, Schwarz A, Ong M et al. Real-time tissue elastography versus FibroScan for noninvasive assessment of liver fibrosis in chronic liver disease. Ultraschall Med 2009; 30(5):478–484
[86] Ferraioli G, Tinelli C, Malfitano A et al. Liver Fibrosis Study Group. Performance of real-time strain-elastography, transient elastography, and asparate-to-platelet ratio index in the assessment of fibrosis in chronic hepatitis C. AJR Am J Roentgenol 2012; 199(1):19–25
[87] Koizumi Y, Hirooka M, Kisaka Y et al. Liver fibrosis in patients with chronic hepatitis C: noninvasive diagnosis by means of real-time tissue elastography —establishment of the method for measurement. Radiology 2011; 258(2): 610–617
[88] Yada N, Kudo M, Morikawa H, Fujimoto K, Kato M, Kawada N. Assessment of liver fibrosis with real-time tissue elastography in chronic viral hepatitis. Oncology 2013; 84 Suppl 1:13–20
[89] Kobayashi K, Nakao H, Nishiyama T et al. Diagnostic accuracy of real-time tissue elastography for the staging of liver fibrosis: a meta-analysis. Eur Radiol 2015; 25(1):230–238
[90] Hong H, Li J, Jin Y et al. Performance of real-time elastography for the staging of hepatic fibrosis: a meta-analysis. PLoS ONE 2014; 9(12):e115702
[91] Wu T, Ren J, Cong SZ et al. Accuracy of real-time tissue elastography for the evaluation of hepatic fibrosis in patients with chronic hepatitis B: a prospective multicenter study. Dig Dis 2014; 32(6):791–799
[92] Fujimoto K, Kato M, Kudo M et al. Novel image analysis method using ultrasound elastography for noninvasive evaluation of hepatic fibrosis in patients with chronic hepatitis C. Oncology 2013; 84 Suppl 1:3–12
[93] Ochi H, Hirooka M, Koizumi Y et al. Real-time tissue elastography for evaluation of hepatic fibrosis and portal hypertension in nonalcoholic fatty liver diseases. Hepatology 2012; 56(4):1271–1278
[94] Berzigotti A. Getting closer to a point-of-care diagnostic assessment in patients with chronic liver disease: controlled attenuation parameter for steatosis. J Hepatol 2014; 60(5):910–912
[95] Sasso M, Beaugrand M, de Ledinghen V et al. Controlled attenuation parameter (CAP): a novel VCTE™ guided ultrasonic attenuation measurement for the evaluation of hepatic steatosis: preliminary study and validation in a cohort of patients with chronic liver disease from various causes. Ultrasound Med Biol 2010; 36(11):1825–1835
[96] Kleiner DE, Brunt EM, Van Natta M et al. Nonalcoholic Steatohepatitis Clinical Research Network. Design and validation of a histological scoring system for nonalcoholic fatty liver disease. Hepatology 2005; 41(6):1313–1321
[97] Brunt EM, Janney CG, Di Bisceglie AM, Neuschwander-Tetri BA, Bacon BR. Nonalcoholic steatohepatitis: a proposal for grading and staging the histological lesions. Am J Gastroenterol 1999; 94(9):2467–2474
[98] Myers RP, Pollett A, Kirsch R et al. Controlled Attenuation Parameter (CAP): a noninvasive method for the detection of hepatic steatosis based on transient elastography. Liver Int 2012; 32(6):902–910

[99] de Lédinghen V, Vergniol J, Foucher J, Merrouche W, le Bail B. Non-invasive diagnosis of liver steatosis using controlled attenuation parameter (CAP) and transient elastography. Liver Int 2012; 32(6):911–918
[100] Sasso M, Tengher-Barna I, Ziol M et al. Novel controlled attenuation parameter for noninvasive assessment of steatosis using Fibroscan(®): validation in chronic hepatitis C. J Viral Hepat 2012; 19(4):244–253
[101] Ferraioli G, Tinelli C, Lissandrin R et al. Controlled attenuation parameter for evaluating liver steatosis in chronic viral hepatitis. World J Gastroenterol 2014; 20(21):6626–6631
[102] de Lédinghen V, Vergniol J, Capdepont M et al. Controlled attenuation parameter (CAP) for the diagnosis of steatosis: a prospective study of 5323 examinations. J Hepatol 2014; 60(5):1026–1031
[103] Kumar M, Rastogi A, Singh T et al. Controlled attenuation parameter for non-invasive assessment of hepatic steatosis: does etiology affect performance? J Gastroenterol Hepatol 2013; 28(7):1194–1201
[104] Ferraioli G, Tinelli C, Lissandrin R et al. Interobserver reproducibility of the controlled attenuation parameter (CAP) for quantifying liver steatosis. Hepatol Int 2014; 8(4):576–581
[105] Carvalhana S, Leitão J, Alves AC, Bourbon M, Cortez-Pinto H. How good is controlled attenuation parameter and fatty liver index for assessing liver steatosis in general population: correlation with ultrasound. Liver Int 2014; 34(6):e111–e117
[106] Ferraioli G, Tinelli C, Lissandrin R et al. Liver Steatosis Study Group. Correlation of the controlled attenuation parameter with indices of liver steatosis in overweight or obese individuals: a pilot study. Eur J Gastroenterol Hepatol 2015; 27(3):305–312

4 Elastography for Focal Liver Disease

Stephanie R. Wilson

4.1 Introduction

Characterizing focal liver masses comprises a significant component of health care costs with substantial impact on patient management both in health and disease. Metastatic liver cancers are the most frequently encountered malignant liver tumors, and patients with common primary cancers of the lung, breast, and colon are at such risk for development of these tumors that frequent surveillance of the liver is standard care in the period following detection and treatment of one of these primary lesions. Primary liver cancer is the fifth most common cancer in the world,[1] and its detection and management place a large demand on imaging, as imaging surveillance of high-risk populations allows for improved detection of lesions while they are still at a small size and amenable to treatment. Added to this concern for the detection of possible malignant liver tumors, however, is the recognition that benign liver tumors and tumorlike liver conditions are also frequent. Although these benign lesions may have typical features on baseline ultrasound, their confident diagnosis is often required to ensure that they are not mistaken for a significant malignant lesion and also to be certain that a significant malignant lesion is not erroneously overlooked. Therefore, many masses incidentally detected on ultrasound are studied further with contrast-enhanced cross-sectional imaging, including magnetic resonance imaging, computed tomography, or ultrasound.

4.2 Noninvasive Diagnosis of Focal Liver Masses

Historically, liver masses were diagnosed by either their surgical excision or biopsy. In the last four decades, however, there has been a progressive trend away from such invasive procedures. We now live in an era of noninvasive liver mass diagnosis. This has been accomplished largely on the basis of information acquired with the use of contrast-agent imaging on computed tomography (CT), magnetic resonance imaging (MRI),[2] and more recently ultrasound (US).[3] This works exceedingly well and, today, only a minority of liver masses are subjected to biopsy to establish their diagnosis.

The noninvasive evaluation of liver masses is important, as benign and insignificant masses are frequently encountered. Hemangioma, the most common benign liver tumor, for example, is present in as many as 20% of patients on autopsy studies.[4,5] They are frequently identified in this era of cross-sectional imaging, where they are often discovered as an incidental finding on CT, MRI, or US examinations performed for unrelated reasons. Noninvasive confirmation of their benign nature allows them to be removed from consideration for clinical management and avoids unnecessary painful biopsy and anxiety.

4.3 Elastography for Liver Mass Diagnosis

Elastography, or elasticity imaging, is a newer noninvasive imaging technology that measures the natural tendency of tissue to resume its original size and shape after being subjected to a deforming force or stress.[6,7] The provision of these stiffness measurements is established as a method of assessing diffuse liver disease, for the determination of the degree of fibrosis through its progression to cirrhosis. It is also established as a method for differentiating hard malignant breast tumors from those that are softer and more likely to be benign. It is known that tumors are generally many times stiffer than their surrounding tissue regardless of their organ of origin, making their response to deformation much different. Therefore, when a mechanical compression or vibration is applied, the tumor deforms less than the surrounding tissue. However, if one compares a cirrhotic liver, which is stiffer than a normal liver, with a tumor, the difference in the stiffness may vary. A tumor that might be hard relative to a normal liver may, in fact, be soft relative to a liver with cirrhosis. Here, we address the application of elastography to the diagnosis of focal liver masses in any liver and the differentiation of those that are malignant from those that are benign.

Numerous approaches to elastography have been described in the literature but three in particular, point shear wave elastography (p-SWE), two-dimensional shear wave elastography (2D-SWE), and strain elastography (SE), are considered best for this application. These different types of elastography are applied differently and their tissue response varies although a similar scientific foundation is common to all.

4.3.1 Shear Wave Elastography

Transient Elastography

Transient elastography (TE), marketed as FibroScan (Echosens, Aix-en-Provence, France), is performed with an ultrasound transducer at the end of a vibrating piston, which produces a vibration of low amplitude and frequency. The transducer is placed blindly (as there is no visual confirmation of the location of the measurement) on the skin surface and the shear wave produced is transmitted through the skin and into the liver up to a depth of about 6 cm. The velocity of the returning pulse is proportional to the tissue stiffness with higher velocities suggestive of stiffer tissue. This blind propagation of a pulse is seemingly suitable for the evaluation of an entire large organ, such as the liver, and may also show stiffness measurements for palpable masses, such as those encountered in the breast. A liver mass, however, is generally not palpable as it is deep to the costal margin, making TE unacceptable for this application.

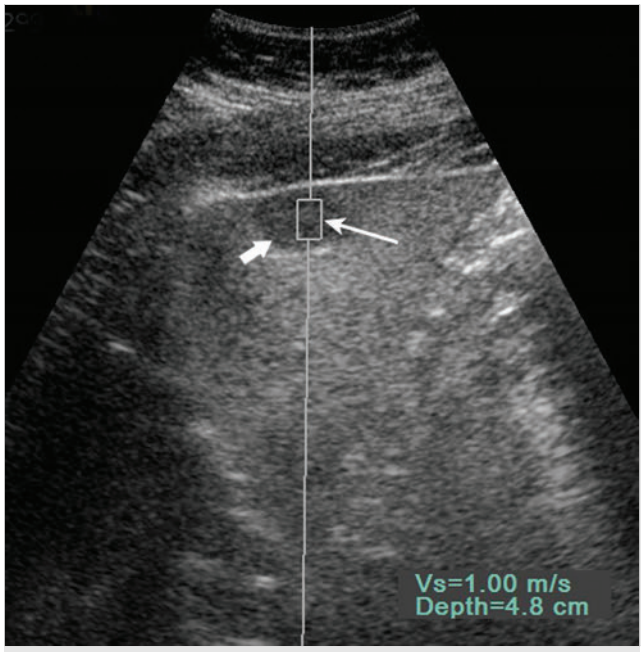

Fig. 4.1 Acoustic radiation force impulse (ARFI) technique for shear wave elastography (SWE). Measurement of velocity of shear wave within the ROI (*long arrow*) of a hypoechoic focal liver mass (*short arrow*) with underlying fatty liver of a 29-year-old woman. This mass is confirmed as a hemangioma on following contrast-enhanced ultrasound. V_s = velocity of shear wave. Depth indicates the distance from the skin to the center of the ROI.

Point Shear Wave Elastography

Point shear wave elastography utilizes acoustic radiation force impulses (ARFI), a newer US elastography technique recently introduced within a conventional ultrasonsograhic device (Acuson S2000, Siemens Medical Solutions, Mountain View, CA) and more recently also on the Philips EPIQ (Philips, Bothel WA). It differs from TE, which applies a pressure manually to the surface of the organ to induce an elastic shear wave. In ARFI, an acoustic radiation pulse is generated in the area of interest by the probe during the real-time B-mode imaging. As with TE, higher shear wave speeds are representative of stiffer tissue. ARFI uses high-energy focused acoustic pulses of short duration (< 1 ms) to excite the tissue in the region of interest, and these pulses displace soft tissue between 1 and 20 µm. These displacements result in shear wave propagation away from the region of excitation, which travel perpendicular to the acoustic push pulse and are detected by using US tracking beams. The speed of the shear waves propagated are measured as a velocity, in meters per second, and the display shows the fixed region of interest and its placement within the tissue under study in grayscale (▶ Fig. 4.1). The measurements, in meters per second, are obtained by placing a region of interest (ROI) box of fixed size within the tissue under direct guidance (▶ Fig. 4.2).

Two-Dimensional Shear Wave Elastography

Two-dimensional shear wave elastography (Aixplorer, Supersonic Imagine, Aix-en-Provence, France) is another advanced elastography system which performs elastography under direct visualization, also using ARFI to generate the pulse, but showing the velocity of shear waves as they are propagated through tissue and producing a color-coded shear wave map in which regions of interest may be placed after the image is frozen (▶ Fig. 4.3). Different colors relate to different tissue stiffnesses, similar to a scale range in color Doppler, and this is helpful to guide placement within the color box of a region of interest box, which can also be manipulated in size. SWE also has a scale, much like a Doppler scale, which can be adjusted up or down to aid in the identification of the stiffer regions within the color box. SWE is measured in meters per second or kilopascals.

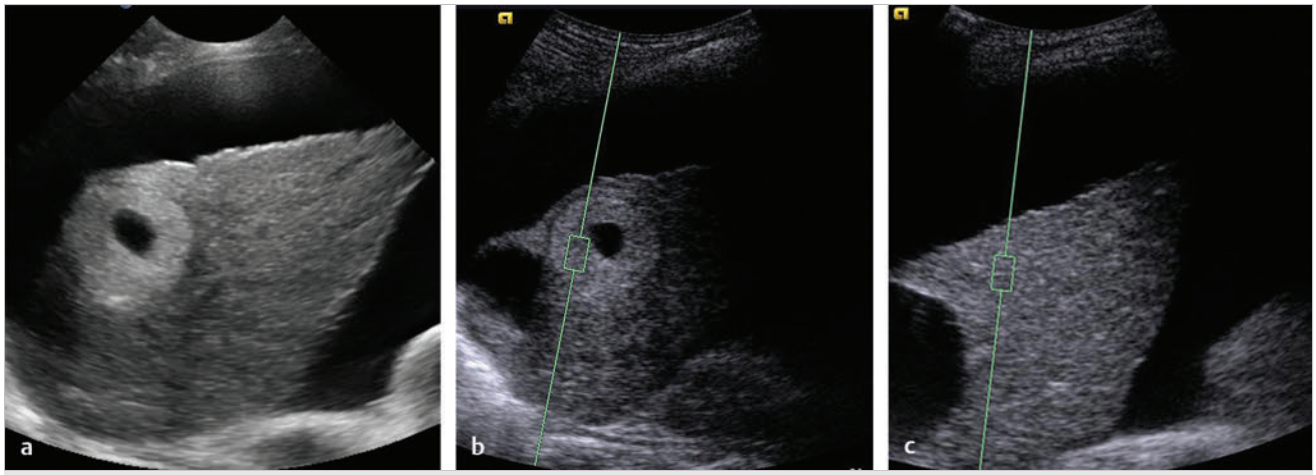

Fig. 4.2 Point shear wave elastography of the liver and a focal liver mass. The patient is a 41-year-old male with hepatitis B virus–related cirrhosis and a known renal cell carcinoma of the kidney. (**a**) Baseline ultrasound shows a cirrhotic liver and ascites. An unusual mass shows a highly echogenic rim and a necrotic or cystic center. (**b**) shows an ARFI measurement from the solid rim, V_s 1.09 m/s. (**c**)The measurement at a similar depth in the liver shows an abnormally high result, consistent with the known cirrhosis. The mass is softer than the cirrhotic liver. The mass is a biopsy proven hepatocellular carcinoma.

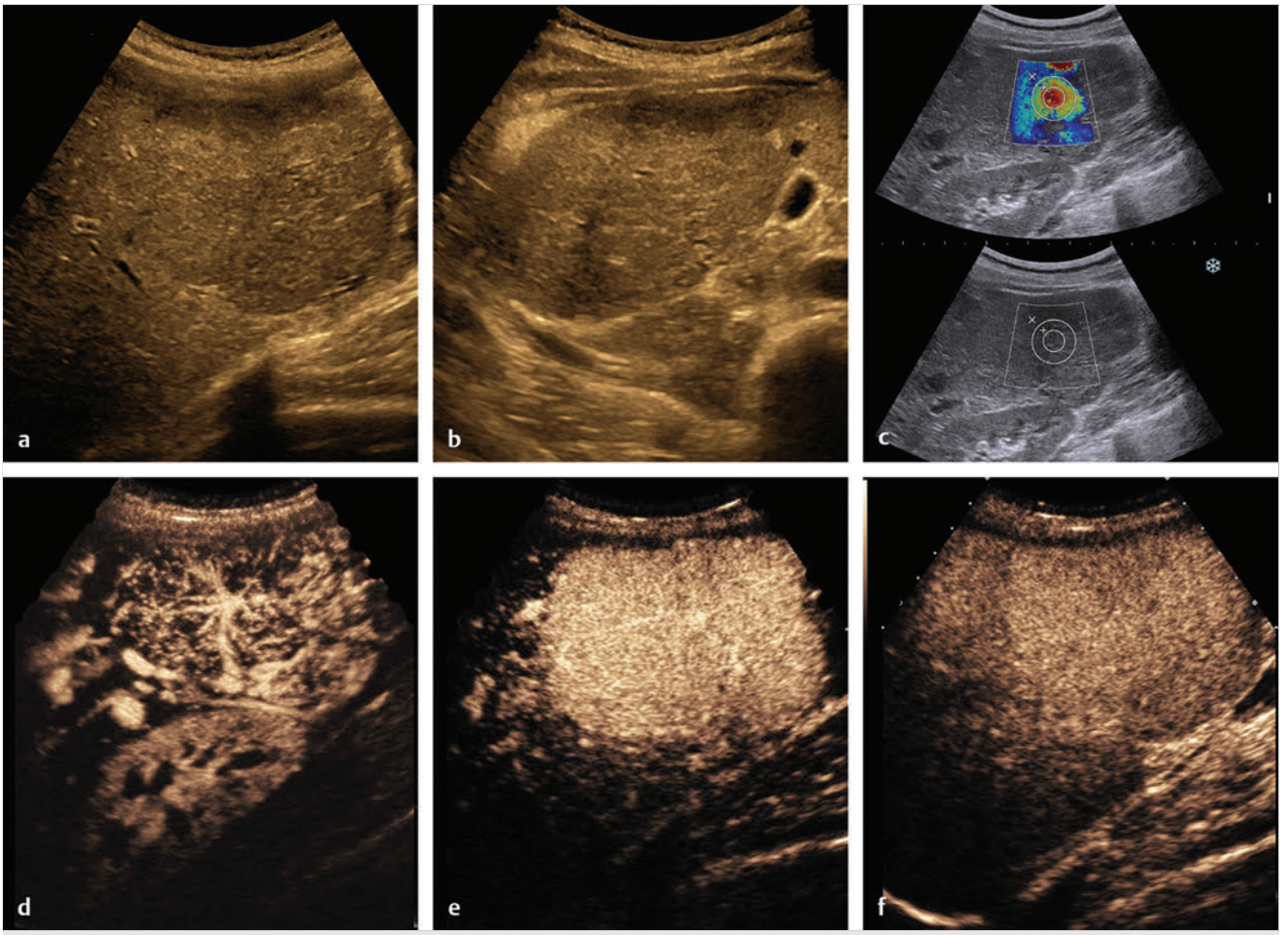

Fig. 4.3 Two-dimensional shear wave elastography and contrast enhanced ultrasound (CEUS)of a focal liver mass. Patient is an asymptomatic young woman with incidental discovery of a bulbous expansive mass in the tip of the right lobe, shown in long axis (**a**) and cross-sectional (**b**) images. (**c**) shows a elastogram from the central portion of the mass where there is a red signal suggesting stiff tissue and likely a scar. (**d**, **e**, **f**) are images from CEUS that show classic features of focal nodular hyperplasia. (**d**) is a MIP (maximum intensity projection) image in the arterial phase showing stellate vascularity. (**e**) At the peak of AP (arterial phase) enhancement, there is uniform hypervascularity. (**f**) A delayed image at 5 minutes shows that the mass has sustained enhancement.

4.3.2 Strain Elastography

Strain elastography (SE) describes a technique whereby an external compression is applied on a tissue and the US images are compared prior to and following the compression. Areas with the least deformation are the stiffest whereas softer tissues show the greatest deformation. This technique is limited in applications related to the liver as the external compression is difficult to apply to an organ deep to the costal margin. Creative investigators, however, have utilized the changes that occur with such maneuvers as normal or exaggerated breathing and changes secondary to cardiac pulsations as sources of compression (▶ Fig. 4.4). Strain elastography is also subjective and does not provide objective measures of tissue stiffness. Further, it only provides relative information about the stiffness of two tissues within the field of view (▶ Fig. 4.5).

4.3.3 Summary

Obviously, only p-SWE and 2D-SWE can directly visualize a focal liver mass to ensure appropriate localization for adequate stiffness calculation. Both have the added positive benefit of performing a standard full liver ultrasound (US) evaluation at the time of the liver mass stiffness determination. Thus, elastography may become a component of a thorough liver US evaluation, which also includes grayscale B-mode imaging and color Doppler. Reproducibility of elastography measurements for focal liver masses is generally possible as long as the masses are well shown on routine US and in a suitable position for interrogation. However, suspending respiration is also required, and, although the time is a brief 3 seconds, this is not possible for some patients.

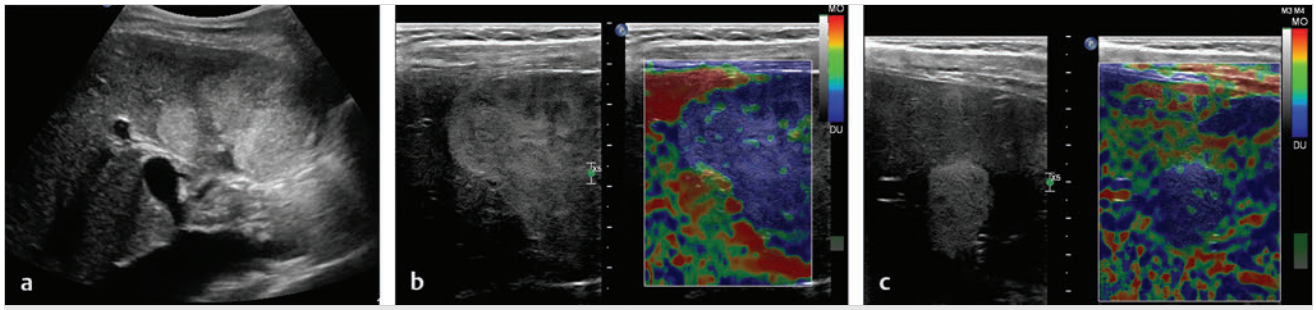

Fig. 4.4 Strain elastography (SE) of a focal liver mass. (**a**) A baseline axial grayscale sonogram on a young asymptomatic woman shows two focal echogenic masses within a normal-looking liver. (**b**) SE is performed of the largest mass while watching the liver during normal quiet respiration. The large mass appears blue (stiff) relative to the softer liver (red/green). (**c**) Similarly the smaller echogenic mass is blue within the surrounding softer red/green liver. These are proven hemangiomata on contrast-enhanced ultrasound imaging.

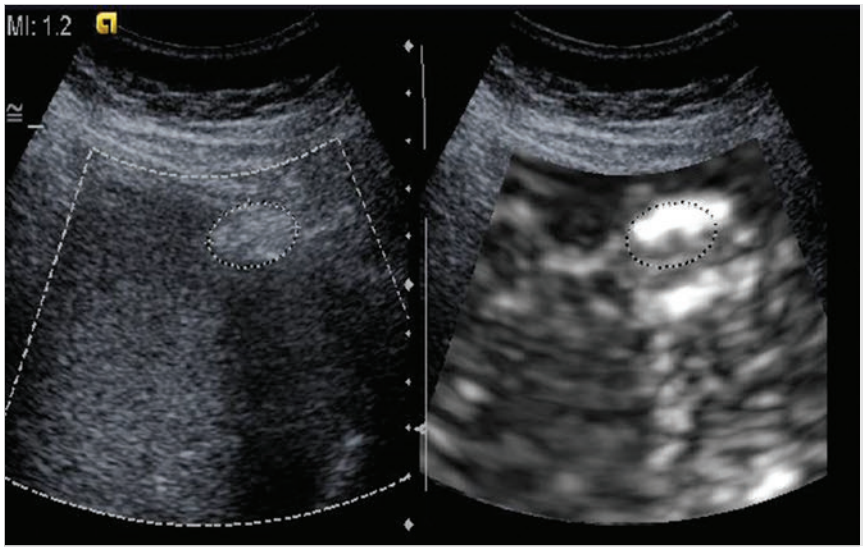

Fig. 4.5 Strain elastography of a focal liver mass displayed in black and white. As this technique shows only stiffness of the mass relative to that of the liver, a black and white display is optimal, as there is no absolute value shown. This mass is a soft fatty deposit within a stiffer liver.

4.4 Value of Elastography in the Evaluation of Focal Liver Disease: What is the Evidence?

Although excellent publications on the use of elastography in the evaluation of diffuse liver disease are now numerous, the publications on its use in evaluation of focal liver disease remain small, and the worldwide consensus opinion on its use for this purpose is undetermined at this time. Choi et al[8] evaluated tumor stiffness with ARFI in 51 patients with 60 focal hepatic lesions, which included 17 hemangiomas, 25 hepatocellular carcinomas (HCCs), 15 metastases and 3 cholangiocarcinomas. The lesions were classified into three groups: group I consisted of metastatic liver tumors and cholangiocarcinomas; group II consisted of HCCs; and group III consisted of hemangiomas. There were no statistical differences among the three groups in terms of tumor stiffness as seen on ARFI-based shear wave elastography images ($p > 0.05$). Although they conclude that by measuring shear wave speed, quantification of stiffness was made possible and showed the potential to differentiate malignant hepatic tumors from hepatic hemangiomas, clearly in their study, there was a big overlap between the groups and in practical terms it is not obvious how the differentiation of a hemangioma from a malignant hepatic tumor is really possible.

Improved boundary definition of tumors with ARFI-generated SWE techniques is also described by Choi et al[8] and also by Fahey et al.[9] These latter investigators describe, in a very small group of patients with abdominal malignancies undergoing US-guided biopsy, including only 7 livers, the mean contrast for suspected HCCs in B-mode images was 2.9 dB (range: 1.5–4.2) versus 7.5 dB (range: 3.1–11.9) in ARFI images, with all HCCs appearing more compliant than regional cirrhotic liver parenchyma. The mean contrast for metastases in B-mode images was 3.1 dB (range: 1.2–5.2) versus 9.3 dB (range: 5.7–13.9) in ARFI images, with all masses appearing less compliant than regional noncirrhotic liver parenchyma. In simplified terms, their small study showed that the metastases were the hardest tissue, the liver was in the middle, and the HCCs were relatively soft.

Prior to working with elastography for characterization of focal liver masses in our own facility, we hypothesized that malignant liver tumors would be hard and easily distinguishable from benign liver tumors, which we anticipated to be softer. However, in our own experience and that of others, this is not a clear case of easy differentiation. In our own published study of

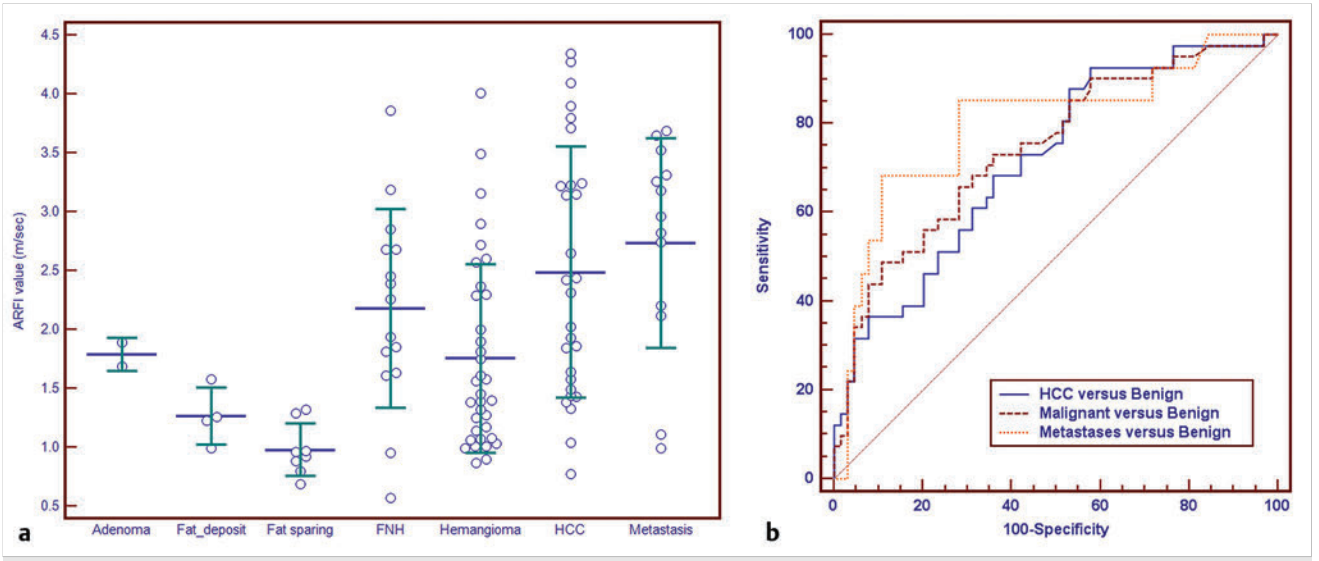

Fig. 4.6 **(a)** Scatterplots of ARFI values of all liver masses. The long horizontal bar is the mean value and the short horizontal bars enclose the standard deviation. (Reproduced with permission from Yu H, Wilson SR. New noninvasive ultrasound techniques: can they predict liver cirrhosis? Ultrasound Q;28:5–11.) (**b**) Comparison of receiver operating characteristic curves for ARFI values in differentiation of the malignant from the benign liver masses, the HCC from the benign liver masses, and the metastases from the benign tumors with the area under the curve 0.744, 0.720, and 0.796 respectively.

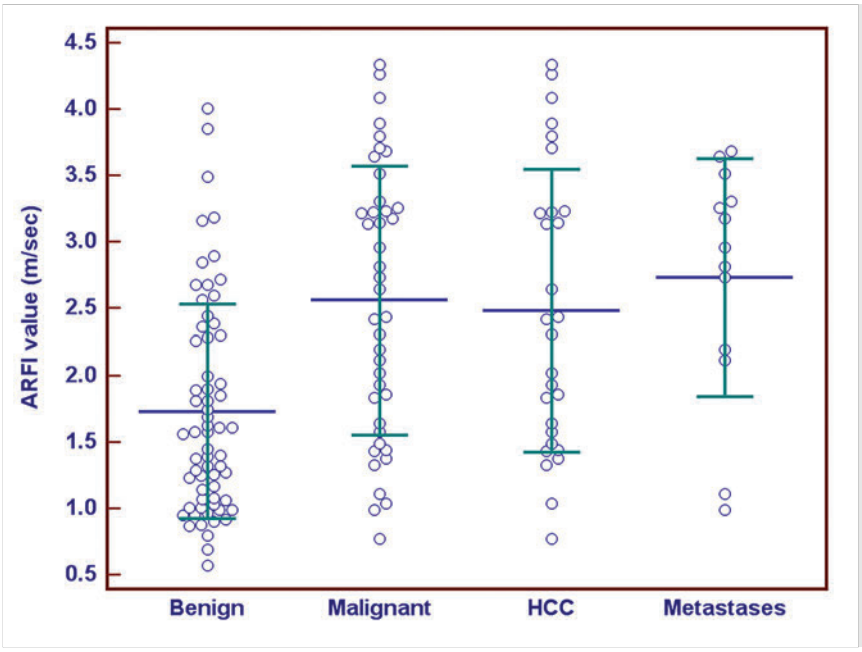

Fig. 4.7 Scatterplots of ARFI values for benign and malignant liver masses, hepatocellular carcinomas (HCCs), and metastases. Long horizontal bar shows mean value and two short horizontal bars show a standard deviation. (Reproduced with permission from Yu H, Wilson SR. New noninvasive ultrasound techniques: can they predict liver cirrhosis? Ultrasound Q;28:5-11.)

ARFI-generated SWE evaluation of 105 masses in 89 patients,[10] there were 28 HCCs, 13 metastases, 35 hemangiomata, 15 focal nodular hyperplasia (FNH), 8 focal fat sparing, 4 focal fat deposits, and 2 adenomas. Successful measurements of mass stiffness were possible in the overwhelming majority of tumors. Receiver operating characteristic (ROC) analysis was determined to pick the optimal cutoff value to show the accuracy of ARFI-generated SWE to separate benign from malignant liver tumors (▶ Fig. 4.6).

Although we did show a statistically significant different ARFI value for benign (1.73 m/sec, standard deviation [SD] 0.78 m/s) and malignant liver tumors (2.57 m/sec, SD 1.01 m/s), the area under the ROC curve was 0.744, suggesting only fair accuracy (54). For differentiation of malignant from benign masses, the sensitivity, specificity, positive predictive value (PPV), and negative predictive value (NPV) were 68% (28/41), 69% (44/64), 58% (28/48), and 77% (44/57), respectively, when 1.9 m/sec was chosen as a cutoff value, reflective of a wide variation of ARFI

values in each diagnosis. For differentiation of metastasis from benign masses, sensitivity, specificity, PPV, and NPV were 69% (9/13), 89% (57/64), 56% (9/16), and 93% (57/61), respectively, when 2.72 m/sec was chosen as a cutoff value. We concluded, therefore, that although ARFI measurements may be helpful to differentiate benign masses from metastases, in particular, ARFI measurements alone do not differentiate benign and malignant masses because of variations in stiffness of all types of masses (▶ Fig. 4.7).

Further, in our own experience, not only is there variation of stiffness measurements among masses with the same diagnosis, there may also be variation of stiffness measurements from within the margins of a single focal mass as well. Not surprisingly, this variability of stiffness determinations within a mass is more easily and frequently shown in large masses, as more ROIs may be reliably placed in a large space. Although this regional variation within a single mass was our impression in our original study,[10] this was not shown sufficiently well for inclusion in our data. The color map on 2D-SWE showing variations in stiffness throughout a mass is, perhaps, more compelling than the numeric values shown on the ARFI scan. For example, the central scar of a FNH will be stiffer than the remainder of the lesion (▶ Fig. 4.3) as will the central sclerosis of a hemangioma and the necrotic zone of a malignant tumor.

4.5 Conclusion

Our conclusions are supported by our personal interaction with our pathologists and our own experience. A small hemangioma, for example, classically is a soft and compressible tumor. However, as these tumors grow, they are susceptible to a variety of changes including thrombosis, sclerosis, hyalinization, calcification, and rare massive cystic degeneration, all of which may change the stiffness of the mass generally making the tumor feel harder.[11] Associated changes in the vascularity of these atypical tumors on CEUS or other imaging are also reflective of these degenerative changes often showing large nonenhanced tumor components which frequently provoke biopsy to obtain the correct diagnosis. These atypical hemangiomas often are not diagnosed with traditional contrast-enhanced imaging and require biopsy. Their atypical features will undoubtedly result in a wide variation in their elastography readings. Similarly, a hepatocellular carcinoma may undergo necrosis resulting in softer portions of a solid tumor, and the inevitable scars found in focal nodular hyperplasia may be tiny or large with different impact on the stiffness of the tumor.

Our results on elastographic characterization of focal liver masses, similar to that of others,[8,9,12] is seemingly different than experience in other organs, such as the breast, prostate,[13] and the pancreas,[14,15] where increasing stiffness seems to correlate strongly with malignant outcome. This great difference in the stiffness of multiple liver tumors with the same histology will undoubtedly be the focus of future research.

References

[1] Bosch FX, Ribes J, Díaz M, Cléries R. Primary liver cancer: worldwide incidence and trends. Gastroenterology 2004; 127(5) Suppl 1:S5–S16

[2] Oliva MR, Saini S. Liver cancer imaging: role of CT, MRI, US and PET. Cancer Imaging 2004; 4 (Spec No A):S42–S46

[3] Brannigan M, Burns PN, Wilson SR. Blood flow patterns in focal liver lesions at microbubble-enhanced US. Radiographics 2004; 24(4):921–935

[4] Ishak KG, Rabin L. Benign tumors of the liver. Med Clin North Am 1975; 59 (4):995–1013

[5] Gandolfi L, Leo P, Solmi L, Vitelli E, Verros G, Colecchia A. Natural history of hepatic haemangiomas: clinical and ultrasound study. Gut 1991; 32(6):677–680

[6] Ophir J, Céspedes I, Ponnekanti H, Yazdi Y, Li X. Elastography: a quantitative method for imaging the elasticity of biological tissues. Ultrason Imaging 1991; 13(2):111–134

[7] Palmeri ML, Wang MH, Dahl JJ, Frinkley KD, Nightingale KR. Quantifying hepatic shear modulus in vivo using acoustic radiation force. Ultrasound Med Biol 2008; 34(4):546–558

[8] Cho SH, Lee JY, Han JK, Choi BI. Acoustic radiation force impulse elastography for the evaluation of focal solid hepatic lesions: preliminary findings. Ultrasound Med Biol 2010; 36(2):202–208

[9] Fahey BJ, Nelson RC, Bradway DP, Hsu SJ, Dumont DM, Trahey GE. In vivo visualization of abdominal malignancies with acoustic radiation force elastography. Phys Med Biol 2008; 53(1):279–293

[10] Yu H, Wilson SR. New noninvasive ultrasound techniques: can they predict liver cirrhosis? Ultrasound Q 2012; 28(1):5–11

[11] Vilgrain V, Boulos L, Vullierme MP, Denys A, Terris B, Menu Y. Imaging of atypical hemangiomas of the liver with pathologic correlation. Radiographics 2000; 20(2):379–397

[12] Heide R, Strobel D, Bernatik T, Goertz RS. Characterization of focal liver lesions (FLL) with acoustic radiation force impulse (ARFI) elastometry. Ultraschall Med 2010; 31(4):405–409

[13] Ginat DT, Destounis SV, Barr RG, Castaneda B, Strang JG, Rubens DJ. US elastography of breast and prostate lesions. Radiographics 2009; 29(7):2007–2016

[14] Lee TH, Cha SW, Cho YD. EUS elastography: advances in diagnostic EUS of the pancreas. Korean J Radiol 2012; 13 Suppl 1:S12–S16

[15] Iglesias-Garcia J, Larino-Noia J, Abdulkader I, Forteza J, Dominguez-Munoz JE. EUS elastography for the characterization of solid pancreatic masses. Gastrointest Endosc 2009; 70(6):1101–1108

5 Elastography of the Breast

Richard G. Barr

5.1 Introduction

Ultrasound is routinely used to evaluate the breast both for screening and diagnostic studies. Initially ultrasound was used to determine if a lesion was cystic or solid,[1,2] but with the criteria described by Stavros,[3] ultrasound has come to play a more important role in breast lesion characterization. These criteria have been incorporated into the ultrasound Breast Imaging–Reporting and Data System (BI-RADS).[4]

Elastography is a relatively new ultrasound technique that can provide additional diagnostic information in breast pathology. Elastography, or elasticity imaging, provides images based on tissue stiffness, rather than anatomical structure. This information was not previously available other than qualitatively with clinical palpation. Physicians have used lesion stiffness based on palpation to help diagnose for thousands of years, realizing that stiff lesions were more likely malignancies.[5] Elastography has the potential to quantify the stiffness of a lesion, which was previously judged only subjectively by physical examination.[6,7,8] Krouskop[9] determined that in vivo there is significant elastographic contrast between cancerous and noncancerous breast lesions. This suggests that elastography could be an excellent technique for characterizing breast lesions as benign or malignant.

There are two types of elastography used to evaluate the breast. Strain elastography (SE) and shear wave elastography (SWE).[10] SE produces images based on the deformation of the tissue from a compression–release force applied externally from the transducer, acoustic radiation force impulse (ARFI), or from a patient source (breathing or heartbeat). SE allows a qualitative assessment of tissue stiffness compared to other tissues in the field of view (FOV). The exact stiffness of the tissue is not obtained with SE. SWE utilizes a special ARFI push pulse that results in the generation of shear waves. The shear wave speed (SWS) is estimated using B-mode to monitor the tissue displacement caused by the shear waves. The SWS is dependent on the tissue stiffness with slower speeds occurring in soft tissues and higher speed in stiffer tissues. The stiffness of the tissue can be displayed as either the shear wave speed (V_s) in meters per second (m/s) or converted to Young's modulus in kilopascals (kPa). Thus, with SWE, a quantitative estimate of stiffness is obtained. SWE can be performed either in a small region of interest (ROI) where one stiffness value is obtained (point shear wave elastography (p-SWE)) or over a wider FOV using color-coding to display the stiffness values (two-dimensional shear wave elastography ([2D-SWE]). A ROI can be placed within the FOV for 2D-SWE to obtain the stiffness value. Three-dimensional strain elastography (3D-SE) and three-dimensional shear wave elastography (3D-SWE) have recently become available for clinical use.

Initially introduced for clinical use in 2003,[11] elastography technology has since improved together with advances in diagnostic ultrasound systems. Some form of breast elastography is available on most commercially available ultrasound systems today. Current elastography systems can not only differentiate between benign and malignant tissue but also can evaluate histological information by depicting the distribution of tissue stiffness. Elastography allows for diagnosis and evaluation not only of masses but also nonmass lesions. It may have the potential to evaluate the therapeutic effect of treatment with anticancer agents. Continuing improvement in image quality, image acquisition technique, and image interpretation has occurred. This chapter discusses the state-of-the art use of elastography of the breast emphasizing the appropriate technique and interpretation needed to obtain consistent accurate results.

The breast has very unique elastic properties that are not seen in other organs. Breast cancers appear larger on elastography than on B-mode imaging, while benign lesions appear smaller.[10] This difference in size has a high predictive value in identifying cancers, using a ratio of elastographic length to B-mode length (the E/B ratio) of ≥ 1 as highly suspicious for a malignancy. Some breast cancers do not propagate shear waves as expected and so care must be taken to accurately assess the results to limit interpretation errors.[12]

Although current modalities of breast imaging, including MRI, ultrasound and mammography, have high sensitivities for detecting breast lesions, they do not have high specificities.[13,14] This has resulted in close monitoring or unnecessary biopsies of many benign lesions. An imaging modality with a high specificity for characterizing malignant lesions such as elastography could significantly decrease the amount of unnecessary biopsies.

In this chapter the principles of elastography are presented in a form easily understood by clinical sonographers and sonologists. A more detailed discussion of these principles can be found in Chapter 2. The techniques required to obtain optimal images with the various methods are discussed with an emphasis on avoiding pitfalls. The interpretation of images obtained using various techniques is discussed and how they relate to each other is explained. A review of the literature and references to other sources of information are provided.

5.2 Overview of Breast Elastography

Elastography should be performed in conjunction with conventional breast ultrasound. It is an additional imaging mode, like color Doppler, to evaluate a breast lesion or nonmass lesion. At this time, elastography cannot be used as a screening technique, but it is an excellent diagnostic technique to characterize a lesion as benign or malignant. Both SE and SWE are FDA approved for determining if a lesion is soft or stiff. Both SE and SWE have been shown to improve characterization of breast abnormalities.[10,12,15,16,17,18,19,20,21,22,23,24] The choice of which to use is a personal preference and is often influenced by experience or equipment availability. Both techniques, SE and SWE, can be performed on an abnormality within a few minutes and can increase confidence of the results if they are concordant. If the results are not concordant, it can be an alert that the lesion is atypical and additional evaluation may be necessary to further characterize it.

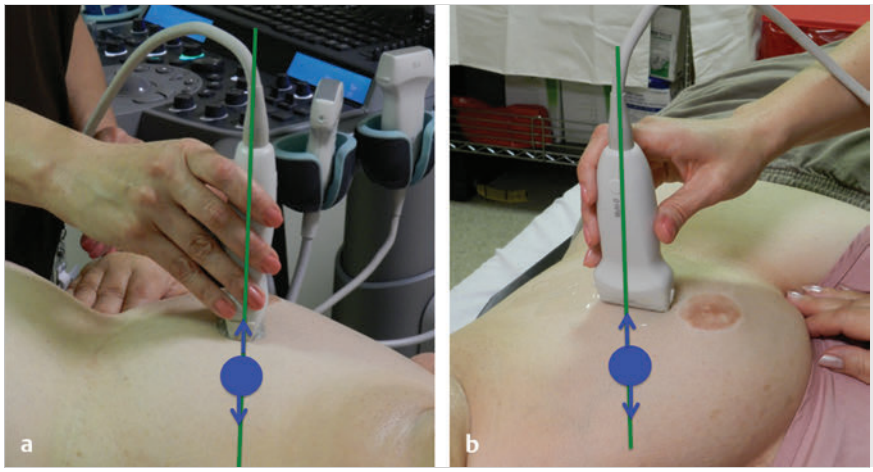

Fig. 5.1 (**a, b**) For optimal elastography results, the patient should be positioned so that the transducer is perpendicular to the table and the patient rolled so that the area of interest moves within the imaging plane during patient respiration. The green line corresponds to the imaging plane. The lesion (*blue circle*) should move within the imaging plane (*arrows*).

Elastography can also be helpful in characterizing isoechoic lesions. If a palpable lesion is not identified on B-mode imaging, the use of elastography can often identify the lesion based on its stiffness. It is not uncommon for it to be difficult to determine if an isoechoic lesion is truly an abnormality or a fat lobule.

It has been suggested that the main advantage of elastography could be improved characterization of BI-RADS category 3 and category 4A lesions. Elastography could be used to upgrade or downgrade these lesions by one BI-RADS score. As elastography continues to improve and more clinical experience is gained, a better understanding of how elastography could be included in the BI-RADS classification will be obtained. Guidelines have been recommended by several organizations.[25,26]

We have used elastography on all our diagnostic breast ultrasound cases for several years and as a research tool for 15 years. In our experience, we have significantly decreased our biopsy rate and significantly increased our positive biopsy rate. The bull's eye artifact has been extremely helpful in increasing confidence that a lesion is a benign complicated cyst and that short-term follow-up or biopsy is not required.[27] Correlation of elastography with pathology has added an additional check for adequacy of our image-guided biopsies.

There are many methods of displaying the elastographic data. Several color scales have been used. In this book we will use the convention of black is stiff and white is soft for SE and red is stiff and blue is soft for SWE. We use the color image in SWE because it depicts the quantitative value of the stiffness and therefore any lesion that is stiff enough to color-code, (i.e., that is above our cutoff value) is easy to identify. We use a grayscale image in SE because we believe we can identify the changes in relative stiffness more accurately than when we use a color image, in which a small change in relative stiffness may be depicted as an abrupt color change. We also believe we are able to measure a lesion more accurately on the elastogram using the grayscale.

5.3 Strain Elastography Imaging

5.3.1 Techniques

The technique of monitoring how a lesion changes shape when an external force is applied is SE. The external force can be patient movement, such as breathing and heartbeat, from ARFI, or from external compression with rhythmic motion of the transducer.[10] In SE the absolute strain value (stiffness) cannot be calculated because the amount of the displacement force cannot be accurately measured. The real-time elasticity image, with a scale based on the relative strain of the tissues in the image, illustrates the strain distribution, indicating the relative stiffness of the tissues. The clinical implications of this are discussed in detail 5.3.8 Interpretation of Results.

An ultrasound pulse (a push pulse) tailored for energy transfer can be used as the source of the displacement. This technique is called acoustic radiation force impulse (ARFI).[28,29] Using ARFI and analyzing the displacement shape changes, a strain image can be obtained. Note that this is different than shear wave imaging where the shear wave speed generated from the pulse is measured.[10]

SE of the breast is performed with a conventional ultrasound unit and standard ultrasound breast transducer. Specific software analysis of frame-to-frame difference in deformation in tissue with mild compression allows for the display of the "softness" or "stiffness" of a lesion.

The technique required to obtain the optimal images varies with the type of elasticity imaging being used as well as the manufacturer of the system. With some manufacturer's systems, very little if any manual compression is needed; with others, a rhythmic compression–release cycle is required. With experience and practice, one can optimize the compression used to obtain optimal image quality.

The algorithm used in compression elastography requires the strain changes to remain within the imaging plane. The same slice of the lesion needs to remain in the imaging plane during the compression–release cycle. Monitoring of the B-mode image to confirm the same slice of the lesion is only displaced in depth during scanning and otherwise is unmoving in the FOV will allow for optimal images. To avoid having the lesion move in and out of the imaging plane, positioning the patient so that an imaginary line through the transducer and lesion is perpendicular to the floor, with patient breathing moving the lesion in the same plane, is helpful (▶ Fig. 5.1). The transducer should not be angled either superiorly or inferiorly or to the right or left (▶ Fig. 5.2). Using SE one cannot be surveying the breast; scanning must be done in one stationary position.

In most systems a dual display is utilized, one with the B-mode image and the other with the elastographic data. The elastographic data can be superimposed over a B-mode image.

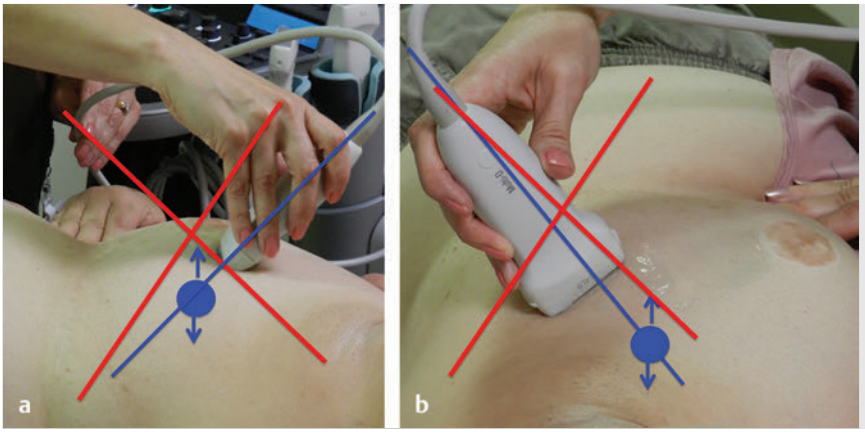

Fig. 5.2 Suboptimal elastography results will be obtained if the transducer is angled. (**a**) The blue line corresponds to the imaging plane. The lesion (*blue circle*) is moving in and out of the imaging plane because the transducer is angled superiorly (angling inferiorly would also be suboptimal). (**b**) The blue line corresponds to the imaging plane. The lesion (*blue circle*) is moving in and out of the imaging plane because the transducer is angled to the left (angling to the right would also be suboptimal).

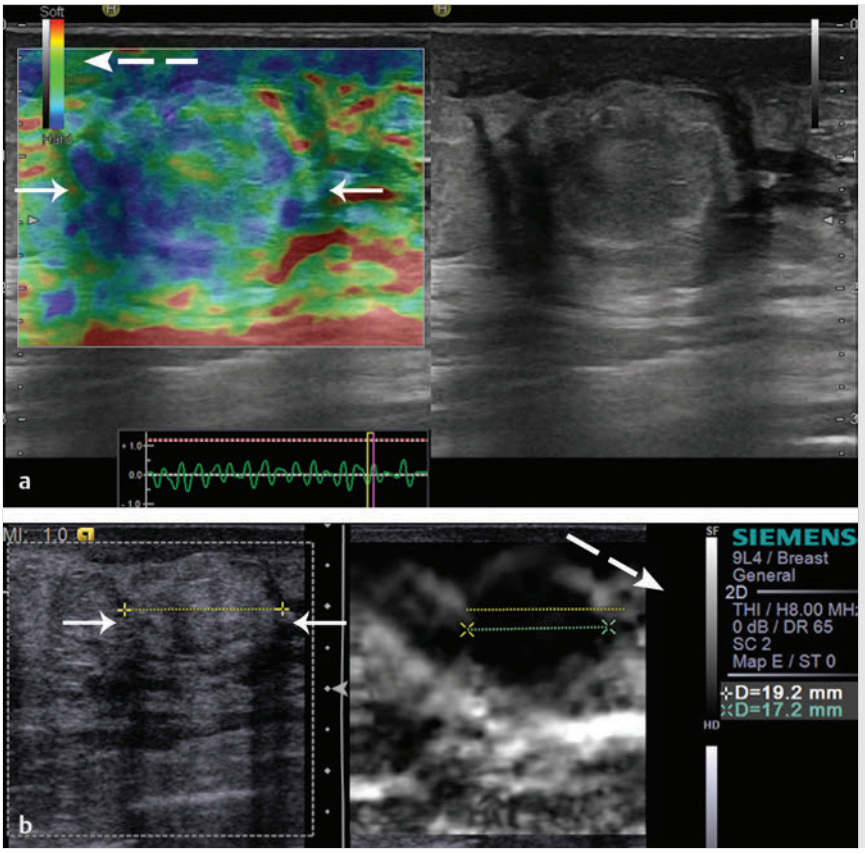

Fig. 5.3 Strain elastography results can be displayed (**a**) using a color-coded display superimposed on a background grayscale B-mode image or (**b**) using a grayscale display without the background grayscale B-mode image. The solid white arrows indicate the lesion and the dash white arrows indicate the display scale, which notes the color that represents soft and the color that represents hard.

In this case, the B-mode image is usually displayed in grayscale and the elastogram in a color (▶ Fig. 5.3). If a grayscale is used, it should not be superimposed on the B-mode image, as the use of two superimposed grayscale maps in one image interferes with interpretation. Preference of maps is often determined by the user's exposure to elastography and interpretation. If color maps are used, be careful to document which color scale you are using, as some have red as stiff and others blue as stiff. The color scale should always be included with the image for accurate interpretation.

5.3.2 Performing an Examination

Strain images are generated from the raw data of B-mode images. Therefore it is important to obtain quality B-mode images before activating the strain mode. It is important to maintain the transducer perpendicular to the skin. Find a scanning window that allows for stable positioning of the transducer with the compression–release cycle.[10] Placing the palm of the hand on the patient helps stabilize the transducer and allows for more sensitive movements (▶ Fig. 5.4).

Better quality elastograms can be obtained if the patient raises the ipsilateral hand above their head; the patient is positioned so the transducer is perpendicular to the floor; motion with respiration moves the lesion within the imaging plane; and the patient refrains from talking during the data acquisition.

Because SE is a relative technique comparing the stiffness values of the tissues within the field of view (FOV), a lesion may appear a different shade of gray (or color) depending on the

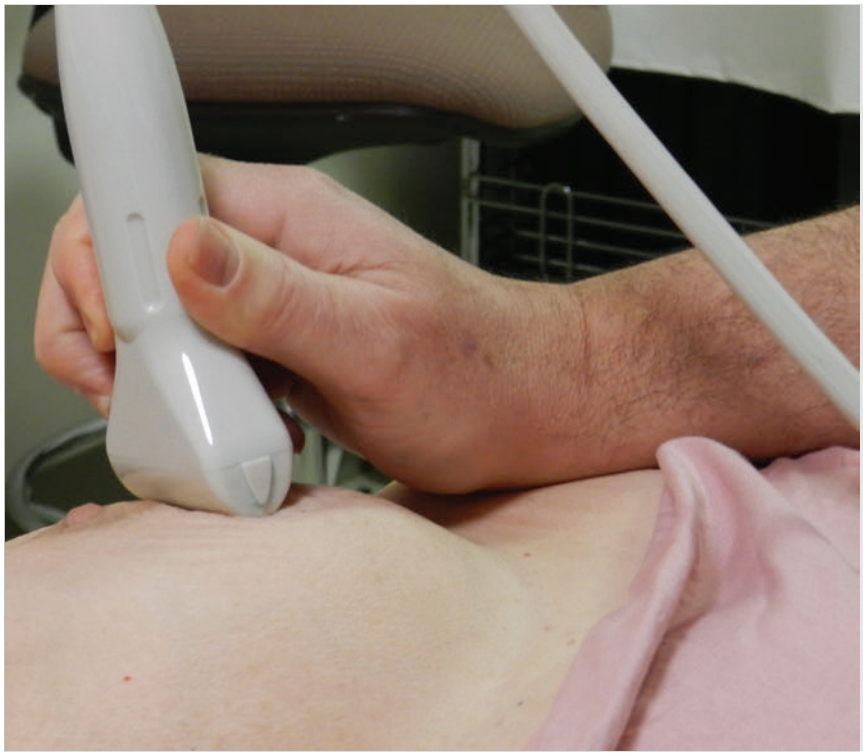

Fig. 5.4 If the sonologist places his or her palm on the patient, it stabilizes the transducer and allows fine control of compression–release by movement of the fingers.

other tissues in the FOV. If only one tissue type is present in the FOV, then the dynamic range of stiffness will be very small. For example if only fat is present in the FOV, some of the fat will code as stiff because it is the stiffest tissue in the FOV even though it is a very soft tissue (▶ Fig. 5.5).

This dynamic range variability of the SE scale can cause difficulty in interpretation. By including some fat, normal dense breast tissue, pectoralis muscle, and the lesion in the elastogram FOV, one can minimize these changes between images. Having a soft tissue (fat) and a harder tissue (muscle) helps maintain a similar dynamic range of grayscale or color display. A large FOV is helpful in image interpretation because including more tissue of differing stiffness will allow for a scale that allows for better differentiation between tissues.

The appropriate amount of compression–release for the system used is critical in obtaining diagnostic elastograms. The presently available systems vary in the amount of compression needed from no manual compression to moderate compression. The amount of compression may vary with the size of the breast or the depth of the lesion. With experience and practice, the compression–release needed for optimal elastogram quality for a given system can be learned. The B-mode image is useful to monitor the amount of tissue displacement.

5.3.3 No-Manual-Compression Systems

Place the probe on the area of interest without consciously applying any vibration/compression. Keep the probe lightly touching the skin and try not to apply pressure. It is important to keep your hands perpendicular with no pressure (minimal precompression) and still on the skin above the area of concern. A technique to confirm that minimal compression has been used has been described in the literature[30] and is detailed section 5.3.4. Usually mild compression is used to obtain B-mode images as it decreases refractive artifacts.

In these no-manual-compression systems the compression–release cycle results from vibration caused by involuntary muscle movements of the sonographer's hand and motion caused by the breathing and heartbeat of the patient. However, in some cases (in patients with large breasts or deep lesions), minimal additional vibration may be required. In patients with small breasts, the motion may still be too great and having the patient hold his or her breath may be helpful.

5.3.4 Minimal- and Moderate-Compression/Vibration Systems

Place the probe on the area of interest and apply very mild rhythmic vibration or compression/decompression making sure not to compress the breast with the transducer (do not apply precompression). Find the "sweet spot" for the ultrasound system and lesion depth by varying the degree and frequency of compression. The amount of compression needed may be between less than 1 mm to 2-3 mm.

Some manufactures have a display bar or number which can help you confirm you are applying the appropriate amount of displacement (compression–release) to generate the elastogram (▶ Fig. 5.6). Some provide a visual scale on the frequency and amount of displacement you are generating. This real-time feedback bar only evaluates the amount of lesion displacement (tissue deformation relative to the lesion). Other factors are important in obtaining optimal images, and so a high quality factor does not mean you will have optimal images.

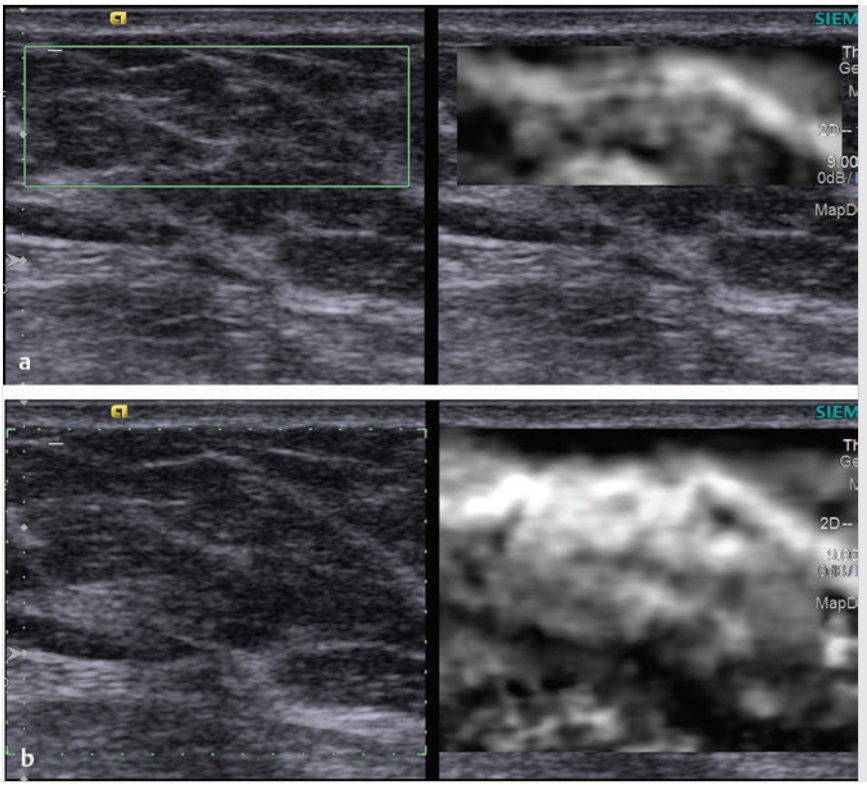

Fig. 5.5 In this elastogram (**a**), the FOV is only fat, which is soft. However, because the stiffness scale in SE is relative, some fat reads as soft (white) while other fat reads as stiff (black). The range of stiffness in the scale is very small. In (**b**), the FOV has been increased to include pectoral muscle. The range of stiffness has been adjusted so that the pectoral muscle is displayed as black and all the fat is displayed as white.

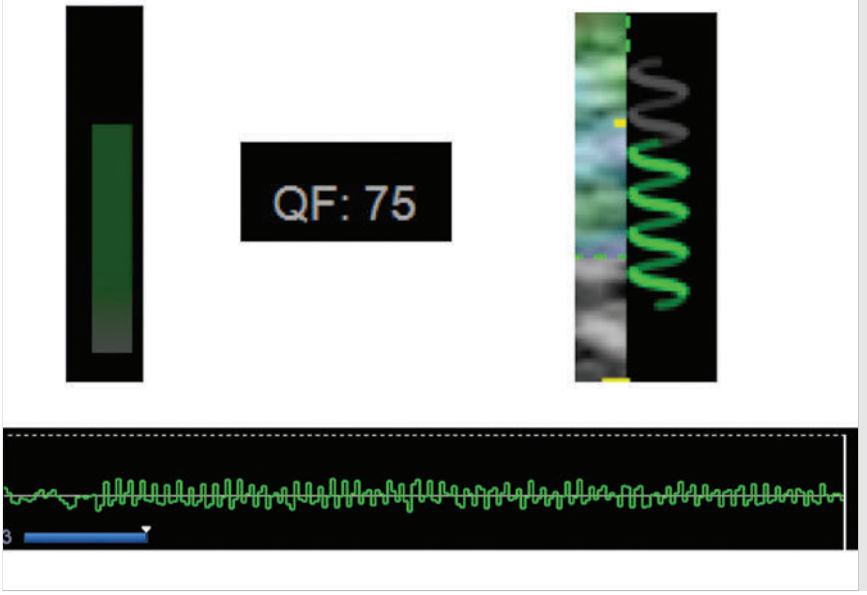

Fig. 5.6 In all systems a compression bar, quality measure, or movement map is provided to guide the sonologist to the appropriate frequency and amount of displacement for the compression–release cycle for that system. Several examples are provided here.

A critical factor in generating a diagnostic elastogram is the amount of pressure you apply with the transducer when scanning. This is called precompression (▶ Fig. 5.7). This is different than the amount of displacement you are generating. If you scan with a "heavy hand," the tissues are compressed and their elastic properties are changed. This precompression markedly changes the image quality and can significantly affect results (▶ Fig. 5.8). This is confirmed with shear wave technology where the shear wave speed can change by a factor of 10 based on precompression. In ▶ Fig. 5.9 we graph the effects of precompression for various tissues. Note that as precompression increases, the differences in shear wave speed between tissue types decreases, leading to less conspicuity between tissues. If enough precompression is applied, all tissues are similar in stiffness and the elastogram is mostly noise.

Generally some precompression is used when obtaining B-mode images as this decreases artifacts. A technique has been demonstrated to allow for consistent application of minimal.[30]

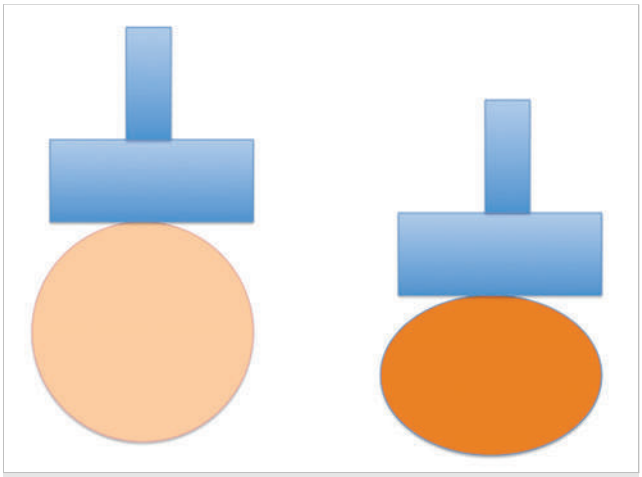

Fig. 5.7 A pictorial diagram demonstrating precompression. The image on the right depicts the breast when precompression is applied; the image on the left depicts the breast when minimal precompression is applied. The addition of precompression makes all tissues stiffer and affects elastography results.

Identify an object in the far field of the image such as a rib. Lift the transducer from the skin. The object will be displaced deeper in the image. When the object is as far in the deep field as possible and there is still adequate contact with the skin for imaging, the elastographic images are obtained. Use of adequate coupling gel is very helpful. This technique has been shown to be highly reproducible both intraoperator and interoperator. This is a similar technique to that used for color Doppler imaging, as precompression can occlude blood vessels. It should be noted that the "quality factor" or "compression bar" used in some manufacturers' equipment to assess adequacy of the amount of displacement does not assess the amount of precompression being applied.

The center of the lesion does not have to be used to obtain the elastogram. In fact it is better if a lesion position is chosen where the lesion measures between 1 and 1.5 cm. This allows for other tissues to be included in the field of view and account for size changes that occur in cancers in elastography. The size changes are discussed in detail in 5.3.8 Interpretation of Results.

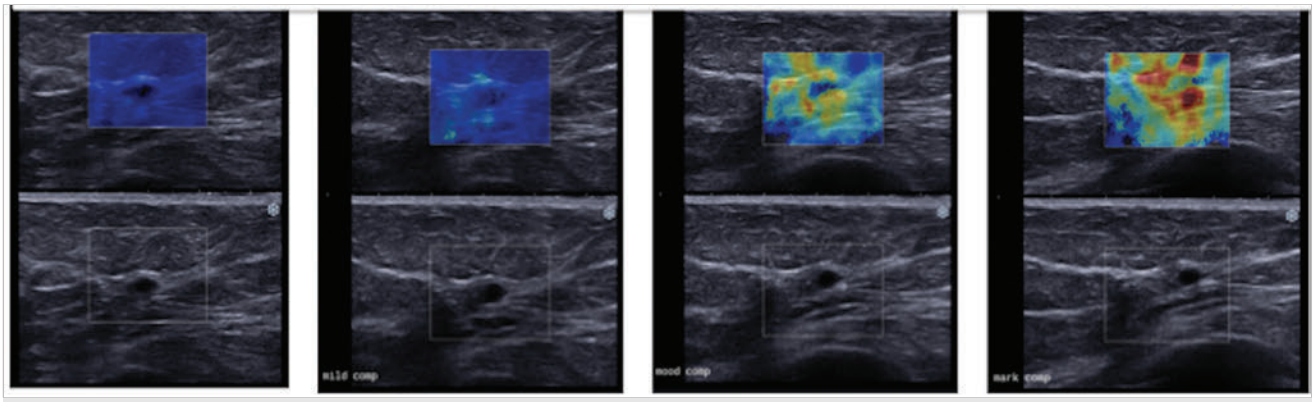

Fig. 5.8 Effect of precompression as seen in this set of images of a benign cyst. No precompression is applied in the image on the left. This color-coding is accurate. Increasing precompression is applied moving to the right. Note the color-coding changes. With enough precompression, the benign cyst has color-coding suggestive of a malignant lesion.

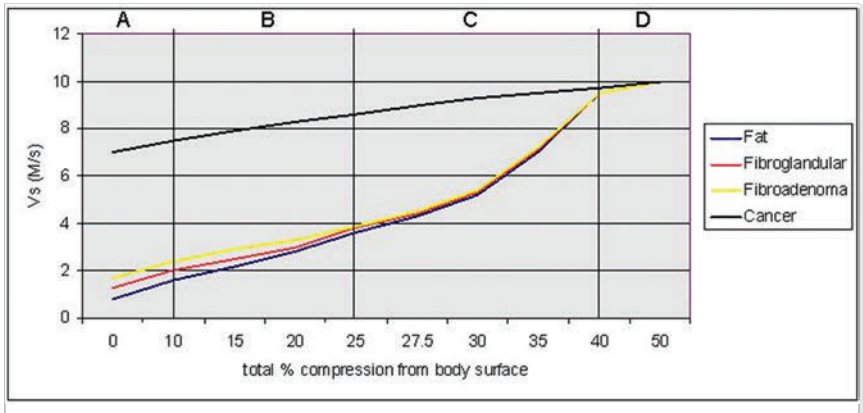

Fig. 5.9 When precompression is applied to breast tissue, the stiffness values increase. This diagram plots the shear wave speed for various breast tissues and pathologies with increasing precompression. Note that the stiffness values increase with precompression, and, if the maximum shear wave speed is used to characterize lesions as benign or malignant, a benign lesion can be made to have the stiffness of a malignancy with precompression. For SE, the differences between tissues are what is displayed. As precompression increases, the difference in stiffness between tissues decreases and therefore the quality of SE results decrease. (Reproduced with permission from Barr RG, Zhang Z. Effects of precompression on elasticity imaging of the breast. J Ultrasound Med 2012; 31:895–902.)

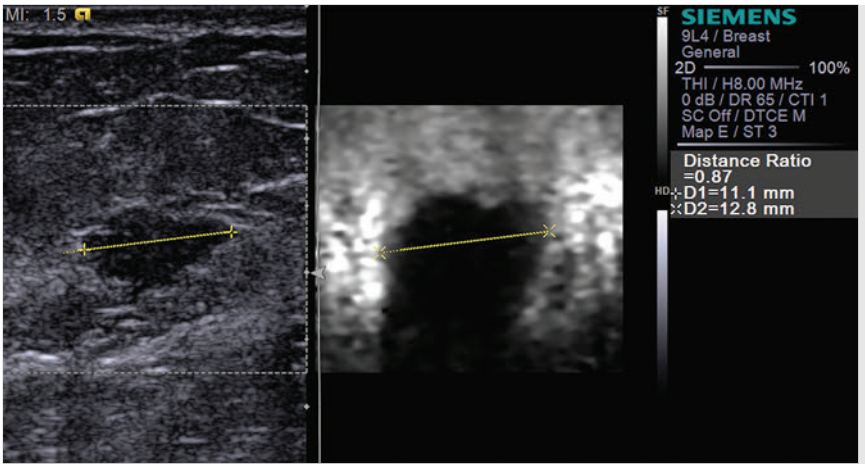

Fig. 5.10 Strain image obtained by using an ARFI pulse as the stress. In this 56-year-old female with an invasive ductal carcinoma (*yellow line*), the B-mode image is presented on the left. The dashed box is the FOV in which the ARFI pulse will generate stress to produce a strain image. This is different than using an ARFI pulse to generate and measure shear waves as in SWE. The image on the right is an strain elastography image. Like all SE images generated with manual compression, the lesion is stiffer than adjacent tissue and appears larger on SE than on B-mode (E/B > 1).

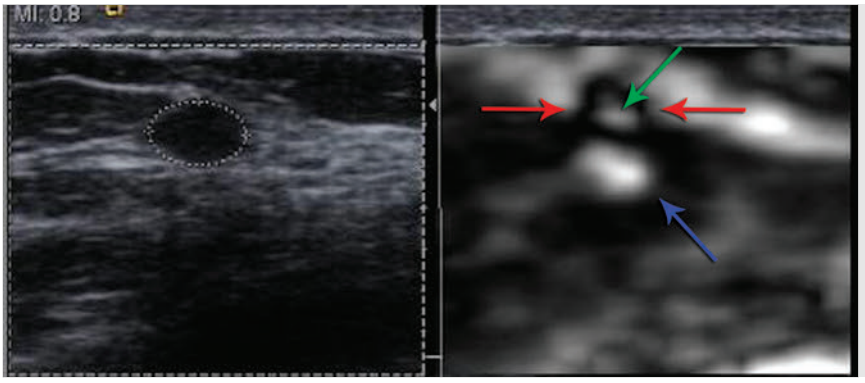

Fig. 5.11 In some systems' strain elastograms, a bull's eye artifact is seen in both simple and complicated cysts. The complicated cyst in the image on left (*dotted white circle*) has the bull's eye artifact seen in the elastogram on the right. The bull's eye artifact is composed of a black outer ring (*red arrows*), a white central signal (*green arrow*) and a distal white area (*blue arrow*). All three components are required to classify the lesion as a benign cystic lesion.

5.3.5 Systems Using ARFI

If an ARFI push pulse is used to generate the tissue displacement (Virtual Touch imaging [VTi], Siemens Ultrasound, Mountain View, CA), no manual displacement should be used. The probe should be held steady and the patient asked to hold their breath and remain motionless during the acquisition. The patient should refrain from talking during data acquisition. The algorithm used to generate the elastogram is similar to SE using manual displacement on the same system. In general the ARFI push pulse is limited and cannot produce displacement deeper than 4 cm with the breast imaging transducer. If the lesion is deeper, a satisfactory elastogram may not be obtained. The images are displayed similar to SE using manual displacement images with the B-mode image on the left and the VTi elastogram on the right. When using an ARFI push pulse to generate a strain image, an ROI is placed at the site of the lesion. The ARFI pulse is only generated within the ROI box, therefore only the ROI box has strain data within it on the elastogram (▶ Fig. 5.10).

5.3.6 Tips and Tricks

- Keep the FOV large to include fat, normal breast tissue, pectoralis muscle if possible, and the lesion. This will maintain a more constant color map (consistent dynamic range of strain values) between images.
- If the lesion is large (> 2 cm) select an image plane where the lesion is between 1 and 1.5 cm to obtain the elastogram.
- Use the B-mode image to determine the amount of tissue displacement being applied.
- Maintain the transducer perpendicular to skin and floor.
- Use the B-mode image to confirm that the scan plane through the lesion remains constant.
- Position the patient so the displacement motion is in the plane of the transducer.
- Do not apply precompression with the transducer.
- Compare the lesion stiffness to that of other tissues (i.e., fat and normal breast tissue).
- Have the patient hold still and maintain uniform shallow breathing. No talking during data acquisition.

5.3.7 Artifacts and Pitfalls

Several artifacts can occur with SE. Some of these artifacts occur when technique is suboptimal, while others can contain diagnostic information.

Bull's Eye Artifact

The Siemens and Philips SE systems have a unique artifact, the *bull's eye artifact*, that occurs with cystic lesions.[27] A different artifact can occur with other systems, the blue-green-red (BGR) artifact, and is described in the next section. The bull's eye artifact is characterized by[1] a black outer ring with[2] a white central area and a[3] white distal spot posterior to the lesion. The shape of the artifact mimics the shape of the cystic lesion. An example of the artifact is shown in ▶ Fig. 5.11, and it is described in detail in Chapter 2.[15,27] This artifact occurs when the fluid in the cyst is moving and there is decorrelation of the signals between images. This artifact has a high predictive value for the lesion

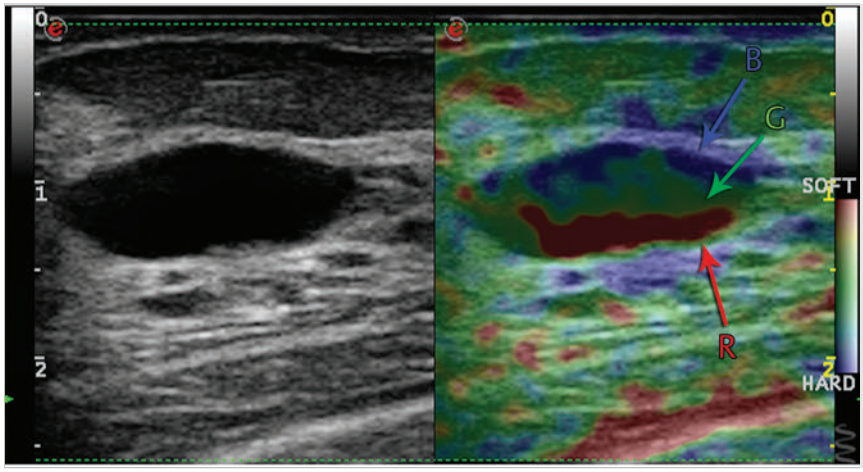

Fig. 5.12 Strain elastogram from a system that produces the blue-green-red (BGR) artifact instead of the bull's eye artifact in simple and complicated cysts.

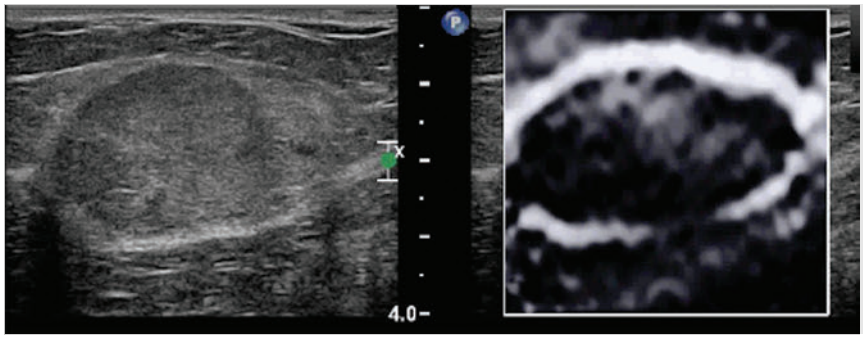

Fig. 5.13 If a lesion moves in and out of the imaging plane, a sliding artifact occurs. This artifact appears as a white ring around the lesion in the elastogram. In this image of a lipoma on the left, the lesion is imaged moving in and out of the imaging plane. In the elastogram on the right, there is a white ring around the lesion, the sliding artifact.

being a benign simple or complicated cyst. If the fluid within the cyst is very viscous, the artifact does not occur. This artifact does not occur in colloid or mucinous cancers. If there is a solid component within the cyst, the solid component will appear stiff and deform the artifact. The artifact can be seen in lesions that appear solid on B-mode imaging but these lesions have been proven to be benign complicated cysts. In these cases the lesions can be aspirated to confirm that they resolve after aspiration. In the case where a solid-appearing lesion on B-mode has the artifact and a core biopsy is performed, notifying the pathologist that a cystic lesion is suspected will help with radiology–pathology correlation as many pathologists do not report cysts routinely in their reports.

The bull's eye artifact has been reported to decrease the number of biopsies performed. In one series, 10% of complicated cysts appeared solid on B-mode and were identified as benign cysts with this technique.[27]

Blue-Green-Red Artifact

Some systems have a different artifact that occurs with cystic lesions: a three-color layered pattern of blue, green, and red (called the *BGR artifact*).[26] An example of this artifact is shown in ▶ Fig. 5.12. This artifact has not been evaluated in detail and the sensitivity and specificity of this artifact has not been reported.

Sliding Artifact

If the lesion is moving in and out of the imaging plane when the SE image is being obtained, a white ring or group of waves occurs around the lesion (▶ Fig. 5.13). This has been named the *sliding artifact*.[10,15] Having the same location of the lesion remain in the imaging plane during the acquisition can eliminate this artifact. Repositioning the patient, using less compression, or having the patient hold his or her breath may help keep the lesion in the scanning plane. This artifact occurs because the lesion is freely moveable within the surrounding tissues and is therefore most likely benign. It can occur with fibroadenomas or lipomas, and has been proposed as a method to determine if there is an invasive component to an intraductal malignancy.[31]

Worm Pattern Artifact

If there is very little variability in the elastic properties of the tissues within the FOV, the dynamic range of the SE scaling is very small and a pattern of varying signal is noted representing noise. This can occur when significant precompression is applied or only one tissue type is present in the FOV (▶ Fig. 5.14). This has been named the *worm pattern*.[10,15] These images do not contain any clinically useful information. This artifact can be eliminated by the use of minimal precompression and including tissue types of varying stiffness within the FOV.

5.3.8 Interpretation of Results

Three methods of interpreting strain images have been proposed: evaluating the size change between the elastogram and the B-mode image (E/B-mode ratio); a 5-point color scale (Tsukuba score); and the ratio of the lesion stiffness to fat stiffness (strain ratio or FLR). The relative stiffness (i.e., is the lesion stiff or soft compared to other breast tissues) can also be helpful clinically in interpreting images.

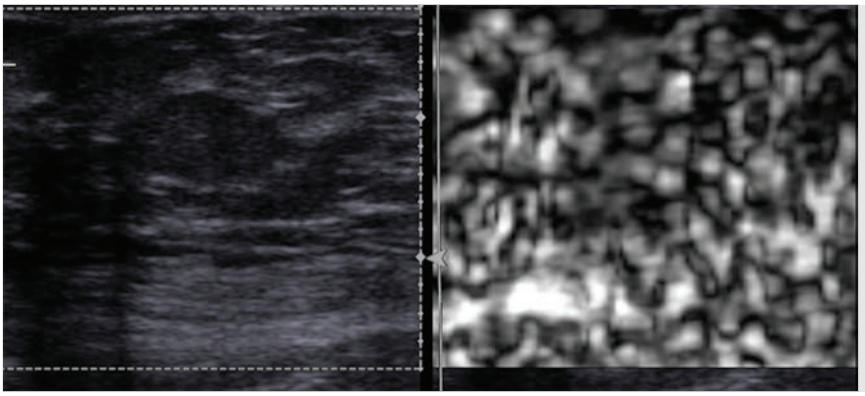

Fig. 5.14 When an image contains only tissues of very similar stiffnesses, as occurs when precompression applied, the elastogram image is all noise. This is depicted as alternating white and black blotches and is called the worm artifact.

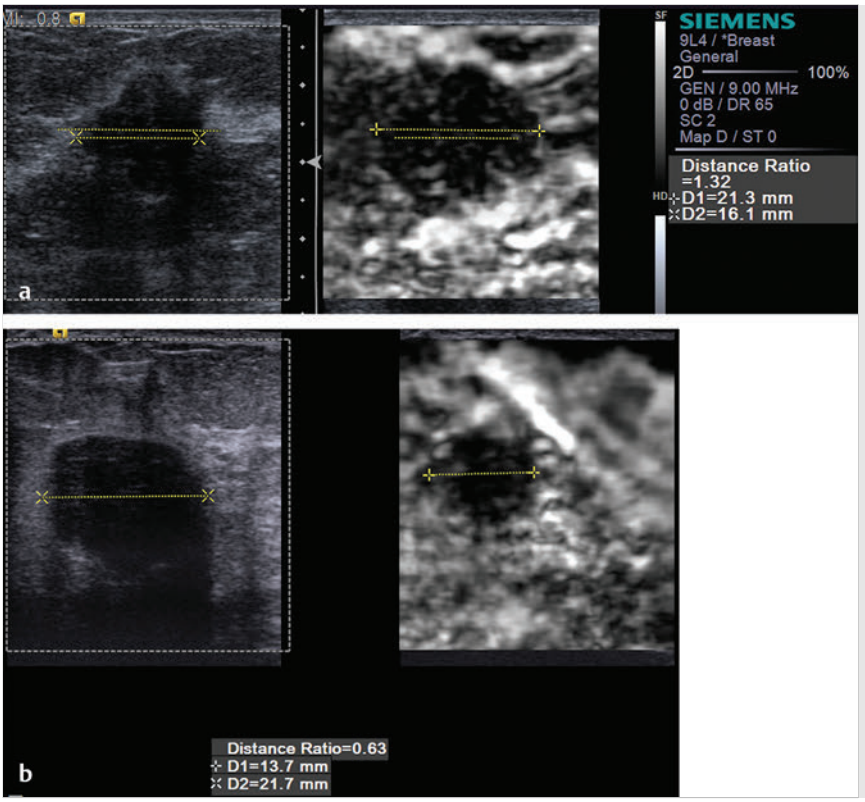

Fig. 5.15 In strain elastography (SE), malignant lesions appear larger in the elastogram than in B-mode imaging, while benign lesions appear smaller. (**a**) An invasive ductal cancer measures 16.1 mm on B-mode imaging and 21.3 mm in the elastogram with an E/B ratio of 1.32. (**b**) A benign fibroadenoma measures 21.7 mm on B-mode imaging and 13.7 mm in the elastogram with an E/B ratio of 0.63.

E/B Ratio

Using a real-time manual displacement strain system displaying the B-mode image and the strain elastogram simultaneously, Hall[32] demonstrated that there was potential to use this technique to characterize breast lesions as benign or malignant. It was noted on SE elastography that benign lesions measured smaller in size than on the corresponding B-mode image while malignant lesions measured larger (▶ Fig. 5.15). They proposed utilizing the ratio of the lesion size on elastography to that on B-mode imaging (E/B ratio) as a diagnostic criterion for benign or malignant lesions.

The location of the lesion within the elastogram does not affect results.[10] Either the lesion length ratio or the lesion area ratio can be used. Measuring the length is usually easier and faster to perform. The lesion is measured in the same position on both the elastogram and B-mode image. The use of a copy, shadow, or mirror function in the measurement technique is helpful. These software keys allow one to measure the lesion on either the B-mode image or elastogram image in a dual mode display and have the length measurement depicted on the opposite image in the exact same position (▶ Fig. 5.16).

This allows for one to determine if the ratio is greater or less than 1 visually. One can then correct the copied or mirrored image measurement to obtain the ratio. This method of interpretation requires that the lesion be visualized well enough to get an accurate measurement on both the B-mode image and the elastogram image. Because cases of ductal carcinoma in situ (DCIS) and lobular cancer are often poorly visualized on B-mode imaging, this technique should not be used unless they are defined masses that can be measured with true distinguishable borders.

Difficulty can occur when measuring the lesion size on the elastogram when a fibroadenoma or fibrocystic lesion is

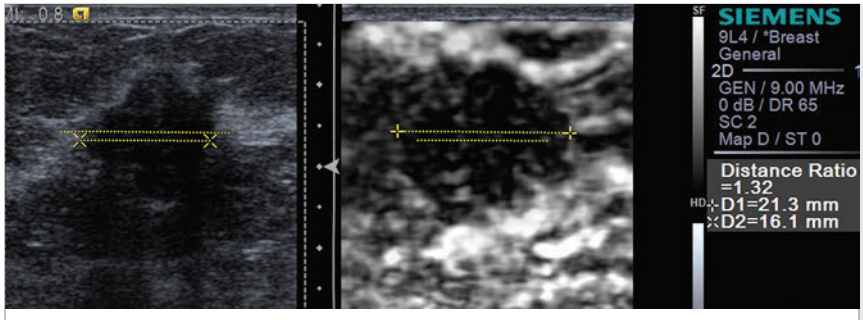

Fig. 5.16 Most vendors have a copy or duplicate function when measuring a lesion. As noted in this case, the lesion was measured on the B-mode image (*x dotted line x*) and then it is duplicated on the elastogram (*dotted lower line*) in the same location. The lesion can then be measured on the elastogram (*+ dotted line +*) and duplicated on the B-mode image (*upper dotted line*). The system then calculates the E/B ratio, which in this case is 1.32 suggesting a malignancy. Some systems copy the measurement made initially on either the B-mode image or the elastogram. The copied measurement can then be adjusted to the correct measurement and the E/B ratio is calculated.

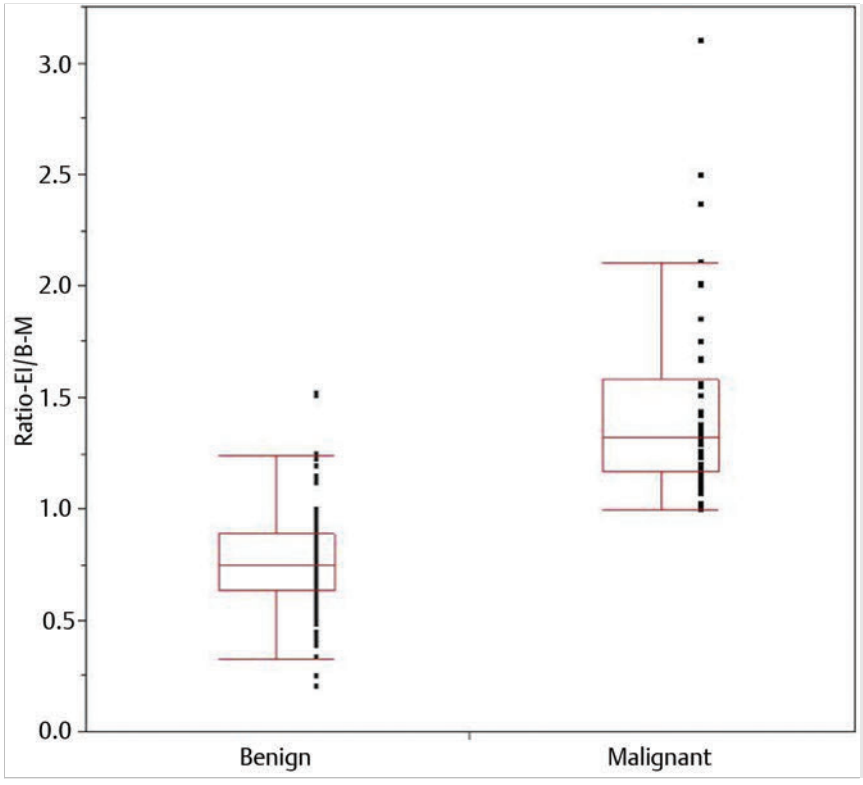

Fig. 5.17 Scatterplot of benign and malignant lesions using the E/B ratio from a large multicenter, international trial. (Reproduced with permission from Barr RG, Destounis S, Lackey LB II, Svensson WE, Balleyguier C, Smith C. Evaluation of breast lesions using sonographic elasticity imaging: a multicenter trial. J Ultrasound Med 2012; 31:281–287.)

present in dense breast tissue. The strain properties of the fibroadenoma or fibrocystic lesion are similar to the background dense breast tissue. Therefore, one may visualize the combination of the lesion and normal dense breast tissue as one lesion, creating a false positive.[10] In a multicenter trial,[16] this accounted for a large number of the false positives decreasing the specificity.

This problem can be avoided by instead comparing the stiffness of the lesion to that of the surrounding tissue; if it is similar to that of surrounding fibroglandular tissue, it is most likely benign. Using the color scale or lesion to fat stiffness ratio methods also may help eliminate this problem on the B-mode or elastogram accurately. When similar lesion length measurements problems occur the use of comparison to adjacent tissue or lesion to fat ratio can be used. Strain images obtained using the ARFI technique can be interpreted using this technique.

Previous studies[16,24,33] have demonstrated that the sensitivity of this technique is quite high (> 98%). ▶ Fig. 5.17 is a box plot of the results. In a large multicenter trial there were 3 cancers out of 222 that had an E/B ratio of < 1. In retrospect of these 3, one lesion was measured incorrectly on B-mode. Another may have been two adjacent lesions, one benign and one malignant, confounding the measurements. The third increased in size in anterior to posterior dimension but got smaller in width. Because cases of DCIS and lobular cancer are often poorly visualized on B-mode imaging, this technique should not be used for them unless they have defined masses that can be measured accurately.

Another confounding factor is the presence of two lesions adjacent to each other. These may appear as one lesion on the B-mode image. Close inspection of the elastogram can distinguish the two lesions (▶ Fig. 5.18). In these cases care must be taken in performing measurements. If different measurements are obtained in different lesion positions, the possibility of the "lesion" being two adjacent lesions should be considered. Always use the results of the larger E/B ratio, and if such a lesion

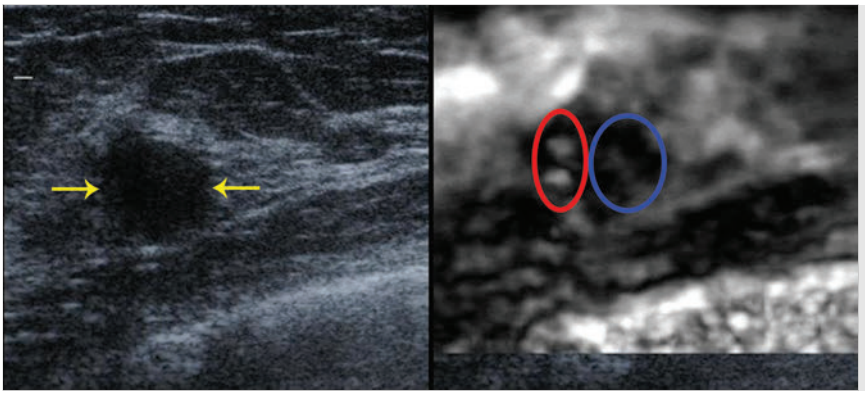

Fig. 5.18 What appears as a single lesion on B-mode imaging can be two adjacent lesions with similar acoustic properties. If the two lesions have different elastic properties, they will appear as two lesions on elastography. As an example, in this figure the B-mode image (left) has "one" lesion (*yellow arrows*) while on the elastogram (right) the "lesion" is two adjacent lesions: a cyst (*red circle*) and a benign fibroadenoma (*blue circle*).

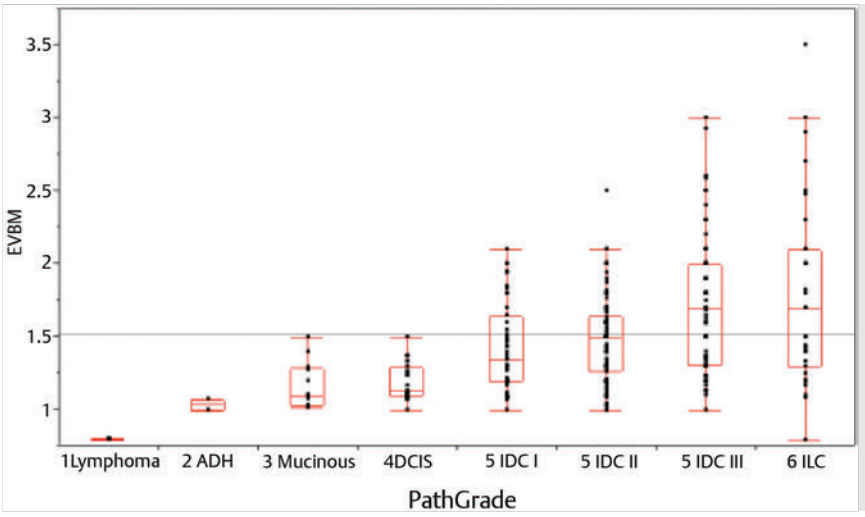

Fig. 5.19 Diagram of E/B ratio for various breast lesions. The E/B ratio increases as the aggressiveness of the tumor increases. (Reproduced with permission from Grajo JR, Barr RG., Strain elastography for prediction of breast cancer tumor grades. J Ultrasound Med 2014; 33:129–134.)

is biopsied, always try to biopsy the portion of the lesion that has the larger E/B ratio.

The E/B ratio has been shown to correlate with tumor grade.[34] The box plots for the E/B ratio for various tumor types and grades are presented in ▶ Fig. 5.19. For less aggressive tumors such as DCIS, mucinous cancer, or colloid cancer, the ratio is close to 1. For invasive ductal cancers the ratio increases with grade and is statistically significant. The clinical utility of this finding is unclear at this time. Some reports suggest a greater specificity with a cutoff value of 1.2. However, with this cutoff value, low-grade malignancies such as DCIS or mucinous cancers can be misclassified as benign, thus trading higher specificity for lower sensitivity.

5-Point Color Scale

A 5-point color scale has been proposed to classify lesions using SE (▶ Fig. 5.20).[11,21] This scale combines the degree of stiffness and E/B ratio of the lesion. In this diagnostic approach, a score from 1 to 5 is assigned based on the color (balance of green and blue, with the color scale set to blue as hard) inside the target lesion and surrounding area on the elastogram, with a higher score indicating a higher diagnostic confidence of malignancy.

If the lesion is soft, it is classified with a score of 1. If the lesion has a mixed hard and soft pattern, it is classified as a 2. If the lesion is hard but smaller on the elastogram than on the B-mode image, it is given a score of 3. Scores of 1 to 3 are classified as benign. When a lesion is hard and the same size on the elastogram and in the B-mode image, the lesion is given a score of 4. If the lesion is hard and larger on the elastogram than on the B-mode image, the lesion is classified as 5 (▶ Fig. 5.21). This technique has been shown to have moderate to substantial interobserver agreement and substantial to perfect intraobserver agreement.[35] There was no significant difference in interobserver and intraobserver agreement concerning lesion size. It is recommended that lesions that are hard and equal in size (score 4) or larger on the elastogram (score 5) are biopsied, similar to the recommendations of Barr.[10,15] If another color scale is used with this technique (such as red as hard), appropriate changes to the colors in the scale need to be made before assigning scores.

Using the 5-point color scale, breast SE has been shown to objectively evaluate tumor or tissue stiffness in addition to morphology and vascularity.[21] Itoh found a sensitivity of 86.5% and a specificity of 89.8% using this technique with a cutoff point between 3 and 4. This technique has been shown to correlate well with the ultrasound BI-RADS score.[36,37] SE has also been shown to visualize nonmass lesions or peritumoral ductal lesions.[21] Multiple studies have found similar results.[38,39,40,41,42] This technique has also been used in the evaluation of suspicious microcalcifications on mammography with 97% sensitivity and 62% specificity in the differentiation of benign and

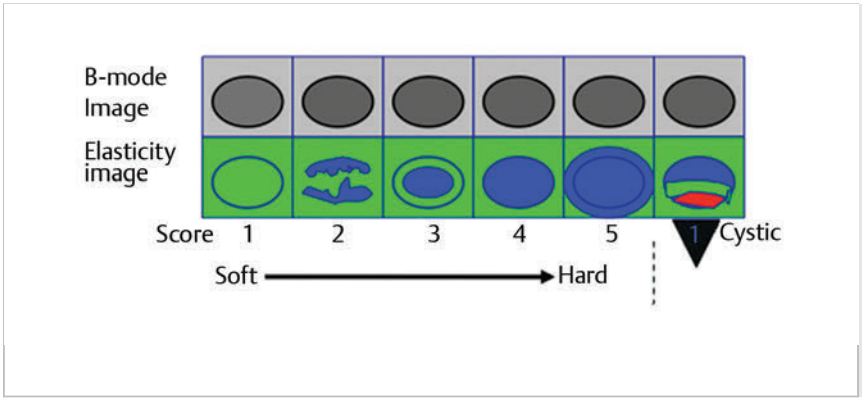

Fig. 5.20 A 5-point color scale has been used to classify breast lesions on SE. In this scale, a soft lesion has a score of 1, a lesion with mixed soft and stiff components is given a score of 2, a lesion that is stiff and smaller on elastography is given a score of 3, a lesion that is stiff and of the same size as B-mode is given a score of 4, and a stiff lesion which is larger on elastography is given a score of 5. In this figure a color scale of blue as stiff and red as soft has been used. Lesions with a score of 1, 2, or 3 are considered benign while a score of 4 or 5 are considered malignant. If the lesion is cystic a tri-color pattern of blue, green, red (BGR) is obtained.

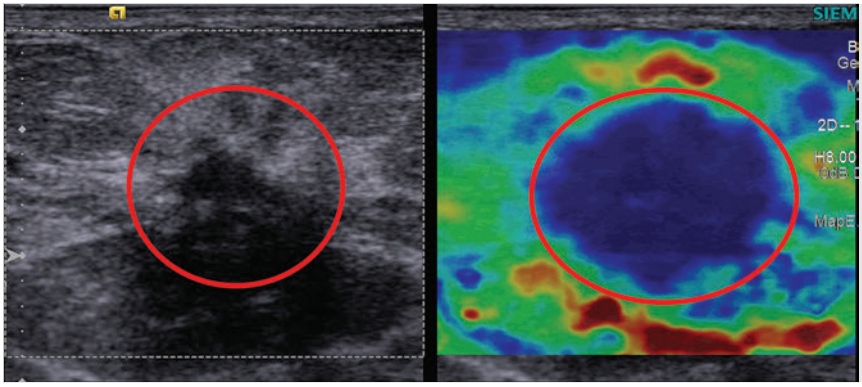

Fig. 5.21 A strain elastogram of an invasive ductal cancer using a color scale with blue as stiff (hard) and red as soft. A red circle has been placed on the malignant lesion. A similar circle has been placed on the corresponding B-mode image to the left. The lesion is larger on the elastogram and stiff (blue) corresponding to a 5-point color score of 5.

malignant microcalcifications.[38] Several articles suggest SE may be most helpful in BI-RADS 3 and BI-RADS 4 lesions by upgrading or downgrading them.[18,40]

Raza[43] reported a prospective clinical trial with a sensitivity of 92.7% and a specificity of 85.8%. Chang et al[44] analyzed factors that affect the accuracy of elasticity scores in a prospective study. They reported that the biggest factor affecting elastography image quality was the breast being thin at the location of the lesion (that is, the target lesion being shallowly located). They mentioned that the accuracy of elastography differed depending on the depth of the lesion and that accuracy control was necessary.

When making a diagnosis using this method, it is important to choose an FOV that includes various tissue types (fat, fibroglandular tissue, pectoralis muscle) and where the lesion accounts for no more than one-fourth of the FOV during imaging. The recommendations for this technique are the same as that for obtaining an E/B ratio. Limitations of this technique include that it is subjective and that it cannot be used for large tumors or large irregular tumors, since the assessment is affected by the ratio of the area of the tumor to that of the surrounding tissue.

Strain Ratio

In an attempt to semiquantify the stiffness measurements, the ratio of breast lesion stiffness to that of subcutaneous fat, whose stiffness properties are fairly constant, has been suggested. This has been called the lesion to fat ratio, strain ratio (SR), or fat to lesion ratio (FLR) and use of it was advocated by Ueno.[23] This ratio can be thought of as a method for numerically evaluating how many times stiffer a target lesion is as compared with subcutaneous fat (▶ Fig. 5.22). To obtain an accurate ratio, the target ROI for the tumor should not protrude from the interior of the tumor in B-mode imaging, and the target ROI for subcutaneous fat should be a circle of sufficient size and limited to fat that does not contain breast tissue.

Since it is possible to evaluate the stiffness of one specific part of a mass by setting the target ROI, it is not only possible to measure the stiffness of very large tumors, but also the stiffness of parts of nonmass abnormalities. The stiffness of a tumor is an approximation. This measurement is easy to perform, and the results of clinical studies using this diagnostic approach have already been reported.

Initial studies[23,45,46] have found this technique valuable in determining if a lesion was benign or malignant. Care must be taken with these measurements, as precompression can significantly change the strain value of fat.[30] As precompression is applied, the stiffness of all tissues increase. However, the stiffness of fat changes more than that of normal breast tissue and lesions. Therefore, with precompression, the strain ratio of lesion to fat will decrease. Care must also be taken that the ROI for the fat measurement contains only fat. The measurements should be taken at the same depth in the image for both the lesion and the fat, as the degree of tissue compression varies with depth.

In addition to performing the measurement of lesion strain to fat strain for one point in a lesion, one vendor offers parametric imaging. In this technique, a ROI is placed in an area of fat and the entire FOV is color-coded based on the ratio of stiffness of each pixel to the stiffness of fat (▶ Fig. 5.23). A color-coded semiquantitative image is obtained over a large FOV. The area with the highest lesion to fat ratio is then identified visually and a measurement at that point is obtained.

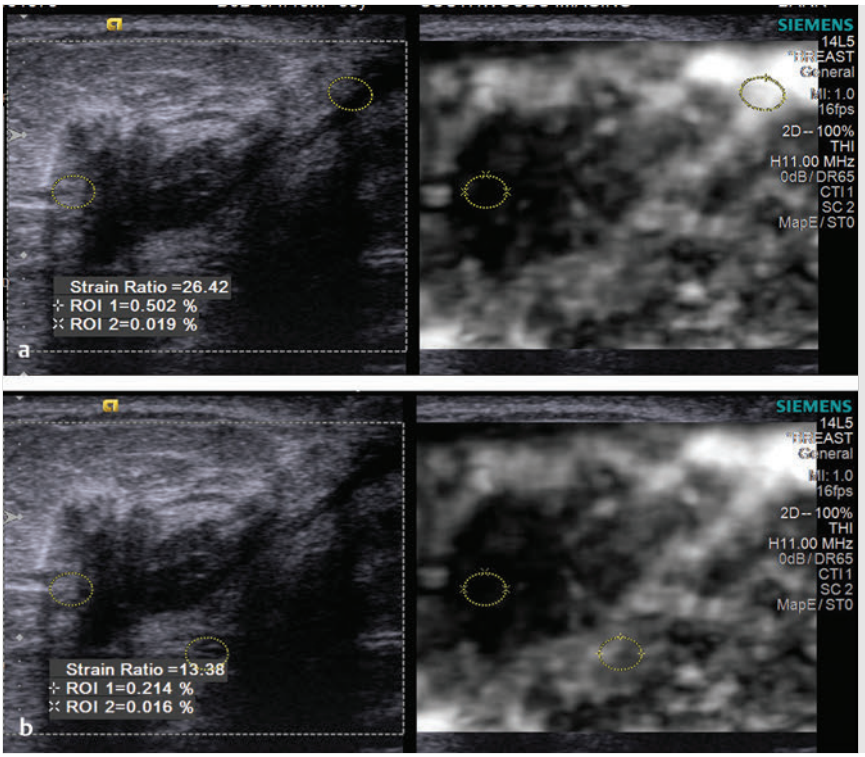

Fig. 5.22 Although SE is qualitative and not quantitative, the lesion to fat ratio, or strain ratio, has been proposed as a semiquantitative method of evaluating elastographic images. The same image is displayed in both (**a**) and (**b**). In both images, a dotted circle has been placed in the lesion as well as in adjacent fat. The selection of fat as reference is important as demonstrated in this case. The strain ratio is 26 in (**a**) and 13 in (**b**). Although both strain ratios are suggestive of a malignant lesion, there is significant difference in the values due to the area of fat selected for strain measurment.

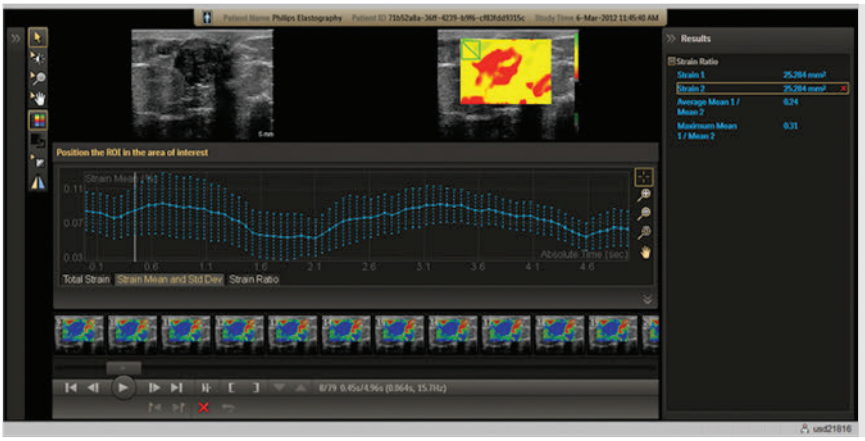

Fig. 5.23 The strain ratio can be performed over a large field of view and displayed as a color-coded map. In this parametric imaging, a ROI is placed on fat (*green square*). The strain ratio is then calculated for each pixel in the FOV, using the strain in the ROI as the reference, and displayed as a color-coded map.

Thomas[46] compared B-mode BI–RADS, the 5-point color scale, and the lesion to fat ratio in 227 breast lesions. Based on the receiver operating characteristic (ROC) curve, they selected a cutoff of 2.455 to distinguish benign from malignant lesions. The mean ratio for malignant lesions was 5.1 ± 4.2, while for benign lesions it was 1.6 ± 1.0 ($p < 0.001$). They found a sensitivity and specificity of 96% and 56% for B-mode imaging, 81% and 89% for the 5-point color scale, and 90% and 89% for the lesion to fat ratio.

Zhi[47] in a similar study compared the lesion to fat ratio and the 5-point color scale in 559 breast lesions. They found the lesion to fat ratio of benign lesions was 1.83 ±1.22 while malignant lesions were 8.38 ± 7.65. These were significantly different ($p < 0.00001$). Based on the ROC curve, they selected a cutoff of 3.05. The area under the curve for the 5-point color system was 0.885, while that for the lesion to fat ratio was 0.944 ($p < 0.05$). In a study by Ueno et al of lesion to fat ratios of 408 lesions,[23] with a cutoff of 4.8, they found a sensitivity of 76.6% and a specificity of 76.8%.

Farrokh[45] reported sensitivity of 94.4% and specificity of 87.3% with a cutoff above 2.9 in a prospective study using the lesion to fat ratio. Alhabshi[48] reported that E/B ratio and strain ratio were the most useful methods of lesion characterization, with a cutoff value of 1.1 for the E/B ratio and a cutoff value of 5.6 for strain ratio, in a study using B-mode, strain pattern (elasticity score), E/B ratio and fat to lesion ratio. Stachs[49] demonstrated the utility of the fat to lesion ratio in 224 breast masses in 215 patients, reporting that the fat to lesion ratio was predominantly higher in malignant tumors, that is, 3.04 ± 0.9 (mean ± standard deviation) for malignant tumors versus 1.91 ± 0.75 for benign tumors.

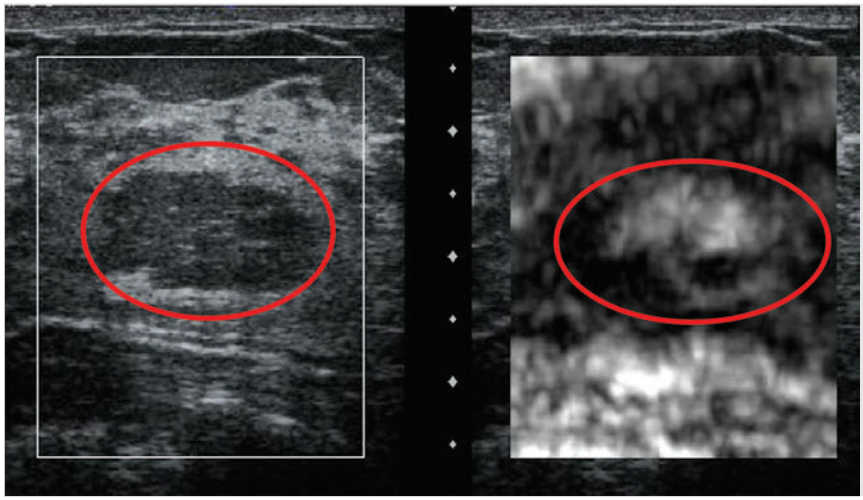

Fig. 5.24 In the B-mode image (left), a lobular isoechoic lesion is identified and was classified as a BI-RADS category 4A lesion. On elastography (right), the lesion is very soft and similar to other fat in the image and represents a fat lobule. It was reclassified as a BI-RADS category 2 lesion.

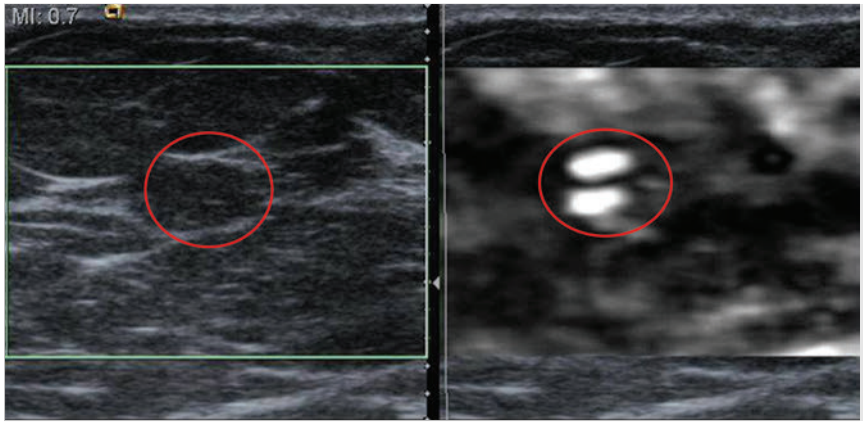

Fig. 5.25 Strain elastography image of a palpable mass that was not identified on B-mode imaging. When a SE image is obtained by placing the transducer over a palpable lesion and a bull's eye artifact (*red circle*) is seen, this confirms the lesion is an isoechoic complicated cyst.

The appropriate cutoff for this technique varies greatly between studies. Using quantitative ARFI, we have been able to change the speed of sound though fatty tissue by a factor of 10 with precompression.[30] As precompression is applied, the stiffness of all tissues increased. However, the stiffness of fat changes more than that of normal breast tissue and lesions; therefore, with precompression the strain ratio of lesion to fat will decrease. Care must also be taken that the FOV for the fat measurement contains only fat. The measurements should be taken at the same tissue depth in the image, as the degree of compression varies with tissue depth. These factors, where not controlled in the studies, may account for the variability of the results. When using this technique, determine the appropriate cutoff value in your lab with your technique and equipment.

Lesion Relative Stiffness

In addition to using the interpretation methods previously discussed to determine if a lesion is benign or malignant, the information about whether the lesion soft or hard or visible on elasticity imaging is clinically helpful in some situations.

It is sometimes difficult to determine if a lobular hypoechoic lesion is a fat lobule on conventional ultrasound. If the lesion is a fat lobule, it will appear very soft on an elastogram and similar to the other fat in the image (▶ Fig. 5.24). If a lesion is difficult to measure, comparing the elasticity of the lesion to dense breast tissue can be helpful. If the elasticity is similar to dense breast tissue, it is probably benign, whereas if it is stiffer than dense breast tissue, it is most likely malignant.

Lesions can be isoechoic to surrounding tissue on B-mode imaging and not be recognized as a lesion. But these lesions may have different strain properties compared to surrounding tissue and can be clearly visualized on SE. This is very common with complicated cysts (▶ Fig. 5.25).

Evaluation of the elasticity image pattern can also define where to best biopsy a lesion (▶ Fig. 5.26), by allowing one to select the hardest location to target the biopsy. The SE pattern can help characterize a complex lesion (▶ Fig. 5.27).

5.3.9 Limitations

Accuracy can differ in measurements between shallow sites and deep sites due to problems associated with variable displacement at different tissue depths. Further improvement of applications and adjustments to imaging methods are needed to overcome these problems. It is possible to use all three interpretation techniques (E/B ratio, 5-point color scale, and lesion to fat ratio) to increase confidence in lesion characterization. If a lesion cannot be measured accurately or is a nonmass lesion

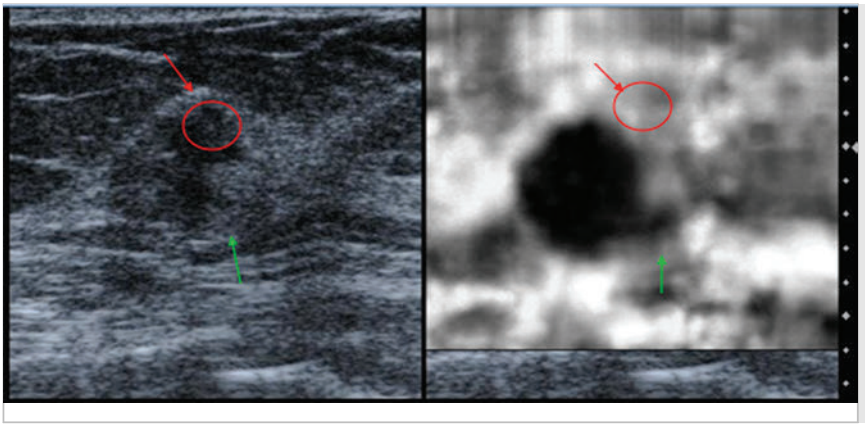

Fig. 5.26 Elastography can be helpful in determining where to perform a biopsy. Selecting the stiffest area should provide better radiology pathology correlation to the surgical specimen. In this case the lesion has three components, an anterior portion (*red circle*), a main portion, and an inferior portion (*green arrow*). The anterior lesion (*red circle*) is soft on the SE image and was a benign fibroadenoma on surgical resection. The main portion and inferior portion (*green arrow*), both very stiff and greater in size than on B-mode imaging (E/B > 1), were invasive ductal cancer on surgical resection. (Reproduced with permission from Barr RG. Sonographic breast elastography: a primer. J Ultrasound Med 2012; 31:773–783.)

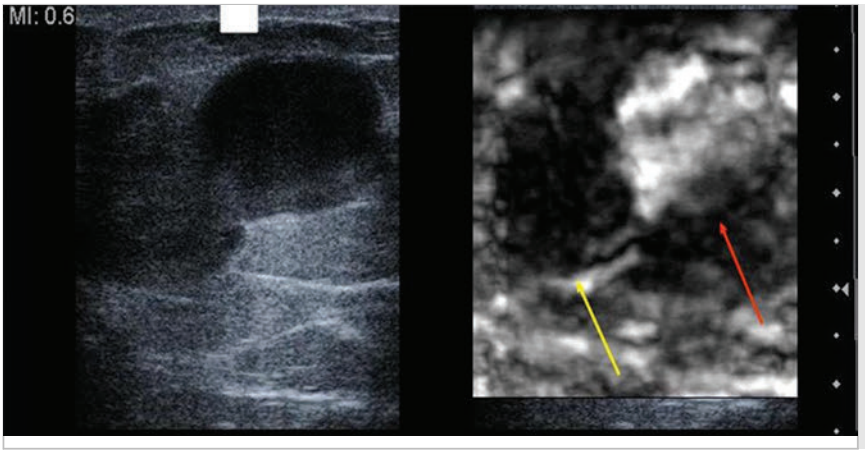

Fig. 5.27 On the B-mode image (left), there is a complex dumbbell-shaped lesion. On SE (right), the portion marked by a yellow arrow is stiff while the portion that is marked by the red arrow is soft. This image is from a 75-year-old woman who presented with a bloody discharge and new mass on mammography. The portion marked by the red arrow was aspirated and was old blood. A bull's eye artifact is not seen because the viscosity of old blood is high enough to prevent a bull's eye artifact. The portion marked by the yellow arrow, biopsied with a 12-gauge needle, was a benign papillary lesion. (Reproduced with permission from Barr RG. Sonographic breast elastography: a primer. J Ultrasound Med 2012; 31:773–783.)

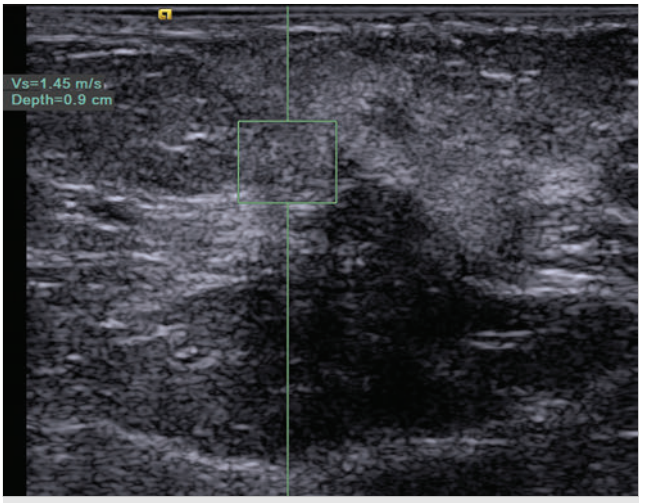

Fig. 5.28 Point shear wave elastography (p-SWE) uses ARFI to determine the shear wave speed in a small ROI. In this example, the square is the ROI where the shear wave speed is calculated. In this case the shear wave speed (V_s) is 1.45 m/s.

and so an E/B ratio cannot be accurately calculated, the other two techniques can be used to characterize the lesion.

At present, reports related to lesion to fat ratios have used significantly different cutoff values. The need for a prospective multicenter study with well-defined acquisition parameters is needed to determine the appropriate cutoff value.

5.4 Shear Wave Elastography Imaging

5.4.1 Techniques

The second major technique to determine the elastic properties of tissue is shear wave speed (SWS) measurement.[26] In this technique an initial ultrasound pulse (push pulse) is applied to the tissue that induces a shear wave perpendicular to the ultrasound beam, and then standard B-mode ultrasound sampling techniques are used to calculate the SWS generated through the tissues (see Chapter 2). From the SWS through the tissues, the strain modulus, called Young's modulus, can be estimated. The speed of the shear wave is proportional to stiffness. The stiffness of a lesion can be displayed as the SWS (V_s in meters per second) or as Young's modulus (in kilopascals).

Various types of shear wave systems are available for clinical use. Using ARFI technology, the SWS can be estimated in a small ROI (approximately 5 × 5 mm). This technique is called point shear wave elastography (p-SWE). An example of this technique is Virtual Touch Quantification (VTQ, Siemens Ultrasound, Mountain View, CA) (▶ Fig. 5.28). By applying multiple ARFI pulses over a larger FOV and color-coding the results, stiffness measurements

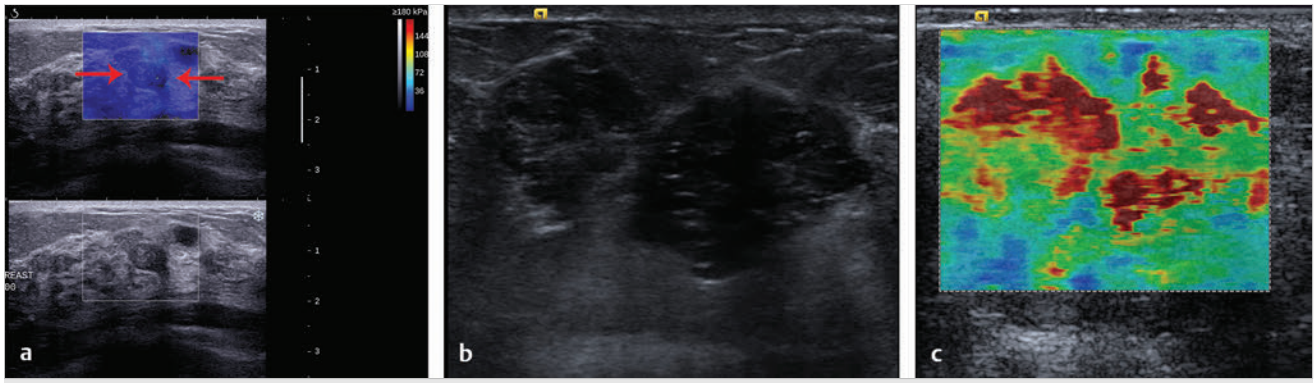

Fig. 5.29 In two-dimensional shear wave elastography (2D-SWE), a larger FOV is placed around the lesion and shear wave speeds are obtained at each pixel within the FOV. The shear wave speeds are then color-coded. A ROI can then be placed in the FOV to obtain the shear wave speed at that location. The color-coded FOV allows for the detection of the area with the highest shear wave speed. (**a**) In this case of a benign fibroadenoma (*red arrows*), the upper image is the elastogram and the lower image is the B-mode image. The shear wave speed of the lesion is 30 kPa (ROI not shown). (**b**) Two adjacent lesions on B-mode imaging and (**c**) the corresponding elastogram. In this case of two adjacent invasive ductal carcinomas, the maximum shear wave speed is 7.5 m/s consistent with a malignant lesion.

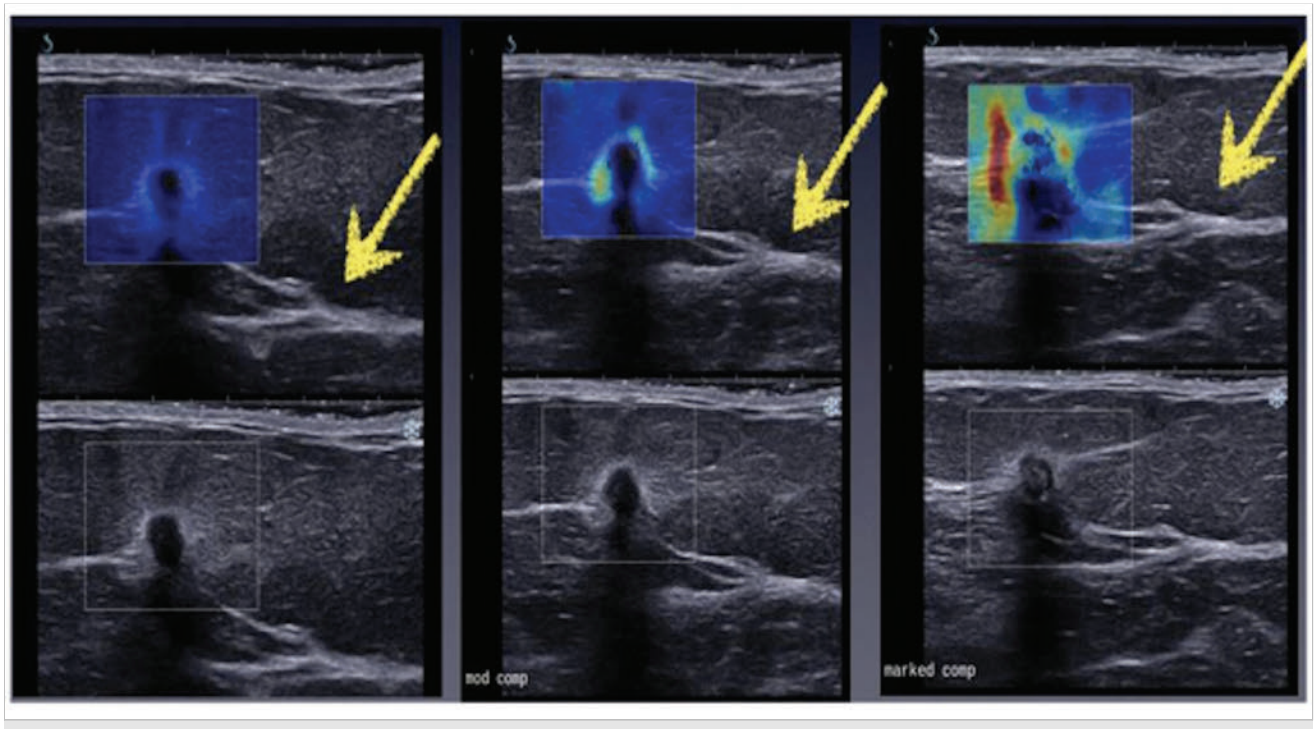

Fig. 5.30 Precompression can affect the shear wave speed of a lesion. In this figure, an invasive ductal cancer is imaged with increasing amounts of precompression (left to right). There are low shear wave speeds in the image with minimal precompression on the left and the shear wave speeds are in the teal color range. As precompression is applied, the tissues surrounding the lesion color-code yellow (middle) and then red (right). The yellow arrows point to a Cooper's ligament. Note that as precompression is applied, the Cooper's ligament moves closer to the transducer (less depth).

over a larger area can be obtained and displayed in a single image. This technique is called two-dimensional shear wave elastography (2D-SWE.) An example of this technique is Virtual Touch IQ (VTIQ, Siemens Ultrasound). A smaller ROI can be placed in the FOV and measurements of the SWS can be obtained. Another technique, real-time 2D-SWE, can be performed when a rapid scanning sequence is used to allow for continuous measurements. An example of this technique is real-time SWE (SuperSonic Imagine, Aix en Provence, France) (▶ Fig. 5.29).

Precompression can markedly change SWS values.[30] ▶ Fig. 5.30 demonstrates the effect of precompression on both a benign and malignant lesion. Note that with precompression even a benign lesion can have high SWS suggestive of a malignant lesion. Precompression also will increase the SWS surrounding a malignant lesion. As previously discussed, the SWS of fat in the breast can be changed by a factor of 10 with precompression. Therefore, it is important not to compress the tissue with the transducer. We recommend using the technique

for applying only minimal precompression, described in section 5.3.4. Minimal- and Moderate-Compression/Vibration Systems.

5.4.2 Performing an Examination

The guidelines for optimal scanning technique for SE also apply to SWE.

As just noted, precompression can change results. To control for this, we recommend using the same technique to acquire images for SWE as for SE.

SWE can be performed in real-time; however, to obtain optimal images, remaining in the same plane for several seconds is required for accurate measurements.

Shear wave generation is depth limited: if a tissue or lesion of interest is deeper than 4 cm, a result may not be obtained. Repositioning of the patient to bring the region of interest (ROI) closer to the transducer may help. If there is no shear wave generation, no color-coding in this area of the elastogram will occur. The results of scanning are color-coded usually with the default color convention of red as hard (stiff) and blue as soft.

However, the stiffness value where color changes occur can be changed (▶ Fig. 5.31). For breast tissues, a color scale with a maximum of 7.7 m/s (180 kPa) is usually used. With this scale, lesions coded green, yellow, and red are stiff within the range of malignancies. When evaluating only benign tissue, decreasing the maximum value of the color scale, for example, to 3.7 m/s (40 kPa) will allow for a greater color differentiation of the stiffness of the benign tissues. However, red will no longer code for a stiffness value suggestive of a malignancy.

Three-dimensional shear wave imaging is available. No studies with the use of 3D-SWE have been published. It is unknown if the volumetric data using the three-dimensional technique will provide additional information or allow for breast screening.

5.4.3 Tips and Tricks

- Keep the FOV slightly larger than the lesion to evaluate the surrounding tissue.
- Maintain the transducer perpendicular to the skin.
- Hold the transducer still and ask the patient to hold breath during measurements.
- Do not apply precompression with the transducer.
- When using real-time shear wave imaging, allow several seconds for the image to stabilize before taking a measurement.

5.4.4 Artifacts and Pitfalls

There are several artifacts that can occur with SWE of the breast. Some of these are due to suboptimal technique. Others may contain diagnostic information.

No Color-Coding (Lack of Shear Wave Signal)

The shear wave is detected by ultrasonic echo signal. Therefore when areas in the B-mode image show extremely low signal, it indicates the echo signal is too low for successful elastographic detection. On the elastogram, these areas are not color-coded. This can also occur with marked shadowing such as seen with ribs, tumors with significant shadowing, and areas with macrocalcifications.[10]

Shear waves do not propagate in simple cysts. Therefore, simple cysts will not be color-coded in SWE (▶ Fig. 5.32). Complicated cysts will support shear waves and they will be color-coded with a low SWS (blue). This artifact can also occur in areas with marked shadowing such as ribs, tumor with significant shadowing and areas of macrocalifications.[10]

In very stiff lesions such as invasive cancers, the shear waves may also not propagate or be able to be measured. In these cases, no results are obtained, and the area in the elastogram is not color-coded (▶ Fig. 5.33), and so no interpretation is possible. However, in general the desmoplastic reaction of the tumor will be stiff surrounding the tumor and a ring of stiffness (yellows or reds) will surround the lesion. Care must be taken when performing the examination as precompression can also create the same appearance of a ring of stiffness in a benign lesion (▶ Fig. 5.8).

Areas deeper than the ARFI pulse can generate shear waves are also not color-coded. For most systems SWE cannot be performed in the breast deeper than 4 cm.

Bang Artifact

If too much pressure is applied with the transducer, a region of stiffness will occur in the near field (▶ Fig. 5.34). Applying less pressure with the transducer can eliminate this artifact. Using adequate coupling gel and allowing a layer of gel to remain between the transducer and skin can be helpful in eliminating this artifact.

5.4.5 Interpretation of Results

Two-Dimensional Shear Wave Elastography

The results with SWE are quantitative and expressed as either the SWS (V_s) in meters per second (m/s) or converted, making some assumptions regarding the tissue, to Young's modulus in kilopascals (kPa). The conversion between the two can be found in Chapter 2.[50] Most equipment allows for display of the results in either form. The default color convention in 2D-SWE is to have the FOV color-coded with red as hard (stiff) and blue as soft. Placement of a small ROI is used to determine the stiffness value at a specific location. Most systems display the maximum, minimum, and mean values, and the standard deviation of the SWS for the pixels within the selected ROI. Both the mean and the maximum values have been used in classification schemes.

The color map overlay on the FOV can be used to identify the area of maximum SWS within or adjacent to the lesion. Note that mean and standard deviation will change depending on the size and placement of the ROI even if the ROI contains the area of maximum stiffness. Often the highest SWS value is in the tissue surrounding the lesion (up to 5 mm from the lesion) and should be used in evaluating the lesion. Examples of both a benign and a malignant lesion are presented in ▶ Fig. 5.29.

Chang et al,[51] in a study of 158 consecutive patients, found the mean elasticity values were significantly higher in malignant masses (153 ± 58 kPa) than benign masses (46 ± 43 kPa) ($p < 0.0001$). They determined an optimal cutoff value of 80 kPa, which resulted in a sensitivity and specificity of 88.8% and 84.9%. The area under the receiver operating characteristic (ROC) curve was 0.898 for conventional ultrasound; 0.932 for

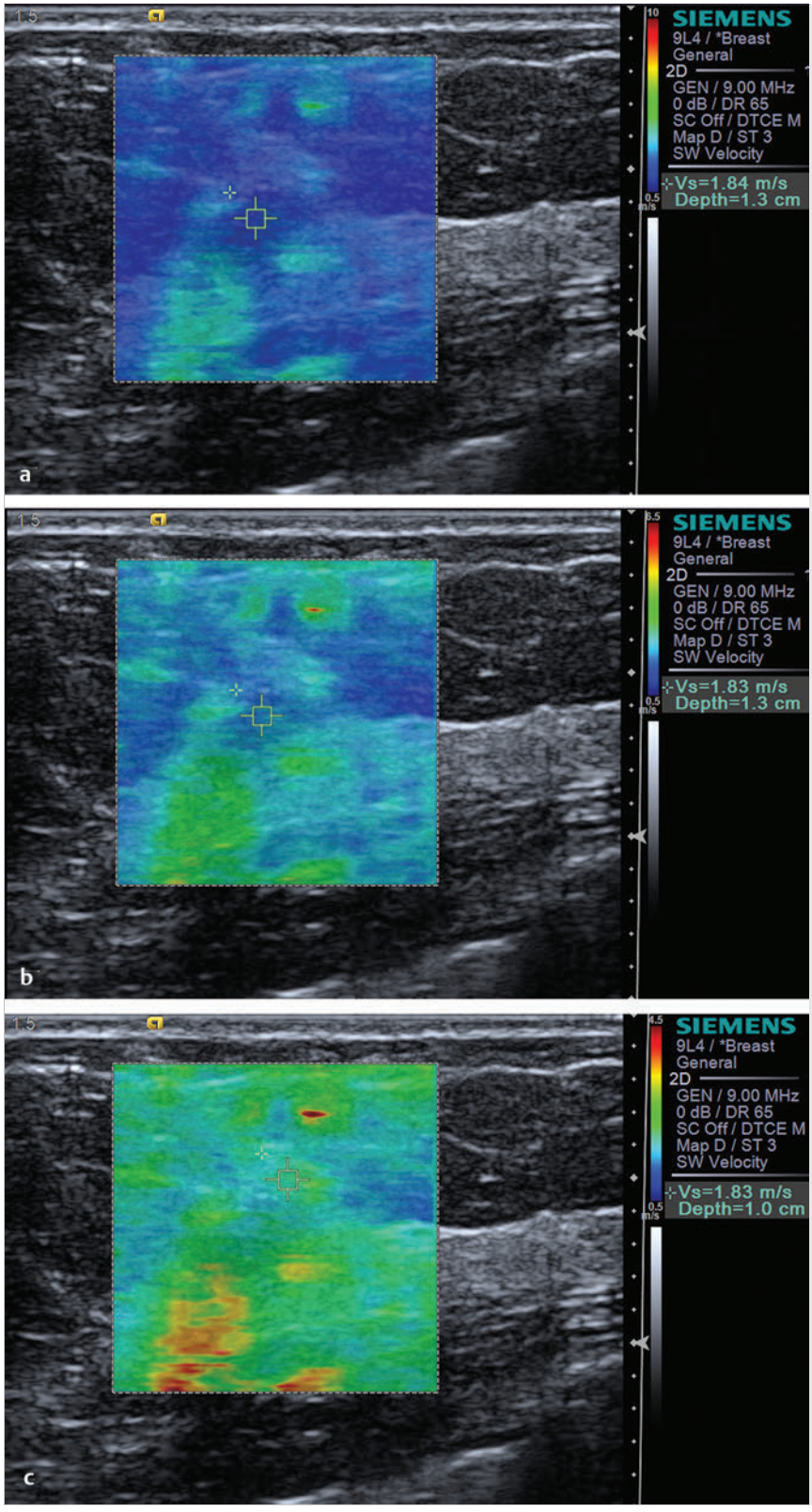

Fig. 5.31 If a lesion is soft, the color scale can be changed to improve the visualization of differences in the shear wave speeds in the FOV. In this series of images, the color scale is decreased from (**a**) 10 m/s to (**b**) 6.5 m/s to (**c**) 4.5 m/s. Note how the coloring in the image changes but the shear wave speed in the ROI remains the same at 1.83 m/s.

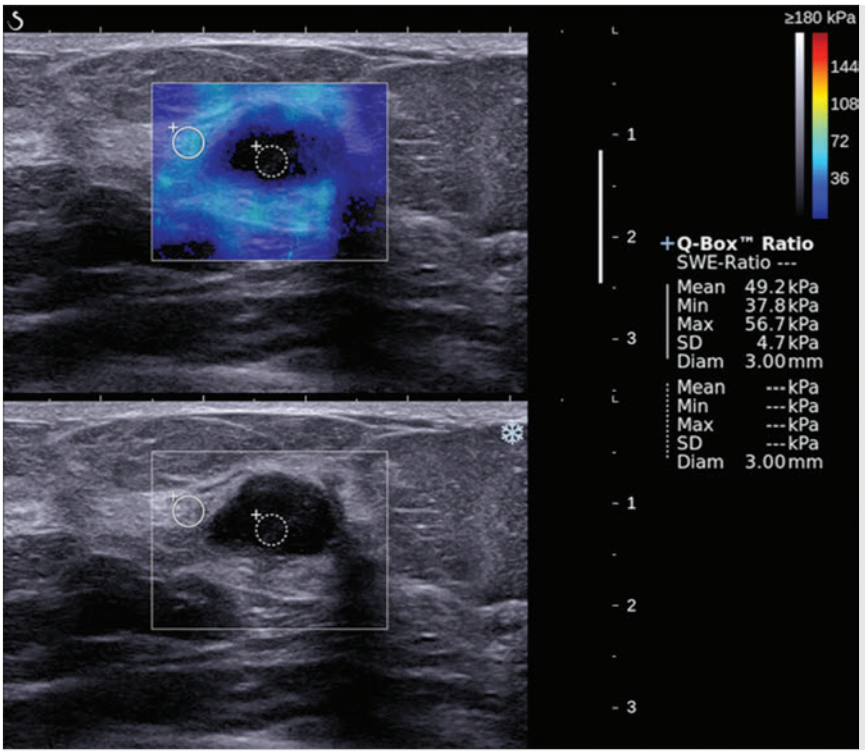

Fig. 5.32 This two-dimensional shear wave elastography image of a simple cyst demonstrates no color-coding of the cyst. Simple cysts do not support shear wave propagation and are therefore not color-coded. Complicated cysts do support shear wave generation and are color-coded soft (blue).

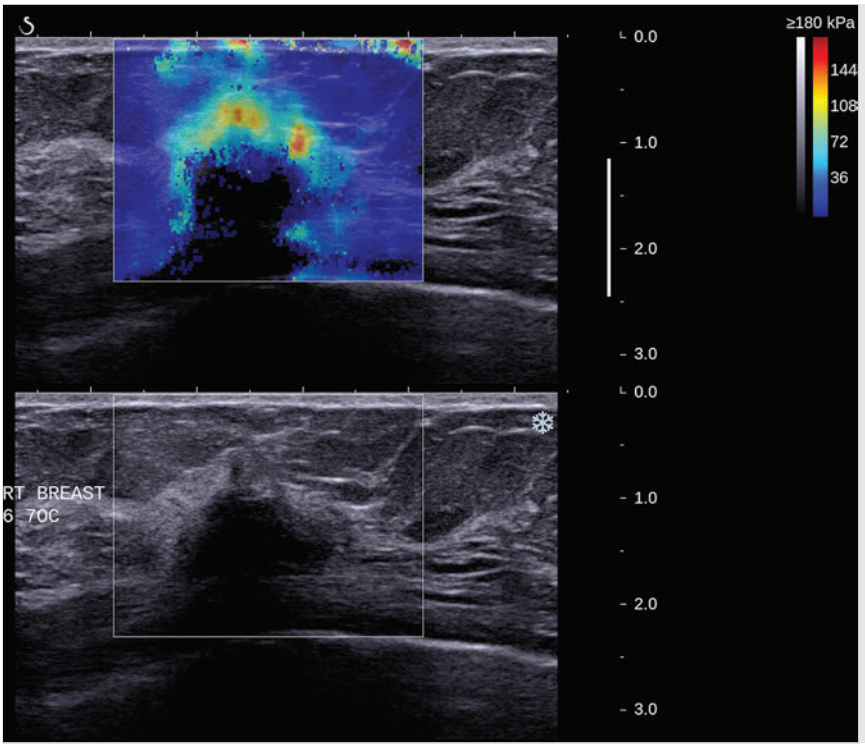

Fig. 5.33 In some cancers shear waves do not propagate as expected and a shear wave speed cannot be obtained. In these cases, the lesion is not color-coded. However, there is often a rim of high stiffness values that can be used to classify the lesion as malignant, as can be seen in this case.

SWE; and 0.982 for the combined data. In a study of 48 breast lesions, Athanasiou et al[52] found similar results with similar stiffness values for benign lesions (45 ± 41 kPa) and malignant lesions (147 ± 40 kPa) (p < 0.001). The results suggest the addition of SWE findings to those of conventional ultrasound could decrease the number of biopsies performed in benign lesions.

In a small series Evans et al[20] found the sensitivity and specificity for SWE (97% and 83%) combined with the results of B-mode imaging to be greater than B-mode imaging alone (87% to 78%). In their series, they used a cutoff value of 50 kPa. They also confirmed that the technique is highly reproducible.

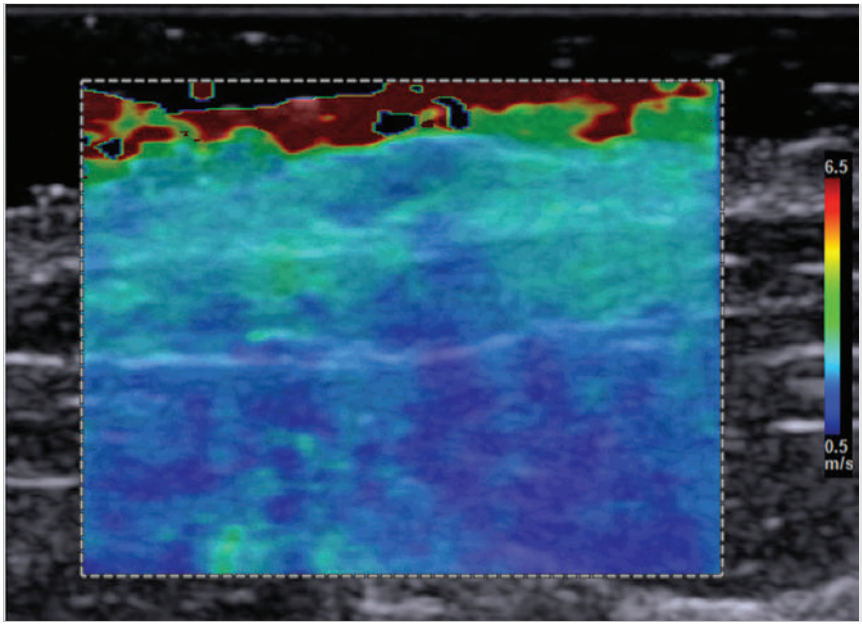

Fig. 5.34 If too much pressure is applied with the transducer (precompression), the near field in shear wave elastogram will appear stiff (red) as in this case. This can be corrected by decreasing the pressure being applied by the transducer.

Based on a recent large multicenter study (BE1), a cutoff value of 80 kPa (5.2 m/s) was determined to distinguish benign from malignant lesions.[17] In this trial, the researchers demonstrated that when SWE was added to BI-RADS classification in B-mode imaging, diagnostic accuracy increased. They found that the evaluation of SWE signal homogeneity and lesion to fat ratios were the best differentiators of benign and malignant lesions. The addition of SWE increased the characterization of lesions over BI-RADS alone, with a sensitivity and specificity of 93.1% and 59.4% in BI-RADS and 92.1% and 70.4% with the addition of SWE. The authors comment that the major value of the addition of SWE is in BI-RADS 3 and 4a lesions, where the SWE results were used to upgrade or downgrade the suspicion of malignancy for these lesions. The same study also included an analysis of reproducibility, which was very high.[53]

The BE1 study rules can be summarized as:

1. Any of the features analyzed in SWE were able to globally improve the diagnostic performance (area under the ROC curves) of the BI-RADS scoring system. This means that SWE features have to be combined with the B-mode features, in order to complement the BI-RADS classification, and should not be used alone in comparison to the BI-RADS classification.
2. The best performing SWE features were the "quantification" of the maximum stiffness of the lesion (inside or on the periphery), as E_{max} measurement Q Box (ROI) or a visual color assessment (5-point color scale).
3. The publication came out with suggested aggressive and conservative rules (i.e., using different stiffness thresholds) to help assess the level of suspicion of the breast masses, depending on their initial BI-RADS score. In the studied population:
   a) All BI-RADS 3 masses with high stiffness (E_{max} > 160kPa [7.3 m/s] or color red with SWE scale at 180 kPa [7.7 m/s]) could have been upgraded to biopsy. This would have enabled the early management of BI-RADS 4 breast cancers.
   b) BI-RADS 4a masses with low stiffness could have been downgraded to follow-up. This would have increased the specificity and positive predicitive value for biopsy of the ultrasound diagnosis.
      a) Aggressive rule: low stiffness would be considered with E_{max} below 80 kPa (5.2 m/s) or light blue color or below with SWE scale set at 180 kPa (7.7 m/s).
      b) Conservative rule: low stiffness would be considered with E_{max} below 30 kPa (3.2 m/s) or dark blue color or below with SWE scale set at 180 kPa (7.7 m/s).
      c) The aggressive rule would have enabled a higher improvement in specificity; however BI-RADS 4 cancers would have been downgraded to follow-up. With the conservative rule, all cancers would have remained in the initial biopsy group with a still significant increase in specificity.

Quantitative SWE using ARFI can be used for characterizing breast masses. In a series of 161 masses including 43 malignancies, using a shear wave speed cutoff of 3.6 m/s (38 kPa), a sensitivity of 91% and a specificity of 80.6% were achieved.[22]

3D-shear wave elastography is in development[15] and but no recommendations can be made at this time for its use.

Point Shear Wave Elastography

When using Virtual Touch Quantification (VTQ, Siemens Ultrasound), where a single measurement is obtained from a small ROI, it is not possible to determine where the area of highest stiffness is located on the B-mode image. Multiple measurements within the lesion and surrounding tissue need to be obtained to acquire optimal measurements. The measurement within the tumor often results in "x.xx" signifying that an adequate shear wave for evaluation was not obtained.[10] Bai et al[54] reported that if a lesion is solid and the reading "x.xx" is obtained, the lesion is most likely a malignancy. With this assumption, they obtained a sensitivity and specificity of 63.4% and 100%.

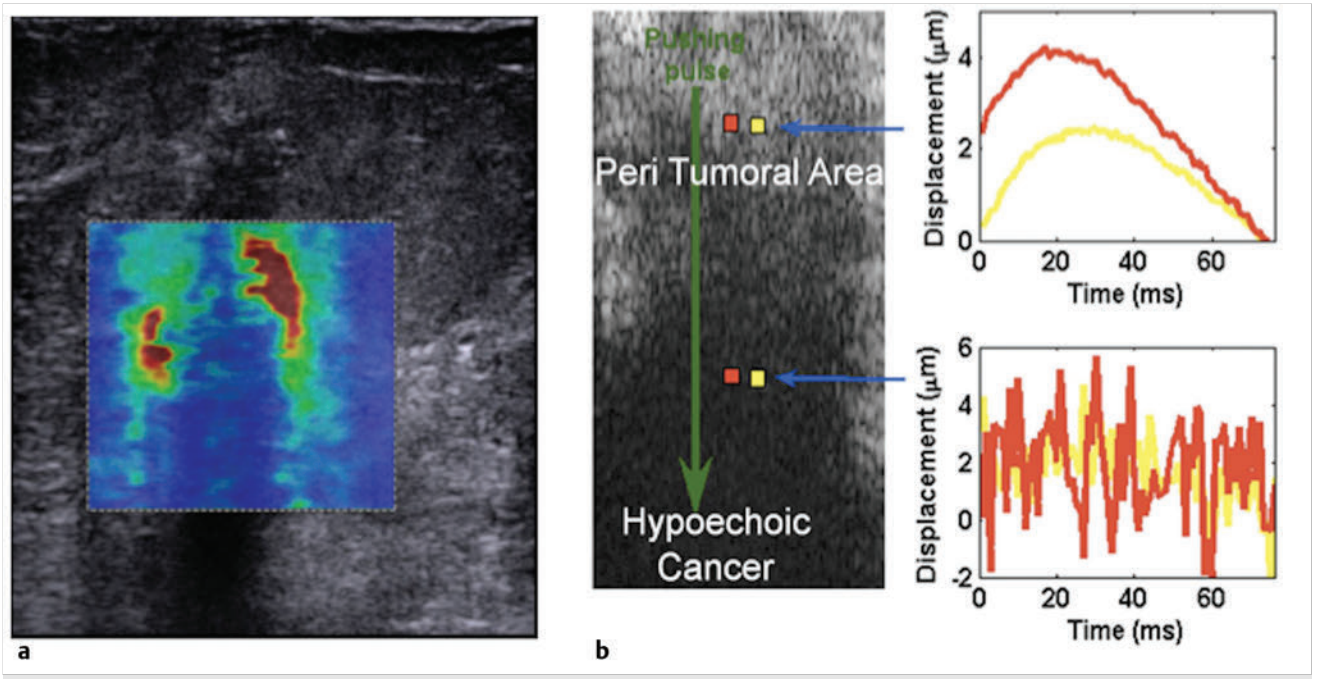

Fig. 5.35 Results from a 57-year-old woman with a palpable mass in her right breast. Mammographic and sonographic workup confirms a Breast Imaging–Reporting and Data System category (BI-RADS) 4B lesion. The lesion is a biopsy-proven poorly differentiated invasive ductal cancer. (**a**) The cancer is the hypoechoic mass in the deeper portion of the image. Two waveforms were obtained using the acoustic radiation force impulse technique. The one taken deeper is from the hypoechoic invasive ductal cancer. The more superficial one is taken in the peritumoral area. Note that the waveform obtained from the cancer is all noise and not interpretable. The waveform in the adjacent peritumoral tissue has more noise than signal in the fat, but the waveform is interpretable and provides a shear wave speed. (**b**) Shear wave image from the same patient. In this image, a color display representing the speed of the shear wave (V_s) is overlaid on the B-mode image. Note that the tumor with just noise in the shear wave signal is color-coded blue, representing a low V_s. This appearance gives the impression that the tumor is soft and so it can be mistaken for a benign lesion. In this case, the peritumoral tissues are coded red (high V_s) in the area where an adequate shear wave signal is obtained. However, not all cases of blue-colored cancers have the peritumoral red ring, which can still result in a false-negative interpretation. (Reproduced with permission from Barr RG. shear wave imaging of the breast: still on the learning curve. J Ultrasound Med 2012; 31:347–350.)

5.5 Quality Factor and/or Confidence Maps

In very hard lesions such as invasive cancers, the shear wave may not propagate in an orderly fashion. No results are therefore obtained and the area with no results is not color-coded. In these areas, interpretation is not possible. However, as previously discussed, in general the desmoplastic reaction of the tumor will be hard surrounding the tumor and appear as a hard (red) halo surrounding the lesion. Even if the entire mass is not coded as hard, heterogeneity of the shear wave image is part of the criteria for a suspicious lesion. Care must be taken with precompression as this can also create the same appearance of a rim of stiffness (halo) around a benign lesion.[30]

In a large number of malignant lesions, the area identified on B-mode as the hypoechoic mass often does not code on SWE because a shear wave is not identified or may code with a low SWS. Bai et al found that 63% of breast malignancies have this finding.[54] Preliminary work in the evaluation of this phenomenon suggests that shear waves may not propagate as expected in some malignant lesions (▶ Fig. 5.35).[55]

Evaluation of the shear waves in these malignant lesions demonstrates significant noise that may be incorrectly interpreted as a low shear wave speed by the algorithm. The addition of a quality measure that evaluates the shear waves generated and determines if they are adequate for an accurate SWS measurement in meters per second or in kilopascals will help in eliminating possible false negative findings (▶ Fig. 5.36).[56]

In a recent study[56] the addition of a quality measure (QM) in shear wave imaging of the breast limited false negative findings (sensitivity without QM, 22/46 (48%, 95% confidence interval [CI]: 33–63%), with QM, 42/46 (91%, 95% CI: 79–98%, $p < 0.0001$)).

5.5.1 Limitations

The shear waves are detected and measured by B-mode ultrasound. When areas in the B-mode image show extremely low signal (anechoic), the echo signal is too low for successful shear wave detection, and these areas are not color-coded in the elastogram. This can occur with marked shadowing such as seen with ribs, tumors with significant shadowing, and areas with macrocalcifications.[10]

Shear waves will not propagate through simple cysts and the cysts, too, will not be color-coded.

5.6 Published Guidelines

Published guidelines for the use of both SE and SWE for evaluation of breast lesions have been produced by the

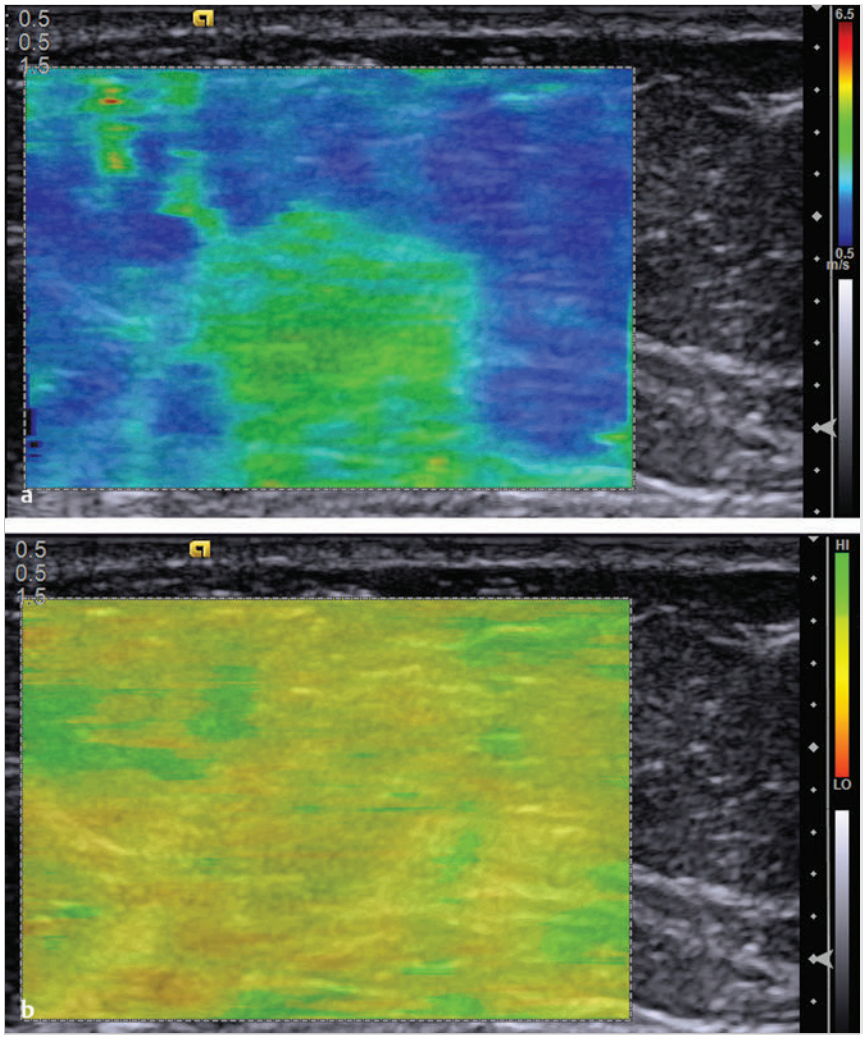

Fig. 5.36 (**a**) Velocity map from a two-dimensional shear wave elastogram from a 64-year-old with an invasive ductal cancer. The maximum shear wave speed is 3.2 m/s suggestive of a benign lesion. However, (**b**) the quality map from the same data demonstrates that the mass has poor shear waves (yellow) and the velocity data should not be assumed as accurate. In general, when the quality map is poor (yellow or red) and the shear wave speed of the lesion is suggestive of a benign lesion, the lesion should be considered malignant (unless it is a simple cyst).

European Federation for Societies for Ultrasound in Medicine and Biology (EFSUMB)[25] and the World Federation for Ultrasound in Medicine and Biology (WFUMB).[26]

5.7 Conclusion

Elasticity imaging of the breast can be performed using several techniques. These techniques all have a high sensitivity and specificity for characterizing breast lesions as benign or malignant. Although the techniques are easy to perform, attention to detail is required to obtain optimal images for interpretation. Each of the techniques has advantages and disadvantages. Further comparative studies are needed to determine which technique or combination of techniques is most appropriate for various clinical problems. The bull's eye artifact seen with SE has been shown to be extremely helpful in characterization of cystic lesions.[27] These techniques are now maturing, but continued work on standardizing them is required.

There are several elastography findings that are unique to the breast. The size change observed in SE as compared to B-mode imaging in both benign (smaller) and malignant lesions (larger) appears to only occur in the breast. Further correlative studies with surgical pathology are needed to determine if the actual size of a malignant tumor is better defined by the elastographic size or the B-mode size. More detailed correlative studies with pathology are needed to determine the exact nature of the stiffness identified on both SE and SWE surrounding malignancies. Preliminary work has demonstrated that the E/B ratio is predictive of tumor grade. Low-grade malignancies such as DCIS, mucinous cancers, or colloid cancers have E/B ratios near 1. Invasive ductal carcinomas have higher E/B ratios and the ratio appears to have some correlation with tumor grade.[34] Similar results have been found with SWE. Evans et al[57] have reported that breast cancers with higher mean stiffness values at SWE had poorer prognostic features. They found that high histological grade, large invasive size, lymph node involvement, tumor type, and vascular invasion all showed statistically significant positive association with high stiffness values. Further investigations need to be performed to determine if this information will prove clinically useful.

The development of 3D-elastography may help to improve lesion characterization and allow for evaluation of larger areas of breast tissue in a time efficient manner. Work is in progress on both 3D-SE (▶ Fig. 5.37; Hitachi Aloka Medical, press release February 7, 2011) and 3D-SWE (▶ Fig. 5.38; Supersonic Imagine, press release March 8, 2011). Evaluation with elastography in the coronal plane and the use of an opacity feature is

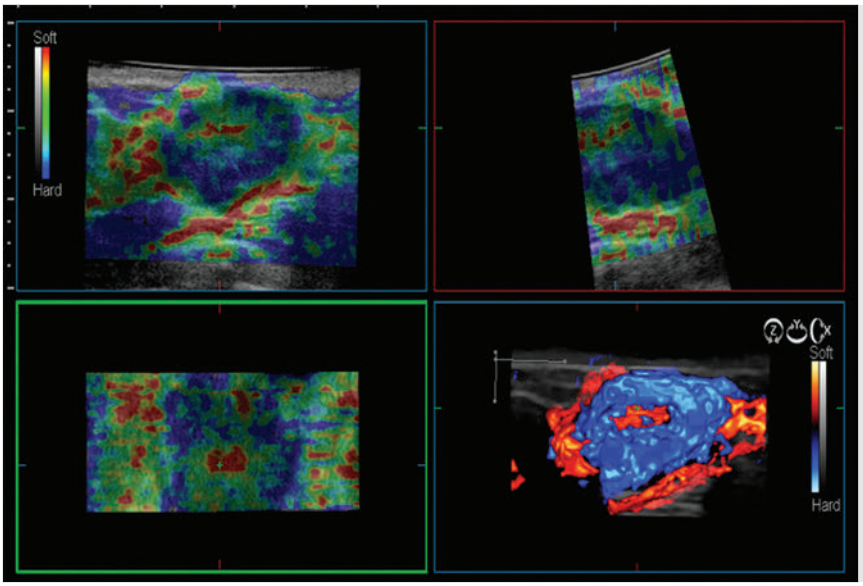

Fig. 5.37 The three-dimensional (3D) strain elastogram of an invasive ductal cancer obtained on a Hitachi system (Hitachi Aloka America, Wallingford, CT) displayed as a 3D rendering. In addition to 3D rendering, 2D slices from the 3D data can be can be displayed in any plane. (Courtesy of Hitachi Aloka Medical, press release of February 7, 2011.)

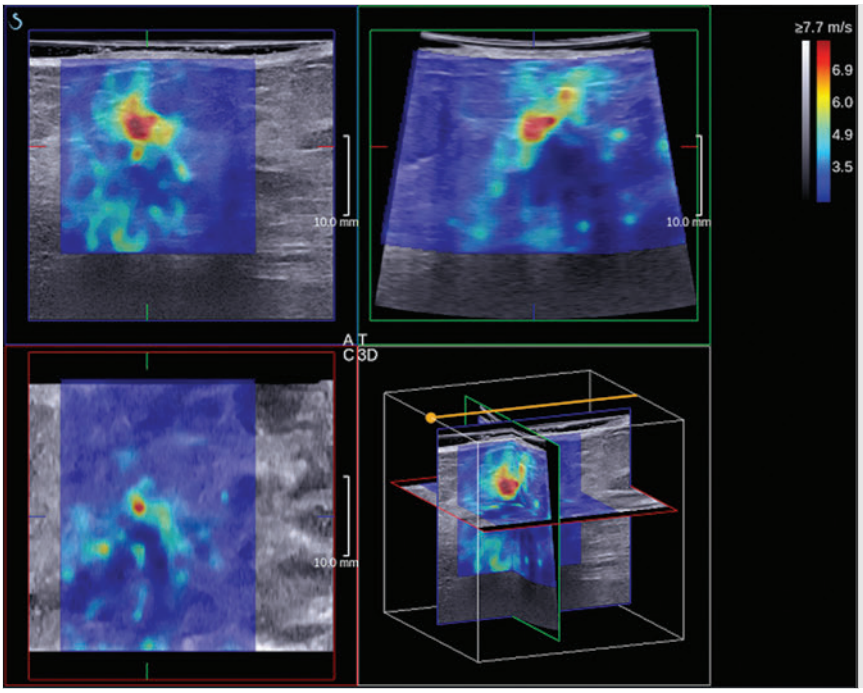

Fig. 5.38 Shear wave imaging can be performed using a three-dimensional (3D) probe allowing evaluation of an entire lesion with one data collection. In this example of an invasive ductal cancer, the image in the upper right is the shear wave elastogram from the imaging plane. The image in the upper left is the image perpendicular to the acquisition plane, whereas the lower left image is the coronal (C) plane. The bottom right image is the 3D depiction. In this case the pixels with high shear wave velocity (suggestive of a malignancy) are color-coded red.

presently being investigated in these systems. With only one acquisition in such systems, the tumor volume can be interrogated for spiculation, extent of invasion, and desmosplastic reaction. This may lead to improved presurgical planning and assessment of effectiveness of chemotherapy. With the ability to evaluate larger areas of the breast in shorter time, this technique may allow for elastography to be incorporated into breast screening exams.

In a large number of malignant breast lesions, the hypoechoic mass on B-mode did not code on SWE, because a shear wave was not identified or noise was detected and given a low SWS. Bai et al found that 63% of breast malignancies have this finding.[54] Preliminary work in the evaluation of this phenomenon suggests that shear waves may not propagate as expected in some malignant lesions (▶ Fig. 5.35).[56]

Evaluation of the shear waves in these malignant lesions demonstrates significant noise, which may be incorrectly interpreted as a low shear wave speed by the algorithm. The addition of a quality measure that evaluates the shear waves generated and determines if they are adequate for an accurate SWS measurement (in m/s or kPa) will help in eliminating possible false negative findings (▶ Fig. 5.36).[56]

There are several methods to obtain and interpret elastography of the breast. No comparative studies have been performed to suggest one method is better than another ▶ Fig. 5.39 summarizes the various methods of interpretation at the

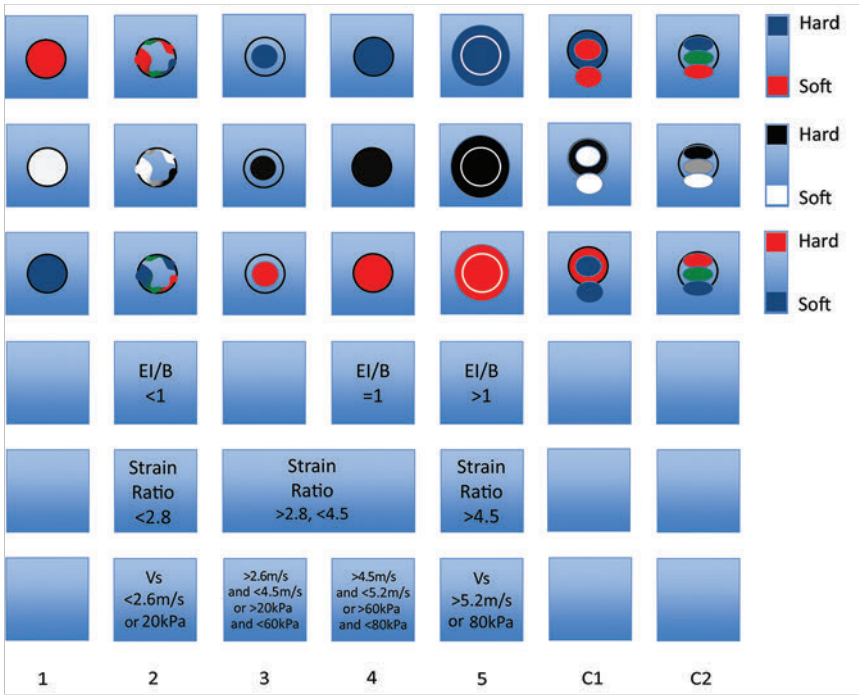

Fig. 5.39 The various methods of interpretation and how they are related based on a BI-RADS classification system.

present time and how they are related based on a BI-RADS classification system. Elastography systems and the applications themselves also continue to evolve, and new tools and new evidence will likely emerge. We anticipate that the direction of development, imaging methods, and diagnostic approaches will change and fragment in the future. It appears that elastography has already become an essential medical tool in the field of breast imaging.

References

[1] Jellins J, Kossoff G, Reeve TS. Detection and classification of liquid-filled masses in the breast by gray scale echography. Radiology 1977; 125(1):205–212

[2] Hilton SV, Leopold GR, Olson LK, Willson SA. Real-time breast sonography: application in 300 consecutive patients. AJR Am J Roentgenol 1986; 147(3): 479–486

[3] Stavros AT, Thickman D, Rapp CL, Dennis MA, Parker SH, Sisney GA. Solid breast nodules: use of sonography to distinguish between benign and malignant lesions. Radiology 1995; 196(1):123–134

[4] American College of Radiology (ACR). ACR BI-RADS (Breast Imaging-Reporting and Data System)—Ultrasound. 4th ed. Reston, VA; American College of Radiology; 2003

[5] Tanter M, Bercoff J, Athanasiou A et al. Quantitative assessment of breast lesion viscoelasticity: initial clinical results using supersonic shear imaging. Ultrasound Med Biol 2008; 34(9):1373–1386

[6] Ophir J, Céspedes I, Ponnekanti H, Yazdi Y, Li X. Elastography: a quantitative method for imaging the elasticity of biological tissues. Ultrason Imaging 1991; 13(2):111–134

[7] Samani A, Zubovits J, Plewes D. Elastic moduli of normal and pathological human breast tissues: an inversion-technique-based investigation of 169 samples. Phys Med Biol 2007; 52(6):1565–1576

[8] Frey H. [Real-time elastography: a new ultrasound procedure for the reconstruction of tissue elasticity][in French] Radiologe 2003; 43(10):850–855

[9] Krouskop TA, Wheeler TM, Kallel F, Garra BS, Hall T. Elastic moduli of breast and prostate tissues under compression. Ultrason Imaging 1998; 20(4):260–274

[10] Barr RG. Sonographic breast elastography: a primer. J Ultrasound Med 2012; 31(5):773–783

[11] Ueno EIA. Diagnosis of breast cancer by elasticity imaging. Eizo Joho Medical. 2004; 36:2–6

[12] Barr RG, Zhang Z. Shear-wave elastography of the breast: value of a quality measure and comparison with strain elastography. Radiology 2015; 275(1): 45–53

[13] Bluemke DA, Gatsonis CA, Chen MH et al. Magnetic resonance imaging of the breast prior to biopsy. JAMA 2004; 292(22):2735–2742

[14] Morrow M. Magnetic resonance imaging in breast cancer: one step forward, two steps back? JAMA 2004; 292(22):2779–2780

[15] Barr RG. Breast Elastography. New York, NY:Thieme Publishers;2015

[16] Barr RG, Destounis S, Lackey LB II, Svensson WE, Balleyguier C, Smith C. Evaluation of breast lesions using sonographic elasticity imaging: a multicenter trial. J Ultrasound Med 2012; 31(2):281–287

[17] Berg WA, Cosgrove DO, Doré CJ et al; BE1 Investigators. Shear-wave elastography improves the specificity of breast US: the BE1 multinational study of 939 masses. Radiology 2012; 262(2):435–449

[18] Chiorean AD, Dudea MM et al. Real-time ultrasound elastography of the breast: state of the art. Medical Ultrasonography 2008; 10:73–82

[19] Cho N, Moon WK, Kim HY, Chang JM, Park SH, Lyou CY. Sonoelastographic strain index for differentiation of benign and malignant nonpalpable breast masses. J Ultrasound Med 2010; 29(1):1–7

[20] Evans A, Whelehan P, Thomson K et al. Quantitative shear wave ultrasound elastography: initial experience in solid breast masses. Breast Cancer Res 2010; 12(6):R104

[21] Itoh A, Ueno E, Tohno E et al. Breast disease: clinical application of US elastography for diagnosis. Radiology 2006; 239(2):341–350

[22] Tozaki M, Isobe S, Sakamoto M. Combination of elastography and tissue quantification using the acoustic radiation force impulse (ARFI) technology for differential diagnosis of breast masses. Jpn J Radiol 2012; 30(8): 659–670

[23] Ueno EI, Bando H, Tohno E, Waki K, Matsumura T. New quantitative method in breast elastography: fat lesion ratio (FLR). Paper presented at 93rd Scientific Assembly and Annual Meeting of the Radiological Society of North America; November 25–30, 2007; Chicago, IL

[24] Destounis S, Arieno A, Morgan R et al. Clinical experience with elasticity imaging in a community-based breast center. J Ultrasound Med 2013; 32(2): 297–302

[25] Cosgrove D, Piscaglia F, Bamber J et al. EFSUMB guidelines and recommendations on the clinical use of ultrasound elastography: part 2: clinical applications. Ultraschall Med 2013; 34(3):238–253

[26] Barr RG, Nakashima K, Amy D et al. WFUMB guidelines and recommendations for clinical use of ultrasound elastography: part 2: breast. Ultrasound Med Biol 2015; 41(5):1148–1160

[27] Barr RG, Lackey AE. The utility of the "bull's-eye" artifact on breast elasticity imaging in reducing breast lesion biopsy rate. Ultrasound Q 2011; 27(3):151–155
[28] Nightingale K, McAleavey S, Trahey G. Shear-wave generation using acoustic radiation force: in vivo and ex vivo results. Ultrasound Med Biol 2003; 29 (12):1715–1723
[29] Nightingale K, Soo MS, Nightingale R, Trahey G. Acoustic radiation force impulse imaging: in vivo demonstration of clinical feasibility. Ultrasound Med Biol 2002; 28(2):227–235
[30] Barr RG, Zhang Z. Effects of precompression on elasticity imaging of the breast: development of a clinically useful semiquantitative method of precompression assessment. J Ultrasound Med 2012; 31(6):895–902
[31] Nakashima K, Moriya T. Comprehensive ultrasound diagnosis for intraductal spread of primary breast cancer. Breast Cancer 2013; 20(1):3–12
[32] Hall TJ, Zhu Y, Spalding CS. In vivo real-time freehand palpation imaging. Ultrasound Med Biol 2003; 29(3):427–435
[33] Barr RG. Real-time ultrasound elasticity of the breast: initial clinical results. Ultrasound Q 2010; 26(2):61–66
[34] Grajo JR, Barr RG. Strain elastography for prediction of breast cancer tumor grades. J Ultrasound Med 2014; 33(1):129–134
[35] Park JSM. Inter and intraobserver agreement in the interpretation of ultrasound elastography of breast lesions. Radiological Society of North America 93rd Scientific Assembly and Annual Meeting; 2007; Chicago, IL.
[36] Chiorean ADM, Dumitriu D et al. Short analysis on elastographic images of benign and malignant breast lesions based on color and hue parameters. Ultraschall Med 2008; 29:OP2–13
[37] Duma MCA, Dudea S et al. Breast lesions: correlations between ultrasound BI-RADS classification and UENO-ITOH elastography score. Ultraschall in der Medizin. 2008;Suppl. 1: OP2–12.
[38] Cho N, Moon WK, Park JS, Cha JH, Jang M, Seong MH. Nonpalpable breast masses: evaluation by US elastography. Korean J Radiol 2008; 9(2):111–118
[39] Scaperrotta G, Ferranti C, Costa C et al. Role of sonoelastography in non-palpable breast lesions. Eur Radiol 2008; 18(11):2381–2389
[40] Tan SM, Teh HS, Mancer JF, Poh WT. Improving B mode ultrasound evaluation of breast lesions with real-time ultrasound elastography—a clinical approach. Breast 2008; 17(3):252–257
[41] Zhi H, Xiao XY, Yang HY et al. Semi-quantitating stiffness of breast solid lesions in ultrasonic elastography. Acad Radiol 2008; 15(11):1347–1353
[42] Zhu QL, Jiang YX, Liu JB et al. Real-time ultrasound elastography: its potential role in assessment of breast lesions. Ultrasound Med Biol 2008; 34(8):1232–1238
[43] Raza S, Odulate A, Ong EM, Chikarmane S, Harston CW. Using real-time tissue elastography for breast lesion evaluation: our initial experience. J Ultrasound Med 2010; 29(4):551–563
[44] Chang JM, Moon WK, Cho N, Kim SJ. Breast mass evaluation: factors influencing the quality of US elastography. Radiology 2011; 259(1):59–64
[45] Farrokh A, Wojcinski S, Degenhardt F. [Diagnostic value of strain ratio measurement in the differentiation of malignant and benign breast lesions] Ultraschall Med 2011; 32(4):400–405
[46] Thomas A, Degenhardt F, Farrokh A, Wojcinski S, Slowinski T, Fischer T. Significant differentiation of focal breast lesions: calculation of strain ratio in breast sonoelastography. Acad Radiol 2010; 17(5):558–563
[47] Zhi H, Xiao XY, Yang HY, Ou B, Wen YL, Luo BM. Ultrasonic elastography in breast cancer diagnosis: strain ratio vs 5-point scale. Acad Radiol 2010; 17 (10):1227–1233
[48] Alhabshi SM, Rahmat K, Abdul Halim N et al. Semi-quantitative and qualitative assessment of breast ultrasound elastography in differentiating between malignant and benign lesions. Ultrasound Med Biol 2013; 39(4):568–578
[49] Stachs A, Hartmann S, Stubert J et al. Differentiating between malignant and benign breast masses: factors limiting sonoelastographic strain ratio. Ultraschall Med 2013; 34(2):131–136
[50] Shiina T, Nightingale KR, Palmeri ML et al. WFUMB guidelines and recommendations for clinical use of ultrasound elastography: Part 1: basic principles and terminology. Ultrasound Med Biol 2015; 41(5):1126–1147
[51] Chang JM, Won JK, Lee KB, Park IA, Yi A, Moon WK. Comparison of shear-wave and strain ultrasound elastography in the differentiation of benign and malignant breast lesions. AJR Am J Roentgenol 2013; 201(2):W347–56
[52] Athanasiou A, Tardivon A, Tanter M et al. Breast lesions: quantitative elastography with supersonic shear imaging—preliminary results. Radiology 2010; 256(1):297–303
[53] Cosgrove DO, Berg WA, Doré CJ et al. BE1 Study Group. Shear wave elastography for breast masses is highly reproducible. Eur Radiol 2012; 22(5):1023–1032
[54] Bai M, Du L, Gu J, Li F, Jia X. Virtual touch tissue quantification using acoustic radiation force impulse technology: initial clinical experience with solid breast masses. J Ultrasound Med 2012; 31(2):289–294
[55] Barr RG. Shear wave imaging of the breast: still on the learning curve. J Ultrasound Med 2012; 31(3):347–350
[56] Barr RG, Zhang Z. Shear-wave elastography of the breast: value of a quality measure and comparison with strain elastography. Radiology 2015; 275(1): 45–53
[57] Evans A, Whelehan P, Thomson K et al. Invasive breast cancer: relationship between shear-wave elastographic findings and histologic prognostic factors. Radiology 2012; 263(3):673–677

6 Elastography of the Thyroid Gland

Vito Cantisani, Hektor Grazhdani, Emanuele David, Fabrizio Calliada, Nicola Di Leo, Mattia DiSegni, Antonio Masciotra, Carlo Catalano, and Ferdinando D'Ambrosio

6.1 Introduction

Thyroid nodules are reported to be found in 33% of adults between the ages of 18 and 65[1] with other studies showing a prevalence of greater than 50% in those over the age of 65.[2] Although most thyroid nodules are benign, the prevalence of thyroid cancer is as high as 5 to 15%,[3] and there has been a 2.4 times increase in the incidence of the thyroid cancer in the last 30 years.[4]

Ultrasound (US) is accurate and precise in the detection of thyroid nodules, but it has a relatively low diagnostic performance for the differentiation between benign and malignant nodules.[5] Even though US features such as micro- or macrocalcifications, marked hypoechogenicity, taller than wide shape, and thick irregular or lobulated margins are correlated with malignancy, they are not highly predictive for this diagnosis.[6,7]

Furthermore, US sensitivity and specificity have considerable variability from study to study and range between 52 and 97% and 26.6 and 83%, respectively.[8,9] The American Thyroid Association guidelines state that: "with the exception of suspicious cervical lymphadenopathy, which is a specific but insensitive finding, no single sonographic feature or combination of features is adequately sensitive or specific to identify all malignant nodules."[10] For this reason, in the cases with normal thyroid-stimulating hormone, fine needle aspiration biopsy (FNAB) is required for the nodules greater than 10 mm or those with suspicious ultrasound signs.[11,12,13] Apart for the large number of FNAB needed due to the high prevalence of thyroid nodules, with eventual repetitions and high costs, this tool is not highly accurate, presenting in various studies with a specificity of 60 to 98% and varying sensitivities from 54 to 90%.[14,15,16] Furthermore, indeterminate and nondiagnostic results are common. As a consequence, a significant number of patients receive unnecessary thyroid surgery, more for diagnostic than for therapeutic purposes. Considering that thyroid surgery has inherent risks, costs, and a certain level of complications, improvement and refinement of noninvasive nodule diagnosis is needed.

Ultrasound elastography is a novel and advanced technique for thyroid characterization on which significant research has been done in the last decade, with over 160 articles published. A firm, or hard, nodule consistency on palpation is associated with a high risk of malignancy. By assessing stiffness as indicator of malignancy, elastography has recently become an additional tool for thyroid nodule differentiation, in combination with conventional US and FNAB.

Techniques of elastography applied to the thyroid principally take two different approaches according to the type of compression force (excitation) used and elasticity evaluation done: the first is freehand strain elastography (SE) with its qualitative and semiquantitative variants, and the second is the quantitative approach of transducer-induced high acoustic pulse shear wave elastography (SWE), which measures the speed of the shear wave generated. SWE can be performed using the acoustic radiation force impulse (ARFI) technology either in a small range of interest (point shear wave elastography, p-SWE) or over a larger field of view using color-coding to visually display the stiffness values (two-dimensional shear wave elastography [2D-SWE]). A small range of interest (ROI) can then be placed at the site of interest and the stiffness value determined in that ROI. In addition, some 2D-SWE can be performed in real-time such as with the Aixplorer from SuperSonic Imagine or the Aplio 500 from Toshiba. There is also a variant of SE with semiquantitative results called *in vivo quasi-static elastography* that uses the internal (physiological) pulsations from neighboring structures–the carotid artery, in the case of the thyroid–to induce the displacement necessary to assess tissue elasticity. In this approach, no external pressure is required.

The guidelines of the European Federation of Societies for Ultrasound in Medicine and Biology (EFSUMB)[17] and those recently published by the World Federation of Societies for Ultrasound in Medicine and Biology (WFUMB)[18] provided a deep analysis of the various elastography techniques and their classifications, which offers clarity in the almost confusing panoply of techniques and denominations offered by the manufacturers.

With the main diagnostic issue being that of thyroid nodules, we will provide an overview of the various available techniques, the main results from the relevant literature and up-to-date research, and the current role of elastography in thyroid nodule characterization. Thereafter we will discuss the elastography of diffuse thyroid disease. Limitations and pitfalls of elastography will also be described.

6.2 Strain Elastography Imaging

6.2.1 Technique

Today strain elastography (SE) is the elastography method most widely available in ultrasound equipment for thyroid evaluation. SE may be performed on longitudinal or axial planes. However, some authors note that transverse (axial) scans through the thyroid are more susceptible to interference from carotid pulsations[19] and, therefore, are less suitable for SE utilizing external force. In these cases, longitudinal scans are preferred, as they are less susceptible to carotid pulsations and they also offer more thyroid gland for reference tissue. Usually a color-coded map of elastographic information indicating relative tissue stiffness is superimposed on the grayscale B-mode image, in what is called real-time SE. The map can also be displayed side-by-side with the B-mode image (twin view). If the elastographic data is displayed using a grayscale map, it is important to turn off the grayscale B-mode image on which it is superimposed, otherwise evaluation is difficult. Nowadays, the offline variants of SE are less used and real-time SE is provided by most manufacturers.

In the elasticity color map, or elastogram, the relatively stiffest structures, usually malignant nodules (with lowest elastic strain or no strain) are displayed in blue or red depending on the color scale used, while the soft, most-deformed tissues (with higher elastic strain) in red or green or blue. Some confusion has arisen because of the different color-coding systems

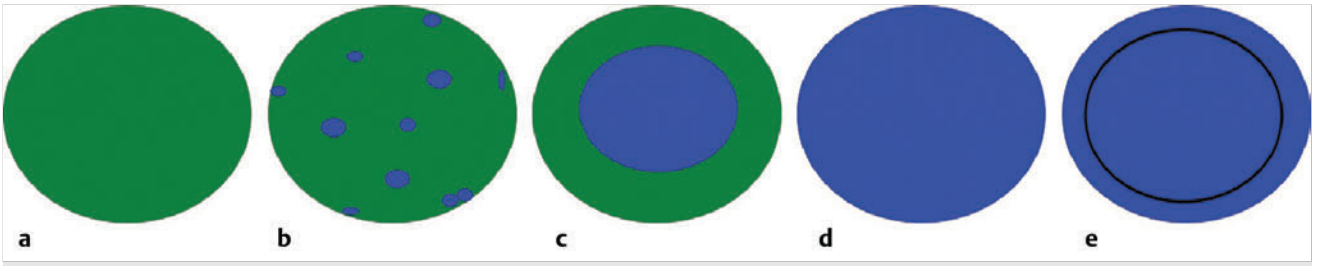

Fig. 6.1 Qualitative strain elastography scores: criteria according to Ueno et al applied to thyroid by Rago et al. (**a**) A score of 1 indicates even elasticity in the whole nodule. (**b**) A score of 2 indicates elasticity in a large part of the nodule. (**c**) A score of 3 indicates elasticity only at the peripheral part of the nodule. (**d**) A score of 4 indicates no elasticity in the nodule. (**e**) A score of 5 indicates no elasticity in the nodule or in the area showing posterior shadowing.

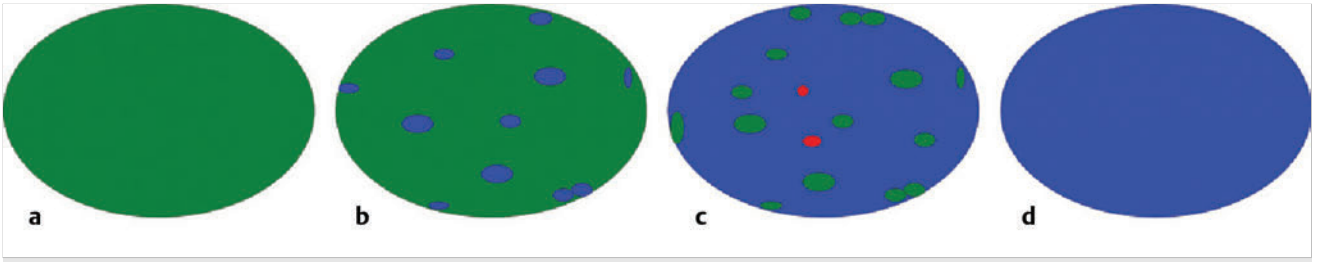

Fig. 6.2 Qualitative strain elastography scores: criteria according to Ito et al applied to the thyroid by Asteria. (**a**) A score of 1 indicates elasticity in the whole examined area. (**b**) A score of 2 indicates elasticity in a large part of the examined area. (**c**) A score of 3 indicates stiffness in a large part of the examined area. (**d**) A score of 4 indicates a nodule without elasticity.

selected by different manufacturers. However, lately, most manufacturers display stiff tissues in blue, soft tissues in red, and the intermediate tissues in green and the array of hues in between. The examiner should keep in mind that the default color scale of the machine can be customized by the user.

Most SE systems provide a color bar or scale to allow the user to optimize the amount of external compressive force applied for optimal imaging on that system.

The mechanical force in some variants of SE is applied internally— the physiologic pulsations of the carotid artery that offer sufficient displacement of the thyroid against the trachea.

SE allows for a qualitative and a semiquantitative assessment of elasticity.

6.2.2 Qualitative Strain Elastography

Scoring systems based on the predominant color pattern of the lesion with 4- or 5-point scales have been proposed as an attempt to standardize SE interpretation. Note that there are various default color scales used by manufacturers, some with blue as stiff and some with red as stiff. It is important to include the color scale when viewing images. In this chapter we will use blue as stiff and red as soft unless otherwise stated.

On SE, classic benign nodules present as soft, represented in the elastogram as red or green, and nodules suspicious for malignancy present as hard (high stiffness), represented in the elastogram as a pattern of blues or mostly blues (stiff).[20,21,22,23,24] Subjective scoring of the predominant color in a nodule, which originated from breast nodule research and has been adopted for the thyroid, uses the breast elastography scale of Itoh et al (▶ Fig. 6.1, ▶ Fig. 6.2)[25,26] or a similar scoring scale (which follows) for thyroid devised by Rubaltelli et al:[23]

- Score 1: homogenously soft
- Score 2: heterogenously soft (▶ Fig. 6.3)
- Score 3A: mixed with peripheral stiff areas
- Score 3B: mixed with central stiff areas
- Score 4: homogenously hard (▶ Fig. 6.4)

For the Rubaltelli scale, scores of 1 and 2 are characteristic of benign nodules, and scores of 3 and 4 are characteristic of malignant nodules, with higher scores having a higher probability of malignancy.[23]

With the Ito scale, scores of 1 and 2 are classified as suggestive for benignity, and higher scores, suspicious for malignancy. Other authors have found that assigning benignity to the score 3 further increases the specificity of the method for cancer detection.[27] Most authors using the Itoh scale consider hard—a score of 4 or 5—suggestive of malignancy, and soft—a score of 1 to 3—suggestive of benign nodules. Neither of the scoring systems appears to be superior.

The subjectively determined score combined with the operator-dependent freehand compression may contribute to interobserver variability.[20,28,29]

6.2.3 Semiquantitative Strain Elastography

Strain Ratio Elastography

Semiquantitative measurements can be obtained by comparing the stiffness of the nodule to that of normal thyroid or muscle.

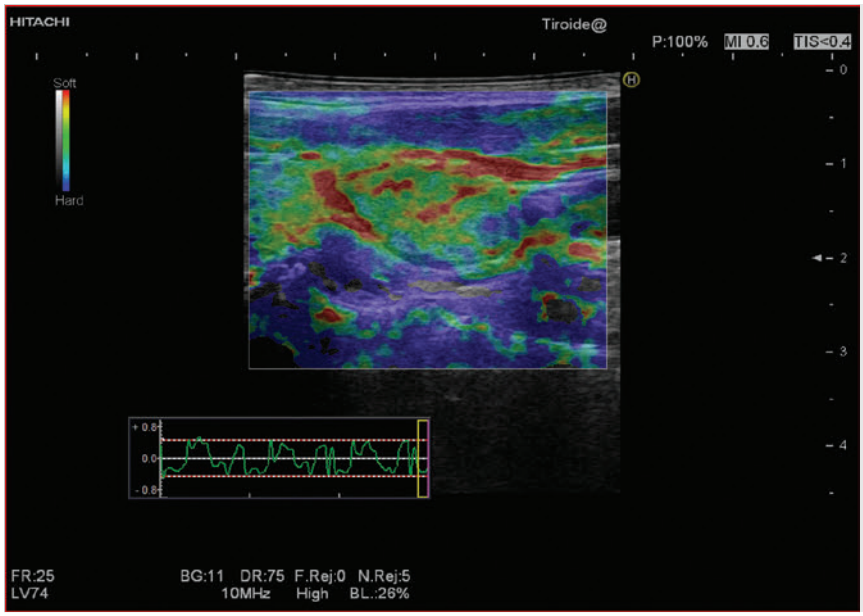

Fig. 6.3 SE of benign thyroid nodule with a score of 2 according to the scale of Asteria.

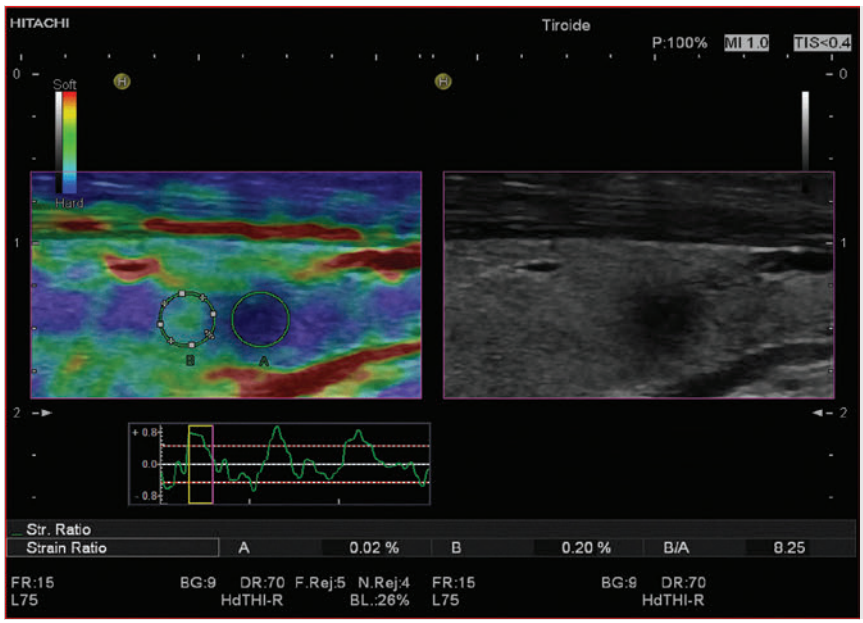

Fig. 6.4 Strain elastography of a malignant thyroid nodule that appears hard, with a strain ratio of 8.25 (in the malignant range).

The calculation of a strain ratio (SR) is obtained by placing a region of interest (ROI) in the normal thyroid parenchyma and a ROI usually on the nodule or any area of the thyroid under investigation. A strain ratio (SR) is generated in real-time by the device or offline by dividing the strain of the normal thyroid parenchyma by that of the nodule.[20,30,31] It is important that the two ROIs be at the same or similar tissue depths, with a difference of less than 10 mm, in order to obviate the effects of strain decay.[19] The SR evaluation does not directly represent the elasticity (i.e., Young's modulus) due to an array of technical reasons (mainly the difficulty of measuring the amount of the applied stress with the freehand techinique)[19] but it does measure how much stiffer the lesion is than normal thyroid.

The published papers to date, with some variation depending on the techniques used, show different cutoff values of SR ranging from 2[20] to 4[32,33,34] with low values assigned to benignity and values above the cutoff suggestive of cancer (▶ Fig. 6.4, ▶ Fig. 6.5, ▶ Fig. 6.6, ▶ Fig. 6.7).

In Vivo Strain Elastography Using Carotid Artery Pulsation

For the carotid artery pulsation SE, a semiquantitative measure similar to the strain ratio, called the elasticity contrast index (ECI), is calculated.[35] In this techinique, the transducer is held still, with slight contact with the skin over the thyroid. The thyroid vibrates because of carotid artery pulsations as the sole strain inductor, while the operator holds the probe in the transverse scan plane over the thyroid, gently and motionlessly. The systolic expansion of the carotid artery compresses the thyroid against the trachea with consequent anteroposterior expansion that is detected and used for strain measurements. US signals in

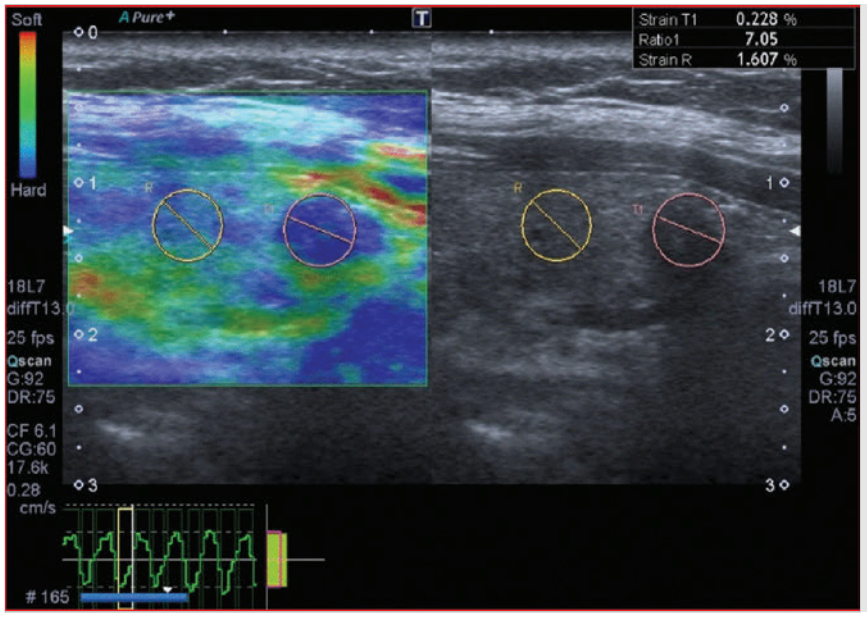

Fig. 6.5 Strain elastography of a papillary carcinoma. The lesion appears blue (hard) with strain ratio of 7.05, thus consistent with its malignant nature.

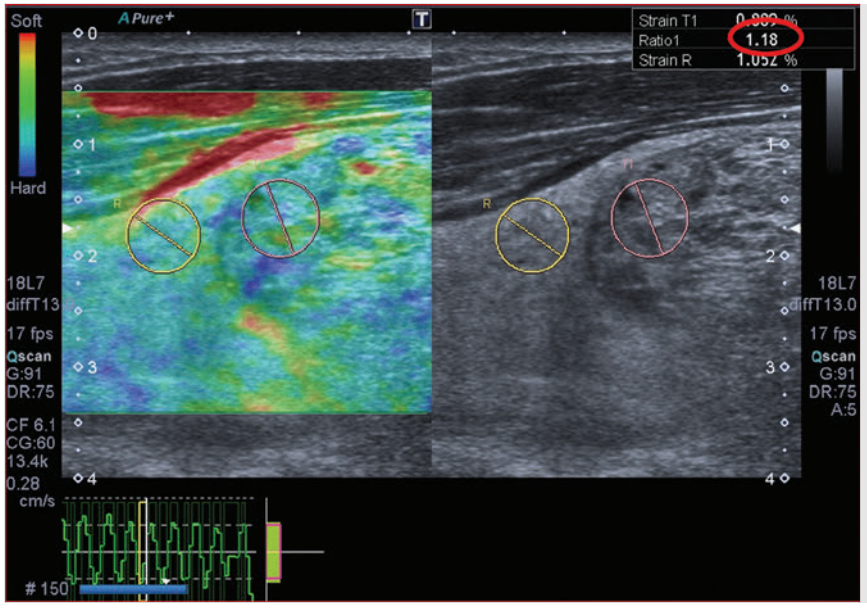

Fig. 6.6 Strain elastography of follicular hyperplasia. The lesion presents with elastographic score 2, with a strain ratio less than 2. Thus it is a benign lesion.

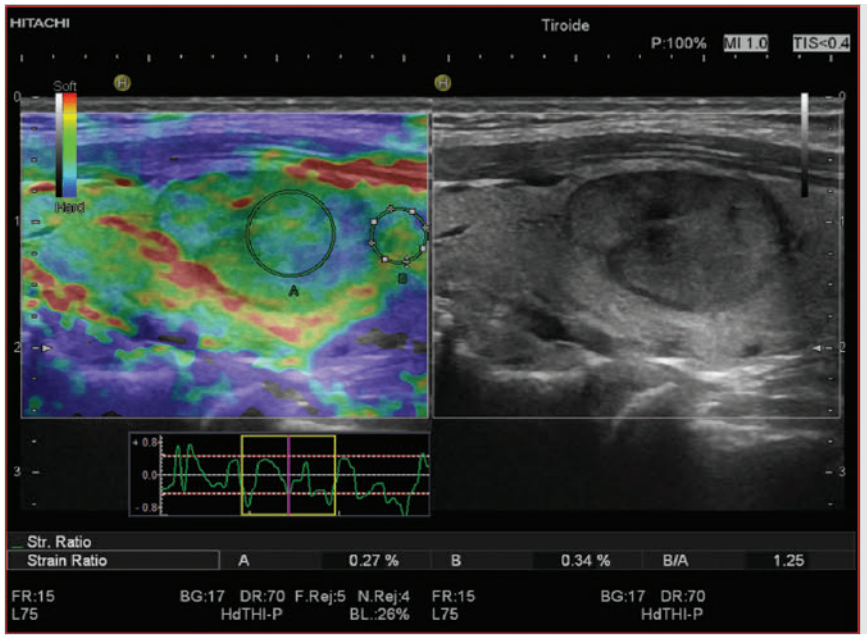

Fig. 6.7 Strain elastography of a benign thyroid nodule that appeared soft, with a strain ratio of 1.25. This corresponded with a final histological diagnosis of a benign nodule.

pre- and postcompression are tracked and strain images are generated.[20,36,37] A ratio of the strain near the carotid artery (a high strain area) divided by the thyroid nodule strain, called the thyroid stiffness index (TSI) or the elasticity contrast index (ECI), is calculated.[20,38,39,40,41] To maximize the efficacy, the software compares the highest strain near the carotid artery with the lowest strain in the nodule.

6.2.4 Tips and Tricks

1. Whatever color-coding is selected, it is important to bear in mind that what is displayed is a representation of the relative stiffness of the tissues in the field of view (FOV) and that SE is by no means capable of measuring absolute values of strain.
2. The measured strain is dependent on the amount of compression, which is always variable in SE. Nowadays, most of the manufacturers provide a real-time quality-assessment indicator during the compression, such as a numeric scale or an elasticity bar, color bar, or cycle-compression bar. By these means the operator obtains a feedback in real-time, whether his compression has reached a range estimated as reliable or if it is advisable to repeat it.
3. Some authors advocate that three different measurements of the SR should be taken and their average should be considered for elasticity assessment.[27,41,42]
4. The ROI for elasticity evaluation in SE should ideally be placed as close as possible to the transducer, as strain diminishes with distance from the transducer. However, the ROI must include the whole nodule and a portion of the surrounding thyroid parenchyma, with some authors advising 5 mm or more of parenchyma around the borders of the nodule.[43]
5. The normal parenchyma is required in the ROI as it serves as the normal reference tissue, whose elasticity is required along with that of the nodule for calculating the strain ratio.
6. The carotid artery and hard tissues, such as muscles and the trachea, should be not be included in the ROI as they notably alter the contrast and the displayed scale of the SE image.
7. During the examination, the patient is asked to extend the neck and stay still without breathing and swallowing for as much time as he or she can.
8. A good quantity of coupling gel is needed for assuring slight skin contact of the transducer. The B-mode focus is positioned at the nodule level or slightly below.
9. An elasticity image scale preset for the thyroid must be used. If not available, some modifications of the displayed elasticity scale may be needed for a correct representation of the thyroid parenchyma and nodule elasticity in the image.
10. The operator applies light freehand compressions in a regular repetitive manner and the quality of these compressions is checked with a graphic scale of quality or numerical values on the screen, depending on the equipment manufacturer. Operator experience is required for a good compression technique. The strain measured depends on amount of compression, and, for correct strain measurements, slight and uniform compressions are needed.

6.2.5 Limitations and Artifacts of SE

Calcifications inside a nodule, being very stiff, alter stiffness measurements and may make the nodule appear as stiff. On the other hand, the presence of colloid and cystic fluid also impair stiffness assessment.[21,29,44,45] The elastography signal inside a cyst is essentially noise due to fluid movement during compression; the result is low-quality strain estimates.[17,20] Thus, if the ROI is placed in a mixed solid and cystic area, the strain measurement is altered.

It has been shown that experienced operators have greater specificity in their results than those without experience.[46]

The pressure of the freehand of different radiologists is difficult to standardize and strain variations due to changes in the amplitude and velocity of compression are unavoidable.[20] Nonuniform compressions produce intraobserver and interobserver variability.[28]

For all elastographic methods, the fact that tissue becomes stiffer as it is stressed by focused compression is an important factor: precompression can result in misleadingly high stiffness readings, especially in superficial tissues.[20,45,47]

The color-coded scoring systems involve subjectivity in evaluation, as seen by the wide variability of performance of SE in different literature reports.[28,29,35]

Isthmic nodule evaluation with SE is limited in efficacy, as these nodules are compressed between the transducer and the trachea, both hard structures, and with very little normal thyroid, which is necessary as it serves as reference tissue.

Carotid artery pulsations adjacent to the thyroid induce deformations in the thyroid that interfere with the freehand compression-release and degrade the strain measurements. This effect is more pronounced with nodules that are adjacent to the carotid artery, especially those that are positioned anterior to the carotid artery, which suffer more from the interference of the carotid pulsation in RTSE evaluation.

Thyroid nodules deep in the posterior thyroid are subject to impaired transmission of compression and so experience less strain, which may make them appear artifactually stiff.[48]

The qualitative visual evaluation of color-coded elastograms is impaired mainly by subjectivity due to operator experience, but also by a certain amount of mottled noise. In SE, error in the estimation of tissue displacement leads to noise in the elastogram.[48] These areas of the elastogram, where accurate strain values cannot be computed, are not color-coded. Noise in elastogram brings about a further increase in the interpretation subjectivity.[20]

The added time needed to complete the elastography evaluation after the ultrasound examination is variable with the different techniques.[20]

The limitations of qualitative SE also apply to strain ratio SE. Further, in situations where the thyroid nodule or multiple nodules are so large that they occupy the whole thyroid lobe, there may not be enough normal thyroid left in the scan for placement of the second ROI to calculate the strain ratio. Also thyroid tissue outside a nodule may not be normal but may present with multinodular goiter or lymphocytic thyroiditis, both conditions with a hard tissue consistency that would alter the strain ratio.[20] These limitations also apply to SE with carotid artery pulsations.

One study found that stronger pressure with the freehand altered results, thus light and uniform compression for all measurements is important.[33]

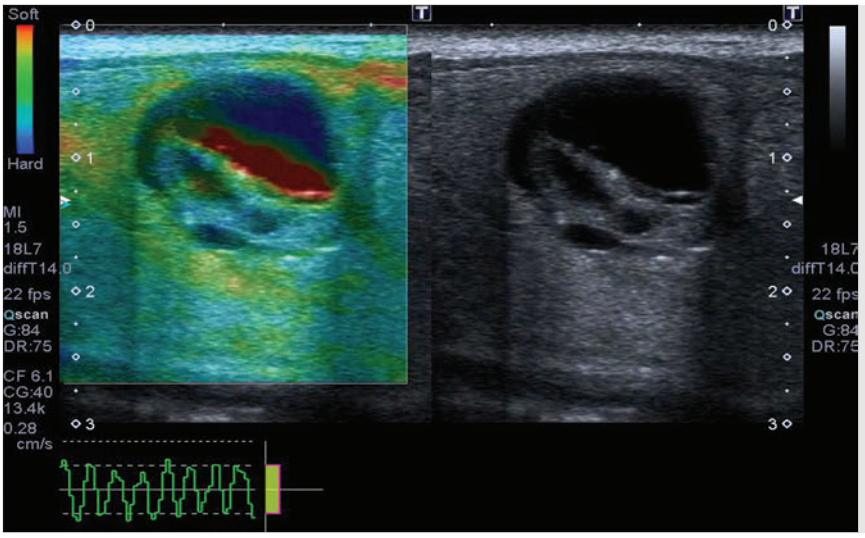

Fig. 6.8 Example of red-green-blue (RGB) sign in a cystic lesion.

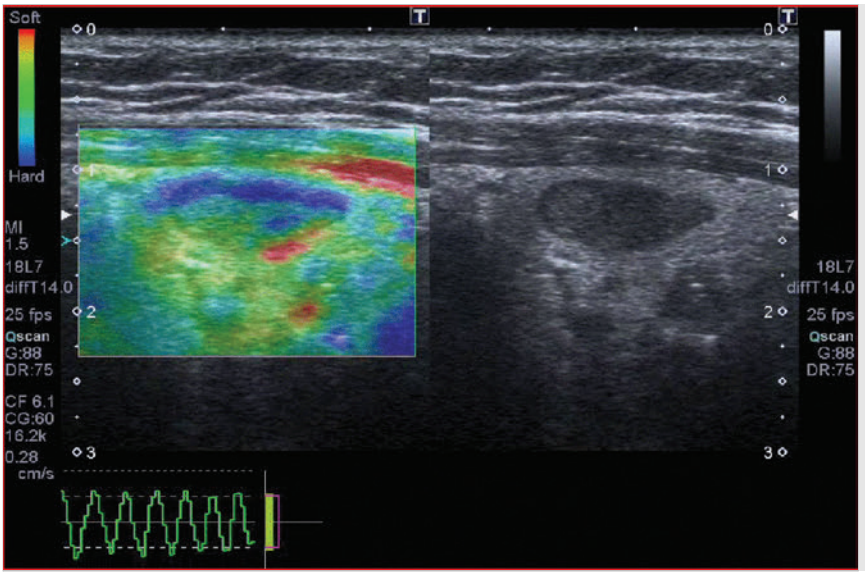

Fig. 6.9 Strain elastography of a FNAC proven thyroid indeterminate nodule (at cytology), which after surgery/at histology was diagnosed as hyperplasia. At qualitative evaluation, the lesion showed the rainbow sign, which can be assigned to score 2 according to Asteria.

To summarize, the literature; the above-mentioned limitations; the many and different technological solutions of SE; and the variable scoring systems, values, and cut-off points make results less comparable and to a certain extent, difficult to assess for validity.[51]

RGB (red-green-blue), or the three-color layer artifact, may appear in the elastograms of cystic lesions from some systems,[50,51] while the bull's eye artifact can be seen in others[52] (▶ Fig. 6.8). In mixed lesions, we also found a so-called rainbow sign (▶ Fig. 6.9).

During the free hand compression, the nodule can slip out of the US imaging plane and the operator does not have the lesion in the elastogram, or has only part of it. This can be corrected by performing the compression right on the lesion, i.e., in the right plane, moving the patient into a different and more stable position, with the chin slightly up on the opposite side, and also asking the patient to hold his breath.

6.2.6 Interpretation of Results

Although SE is reported to have high accuracy, as the number of studies, patients, and nodules have increased, more cautious results and suggestions for thyroid SE have emerged. There may be a preselection bias in these studies as some evaluate all patients with nodules while others evaluate a selected group of patients who had a high probability of malignancy based on B-mode findings.

Over time, some studies achieved lower sensitivities and positive predictive values around 80%,[27] but high to very high negative predictive values remain common to all studies, some reaching 99%.[19] Most authors used SE with scoring for their qualitative analysis, which was an attempt towards systematization of the SE method for reading elastograms; however, as reported in different studies,[23,44,53,54] scoring did not offer a

high and reproducible performance, and its utility has become a subject of debate.[55]

The discrepancies in performance of SE may also be related to the imperfection of the reference gold standard (fine needle aspiration biopsy [FNAB]) used in most studies, and only a few studies have used postsurgery histology as a reference standard.[56]

In a meta-analysis, 8 studies of qualitative SE, selected on the basis of a high rating in quality assessment, with a total of 639 thyroid nodules, were analyzed.[57] For the diagnosis of malignant thyroid nodules with elastography, the overall mean sensitivity of the 8 studies was 92% (95% confidence interval [CI], 88–96%) and the overall mean specificity was 90% (95% CI, 85–95). A significant heterogeneity was found for specificity in the different studies. Furthermore, the patient population was highly selected with a 24% prevalence of malignancy, which does not reflect typical clinical practice.

The encouraging initial results of qualitative SE were challenged by conflicting reports.[46,58] In a large retrospective study[26] of 703 nodules (217 malignant), SE was assessed with two different elastogram scoring systems. The results showed inferior performance of SE (sensitivity 65.4%, negative predictive value [NPV] 79.1%), compared with grayscale B-mode features in combination (sensitivity 91.7%, NPV 94.7%), so the authors concluded that elastography was not useful in recommending for fine needle aspiration cytology (FNAC). Similarly, another study,[58] based on 237 thyroid nodules (58 malignant), reported lower performance of SE in comparison with grayscale B-mode ultrasound.

On the contrary, a recent study[59] found good accuracy of SE (84%, odds ratio (OR) 29) in a cohort of 132 thyroid nodules with 40 malignancies. With regard to qualitative SE, a review and systematic meta-analysis based on Asteria's classification[60] applied in 20 studies including thyroid nodules was published. Pooled results of elastography showed a summary sensitivity of 85% (95% CI, 79–90%) and specificity of 80% (95% CI, 73–86%). The respective pooled negative predictive and positive predictive values were 97% (95% CI, 94–98%) and 40% (95% CI, 34–48%), respectively. The authors concluded that qualitative elastography has a fair specificity and sensitivity for diagnostic accuracy. Its major strength is the detection of benignity, especially when only completely soft nodules qualify as benign. The outcome of their analysis (pooled NPV 97%) shows that fine needle aspiration could safely be omitted in patients referred for analysis of their thyroid nodule when elastography shows it to be completely soft. This could prevent unnecessary invasive diagnostic procedures in a substantial portion of patients.

When combined in a single evaluation, the elastographic and B-mode ultrasound findings improved diagnostic performance, as shown by two additional studies[61,62] that demonstated increased sensitivity and negative predictive values. The multicenter study of Trimboli et al[62] with 498 nodules observed added value for B-mode ultrasound when combined with qualitative SE, reporting increased sensitivity for malignancy detection and a better selection of nodules needing cytology evaluation with FNAC.

In comparison with the contradictory results of qualitative SE in identifying malignancy, consistently improved results seemed to be obtained with semiquantitative SE. A study[27] found that in benign nodules, SR was 2.59 ± 2.12 and in malignant ones 9.10 ± 7.02. In another more recent study[64] on 97 patients using the Q-elastography technique (Toshiba) for the prediction of malignancy and with a SR cutoff value ≥ 2, sensitivity, specificity, positive predictive value (PPV), and NPV of 97.3%, 91.7%, 87.8%, and 98.2%, respectively, were obtained.

Wang et al[45] found the best SR cutoff value for suspicion of malignancy with different strain elastographic techniques was 3.79 with 97.8% sensitivity and 85.7% specificity. The area under the curve for the strain ratio was 0.92, whereas that for the 4-point scoring of real-time strain elastography (RTSE) was 0.85. For grayscale B-mode ultrasound features, microcalcification had the highest area under the curve, 0.72. Ding et al[31] reported the best SR cutoff points of two evaluations were 3.5 (82% sensitivity, 72% specificity) and 4.225 (81% sensitivity, 83% specificity).

However, at least one study found low accuracy for SR evaluation. Another study (conducted on a different machine) found that adding SR to the color-scale classification results does not improve the diagnosis; on the contrary, the association of the two brought about a lower diagnostic efficacy.[19,63,64]

Even more recently with the respect to the use of SR in diagnosis of malignancies, two comprehensive meta-analyses were published. In the first meta-analysis, published by Razavi et al,[65] both qualitative (elasticity score) and SR results were provided. In the paper, relevant information on more than 2624 patients and 3531 thyroid nodules (927 malignant and 2604 benign) in 24 studies were provided. Six ultrasound features (echogenicity, calcifications, margins, halo sign, shape, and color Doppler flow pattern) were compared with the elasticity score and strain ratio. The respective sensitivities and specificities were as follows: elasticity score, 82% and 82%; strain ratio, 89% and 82%; hypoechogenicity, 78% and 55%; microcalcifications, 50% and 80%; irregular margins, 66% and 81%; absent halo sign, 56% and 57%; nodule vertical development, 46% and 77%; and intranodular vascularization, 40% and 61%. They showed and confirmed that elastography appears to be both more sensitive and specific than each of the ultrasound features in thyroid nodule differentiation.

In a more recent study, Sun et al[66] performed a meta-analysis extending the previous meta-analyses to assess the diagnostic power of elastography in differentiating benign and malignant thyroid nodules using elasticity scores and SR assessments. A total of 5481 nodules in 4468 patients for elasticity score studies and 1063 nodules in 983 patients for SR studies published up until January 2013 were analyzed. The overall mean sensitivity and specificity of elastography for differentiation of thyroid nodules were 79% for elasticity-score assessment and 85% and 80% for strain-ratio assessment, respectively. The areas under the curve for the elasticity score and strain ratio were 0.8941 and 0.9285. Another issue is the role of SE in the evaluation of thyroid nodules of indeterminate FNAC.[43,52,53] In two studies[67,68] SE was reported as an accurate tool for the evaluation of nodules with indeterminate or nondiagnostic cytology and therefore potentially useful in selecting patients who are candidates for surgery. However, these results were not confirmed in another study that suggested the need for quantitative analytical assessment of nodule stiffness to improve SE efficacy.[69] A meta-analysis of qualitative SE published by Trimboli et al[62] achieved an area under the curve of 0.77 and concluded that SE has suboptimal diagnostic accuracy to diagnose thyroid

nodules previously classified as indeterminate. They advised further studies using other elastographic approaches and using combined RTSE and B-mode ultrasonography. More recently, Cantisani et al reported better results with an accuracy of 89.8% by using strain ratio SE.[55]

6.2.7 Drawbacks of SE

Freehand elastography (i.e., manual probe-mediated compression of the tissue) has intrinsic limitations related to the experience on the operator, the conformation of the patient's neck, and carotid artery pulsation. All these factors may influence the acquisition results. Operator experience also influences the assignment of elasticity scores using color scales, thus failing to insure objective and reproducible elastogram interpretation, and so, score assignment.

An early study focused on interobserver agreement of SE published by Park et al[28] reported no or poor interobserver agreement with the use of the Itoh scale for scoring. Subsequent studies reported good results for the SE 4-point scale with almost perfect interobserver agreement[47,59,70,71] and good intraobserver agreement.[72] One study found the interobserver agreement with use of the 4-point scale better than that with the use of the Thyroid Imaging–Reporting and Data System (TI-RADS) score.[71] Given the availability of scoring scales with 3 steps up to 6 steps, some authors advocate the use of simple scoring systems to obviate the interobserver variability.[19]

An attempt to develop an even more reproducible method of evaluation to use the strain ratio.[73] However, even in this case, the selection of the ROIs for calculating the SR is manual and may lead to error. A learning curve and experience influence the interobserver and intraobserver agreement, but when a standardized protocol is used in making compressions and selecting ROIs, the results were very good.[20,73]

Most papers showed no dependency of the elasticity assessment score on the nodule size.[20,24,44,71,74] However 2 studies had worse performance of SE with nodules < 1 cm in comparison with nodules > 1 cm[26,34] and 2 other studies reported unacceptable accuracy of qualitative SE for nodules < 5 mm.[44,75] On the contrary, a study[45] with 51 small solid nodules of 3 to 10 mm suggested that SE seemed to be useful even in small nodules: sensitivity 91%, specificity 89%, PPV 94%, and NPV 85%. Nodules > 3.5 cm have been reported not to be suitable for SE evaluation as they are larger than the possible ROI.[41,76]

Papillary carcinoma and its variants are the most common thyroid malignancies; the second most common histology is follicular carcinoma. A number of studies have documented that SE cannot differentiate follicular carcinoma from benign nodules[44,47,51,79,70,76] as it presents as elastic in almost half of the cases. In Bojunga et al's meta-analysis,[57] the authors' remark that most malignant nodules missed by elastography were follicular carcinomas, which can be soft and difficult to differentiate from benign nodules.

Furthermore, medullary, nondifferentiated, and metastatic carcinoma can also present as soft and cannot be diagnosed with elastography.[53,76] However, another study[74] found SE to be useful for predicting malignancy in nodules with nondiagnostic cytological findings by analyzing 101 patients with at least one indeterminate nodule. The authors reported a better performance of SE than ultrasound and the potential capability of SE for reducing unnecessary surgery.

Cystic areas produce artifacts at elastography, and evaluation of mixed cystic and solid nodules should be focused on the solid areas, whose small dimensions may not be suitable for elasticity assessment. Also when part of a nodule consists of benign tissue and the other portion is malignant, evaluation with elastography is difficult.

A study showed that a microcarcinoma (< 10 mm) in a very hard nodule with score 4 or 5 has a predilection to extrathyroid extension,[77] although another study did not find an increased risk of neck lymph node metastases in such type of nodules.[78]

With freehand SE, it is not possible to have equal compression–release cycles and to maintain exactly the same initial compression, and these variabilities confer variation in the strain and in the elastographic image.[20,28,35,76] Therefore complying with the quality indicator on the screen while executing freehand compression is crucial for an accurate evaluation of elasticity. Experience is needed for performing compression–release cycles that lead to reproducible and reliable elasticity readings. A study report claims that for liver elastography, an operator with experience of over 500 examinations produces better results.[79] However, to date, only one study evaluated the learning curve in the thyroid setting, showing a very steep learning curve, with constant and reproducible results after only 7 patients.[80]

Out-of-plane motion of the nodule during the compression–release cycles can impair strain measurements. Some manufacturers offer combined autocorrelation methods to address this issue.[19]

Because SE displays the relative strain of the tissues (in comparison of one against the other in the field of view) in color-coded elastograms, it is important to select a field of view (FOV) large enough to include healthy thyroid tissue, which serves as the standard for normal thyroid tissue strain. On the other hand, for nodules with an anterior position in the gland, the strap muscles should be left out of the FOV due to their stiffness, as they alter the measure of relative strain in the elasticity image; a malignant nodule may appear as soft (relative to the stiff strap muscles).

Another fact is that the strain values obtained during elastography can cover a very large range of values, much larger than the low range that can be displayed on a color-coded elastogram.[49] For this reason, an elastogram whose range of values has been optimized for a rather soft material will not display the variations in hard materials such as nodules and cancers well. Therefore, customization of the display scale according to the stiffness of the material under investigation is needed to obtain quality elastograms.[49] On the contrary, a strain ratio considers in the computation the full range of strain values and therefore may be more accurate. See the selected studies results in ▶ Table 6.1 and ▶ Table 6.2.

6.2.8 Interpretation of Results of Internal Quasi-Static Strain Elastography

This technique, also called in vivo carotid artery compression elastography, may provide, depending on the equipment, a thyroid stiffness index, or systolic thyroid strain index, (TSI) and an

Table 6.1 Diagnostic performance in malignancy detection of strain elastography with color-coded scale for elasticity evaluation, in selected studies

Study	No. of nodules	Sensitivity (%)	Specificity (%)	Reference standard
Rago et al 2007[24]	92	97	100	Surgery
Asteria et al 2008[54]	86	94	81	FNAB or surgery
Tranquart et al 2008[81]	108	100	93	FNAB
Hong et al 2009[44]	145	88	90	Surgery
Rubaltelli et al 2009[23]	51	82	86	FNAB or surgery
Lippolis et al 2011[69]	102	89	6	Presurgery of indeterminate cytology (follicular)
Moon et al 2012[78]	703	65	58	FNAB or surgery
Azizi et al 2013[82]	912	80	70	FNAB or surgery
Ko et al 2013[46]	367	89	81	FNAB or surgery
Mehrotra et al 2013[83]	146	90	79	FNAB or surgery
Ragazzoni et al 2012[59]	132	85	83	Surgery
Razavi et al 2013[65]	3531	82	82	FNAB or surgery
Nell et al 2015[60]	3908	79–90	73–86	FNAB or surgery
Sun et al 2015[66]	5481	79	85	FNAB or surgery

Abbreviation: FNAB, fine needle aspiration biopsy.

Table 6.2 Diagnostic performance of semi quantitative SE with strain ratio for elasticity evaluation, in selected studies

Study	No. of nodules	Sensitivity (%)	Specificity (%)	Reference standard
Dighe et al 2008*,[36]	62	100	79	FNAB or surgery
Cakir et al 2011[32]	391	73	70	Surgery
Cantisani et al 2012[63]	97	97.3	91.7	Surgery
Razavi et al 2013[65]	3531	89	82	FNAB or Surgery
Cantisani et al 2014[73]	354	93	92	FNAB or Surgery
Sun et al 2014[66]	54–81	85	80	FNAB or Surgery

*Dighe et al used carotid artery compression strain elastography.

Abbreviation: FNAB, fine needle aspiration biopsy.

elasticity contrast index (ECI). The TSI requires a FOV placed in axial direction, covering both the nodule and the carotid artery. The software calculates a ratio (TSI): the strain of the carotid artery, which is very stiff, divided by the lowest strain inside the nodule.[19,36,38,84]

Among the few reports in the literature involving internal quasi-static SE is a significant study that obtained the value of TSI (called in this study, systolic TSI) of benign nodules at 6.82 ± 3.54 and 18.43 ± 5.99 in the malignancies, with a cutoff value of 10 yielding best performance,[20,38] with sensitivity of 100% and specificity of 79.5%.

The elasticity contrast index (ECI, or SR) method, called Elastoscan (Samsung), again uses a quasi-static, steady-state physiologic excitation technique based on carotid pulsations to induce the strain.[19,35,85] The software measures the strain in a FOV that includes the nodule and adjacent normal thyroid. Thereafter, strain differences in the FOV are represented as a color-coded map and an elasticity contrast index is computed which is high for malignancies and low for benign nodules.[19,36,81] The operator holds the transducer in transverse scan, with only minimal pressure and waits to obtain a steady state, while the quality of the technique is shown by a scale indicator on the screen.[81] The operator then draws a FOV that comprises the nodule and some tissue around it or is located only within the nodule (▶ Fig. 6.10).[81] Some authors suggest that two measurements be taken with the highest one being considered for diagnosis.[35,86]

A cutoff ECI value of 3 resulted as an accurate method for predicting the malignant nature of the nodules.[84] Other studies showed good reproducibility with an excellent interobserver agreement and a steep learning curve with an experience of just about 30 examinations needed to obtain accurate and reproducible results.[20] Limitations and lower accuracy of results from performance of carotid artery compression elastography are related to the variabilities of carotid pulsations in states such as age, heart failure, systemic hypertension, severe pulmonary hypertension, atrial fibrillation, atherosclerosis, and pregnancy.[35,85] Selected studies results are in ▶ Table 6.3.

Table 6.3 Diagnostic performance of ECI elastography and cutoff values for malignancy detection in selected studies

Study	Cutoff value for malignancy	Sensitivity (%)	Specificity (%)
Luo 2012[40]	>0.6	95	74
Dighe 2013[39]	>3.6	100	60
Cantisani 2014[73]	>3	91	90
Kim 2014[86]	>3.1	81	64

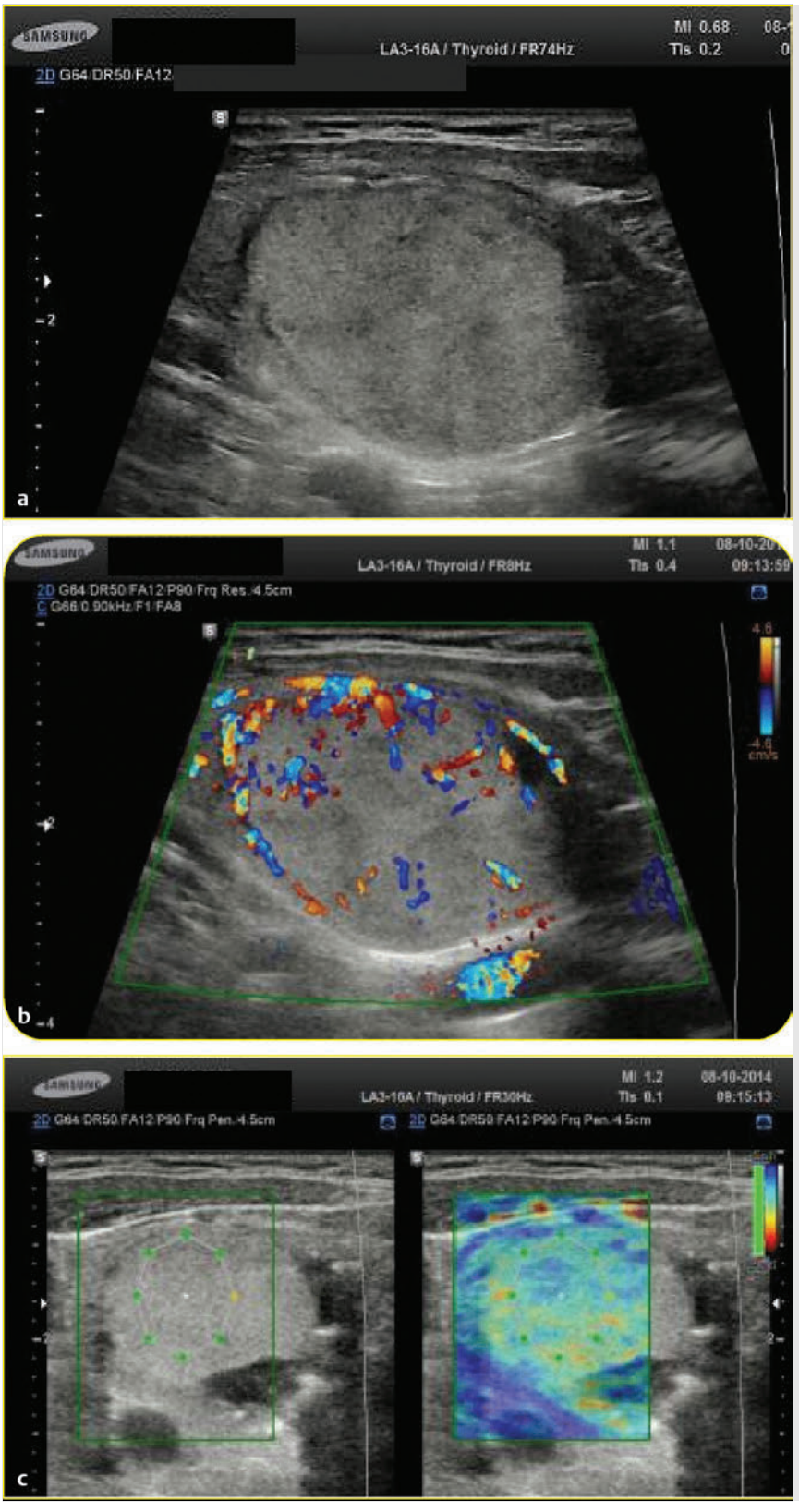

Fig. 6.10 Follicular adenoma. (**a**) At baseline ultrasound, the lesion appears isoechoic with a tiny halo. (**b**) At color Doppler, the nodule shows peri-intraleisonal vascularization corresponding to Pattern III. (**c**) Elasticity contrast index (ECI) evaluation at Elastoscan was lower than 3 and thus consistent with benignity of the lesion.

6.3 Shear Wave Elastography Imaging

6.3.1 Techniques

In shear wave elastography an external acoustic radiation force push pulse, generated by the probe itself, induces transverse shear waves inside a tissue. The induced shear wave speed is directly proportional to the stiffness of the tissue. The ultrasound machine is able to measure the shear wave speed in meters per second (m/s) or, making some assumptions, calculates the stiffness as Young's modulus in kilopascals (kPa). Most systems allow the user to choose whether the stiffness value is displayed as shear wave speed or Young's modulus.

Some systems measure the shear wave speed within a preselected fixed small ROI with display of the shear wave speed within that ROI; this is called point shear wave elastography (p-SWE). Other systems offer the possibility of displaying a color-coded velocity (speed) map in a larger FOV superimposed on the corresponding B-mode image with more flexibility to select the ROI size manually, called 2D-shear wave elastography (2D-SWE). Some systems allow for real-time 2D-SWE assessment such as those from SuperSonic Imagine. With real-time 2D-SWE, it is important to stay stationary on the area of concern for several seconds to get an accurate measurement.

The quantitative nature of SWE, unlike the subjective qualitative nature of SE, and the fact that the acoustic pulse moves the tissue, not an operator's hand with its variability, may improve the consistency and accuracy SWE results over those of SE. Indeed, in p-SWE, the stiffness can be evaluated without a reference area which is required in SE, making it suitable for a direct and quantitative elasticity assessment of thyroid lesions.

Toshiba uses a Doppler tracking method to calculate shear wave speed. In this technique, a push pulse generates downward displacement, inducing shear waves parallel to each raster, which can be detected by the color Doppler in order to measure the speed of traveling shear wave. It can be displayed in three different modes, described as follows.

Velocity Mode

In this mode, the parametric (color) shear wave velocities are shown in the selected window (FOV), colored according to the color Doppler scale, with the size of window adjusted according to the lesion size. It is recommended that the whole lesions be inside the window. The displayed shear wave velocity window is overlaid on the corresponding B-mode image. It allows one to measure the shear wave speed at any point in the entire window by selecting a ROI (▶ Fig. 6.11a).

Stiffness Mode

Similar to the velocity mode, the stiffness mode displays the stiffness in the entire window by using mathematical calculations. Then by selecting a ROI, the system measures the absolute stiffness value in kilopascals of said ROI. This system allows for the measurement of stiffness values in several ROIs, depending on the lesion size and structure, and in addition, calculation of the mean stiffness value and standard deviation (SD) of every stiffness value for a ROI (▶ Fig. 6.11b).

Propagation Mode

Propagation mode is a quality control map, a display of shear wave propagation lines in the selected window (FOV), in order to guide a precise positioning of the ROI(s) for reliable measurements (▶ Fig. 6.11c).

If the propagation lines are parallel to each other, the detection is valid and the ROI can be placed at that site. The measurement of the shear wave velocity and stiffness value (kPa) are, in this case, reliable and accurate. On the other hand if the propagation lines are not parallel, or are distorted, the positioning of the ROI is not recommended as the measurements are bound to be less reliable. In the latter case, it is recommended that one selects another part of the lesion to perform measurements.

According to our preliminary experience, this propagation map provides additional information to support an accurate reading of the shear wave speed, and increases the reproducibility of readings.

Point Shear Wave Elastography

With point shear wave elastography (p-SWE), an ARFI technique, a standard ROI of 5 × 5 mm is placed inside the nodule avoiding cystic or calcified areas, while the patient holds his or her breath and the operator exerts only minimal pressure with the probe.[19,87,88] Healthy thyroid parenchyma should not be included in the ROI. The software displays the velocity together with the depth of the ROI. High stiffness values correspond to high velocities.[19,88,89] In the experience of some researchers, 10 measurements were needed to obtain an average which yielded a reliable accuracy.[19,88] Another research group had good results with 5 measurements.[90]

6.3.2 Two-Dimensional Shear Wave Elastography

In 2D-SWE, the color (or, optionally, grayscale) display (overlayed on the B-mode image) indicates the shear wave speeds in meters per second (or are converted to Young's moduli in kilopascals) in the FOV. ROIs can then be placed on the stiffest part of a lesion and on adjacent fat to obtain quantitative readouts as well as ratios for tissues in those ROIs. Cancers tend to be stiff and also more heterogeneous than benign lesions, and often the stiffness seems to be most marked at and around the periphery of the mass.

When the elasticity cannot be estimated in an area of the FOV, the color display is switched off in that area and the underlying B-mode image (usually black) is revealed. This should not be mistaken for a low value that signifies a soft region. Reasons for the absence of shear wave signals include situations where the system cannot measure the stiffness because the tissue is not vibrating enough and so the amplitude of the shear wave is too low and is lost in noise.

Biological conditions where the shear wave cannot be imaged are also encountered, such as when the speed of the shear wave speed is too high to be captured (e.g., in extremely stiff cancers), or when the interrogating beam cannot penetrate to the mass, for example, in regions that are shadowed-out, typically in the deeper parts of scirrhous cancers. A practical rule is that the

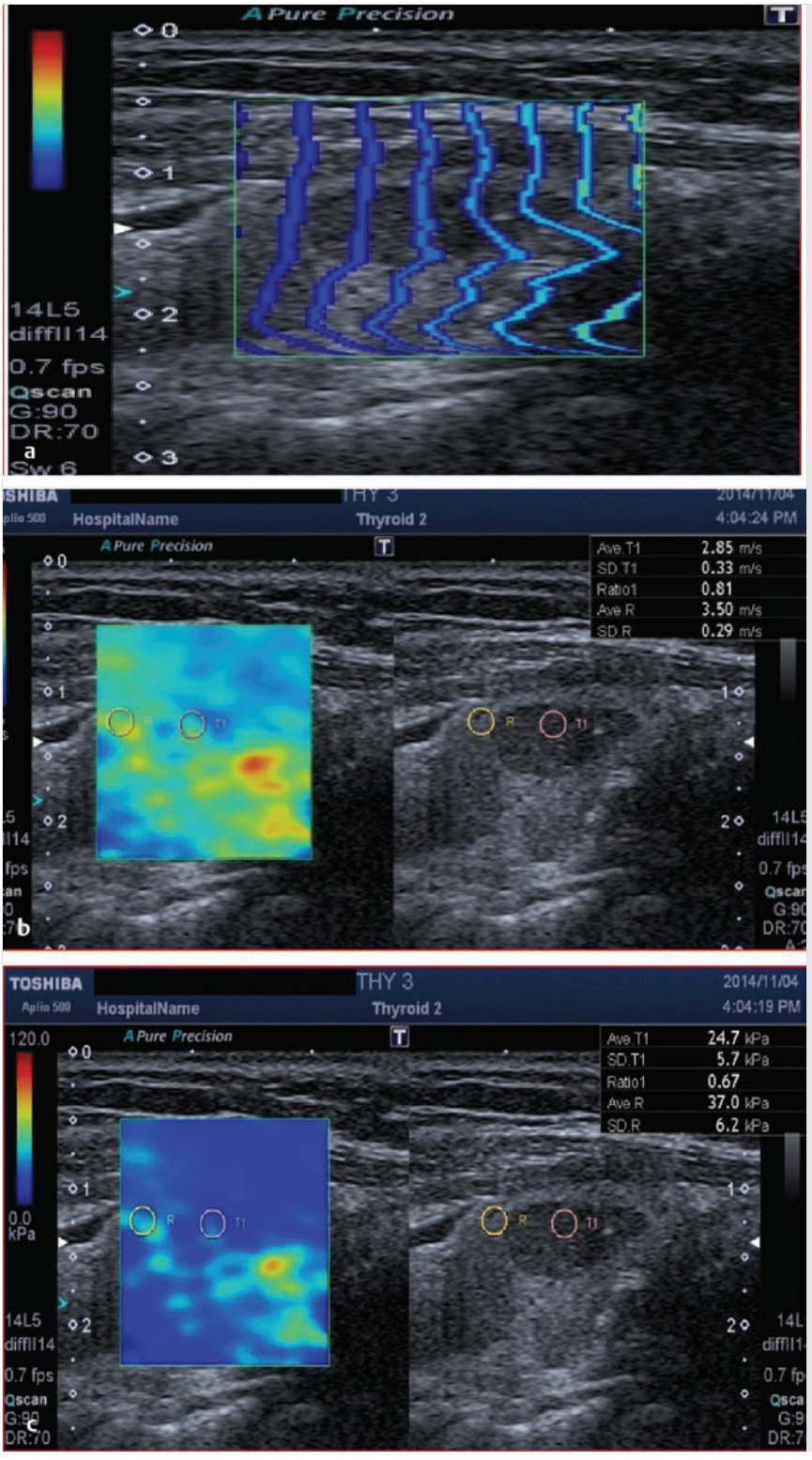

Fig. 6.11 Shear wave elastography of follicular hyperplasia. (**a**) Propagation mode for the assessment of the validity of the measurement. (**b**) The lesion presents low elasticity values. (**c**) Stiffness values calculated in kPa are also shown.

stiffest part of the mass or surroundings is definitive. As with strain elastography, genuinely soft cancers do occur, albeit rarely; these appear as soft masses rather than as a void in the color display.

Cysts deserve special mention: nonviscous fluids do not support shear waves and so they appear as color voids, usually seen as black regions where the anechoic B-mode layer shows through. However, when the fluid is viscous, shear wave signals may be seen and would indicate a soft region.[17]

6.3.3 Limitations of ARFI-Based Systems

In ARFI-based systems, as in all other elastography techniques, pressure applied by the probe alters the measurements.[20,91,92]

Therefore experience is required to perform reliable examinations even in the case of ARFI quantification.[61] Liberal use of ultrasound coupling gel can help.

Also the ROI of ARFI quantification is not modifiable and it is available with two measures: 5 × 6 mm and 20 × 20 mm. For this reason, the ROI enclosing a small nodule would include adjacent normal thyroid and this would result in altered measurements. As in other elastography techniques, cystic areas and calcifications yield false results. However, peculiar to ARFI, the use of the standard size ROI sometimes makes it impossible to exclude fluid and calcified areas of a nodule.

6.3.4 Tips and Tricks

1. Shear wave elastography is performed with a linear probe held with slight pressure and the patient in breath-hold.[19]
2. The quantitative evaluation is switched on and the color-coded image is displayed in a split screen together with the grayscale B-mode ultrasound image, which is common to most systems. The color representation of SWE is the opposite of SE, soft tissue is shown in blue and stiff (hard) tissue is shown in red. However, the user can customize.
3. Quantification is expressed either as shear wave speed (in meters per second) or Young's modulus (in kilopascals). These are easily converted from one to the other, as discussed in Chapter 2.
4. The elastogram ROI should include as much of the nodule as possible and only a little of the surrounding normal thyroid.
5. In the elasticity image there can be areas with no color that may be due to fluid content or technical problems.[19]
6. Some authors recommend, for every nodule, the acquisition of three cine loops of at least 10 seconds' duration.[89]
7. Choosing a correct preset is important for acquiring accurate measurements, and in the case of the thyroid, the preset should be 0–180 kPa.[19] Of importance is also increasing the elasticity color gain to its maximum until noise starts to appear, because this will aid in acquiring elastograms with good intensity of color.
8. The operator should be careful in maintaining the transducer still and with only slight contact with the skin, as pressure of the transducer causes artifacts of increased stiffness.[67]

Some authors claim that SuperSonic Imagine is an operator independent and reproducible technique.[50,93] However, only a small number of studies have been published so far regarding nodule evaluation with SuperSonic Imagine imaging; therefore future multicenter studies are warranted to better clarify this issue.

6.3.5 Artifacts and Pitfalls of SWE

If the system cannot calculate an adequate shear wave speed for given pixels, they are not colored. This can occur when there is significant noise, a very stiff lesion, or a simple cyst. Simple cysts do not support shear waves while complicated cysts do.[94]

A vertical artifact that appears as a pattern of red in the near field may reduce on minimizing compression.[20,91,92]

With increasing pressure of the transducer, the stiffness increases rapidly, due to nonlinear elastic effects,[19] and the nodules in the isthmus, compressed against the tracheal cartilages, suffer most from this effect. To avoid this artifactually increased stiffness in the isthmic nodules, some authors recommend the use of paracoronal scanning in order to avoid compressing the nodules against the trachea.[95]

Calcified and cystic areas, as in other types of elastography, alter the measurements in SWE as well.

6.3.6 Interpretation of Results of SWE

Elasticity of the thyroid gland depends on the structural properties of the matrix of tissues (cells, membranes, extravascular matrix, microvessels, etc.), whereas in conventional B-mode ultrasound, it is the microscopic structure that determines reflectivity. This means that in elastography, there is image contrast based on histologic tissue structure, enabling the differentiation of normal gland tissues from that of nodules and parenchymal diseases.

At SE the normal thyroid has a soft appearance, homogeneously green and at times green/red/yellow. A variability in elastographic appearance of the normal gland could be an expression of the normal balance between parenchymal hyperplasia and involution, producing deviations from the usual histological pattern.[76]

A few SWE papers report normal velocity values in the gland of 2.0 ± 0.40 m/s.[90,96] For real-time 2D-SWE using SuperSonic Imagine (SSI), reports of normal thyroid values are at 20.8 ± 10.4 kPa.[97]

Studies using SWE for differentiating benign (▶ Fig. 6.12, ▶ Fig. 6.13) and malignant thyroid nodules reported various cutoff values ranging from 34.5 kPa[91] to a best cutoff at 65 kPa[93]and 66 kPa.[97,98] Different cutoff values were reported in various studies and they were associated with different diagnostic performance. A group of researchers found that by increasing the cutoff value from 10.3 kPa to 132 kPa, the specificity changed from 8.9 % to 100%.[91] Another study reported that a mean stiffness value of > 85 kPa or a maximum value > 94 kPa are independent predictors of malignancy.[99] Two studies found that SSI can differentiate thyroid nodules, even in the presence of autoimmune thyroiditis.[95,100]

The shear wave speed (SWS) measured by ARFI is demonstrated[89] as being significantly higher in malignant lesions than benign ones, with a value higher than 2.87 m/s strongly suggestive for suspicious lesions.[20,89] One study[89] reported that the SWSs of benign (▶ Fig. 6.14) and malignant thyroid nodules were 2.34 ± 1.17 m/s (range: 0.61–9.00 m/s) and 4.82 ± 2.53 m/s (range: 2.32–9.00 m/s), respectively ($p < 0.001$). These results were similar to other studies in which cutoff values in the range of 2.55 to 2.75 m/s were reported.[88,96,101,102,103]

6.4 Comparison of Strain Elastography and Shear Wave Elastography

Only a few papers have been published that compare the value of SE and SWE. Liu et al compared SWE and qualitative SE using a 5-grade color scale assessment to discriminate 64 focal thyroid nodules in 49 patients with surgical pathology.[43] Of the 64 nodules, 19 were papillary thyroid carcinomas and 45 were

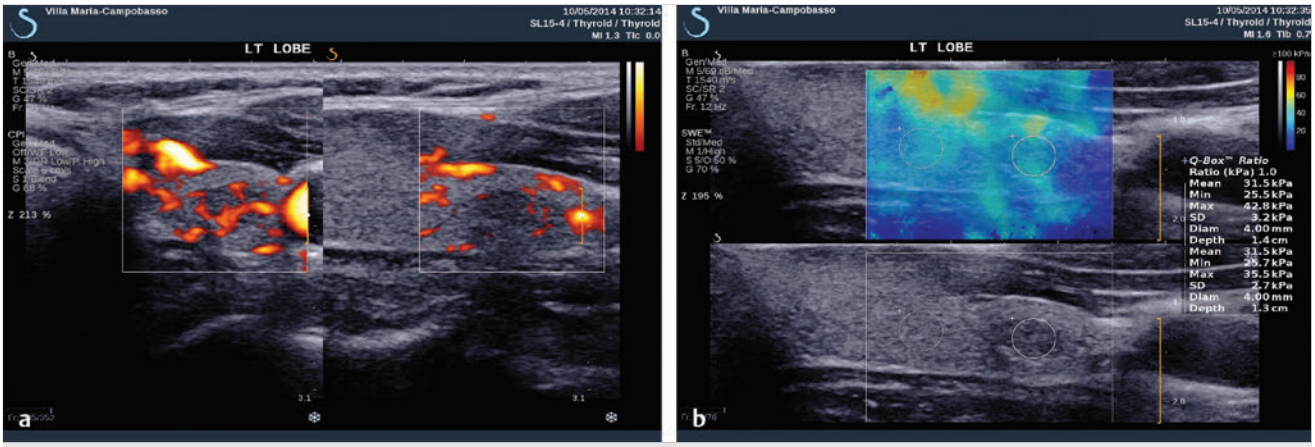

Fig. 6.12 Follicular hyperplasia. (**a**) SuperSonic Imagine imaging: lesion is located in the lower pole of the left lobe, which appears slightly hypoechoic with a few intranodular vessels at power Doppler. **(b)** At shear wave elastography the lesion presents similar values of stiffness as the surrounding normal parenchyma.

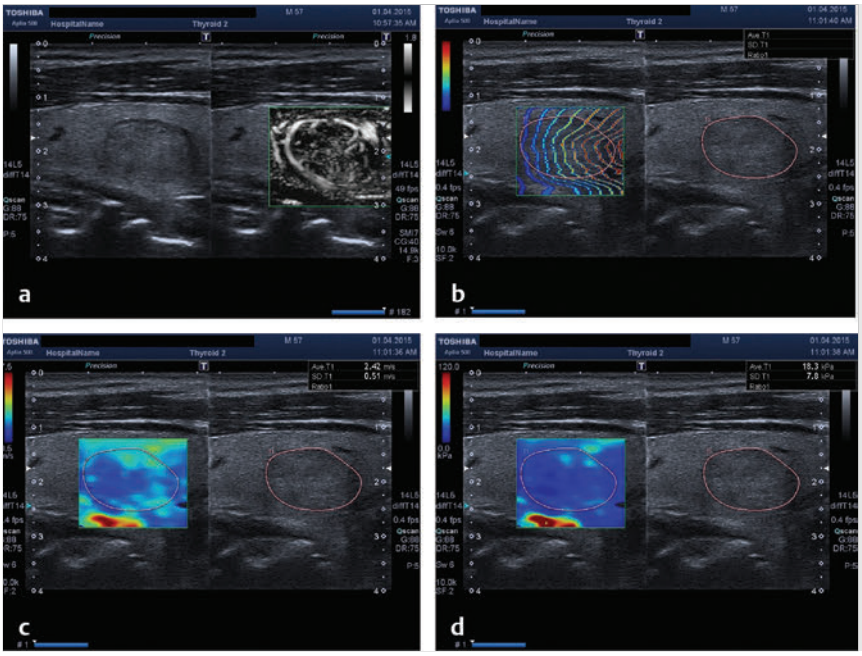

Fig. 6.13 Follicular hyperplasia. (**a**) At baseline ultrasound, the lesion appears isoechoic with a tiny and regular hypoechoic halo (right side) with pattern III at SMI (Superb Microvascular Imaging). (**b**) Propagation wave modulus. (**c, d**) The lesion showed low values at SWE.

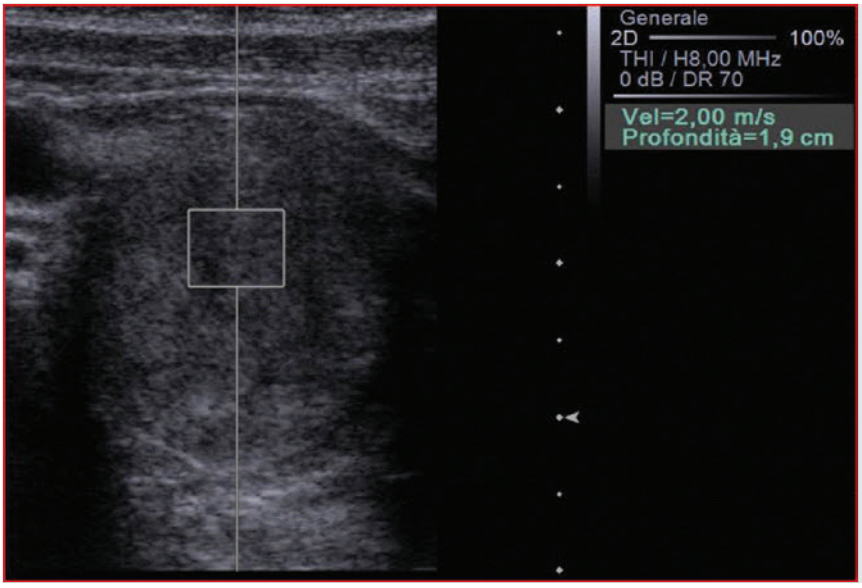

Fig. 6.14 ARFI-based SWE of follicular adenoma.

Table 6.4 Diagnostic performance of ARFI quantification in the detection of malignancies in selected studies

Study	Cutoff value for malignancy	Sensitivity (%)	Specificity (%)
Zhang 2012[89]	2.87 m/sec	75	82
Gu 2012[101]	2.55 m/sec	86	93
Zhan 2013[104]	2.85 m/sec	94	85
Zhang 2014[105]	2.9 m/sec	91	85

Table 6.5 Diagnostic performance of SWE and cutoff values for malignancy detection in selected studies

Study	Cutoff value for malignancy	Sensitivity (%)	Specificity (%)
Sebag 2010[93]	65 kPa	85	94
Bhatia 2012[91]	42 kPa	53	78
Veyrieres 2012[97]	66 kPa	80	91
Carneiro 2013[106]	34.5 kPa	77	71
Kim 2013[107]	62 kPa	67	72
Park 2015[99]	85 kPa	54	88

benign. Using the most accurate cutoff, 38.3kPa for the mean value to predict malignancy, the diagnostic specificity, sensitivity, accuracy, positive predictive value, and negative predictive value of SWE and SE were 68.4% versus 79.0%, 86.7% versus 84.4%, 81.3% versus 78.1%, 68.4% versus 64.7%, and 86.7% versus 83.3%, respectively (p values from 0.683–1.000). They concluded that SWE was a promising tool and can be performed in differentiating thyroid nodules with comparable results to RTSE, being slightly lower in sensitivity and slightly higher in specificity than the latter. Bojunga et al compared 2D-SWE and qualitative SE in 158 nodules in 138 patients.[88] No significant difference of diagnostic accuracy for the diagnosis of malignant thyroid nodules was shown between RTSE and SWE (0.74 versus 0.69, p = 0.54) and the combination of RTSE with SWE did not improve diagnostic accuracy. Selected studies results are in ▶ Table 6.4 and ▶ Table 6.5.

6.5 Diffuse Thyroid Diseases

Chronic autoimmune thyroiditis (Hashimoto's thyroiditis), Graves' disease, and multinodular goiter are usually diagnosed on the basis of clinical and laboratory findings, with the complement of ultrasound. They present histological alterations associated with increased stiffness as shown in literature reports. A variability in elastographic appearance could be an expression of the different stages of inflammation and sclerotic involution although the general tendency is that of a diffusely stiff gland. A study group[90] reported in two studies statistically significant differences in SWE stiffness between normal subjects and patients with autoimmune pathology (Graves' disease and chronic autoimmune thyroiditis) with values of 2.07 ± 0.44 m/s versus 2.68 ± 0.50 m/s, $p < 0.001$. They suggest that SWE seems to be able to predict with sufficient accuracy the presence of diffuse thyroid disease (area under receiver operating characteristic curve of 0.80), with 5 measurements needed for obtaining a reliable median value. Magri et al[95] applied SWE in 75 patients with a benign thyroid nodule at cytology: 33 with Hashimoto's thyroiditis (HT) and 42 with uni- or multinodular goiter. They report that the SWE stiffness of the extranodular tissue was greater, though not statistically significant, in the HT than in the non-HT group (24.0 ± 10.5 kPa versus 20.8 ± 10.4 kPa; $p = 0.206$).

More recently Menzilcioglu[107] evaluated the accuracy of the strain ratio at RTSE, with the strap muscles as reference measurement, in order to calculate the cut off point for the diagnosis of chronic autoimmune thyroiditis (CAT). The strain ratio was higher in CAT than in normal thyroid parenchyma in RTSE. The authors concluded that this method seems to be a useful method for the assessment of CAT with RTSE but it needs further evaluation on larger populations.

In subacute (granulomatous or de Quervain's) thyroiditis, two studies found the inflammatory areas to be stiff.[108] When focal, the inflammatory areas, being harder than the ones encountered in Hashimoto's thyroiditis, should be included in the differential diagnosis of carcinoma.[19,109] The appearance is significantly different from multinodular goiter but not from cancer. Riedel (chronic) thyroiditis is characterized by extremely stiff parenchyma, with values of 143–281 kPa.[19]

6.6 Future Prospects

Future technical developments, such automatic assisted strain elastography and three-dimensional (3D) elasticity imaging with 3D probes, are warranted to make elastography more reproducible and effective. Initial data in the thyroid as well as the breast and testis reported interesting results for in vivo 3D strain elastography imaging in order to reduce noise and to help differentiate cystic and solid lesions.[110] Ideally this seems particularly useful for minimally invasive treatments such as high-frequency focused ultrasound (HIFU) and radio frequency ablation (RFA). According to our preliminary experience,[111] it is feasible with 3D elastography to reconstruct different 2D planes from the 3D whole nodule elastographic data set. However, in our opinion, further technical refinements are still needed in order to ensure more reliability and reproducibility. Research studies are of auspices to determine its clinical role. (▶ Fig. 6.15, ▶ Fig. 6.16, ▶ Fig. 6.17).

6.7 Published Guidelines

To date the only published guidelines are the European Federation of Societies for Ultrasound in Medicine and Biology (EFSUMB) Guidelines and Recommendations with regard to thyroid ultrasound elastography. The guidelines recommend as practical points that both SE and SWE elastography may be performed with no patient preparation but require dedicated equipment. They recommend use of elastography as an additional tool to conventional ultrasound evaluation and to guide follow-up of lesions previously diagnosed as benign at FNA.

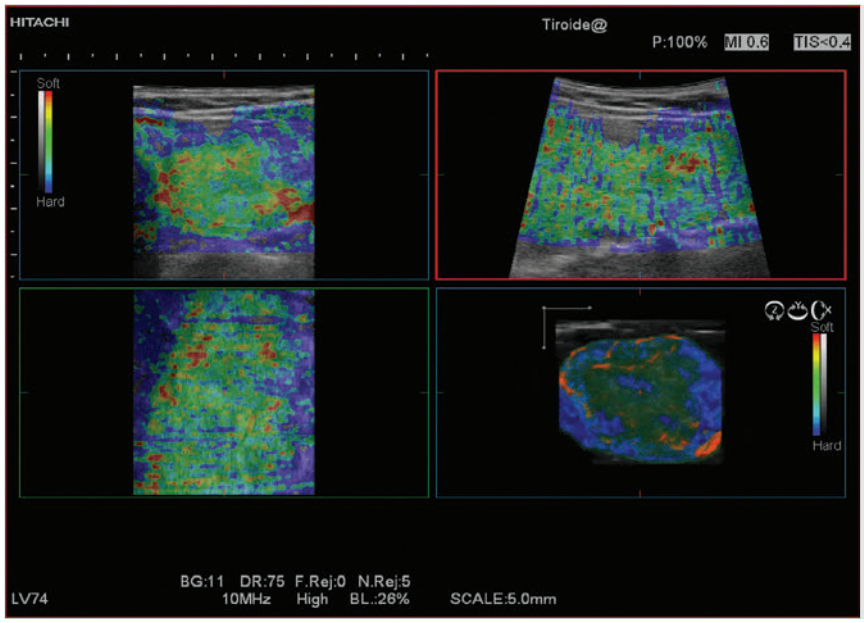

Fig. 6.15 Follicular adenoma: elastograms of different planes through the lesion are obtained with 3D elastography.

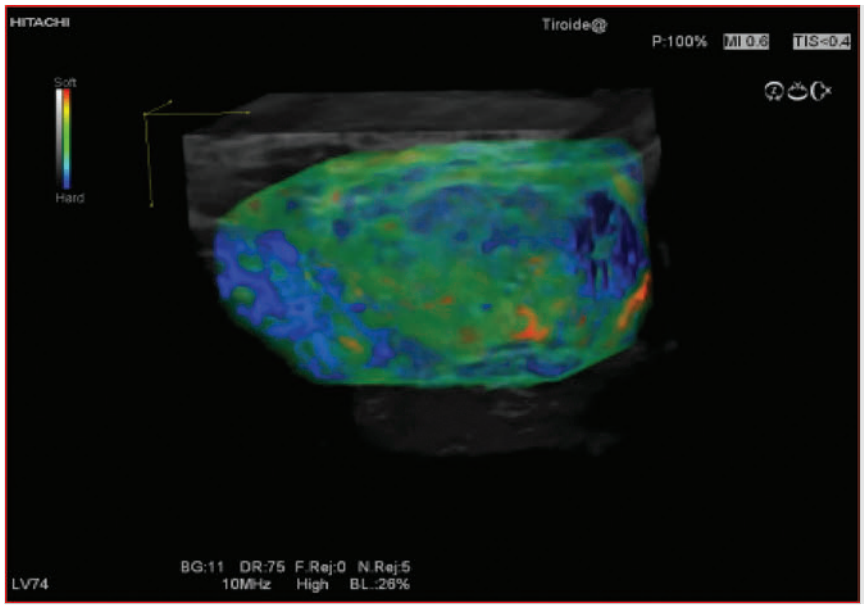

Fig. 6.16 Three-dimensional elastography volume rendering clearly shows that the thyroid nodule is predominantly soft with regular and defined margins.

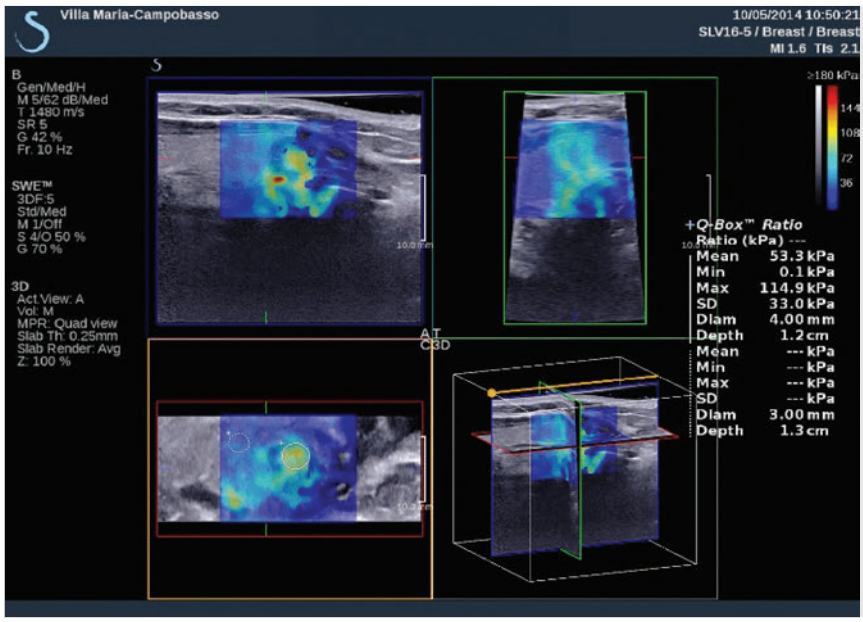

Fig. 6.17 Three dimensional SuperSonic Imagine imaging of a papillary carcinoma.

6.8 Conclusion

Elastography, both SE and SWE, is a valid and useful additional tool to color Doppler in thyroid evaluation as proven by the update of the literature and by EFSUMB guidelines. However, to achieve prompt and reliable elastography, adequate training, suitable parameters for both strain and shear wave elastography, adequate equipment, and clinical appropriateness of examination are necessary. Our suggestion is to minimize precompression and vertical artifacts, to check ROI size and positions, to avoid areas with artifacts or with gross calcifications or cystic areas, and to instruct patients to cooperate properly.

To date, more data are present in the literature in favor of SE in terms of sensitivity, while SWE could be considered more reproducible, with similar specificity for thyroid nodule differentiation, and indicated more for diffuse thyroid diseases. Elastography showed the highest sensitivity, specificity, and NPV for the diagnosis of papillary carcinoma from benign nodules.

However, when we deal with thyroid nodule differentiation, we have to take into account that not all of the malignant thyroid nodules are stiff; they may be soft or heterogeneous. Follicular carcinomas can be soft and difficult to differentiate from benign nodules, although some good results have also been reported both with strain ratio SE[55] and with SWE.[112] In the latter paper a cutoff value of 22.30 kPa can help differentiate malignant from benign follicular thyroid lesions with a sensitivity of 82%, a specificity of 88%, and positive and negative predictive values of 75% and 91%, respectively.

To date only a few papers on medullary thyroid tumors have been reported. Andrioli et al recently reported their experience with 18 histologically proven medullary thyroid cancers (MTCs), that at qualitative SE most MTCs presented as a soft elastographic pattern. Therefore, qualitative elastography was reported not to be useful to add information in pointing out MTC on the basis of its hardness.[113]

Future technical developments to reduce even more the interobserver and intraobserver variability are warranted.

In conclusion, multicenter studies, and periodic evaluation by international experts consensus panels are warranted to better define the role of each technique, and the right workup for patients with both thyroid nodule and diffuse thyroid disease.

References

[1] Reiners C, Wegscheider K, Schicha H et al. Prevalence of thyroid disorders in the working population of Germany: ultrasonography screening in 96,278 unselected employees. Thyroid 2004; 14(11):926–932

[2] Brander A, Viikinkoski P, Nickels J, Kivisaari L. Thyroid gland: US screening in a random adult population. Radiology 1991; 181(3):683–687

[3] Tunbridge WM, Evered DC, Hall R et al. The spectrum of thyroid disease in a community: the Whickham survey. Clin Endocrinol (Oxf) 1977; 7(6):481–493

[4] Davies L, Welch HG. Increasing incidence of thyroid cancer in the United States, 1973–2002. JAMA 2006; 295(18):2164–2167

[5] Iannuccilli JD, Cronan JJ, Monchik JM. Risk for malignancy of thyroid nodules as assessed by sonographic criteria: the need for biopsy. J Ultrasound Med 2004; 23(11):1455–1464

[6] Hoang JK, Lee WK, Lee M, Johnson D, Farrell S. US features of thyroid malignancy: pearls and pitfalls. Radiographics 2007; 27(3):847–860, discussion 861–865

[7] Moon H-G, Jung E-J, Park ST et al. Role of ultrasonography in predicting malignancy in patients with thyroid nodules. World J Surg 2007; 31(7): 1410–1416

[8] Fish SA, Langer JE, Mandel SJ. Sonographic imaging of thyroid nodules and cervical lymph nodes. Endocrinol Metab Clin North Am 2008; 37(2):401–417, ix

[9] Kim HG, Moon HJ, Kwak JY, Kim EK. Diagnostic accuracy of the ultrasonographic features for subcentimeter thyroid nodules suggested by the revised American Thyroid Association guidelines. Thyroid 2013; 23(12): 1583–1589

[10] Cooper DS, Doherty GM, Haugen BR et al. American Thyroid Association (ATA) Guidelines Taskforce on Thyroid Nodules and Differentiated Thyroid Cancer. Revised American Thyroid Association management guidelines for patients with thyroid nodules and differentiated thyroid cancer. Thyroid 2009; 19(11):1167–1214

[11] Cooper DS, Doherty GM, Haugen BR et al. American Thyroid Association Guidelines Taskforce. Management guidelines for patients with thyroid nodules and differentiated thyroid cancer. Thyroid 2006; 16(2):109–142

[12] Gharib H, Papini E, Paschke R et al. AACE/AME/ETA Task Force on Thyroid Nodules. American Association of Clinical Endocrinologists, Associazione Medici Endocrinologi, and European Thyroid Association Medical Guidelines for Clinical Practice for the Diagnosis and Management of Thyroid Nodules. Endocr Pract 2010; 16 Suppl 1:1–43

[13] Hegedüs L. Clinical practice: the thyroid nodule. N Engl J Med 2004; 351 (17):1764–1771

[14] Tee YY, Lowe AJ, Brand CA, Judson RT. Fine-needle aspiration may miss a third of all malignancy in palpable thyroid nodules: a comprehensive literature review. Ann Surg 2007; 246(5):714–720

[15] Peng Y, Wang HH. A meta-analysis of comparing fine-needle aspiration and frozen section for evaluating thyroid nodules. Diagn Cytopathol 2008; 36 (12):916–920

[16] Oertel YC, Miyahara-Felipe L, Mendoza MG, Yu K. Value of repeated fine needle aspirations of the thyroid: an analysis of over ten thousand FNAs. Thyroid 2007; 17(11):1061–1066

[17] Bamber J, Cosgrove D, Dietrich CF et al. EFSUMB guidelines and recommendations on the clinical use of ultrasound elastography. Part 1: Basic principles and technology. Ultraschall Med 2013; 34(2):169–184

[18] Shiina T, Nightingale KR, Palmeri ML et al. WFUMB guidelines and recommendations for clinical use of ultrasound elastography: Part 1: basic principles and terminology. Ultrasound Med Biol 2015; 41(5):1126–1147

[19] Dudea SM, Botar-Jid C. Ultrasound elastography in thyroid disease. Med Ultrasound 2015; 17(1):74–96

[20] Cantisani V, Consorti F, Guerrisi A et al. Prospective comparative evaluation of quantitative-elastosonography (Q-elastography) and contrast-enhanced ultrasound for the evaluation of thyroid nodules: preliminary experience. Eur J Radiol 2013; 82(11):1892–1898

[21] Rago T, Vitti P. Potential value of elastosonography in the diagnosis of malignancy in thyroid nodules. Q J Nucl Med Mol Imaging 2009; 53(5): 455–464

[22] Ueno E, Itoh A. Diagnosis of breast cancer by elasticity imaging. Eizo Joho Medical 2004; 36(12):2–6

[23] Rubaltelli L, Corradin S, Dorigo A et al. Differential diagnosis of benign and malignant thyroid nodules at elastosonography. Ultraschall Med 2009; 30 (2):175–179

[24] Rago T, Santini F, Scutari M, Pinchera A, Vitti P. Elastography: new developments in ultrasound for predicting malignancy in thyroid nodules. J Clin Endocrinol Metab 2007; 92(8):2917–2922

[25] Itoh A, Ueno E, Tohno E et al. Breast disease: clinical application of US elastography for diagnosis. Radiology 2006; 239(2):341–350

[26] Moon HJ, Sung JM, Kim EK, Yoon JH, Youk JH, Kwak JY. Diagnostic performance of gray-scale US and elastography in solid thyroid nodules. Radiology 2012; 262(3):1002–1013

[27] Ning CP, Jiang SQ, Zhang T, Sun LT, Liu YJ, Tian JW. The value of strain ratio in differential diagnosis of thyroid solid nodules. Eur J Radiol 2012; 81(2):286–291

[28] Park SH, Kim SJ, Kim EK, Kim MJ, Son EJ, Kwak JY. Interobserver agreement in assessing the sonographic and elastographic features of malignant thyroid nodules. AJR Am J Roentgenol 2009; 193(5):W416–W423

[29] Kim JK, Baek JH, Lee JH et al. Ultrasound elastography for thyroid nodules: a reliable study? Ultrasound Med Biol 2012; 38(9):1508–1513

[30] Vorländer C, Wolff J, Saalabian S, Lienenlüke RH, Wahl RA. Real-time ultrasound elastography—a noninvasive diagnostic procedure for evaluating dominant thyroid nodules. Langenbecks Arch Surg 2010; 395(7):865–871

[31] Ding J, Cheng HD, Huang J, Zhang Y, Liu J. An improved quantitative measurement for thyroid cancer detection based on elastography. Eur J Radiol 2012; 81(4):800–805

[32] Cakir B, Aydin C, Korukluoğlu B et al. Diagnostic value of elastosonographically determined strain index in the differential diagnosis of benign and malignant thyroid nodules. Endocrine 2011; 39(1):89–98
[33] Ciledag N, Arda K, Aribas BK, Aktas E, Köse SK. The utility of ultrasound elastography and MicroPure imaging in the differentiation of benign and malignant thyroid nodules. AJR Am J Roentgenol 2012; 198(3):W244-W249
[34] Xing P, Wu L, Zhang C, Li S, Liu C, Wu C. Differentiation of benign from malignant thyroid lesions: calculation of the strain ratio on thyroid sonoelastography. J Ultrasound Med 2011; 30(5):663–669
[35] Zhang FJ, Han RL, Zhao XM. The value of virtual touch tissue image (VTI) and virtual touch tissue quantification (VTQ) in the differential diagnosis of thyroid nodules. Eur J Radiol 2014; 83(11):2033–2040
[36] Lim DJ, Luo S, Kim MH, Ko SH, Kim Y. Interobserver agreement and intraobserver reproducibility in thyroid ultrasound elastography. AJR Am J Roentgenol 2012; 198(4):896–901
[37] Dighe M, Bae U, Richardson ML, Dubinsky TJ, Minoshima S, Kim Y. Differential diagnosis of thyroid nodules with US elastography using carotid artery pulsation. Radiology 2008; 248(2):662–669
[38] Luo S, Kim EH, Dighe M, Kim Y. Screening of thyroid nodules by ultrasound elastography using diastolic strain variation. Conf Proc IEEE Eng Med Biol Soc 2009; 2009:4420–4423
[39] Dighe M, Kim J, Luo S, Kim Y. Utility of the ultrasound elastographic systolic thyroid stiffness index in reducing fine-needle aspirations. J Ultrasound Med 2010; 29(4):565–574
[40] Dighe M, Luo S, Cuevas C, Kim Y. Efficacy of thyroid ultrasound elastography in differential diagnosis of small thyroid nodules. Eur J Radiol 2013; 82(6): e274–e280
[41] Luo S, Lim DJ, Kim Y. Objective ultrasound elastography scoring of thyroid nodules using spatiotemporal strain information. Med Phys 2012; 39(3): 1182–1189
[42] Wang HL, Zhang S, Xin XJ et al. Application of real-time ultrasound elastography in diagnosing benign and malignant thyroid solid nodules. Cancer Biol Med 2012; 9(2):124–127
[43] Mona A, EL-Hariri MA, Taha TF, Tawab MA, Magid AM, Shiekh AF. The clinical value of ultrasound elastography in predicting malignant thyroid nodules. Egypt J Radiol Nucl Med 2014; 45:353–359
[44] Liu BX, Xie XY, Liang JY et al. Shear wave elastography versus real-time elastography on evaluation thyroid nodules: a preliminary study. Eur J Radiol 2014; 83(7):1135–1143
[45] Hong Y, Liu X, Li Z, Zhang X, Chen M, Luo Z. Real-time ultrasound elastography in the differential diagnosis of benign and malignant thyroid nodules. J Ultrasound Med 2009; 28(7):861–867
[46] Wang Y, Dan HJ, Dan HY, Li T, Hu B. Differential diagnosis of small single solid thyroid nodules using real-time ultrasound elastography. J Int Med Res 2010; 38(2):466–472
[47] Ko SY, Kim EK, Sung JM, Moon HJ, Kwak JY. Diagnostic performance of ultrasound and ultrasound elastography with respect to physician experience. Ultrasound Med Biol 2014; 40(5):854–863
[48] Merino S, Arrazola J, Cárdenas A et al. Utility and interobserver agreement of ultrasound elastography in the detection of malignant thyroid nodules in clinical care. AJNR Am J Neuroradiol 2011; 32(11):2142–2148
[49] Bhatia KS, Rasalkar DP, Lee YP et al. Cystic change in thyroid nodules: a confounding factor for real-time qualitative thyroid ultrasound elastography. Clin Radiol 2011; 66(9):799–807
[50] Garra BS. Elastography: current status, future prospects, and making it work for you. Ultrasound Q 2011; 27(3):177–186
[51] Hegedüs L. Can elastography stretch our understanding of thyroid histomorphology? J Clin Endocrinol Metab 2010; 95(12):5213–5215
[52] Barr RG, Lackey AE. The utility of the "bull's-eye" artifact on breast elasticity imaging in reducing breast lesion biopsy rate. Ultrasound Q 2011; 27(3): 151–155
[53] Barr RG. Breast Elastography. New York, NY: Thieme; 2014
[54] Shuzhen C. Comparison analysis between conventional ultrasonography and ultrasound elastography of thyroid nodules. Eur J Radiol 2012; 81(8):1806–1811
[55] Asteria C, Giovanardi A, Pizzocaro A et al. US-elastography in the differential diagnosis of benign and malignant thyroid nodules. Thyroid 2008; 18(5): 523–531
[56] Cantisani V, Ulisse S, Guaitoli E et al. Q-elastography in the presurgical diagnosis of thyroid nodules with indeterminate cytology. PLoS ONE 2012; 7 (11):e50725
[57] Rivo-Vázquez Á, Rodríguez-Lorenzo Á, Rivo-Vázquez JE et al. The use of ultrasound elastography in the assessment of malignancy risk in thyroid nodules and multinodular goitres. Clin Endocrinol (Oxf) 2013; 79(6):887–891
[58] Bojunga J, Herrmann E, Meyer G, Weber S, Zeuzem S, Friedrich-Rust M. Real-time elastography for the differentiation of benign and malignant thyroid nodules: a meta-analysis. Thyroid 2010; 20(10):1145–1150
[59] Unlütürk U, Erdoğan MF, Demir O, Güllü S, Başkal N. Ultrasound elastography is not superior to grayscale ultrasound in predicting malignancy in thyroid nodules. Thyroid 2012; 22(10):1031–1038
[60] Ragazzoni F, Deandrea M, Mormile A et al. High diagnostic accuracy and interobserver reliability of real-time elastography in the evaluation of thyroid nodules. Ultrasound Med Biol 2012; 38(7):1154–1162
[61] Nell S, Kist JW, Debray TP et al. Qualitative elastography can replace thyroid nodule fine-needle aspiration in patients with soft thyroid nodules: a systematic review and meta-analysis. Eur J Radiol 2015; 84(4):652–661
[62] Shao J, Shen Y, Lu J, Wang J. Ultrasound scoring in combination with ultrasound elastography for differentiating benign and malignant thyroid nodules. Clin Endocrinol (Oxf) 2015; 83(2):254–260
[63] Trimboli P, Guglielmi R, Monti S et al. Ultrasound sensitivity for thyroid malignancy is increased by real-time elastography: a prospective multicenter study. J Clin Endocrinol Metab 2012; 97(12):4524–4530
[64] Cantisani V, D'Andrea V, Biancari F et al. Prospective evaluation of multiparametric ultrasound and quantitative elastosonography in the differential diagnosis of benign and malignant thyroid nodules: preliminary experience. Eur J Radiol 2012; 81(10):2678–2683
[65] Chong Y, Shin JH, Ko ES, Han BK. Ultrasonographic elastography of thyroid nodules: is adding strain ratio to colour mapping better? Clin Radiol 2013; 68(12):1241–1246
[66] Razavi SA, Hadduck TA, Sadigh G, Dwamena BA. Comparative effectiveness of elastographic and B-mode ultrasound criteria for diagnostic discrimination of thyroid nodules: a meta-analysis. AJR Am J Roentgenol 2013; 200(6): 1317–1326
[67] Sun J, Cai J, Wang X. Real-time ultrasound elastography for differentiation of benign and malignant thyroid nodules: a meta-analysis. J Ultrasound Med 2014; 33(3):495–502
[68] Rago T, Scutari M, Santini F et al. Real-time elastosonography: useful tool for refining the presurgical diagnosis in thyroid nodules with indeterminate or nondiagnostic cytology. J Clin Endocrinol Metab 2010; 95(12):5274–5280
[69] Garino F, Deandrea M, Motta M et al. Diagnostic performance of elastography in cytologically indeterminate thyroid nodules. Endocrine 2015; 49(1): 175–183
[70] Lippolis PV, Tognini S, Materazzi G et al. Is elastography actually useful in the presurgical selection of thyroid nodules with indeterminate cytology? J Clin Endocrinol Metab 2011; 96(11):E1826–E1830
[71] Friedrich-Rust M, Meyer G, Dauth N et al. Interobserver agreement of Thyroid Imaging Reporting and Data System (TIRADS) and strain elastography for the assessment of thyroid nodules. PLoS ONE 2013; 8(10): e77927
[72] Calvete AC, Rodríguez JM, de Dios Berná-Mestre J, Ríos A, Abellán-Rivero D, Reus M. Interobserver agreement for thyroid elastography: value of the quality factor. J Ultrasound Med 2013; 32(3):495–504
[73] Monpeyssen H, Tramalloni J, Poirée S, Hélénon O, Correas JM. Elastography of the thyroid. Diagn Interv Imaging 2013; 94(5):535–544
[74] Cantisani V, Grazhdani H, Ricci P et al. Q-elastosonography of solid thyroid nodules: assessment of diagnostic efficacy and interobserver variability in a large patient cohort. Eur Radiol 2014; 24(1):143–150
[75] Cappelli C, Pirola I, Gandossi E et al. Real-time elastography: a useful tool for predicting malignancy in thyroid nodules with nondiagnostic cytologic findings. J Ultrasound Med 2012; 31(11):1777–1782
[76] Hong YR, Wu YL, Luo ZY, Wu NB, Liu XM. Impact of nodular size on the predictive values of gray-scale, color-Doppler ultrasound, and sonoelastography for assessment of thyroid nodules. J Zhejiang Univ Sci B 2012; 13(9):707–716
[77] Oliver C, Vaillant-Lombard J, Albarel F et al. What is the contribution of elastography to thyroid nodules evaluation? Ann Endocrinol (Paris) 2011; 72 (2):120–124
[78] Wu HX, Zhang BJ, Wang J, Zhu BL, Zang YP, Cao YL. Conventional ultrasonography and real-time ultrasound elastography in the differential diagnosis of degenerating cystic thyroid nodules mimicking malignancy and papillary thyroid carcinomas. Asian Pac J Cancer Prev 2013; 14(2):935–940
[79] Moon HJ, Kim EK, Yoon JH, Kwak JY. Clinical implication of elastography as a prognostic factor of papillary thyroid microcarcinoma. Ann Surg Oncol 2012; 19(7):2279–2287

[80] Castéra L, Foucher J, Bernard PH et al. Pitfalls of liver stiffness measurement: a 5-year prospective study of 13,369 examinations. Hepatology 2010; 51(3): 828–835
[81] Tatar IG, Kurt A, Yilmaz KB, Akinci M, Kulacoglu H, Hekimoglu B. The learning curve of real-time elastosonography: a preliminary study conducted for the assessment of malignancy risk in thyroid nodules. Med Ultrasound 2013; 15(4):278–284
[82] Azizi G, Keller J, Lewis M, Puett D, Rivenbark K, Malchoff C. Performance of elastography for the evaluation of thyroid nodules: a prospective study. Thyroid 2013; 23(6):734–740
[83] Mehrotra P, McQueen A, Kolla S, Johnson SJ, Richardson DL. Does elastography reduce the need for thyroid FNAs? Clin Endocrinol (Oxf) 2013; 78(6): 942–949
[84] Bae U, Dighe M, Dubinsky T, Minoshima S, Shamdasani V, Kim Y. Ultrasound thyroid elastography using carotid artery pulsation: preliminary study. J Ultrasound Med 2007; 26(6):797–805
[85] Cantisani V, Lodise P, Di Rocco G et al. Diagnostic accuracy and interobserver agreement of Quasistatic Ultrasound Elastography in the diagnosis of thyroid nodules. Ultraschall Med 2015; 36(2):162–167
[86] Kim MH, Luo S, Ko SH, Jung SL, Lim DJ, Kim Y. Elastography can effectively decrease the number of fine-needle aspiration biopsies in patients with calcified thyroid nodules. Ultrasound Med Biol 2014; 40(10):2329–2335
[87] Friedrich-Rust M, Sperber A, Holzer K et al. Real-time elastography and contrast-enhanced ultrasound for the assessment of thyroid nodules. Exp Clin Endocrinol Diabetes 2010; 118(9):602–609
[88] Bojunga J, Dauth N, Berner C et al. Acoustic radiation force impulse imaging for differentiation of thyroid nodules. PLoS ONE 2012; 7(8):e42735
[89] Zhang YF, Xu HX, He Y et al. Virtual touch tissue quantification of acoustic radiation force impulse: a new ultrasound elastic imaging in the diagnosis of thyroid nodules. PLoS ONE 2012; 7(11):e49094
[90] Sporea I, Sirli R, Bota S, Vlad M, Popescu A, Zosin I. ARFI elastography for the evaluation of diffuse thyroid gland pathology: preliminary results. World J Radiol 2012; 4(4):174–178
[91] Bhatia KS, Tong CS, Cho CC, Yuen EH, Lee YY, Ahuja AT. Shear wave elastography of thyroid nodules in routine clinical practice: preliminary observations and utility for detecting malignancy. Eur Radiol 2012; 22(11):2397–2406
[92] Lyshchik A, Higashi T, Asato R et al. Elastic moduli of thyroid tissues under compression. Ultrason Imaging 2005; 27(2):101–110
[93] Sebag F, Vaillant-Lombard J, Berbis J et al. Shear wave elastography: a new ultrasound imaging mode for the differential diagnosis of benign and malignant thyroid nodules. J Clin Endocrinol Metab 2010; 95(12):5281–5288
[94] Barr RG, Zhang Z. Shear-wave elastography of the breast: value of a quality measure and comparison with strain elastography. Radiology 2015; 275(1): 45–53
[95] Magri F, Chytiris S, Capelli V et al. Shear wave elastography in the diagnosis of thyroid nodules: feasibility in the case of coexistent chronic autoimmune Hashimoto's thyroiditis. Clin Endocrinol (Oxf) 2012; 76(1):137–141
[96] Friedrich-Rust M, Romenski O, Meyer G et al. Acoustic Radiation Force Impulse-Imaging for the evaluation of the thyroid gland: a limited patient feasibility study. Ultrasonics 2012; 52(1):69–74
[97] Veyrieres JB, Albarel F, Lombard JV et al. A threshold value in Shear Wave elastography to rule out malignant thyroid nodules: a reality? Eur J Radiol 2012; 81(12):3965–3972
[98] Slapa RZ, Piwowonski A, Jakubowski WS et al. Shear wave elastography may add a new dimension to ultrasound evaluation of thyroid nodules: case series with comparative evaluation. J Thyroid Res 2012; 2012:657147
[99] Park AY, Son EJ, Han K, Youk JH, Kim JA, Park CS. Shear wave elastography of thyroid nodules for the prediction of malignancy in a large scale study. Eur J Radiol 2015; 84(3):407–412
[100] Kim I, Kim EK, Yoon JH et al. Diagnostic role of conventional ultrasonography and shearwave elastography in asymptomatic patients with diffuse thyroid disease: initial experience with 57 patients. Yonsei Med J 2014; 55(1):247–253
[101] Gu J, Du L, Bai M et al. Preliminary study on the diagnostic value of acoustic radiation force impulse technology for differentiating between benign and malignant thyroid nodules. J Ultrasound Med 2012; 31(5):763–771
[102] Hou XJ, Sun AX, Zhou XL et al. The application of Virtual Touch tissue quantification (VTQ) in diagnosis of thyroid lesions: a preliminary study. Eur J Radiol 2013; 82(5):797–801
[103] Han R, Li F, Wang Y, Ying Z, Zhang Y. Virtual Touch tissue quantification (VTQ) in the diagnosis of thyroid nodules with coexistent chronic autoimmune Hashimoto's thyroiditis: a preliminary study. Eur J Radiol 2015; 84 (2):327–331
[104] Zhan J, Diao XH, Chai QL, Chen Y. Comparative study of acoustic radiation force impulse imaging with real-time elastography in differential diagnosis of thyroid nodules. Ultrasound Med Biol 2013; 39(12):2217–2225
[105] Carneiro-Pla D. Ultrasound elastography in the evaluation of thyroid nodules for thyroid cancer. Curr Opin Oncol 2013; 25(1):1–5
[106] Kim H, Kim JA, Son EJ, Youk JH. Quantitative assessment of shear-wave ultrasound elastography in thyroid nodules: diagnostic performance for predicting malignancy. Eur Radiol 2013; 23(9):2532–2537
[107] Menzilcioglu MS, Duymus M, Gungor G et al. The value of real-time ultrasound elastography in chronic autoimmune thyroiditis. Br J Radiol 2014; 87 (1044):20140604
[108] Xie P, Xiao Y, Liu F. Real-time ultrasound elastography in the diagnosis and differential diagnosis of subacute thyroiditis. J Clin Ultrasound 2011; 39(8): 435–440
[109] Andrioli M, Persani L. Elastographic techniques of thyroid gland: current status. Endocrine 2014; 46(3):455–461
[110] Chen L, Freeman SJ, Gee AH et al. Initial clinical experience of an ultrasonic strain imaging system with novel noise-masking capability. Br J Radiol 2010; 83(992):702–706
[111] Cantisani V, Grazhdani H, Drakonaki E et al. Strain US elastography for the characterization of thyroid nodules: advantages and limitation. Int J Endocrinol 2015; 2015:908575
[112] Samir AE, Dhyani M, Anvari A et al. Shear-wave elastography for the preoperative risk stratification of follicular-patterned lesions of the thyroid: diagnostic accuracy and optimal measurement plane. Radiology 2015; 277 (2):565–573
[113] Andrioli M, Trimboli P, Amendola S et al. Elastographic presentation of medullary thyroid carcinoma. Endocrine 2014; 45(1):153–155

7 Elastography of the Prostate

Jean-Michel Correas and Olivier Hélénon

7.1 Introduction

Prostate cancer (PCa) is a public health issue because it is the cancer with the highest incidence rate and the second leading cause of cancer death in men (the first being lung cancer). There were around 790,000 cases in the United States in 2012, with 241,740 being new cases.[1] These figures are slightly higher than those for breast cancer for the same year. In France, the number of new cases was estimated to have been 71,000 in 2011 with a significantly increasing rate (+8.5% every year between 2000 and 2005). This is as a result of the combined aging of the population, improvement in diagnostic techniques, and increased monitoring of prostatic specific antigen (PSA) levels.[2] The number of new cases is around 3.3 times higher than that of colorectal cancer, while the number of deaths related to PCa was estimated to be 8,700 in 2011, almost identical to that of colorectal cancer (9,200 deaths). Despite improvement in diagnosis due to progress in imaging techniques and greater efficacy in treatment, the specific mortality rate is only falling slightly, but this fall is constant (-2.5% per year for the period 2000–2005). There is no systematic screening. Individual screening relies on an annual digital rectal examination (DRE) and PSA level monitoring. Detection and characterization of prostate nodules using ultrasound or magnetic resonanace imaging (MRI) remain difficult to carry out.[3]

7.2 Prostate Cancer Screening

PCa systematic screening has been challenged again following the publication of the recent recommendations by the French National Authority for Health (HAS).[2] The aim of systematic screening is to detect a clinically significant cancer in healthy men, hopefully a curable lesion at an early stage, thereby improving the prognosis of the disease. Its benefits must be greater than its drawbacks, which include complications related to treatment (urinary incontinence, impotence, radiation cystitis or proctitis), to diagnostic methods (hematuria, rectal hemorrhage, urinary retention, postbiopsy prostatitis, complications due to MRI and administration of contrast agents, PSA false positives), to the psychological impact of this diagnosis, and finally to false positives of MRI examinations. The limits of screening stem from the lack of an effective and simple test to pinpoint men with a risk of cancer high enough to justify continuing the diagnostic procedure with more aggressive tests. Screening may concern either an entire population based on age (systematic screening) or a target population considered to be at high risk. Screening is considered to be organized, when it concerns an entire population actively recruited, or individual, when the population is recruited when treatment is sought. In France, just as in the United States or the United Kingdom, there is no systematic screening, because of the lack of proof that the specific death rate can be reduced.[4] We cannot, however, rule out the role played by extending individual screening through combining PSA level screening to DRE in light of the recent fall in specific death rate. However, individual screening for PCa may be offered to men over 50 without a predisposition, after disclosing the benefits and risks to the patient. For high-risk patients (first degree family history, African American patients), screening may even start earlier, at age 40. Individual screening for PCa is based on DRE and PSA levels. However, increase of PSA levels is not specific to PCa and can be related to prostatic hyperplasia, acute and chronic prostatitis, or prostate trauma (caused by cystoscopy, resection, or biopsies). Moreover, there are significant PCas with PSA levels lower than the threshold of 4 ng/ml.

7.3 Prostate Cancer Diagnosis

PCa may be suspected if the PSA level is abnormal or increasing, or if the DRE is abnormal. Further tests are then carried out, which in most cases mean a transrectal ultrasound-guided biopsy. Prostate biopsy also allows estimating the tumor volume (number and spatial dispersion of the positive cores, length of the tumor in each positive sample) and its aggressiveness (Gleason score [GS] and invasion of the capsule or the neurovascular bundles). However, this approach has several limitations. PSA screening leads to a substantial number of unnecessary biopsies in patients with no cancer or with indolent cancer that does not need immediate treatment, with an estimated over-detection rate ranging from 27 to 56%.[5] The false negative rate of prostate biopsy varies from 17 to 21% in patients with a negative first series of biopsies.[4,6] Many urologists are now facing a dilemma when patients present with an abnormal level of PSA and negative biopsies: when should one stop and when should one continue carrying out biopsies?[7] Finally, although PSA levels and biopsy results are correlated with the clinical stage, tumor volume, and histological tumor grade, the information provided is limited for predicting the tumor mass and its aggressiveness in each patient.[5] The increase in the number of core biopsies (saturation biopsies up to 40) improves PCa detection and offers a better estimation of the tumor volume and GS,[8,9] but it has many limitations including increased cost and morbidity, and over-diagnosis and overtreatment of microscopic tumor foci;[10,11] saturation biopsies cannot really rule out PCa.[8,9] MRI recently provided interesting results in terms of detecting and locating tumors.[12] Multiparametric MRI (mp-MRI), combining T2-weighted imaging and functional sequences, has become a major modality for tumor detection and staging,[12] particularly in candidates for radical prostatectomy (RP), with areas under the receiver operating characteristic (ROC) curve over 0.9.[13,14,15] Other interesting results have been published on patient series having a first negative biopsy and an elevated PSA level.[16]

One clinical study has reported that mp-MRI could improve the positive biopsy rate in patients with a visible MRI anterior lesion.[17] However, MRI performance varies depending on which combination of positive features is selected for cancer diagnosis between T2-weighted sequence, diffusion sequence (including apparent diffusion coefficient [ADC] calculation), dynamic contrast-enhanced sequence, and sometimes spectro-MRI. If

the sensitivity of mp-MRI is high, its specificity remains low especially because it is affected by the increased vascularity of the normal inner gland and coexisting benign prostatic hyperplasic nodules. Also while its sensitivity is high for large (> 1 cm^3) and high GS PCa (≥ 6),[18] its remains low for the detection of small lesions of limited GS (< 6) and there is little information to help distinguish between aggressive and indolent tumors.[19] Computer-aided diagnosis systems may help in standardizing the interpretation of images and in defining thresholds for distinguishing aggressive tumors.[20] Different scoring systems combining the different sequences exist today: the subjective 5-point Likert score,[13] the Prostate Imaging—Reporting and Data System (PI-RADS), and the morphology-location-signal (MLS) intensity.

In a recent study comparing these different scoring systems,[21] the Likert scoring system exhibited significantly higher diagnostic performance for the characterization of prostate lesions than the other two systems. This study also reported a poor to moderate interobserver agreement for categorization of prostate lesions visible at mp-MRI as benign or malignant for all scoring systems. Conventional transrectal ultrasound (TRUS) B-mode imaging has also been studied to assess its performance for PCa diagnosis. However, its sensitivity and specificity were very limited ranging between 40 to 50% for PCa detection, and were not significantly improved by the use of color or power Doppler.[22,23] Contrast-enhanced ultrasound is still under evaluation and has proven to sensitize prostate biopsy;[24] however, it requires an intravenous injection.

Prostate harboring PCas are usually stiffer than "normal" prostate, and this feature plays a major role during DRE.[25] However, DRE is not suitable for PCa diagnosis as its findings are subjective, its interobserver variability is very important,[26] and it is not an accurate method for staging disease and locating the different foci accurately,[27] which are two factors mandatory for planning primary therapy. An imaging technique able to map tissue elasticity could therefore be useful in detecting and locating cancer areas within the prostate.

7.4 Why Measure Prostate Tissue Elasticity for Prostate Cancer Diagnosis?

Up until recently, conventional imaging techniques did not provide any information about in vivo elastic properties of organs. However, the elasticity (or equivalently, the stiffness) of tissues in the body changes as diseases progress over several months and/or decades depending on the speed of the disease progression. PCa tissue becomes stiffer than the surrounding healthy prostate tissue due to several changes. There is an increase in cellular density and in microvascularization, destroying the glandular architecture[28] and triggering wound repair. This process is characterized by the stromal reaction[28,29] and the deposition of collagen in the stroma surrounding the cancer.[30] This deposition of collagen also significantly increases with an increasing Gleason score[31,32] and is linked to a significant reduction in the acinar area in the PCa stroma. All these changes contribute to the increased stiffness of tissue affected by PCa.[33]

Several studies focused on ex vivo samples mainly due to the engineering challenges of deploying mechanical devices to measure stiffness in vivo. The results of the different mechanical studies performed ex vivo on prostate tissue samples are summarized in ▶ Table 7.1.[33,34,35,36,37,38] In the late 1990s Krouskop et al[34] started a mechanical assessment of prostate tissue. A significant difference between normal and cancerous prostate tissue stiffness was demonstrated.[35,37,38] Moreover, the increase in tissue stiffness was correlated to the aggressiveness of the disease as evaluated with the Gleason score (GS)[37] and the disease severity.[38] This fact is an important finding, as elasticity could help differentiate clinically significant cancer from insignificant disease. Benign prostatic hyperplasia (BPH) nodules can often induce false positive diagnosis when using DRE and/or TRUS imaging, revealing the presence of prostate nodules at B-mode imaging. Young's moduli for BPH nodules versus those for cancerous tissues nodules reported in two of these studies are significantly different.[33,38]

Table 7.1 Measurement of tissue elasticity using mechanical techniques

Study	Year	Study design	# Specimens	Tissue stiffness range (kPa)		
				Normal	BPH	PCa
Krouskop et al[34]	1998	1 from patient with RP	–	55–71	36–41	96–241
Phipps et al[33]	2005	83 samples from 22 patients with RP	11 BPH 11 PCa	–	100	118
Zhang et al[36]	2008	17 samples from 8 RP peripheral zones	8 normal 9 PCa	15.9 ± 5.9	–	40.4 ± 15.7
Hoyt et al[35]	2008	17 samples from 8 RP specimens	8 normal 9 PCa	3.8–25	–	7.8–40.6
Ahn et al[37]	2010	46 RP specimens	–	17.0 ± 9	–	24.1 ± 14.5
Carson et al[38]	2011	23 RP specimens, 6 autopsy specimens	–	41.1	36.8	30.9–71.0

Abbreviations: BPH, benign prostatic hyperplasia; PCa, prostate cancer; RP, radical prostectomy; #, number of.

Despite the limitations of ex vivo studies, these encouraging results, together with the wide use of TRUS for guiding systematic biopsy, prompted the development of an ultrasound-based elasticity imaging for the prostate gland.

7.5 Prostate Elastography Techniques

Several ultrasound-based methods were developed in the recent years to measure in vivo prostate tissue elasticities and provide an elasticity map. They improve both prostate lesion characterization and PCa detection; in particular, this approach can be extremely useful for prostate lesions, disclosing lesions on the elasticity map which are not visible in conventional TRUS imaging (isoechogenic lesions) or other imaging modalities such as MRI. In fact, it is of importance to understand that isoechogenic lesions can be detected with prostate elastography, as the displayed information does not rely on backscattered signals. Elastography may therefore have two major indications: to provide additional information for the characterization of prostate lesions and to improve the detection of PCas.

Two concepts are currently used for ultrasound elastography: the analysis of the strain or deformation of a tissue created by a mechanical force (static/quasistatic elastography or strain elastography [SE]) and the analysis of the propagation speed of a shear wave (shear wave elastography [SWE]) which is linked to tissue elasticity.

7.5.1 Strain Elastography

In prostate strain elastography, an external stress is applied on the patient's rectal wall adjacent to the prostate peripheral zone by using the endocavity transducer as a compression device. There are technical issues that arise with the prostate application of strain elastrography. The first issue is related to obtaining homogeneity of the tissue deformation due to the use of a microconvex endfire transducer. The compression–release cycles should be applied without changing the imaging plane in order to avoid slippage artifacts. This might be difficult with the length of the transducer and its microconvex shape. A water-filled balloon placed between the imaging probe and the rectal wall can be used to improve the homogeneity of the deformation.[39] The second issue is related to the position of the FOV. Indeed, the stiffness color scale is automatically distributed from the lowest to the highest strain found in the image plane. The display depends upon the range of stiffness found in the stiffness region of interest (ROI). This is why the size and position of the stiffness box may induce artifactual variation of the displayed strain and the ROI should cover the entire gland and the surrounding tissues. The third issue is related to the lack of true quantitative information. The stiffness threshold cannot be defined, and only qualitative images are provided to the clinician. The value of semiquantitative information that can be derived by measuring the strain ratio between two regions of interest (usually one considered "normal" in terms of stiffness and one considered "abnormal") is limited. The strain for each pixel is color-coded (or grayscale-coded) and displayed as overlay on the B-mode image. This technique became available on endocavity probes to allow prostate scanning several years ago.

Acquisition and Interpretation

Prostate strain elastography is conducted after a complete B-mode and color Doppler examination conducted in the transverse and sagittal planes, in order to measure prostate volume, identify suspicious areas in the peripheral gland (mostly hypoechoic and sometimes hypervascular), and analyze the periprostatic space (including the seminal vesicles). Strain elastography mode is activated and each suspicious focal lesion is analyzed during slight compression–release cycles induced by the transrectal probe, while the patient is lying in a left lateral position. The entire gland can also be studied for detection of stiff areas typically in the transverse plane. The Quality Index (quality factor) allows controls to ensure appropriate speed and pressure of the compression–release cycle.

Stiff tissues exhibit a reduced strain color-coded in blue, while soft tissues have an increased strain color-coded in red. The normal strain elastography pattern of the peripheral zone is of intermediate elasticity (▶ Fig. 7.1), while the inner gland (mostly the transition zone) shows more heterogeneity and exhibits an increasing stiffness with growing age and volume[40] (▶ Fig. 7.1b). Hypoechoic lesions coded in blue are highly suspicious to be malignant (▶ Fig. 7.2).

Limitations

Prostate strain elastography is facing some challenges, such as the lack of uniform compression over the entire gland, the operator dependency, and the requirement of significant training in order to improve reproducibility and limit artifacts. One of the greatest limiting factors is the difficulty in mastering the technique required to obtain appropriate and reproducible strain elastograms. The interobserver agreement in detecting cancer can show a moderate agreement between readers, as demonstrated by low kappa values.[41] Even in experienced hands, up to 32% strain elastographic acquisitions can be judged to be unevaluable due to technical problems, such as slippage of the compression plane.[41,42] The mismatch between the pre- and postcompression planes results in wrong estimation of the tissue elasticity, but this artifact is reduced with training and balloon interposition. Benign prostatic hyperplasia is responsible for most of the false positive elastography evaluation.[41] Stiff areas can also result from inflammatory prostate disease and can be detected in up to 40% of the patients in whom cancer was not detected.[43]

Compression of the prostate from the rectum may prevent transmission of sufficient deformation through the entire prostate, more specifically the anterior region of the prostate. It should be noted that the compression applied to the posterior regions and the subsequent deformation is necessarily different from that at the anterior region (due to depth); the same mechanism applies with the base and the apex due to the different angulation of the endfire transducer. This may affect the strain elastography dectection rates (DRs), that were reported to be lower in the anterior region of the prostate than in the posterior region, and also lower in the prostatic base compared with the apical region, as shown by several studies.[39,44,45,46]

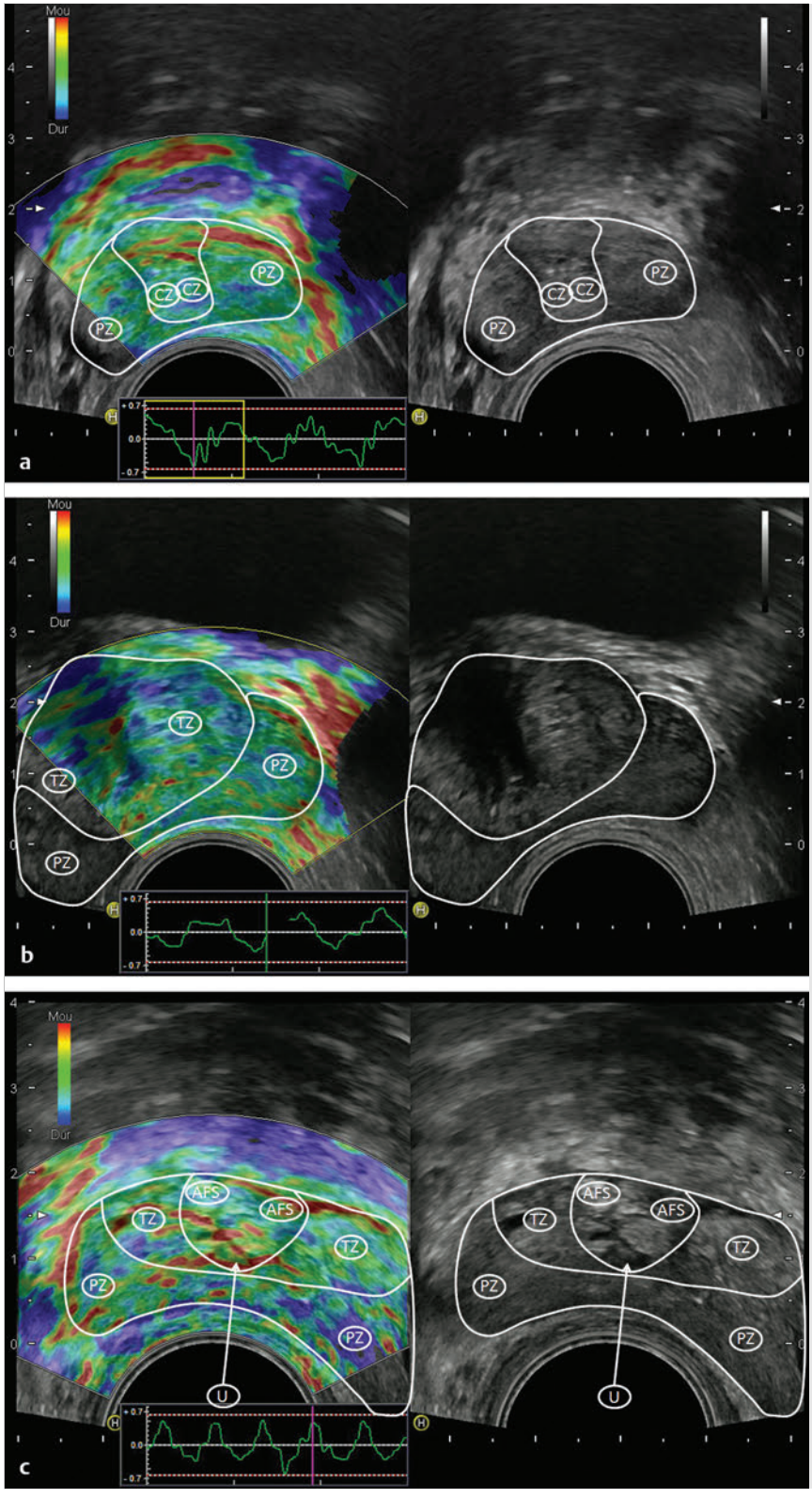

Fig. 7.1 Typical distribution of elasticity pattern using strain elastography in a 60-year-old patient with moderate benign prostatic hyperplasia (BPH). **(a)** Prostate base, transverse view, left lateral rotation of the transducer. The peripheral zone (PZ) is coded with green and red colors due to soft to intermediate tissue stiffness. Some blue colors are seen at the edges of the gland corresponding to nondeformation artifacts. At the most upper and anterior part of the gland, it is difficult to separate the central zone (CZ) from the anterior fibromuscular stroma. The pericapsular elastic border is coded in red (soft) and can be seen anteriorly. **(b)** Prostate mid-gland, transverse view, left lateral rotation of the transducer. The peripheral zone (PZ) appears larger with the same elasticity pattern. The transition zone (TZ) exhibits a more heterogeneous pattern due to BPH development with some blue colors due to stiffer areas. The pericapsular elastic border is coded in red (soft) and can be seen laterally. **(c)** Prostate apex, transverse view, slight right lateral rotation of the transducer. The peripheral zone (PZ) is mainly coded in green due to intermediate elasticity. The pericapsular elastic border is coded in red (soft) and can be seen anteriorly. Note the heterogeneous pattern of the urethra with peripheral ring-shaped lines. AFS, anterior fibromuscular stroma; U, urethra.

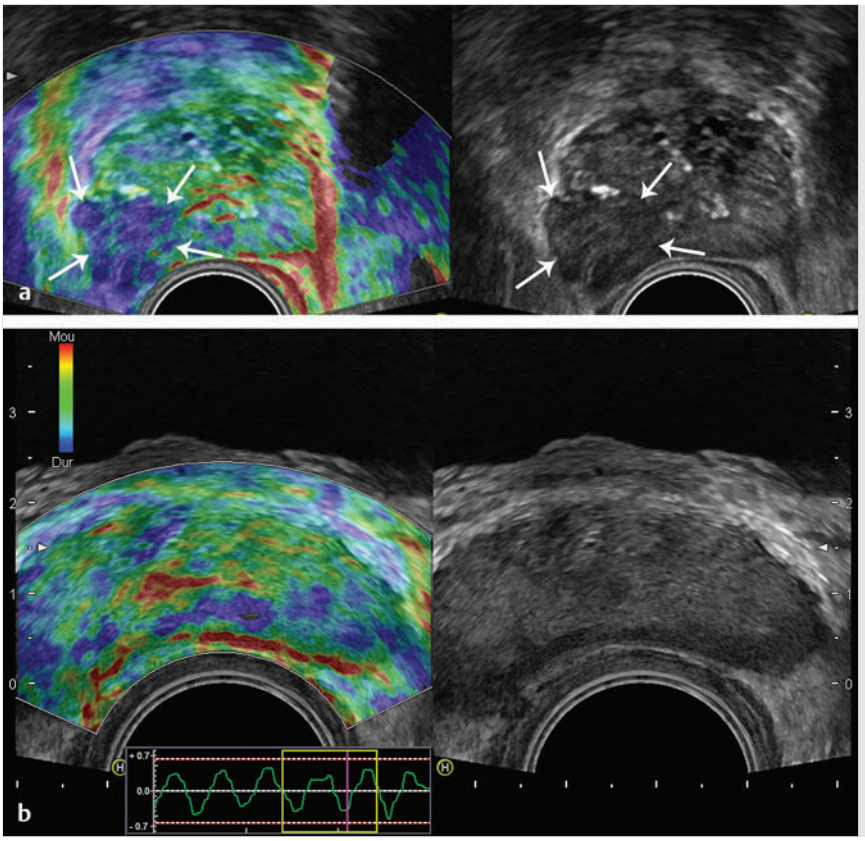

Fig. 7.2 Prostate cancer pattern at strain elastography. **(a)** Typical hypoechogenic nodule developed in the posterior peripheral zone, with typical stiff pattern color-coded in blue (*arrows*); note that the cancer is certainly invading the capsule. **(b)** Diffuse prostate cancer invading the entire gland corresponding to a Gleason score 7 lesion. This diagnosis is difficult and was initially missed by the magnetic resonance imaging (MRI) study. However, the strain elastogram revealed the presence of abnormal stiff areas coded in blue distributed all over the peripheral and transition zones. This pattern was very stable with the compression–release cycles.

7.5.2 Shear Wave Elastography

Unlike strain elastography (SE), shear wave elastography, or SWE, requires no compression on the rectal wall to produce elastograms. This technique is based on the measurement of shear wave velocity propagating through the tissues.[47] It belongs to the field of multiwave imaging as it combines two different waves: one (shear wave) that provides stiffness information and another (ultrasonic wave) that captures the propagation of the shear wave. Thanks to the combination of these two waves, shear wave elastography provides a dynamic quantitative map of soft tissues' viscoelastic properties in quasireal-time. It is important to know that the prostate can be easily displaced by perineal muscle contractions and/or by the endocavity transducer introduction and displacements. Despite the low frame rate, the quasireal-time acquisition is truly helpful in scanning the prostate. Mean elasticities are averaged from a region of interest (ROI) and can be displayed in kilopascals (kPa) or in meters per second (m/s) (if shear wave speeds are displayed). The shear wave speed (in m/s) or the Young's modulus (in kPa) is color-coded for each pixel and displayed as an overlay on the B-mode image.

Stiff tissues are color-coded in red, while soft tissues appear in blue. The elasticity values (mean, standard deviation, minimum, and maximum) are then calculated for each ROI (▶ Fig. 7.4a). The ratio between the mean values of two ROIs placed in a suspicious region and in the adjacent normal peripheral zone can be calculated (▶ Fig. 7.4a). This technology became available on endfire endocavity transducers only recently, explaining the limited number of published papers.

Acquisition and Interpretation

Prostate SWE is also conducted after a complete evaluation of the prostate using B-mode and color Doppler imaging in a patient lying in a left lateral position. SWE mode is activated and each suspicious focal lesion is analyzed avoiding any pressure on the transducer. Optimized settings should include maximized penetration and appropriate elasticity scale (70 to 90 kPa). The entire gland can also be scanned for detection of stiff areas in the transverse plane. The SWE box is enlarged to the maximum in order to cover half of the gland on a transverse plane. Thus, each side of the prostate is scanned separately and stored from base to apex in 2 separate cine loops. For each plane, the transducer is maintained in a steady position for 3 to 4 seconds until stabilization of the signals occurs. Hypoechoic lesions coded in red are highly suspicious to be malignant. The digital cine loop can be reviewed and the ROI can be positioned on suspicious areas detected either at the B-mode scan or during the SWE detection scan, even during the review process. The elasticity values (mean, standard deviation, minimum, and maximum) are then calculated for each ROI.

In young patients without prostatic disorder, the peripheral and central zones are coded in blue with a very homogeneous pattern (with stiffness values ranging from 15 to 25 kPa), while the transition zone exhibits stiffness below 30 kPa (▶ Fig. 7.3). With the development of benign prostatic hyperplasia, the peripheral zone remains soft with a very homogeneous color encoding in blue (soft tissue), while the transition zone becomes hard (red color) with a heterogeneous color pattern; elasticity values range from 30 to 180 kPa[48] (▶ Fig. 7.3).

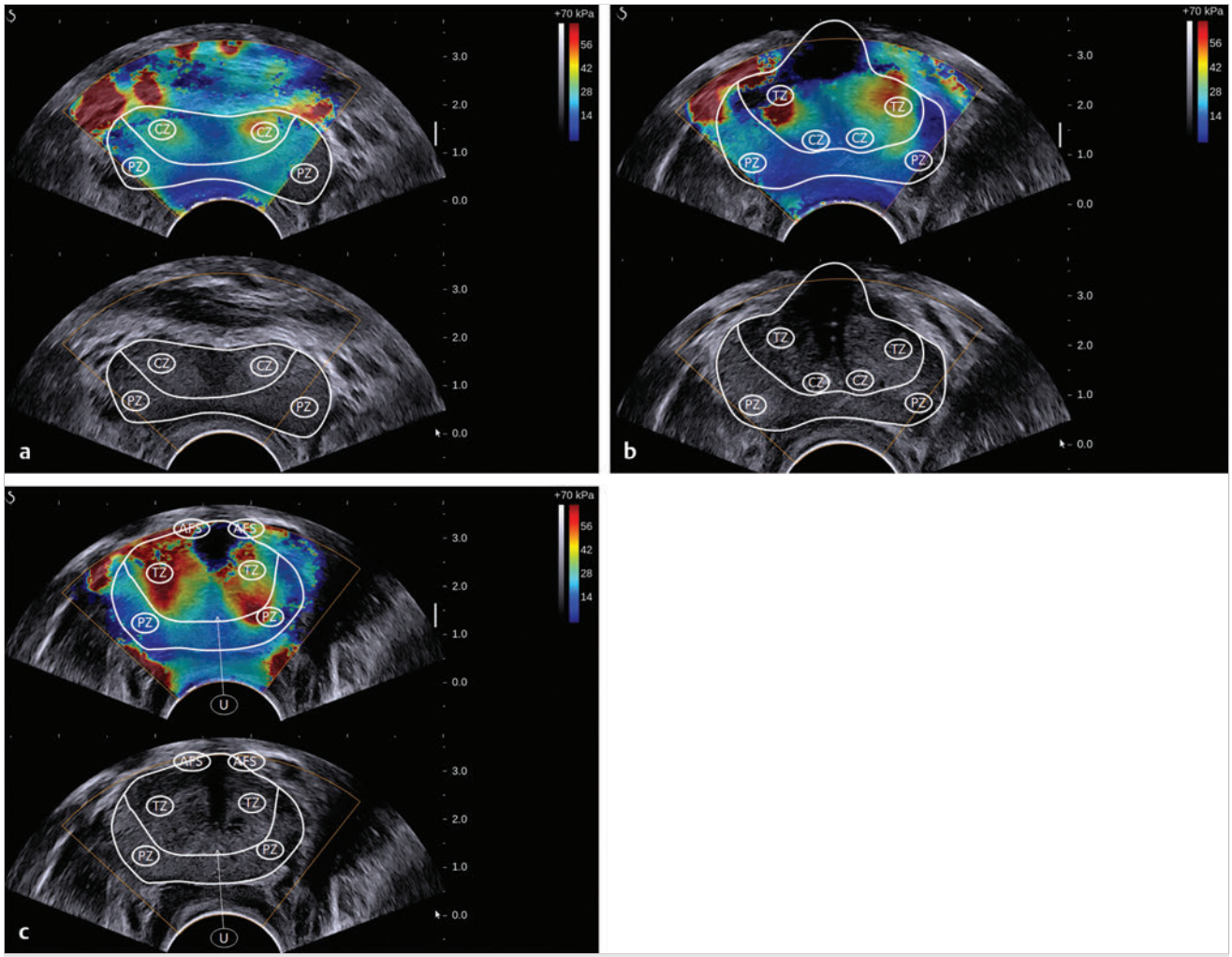

Fig. 7.3 Typical distribution of elasticity pattern using shear wave elastography in a 35-year-old patient with minimal benign prostatic hyperplasia (BPH), from base to apex. (**a**) Prostate base, transverse view. The peripheral zone (PZ) is homogeneously soft and, thus, is coded with blue colors. The mean stiffness values are typically below 30 kPa. The central zone (CZ) remains rather homogeneous due to minimal development of BPH and appears slightly stiffer with mean values ranging from 20 to 30 kPa. Note that the space between the rectal wall and the posterior peripheral zone is coded in blue reflecting the minimal pressure induced by the endocavity transducer. (**b**) Prostate mid-gland, transverse view. The peripheral zone appears larger and remains homogeneous with typical soft pattern and mean stiffness values below 30 kPa. The central zone is still visible posteriorly and is rather homogeneous due to minimal development of BPH, appearing slightly stiffer with mean values ranging from 20 to 35 kPa. The transition zone (TZ) appears more heterogeneous due to BPH development. (**c**) Prostate apex, transverse view. The peripheral zone exhibits the same homogeneous soft pattern with mean stiffness values below 30 kPa. The transition zone appears heterogeneous due to BPH development and some anterior nodules are displayed at SWE with mean stiffness values of 30 to 55 kPa. Due to limited anterior penetration of SWE, the anterior fibromuscular stroma is not color-coded. AFS, anterior fibromuscular stroma; U, urethra.

SWE reproducibility has been studied in a single paper and showed an excellent overall intraobserver reproducibility (intraclass correlation [ICC] = 0.876), with minimal impact of ROI location, prostate volume, and clinical variables (ICC = 0.826–0.917).[49] The real-time capability of SWE allows one to sweep through the whole gland and to perform detection of stiff foci that are not always displayed in the B-mode image (▶ Fig. 7.4, ▶ Fig. 7.5). PCas usually appear as stiffer areas than the surrounding tissue (▶ Fig. 7.5). Targeted biopsy can be performed under SWE guidance to increase the detection rate of cancer. Despite the slow frame rate, the real-time capability of SWE is helpful in optimizing the needle tract, and targeting the stiffest area of the nodule that sometimes does not strictly correlate with the B-mode findings (▶ Fig. 7.6).

Limitations

Prostate SWE is also facing some challenges. When a stiff area is encountered, the operator should release any pressure on the rectum to be sure that the stiffer pattern does not result from excessive pressure on the endfire transducer; however, some pressure cannot be avoided when scanning the apex as the transducer is reclined or when scanning a large hypertrophic prostate that protrudes into the rectal lumen. In cases of excessive pressure, the peripheral zone sitting just against the transducer appears stiff. SWE has other limitations, such as slow frame rate, a small SWE box, image stabilization, and penetration issues. In the presence of macrocalcifications, the elasticity values are increased (▶ Fig. 7.7). The shear wave pulse

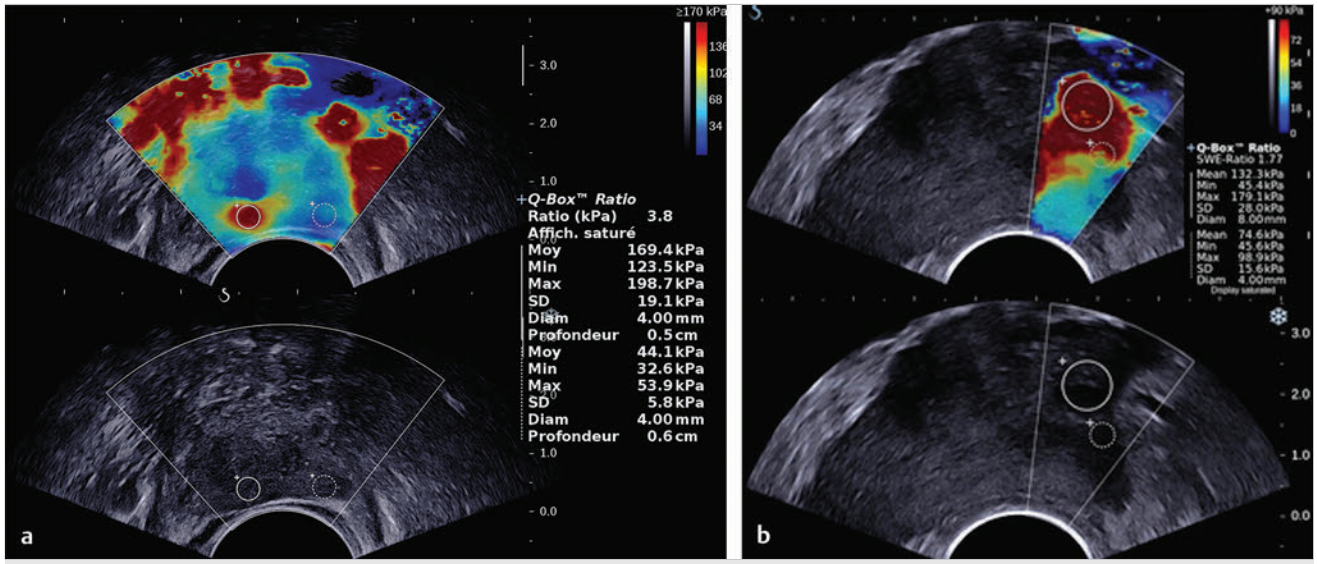

Fig. 7.4 Shear wave elastography (SWE) typical pattern of prostate cancer. (**a**) The posterior peripheral zone at the apex appeared slightly hypoechogenic. SWE reveals a very stiff nodular area; the mean stiffness of the lesion is 169 kPa while the contralateral peripheral zone stiffness is at 44 kPa; the stiffness ratio is 3.8. SWE allows quantitative measurements of tissue stiffness using ROI. For prostate SWE, the typical scale of displayed elasticity values is set to 50 to 70 kPa. Note that the posterior periprostatic space is color-coded in blue demonstrating the minimal pressure of the endocavity transducer. Prostate biopsy confirmed the presence of a Gleason score 8 adenocarcinoma. (**b**) The diagnosis of anterior prostate cancer is more difficult. In this patient, the anterior peripheral zone was slightly hypoechogenic. SWE reveals a very stiff nodular area; the mean stiffness of the lesion is 169 kPa while the contralateral peripheral zone stiffness is at 132 kPa; the adjacent posterior peripheral zone is color-coded in light blue, corresponding to stiffness values below 35 kPa. Prostate biopsy confirmed the presence of a Gleason score 7 adenocarcinoma.

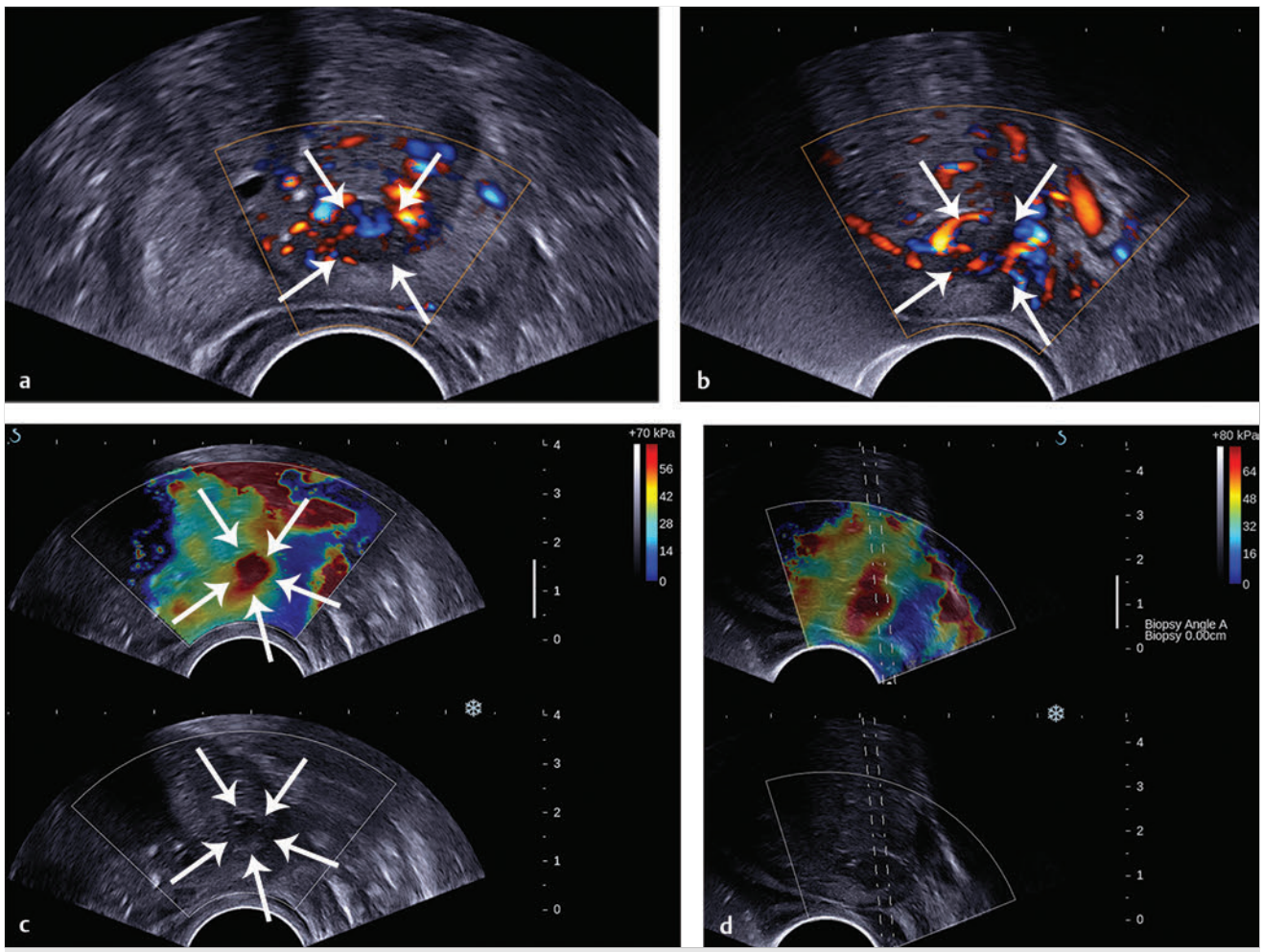

Fig. 7.5 The additional value of shear wave elastography (SWE) for prostate cancer diagnosis and biopsy. (**a,b**) Prostate B-mode and directional power Doppler TRUS did not detect any lesion in the peripheral zone; a single hypervascular nodule was seen in the transition zone sitting next to the posterior surgical capsule and exhibited some strong hypervascularity (*white arrows*) in the transverse plane (**a**) and the sagittal plane (**b**). (**c**) During the detection scan from base to apex, SWE revealed a very stiff nodular area (red pattern) in the peripheral zone at mid-gland level. The area was previously seen at B-mode imaging as a pseudo-cystic hypoechogenic area and was not initially considered as a potential target. (**d**) SWE-targeted biopsy inside this lesion confirmed the presence of a Gleason score 6 adenocarcinoma. All other cores were negative.

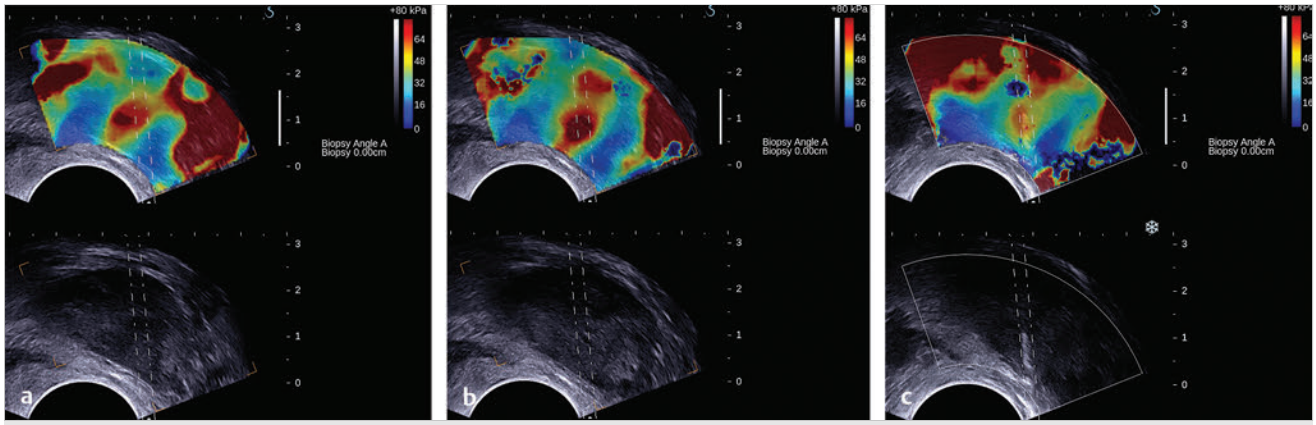

Fig. 7.6 Shear wave elastography (SWE)–targeted biopsies. (**a**) This prostate lesion was poorly seen at B-mode imaging but easily detected at SWE. The dotted lines indicate the needle tract. This angulation is suboptimal, as the tract is not targeting the stiffest area of the lesion. (**b**) After bending the transducer, the route was optimized and the tract was covering most of the stiffest part of the lesion. (**c**) The needle tract was passing exactly in the lesion. SWE-targeted biopsy is of interest particularly when the lesion cannot be seen at B-mode imaging.

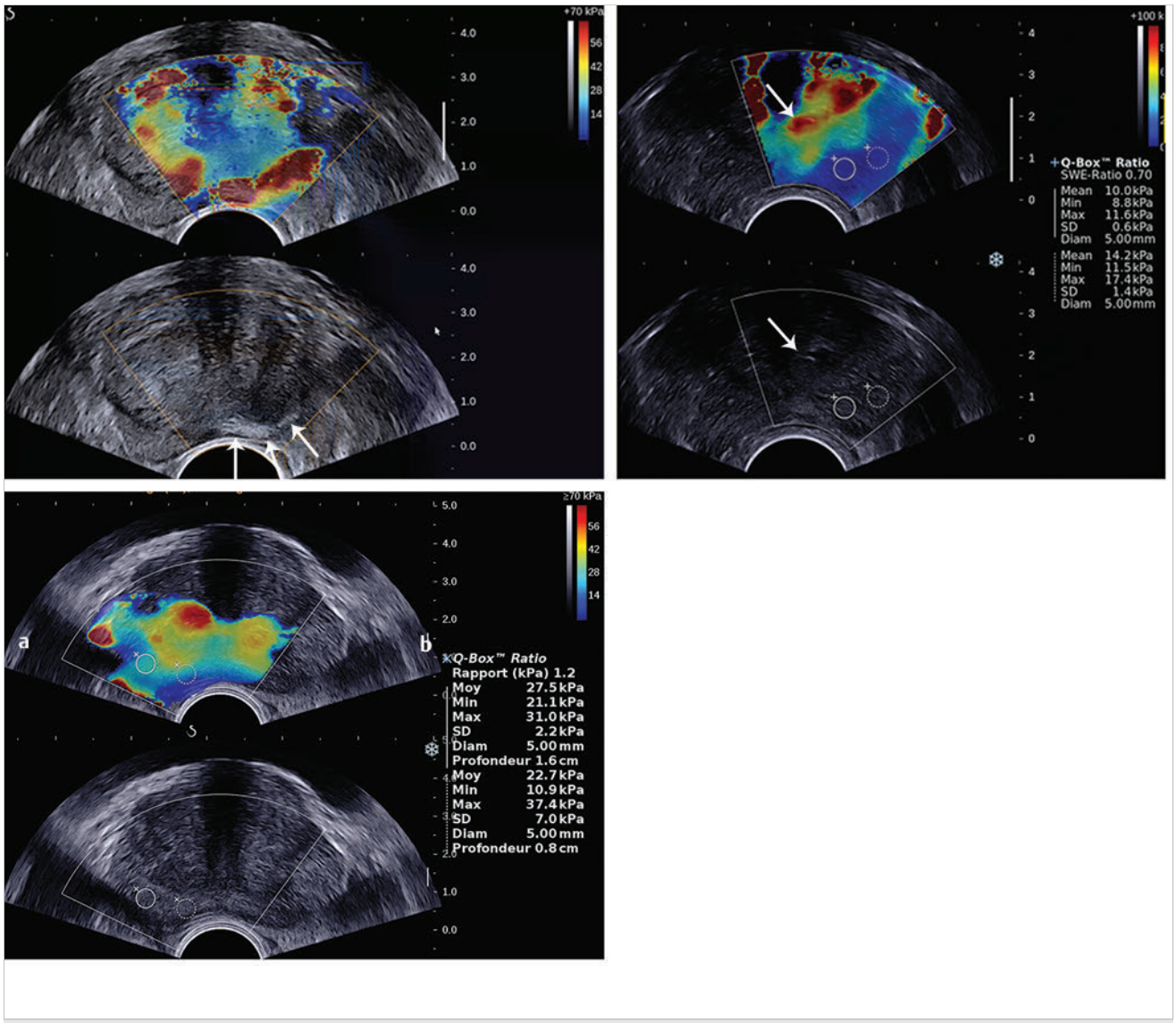

Fig. 7.7 Prostate elastography: pitfalls and limits. (**a**) Shear wave elastography (SWE): increased stiffness due to massive calcifications at the limit between peripheral and transition zones (*arrows*). (**b**) Sometimes, the calcifications are less visible and the SWE pattern should always be analyzed in conjunction with the B-mode image (*arrow*). (**c**) SWE: large benign prostate hyperprophy attenuating the ultrasound beam, and particularly the shear waves. There is no mapping of elasticities below 2 to 3 cm in the anterior part of the prostate.

Table 7.2 Literature review of prostate elastography studies prior to radical prostatectomy for diagnostic performance per patients and per core

Study	Year	Technique	Patients	# PCa	Sen (%)	Spef (%)	PPV (%)	NPV (%)	Acc (%)
Pallwein et al[51]	2007	Strain	16	35	87	92	80	95	92
Tsutsumi et al[42]	2007	Strain	51	77	82	60	–	–	–
Sumura et al[52]	2007	Strain	17	–	74	88	–	–	–
Salomon et al[53]	2008	Strain	109	451	75	77	88	59	76
Tsutsumi et al[39]	2010	Strain	55	115	73	89	81	84	83
Walz et al[54]	2011	Strain	28	88	73	79	67	83	77
Walz et al[55]	2011	Strain	32	–	72	81	67	85	–
Brock et al[56]	2011	Strain	229	894	66	72	81	53	68
Junker et al[45]	2012	Strain	39	48	83	–	–	–	–
Pelzer et al[57]	2013	Strain	50	–	–	–	–	–	–
Brock et al[58]	2013	Strain	86	56	49	74	78	51	62
Junker et al[46]	2014	Strain	39	61	67	–	–	–	–
Zhu et al[59]	2014	Strain	56	–	67	89	–	–	83
Boehm et al[48]	2015	SWE	60	60	81	69	67	82	74

Abbreviations: Acc, Accuracy; NPV, negative predictive value; PCa, prostate cancer; PPV, positive predictive value; Sen, sensitivity; Spef, specificity; #, number of.

penetrates 3 to 4 cm. In a large prostate, this may not penetrate deep enough to measure the anterior zone of the large prostate[48,50] (▶ Fig. 7.7c).

Both SWE and SE techniques also suffer from the same intrinsic limitations: not all cancers are stiff and not all stiff lesions are cancers (particularly in the presence of calcifications and fibrous changes). This is why the analysis of the B-mode pattern of the stiff areas remains mandatory.

7.6 Literature Review

Several studies attest to the value of both SE and SWE as shown in ▶ Table 7.2, ▶ Table 7.3 and ▶ Table 7.5. Three different applications can be identified: first, characterization of an abnormal area detected at either B-mode imaging, color Doppler US, or even at a previous MRI examination; second, detection of a lesion not seen with any previous imaging technique; and third, biopsy targeting. Prostate elastography requires specific training; the learning curve may be longer for SE due to the variability of constraint applied with the transducer. Some of the discrepancies in the literature arise from the poorer performance of the earliest implementations, and more up-to-date systems seem to be easier to use and to provide more consistent results. However, it is interesting to note that most US manufacturers are developing SWE techniques and should be extending their use to the endocavity transducers.

7.6.1 Comparison of Elastography to Radical Prostatectomy for Diagnosis of Prostate Cancer

Since systematic biopsies may miss PCa, many studies[39,42,45,46,48,51,52,53,54,55,56,57,58,59] have been conducted using RP as the gold standard to assess the overall accuracy of strain elastography for PCa diagnosis. A comparison with RP specimens allows for the exact localization, volume, histological type, and extracapsular extension of PCa lesions to be determined. Investigators scanning this group of patients might be biased knowing that RP is scheduled.

Table 7.3 Literature review of prostate elastography (strain and SWE) studies prior to systematic biopsy for diagnostic performance per patients and per core

Study	Year	Technique	N	# PCa	Per patient (%)					# Core	Per core (%)				
					Sen	Spef	PPV	NPV	Acc		Sen	Spef	PPV	NPV	Acc
Konig et al[60]	2005	Strain	404	151	84	–	–	–	–	906	51	67	49	68	61
Pallwein et al[61]	2008	Strain	492	125	89	72	62	91	77	2952	69	89	51	95	87
Kamoi et al[62]	2008	Strain	107	40	68	81	68	81	76	940	75	77	88	59	76
Miyagawa et al[41]	2009	Strain	311	95	73	–	–	–	–	1539	50	53	22	81	53
Brock et al[44]	2012	Strain	178	91	51	–	–	–	–	1068	61	68	32	89	68
Barr et al[50]	2012	SWE	53	26	100	–	–	–	–	318	96	96	69	99	96
Ahmad et al[63]	2013	SWE	50	33	–	–	–	–	–	626	92	89	95	83	91
Woo et al[64]	2015	SWE	97	26	–	–	–	–	–	1058	43	81	13	95	70
Correas et al[65]	2015	SWE	184	68	93	63	59	94	74	–	96	85	48	99	85
Boehm et al[66]	2015	SWE	95	38	95	67	49	90	58	–	–	–	–	–	–

Abbreviations: Acc, Accuracy; N, number of patients; NPV, negative predictive value; PCa, prostate cancer; PPV, positive predictive value; Sen, sensitivity; Spef, specificity; SWE, shear wave elastography; PCa, prostate cancer; #, number of.

The most important studies are summarized in ▶ Table 7.2. In 2011, Brock et al conducted the largest one on strain elastography, including a total of 229 patients with biopsy-proven PCa prospectively screened for cancer-suspicious areas and extracapsular extension using grayscale ultrasound and strain elastography.[56] Among the 1374 sectors evaluated, pathology reported the presence of cancer in 894 (62%) patients and extracapsular extension in 47 patients. Strain elastography correctly detected 594 (66%) and grayscale ultrasound 215 (24%) cancer-suspicious lesions. Strain elastography sensitivity and specificity were 66% and 72%, respectively (▶ Table 7.2), compared to 24% and 90% respectively for grayscale ultrasound. Elastography identified the largest site-specific tumor focus in 68% of patients. Extracapsular extension was identified with a sensitivity of 38% and specificity of 96% using strain elastography compared to 15% and 97%, respectively, using grayscale ultrasound. Most studies reported a significant improvement in PCa identification (▶ Table 7.2); indeed, Zhang et al[67] performed a meta-analysis using seven published studies,[39,42,52,53,54,56,68] which included a total of 508 patients to assess the diagnostic performance of strain elastography using RP as the gold standard and established that the pooled sensitivity and specificity were 72% (95% confidence interval [CI]: 70–74%) and 76% (95% CI:74–78%), respectively. They concluded that strain elastography imaging has high accuracy in the detection of PCas. Several studies[39,45,46,52,59] also showed that the PCa detection rates of strain elastography are dependent on tumor size, tumor volume, localization, histological type, and extracapsular extension. Strain elastography was found to be more sensitive in detecting PCa lesions with higher GSs, with large volumes, extracapsular extension, and located in the peripheral zone and the apical part.

Boehm et al studied the capability of SWE to localize PCa lesions prior to RP and also assessed the elasticity threshold for cancer foci detection.[48] They showed that SWE allows the identification of cancer foci based on tissue stiffness differences and that reliable cutoffs can be established, allowing examiner independent localization of PCa foci.

In recent years, the concept of focal therapy has gained more and more interest.[69] The aim of focal therapy is to provide treatment to the PCa lesion without treating the entire prostate, because this approach would reduce significantly treatment side effects by leaving the sensible structures, such as the neurovascular bundle or the urinary sphincter, untouched. The limitations of focal therapy for PCa are the multifocal nature of the disease, as well as the problem of correct identification and localization of the PCa lesions by prostate biopsy and/or imaging.[70] The main PCa lesion is usually called the PCa index lesion and is considered to be responsible for possible metastatic progression and cancer-specific death.[70] The goal of focal therapy is to treat this index lesion only. Walz et al evaluated the ability of strain elastography to identify the PCa index lesion, and they observed a low sensitivity of 59%, whereas systematic biopsies had a sensitivity of 68%.[55] They concluded that, if focal therapy had been based on strain elastography alone, only 60% of all patients would have received satisfactory treatment of the index lesion, whereas 40% of the patients would have been undertreated. However they also noticed that combining biopsy data with strain elastography would have increased the sensitivity to 85%.

7.6.2 Comparison of Elastography to Systematic Biopsies for Diagnosis of Prostate Cancer

▶ Table 7.3 summarizes the studies assessing the diagnostic performance of elastography compared with randomized biopsies. Strain elastography studies reported average to good diagnostic performance while SWE reported better diagnostic performance; accuracies, sensitivities, and negative predictive values (NPVs) ranged from 61 to 87% and 70 to 96%, 50 to 75% and 92 to 96% (except for Woo et al), and 59 to 95% and 83 to 99%, respectively, for strain elastography and SWE. These improvements can be attributed to the higher reproducibility of SWE and its quantitative nature. Miyagawa et al[41] performed a per core histology analysis and compared the results with strain elastography data on 311 patients. Among the 1528 (65%) acquisitions that could be analyzed, 805 cores were found negative and 733 positive in biopsy histology. Of the 733 positive cores, only 158 were diagnosed as cancers; of the remaining 575 elastography-positive acquisitions with biopsy negative, 424 (74%) images were considered to show prostatic hyperplasia.

SWE is a more recent technique and fewer papers can be found in the literature (▶ Table 7.4). In all studies, Young's modulus values of PCa were statistically significantly higher when compared with Young's modulus values of benign lesions ($p < 0.002$ in all studies) (▶ Table 7.4). Barr et al[50] showed that the Young's modulus value difference between benign lesions were all not statistically significant: benign versus atypia ($p = 0.818$), benign versus acute inflammation ($p = 0.606$), benign versus chronic inflammation ($p = 0.0509$), and acute inflammation versus chronic inflammation ($p = 0.096$) while Woo et al[64] showed a significant difference between normal prostate tissue and chronic inflammation ($p = 0.021$). Two studies

Table 7.4 Literature review of prostate shear wave elastography: mean stiffness and standard deviation for benign and malignant tissues (for all GS and GS 6, 7, 8, and 9 lesions).

Study	Year	N	# PCa	Benign tissue†				p	Malignant tissue‡				
				All	Norm	Infla	PIN		All	GS 6	GS 7	GS 8	GS 9
Barr et al[50]	2012	53	26	22±12	–	–	–	0.0001	58±21	–	–	–	–
Ahmad et al[63]	2013	50	33	75±47	–	–	83±39	0.0001	134±58	95±29	163±63	113±20	–
Woo et al[64]	2015	97	26	33±18	32±17	46±38	26±11	0.002	55±46	33±19	55±49	57±40	88±64
Correas et al[65]	2015	184	68	21±6	–	–	–	<0.0001	60±20	45±7	60±20	70±29	125±29
Boehm et al[66]	2015	95	38	42±20	–	–	–	<0.0001	88±40	–	–	–	–

† For Barr et al. and Correas et al. Gleason Score 6 lesions were considered PCa.
‡ For Boem et al., Ahmad et al, and Woo et al. Gleason Score 6 lesions were considered as noncancerous lesions.
Abbreviations: GS, Gleason score; Infla, inflammation; N, number of patients; Norm, normal; PIN, prostatic intraepithelial neoplasia; p, p-value; PCa, prostate cancer; #, number of lesions.

showed a statistically significant linear trend of SWE elasticity with Gleason scores (Spearman's rank correlation coefficient, $\rho = 0.343$ in Woo et al[64] and $\rho = 0.282$ in Correas et al[65] both with $p < 0.001$). In addition, aggressive PCa exhibited statistically significantly higher tissue stiffness ($p < 0.01$ in all studies) than indolent PCa in several studies.[63,64,65] Boehm et al[48] reported that false-positive results or false-negative results were observed in the anterior and transition zone of the prostate gland. In the largest study,[65] including 184 patients, we obtained sensitivity, specificity, positive predictive values, and negative predictive values of 97%, 70%, 70%, and 97%, respectively, for a 35 kPa cutoff for diagnosing PCa with GS ≥ 6.[65] This threshold is very similar to the one found in the Barr et al[50] study (37 kPa); however, it is lower than the ones found in Ahmad et al,[63] Woo et al,[64] and Boehm et al[48] studies of 70 kPa, 43 kPa, and 50 kPa, respectively. In these latter studies GS 6 lesions were considered as noncancerous lesions in the statistical analysis. This consideration also explains why, in the Ahmad et al and Boehm et al[48] studies, overall malignant and overall benign tissue mean elasticity values were higher than in Barr et al[50] and Correas et al.[65] (▶ Table 7.4).

7.6.3 Comparison of Elastography-Targeted Biopsy with Systematic Biopsy on Prostate Cancer Detection Rates

The additional value of elastography-targeted biopsies has been widely studied in recent years (▶ Table 7.5). Most of the studies are comparing the current standard of systematic 10 to 12 core biopsy schemes with image-targeted biopsies and/or with the combination of both systematic and image-targeted biopsies. All studies are concordant and show an increase of the overall DRs over the systematic biopsy scheme, when systematic and targeted biopsies were combined. This increase in per patient and per core DRs varies between 1 to 10% and 2 to 6%, respectively (▶ Table 7.5).

Only one study (Boehm et al[66]) was performed with SWE and showed that patients with the presence of suspicious SWE findings are at a 6.4-fold higher risk to harbor a clinically significant PCa and that SWE-targeted biopsies increased the per patient DR by 4%. However, most studies also reported that a non-negligible number of patients with clinically significant PCa[66,71] might be missed performing only elastography-targeted biopsies. Therefore, elastography-targeted biopsy cores should be performed in combination with systematic biopsies.

7.6.4 Comparison of Elastography to MRI for Prostate Cancer Diagnosis

A systematic literature review was conducted by Van Hove et al[71] whose aim was to gather the current evidence in favor of or against image-targeted biopsies in PCa in order to draw clinically relevant conclusions. This review included several imaging technologies including contrast-enhanced ultrasound imaging, histoscanning, MRI, and strain elastography.[43,44,73,75,78] Invariably, all imaging techniques showed an increased DR when combining systematic biopsies with targeted biopsies. This suggests that targeted biopsy should be combined with systematic biopsy using the most effective diagnostic procedure, especially in the case of repeated biopsy.

Brock et al[80] performed a study to determine whether fusion of mp-MRI combined with transrectal strain elastography could improve the visualization of PCa lesions compared to mp-MRI alone. mp-MRI alone exhibited a sensitivity and specificity of 65% and 56%, respectively, while mp-MRI combined with strain elastography increased the performance to 72% and 66%, respectively. They concluded that the mp-MRI and strain elastography combination improved PCa visualization and biopsy-guided PCa detection.

Limiting the literature to comparisons with histopathological whole mount sections, Boehm et al[66] concluded that SWE diagnostic performance is comparable to that of MRI[81] with

Table 7.5 Detection rates per patient and per core of prostate elastography (strain and SWE) with systematic biopsies (SB), with targeted biopsies (TB), and with both (SB + TB)

Study	Year	Technique	N	Study design	# SB	# TB	DR per patient (%)			DR per core (%)		
							SB	TB	SB + TB	SB	TB	SB + TB
Konig et al[60]	2005	Strain	404	SB + TB	10	≤ 4	–	31	37	–	–	–
Pallwein et al[43]	2007	Strain	230	SB + TB	10	≤ 5	25	30	35	6	13	8
Nelson et al[72]	2007	Strain	137	SB + TB	8	≤ 4	40	24	44	12	20	14
Kamoi et al[62]	2008	Strain	107	SB + TB	10	≤ 4	31	29	37	15	55	19
Aigner et al[73]	2010	Strain	94	SB + TB	10	≤ 5	19	21	28	5	24	8
Kapoor et al[74]	2011	Strain	15	SB + TB	10	≤ 4	67	73	73	37	67	43
Ganzer et al[75]	2012	Strain	139	SB + TB	10	≤ 4	47	32	53	11	22	14
Brock et al[44]	2012	Strain	353	Mixed	10	≤ 10	39	51	45	–	–	–
Zhang et al[76]	2012	Strain	148	SB + TB	12	≤ 4	–	41	44	14	76	19
Taverna et al[77]	2013	Strain	102	SB	13	–	32	1	33	–	–	–
Salomon et al[78]	2014	Strain	1024	SB + TB	10	≤ 4	39	29	46	–	–	–
Nygård et al[79]	2014	Strain	127	SB + TB	10–12	≤ 4	48	24	50	18	28	20
Boehm et al[66]	2015	SWE	95	SB + TB	6–18	≤ 3	36	28	40	9	11	9

Abbreviations: DR, detection rate(s); N, number of patients; SB, systematic biopsies; SWE, shear wave elastography; TB, targeted biopsies.

sensitivity, specificity, and accuracy of 81%, 69% and 74%, respectively.

7.7 Future Perspectives

Prostate elastography should become an additional US modality for routine prostate examination and biopsy procedures, in order to target suspicious areas and increase prostate biopsy detecton rates. It can be used to complement B-mode and color Doppler TRUS for routine scanning of the prostate, but it requires specific training. SWE provides quantitative values of prostate tissue stiffness and reliable elasticity cutoffs and seems more reproducible. The major advantage of the shear wave technology is the lack of variability due to prostate deformation required by the strain technology. It is interesting to note that most US companies involved with strain elastography are developing SWE technology. SWE also enables the development of three-dimensional prostate elastography with multiplanar reconstruction, and MRI fusion to volumetric US including elastography. These new modalities should include guiding capabilities in order to target biopsies to the most suspicious areas. The improvements in PCa detection are mandatory for the development of focal therapy.

References

[1] American Cancer Society. Estimated numbers of new cases of selected cancers by state, US 2012. In: Cancer Facts and Figures 2012. www.cancer.org.

[2] Cancer de la prostate: identification des facteurs de risque et pertinence d'un dépistage par dosage de l'antigène spécifique prostatique (PSA) de populations d'hommes à haut risque ? Haute Autorité de Santé 2012.

[3] Ahmed HU, Arya M, Freeman A, Emberton M. Do low-grade and low-volume prostate cancers bear the hallmarks of malignancy? Lancet Oncol 2012; 13 (11):e509–e517

[4] Singh H, Canto EI, Shariat SF et al. Predictors of prostate cancer after initial negative systematic 12 core biopsy. J Urol 2004; 171(5):1850–1854

[5] Kelloff GJ, Choyke P, Coffey DS; Prostate Cancer Imaging Working Group. Challenges in clinical prostate cancer: role of imaging. AJR Am J Roentgenol 2009; 192(6):1455–1470

[6] Mian BM, Naya Y, Okihara K, Vakar-Lopez F, Troncoso P, Babaian RJ. Predictors of cancer in repeat extended multisite prostate biopsy in men with previous negative extended multisite biopsy. Urology 2002; 60(5):836–840

[7] Djavan B, Remzi M, Marberger M. When to biopsy and when to stop biopsying. Urol Clin North Am 2003; 30(2):253–262, viii– viii.

[8] Delongchamps NB, Haas GP. Saturation biopsies for prostate cancer: current uses and future prospects. Nat Rev Urol 2009; 6(12):645–652

[9] Giannarini G, Autorino R, di Lorenzo G. Saturation biopsy of the prostate: why saturation does not saturate. Eur Urol 2009; 56(4):619–621

[10] Girouin N, Mège-Lechevallier F, Tonina Senes A et al. Prostate dynamic contrast-enhanced MRI with simple visual diagnostic criteria: is it reasonable? Eur Radiol 2007; 17(6):1498–1509

[11] Ashley RA, Inman BA, Routh JC, Mynderse LA, Gettman MT, Blute ML. Reassessing the diagnostic yield of saturation biopsy of the prostate. Eur Urol 2008; 53(5):976–981

[12] Lemaitre L, Puech P, Poncelet E et al. Dynamic contrast-enhanced MRI of anterior prostate cancer: morphometric assessment and correlation with radical prostatectomy findings. Eur Radiol 2009; 19(2):470–480

[13] Dickinson L, Ahmed HU, Allen C et al. Magnetic resonance imaging for the detection, localisation, and characterisation of prostate cancer: recommendations from a European consensus meeting. Eur Urol 2011; 59(4):477–494

[14] Vargas HA, Akin O, Afaq A et al. Magnetic resonance imaging for predicting prostate biopsy findings in patients considered for active surveillance of clinically low risk prostate cancer. J Urol 2012; 188(5):1732–1738

[15] Dickinson L, Ahmed HU, Allen C et al. Scoring systems used for the interpretation and reporting of multiparametric MRI for prostate cancer detection, localization, and characterization: could standardization lead to improved utilization of imaging within the diagnostic pathway? J Magn Reson Imaging 2013; 37(1):48–58

[16] Cheikh AB, Girouin N, Colombel M et al. Evaluation of T2-weighted and dynamic contrast-enhanced MRI in localizing prostate cancer before repeat biopsy. Eur Radiol 2009; 19(3):770–778

[17] Puech P, Rouvière O, Renard-Penna R et al. Prostate cancer diagnosis: multiparametric MR-targeted biopsy with cognitive and transrectal US-MR fusion guidance versus systematic biopsy—prospective multicenter study. Radiology 2013; 268(2):461–469

[18] Vargas HA, Akin O, Shukla-Dave A et al. Performance characteristics of MR imaging in the evaluation of clinically low-risk prostate cancer: a prospective study. Radiology 2012; 265(2):478–487

[19] Turkbey B, Choyke PL. Multiparametric MRI and prostate cancer diagnosis and risk stratification. Curr Opin Urol 2012; 22(4):310–315

[20] Niaf E, Lartizien C, Bratan F et al. Prostate focal peripheral zone lesions: characterization at multiparametric MR imaging—influence of a computer-aided diagnosis system. Radiology 2014; 271(3):761–769

[21] Vaché T, Bratan F, Mège-Lechevallier F, Roche S, Rabilloud M, Rouvière O. Characterization of prostate lesions as benign or malignant at multiparametric MR imaging: comparison of three scoring systems in patients treated with radical prostatectomy. Radiology 2014; 272(2):446–455

[22] Norberg M, Egevad L, Holmberg L, Sparén P, Norlén BJ, Busch C. The sextant protocol for ultrasound-guided core biopsies of the prostate underestimates the presence of cancer. Urology 1997; 50(4):562–566

[23] Beerlage HP, Aarnink RG, Ruijter ET et al. Correlation of transrectal ultrasound, computer analysis of transrectal ultrasound and histopathology of radical prostatectomy specimen. Prostate Cancer Prostatic Dis 2001; 4(1):56–62

[24] Kundavaram CR, Halpern EJ, Trabulsi EJ. Value of contrast-enhanced ultrasonography in prostate cancer. Curr Opin Urol 2012; 22(4):303–309

[25] Zhai L, Madden J, Foo WC et al. Characterizing stiffness of human prostates using acoustic radiation force. Ultrason Imaging 2010; 32(4):201–213

[26] Smith DS, Catalona WJ. Interexaminer variability of digital rectal examination in detecting prostate cancer. Urology 1995; 45(1):70–74

[27] Baumgart LA, Gerling GJ, Bass EJ. Characterizing the range of simulated prostate abnormalities palpable by digital rectal examination. Cancer Epidemiol 2010; 34(1):79–84

[28] Dvorak HF. Tumors: wounds that do not heal: similarities between tumor stroma generation and wound healing. N Engl J Med 1986; 315(26):1650–1659

[29] Tuxhorn JA, Ayala GE, Rowley DR. Reactive stroma in prostate cancer progression. J Urol 2001; 166(6):2472–2483

[30] Tuxhorn JA, Ayala GE, Smith MJ, Smith VC, Dang TD, Rowley DR. Reactive stroma in human prostate cancer: induction of myofibroblast phenotype and extracellular matrix remodeling. Clin Cancer Res 2002; 8(9):2912–2923

[31] Burns-Cox N, Avery NC, Gingell JC, Bailey AJ. Changes in collagen metabolism in prostate cancer: a host response that may alter progression. J Urol 2001; 166(5):1698–1701

[32] Zhang Y, Nojima S, Nakayama H, Jin Y, Enza H. Characteristics of normal stromal components and their correlation with cancer occurrence in human prostate. Oncol Rep 2003; 10(1):207–211

[33] Phipps S, Yang TH, Habib FK, Reuben RL, McNeill SA. Measurement of tissue mechanical characteristics to distinguish between benign and malignant prostatic disease. Urology 2005; 66(2):447–450

[34] Krouskop TA, Wheeler TM, Kallel F, Garra BS, Hall T. Elastic moduli of breast and prostate tissues under compression. Ultrason Imaging 1998; 20(4):260–274

[35] Hoyt K, Castaneda B, Zhang M et al. Tissue elasticity properties as biomarkers for prostate cancer. Cancer Biomark 2008; 4(4–5):213–225

[36] Zhang M, Nigwekar P, Castaneda B et al. Quantitative characterization of viscoelastic properties of human prostate correlated with histology. Ultrasound Med Biol 2008; 34(7):1033–1042

[37] Ahn BM, Kim J, Ian L, Rha KH, Kim HJ. Mechanical property characterization of prostate cancer using a minimally motorized indenter in an ex vivo indentation experiment. Urology 2010; 76(4):1007–1011

[38] Carson WC, Gerling GJ, Krupski TL, Kowalik CG, Harper JC, Moskaluk CA. Material characterization of ex vivo prostate tissue via spherical indentation in the clinic. Med Eng Phys 2011; 33(3):302–309

[39] Tsutsumi M, Miyagawa T, Matsumura T et al. Real-time balloon inflation elastography for prostate cancer detection and initial evaluation of clinicopathologic analysis. AJR Am J Roentgenol 2010; 194(6):W471-W476

[40] Goddi A, Sacchi A, Magistretti G, Almolla J. Transrectal real-time elastography of the prostate: normal patterns. J Ultrasound 2011; 14(4):220–232

[41] Miyagawa T, Tsutsumi M, Matsumura T et al. Real-time elastography for the diagnosis of prostate cancer: evaluation of elastographic moving images. Jpn J Clin Oncol 2009; 39(6):394–398
[42] Tsutsumi M, Miyagawa T, Matsumura T et al. The impact of real-time tissue elasticity imaging (elastography) on the detection of prostate cancer: clinicopathological analysis. Int J Clin Oncol 2007; 12(4):250–255
[43] Pallwein L, Mitterberger M, Struve P et al. Comparison of sonoelastography guided biopsy with systematic biopsy: impact on prostate cancer detection. Eur Radiol 2007; 17(9):2278–2285
[44] Brock M, von Bodman C, Palisaar RJ et al. The impact of real-time elastography guiding a systematic prostate biopsy to improve cancer detection rate: a prospective study of 353 patients. J Urol 2012; 187(6):2039–2043
[45] Junker D, Schäfer G, Aigner F et al. Potentials and limitations of real-time elastography for prostate cancer detection: a whole-mount step section analysis. ScientificWorldJournal 2012; 2012:193213
[46] Junker D, Schäfer G, Kobel C et al. Comparison of real-time elastography and multiparametric MRI for prostate cancer detection: a whole-mount step-section analysis. AJR Am J Roentgenol 2014; 202(3):W263–9
[47] Bercoff J, Tanter M, Fink M. Supersonic shear imaging: a new technique for soft tissue elasticity mapping. IEEE Trans Ultrason Ferroelectr Freq Control 2004; 51(4):396–409
[48] Boehm K, Salomon G, Beyer B et al. Shear wave elastography for localization of prostate cancer lesions and assessment of elasticity thresholds: implications for targeted biopsies and active surveillance protocols. J Urol 2015; 193 (3):794–800
[49] Woo S, Kim SY, Lee MS, Cho JY, Kim SH. Shear wave elastography assessment in the prostate: an intraobserver reproducibility study. Clin Imaging 2015; 39 (3):484–487
[50] Barr RG, Memo R, Schaub CR. Shear wave ultrasound elastography of the prostate: initial results. Ultrasound Q 2012; 28(1):13–20
[51] Pallwein L, Mitterberger M, Struve P et al. Real-time elastography for detecting prostate cancer: preliminary experience. BJU Int 2007; 100(1):42–46
[52] Sumura M, Shigeno K, Hyuga T, Yoneda T, Shiina H, Igawa M. Initial evaluation of prostate cancer with real-time elastography based on step-section pathologic analysis after radical prostatectomy: a preliminary study. Int J Urol 2007; 14(9):811–816
[53] Salomon G, Köllerman J, Thederan I et al. Evaluation of prostate cancer detection with ultrasound real-time elastography: a comparison with step section pathological analysis after radical prostatectomy. Eur Urol 2008; 54(6):1354–1362
[54] Walz J, Marcy M, Maubon T et al. [Real time elastography in the diagnosis of prostate cancer: comparison of preoperative imaging and histology after radical prostatectomy] Prog Urol 2011; 21(13):925–931
[55] Walz J, Marcy M, Pianna JT et al. Identification of the prostate cancer index lesion by real-time elastography: considerations for focal therapy of prostate cancer. World J Urol 2011; 29(5):589–594
[56] Brock M, von Bodman C, Sommerer F et al. Comparison of real-time elastography with grey-scale ultrasonography for detection of organ-confined prostate cancer and extra capsular extension: a prospective analysis using whole mount sections after radical prostatectomy. BJU Int 2011; 108(8 Pt 2):E217–E222
[57] Pelzer AE, Heinzelbecker J, Weiß C et al. Real-time sonoelastography compared to magnetic resonance imaging using four different modalities at 3.0 T in the detection of prostate cancer: strength and weaknesses. Eur J Radiol 2013; 82(5):814–821
[58] Brock M, Eggert T, Palisaar RJ et al. Multiparametric ultrasound of the prostate: adding contrast enhanced ultrasound to real-time elastography to detect histopathologically confirmed cancer. J Urol 2013; 189(1):93–98
[59] Zhu Y, Chen Y, Qi T et al. Prostate cancer detection with real-time elastography using a bi-plane transducer: comparison with step section radical prostatectomy pathology. World J Urol 2014; 32(2):329–333
[60] König K, Scheipers U, Pesavento A, Lorenz A, Ermert H, Senge T. Initial experiences with real-time elastography guided biopsies of the prostate. J Urol 2005; 174(1):115–117
[61] Pallwein L, Mitterberger M, Pinggera G et al. Sonoelastography of the prostate: comparison with systematic biopsy findings in 492 patients. Eur J Radiol 2008; 65(2):304–310
[62] Kamoi K, Okihara K, Ochiai A et al. The utility of transrectal real-time elastography in the diagnosis of prostate cancer. Ultrasound Med Biol 2008; 34(7): 1025–1032
[63] Ahmad S, Cao R, Varghese T, Bidaut L, Nabi G. Transrectal quantitative shear wave elastography in the detection and characterisation of prostate cancer. Surg Endosc 2013; 27(9):3280–3287
[64] Woo S, Kim SY, Cho JY, Kim SH. Shear wave elastography for detection of prostate cancer: a preliminary study. Korean J Radiol 2014; 15(3):346–355
[65] Correas JM, Tissier AM, Khairoune A et al. Prostate cancer: diagnostic performance of real-time shear-wave elastography. Radiology 2015; 275(1):280–289
[66] Boehm K, Budäus L, Tennstedt P et al. Prediction of significant prostate cancer at prostate biopsy and per core detection rate of targeted and systematic biopsies using real-time shear wave elastography. Urol Int 2015; 95(2):189–196
[67] Zhang B, Ma X, Zhan W et al. Real-time elastography in the diagnosis of patients suspected of having prostate cancer: a meta-analysis. Ultrasound Med Biol 2014; 40(7):1400–1407
[68] Pallwein L, Mitterberger M, Gradl J et al. Value of contrast-enhanced ultrasound and elastography in imaging of prostate cancer. Curr Opin Urol 2007; 17(1):39–47
[69] Ward JF. Contemporary outcomes of focal therapy in prostate cancer: what do we know so far... World J Urol 2010; 28(5):593–597
[70] Ahmed HU. The index lesion and the origin of prostate cancer. N Engl J Med 2009; 361(17):1704–1706
[71] van Hove A, Savoie PH, Maurin C et al. Comparison of image-guided targeted biopsies versus systematic randomized biopsies in the detection of prostate cancer: a systematic literature review of well-designed studies. World J Urol 2014; 32(4):847–858
[72] Nelson ED, Slotoroff CB, Gomella LG, Halpern EJ. Targeted biopsy of the prostate: the impact of color Doppler imaging and elastography on prostate cancer detection and Gleason score. Urology 2007; 70(6):1136–1140
[73] Aigner F, Pallwein L, Junker D et al. Value of real-time elastography targeted biopsy for prostate cancer detection in men with prostate specific antigen 1.25 ng/ml or greater and 4.00 ng/ml or less. J Urol 2010; 184(3):913–917
[74] Kapoor A, Kapoor A, Mahajan G, Sidhu BS. Real-time elastography in the detection of prostate cancer in patients with raised PSA level. Ultrasound Med Biol 2011; 37(9):1374–1381
[75] Ganzer R, Brandtner A, Wieland WF, Fritsche HM. Prospective blinded comparison of real-time sonoelastography targeted versus randomised biopsy of the prostate in the primary and re-biopsy setting. World J Urol 2012; 30(2): 219–223
[76] Zhang Y, Tang J, Li YM et al. The contribution of strain patterns in characterization of prostate peripheral zone lesions at transrectal ultrasonography. Acta Radiol 2012; 53(1):119–126
[77] Taverna G, Magnoni P, Giusti G et al. Impact of real-time elastography versus systematic prostate biopsy method on cancer detection rate in men with a serum prostate-specific antigen between 2.5 and 10 ng/mL. ISRN Oncol 2013; 2013:584672
[78] Salomon G, Drews N, Autier P et al. Incremental detection rate of prostate cancer by real-time elastography targeted biopsies in combination with a conventional 10-core biopsy in 1024 consecutive patients. BJU Int 2014; 113 (4):548–553
[79] Nygård Y, Haukaas SA, Halvorsen OJ et al. A positive real-time elastography is an independent marker for detection of high-risk prostate cancers in the primary biopsy setting. BJU Int 2014; 113 5b:E90–E97
[80] Brock M, Roghmann F, Sonntag C et al. Fusion of magnetic resonance imaging and real-time elastography to visualize prostate cancer: a prospective analysis using whole mount sections after radical prostatectomy. Ultraschall Med 2015; 36(4):355–361
[81] Wu LM, Xu JR, Ye YQ, Lu Q, Hu JN. The clinical value of diffusion-weighted imaging in combination with T2-weighted imaging in diagnosing prostate carcinoma: a systematic review and meta-analysis. AJR Am J Roentgenol 2012; 199(1):103–110

8 Elastography of the Lymph Nodes

Nitun Chaubal, Anupam Bam, and Ketki Khadtare[1]

8.1 Introduction

This chapter is intended to serve as a guide to the use of elastography in characterizing lymphadenopathy. Conventional clinical methods, including manual palpation, B-mode (grayscale) ultrasound, and Doppler ultrasound have their limitations in characterization of lymph nodes. Hence, there is a need to explore other noninvasive imaging techniques for this purpose. At present, elastography is such a technique, which is mainly useful for evaluation of superficial groups of lymph nodes, that is, cervical, axillary, and inguinal groups.

Out of 400 to 450 lymph nodes present in the human body, cervical nodes form one of the major groups (60 to 70 in number) that are frequently involved in inflammatory and neoplastic diseases.[1] Among the various lymph node pathologies, metastasis causes the most apparent change in consistency of the node. Diagnosis of nodal involvement in metastasis is critical for management of many cancers. Thus, this chapter mainly deals with usefulness of elastography to distinguish between benign and malignant diseases of cervical lymph nodes.

8.2 Conventional Ways of Diagnosing Lymphadenopathy

Lymph nodes are the guardians at checkpoints in the human body and send alarm signals in response to many pathologic conditions. Often, they are the first organs that become clinically detectable due to secondary involvement in diseases like infections, inflammatory conditions, and metastases. Status of lymph node involvement can be the most powerful prognostic indicator in the case of certain malignancies such as breast carcinoma, and it can influence management in such cases.[2] Localized, or regional, lymphadenopathy indicates involvement of specific anatomical areas. For example, occipital lymph nodes are frequently involved in infections of the scalp, while left supraclavicular nodal involvement indicates primary malignancy in the gastrointestinal tract (Virchow's node). Generalized lymphadenopathy may point to lymphoma or to nonmalignant systemic disorders, such as certain infections (HIV, infectious mononucleosis, etc.) and connective tissue disorders.[3,4] Thus, the clinical importance of detection and characterization of enlarged lymph nodes and its eventual impact on patient management cannot be overemphasized.

Conventionally, manual palpation and ultrasonographic evaluation (B-mode and Doppler) are used for detection of lymph node abnormalities. Invasive techniques (like ultrasound-guided fine needle aspiration cytology and core needle biopsy), though being sensitive and specific for detecting macrometastases, have serious limitations in case of micrometastases.[5]

Manual palpation gives information about size, temperature, tenderness, and consistency of the nodes. Though it is a good fundamental technique, it fails to assess the internal structure of the nodes and has practical limitations in the evaluation of nodes situated deep to the skin. The sensitivity and specificity of manual palpation for detecting malignant lesions is low (64% and 85%, respectively).[6]

Ultrasound imaging of lymph nodes (B-mode and Doppler) can assess the internal structure of the nodes and their vascularity. It helps to characterize clinically suspicious nodes and to identify occult nodes.[7] These ultrasonographic techniques and their limitations are briefly described here.

8.2.1 B-Mode Ultrasound

With the advent of better resolution ultrasound machines and high-frequency probes with smaller footprints, the sensitivity of ultrasound to detect lymph nodes has increased manifold. These advances have also made the detailed study of the size, shape and internal structure (with respect to overall echogenicity, presence of central echogenic hilum, calcifications, margin definition and regularity, intranodal necrosis, and focal cortical hypertrophy) of lymph nodes possible, which contributes substantially to their characterization.

Lymph node size, as represented by its short axis diameter, has been considered as one of the criteria to differentiate malignant lymph nodes from benign ones (▶ Fig. 8.1). Various cutoffs ranging from 5 to 30 mm have been described. However, this criterion, being an absolute value, depends on lymph node location and has either low sensitivity or low specificity.[8,9,10] A short-to-long axis diameter ratio of 0.5 is a more useful parameter with moderate sensitivity, specificity, and overall accuracy of 75%, 81%, and 79%, respectively.[11] Absence of a hyperechoic hilum (▶ Fig. 8.2) is characteristic of metastatic lymph nodes, with specificity and sensitivity of 88% and 90%, respectively, for detection of metastasis from papillary thyroid carcinoma.[12] Yet, in general, it is not a definite criterion for differentiating between malignant and benign lymph nodes.[8,11] Calcifications in lymph nodes are almost exclusively due to metastases from medullary and papillary carcinoma of the thyroid, besides those seen with benign diseases such as tuberculosis.[8] This feature has a high specificity for metastasis but a low sensitivity.[11] Eccentric cortical hypertrophy due to focal tumor infiltration is a useful sign to identify metastatic nodes. Metastatic lymph nodes are predominantly hypoechoic relative to adjacent musculature, as are reactive, lymphomatous, or tuberculous nodes. However, metastatic nodes from papillary or medullary carcinoma of the thyroid are usually hyperechoic.[8] Intranodal necrosis may be found in tuberculosis and abscessed lymphadenopathy, along with metastatic nodes.[8]

8.2.2 Doppler Ultrasound

Doppler ultrasound evaluation of lymph nodes involves assessment of vascular distribution as well as vascular resistance within a lymph node.

[1] *Acknowledgment:* We are grateful for the valuable input of Dr Mukund Joshi, Mumbai, India.

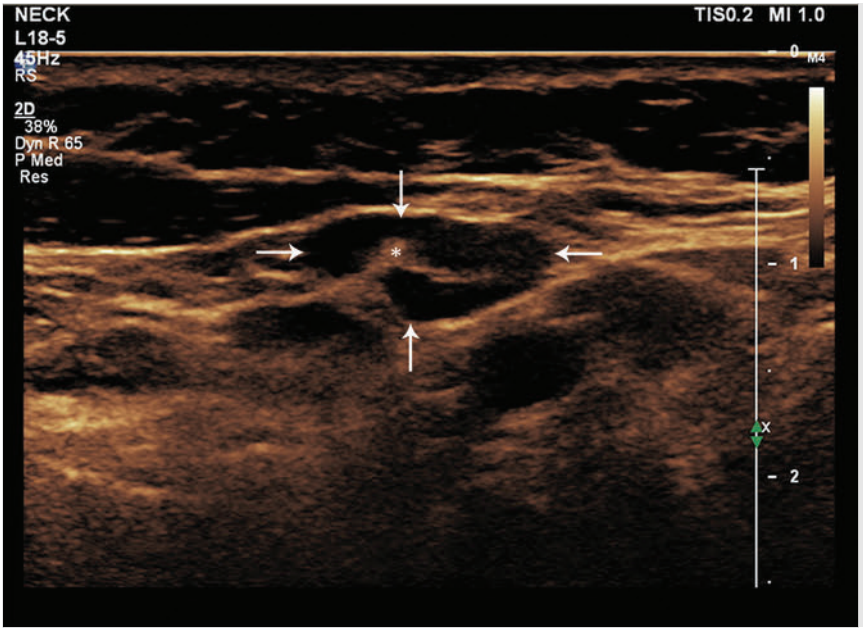

Fig. 8.1 B-mode ultrasound image of the neck showing a less than 1 cm lymph node (*arrows*). The node with an echogenic hilum (*asterisk*), which is one of the characteristics of a benign lymph node, measures around 0.8 × 0.5 cm.

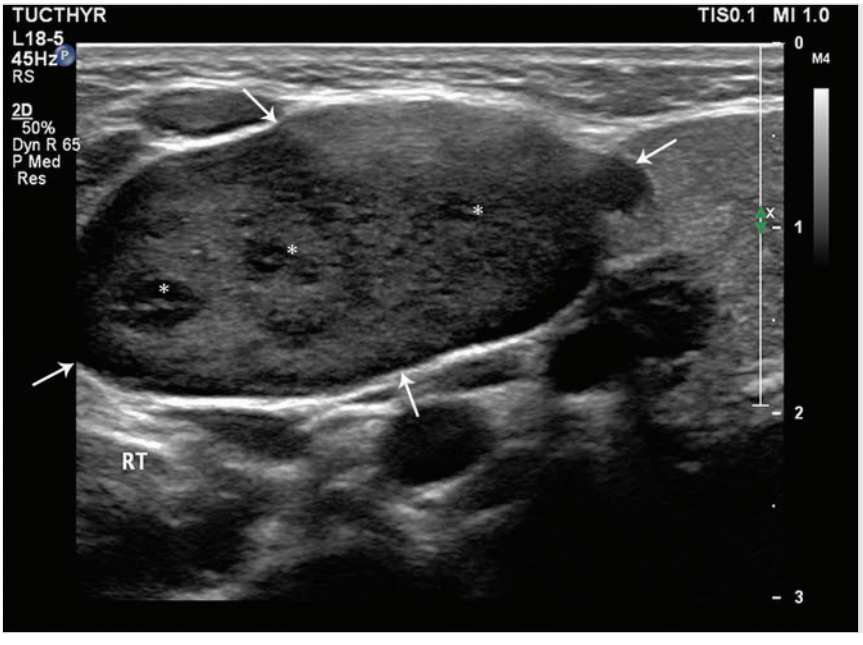

Fig. 8.2 B-mode ultrasound image of the neck showing a lymph node (*arrows*) with loss of central hilum and presence of internal hypoechoic nodules (*asterisks*). The node measures around 2.5 × 1.5 cm. These findings indicate malignancy.

Vascular Distribution

Evaluation of the vascular pattern of cervical lymph nodes shows a hilar type of flow (▶ Fig. 8.3) or absence of vascularity in the case of normal and reactive nodes. Peripheral or mixed vascularity is common in metastatic nodes (▶ Fig. 8.4). This criterion has moderate to high specificity (76%–99%) but low sensitivity (47%).[11,13]

Vascular Resistance

A high nodal vascular resistance (pulsatility index [PI] > 1.6 and resistivity index [RI] > 0.8) is generally indicative of metastatic lesions, while normal and reactive nodes tend to have PI < 1.6 and RI < 0.8.[13] In view of the low sensitivity (47% and 55%, respectively[14]) of these indices and the technical difficulties involved in obtaining suitable and/or repeatable values, their role in routine clinical practice is limited.

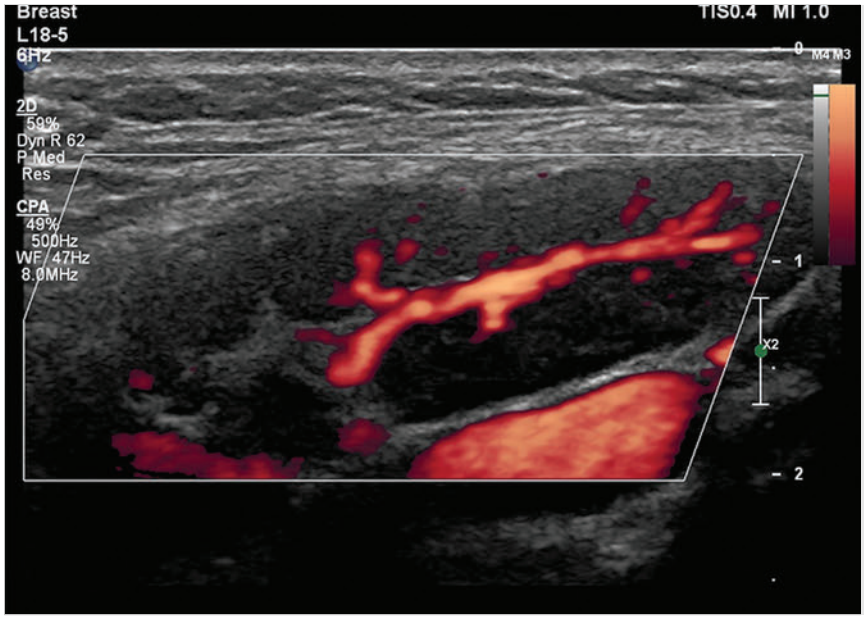

Fig. 8.3 Power Doppler ultrasound image of a benign lymph node showing normal branched hilar flow.

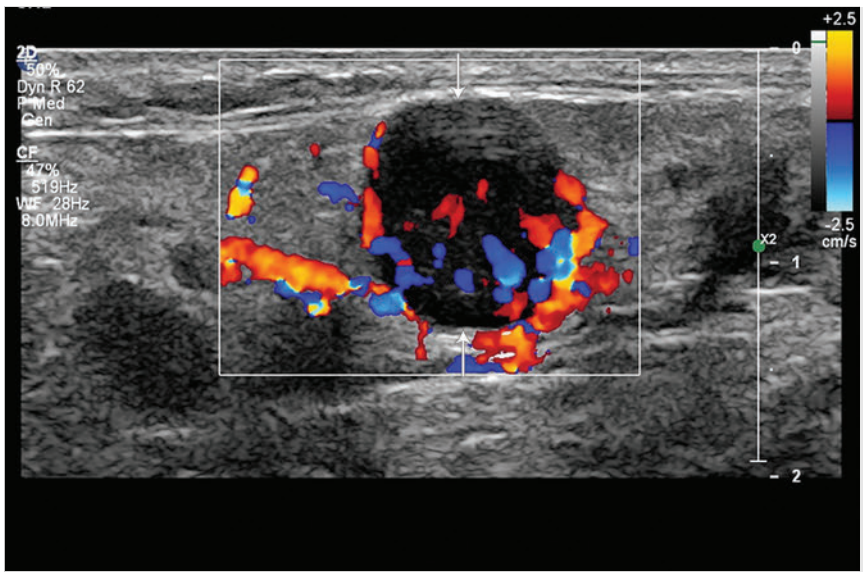

Fig. 8.4 Color Doppler ultrasound image showing mixed peripheral-central flow in a lymph node, a feature favoring malignancy. Also, note the round shape of the node (*arrows*).

Considering the limitations of the above modalities, there is a need to further improve diagnostic accuracy. Ultrasound elastography is a potential tool to fill this void.

8.3 Elastography for Diagnosis of Lymphadenopathy

Various studies have shown the usefulness of elastography in differentiating benign from malignant cervical lymph nodes.[11, 15] Simultaneous use of B-mode ultrasound, Doppler ultrasound, and elastography in various combinations could potentially improve diagnostic performance for lymphadenopathy.[1] There are two main elastography techniques—strain imaging and shear wave imaging—that are widely used for the assessment of suspicious lymph nodes.

8.3.1 Strain Elastography Imaging

Strain elastography imaging is the more commonly used elastography technique for the study of lymph nodes. It is also known by the names of sonoelastography, real-time tissue elastography (RTE), tissue type imaging (TTI), and real-time sonoelastography (RTSE).[16] The technique has been described in detail in Chapter 2. Here, its use pertinent to the study of lymph nodes is discussed.

Techniques

Strain imaging is commonly used for evaluating cervical lymph nodes. The anatomy of cervical nodes is shown in ▶ Fig. 8.5 for reference. According to the 2009 American Joint Committee on Cancer (AJCC) classification, cervical lymph nodes are classified into seven anatomical levels.[17] Elastography is helpful for

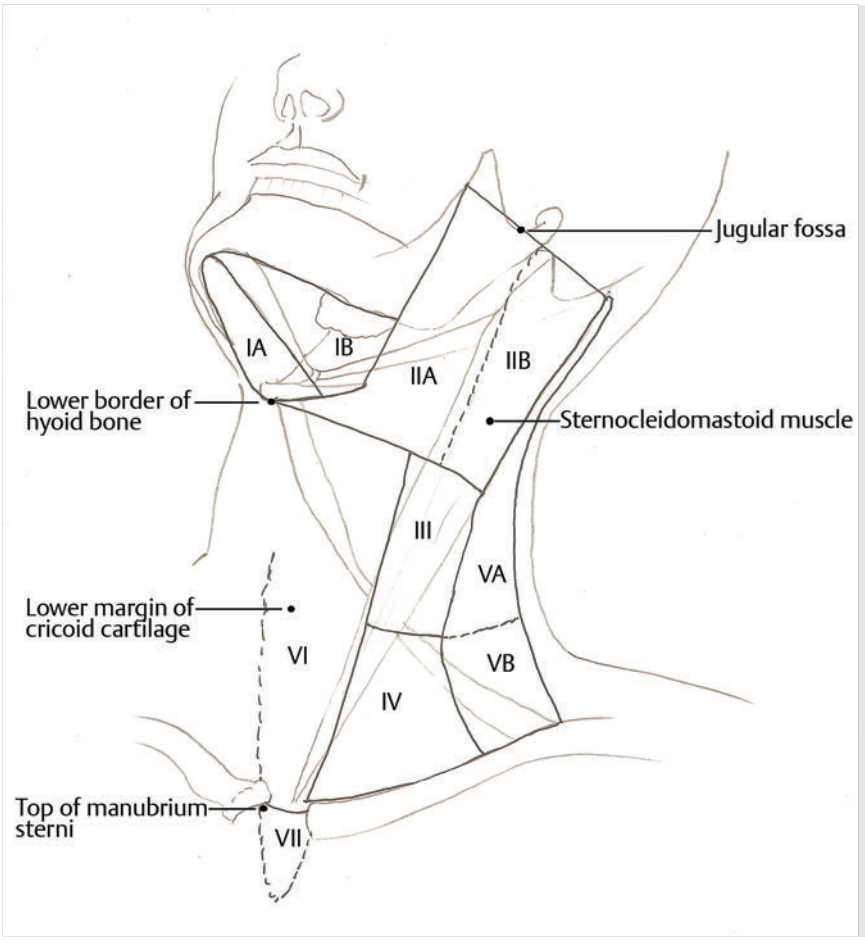

Fig. 8.5 Anatomical levels of cervical lymph nodes (Reproduced with permission from AJACC Cancer Staging Manual, 7th edition).[17] Level I: submental (IA) and submandibular (IB); level IIA and IIB: upper jugular; level III: middle jugular; level IV: lower jugular; level VA and VB: posterior triangle group; level VI: anterior compartment group; and level VII: superior mediastinal group.

examining nodes of all the levels except for level VII, as level VII nodes are not accessible for ultrasound evaluation. The technique of performing cervical node strain elastography is discussed below. Practical tips include:

- Position the patient similar to routine neck ultrasound imaging with neck extended over a pillow.
- Hold probe perpendicular to the skin and apply a steady compression in the direction of ultrasound beam, followed by a slow release (decompression).
- Apply adequate compression as guided by the compression bar. It should be at least at three-fourths of its maximum height.
- Choose a field of view (FOV) so as to include the target lymph node and the surrounding tissue in approximately equal proportions.
- Select an image with optimum FOV and compression for further analysis.
- For the strain ratio (SR) calculation, select a small region of interest (ROI) that includes the hardest area of the node.
- Use the freehand technique for all neck lymph node levels except level VII.
- Adopt a similar technique for examining various superficial lymph nodes with an appropriate change in patient position during examination.

Patient Positioning and Initial Examination

The patient is made to lie comfortably in a supine position similar to that adopted for a standard neck ultrasound examination with neck slightly extended over a pillow. The examination begins with B-mode neck ultrasound using a linear array probe with a wide range of ultrasound frequency (5–18 MHz). After a systematic assessment of the position, size, and B-mode characteristics of each lymph node, the elastography mode is switched on and using the same probe the elastogram is obtained. A dual panel image is displayed, allowing one to see the B-mode image alongside the elastogram.[1,11,18,19]

Acquisition of Elastograms

The freehand technique for acquiring elastograms in described in ▶ Fig. 8.6. The probe is placed perpendicular to the skin surface overlying the lymph node under assessment. The patient is asked to avoid swallowing and hold his or her breath to prevent movement of the lymph node. A small precompressive force is applied to stabilize the node and hence to minimize its lateral movement. Unlike thyroid elastography, using intrinsic compression from carotid artery pulsations is not feasible for lymph nodes at all levels. Furthermore, due to their mobility, lymph nodes tend to get laterally displaced by arterial pulsations. Therefore, a freehand steady compressive force is applied with

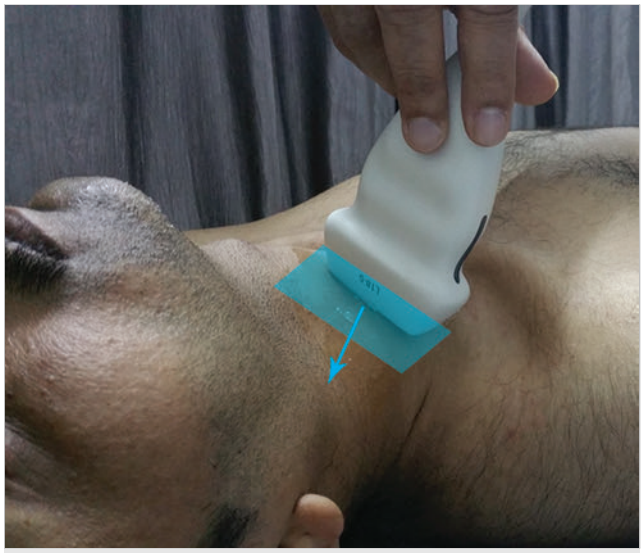

Fig. 8.6 The freehand technique of acquisition of data for an elastogram. A linear ultrasound probe is held perpendicular to the plane parallel to the skin overlying a cervical lymph node (*blue polygon*). A constant precompression is applied to fix the node against the underlying structures and a controlled compression is applied in the direction of propagation of the ultrasound waves (*blue arrow*) followed by decompression. A cine loop of elastograms is recorded during a few such cycles of compression–release. In the figure, level IV nodes lying adjacent to the sternal head of the sternocleidomastoid muscle are being investigated in a transverse direction.

the probe followed by steady release. Images are obtained as a cine loop during multiple compression–release cycles. A compression scale displayed by the side of the image helps to optimize the compressive force. Different manufacturers have different grading systems for the compressive force, but in general a 75% rise in the display bar or a quality factor of 3 or 4 is considered optimal. An image with optimal compression is chosen for further assessment.[11,18,19,20]

The field of view (FOV) of the elastography map (elastogram) is chosen such that it includes the target lymph node and the surrounding reference tissue in the same plane in almost equal proportions. Ideally, at least 5 mm of surrounding reference tissue beyond the lymph node margins should be included. The upper margin of the FOV is kept as close to the probe as possible. Surrounding tissues which can interfere or alter the strain ratio calculations, like bones and vessels, are excluded from the FOV.[1,18,20]

The Elastogram

Two types of elastograms are utilized for evaluation, grayscale and color, of which the latter is preferred. On the grayscale elastogram, hard and soft areas appear dark and bright, respectively. On the color elastogram, red represents the softest and blue represents the hardest areas, while intermediate stiffness is indicated by green. These colors represent relative hardness of the tissues on the elastogram. Many manufacturers provide an option of a color scale which is reversed with respect to the above-mentioned one; that is, where blue represents hardest areas and red, softest (▶ Fig. 8.7).[21]

Interpretation of elastograms can be done in two ways: qualitative and quantitative. For qualitative analysis, elastograms are given various grades (an elasticity score [ES]) based on their appearance. For quantitative analysis, a strain ratio (SR), or strain index (SI), is calculated. The SR represents the ratio of the strain of a reference tissue to that of the lymph node of interest in the ROI.[20] Most often, cervical muscles are used as reference tissue. Different cutoffs for SR have been suggested.

The following sections describe the two types of elastograms and the various grading systems used in evaluating them.

Grayscale Elastograms

When using grayscale elastograms it is important to turn off the background B-mode grayscale image so only the grayscale elastogram is displayed.

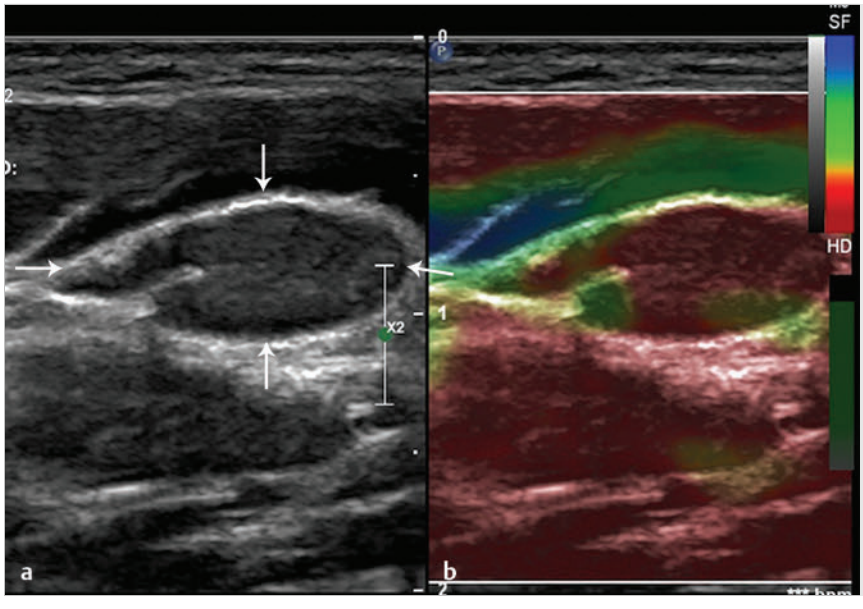

Fig. 8.7 Color elastogram of a lymph node (*arrows*) with an inverted color scale, in which red indicates stiff areas while blue indicates soft areas. (**a**) B-mode ultrasound image and (**b**) corresponding color elastogram. Red (stiff) areas are seen filling this node almost entirely. Note that shape and minor-to-major axis ratio of the node are typical of a benign node.

Table 8.1 Four-point grading system for grayscale elastograms, according to Lyshchik et al[11]

Criterion	Score	1	2	3	4
Node visualization		Not visible	Barely visible	Partially visible	Intensely visible
Brightness index		Very dark	Substantially darker	Slightly darker	Same or brighter
Margin regularity		Regular	Slightly irregular	Moderately irregular	Very irregular
Margin definition		Distinct, > 50%		Indistinct, < 50%	

One of the methods adopted by Lyshchik et al to evaluate elastograms for lymph node visibility, relative brightness, margin regularity, and margin definition uses a 4-point rating scale (▶ Table 8.1).

It has been found that the majority of the benign nodes are barely visible (visualization score < 3) and have the same brightness as the surrounding structures (brightness index > 2) (▶ Fig. 8.8), while metastatic lymph nodes are partially or very visible (visualization score > 2) and appear substantially darker as compared to the surrounding muscle (brightness index ≤ 2) (▶ Fig. 8.9). This is because while metastatic lymph nodes are relatively stiffer than the surrounding muscle, there is not much difference between the stiffness of benign lymph nodes and muscle. Due to the same differences in relative stiffness, the margins of the metastatic lymph nodes appear more regular and distinct (regularity score and definition score 1 or 2) than the margins of the benign lymph nodes. This could also be attributed to the desmoplastic reaction surrounding metastases. These qualitative criteria have low diagnostic accuracy.[11]

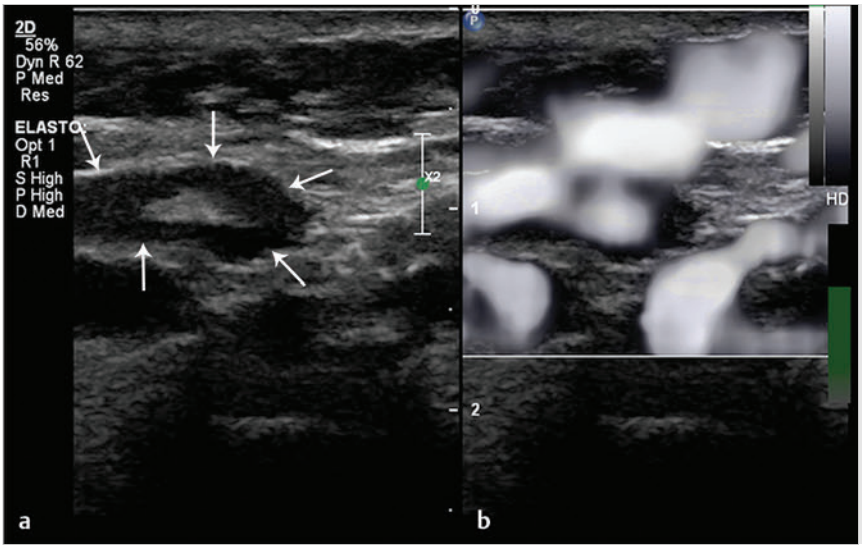

Fig. 8.8 Grayscale elastogram of benign lymph node. (**a**) B-mode ultrasound image showing a cervical lymph node (*arrows*) with a short-axis diameter of 5 mm and a short-to-long-axis diameter ratio smaller than 0.5. (**b**) On the corresponding grayscale elastogram, the node looks as bright as the surrounding muscle.

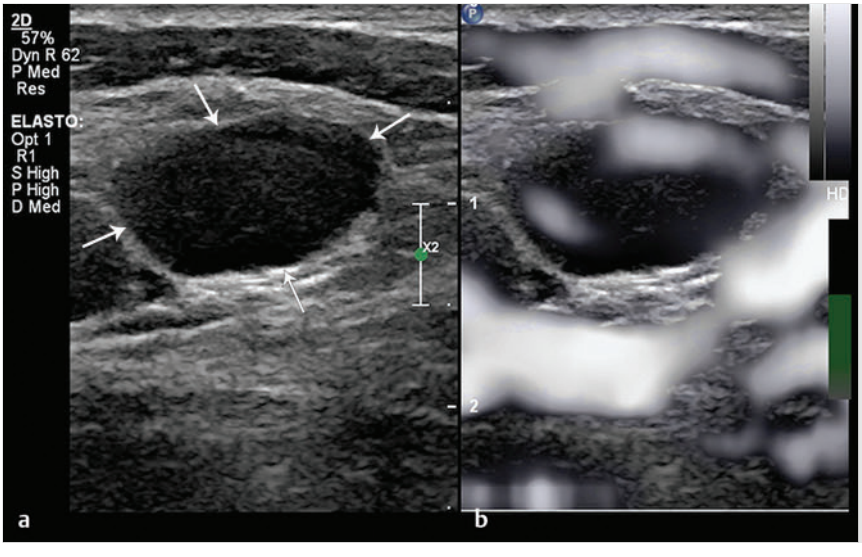

Fig. 8.9 Grayscale elastogram of metastatic lymph node. (**a**) B-mode ultrasound image showing a cervical lymph node (*arrows*) with a short-axis diameter of 8 mm and a short-to-long axis diameter ratio greater than 0.5. (**b**) Corresponding grayscale elastogram. The major portion of the lymph node is darker than the surrounding muscle.

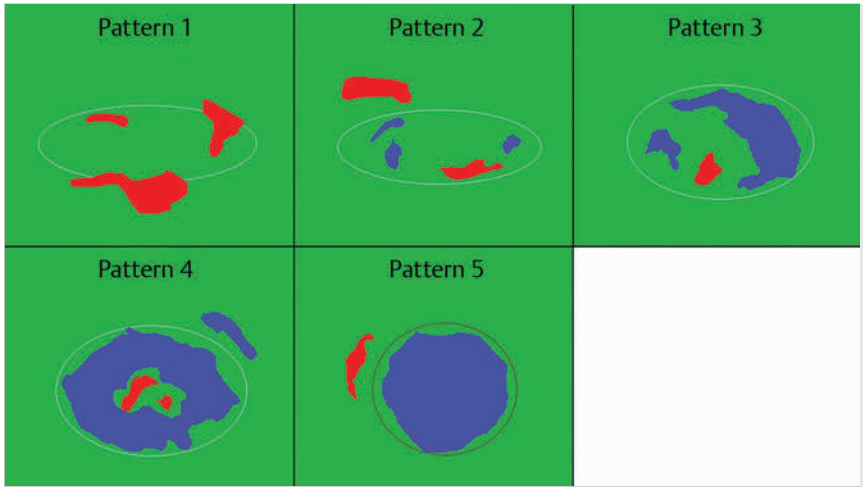

Fig. 8.10 Schematic showing elastogram color pattern as suggested by Alam et al.[1] Pattern 1: absent or very small blue area. Pattern 2: small scattered blue areas, total blue area < 45%. Pattern 3: large blue area(s), total blue area ≥ 45%. Pattern 4: peripheral blue area and central green area, suggesting central necrosis. Pattern 5: blue area with or without a green rim.

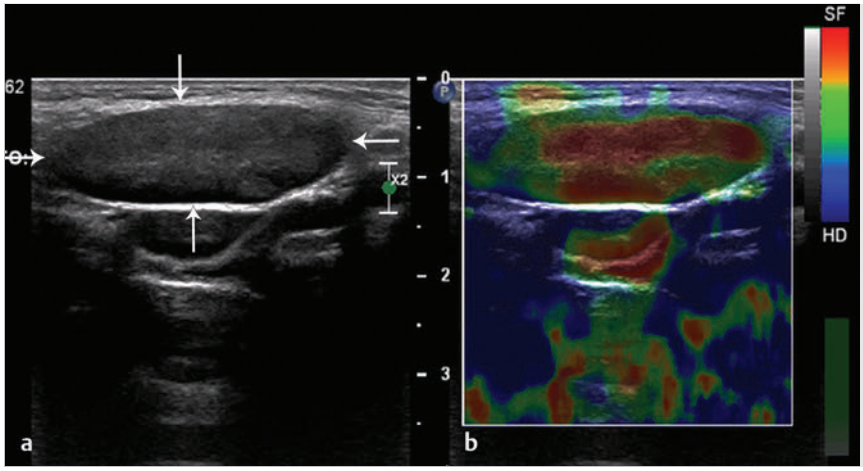

Fig. 8.11 Split-screen (**a**) B-mode ultrasound image and (**b**) corresponding strain elastogram of a benign lymph node (*arrows*). The elastogram shows that almost the entire lymph node is filled with shades of green and red (pattern 1).

Color Elastograms

Color elastograms often allow better visual distinction between normal and pathologic areas. Various scoring and grading systems have been described for the interpretation of color elastograms.[1,15,20,21,22,23,24,25] The system proposed by Alam et al seems to be the most accurate (sensitivity, 83%, and specificity,100%).[1] It is described here in detail. Other noteworthy grading systems are briefly described thereafter.

For the analysis of a color elastogram, an image with optimum compression force is first chosen. The color scale commonly used for color elastograms is shown in ▶ Fig. 8.10.

The percentage of area with high stiffness (i.e., blue area) in an elastogram can be estimated offline using certain image analysis software (e.g., Image J developed by the National Institutes of Health[26]) or can be determined subjectively (less accurate). Based on the distribution and percentage of blue area, elastograms are divided into five patterns (▶ Fig. 8.11, ▶ Fig. 8.12, ▶ Fig. 8.13, ▶ Fig. 8.14, ▶ Fig. 8.15, ▶ Table 8.2).

Each elastogram is identified with one of the five patterns depending on the distribution of the blue area in the lymph node. The cutoff line for reactive versus metastatic lymph nodes lies between patterns 2 and 3. Patterns 3 to 5 are considered metastatic. It may be noted that the sensitivity, specificity, and accuracy of a combination of B-mode ultrasound and elastography for detection of metastatic nodes have been reported to be 92%, 94%, and 93%, respectively. Hence, the combination is potentially superior to each individual technique for the diagnosis of metastatic lymph nodes.[1]

Table 8.2 Patterns and scoring system for color elastograms, according to Alam et al[1]

Pattern	Score	Description	Elastographic diagnosis
1	2	Absent or very small blue area(s)	Reactive
2	4	Small scattered blue area(s), total blue area < 45%	Reactive
3	6	Large blue area(s), total blue area ≥ 45%	Malignant
4	8	Peripheral blue area and central green area, suggesting central necrosis	Malignant
5	10	Blue area with or without a green rim	Malignant

Note: Blue represents hard (stiff) and red (soft).

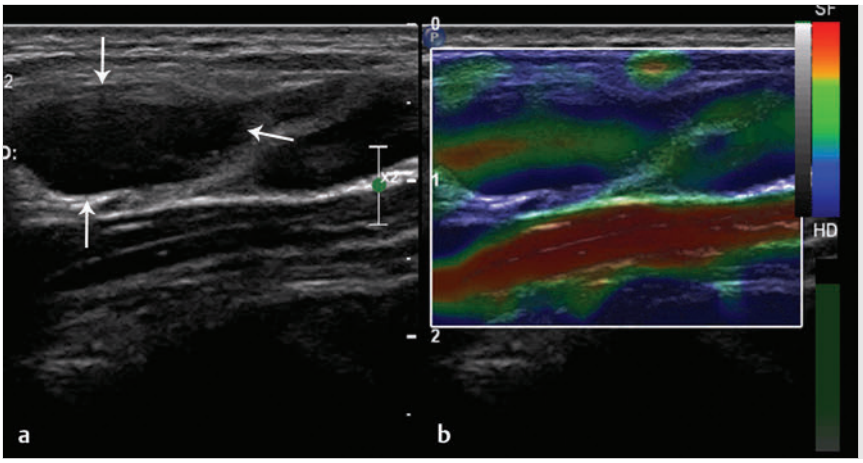

Fig. 8.12 Split-screen B-mode ultrasound image (**a**) and corresponding strain elastogram (**b**) of a benign lymph node (*arrows*). The elastogram shows blue areas roughly representing < 45% of the lymph node (pattern 2).

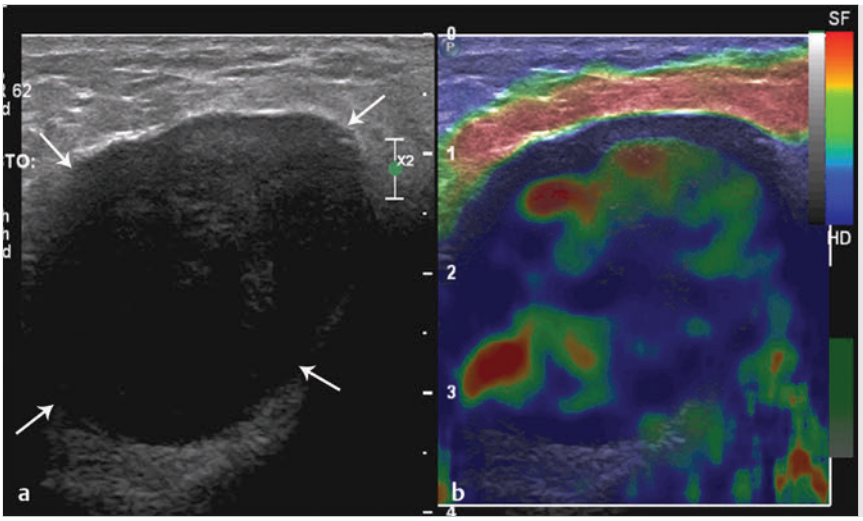

Fig. 8.13 Split-screen (**a**) B-mode ultrasound image and (**b**) corresponding strain elastogram of a metastatic lymph node (*arrows*). The elastogram shows blue areas accounting for more than 45% of the lymph node (pattern 3).

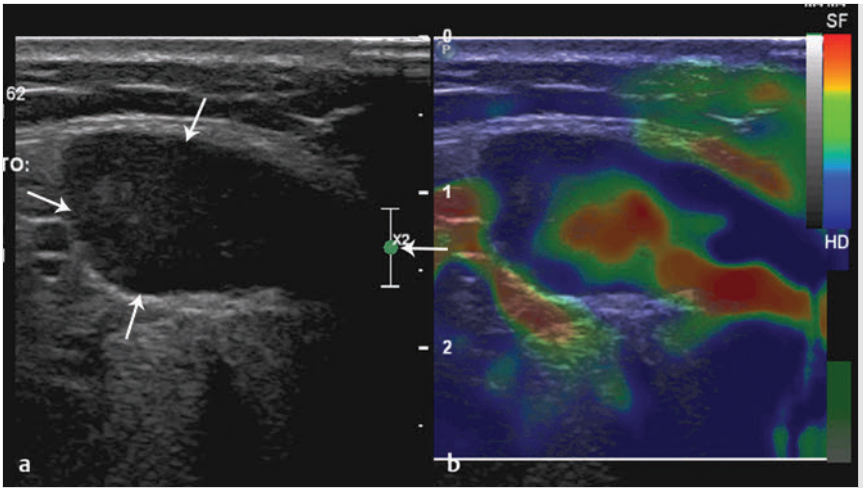

Fig. 8.14 Split-screen (**a**) B-mode ultrasound image and (**b**) corresponding strain elastogram of a metastatic lymph node (*arrows*). The elastogram shows a rim of blue (stiff) areas in the periphery of the lymph node with central red and green (soft) hues indicating liquefactive necrosis (pattern 4).

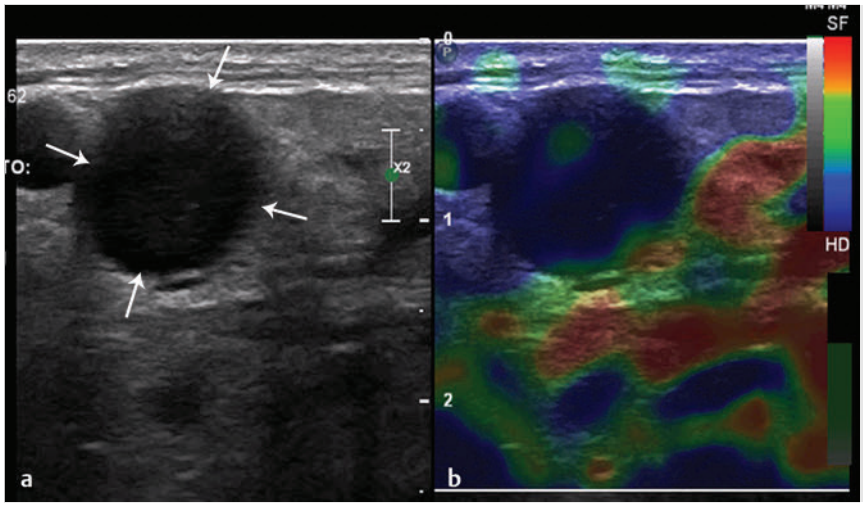

Fig. 8.15 Split-screen (**a**) B-mode ultrasound image and (**b**) corresponding strain elastogram of a metastatic lymph node (*arrows*). The elastogram shows the node appearing almost entirely blue, that is, hard (pattern 5).

Furukawa et al evaluated the usefulness of elastography for detection of cervical lymph node metastasis in patients with head and neck cancers. Their grading system is described in ▶ Table 8.3. Pattern 1 and 2 are generally seen with benign or reactive nodes while metastatic nodes show patterns 3 and 4.[15,27]

Another scoring system proposed by Lenghel et al (▶ Table 8.4) tries to incorporate correlation between elastographic and B-mode (echogenicity) findings and intranodal structural changes, such as liquefaction and focal metastatic deposits, into the existing systems. Using pattern 3 (benign) and pattern 4 (malignant) as a cutoff line to distinguish benign and malignant lymph nodes, this system reports a high specificity (96.67%) but a lower sensitivity (66.67%). It is also observed that lymphomatous nodes are more likely to show a benign appearance on elastography due to their low stiffness.[23]

Strain Ratio

The quantitative index that can be calculated for interpreting elastograms is known as the strain ratio (SR), or strain index (SI) (described in Chapter 2). It provides a semiquantitative method to assess the stiffness of the lymph nodes relative to the surrounding tissue. It is the ratio of absolute strain in a reference tissue to the absolute strain in the lymph node under investigation. In the cervical region, skeletal muscles in the vicinity of the node are taken as the reference tissue. For calculation of SR, two ROIs are placed within the elastogram obtained with optimum compressive force; one over the reference muscle and the other over the lymph node (▶ Fig. 8.16). The standard size of these ROIs is 5 to 10 mm square. Care must be taken to place both the ROIs within 10 mm depth of each other to avoid depth-associated stress decay.[11]

From a knowledge of strain elastography, one can understand that a softer node will typically show a low SR (▶ Fig. 8.17), while a hard node will have a higher SR (▶ Fig. 8.18, ▶ Fig. 8.19). Based on this, different cutoff values of SR have been proposed to differentiate between benign and malignant lymph node lesions (▶ Table 8.5). Based on sensitivity and specificity values, a cutoff of 1.5 seems reasonable. However, further large-scale studies would certainly help to validate these findings and to establish a more accurate cutoff value.

Subcutaneous fat may be used as a reference tissue for evaluating axillary lymph nodes. As fatty tissue is softer than skeletal muscle, it will display more strain as compared to muscle with the same applied pressure. Therefore, a higher cutoff of 2.3 for the SR may be used for detection of malignant lymph nodes.[28] However, this value certainly requires further interrogation and validation with clinical studies.

Table 8.3 Patterns for color elastograms, proposed by Furukawa et al[15,27]

Pattern	Description
1	80% or more of the cross-sectional area of the lymph node is red or green, i.e., soft
2	50% to < 80% of the cross-sectional area of the lymph node is red or green
3	50% to < 80% of the cross-sectional area of the lymph node is blue
4	≥ 80% of the cross-sectional area of the lymph node is blue, i.e., hard

Note: Blue represents hard (stiff) and red (soft).

Table 8.4 Color elastogram scoring system, proposed by Lenghel et al[23]

Pattern	Description
1	No or minimum blue area (suggestive of soft consistency similar to the surrounding tissues)
2	< 50% blue area, no individualized hypoechoic nodules
3	< 50% blue area, individualized soft hypoechoic nodules present
4	< 50% blue area, individualized hard hypoechoic nodules present
5	50%-100% blue area, no individualized hypoechoic nodules
6	50%-100% blue area, individualized hard hypoechoic nodules present
7	Blue area covers the whole nodules and extends into the soft tissues
8	Blue (hard) nodule containing fluid areas (suggestive of liquefactive necrosis)

Note: Blue represents hard (stiff) and red (soft).

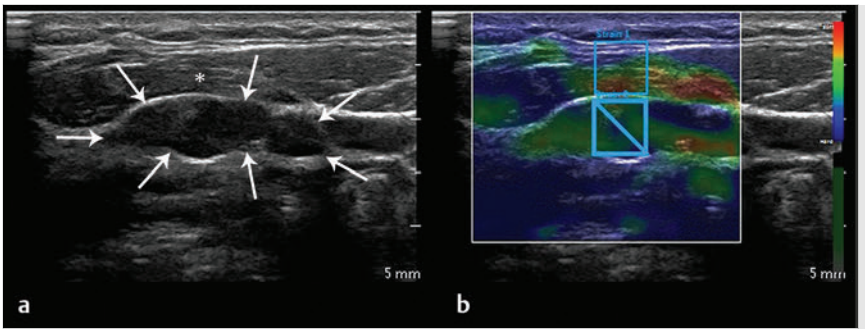

Fig. 8.16 Calculation of strain ratio (SR). (**a**) B-mode ultrasound image of a benign lymph node and (**b**) corresponding strain elastogram showing color pattern 1. The SR is calculated by placing a 5 × 5 mm ROI over the adjacent muscle (*asterisk*), while keeping the other ROI inside the node (*arrows*). In this case, an SR of 0.89 was calculated.

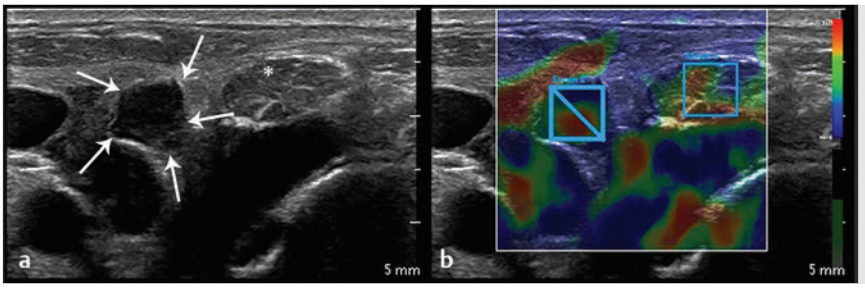

Fig. 8.17 Split-screen (**a**) B-mode ultrasound image and (**b**) corresponding strain elastogram of a tuberculous lymph node (*arrows*) showing pattern 2 on elastogram. A strain ratio (SR) of 1.21 was obtained by comparing the strain of the node with that of the surrounding muscle (*asterisk*).

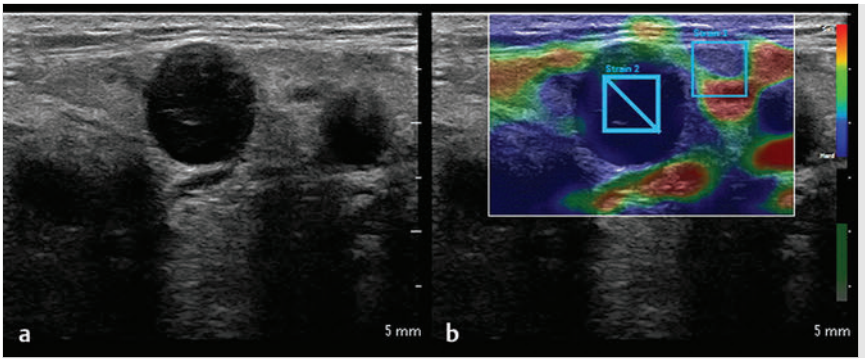

Fig. 8.18 Split-screen (**a**) B-mode ultrasound image and (**b**) strain elastogram of a metastatic lymph node showing pattern 5 on the elastogram. A strain ratio of 3.82 was calculated.

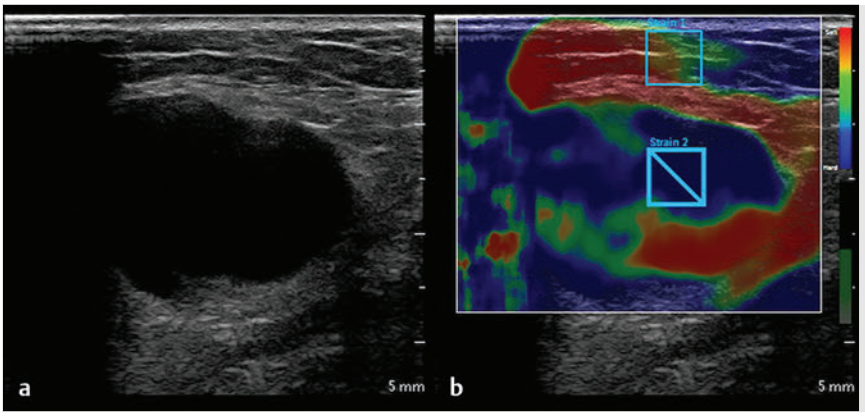

Fig. 8.19 Split-screen (**a**) B-mode ultrasound image and (**b**) strain elastogram of a metastatic lymph node showing pattern 3 on the elastogram. A strain ratio of 6.2 was calculated.

Table 8.5 Different proposed cutoff values of strain ratio (SR) and their diagnostic utility

SR cutoff	Lymph node region	Sensitivity (%)	Specificity (%)	Study
1.5	Cervical	85	98	Lyshchik et al[11]
2.45	Cervical	93.8	89.5	Arda et al[38]
1.5	Cervical	92.8	53.4	Tan et al[39]
1.78	Cervical	98.1	64.9	Teng et al[40]
2.395	Cervical, supraclavicular, axillary, inguinal	78.41	98.51	Zhang et al[41]
2.3	Axillary	82.8	56.3	Choi et al[28]
1.54*	Axillary	100	48	Taylor et al[42]

*The original article mentions a value of 0.65, which is the ratio of node strain to tissue strain. The reciprocal of 0.65 is the equivalent of the SR referred to in the text, that is, 1.54.

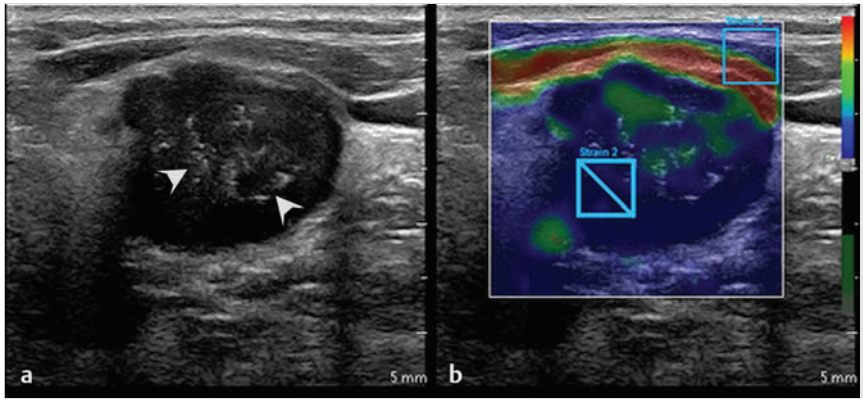

Fig. 8.20 Split-screen (**a**) B-mode ultrasound image and (**b**) corresponding strain elastogram of a known tuberculous lymph node with fibrosis and calcifications (*arrowheads*). The B-mode image shows loss of the central echogenic hilum and presence of calcific foci, while the elastogram shows color pattern 3. A strain ratio of 3.1 was calculated. Thus, both the B-mode and elastogram findings falsely indicate a metastatic region.

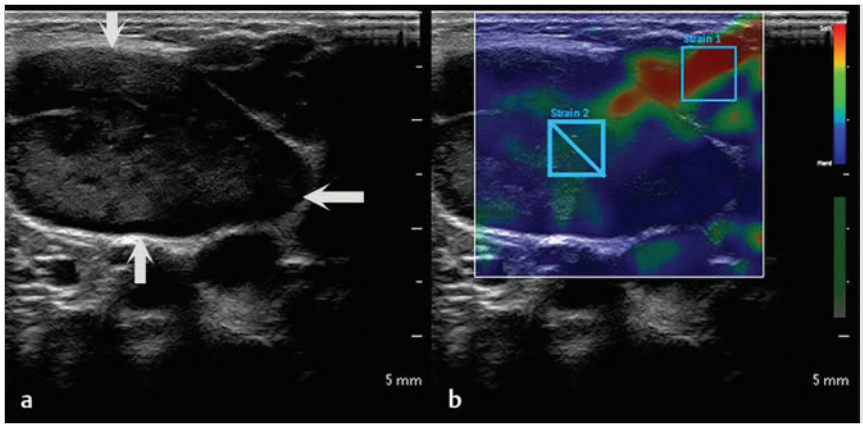

Fig. 8.21 Split-screen (**a**) B-mode ultrasound image and (**b**) corresponding strain elastogram of a known lymphomatous lymph node (*arrows*). The B-mode image shows loss of fatty hilum and cortical heterogeneity, while the elastogram shows color pattern 3. A strain ratio of 1.36 was calculated, which is less than the cutoff of 1.50 for malignant lymph nodes (false negative).

Limitations of Strain Imaging

Strain imaging appears to be a promising technique for lymph node characterization, especially for diagnosis of metastases. However, limitations in this emerging technology should be assessed carefully before its widespread acceptance.

- Cervical, axillary and inguinal lymph nodes are easily evaluated by ultrasound elastography. However, mediastinal and abdominal lymph nodes are not readily accessible. Endoscopic ultrasound elastography has proven to be useful for the evaluation of mediastinal and perigastric nodes.
- Nonaxial and out-of plane motion of the lymph node during image acquisition may create variations in the strain calculations.
- Optimum compression force is an important factor in freehand elastography. Due to its highly subjective nature, it may produce interobserver and intraobserver variability and adversely affect reproducibility.
- Box (ROI) size, shape, and distance from the transducer may induce variation in the SR calculation. There may be variation in implementation of the technique by different manufacturers.[11,20]
- The elastographic patterns as well as the strain ratios are relative to the elastographic properties of the surrounding tissues, which are assumed to be normal. Hence, pre-existing tissue disorders and postexcision fibrosis in these tissues may interfere with elastographic analysis.
- Presence of large blood vessels complicates the elastographic evaluation by inducing loss of pressure homogeneity and distorting the elastogram.
- Benign reactive lymph nodes have stiffness similar to surrounding soft tissues while malignant lymph nodes tend to be harder. However, a few nonmalignant pathologies like tuberculosis may have an overlapping appearance. A tuberculous lymph node with necrosis and liquefaction will appear softer, while one with fibrosis, scarring, or calcification may display harder areas (▶ Fig. 8.20).[20]
- The elastographic appearance in relapsing or chronic lymphadenitis and in rare benign diseases such as Kikuchi or Kimura's disease is not well studied. The effect of various therapies on elastographic appearance of lymph nodes also needs further evaluation.[20]
- Most malignant lymph nodes are harder than surrounding normal tissue. However, lymphomatous nodes tend to be softer (▶ Fig. 8.21).[23]
- Determining the percentage of hard area is largely subjective and depends on various factors such as the operator's experience and the scoring system used. These may induce a considerable amount of intraobserver and interobserver variability. Use of dedicated image processing software to measure the percentage of hard tissue probably reduces this source of measurement bias. Strain ratios are semi-quantitative and have better accuracy than scoring systems.
- Focal deposits within a lymph node that are small are either overlooked or the lymph node is given a score similar to benign nodes. Necrotic soft areas in some metastatic nodes alter their score. These shortcomings can be eliminated by adopting a scoring system which incorporates focal deposits and necrotic areas.[23]

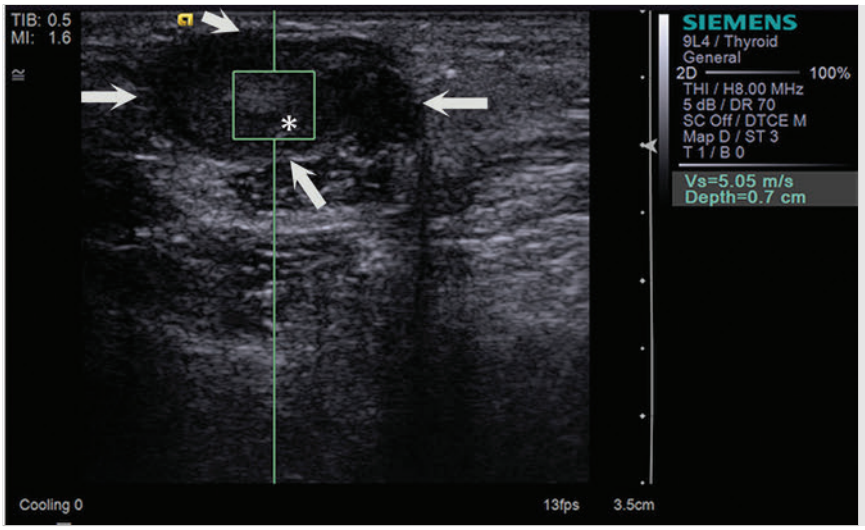

Fig. 8.22 Image acquisition for p-SWE of a known metastatic lymph node. A 5 × 6 mm ROI box (*asterisk*) is placed at a suspicious region inside a cervical node (*arrows*). The shear wave speed (V_s) of 5.05 m/s indicates malignancy.

Some of the above limitations can potentially be overcome by using shear wave imaging.

8.3.2 Shear Wave Elastography Imaging

Shear wave elastography for lymph nodes is a novel technique that allows real-time assessment of lymph node stiffness in absolute quantitative terms. Thus, it overcomes the intrinsic limitations associated with strain elastography, which provides only qualitative and semiquantitative data (in the form of the elastogram and the strain ratio, respectively). Unlike strain elastography, which involves the application of freehand manual compression, shear wave elastography involves application of a radiation force by the probe rather than the operator, which results in greater reproducibility.[29] This has been discussed in detail in Chapter 3. Only relevant parts are discussed here.

Techniques

The variations of shear wave imaging which are used for lymph node assessment include acoustic radiation force impulse (ARFI) and SuperSonic Imagine (SSI) imaging amongst others. The technique of image acquisition with shear wave imaging is summarized here:

- Position the patient similar to routine neck ultrasound imaging with the neck extended over a pillow.
- Hold the probe still, perpendicular to the skin, with just enough compression to establish a complete contact with the underlying node using copious coupling gel.
- In case of ARFI imaging (point shear wave imaging), put the ROI blindly over a suspected lesion within a lymph node to get values of shear wave velocity in meters per second.
- On the other hand, in SSI imaging and two-dimensional shear wave imaging, which have the advantage of displaying a color map of tissue stiffness, place the ROI in the hardest visible region of the node to calculate the SR.
- Use this technique for all neck lymph node levels except level VII.

Acoustic Radiation Force Impulse Imaging

Acoustic radiation force impulse (ARFI) imaging utilizes shear waves generated by a pushing beam of ultrasound energy. The technique can be used in two ways: point shear wave imaging (p-SWE) and two-dimensional shear wave imaging (2D-SWE). In p-SWE, a small ROI box is placed at the site where the stiffness value is desired. After initiating the pulse, a stiffness value of the tissues in the ROI is provided. In 2D-SWE, a large field of view (FOV) is placed and multiple ARFI pulses are used to provide a color-coded display of the stiffness values of all the tissues in the FOV. A smaller ROI(s) can then be placed in the FOV to obtain stiffness values at specific locations. The position of the patient during the examination is same as that for a routine neck ultrasound. The probe is applied with a minimum amount of pressure so as to make complete contact with the cervical lymph nodes without significantly altering tissue stiffness. The ROI, typically a 5 × 5 mm box, is placed over the lesion and the quantitative shear wave speed (in meters per second) is determined (▶ Fig. 8.22).[30] Real-time elastograms are currently unavailable in this technique. Various studies have come up with various cutoffs in their analysis.[31,32,33] This warrants further large-scale studies to develop a widely acceptable and accurate cutoff.

SuperSonic Imagine Imaging

SSI (SuperSonic Imagine) imaging is a 2D-SWE technique that provides real-time quantitative shear modulus mapping of an organ in less than 30 ms. It generates supersonic impulses that induce shear waves, which are then tracked throughout the entire window (FOV) using an ultrafast scanner and sophisticated postprocessing software. This system displays real-time, color-coded elastograms in terms of either shear wave speed (in meters per second [m/s]) or shear (or elastic) modulus (in kilopascals [kPa]). Quantitative measurements of the shear modulus (SM) can be obtained using static elastograms.[2,34,35]

Like strain elastography, SSI imaging of cervical lymph nodes is also performed in a position similar to that for conventional ultrasound, namely, with the patient lying supine with the neck

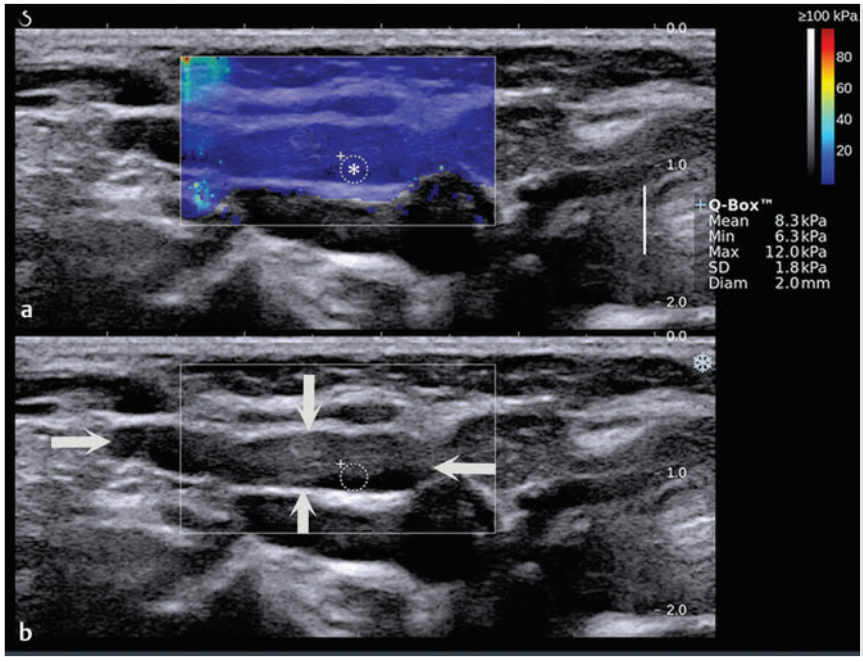

Fig. 8.23 (**a**) 2D-shear wave elastogram and (**b**) corresponding B-mode ultrasound image of a benign lymph node (*arrows*). The elastogram shows a homogeneous blue (soft) hue. Placement of Qbox (ROI box, *asterisk*) in the hardest region gives values of different shear modulus parameters. Here, a low shear (elasticity) modulus (maximum shear modulus [SM] 12.0 kPa) can be observed.

slightly extended. After obtaining a B-mode image (using copious coupling gel) with a linear probe (4–15 MHz), shear wave mode is selected. After application of the transducer, it is held still and normally over the lymph node under investigation with minimal pressure to allow the shear wave image to consolidate, which usually takes 2 or 3 seconds. Any significant pressure by the probe can increase tissue stiffness and thus give false positive high values. The patient may be asked to hold his or her breath in order to minimize motion-related inhomogeneity. While obtaining elastography images, default elasticity settings of acoustic impulse intensity, kilopascal display scale (0 to 180 kPa), smoothing, and persistence can be used. In this mode, the B-mode and shear wave elasticity images are displayed on the screen in two adjacent panels. The color scale can be adjusted to a lower maximum in kilopascals for better color differentiation of the tissues in the elasticity image. The system allows for stiffness values to be displayed in meters per second (m/s) if desired. The elastography color map, where hard (stiff) areas are indicated in red and soft areas are indicated in blue, is superimposed over the grayscale B-mode image. A ROI box (Qbox in SSI) is placed over an artifact-free area which appears to be the stiffest in the node. The size of the ROI can be varied; however, a minimum size of 2 mm x 2 mm is prescribed.[2,35]

After placement of the ROI, a quantitative elasticity map is constructed (▶ Fig. 8.23), displaying the shear modulus of every pixel of the image in kilopascals (kPa), by measuring the speed of the propagation of the shear wave at that point. The software generates a list of quantitative parameters (minimum SM [kPa], maximum SM [kPa], mean SM [kPa], standard deviation of SM [kPa], and diameter of the ROI) out of which the maximum SM value is considered for analysis since it helps detect focal cortical metastases better.[5,35] Higher shear modulus values for nodes suggest malignancy (▶ Fig. 8.24), while benign nodes show lower shear modulus values (▶ Fig. 8.23).

For the evaluation of cervical lymph nodes to differentiate between benign and malignant lymph nodes, the mean SM with a cutoff of 30.2 kPa has a 41.9% sensitivity and 100% specificity, while the max SM with a cutoff of 45 kPa has a 48.4% sensitivity and 91.8% specificity.[35] A study revealed a better sensitivity (91%) and a comparable specificity (97%) of max SM with a cutoff value of 19.44 kPa.[29] In case of axillary lymph node evaluation, the same indices show similar sensitivity and specificity with slightly different cutoff values.[5] Universal standardization of these cutoffs needs further validation in large-scale studies.

Limitations of Shear Wave Imaging

Shear wave imaging has clear advantages over strain imaging by virtue of being quantitative and user independent. Yet, it suffers from certain limitations.

- The max SM values may vary with the histology of the malignancy. Lymphomatous lymph nodes may appear softer (as low as 23kPa) and hence contribute to false-negative results. False-negative results may also be obtained due to focal cortical metastatic foci too small to be detected by SWE.
- Shear wave measurements are accurate only up to 3 cm depth from the skin, as the shear wave signal tends to attenuate rapidly beyond this depth.[5]

8.4 Future Prospects

Endoscopic ultrasound (EUS) elastography addresses the major limitation of inaccessibility of visceral lymph nodes to elastographic evaluation (▶ Fig. 8.25). It is a novel, noninvasive technique with minimum added cost and no added complications. It has been used to investigate mediastinal, perigastric, and peripancreatic lymph nodes. During examination, extrinsic compression is not required (and also may not be feasible) as intrinsic compression by respiratory movements and vascular pulsations can be utilized for elastogram acquisition. This limits the use of strain imaging for EUS. Software-assisted analysis

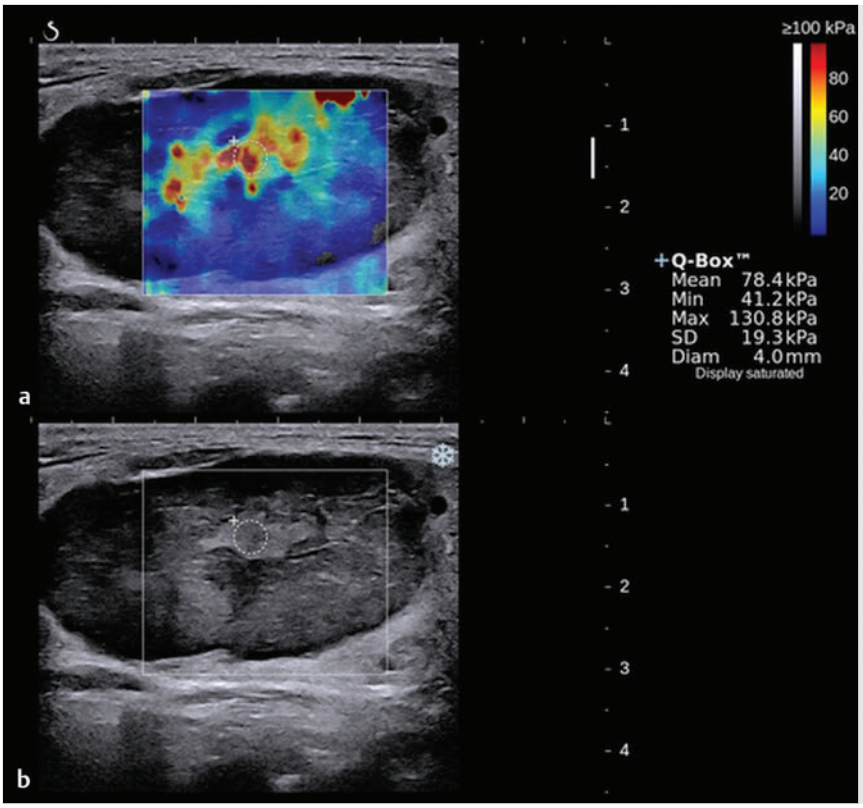

Fig. 8.24 (**a**) 2D-shear wave elastogram and (**b**) corresponding B-mode ultrasound image of a metastatic lymph node. The B-mode image shows the loss of fatty hilum and cortical heterogeneity while the elastogram reveals heterogeneous, high stiffness (red) areas. The maximum shear modulus (max SM) value of 130.8 kPa suggests a metastatic region.

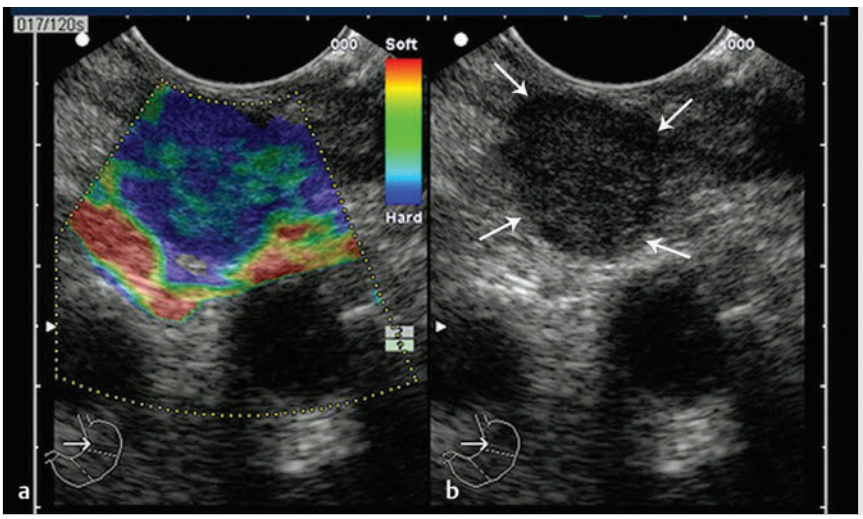

Fig. 8.25 Endoscopic ultrasound (EUS) of perigastric lymph node (*arrows*). (**a**) Strain elastogram and (**b**) corresponding B-mode image. The elastogram shows hard areas (blue) covering approximately > 45% of the node. The B-mode image shows a rounded node with loss of hilar echoes. The findings suggest malignancy. (Image courtesy of Dr Pankaj Dhawan, Mumbai, India.)

can be applied to increase the accuracy and reproducibility of EUS.[36] EUS may prove superior to B-mode US for the differential diagnosis of benign and malignant lymph nodes.[36,37] It provides valuable complementary information to EUS-guided fine needle aspiration cytology (FNAC) and can also serve as a promising tool to guide sampling. This may increase the yield in metastasis cases with necrotic areas or partial invasion.

Other potential uses of elastography to assess lymph nodes include elastography-guided FNAC or biopsy, incorporation of other ultrasound technologies like volumetric ultrasound (three-dimensional [3D] ultrasound) in elastography, and fusion of other imaging techniques with elastography.

8.5 Conclusion

Elastography seems to be a more promising tool for characterization of lymph nodes as compared to conventional noninvasive imaging modalities. The clinical utility of elastography will further increase as future advances in image acquisition and reconstruction algorithms take place. It can contribute noninvasive, prognostic information for more accurate preoperative assessment. It can also be a valuable guiding tool for performing percutaneous procedures for lymph node sampling. In particular, shear wave elastography is a quantifiable, user-independent, and reproducible method. However, its usefulness

needs to be further evaluated in large, prospective, multicenter studies. Also, whether elastography eventually obviates the need for certain lymph node biopsies remains to be seen. EUS is a futuristic modality of assessing anatomically difficult nodes.

References

[1] Alam F, Naito K, Horiguchi J, Fukuda H, Tachikake T, Ito K. Accuracy of sonographic elastography in the differential diagnosis of enlarged cervical lymph nodes: comparison with conventional B-mode sonography. AJR Am J Roentgenol 2008; 191(2):604–610

[2] Evans A, Rauchhaus P, Whelehan P et al. Does shear wave ultrasound independently predict axillary lymph node metastasis in women with invasive breast cancer? Breast Cancer Res Treat 2014; 143(1):153–157

[3] Fauci A, Braunwald E, Kasper D, et al. Harrison's Principles of Internal Medicine. 17th ed. New York, NY: McGraw-Hill; 2008.

[4] Munjal YP, Sharma SK, Agarwal AK, et al, eds. API Textbook of Medicine. 9th ed. London, England: JP Medical Ltd; 2012.

[5] Tourasse C, Dénier JF, Awada A, Gratadour A-C, Nessah-Bousquet K, Gay J. Elastography in the assessment of sentinel lymph nodes prior to dissection. Eur J Radiol 2012; 81(11):3154–3159

[6] Haberal I, Çelik H, Göçmen H, Akmansu H, Yörük M, Özeri C. Which is important in the evaluation of metastatic lymph nodes in head and neck cancer: palpation, ultrasonography, or computed tomography? Otolaryngol Head Neck Surg 2004; 130(2):197–201

[7] Som PM, Curtin HD. Head and Neck Imaging. 4th ed. Philadelphia, PA: Elsevier Health Sciences; 2003.

[8] Dudea SM, Lenghel M, Botar-Jid C, Vasilescu D, Duma M. Ultrasonography of superficial lymph nodes: benign vs. malignant. Med Ultrasound 2012; 14(4): 294–306

[9] Ying M, Ahuja A, Metreweli C. Diagnostic accuracy of sonographic criteria for evaluation of cervical lymphadenopathy. J Ultrasound Med 1998; 17(7):437–445

[10] van den Brekel MWM, Castelijns JA, Snow GB. The size of lymph nodes in the neck on sonograms as a radiologic criterion for metastasis: how reliable is it? AJNR Am J Neuroradiol 1998; 19(4):695–700

[11] Lyshchik A, Higashi T, Asato R et al. Cervical lymph node metastases: diagnosis at sonoelastography—initial experience. Radiology 2007; 243(1):258–267

[12] Rosário PWS, de Faria S, Bicalho L et al. Ultrasonographic differentiation between metastatic and benign lymph nodes in patients with papillary thyroid carcinoma. J Ultrasound Med 2005; 24(10):1385–1389

[13] Steinkamp HJ, Wissgott C, Rademaker J, Felix R. Current status of power Doppler and color Doppler sonography in the differential diagnosis of lymph node lesions. Eur Radiol 2002; 12(7):1785–1793

[14] Na DG, Lim HK, Byun HS, Kim HD, Ko YH, Baek JH. Differential diagnosis of cervical lymphadenopathy: usefulness of color Doppler sonography. AJR Am J Roentgenol 1997; 168(5):1311–1316

[15] Furukawa MK, Kubota A, Hanamura H, Fujita Y, Furukawa M. Diagnosis of cervical lymph node metastasis of head and neck squamous cell carcinoma. MEDIX (Suppl.) 2007:20–23.

[16] Smajlovic F, Carovac A, Bulja D. Sonoelastography : the method of choice for evaluation of tissue elasticity. J Health Sci 2011; 1(1):50–55

[17] Edge SB, Byrd DR, Compton CC, Fritz AG, Greene FL. AJCC Cancer Staging Manual. 7th ed. New York, NY: Springer-Verlag; 2009.

[18] Hefeda MM, Badawy ME. Can ultrasound elastography distinguish metastatic from reactive lymph nodes in patients with primary head and neck cancers? Egypt. J. Radiol. Nucl. Med. 2014; 45(3):715-722

[19] Fu Y, Shi Y-F, Yan K, Wang Y-J, Yang W, Feng G-S. Clinical value of real-time elastography in patients with unexplained cervical lymphadenopathy: quantitative evaluation. Asian Pac J Cancer Prev 2014; 15(13):5487–5492

[20] Dudea SM, Botar-Jid C, Dumitriu D, Vasilescu D, Manole S, Lenghel ML. Differentiating benign from malignant superficial lymph nodes with sonoelastography. Med Ultrasound 2013; 15(2):132–139

[21] Ishibashi N, Yamagata K, Sasaki H et al. Real-time tissue elastography for the diagnosis of lymph node metastasis in oral squamous cell carcinoma. Ultrasound Med Biol 2012; 38(3):389–395

[22] Bhatia KSS, Cho CCM, Yuen Y-H, Rasalkar DD, King AD, Ahuja AT. Real-time qualitative ultrasound elastography of cervical lymph nodes in routine clinical practice: interobserver agreement and correlation with malignancy. Ultrasound Med Biol 2010; 36(12):1990–1997

[23] Lenghel LM, Bolboacă SD, Botar-Jid C, Băciuț G, Dudea SM. The value of a new score for sonoelastographic differentiation between benign and malignant cervical lymph nodes. Med Ultrasound 2012; 14(4):271–277

[24] Rago T, Santini F, Scutari M, Pinchera A, Vitti P. Elastography: new developments in ultrasound for predicting malignancy in thyroid nodules. J Clin Endocrinol Metab 2007; 92(8):2917–2922

[25] Moon HJ, Kim E-K, Yoon JH, Kwak JY. Clinical implication of elastography as a prognostic factor of papillary thyroid microcarcinoma. Ann Surg Oncol 2012; 19(7):2279–2287

[26] Image J. Image processing and analysis in Java. Available at: rsb.info.nih.gov/ij/. Accessed May 5, 2015.

[27] Furukawa MK, Kubota A, Hanamura H, Furukawa M. [Clinical application of real-time tissue elastography to head and neck cancer—evaluation of cervical lymph node metastasis with real-time tissue elastography] Nippon Jibiinkoka Gakkai Kaiho 2007; 110(7):503–505–505

[28] Choi JJ, Kang BJ, Kim SH et al. Role of sonographic elastography in the differential diagnosis of axillary lymph nodes in breast cancer. J Ultrasound Med 2011; 30(4):429–436

[29] Choi YJ, Lee JH, Lim HK et al. Quantitative shear wave elastography in the evaluation of metastatic cervical lymph nodes. Ultrasound Med Biol 2013; 39 (6):935–940

[30] Choi YJ, Lee JH, Baek JH. Ultrasound elastography for evaluation of cervical lymph nodes. In: Ultrasonography. 2015 Jul; 34(3): 157-164

[31] Fujiwara T, Tomokuni J, Iwanaga K, Ooba S, Haji T. Acoustic radiation force impulse imaging for reactive and malignant/metastatic cervical lymph nodes. Ultrasound Med Biol 2013; 39(7):1178–1183

[32] Tamaki K, Tamaki N, Kamada Y et al. Non-invasive evaluation of axillary lymph node status in breast cancer patients using shear wave elastography. Tohoku J Exp Med 2013; 231(3):211–216

[33] Meng W, Xing P, Chen Q, Wu C. Initial experience of acoustic radiation force impulse ultrasound imaging of cervical lymph nodes. Eur J Radiol 2013; 82 (10):1788–1792

[34] Bercoff J, Tanter M, Fink M. Supersonic shear imaging: a new technique for soft tissue elasticity mapping. IEEE Trans Ultrason Ferroelectr Freq Control 2004; 51(4):396–409

[35] Bhatia KSS, Cho CCM, Tong CSL, Yuen EHY, Ahuja AT. Shear wave elasticity imaging of cervical lymph nodes. Ultrasound Med Biol 2012; 38(2):195–201

[36] Săftoiu A, Vilmann P, Ciurea T et al. Dynamic analysis of EUS used for the differentiation of benign and malignant lymph nodes. Gastrointest Endosc 2007; 66(2):291–300

[37] Paterson S, Duthie F, Stanley AJ. Endoscopic ultrasound-guided elastography in the nodal staging of oesophageal cancer. World J Gastroenterol 2012; 18 (9):889–895

[38] Arda K, Ciledag N, Gumusdag P. Differential diagnosis of malignant cervical lymph nodes at real-time ultrasonographic elastography and Doppler ultrasonography. Hung Radiol Online 2010; 1:10–13

[39] Tan R, Xiao Y, He Q. Ultrasound elastography: its potential role in assessment of cervical lymphadenopathy. Acad Radiol 2010; 17(7):849–855

[40] Teng D-K, Wang H, Lin Y-Q, Sui G-Q, Guo F, Sun L-N. Value of ultrasound elastography in assessment of enlarged cervical lymph nodes. Asian Pac J Cancer Prev 2012; 13(5):2081–2085

[41] Zhang Y, Lv Q, Yin Y et al. The value of ultrasound elastography in differential diagnosis of superficial lymph nodes. Front Med China 2009; 3(3):368–374

[42] Taylor K, O'Keeffe S, Britton PD et al. Ultrasound elastography as an adjuvant to conventional ultrasound in the preoperative assessment of axillary lymph nodes in suspected breast cancer: a pilot study. Clin Radiol 2011; 66(11): 1064–1071

9 Elastography of the Spleen, Pancreas, and Kidneys

Mirko D'Onofrio, Vito Cantisani, Emilio Quaia, Riccardo De Robertis, Costanza Bruno, Stefano Crosara, Valentina Ciaravino, Antonio Giulio Gennari, Michele Pontello, Giuseppe Schillizzi and Roberto Pozzi Mucelli

9.1 Introduction

Although much research has been performed evaluating the liver using elastography, especially for assessment of liver fibrosis, elastography can also be performed on other abdominal organs. This chapter reviews elastography of the spleen, pancreas, and kidney.

Strain elastography (SE), point shear wave elastography (p-SWE), and 2D-shear wave elastography (2D-SWE) are all implemented on conventional ultrasound systems and stiffness values can be obtained from other abdominal organs, using B-mode ultrasound for localization. For vibration-controlled transient elastography (VCTE), which does not have conventional ultrasound available in its system, localization of areas to assess stiffness is more problematic. As in many other organs, disease states in abdominal organs present with changes in stiffness, with malignancy substantially stiffer than normal tissues. With all abdominal organs, respiration causes motion, which is problematic in obtaining accurate stiffness values.

9.2 Spleen

Ultrasonography has long been used as a noninvasive and rapid diagnostic modality for solid organs in the upper abdomen, including the spleen. The need to evaluate solid organs in the upper abdomen using noninvasive methods and to monitor several chronic disorders of abdominal organs has led to the development of a new technique, ultrasound elastography.

Ultrasound elastography (or more commonly elastography) is a novel method to visualize and quantify the stiffness of a tissue. Since pathologic conditions such as inflammation and tumors can change tissue elasticity, elastrography can be used to differentiate pathologic from normal tissue and monitor the progress of some chronic pathologic conditions. The degree of deformation of the underlying soft tissue in response to compression is calculated to estimate the tissue stiffness (not true elasticity) in kilopascals.[1,2] Three main forms of elastography are present nowadays in clinical practice: vibration-controlled transient elastography (VCTE), strain elastography (SE), and shear wave elastography (SWE). Other important implementations are to be expected as the field matures. In strain elastography (SE), known as quasi-static elastography, the tissue deformation produced by external compressive force with a probe or by endogenous stress such as arterial pulsations reveals the physical properties of soft tissue. It does so by characterizing the differences in stiffness between the tissue of interest and the surrounding normal tissue on the basis of a uniform (mechanically induced) strain on these tissues during B-mode scanning. The data can then be used to form an image that is coded in color or in grayscale to show the pattern of strain, which is inversely related to tissue stiffness and can be assessed subjectively.[3] Shear wave elastography (SWE) is a technique that assesses the mechanical properties of a tissue by monitoring the speed of shear wave propagation originating from said tissue on deformation. It does so with low-frequency waves that are generated by mechanical knocks with a probe (VCTE) or by the acoustic radiation force impulses (ARFIs).[4,5] This method can visualize not only the distribution of stiffness over tissues, but can also quantify the stiffness of a tissue. Moreover, the method does not require any direct touching or compression. To date, a limited number of papers have been published to evaluate the use of elastography in abdominal organs other than the liver in clinical practice.

9.2.1 Examination Technique

Strain Elastography

Limited evaluation of SE has been performed on the spleen.

Shear Wave Elastography

The reported mean elasticity values of normal spleen, calculated by means of SWE, were 2.9 ± 1.8 kPa (range, 1–10 kPa); the mean elasticity values for the spleen did not exhibit a significant difference between the sexes and among ages.[6] Similarly, Ferraioli et al showed that in 4,172 measurements of spleen stiffness values obtained, those from men were not significantly different than from women. Both in men and women, the spleen showed higher stiffness (▶ Fig. 9.1) with respect to the liver.[7]

Some technical issues to address in an elastographic examination tailored to the spleen have been proposed by Karlas et al. They found that diagnostic accuracy of p-SWE is affected by the ROI angle with respect to the spleen, and the lowest variation of the elastographic value was found when the ROI position was placed perpendicular to the central portion of the transducer surface.[8] When obtaining a measurement, the patient should hold his or her breath similar to when performing a liver fibrosis study. It is unknown if the measurements are dependent on the prandial state, as they are with the liver. However, it is expected that splenic stiffness may increase with the increased blood flow after eating.

When using VCTE, an ultrasound system is required to localize the spleen and provide guidance for the VCTE measurement. If ascites is present, VCTE measurements cannot be made since the mechanically induced shear waves do not transmit in ascites.

9.2.2 Clinical Applications

The main application of elastography in the study of the spleen is in the evaluation of cirrhotic patients in order to determine the risk of portal hypertension.[9,10,11] Recent studies have shown that spleen stiffness correlates with hepatic fibrosis (HF), portal hypertension (PH), and the risk of esophageal varices (EV) in patients with chronic liver disease. In particular, there are changes in spleen morphology noted among patients with cirrhosis, including hyperplasia of splenic histiocytes, lengthening of

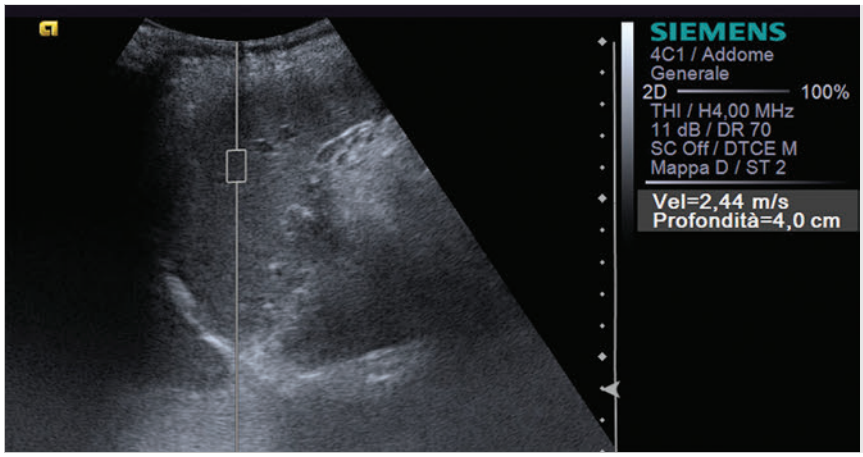

Fig. 9.1 Shear wave speed of the spleen.

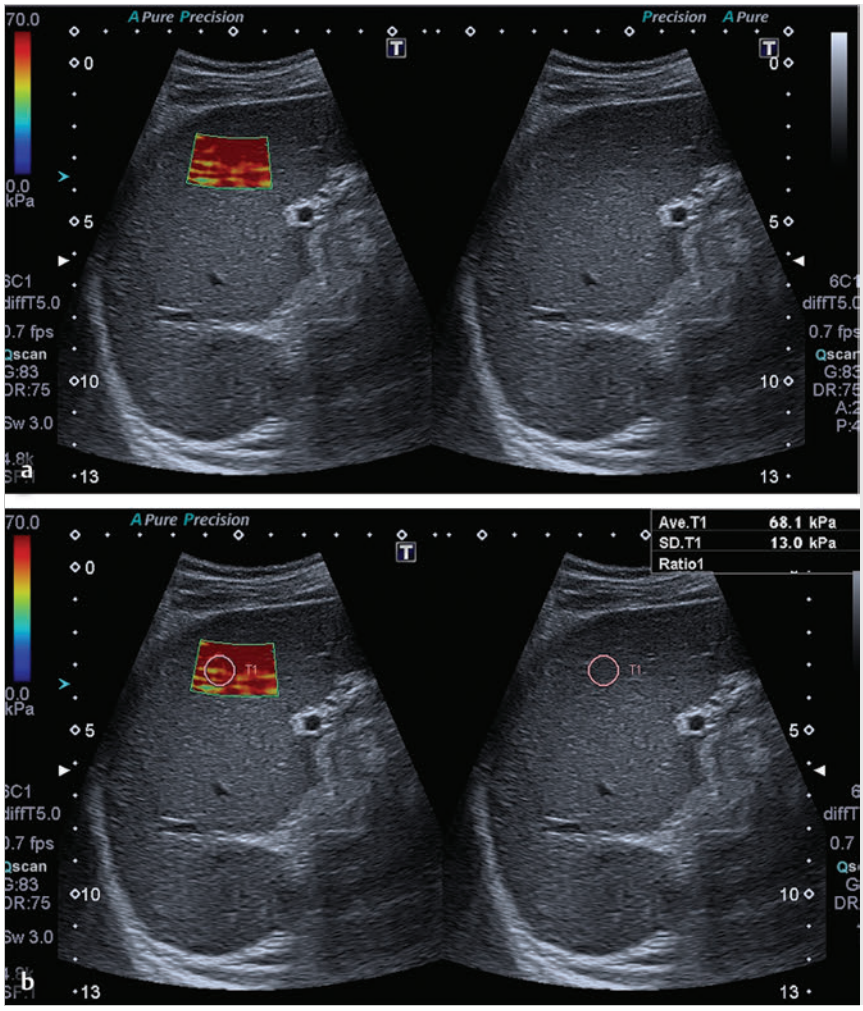

Fig. 9.2 (**a**, **b**) Cirrhotic patient with portal hypertension. The spleen is enlarged and stiff.

arterial terminals, increased splenic white pulp volume, fibrosis between splenic trabecular structures, and increased splenic red pulp blood volume from congestion with blood. The increased spleen stiffness (▶ Fig. 9.2) in portal hypertension is likely due to spleen congestion that, by itself, leads to increased organ stiffness.[12,13] Piscaglia et al[11] calculated that the median ARFI-VTQ (Virtual Touch Quantification, a p-SWE technique) values in the spleen were 2.33 m/s in normal subjects, 2.62 m/s in patients with chronic hepatitis demonstrated by transient elastography (TE) (namely < 13 kPa), and 3.36 m/s in those with cirrhosis (TE > 13 kPa) ($p < 0.005$) among groups and for paired comparisons, thus confirming the hypothesis that an increase in splenic stiffness occurs with the development of portal hypertension. The derived splenohepatic index in the various groups (obtained by multiplying the shear wave speed [SWS] value calculated in the liver by the SWS value calculated in the

spleen and dividing the result by 100, in order to correlate these two values) were 2.61 m/s, 3.77 m/s, and 8.13 m/s, respectively. The diagnostic accuracy of the ARFI-VTQ splenohepatic index for the diagnosis of cirrhosis produced higher area under the receiver operating characteristic (AUROC) curve values (0.945) than the assessment of liver stiffness in the right or left liver lobe or in the spleen. The best cutoff has been proven to be 4.90 m/s (sensitivity 95.2%, specificity 80.9%, positive predictive value [PPV] 81.6%, negative predictive value [NPV] 95.0%).[11]

Moreover, Colecchia et al[9] conducted stiffness measurements of the spleen and liver by means of transient elastography (TE, a VCTE technique) in 100 patients with hepatitis C virus [HCV]–related cirrhosis and compared its performance in predicting portal hypertension (PH) and esophageal varices (EV) to other parameters, including the hepatic vein pressure gradient (HVPG) and noninvasive scores of PH and EV, such as the platelet count/spleen diameter ratio and the score of liver stiffness and the platelet count/spleen diameter ratio. They concluded that the spleen and liver stiffness measurements were more accurate than the other parameters and suggested their use as a noninvasive assessment and in monitoring PH and EV.[9]

A recent systematic review and meta-analysis of 12 studies on the diagnostic performance of elastography techniques in the evaluation of spleen stiffness showed that sensitivity (78%) and specificity (76%) were good, and its likelihood ratio for the presence or absence of EV based on spleen stiffness measurement were modest. Likewise, the diagnostic performance of spleen stiffness measurement for detecting the presence of clinically significant EV also was good, but not at levels that would suggest low false-positive and false-negative diagnostic rates. In this systematic review and meta-analysis published by Singh et al, no differences were found in the diagnostic performance of TE and acoustic radiation force impulse (ARFI) SWE imaging in subgroup analyses.[14]

The results of these studies show that the reproducibility of spleen stiffness measurements in different populations depends on the expertise of the operator, and, in order to achieve a good agreement between measurements, a training period is required. Another disadvantage includes the relativity of the indirect evaluation. Therefore, although useful, and promising, the current techniques of spleen stiffness measurement are suboptimal at this time to replace esophagogastroduodenoscopy (EGD) as the screening modality of choice for detecting the presence and size of EV.

Further studies with larger series of patients should be performed to compare the elasticity values of normal and pathologic tissues to determine the diagnostic role of those techniques.

There is minimal information available for the use of elastography in focal splenic masses.

9.3 Pancreas

The use of elastosonography for the evaluation of the pancreas is still under validation, with a relatively low number of published studies, and with some equivocal and not always concordant results. Two main techniques can be used for the elastographic evaluation of the pancreas, SE and SWE, which include TE, p-SWE, 2D-SWE, and 3D-SWE. These techniques are explained in detail in Chapters 2 and 3.

Elastosonography of the pancreas can be obtained with either an endoscopic or transabdominal approach; the first is frequently used as a part of a comprehensive endoscopic ultrasound (EUS) evaluation, while the latter is a recent technical improvement of conventional ultrasound (US), which needs further evaluation to be considered in clinical practice. The percutaneous approach, although easier and practicable for most specialists, has the same intrinsic limitations of the conventional ultrasound examination, such as the presence of bowel gas.

9.3.1 Examination Technique

Strain Elastography

SE is a quasi-static strain imaging technique that can be applied in the EUS evaluation of the pancreas. This technique can measure the elastic modulus, a measure of the stress applied to tissue structure relative to the strain, or deformation, produced by passive internal physiologically-induced forces (real-time strain elastography [RTSE]).[15]

SE provides a qualitative assessment of strain across the field of view via a colorimetric map. Tools to quantitatively analyze image characteristics, such as to calculate strain ratios, are available.

The field of view (FOV) must be large enough to include both the target tissue and the surrounding normal pancreatic tissue for a proper comparison. Both longitudinal and radial echoendoscopes can be used for RTSE. EUS elastography needs the proper positioning of the endoscopic probe within the gastric and/or duodenal lumen to obtain a reliable evaluation; moreover, adequate pressure must be obtained with the manipulation of the endoscopic probe, but in most cases very little additional compression is required, as the pulsatory impulse of peripancreatic vessels are sufficient to achieve a valid elastographic evaluation.[15]

Each pixel in the elastographic FOV is displayed with a hue that represents the relative strain value (hardness) of the tissue. In most of the equipment, the strain value is presented through a chromatic map (red–green–blue) in which hard tissues are shown in dark blue/blue, while soft tissues are displayed in red/green; color maps are dynamically displayed as a transparent overlay superimposed on the grayscale EUS image.[15] Various color or grayscale maps can be used and the color map should be included with the images for correct stiffness assessment.

In transabdominal strain elastography, it is difficult to apply the correct compression–release to get diagnostic information and achieving this can be heavily limited by bowel gas. This procedure comes with a long learning curve and is highly operator dependent.

Shear Wave Elastography

Acoustic radiation force impulses (ARFIs) are used to induce shear waves in tissues in SWE, and ARFI generation is available as a technical improvement of ultrasound scanners for transabdominal elastography. ARFI generation is independent from external manual compression and therefore suitable for use in the evaluation of deep abdominal organs such as the pancreas. ARFI-based SWE is a new ultrasound tool able to evaluate the stiffness of deep tissues.[16] Tissues, responses to these forces are ultrasound-induced focused radiation force impulses or Mach cone–induced localized microscopic displacements in the

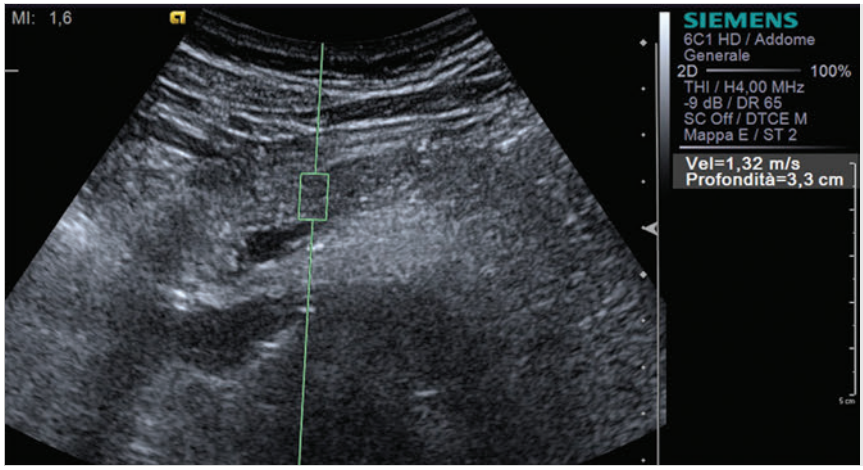

Fig. 9.3 Shear wave speed of the pancreas.

selected target FOV (longitudinal waves and shear waves). Both the displacement and the shear waves speed (SWS) depend on the viscoelastic properties of the tissue, which are directly correlated to the resistance to wave propagation.

SWE can provide both a qualitative assessment of displacements through a visual assessment of grayscale or color maps (ARFI Virtual Touch Tissue Imaging, ARFI-VTI) and a quantitative evaluation of SWS through a numerical representation expressed in meters per second (ARFI Virtual Touch Quantification, ARFI-VTQ). The stiffer a tissue is, the faster will be the SWS.

Transabdominal US elastographic examination technique has no particular technical differences with conventional transabdominal US examination.

9.3.2 Clinical Applications

Healthy Pancreas

The pancreas is histologically composed of a variable admixture of soft components, including pancreatic acini and fatty tissue. As a consequence, healthy pancreas is characterized by a homogeneously green pattern, represented by a predominance of green areas at qualitative visual analysis of EUS and elastographic examination.[17,18,19,20,21,22] In older people, fat and connective tissue progressively deposit within the pancreas, increasing its echogenicity, so that at elastographic study the pancreas itself becomes heterogeneous.[16]

Furthermore the elastographic study can help in the differentiation between the ventral primordium of the pancreas (developed from a dorsal and a ventral primordium) and a neoplastic or inflammatory pathology. The ventral primordium of pancreas can be visible above pancreatic surrounding tissue as a hypoechoic structure with a band-shape. This hypoechoic structure can be confused with other diseases such as inflammation or tumors; elastography can demonstrate the same tissue properties between these two parts of the healthy pancreas.[16]

The semiquantitative evaluation of EUS elastography–derived histograms have reported high strain values, with a mean value of about 110 (based on a range from 0 [hardest] to 255 [softest]) in the pancreas of healthy subjects below 60 years of age; pancreatic stiffness can increase with age, with a mean value of about 80 over 60 years of age.[23,24]

The mean SWS of the healthy pancreas at ARFI-VTQ (▶ Fig. 9.3) is around 1.20 and 1.40 m/s.[25,26,27]

Inflammatory Diseases

Acute pancreatitis can be histopathologically divided into edematous and necrohemorragic variants. While the first is characterized by the presence of interstitial edema, congestion, and leucocytic infiltration, the second one presents with tissue destruction, fat necrosis, and hemorrhage. In both cases, the consistency of the pancreatic parenchyma during acute inflammation becomes softer than that of the healthy pancreas as a consequence of edema or necrosis, and this feature could theoretically be identified with elastosonography.

Necrosis can be identified at EUS elastography as blue (soft) areas.[28] Unfortunately, literature data regarding ARFI-VTQ are controversial. Some authors have reported that the sensitivity and specificity of ARFI-VTQ can reach 100% and 98%, respectively, for this diagnosis of acute pancreatitis, using a cutoff value of 1.63 m/s (being the mean SWS value for the patients with acute pancreatitis and significantly higher than the value for the control group [$p < 0.001$]);[29] others have reported that SWS values tend to be higher in acute pancreatitis (3.28 m/s) than in chronic pancreatitis (1.25 m/s),[26] a finding that is fairly unusual if correlated to the typical histopathologic findings of these entities (i.e., presence of edema and/or necrosis versus fibrosis).

Chronic pancreatitis is characterized by atrophic changes, fibrosis, and frequently by the presence of parenchymal calcifications and intraductal calculi, which harden the consistency of the pancreas.

In patients with suspected chronic pancreatitis a direct linear correlation with a high area under the curve (AUC) and accuracy value has been reported between the number of EUS criteria for the diagnosis of chronic pancreatitis according to the Rosemont classification[30] and the EUS strain ratio.[32] At visual qualitative EUS elastography chronic pancreatitis usually presents a predominant hard (blue) pattern,[17,19,20] despite a heterogeneous mixed-color pattern or even a homogeneously soft (green) pattern having been reported.[17,19,20]

Semiquantitative analysis of pancreatic stiffness through a histogram-derived analysis in patients with chronic pancreatitis provides values around 30 (based on a range from 0 [hardest] to 255[softest]), which are significantly lower than that of healthy patients, even of elderly age.[23] A linear correspondence between quantitative EUS elastography results and the grade of pancreatic fibrosis assessed at histopathologic analysis has been reported.[32]

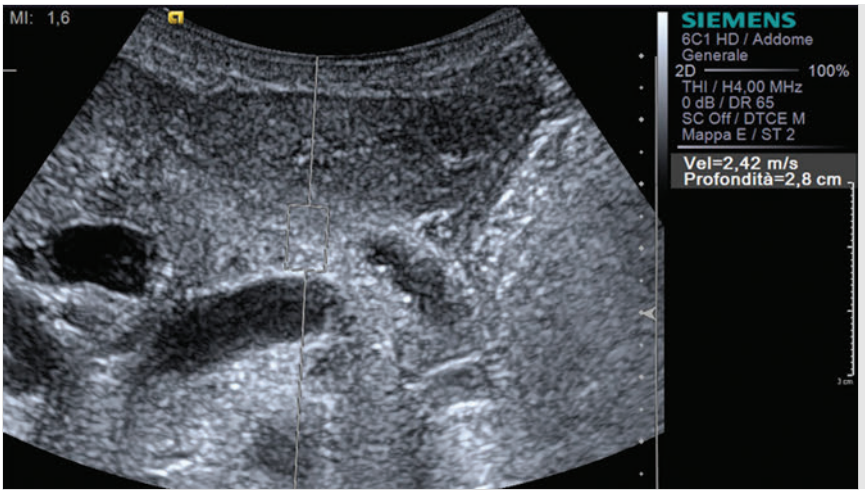

Fig. 9.4 Shear wave speed in obstructive chronic pancreatitis.

At quantitative transabdominal elastography, patients with chronic pancreatitis generally present high SWS values (▶ Fig. 9.4), despite differences in the precise cutoff value that have been reported.[26,33]

One major issue in patients with focal chronic pancreatitis is the differentiation from pancreatic ductal adenocarcinoma (PDAC), given that parenchymal fibrosis, calcifications, and intraductal calculi, which are frequently present in patients with chronic pancreatitis, produce a hard (blue) elastographic pattern, comparable with that of highly fibrotic malignant lesions, such as PDAC. Moreover, at present no universally accepted numerical cutoff values for both quantitative EUS elastography and ARFI-VTQ exist for the differentiation between chronic pancreatitis and PDAC.

As a consequence, despite some authors having reported enthusiastic results,[20] further studies have proven that EUS elastography has low specificity and sensitivity (< 70%) in the differential diagnosis[17,19] between chronic pancreatitis and PDAC.

Nevertheless, some authors have proposed the use of semiquantitative evaluation methods to improve this distinction by means of EUS elastography: for example, the strain ratio of PDAC seems to be higher than that of mass-forming pancreatitis (45.23 versus 5.78).[19] The histogram analysis of SWS values have also reported good results for this distinction: chronic pancreatitis presents higher strain for the average hue histograms as compared to PDAC.[34,35]

Pancreatic involvement in cystic fibrosis leads to acinar cell destruction, fibrosis, and exocrine insufficiency. Patients with pancreatic insufficiency related to cystic fibrosis have significantly lower SWS values assessed with ARFI-VTQ as compared to patients with preserved pancreatic function.[36]

Autoimmune pancreatitis (AIP) is an autoimmune form of chronic and/or relapsing pancreatitis characterized by dense lymphoplasmacytic periductal infiltration. Its qualitative elastographic findings are indistinguishable from those of chronic pancreatitis, presenting a hard (blue) pattern at RTSE; nevertheless, AIP can be distinguished from PDAC based on the presence of a diffuse hard pattern, while on the contrary, PDAC usually presents as a focal blue area.[37]

Solid Neoplasms

EUS elastography is a good method for the detection of solid pancreatic lesions, with sensitivity, specificity, positive predictive value, negative predictive value, and accuracy of 100%, 85.5%, 90.7%, 100% and 94%, respectively.[21]

At visual analysis, EUS elastography seems to be able to adequately distinguish between normal pancreas and pancreatic neoplasms, given that these latter generally present as hard (blue) areas as compared to the soft (green) healthy parenchyma. As a consequence, a green-predominant pattern has been reported to be able to exclude the presence of a pancreatic solid lesion with a high accuracy.[17,21,38] Moreover, the mean elasticity value of the healthy pancreas seems to be significantly higher than that of PDAC (0.53% versus 0.02%, respectively; $p < 0.0001$).[39]

Nevertheless, the clinical usefulness of visual assessment seems to be limited, since most pancreatic lesions are harder than the surrounding parenchyma, independent of their histopathologic nature.[18]

SWS quantification using p-SWE has been proven to be able to distinguish between the pancreas harboring pancreatic cancer, which presents high SWS values (1.51 ± 0.45 m/s) and the pancreas without cancer (1.43 ± 0.28 m/s), thus improving the detection of PDAC.[40]

Some authors have tried to discriminate between different solid pancreatic lesions using elastosonography, but the results are poor and controversial. While some authors reported good results, with high sensitivity and specificity values (reaching 100% and almost 70%) for the differential diagnosis of malignant pancreatic masses using EUS elastography,[41,42] other studies[19,20,34] have proven that EUS elastography has a limited value.

Malignant lesions seem to be characterized by higher mean echogenicity at ARFI-VTI when compared to benign lesions:[43] in fact it has been demonstrated that the mean echogenicity score of the malignant lesions (3.7 ± 1.0) was higher than that of the benign lesions (3.1 ± 0.4; p = 0.023). On the contrary, although a no statistical difference has been reported on ARFI-VTQ images between benign and malignant lesions (2.4 ± 1.1 m/s versus 3.3 ± 1.0 m/s; p = 0.101), the mean SWS difference between the lesions and the adjacent parenchyma was higher for malignant lesions (1.5 ± 0.8 m/s) as compared to benign lesions (0.4 ± 0.3 m/s).

Pancreatic ductal adenocarcinoma (PDAC) is a solid firm mass, stiffer than the adjacent parenchyma and characterized by intense desmoplasia with a highly fibrotic aspect at histopathologic evaluation. As a consequence, at EUS elastosonography,

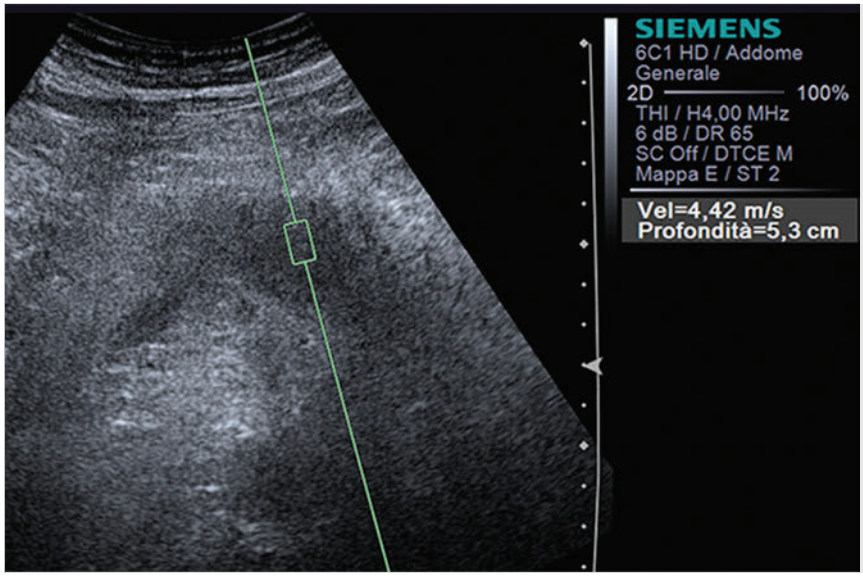

Fig. 9.5 Shear wave speed of a ductal adenocarcinoma of the pancreatic body.

PDAC usually presents a hard pattern.[17,18,19,20,21] At SWS quantification (▶ Fig. 9.5), PDAC is generally characterized by high values.[44] The use of elastography with SWS quantification in the study of a pancreatic mass can lead to suspicion of a ductal adenocarcinoma based on the lesion stiffness (▶ Fig. 9.6).

Pancreatic neuroendocrine tumors (PanNETs) have a variable aspect at EUS elastography: they can present a predominantly hard (blue) pattern, slightly harder than the surrounding parenchyma;[17,18,19,20] a mixed pattern, with a central green area surrounded by blue tissue;[19,20] or even a homogeneous soft (green) pattern.[19,20] At transabdominal elastography, PanNETs are usually harder or slightly harder than normal pancreatic parenchyma.[44]

Pancreatic metastases, rare solid pancreatic lesions, present a heterogeneously hard (blue) pattern.[20,21]

Cystic Neoplasms

Pancreatic cystic tumors can be divided into serous neoplasms, mucinous cystic neoplasms, intraductal papillary mucinous neoplasms (IPMNs), and solid pseudopapillary tumors. Cystic tumors are usually characterized at imaging based on their morphology and architecture. Nevertheless, their definite diagnosis often requires the analysis of their content by means of EUS-guided fine needle aspiration: serous cystadenoma is characterized by a simple fluid content, whereas mucinous cystic neoplasms and IPMNs present a complex and viscous content.[45]

Although mechanical longitudinal waves propagate through both solids and liquids, shear waves are markedly attenuated in liquids, in which only longitudinal waves or the shear waves reflected at the solid–fluid interface can be measured. However, the wide range of different fluids in vivo, with heterogeneous viscosities and composition (for example, presence of suspended particles), may generate different responses at elastography.

Experimental studies[46] have reported that simple fluids, such as water, are characterized by nonnumerical values at ARFI-VTQ and displayed as "XXXX/0" by the US equipment, while complex fluids are characterized by numerical values. This is due to simple fluids not supporting shear waves while complex fluids that have increased viscosity support shear waves.

In vivo applications of ARFI-VTQ to cystic pancreatic lesions have reported that serous cystadenomas often present nonnumerical values ("XXXX/0"), while mucinous cystic neoplasms often present numerical values.[47,48] The presence of at least two ARFI-VTQ measurements with numerical results (different from "XXXX/0") out of five total measurements yielded a sensitivity, specificity, positive predictive value, negative predictive value, and accuracy of 68.8%, 77.3%, 68.8%, 77.3%, and 73.7%, respectively, for distinguishing between mucinous and serous cystic neoplasms. The prevalence of measurements with numerical results irrespective of the total number of measurements provided the following sensitivity, specificity, positive predictive value, negative predictive value, and accuracy values for this distinction: 37.5%, 100%, 100%, 68.8%, and 73.3%.[49] ARFI-VTQ can therefore be potentially able to improve the characterization of pancreatic cystic lesions, providing a noninvasive analysis of their fluid content (▶ Fig. 9.7).

Prediction of Postoperative Pancreatic Fistula

Despite technical improvements of pancreatic surgery, postoperative pancreatic fistula (POPF) remains one of the most common complications after pancreaticoduodenectomy.[50]

The incidence of POPF is related to several predisposing factors, including the consistency of the pancreatic parenchyma: a soft pancreas will more likely develop POPF than a pancreas with a hard consistency.[50] This finding has been confirmed by studies conducted with ARFI-VTQ: the incidence of POPF was significantly higher in patients presenting a mean pancreatic SWS below 1.54 m/s than in those presenting a "hard" pancreas (≥ 1.54 m/s).[51,52]

9.4 Kidney

The kidney is a complex, highly perfused (1.2 L/min corresponding to 20% of cardiac output; 400 mL/min/100 g), and anisotropic organ, so the intrinsic geometry of the tissue and its degree of anisotropy are primary factors of varying elasticity.[53,54] Renal cortex anatomy is not organized in linear structures,

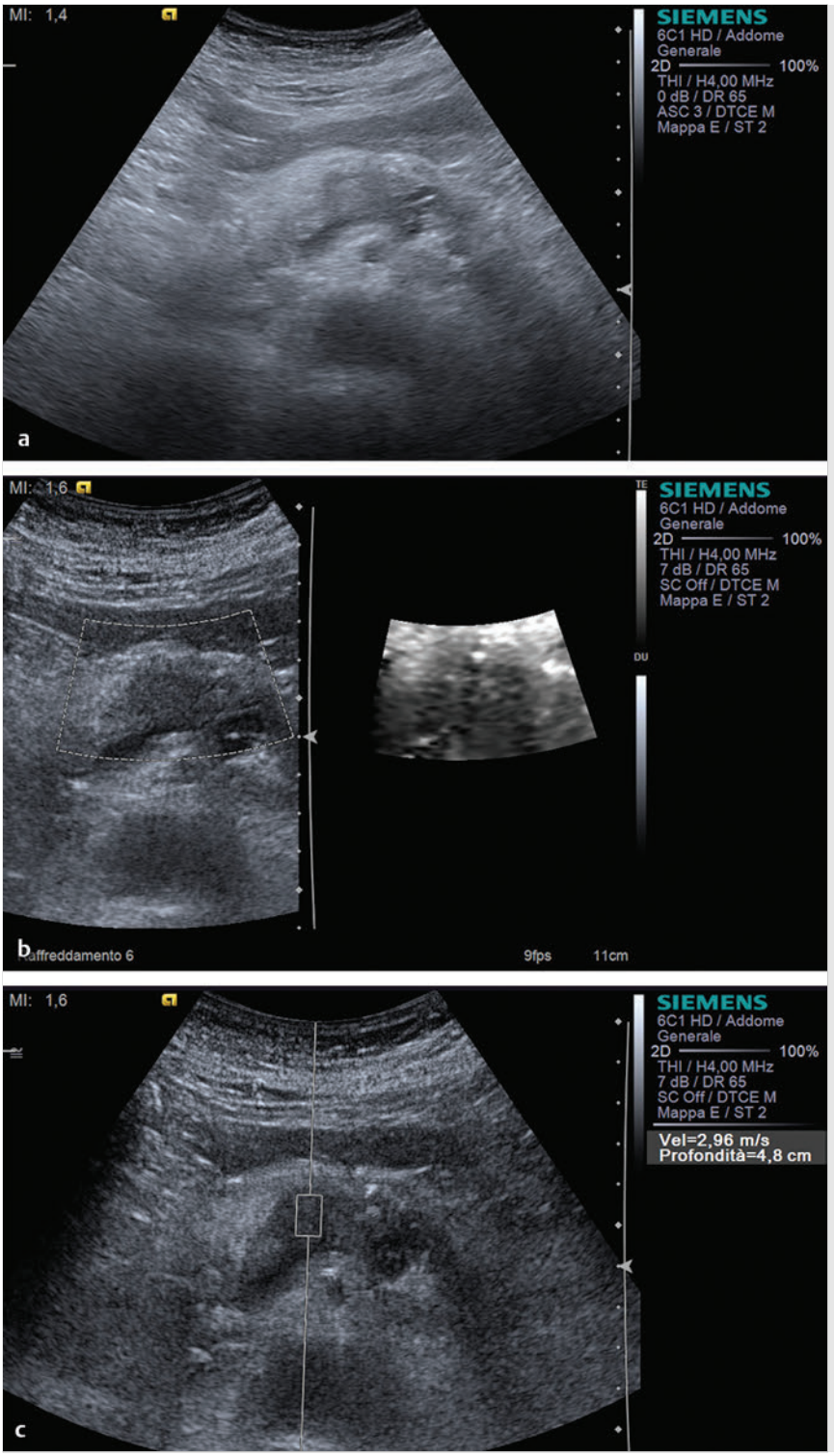

Fig. 9.6 Ductal adenocarcinoma. (**a**) At B-mode imaging, it appears as an ill-defined hypoechoic area in the pancreatic body. (**b**) At SWE imaging, the lesion is black due to relative stiffness (**c**) with high shear wave speeds at quantification.

since glomeruli are spherical and proximal and distal tubules have convoluted shapes.[55] On the other hand, the predominant perpendicular orientation of Henle loops and vasa recta within the renal medulla in respect to the capsule produces a high degree of anisotropy. Therefore, when the acoustic radiation force impulses are sent parallel to these structures, the shear waves induced propagate at a lower speed resulting in an underestimation of renal tissue stiffness. Conversely, when the acoustic radiation force impulses are sent perpendicular to these structures, the shear waves propagate at a higher speed resulting in overestimation of renal tissue stiffness.[53] For all these reasons, a precise identification of the renal segments to be sampled and their orientation to the US beam is mandatory when performing renal elastography.[54]

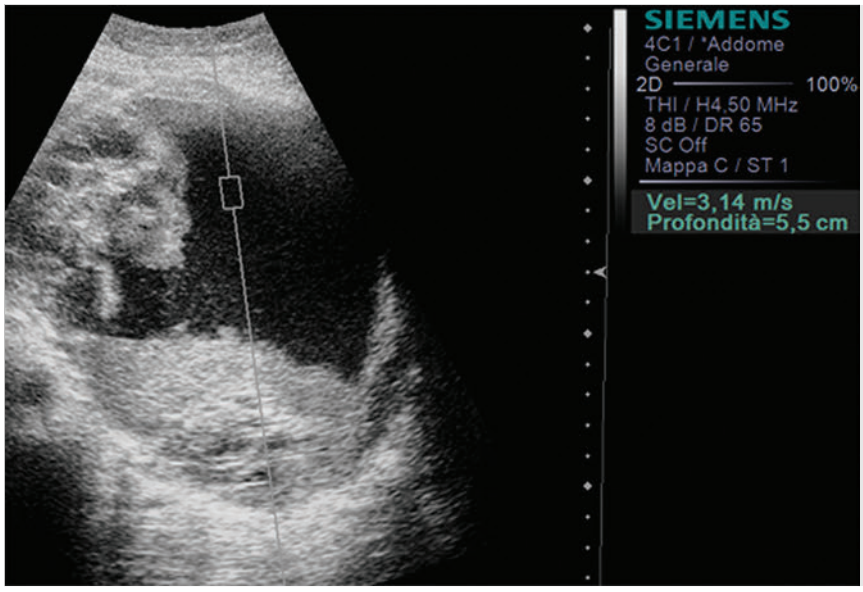

Fig. 9.7 Mucinous cystadenocarcinoma, showing shear wave speeds in the mucous intracystic fluid.

9.4.1 Examination Technique

There is no standardized method to perform a renal elastography examination. Even though it seems to be easier to perform it with the patient lying in a prone position,[56,57] there is not a consensus between authors, some of them preferring the lateral position,[57,58] while others prefer the supine position.[59,60] Children usually do not maintain the correct decubitus position so the evaluation is always challenging. On the other hand, when assessing a transplanted patient, the supine position is typically used.[61] Moreover, in this patient type, it is important to be aware of the relationship between the applied transducer force and the shear wave speed (SWS),[62] as it is known that the elastic modulus of a biological tissue becomes progressively greater with increasing strain.[63]

Breath-holding minimizes motion artifacts and leads to a more accurate evaluation. The applied probe frequencies are also important and should be chosen on a case-by-case basis, especially in children given their varying body size: a lower-frequency probe could be used both for adults and older children, whereas a high-frequency probe should be specifically dedicated to children under 5 years of age.[59] One of the main issues in acquiring reproducible elasticity values on native kidney is the depth of the tissue under investigation, which does not always allow proper SW generation and acquisition.[53] Moreover, particular attention has to be paid to the degree of bladder filling in the elastography examination of transplanted kidney,[55] which should be evaluated after micturition.

Strain Elastography

Strain elastography techniques are not adequate for the measurement of renal tissue stiffness for two main reasons: first, kidneys are deep organs and therefore there is no direct access to apply an external compression easily; second, the kidney is heterogeneous so there is no normal tissue to compare abnormalities–therefore this technique does not provide quantitative data on renal stiffness.[53] Similarly, elastography systems without US guidance are also inappropriate due to the absence of B-mode control, so it is extremely difficult and hazardous to adequately position the ROI on the renal parenchyma (due to the lack of a rigid support for the probe, such as the rib cage).[53]

Shear Wave Elastography

The ARFI-SWE and Supersonic Imagine SWE (real-time 2D-SWE) are more promising for kidney stiffness evaluation because it is possible to selectively sample the cortex or the medulla, avoiding the perirenal tissue and the renal sinus, and avoiding also the use of external compression, but measurements are affected by anisotropy and organ vascular pressure.[53]

On elastography examination, the normal kidney shows higher tissue stiffness values than normal liver and pancreas.[27,64] Furthermore many factors seem to influence renal tissue stiffness measurement including patient gender, age, height, weight, and body mass index (BMI). An increase in renal tissue elasticity is related to increased urinary pressure, which determines an increase in anisotropy of the renal cortex (▶ Fig. 9.8) with no significant changes in renal medulla.[55] The occlusion of the renal artery induces a significant decrease of elasticity; conversely, the occlusion of the renal vein induces a severe increase of elasticity in all compartments.[55]

A thorough assessment of all these factors is essential to reduce the intrinsic variability of in vivo measurements, and to increase the reproducibility of the examination results. Anisotropy and vasculature effects on stiffness measurement could be partially overcome by placing the region of interest (ROI) entirely in the outer renal cortex, with the external border close to the capsule. This excludes the medulla, the stroma, and the great vessels from the ROI, to limit the percentage of collecting cavities within the ROI itself, and minimizes the influence of the calyx pressure on SWS values.[65] The reported normal mean SWS for adult kidneys range from 2.24 to 2.37 m/s with no difference between right and left kidney[25,27] but with a high standard deviation (~0.7 m/s).[27] It would be risky in clinical practice to compare values measured using two different ultrasound systems, and the threshold values proposed in the literature should be used only if obtained by the same ultrasound system.[66]

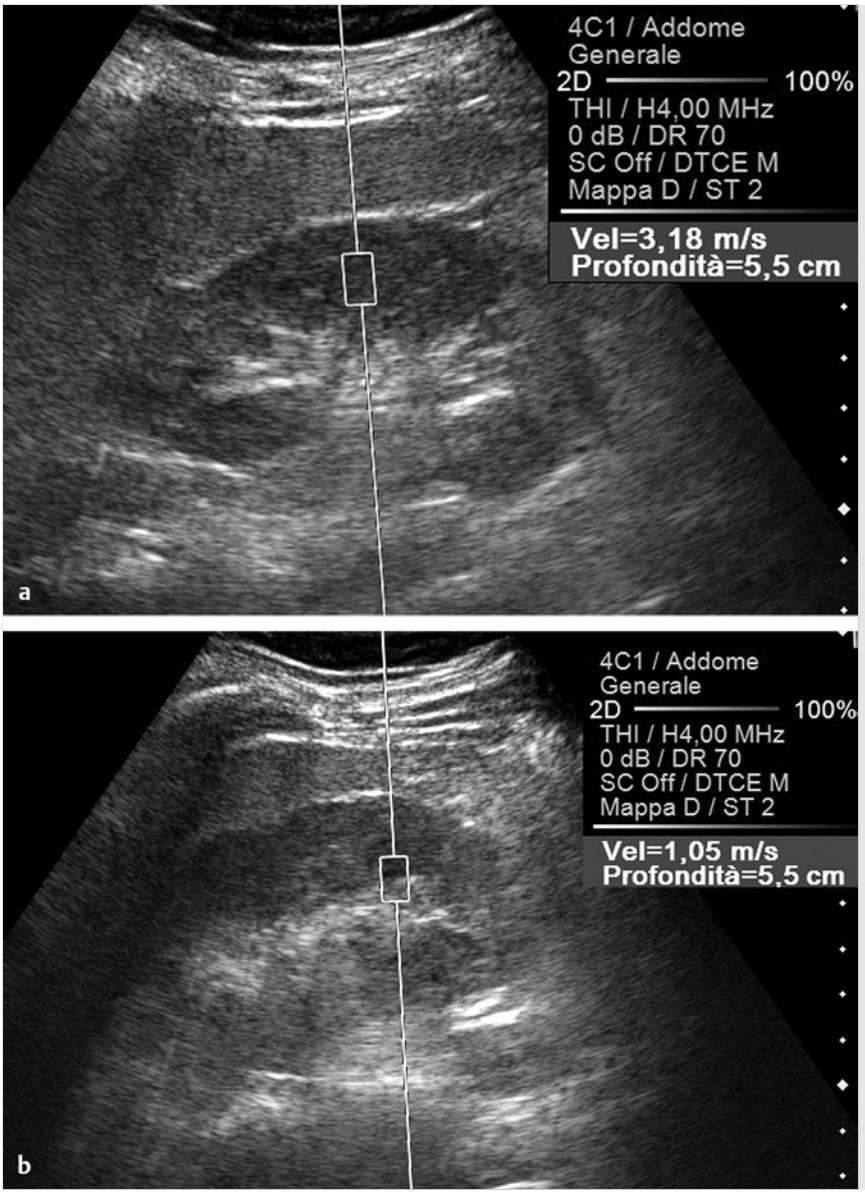

Fig. 9.8 Shear wave speeds are higher in (**a**) the cortex than in (**b**) the medulla, due to the different anatomical organization of these areas of the kidney. Shear wave speeds found in the cortex are higher than those found in other organs.

The majority of incidentally-found renal lesions are small, simple, benign cysts and require no treatment.[67] As a general rule, fluid can greatly alter the tissue stiffness inside the ROI and a lesion with a cystic component cannot be adequately assessed.[68,69,70]

9.4.2 Clinical Applications

Detection of Renal Damage in Children

Low weight at birth and premature birth have been associated with focal segmental glomerulosclerosis.[71,72,73] Chronic kidney disease (CKD) in children older than 2 years is defined as a progressive impairment of renal function in which, for a period of over 3 months, the glomerular filtration rate (GFR) is reduced below 60 mL/min/m^2 with or without abnormalities in the composition of the blood or urine, in imaging studies, or in kidney biopsy.[74] Kidneys that are frequently exposed to urinary tract infection (UTI) may develop renal parenchymal damage that ultimately may lead to development of hypertension and chronic renal failure.[75,76]

The most frequent urinary tract abnormality that predisposes children to pyelonephritis and kidney scarring is high-grade vesicouretreral reflux (VUR).[75,76,77] To date, dimercaptosuccinic acid (DMSA) scintigraphy is the gold standard imaging method for the detection and follow-up of renal damage.[78] Although low (< 0.01 mSv), radiation exposure is unavoidable with scintigraphy, and must be taken into account when dealing with a pediatric population. A statistically significant difference was shown between the SWS values of absolutely normal kidneys, the contralateral kidney of the patients with unilateral disease, and the kidney affected by VUR.[65] The mean SWS values obtained from affected kidneys (5.70 ± 1.71 m/s) were significantly higher than those measured in both contralateral (4.09 ± 0.97 m/s, $p < 0.0001$) and healthy kidneys (3.13 ± 0.09 m/s, $p < 0.0001$). Among the affected kidneys, the difference between the mean SWS values obtained from kidneys with primary (i.e., occurring in an otherwise normal urinary tract) reflux (5.35 ± 1.72 m/s) and those obtained from kidneys with secondary (secondary to anatomical and/or functional abnormalities

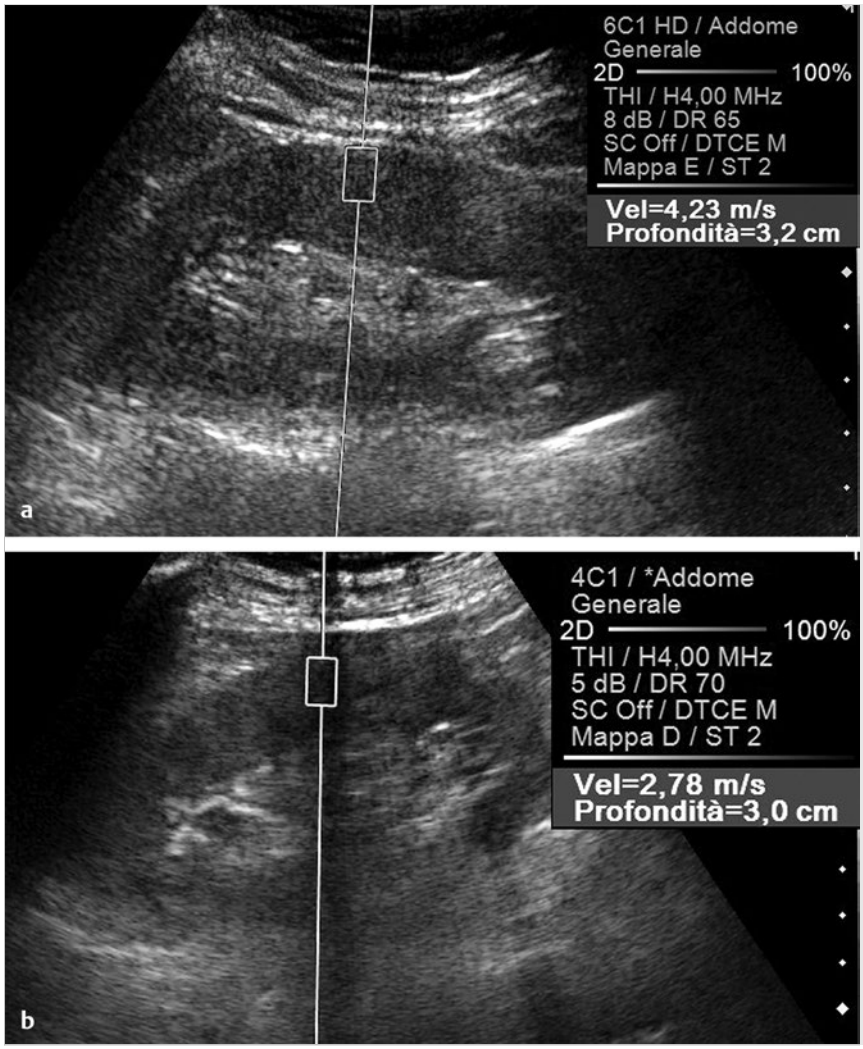

Fig. 9.9 Shear wave speeds are higher (**a**) in kidneys affected by early stage chronic disease than (**b**) in healthy ones.

such as posterior urethral valves or neurogenic bladder) reflux (6.59 ± 1.45 m/s) was significant, too (p = 0.038).

The accuracy of SWE in differentiating between affected, contralateral, and healthy kidneys ranged from 80.3 to 97.1%.[65] This suggests that elasticity decreases and stiffness increases in high-grade hydronephrotic kidneys[65,79]. Moreover a low-grade fibrosis is present in the contralateral kidney due to hyperfiltration damage and consequent sclerotic changes.[65,80,81]

In a preliminary study, SWS values in healthy patients were higher compared with that of patients with renal scarring, with the damaged region having lower SWS values compared with the overall SWS values of the same kidney, and with the lowest SWS values found in the most damaged kidneys in comparison to healthy kidneys.[82] Moreover, significant differences in SWS values were found in non-refluxing patients, in patients with low-grade reflux, and in patients with high-grade reflux, with the latter having the lowest and the former the highest values.[82]

Measurement of Renal Fibrosis in Patients with Chronic Kidney Disease

Chronic kidney disease (CKD) is defined as a reduced glomerular filtration rate, increased urinary albumin excretion, or both,[83] due to progressive glomerulosclerosis, vascular sclerosis, and tubulointerstitial injury with interstitial fibrosis. The CKD incidence and prevalence are increasing in developed countries, particularly in patients with diabetes and hypertension-related nephropathies.[84] Particularly, the risk for cardiovascular disease is notably increased in individuals with CKD.[85] Because it is a progressive disease, CKD may lead to end-stage renal failure, with increase of health cost and extensive morbidity and mortality. As in most types of kidney diseases, CKD progression is characterized by a progressive fibrotic process, which may involve first either glomeruli (glomerulosclerosis) or the interstitial space (interstitial fibrosis) depending on the underlying initial nephropathy.[86,87] The progression of CKD is related to intrarenal fibrosis, and sequential measurement of renal tissue stiffness by elastography could help in following the progression of renal fibrosis. As sensitive laboratory markers are missing, currently renal biopsy is the reference standard for renal fibrosis staging.[88] Detecting intrarenal fibrosis and quantifying its progression with noninvasive methods such as elastography (▶ Fig. 9.9) could be useful to nephrologists since renal biopsy is an invasive technique, susceptible to sampling errors and not feasible for longitudinal monitoring.[89]

Early studies, however, are contradictory: some have not shown a consistent relationship between renal tissue stiffness measured by SWS and renal fibrosis.[85,90] Wang et al, in fact,

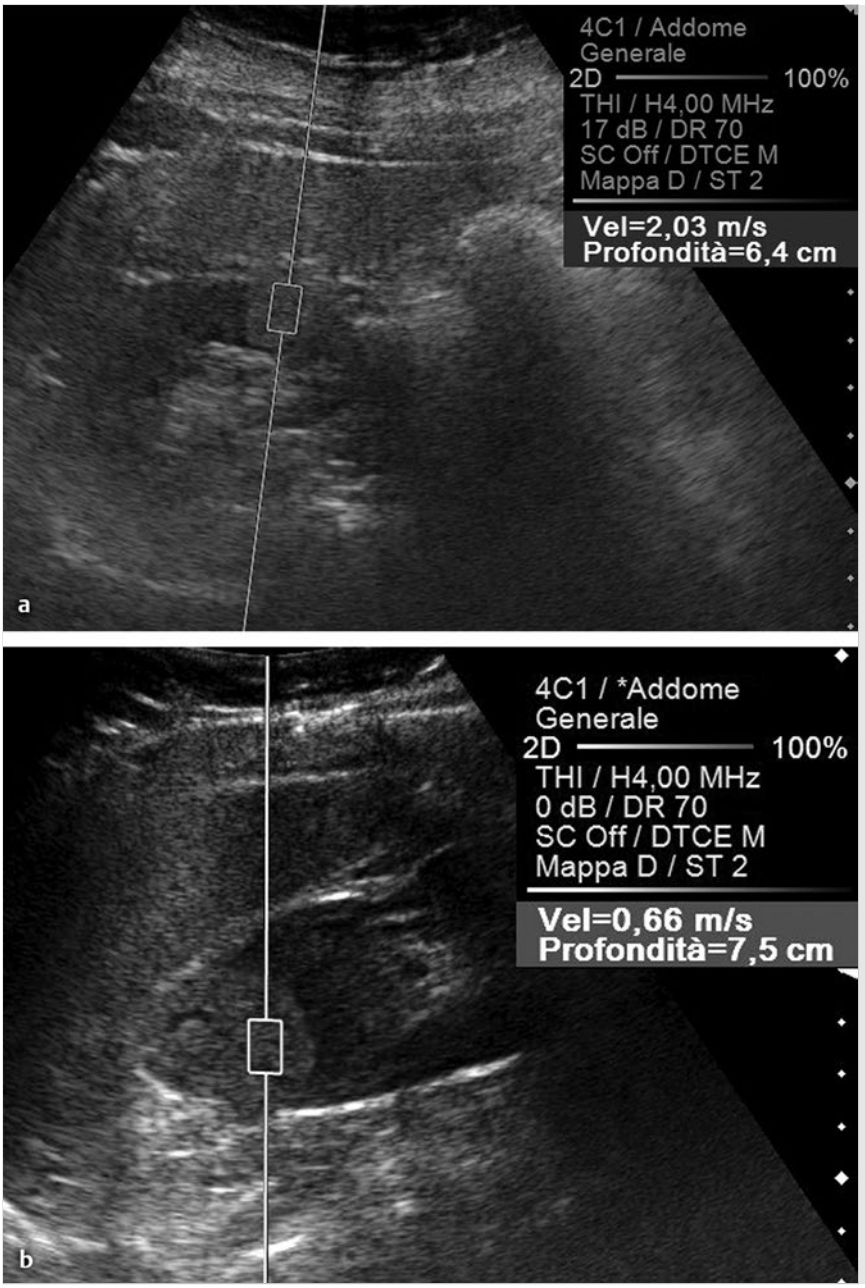

Fig. 9.10 Preliminary results indicate that acoustic radiation force impulse (ARFI) shear wave elastography can be useful in the differentiation of malignant (**a**) clear cell carcinoma from benign (**b**) oncocytoma. Malignant lesions show a stiffer pattern than benign ones, characterized by higher shear wave speeds.

demonstrated that SWS values did not show significant correlations with CKD stage and fibrosis indicators despite using standardized measurement methods.[85] The reason for this finding could be that, as CKD progresses, renal fibrosis increases gradually, whereas intrarenal blood perfusion decreases simultaneously.[91] The two factors contribute oppositely to the stiffness of renal tissue. Renal perfusion impairment, therefore, may counterbalance to some extent the stiffness increase due to fibrosis.[85] In the study by Cui et al[90] the ARFI-VTQ values of the mild and moderate fibrosis groups were significantly increased ($p < 0.01$) compared to the nonfibrosis group; however, there was no significant difference between the ARFI-VTQ values of the mild and moderate fibrosis groups ($p > 0.05$). According to the receiver operating characteristic (ROC) curve, a ARFI-VTQ value of renal parenchyma of > 1.67 m/sec was determined to be an indicator of renal fibrosis, with a sensitivity of 86.3% and a specificity of 83.3%, but with no possibility to distinguish different degrees of fibrosis.

Assessment of Renal Allograft Interstitial Disease

Elastography is a rapid and noninvasive method to measure the progression of renal allograft interstitial disease due to interstitial fibrosis and tubular atrophy, leading to renal transplant failure. The renal tissue stiffness does not show significant correlation with parameters of renal function such as serum creatinine, glomerular filtration rate, and blood pressure. However, patients with increased serum creatinine showed statistically significant higher renal tissue stiffness as compared to stable patients.[91] Indeed, while CKD progresses, renal fibrosis increases[92] leading to increased elastographic values up

to 9.4–9.5 kPa (compared to 4.4–4.5 kPa of the normal kidney). Moreover, there is a significant correlation between the Young's modulus of the cortical parenchyma of the renal allograft estimated through strain elastography and the cortical fibrosis on biopsy.[92] Nonetheless, impaired renal function or interstitial fibrosis have limited influence on renal tissue stiffness, since most renal diseases affect several compartments of the renal tissue and interstitial fibrosis is only one factor which contributes to the deterioration of renal function.

Assessment of Renal Tumors

Angiomyolipoma and renal cell carcinoma (RCC) represent the most common benign and malignant tumors of the kidney, respectively, and an accurate differentiation between these two lesions is essential. Real-time strain elastography may be useful (▶ Fig. 9.10) to differentiate angiomyolipomas from renal cell carcinomas.[93] During breath-holding after deep inspiration, the compression with the transducer followed by release is repeated until a stable image is obtained.[93] The elastogram is displayed over the B-mode image with a color scale in which red represents the greatest strain (softest tissue component), green average strain (intermediate tissue component), and blue no strain (hardest tissue component). Four elastographic patterns were described[93]: type 1, completely soft lesion (mixture of green, yellow, and red without evidence of stiffness); type 2, predominantly soft lesion (some areas of stiffness coded in blue); type 3, predominantly stiff lesion (some soft areas but with > 50% stiff areas coded in blue); and type 4, completely stiff lesion with little or no strain. Type 3 and 4 are more common in RCC.[93] A possible exception is represented by the chromophobe isthological pattern of RCC that may simulate a benign lesion because of the predominant strain (type 2). In a recent paper, a cutoff value of 2.34 m/s was proposed to differentiate benign renal lesions from malignant renal tumors with sensitivity and specificity of 88% and 54%, respectively.[94]

9.5 Conclusion

Elastography is an easy to perform diagnostic technique based on complex physical interactions, which prove its clinical utility outside the liver during ultrasound of the abdomen especially in studying the spleen, the pancreas, and the kidneys. It is better suited for characterization than for detection of pathologies. Elastography is a promising technique that hopefully will add diagnostic information in clinical practice, guiding treatment decisions and patient follow-up, and monitoring the changes in stiffness related with pathologic events. For some applications, such as in the pancreas and kidney, some limitations come from the explorability of the organ and the intrinsic complexity of parenchyma, respectively.

References

[1] Frey H. [Real-time elastography: a new ultrasound procedure for the reconstruction of tissue elasticity][in German] Radiologe 2003; 43(10):850–855

[2] Itoh A, Ueno E, Tohno E et al. Breast disease: clinical application of US elastography for diagnosis. Radiology 2006; 239(2):341–350

[3] Cosgrove D, Piscaglia F, Bamber J et al; EFSUMB. EFSUMB guidelines and recommendations on the clinical use of ultrasound elastography. Part 2: Clinical applications. Ultraschall Med 2013; 34(3):238–253

[4] Nightingale K, Soo MS, Nightingale R, Trahey G. Acoustic radiation force impulse imaging: in vivo demonstration of clinical feasibility. Ultrasound Med Biol 2002; 28(2):227–235

[5] Palmeri ML, Wang MH, Dahl JJ, Frinkley KD, Nightingale KR. Quantifying hepatic shear modulus in vivo using acoustic radiation force. Ultrasound Med Biol 2008; 34(4):546–558

[6] Arda K, Ciledag N, Aktas E, Aribas BK, Köse K. Quantitative assessment of normal soft-tissue elasticity using shear-wave ultrasound elastography. AJR Am J Roentgenol 2011; 197(3):532–536

[7] Ferraioli G, Tinelli C, Lissandrin R et al; Elastography Study Group. Ultrasound point shear wave elastography assessment of liver and spleen stiffness: effect of training on repeatability of measurements. Eur Radiol 2014; 24(6):1283–1289

[8] Karlas T, Pfrepper C, Wiegand J et al. Acoustic radiation force impulse imaging (ARFI) for non-invasive detection of liver fibrosis: examination standards and evaluation of interlobe differences in healthy subjects and chronic liver disease. Scand J Gastroenterol 2011; 46(12):1458–1467

[9] Colecchia A, Montrone L, Scaioli E et al. Measurement of spleen stiffness to evaluate portal hypertension and the presence of esophageal varices in patients with HCV-related cirrhosis. Gastroenterology 2012; 143(3):646–654

[10] Hirooka M, Ochi H, Koizumi Y et al. Splenic elasticity measured with real-time tissue elastography is a marker of portal hypertension. Radiology 2011; 261(3):960–968

[11] Piscaglia F, Salvatore V, Di Donato R et al. Accuracy of VirtualTouch acoustic radiation force impulse (ARFI) imaging for the diagnosis of cirrhosis during liver ultrasonography. Ultraschall Med 2011; 32(2):167–175

[12] Bolognesi M, Merkel C, Sacerdoti D, Nava V, Gatta A. Role of spleen enlargement in cirrhosis with portal hypertension. Dig Liver Dis 2002; 34(2):144–150

[13] Mejias M, Garcia-Pras E, Gallego J, Mendez R, Bosch J, Fernandez M. Relevance of the mTOR signaling pathway in the pathophysiology of splenomegaly in rats with chronic portal hypertension. J Hepatol 2010; 52(4):529–539

[14] Singh S, Eaton JE, Murad MH, Tanaka H, Iijima H, Talwalkar JA. Accuracy of spleen stiffness measurement in detection of esophageal varices in patients with chronic liver disease: systematic review and meta-analysis. Clin Gastroenterol Hepatol 2014; 12(6):935–9–45.e4

[15] Dietrich CF, Săftoiu A, Jenssen C. Real time elastography endoscopic ultrasound (RTE-EUS), a comprehensive review. Eur J Radiol 2014; 83(3):405–414

[16] D'Onofrio M, Crosara S, De Robertis R, et al. Pancreas. In: Calliada F, Canepari M, Ferraioli G, Filice C, eds. Sonoelastography: main clinical applications. Pavia, Italy: Edimes; 2012:39–47

[17] Janssen J, Schlörer E, Greiner L. EUS elastography of the pancreas: feasibility and pattern description of the normal pancreas, chronic pancreatitis, and focal pancreatic lesions. Gastrointest Endosc 2007; 65(7):971–978

[18] Hirche TO, Ignee A, Barreiros AP et al. Indications and limitations of endoscopic ultrasound elastography for evaluation of focal pancreatic lesions. Endoscopy 2008; 40(11):910–917

[19] Itokawa F, Itoi T, Sofuni A et al. EUS elastography combined with the strain ratio of tissue elasticity for diagnosis of solid pancreatic masses. J Gastroenterol 2011; 46(6):843–853

[20] Giovannini M, Thomas B, Erwan B et al. Endoscopic ultrasound elastography for evaluation of lymph nodes and pancreatic masses: a multicenter study. World J Gastroenterol 2009; 15(13):1587–1593

[21] Iglesias-Garcia J, Larino-Noia J, Abdulkader I, Forteza J, Dominguez-Munoz JE. EUS elastography for the characterization of solid pancreatic masses. Gastrointest Endosc 2009; 70(6):1101–1108

[22] Lee TH, Cha SW, Cho YD. EUS elastography: advances in diagnostic EUS of the pancreas. Korean J Radiol 2012; 13 Suppl 1:S12–S16

[23] Janssen J, Papavassiliou I. Effect of aging and diffuse chronic pancreatitis on pancreas elasticity evaluated using semiquantitative EUS elastography. Ultraschall Med 2014; 35(3):253–258

[24] Săftoiu A, Vilmann P, Gorunescu F et al. Neural network analysis of dynamic sequences of EUS elastography used for the differential diagnosis of chronic pancreatitis and pancreatic cancer. Gastrointest Endosc 2008; 68(6):1086–1094

[25] Gallotti A, D'Onofrio M, Pozzi Mucelli R. Acoustic radiation force impulse (ARFI) technique in ultrasound with Virtual Touch tissue quantification of the upper abdomen. Radiol Med (Torino) 2010; 115(6):889–897

[26] Mateen MA, Muheet KA, Mohan RJ et al. Evaluation of ultrasound based acoustic radiation force impulse (ARFI) and eSie touch sonoelastography for diagnosis of inflammatory pancreatic diseases. JOP 2012; 13(1):36–44

[27] Goertz RS, Amann K, Heide R, Bernatik T, Neurath MF, Strobel D. An abdominal and thyroid status with Acoustic Radiation Force Impulse Elastometry—a feasibility study: Acoustic Radiation Force Impulse Elastometry of human organs. Eur J Radiol 2011; 80(3):e226–e230
[28] Dietrich CF. Real-time tissue elastography: multiple clinical applications, multiple clinical solutions. Endosk Heute 2012; 24:177–212
[29] Göya C, Hamidi C, Hattapoğlu S et al. Use of acoustic radiation force impulse elastography to diagnose acute pancreatitis at hospital admission: comparison with sonography and computed tomography. J Ultrasound Med 2014; 33 (8):1453–1460
[30] Catalano MF, Sahai A, Levy M et al. EUS-based criteria for the diagnosis of chronic pancreatitis: the Rosemont classification. Gastrointest Endosc 2009; 69(7):1251–1261
[31] Iglesias-Garcia J, Domínguez-Muñoz JE, Castiñeira-Alvariño M, Luaces-Regueira M, Lariño-Noia J. Quantitative elastography associated with endoscopic ultrasound for the diagnosis of chronic pancreatitis. Endoscopy 2013; 45(10): 781–788
[32] Itoh Y, Itoh A, Kawashima H et al. Quantitative analysis of diagnosing pancreatic fibrosis using EUS-elastography (comparison with surgical specimens). J Gastroenterol 2014; 49(7):1183–1192
[33] Yashima Y, Sasahira N, Isayama H et al. Acoustic radiation force impulse elastography for noninvasive assessment of chronic pancreatitis. J Gastroenterol 2012; 47(4):427–432
[34] Săftoiu A, Vilmann P, Gorunescu F et al; European EUS Elastography Multicentric Study Group. Accuracy of endoscopic ultrasound elastography used for differential diagnosis of focal pancreatic masses: a multicenter study. Endoscopy 2011; 43(7):596–603
[35] Săftoiu A, Vilmann P, Gorunescu F et al; European EUS Elastography Multicentric Study Group. Efficacy of an artificial neural network-based approach to endoscopic ultrasound elastography in diagnosis of focal pancreatic masses. Clin Gastroenterol Hepatol 2012; 10(1):84–90.e1
[36] Friedrich-Rust M, Schlueter N, Smaczny C et al. Non-invasive measurement of liver and pancreas fibrosis in patients with cystic fibrosis. J Cyst Fibros 2013; 12(5):431–439
[37] Dietrich CF, Hirche TO, Ott M, Ignee A. Real-time tissue elastography in the diagnosis of autoimmune pancreatitis. Endoscopy 2009; 41(8):718–720
[38] Schrader H, Wiese M, Ellrichmann M et al. Diagnostic value of quantitative EUS elastography for malignant pancreatic tumors: relationship with pancreatic fibrosis. Ultraschall Med 2012; 33(7):E196–E201
[39] Lee TH, Cho YD, Cha SW et al. Endoscopic ultrasound elastography for the pancreas in Korea: a preliminary single center study. Clin Endosc 2013; 46 (2):172–177
[40] Kawada N, Tanaka S, Uehara H et al. Potential use of point shear wave elastography for the pancreas: a single center prospective study. Eur J Radiol 2014; 83(4):620–624
[41] Giovannini M, Hookey LC, Bories E, Pesenti C, Monges G, Delpero JR. Endoscopic ultrasound elastography: the first step towards virtual biopsy? Preliminary results in 49 patients. Endoscopy 2006; 38(4):344–348
[42] Pei Q, Zou X, Zhang X, Chen M, Guo Y, Luo H. Diagnostic value of EUS elastography in differentiation of benign and malignant solid pancreatic masses: a meta-analysis. Pancreatology 2012; 12(5):402–408
[43] Park MK, Jo J, Kwon H et al. Usefulness of acoustic radiation force impulse elastography in the differential diagnosis of benign and malignant solid pancreatic lesions. Ultrasonography 2014; 33(1):26–33
[44] Uchida H, Hirooka Y, Itoh A et al. Feasibility of tissue elastography using transcutaneous ultrasonography for the diagnosis of pancreatic diseases. Pancreas 2009; 38(1):17–22
[45] Eisendrath P, Ibrahim M. How good is fine needle aspiration? What results should you expect? Endosc Ultrasound 2014; 3(1):3–11
[46] D'Onofrio M, Gallotti A, Falconi M, Capelli P, Mucelli RP. Acoustic radiation force impulse ultrasound imaging of pancreatic cystic lesions: preliminary results. Pancreas 2010; 39(6):939–940
[47] D'Onofrio M, Gallotti A, Salvia R, Capelli P, Mucelli RP. Acoustic radiation force impulse (ARFI) ultrasound imaging of pancreatic cystic lesions. Eur J Radiol 2011; 80(2):241–244
[48] D'Onofrio M, Gallotti A, Martone E, Pozzi Mucelli R. Solid appearance of pancreatic serous cystadenoma diagnosed as cystic at ultrasound acoustic radiation force impulse imaging. JOP 2009; 10(5):543–546
[49] D'Onofrio M, Crosara S, Canestrini S et al. Virtual analysis of pancreatic cystic lesion fluid content by ultrasound acoustic radiation force impulse quantification. J Ultrasound Med 2013; 32(4):647–651
[50] Bassi C, Dervenis C, Butturini G et al; International Study Group on Pancreatic Fistula Definition. Postoperative pancreatic fistula: an international study group (ISGPF) definition. Surgery 2005; 138(1):8–13
[51] Harada N, Ishizawa T, Inoue Y et al. Acoustic radiation force impulse imaging of the pancreas for estimation of pathologic fibrosis and risk of postoperative pancreatic fistula. J Am Coll Surg 2014; 219(5):887–94.e5
[52] Lee TK, Kang CM, Park MS et al. Prediction of postoperative pancreatic fistulas after pancreatectomy: assessment with acoustic radiation force impulse elastography. J Ultrasound Med 2014; 33(5):781–786
[53] Grenier N, Gennisson JL, Cornelis F, Le Bras Y, Couzi L. Renal ultrasound elastography. Diagn Interv Imaging 2013; 94(5):545–550
[54] Ozkan F, Menzilcioglu MS, Duymus M, Yildiz S, Avcu S. Acoustic radiation force impulse elastography for evaluating renal parenchymal stiffness in children. Pediatr Radiol 2015; 45(3):461
[55] Gennisson JL, Grenier N, Combe C, Tanter M. Supersonic shear wave elastography of in vivo pig kidney: influence of blood pressure, urinary pressure and tissue anisotropy. Ultrasound Med Biol 2012; 38(9):1559–1567
[56] Guo LH, Xu HX, Fu HJ, Peng A, Zhang YF, Liu LN. Acoustic radiation force impulse imaging for noninvasive evaluation of renal parenchyma elasticity: preliminary findings. PLoS ONE 2013; 8(7):e68925
[57] Zheng XZ, Yang B, Fu NH. Preliminary study on the kidney elasticity quantification in patients with chronic kidney disease using virtual touch tissue quantification. Iran J Radiol 2015; 12(1):e12026
[58] Bob F, Bota S, Sporea I, Sirli R, Petrica L, Schiller A. Kidney shear wave speed values in subjects with and without renal pathology and inter-operator reproducibility of acoustic radiation force impulse elastography (ARFI)—preliminary results. PLoS ONE 2014; 9(11):e113761
[59] Lee MJ, Kim MJ, Han KH, Yoon CS. Age-related changes in liver, kidney, and spleen stiffness in healthy children measured with acoustic radiation force impulse imaging. Eur J Radiol 2013; 82(6):e290–e294
[60] Zaffanello M, Piacentini G, Bruno C, Brugnara M, Fanos V. Renal elasticity quantification by acoustic radiation force impulse applied to the evaluation of kidney diseases: a review. J Investig Med 2015; 63(4):605–612
[61] Arndt R, Schmidt S, Loddenkemper C et al. Noninvasive evaluation of renal allograft fibrosis by transient elastography—a pilot study. Transpl Int 2010; 23(9):871–877
[62] Syversveen T, Midtvedt K, Berstad AE, Brabrand K, Strøm EH, Abildgaard A. Tissue elasticity estimated by acoustic radiation force impulse quantification depends on the applied transducer force: an experimental study in kidney transplant patients. Eur Radiol 2012; 22(10):2130–2137
[63] Wells PN, Liang HD. Medical ultrasound: imaging of soft tissue strain and elasticity. J R Soc Interface 2011; 8(64):1521–1549
[64] Syversveen T, Brabrand K, Midtvedt K et al. Assessment of renal allograft fibrosis by acoustic radiation force impulse quantification—a pilot study. Transpl Int 2011; 24(1):100–105
[65] Bruno C, Caliari G, Zaffanello M et al. Acoustic radiation force impulse (ARFI) in the evaluation of the renal parenchymal stiffness in paediatric patients with vesicoureteral reflux: preliminary results. Eur Radiol 2013; 23(12): 3477–3484
[66] Franchi-Abella S, Elie C, Correas JM. Ultrasound elastography: advantages, limitations and artefacts of the different techniques from a study on a phantom. Diagn Interv Imaging 2013; 94(5):497–501
[67] Gill IS, Aron M, Gervais DA, Jewett MA. Clinical practice: small renal mass. N Engl J Med 2010; 362(7):624–634
[68] Popescu A, Săftoiu A. Can elastography replace fine needle aspiration? Endosc Ultrasound 2014; 3(2):109–117
[69] Kim JK, Baek JH, Lee JH et al. Ultrasound elastography for thyroid nodules: a reliable study? Ultrasound Med Biol 2012; 38(9):1508–1513
[70] Bhatia KS, Rasalkar DP, Lee YP et al. Cystic change in thyroid nodules: a confounding factor for real-time qualitative thyroid ultrasound elastography. Clin Radiol 2011; 66(9):799–807
[71] Kwinta P, Klimek M, Drozdz D et al. Assessment of long-term renal complications in extremely low birth weight children. Pediatr Nephrol 2011; 26(7): 1095–1103
[72] Zaffanello M, Brugnara M, Bruno C et al. Renal function and volume of infants born with a very low birth-weight: a preliminary cross-sectional study. Acta Paediatr 2010; 99(8):1192–1198
[73] Ikezumi Y, Suzuki T, Karasawa T et al. Low birthweight and premature birth are risk factors for podocytopenia and focal segmental glomerulosclerosis. Am J Nephrol 2013; 38(2):149–157
[74] Hogg RJ, Furth S, Lemley KV et al; National Kidney Foundation's Kidney Disease Outcomes Quality Initiative. National Kidney Foundation's Kidney Disease Outcomes Quality Initiative clinical practice guidelines for chronic

kidney disease in children and adolescents: evaluation, classification, and stratification. Pediatrics 2003; 111 (6 Pt 1):1416–1421
[75] Soylu A, Demir BK, Türkmen M et al. Predictors of renal scar in children with urinary infection and vesicoureteral reflux. Pediatr Nephrol 2008; 23(12): 2227–2232
[76] Elder JS, Peters CA, Arant BS, Jr et al. Pediatric Vesicoureteral Reflux Guidelines Panel summary report on the management of primary vesicoureteral reflux in children. J Urol 1997; 157(5):1846–1851
[77] Lee HY, Soh BH, Hong CH, Kim MJ, Han SW. The efficacy of ultrasound and dimercaptosuccinic acid scan in predicting vesicoureteral reflux in children below the age of 2 years with their first febrile urinary tract infection. Pediatr Nephrol 2009; 24(10):2009–2013
[78] Rushton HG, Majd M. Dimercaptosuccinic acid renal scintigraphy for the evaluation of pyelonephritis and scarring: a review of experimental and clinical studies. J Urol 1992; 148 (5 Pt 2):1726–1732
[79] Sohn B, Kim MJ, Han SW, Im YJ, Lee MJ. Shear wave velocity measurements using acoustic radiation force impulse in young children with normal kidneys versus hydronephrotic kidneys. Ultrasonography 2014; 33(2):116–121
[80] Brenner BM, Meyer TW, Hostetter TH. Dietary protein intake and the progressive nature of kidney disease: the role of hemodynamically mediated glomerular injury in the pathogenesis of progressive glomerular sclerosis in aging, renal ablation, and intrinsic renal disease. N Engl J Med 1982; 307(11):652–659
[81] Hostetter TH, Rennke HG, Brenner BM. Compensatory renal hemodynamic injury: a final common pathway of residual nephron destruction. Am J Kidney Dis 1982; 1(5):310–314
[82] Göya C, Hamidi C, Ece A et al. Acoustic radiation force impulse (ARFI) elastography for detection of renal damage in children. Pediatr Radiol 2015; 45(1): 55–61
[83] Levey AS, de Jong PE, Coresh J et al. The definition, classification, and prognosis of chronic kidney disease: a KDIGO Controversies Conference report. Kidney Int 2011; 80(1):17–28
[84] El Nahas M. The global challenge of chronic kidney disease. Kidney Int 2005; 68(6):2918–2929
[85] Wang L, Xia P, Lv K et al. Assessment of renal tissue elasticity by acoustic radiation force impulse quantification with histopathological correlation: preliminary experience in chronic kidney disease. Eur Radiol 2014; 24(7):1694–1699
[86] Chatziantoniou C, Boffa JJ, Tharaux PL, Flamant M, Ronco P, Dussaule JC. Progression and regression in renal vascular and glomerular fibrosis. Int J Exp Pathol 2004; 85(1):1–11
[87] Ricardo SD, van Goor H, Eddy AA. Macrophage diversity in renal injury and repair. J Clin Invest 2008; 118(11):3522–3530
[88] Anvari A, Barr RG, Dhyani M, Samir AE. Clinical application of sonoelastography in thyroid, prostate, kidney, pancreas, and deep venous thrombosis. Abdom Imaging 2015; 40(4):709–722
[89] Bosmans JL, Ysebaert DK, Verpooten GA. Chronic allograft nephropathy: what have we learned from protocol biopsies? Transplantation 2008; 85(7) Suppl: S38–S41
[90] Cui G, Yang Z, Zhang W et al. Evaluation of acoustic radiation force impulse imaging for the clinicopathological typing of renal fibrosis. Exp Ther Med 2014; 7(1):233–235
[91] Syversveen T, Brabrand K, Midtvedt K, Strøm EH, Hartmann A, Berstad AE. Non-invasive assessment of renal allograft fibrosis by dynamic sonographic tissue perfusion measurement. Acta Radiol 2011; 52(8):920–926
[92] Orlacchio A, Chegai F, Del Giudice C et al. Kidney transplant: usefulness of real-time elastography (RTE) in the diagnosis of graft interstitial fibrosis. Ultrasound Med Biol 2014; 40(11):2564–2572
[93] Tan S, Özcan MF, Tezcan F et al. Real-time elastography for distinguishing angiomyolipoma from renal cell carcinoma: preliminary observations. AJR Am J Roentgenol 2013; 200(4):W369–75
[94] Göya C, Daggulli M, Hamidi C et al. The role of quantitative measurement by acoustic radiation force impulse imaging in differentiating benign renal lesions from malignant renal tumours. Radiol Med (Torino) 2015; 120(3): 296–303

10 Elastography of the Musculoskeletal System

Richard G. Barr, Amy M. Lex, and Nelson A. Hager

10.1 Introduction

B-mode ultrasound is becoming widely utilized as a first-line approach for evaluation of musculoskeletal (MSK) problems because of its high level of patient acceptance, high imaging resolution, real-time imaging, and relatively low cost.[1,2] The real-time imaging ability of ultrasound allows for the dynamic evaluation of the MSK system, comparison with the contralateral side, and scanning at the point of tenderness. Recently a new ultrasound mode, elastography, has become available. Elastography can assess the mechanical properties of tissue adding a new dimension to ultrasound imaging of the MSK system.

Tendons are some of the stiffest organs in the body. When tendons and ligaments become injured (sprained, strained, torn, or partially torn) or diseased, they become softer. When contracted, muscles become stiffer, which can be monitored with elastography. Most of the MSK system is anisotropic, meaning that its physical properties vary depending on direction so that when it is evaluated with ultrasound at different angles of insonation, it has a different appearance. Tendons and ligaments in particular exhibit anisotropic properties, and it is important to direct the ultrasound beam perpendicular to these structures so that one does not confuse their normal appearance with pathology. It may be necessary to heel-toe, or rock, the transducer to achieve a representative image. It is also important to know that tendon attachments are often naturally hypoechoic. To obtain adequate strain or shear wave elastograms, these features require different methods than those used for other organs in the body.

Structures with anisotropy have different acoustic properties in different directions, as just mentioned. It is important to have the transducer perpendicular to the structure so the angle of incidence of the beam is near 90 degrees. When the angle of incidence is not near 90 degrees, the structure may be hypoechoic due to refraction with no return of shear waves, and can simulate pathology. The effects of anisotropy on tendons or muscles are demonstrated in ▶ Fig. 10.1. In ▶ Fig. 10.1a, the transducer is placed on a tendon that is curved. In the ultrasound image ▶ Fig. 10.1b, the portion of the tendon that is perpendicular to the ultrasound beam (black) will appear normal with the linear structure of the tendon identifiable. However, in the portion where the angle of incidence is not 90 degrees (red), the linear structure of the tendon will not be identifiable and the tendon may appear hypoechoic and abnormal.

Both strain (SE) and shear wave elastography (SWE) have been applied to the MSK system. Chapter 2 details the basic science of both strain and shear wave elastography, as well as other references.[3] Here we will highlight the unique features needed for performing adequate elastography on the MSK system. There are unique features of elastography when performed on the MSK system.

Disease alters the biomechanical properties of muscles and tendons. The elasticity of tissues of the MSK system is altered in neoplastic conditions and in nonneoplastic disorders (e.g., injury, strain and/or sprain, tissue tear) such as tendinopathy, neuromuscular disease, or during wound healing.[4,5,6,7,8]

After discussion of strain and shear wave principles unique to the MSK system, we will review various applications of elastography in the MSK system. Several review papers are available on elastography of the MSK system.[9,10,11]

10.2 Strain Imaging

10.2.1 Techniques

In strain elastography (SE) a stress is applied to the tissue (the transducer is the compression source) and how the tissue responds to that stress is measured with B-mode ultrasound. Stiff tissues do not deform significantly while soft tissues deform significantly. The compression–release used to generate the stress varies with each ultrasound system, with some requiring minimal or no compression and others requiring compression of 1 to 2 mm and release. Most systems have a confidence scale that allows the users to monitor the amount of displacement; therefore you need to apply the appropriate amount of compression for accurate elastograms.[12]

SE is a relative technique. The stiffness of the tissue of interest in strain elastography is relative to the other tissues in the field of view (FOV). A grayscale or color scale is used to display the relative stiffness of the tissues in the FOV. Since tendons and ligaments are hard unless injured, using a color display with blue for hard and moving to green and then to red for soft can be helpful to indicate injury and/or disease. When using a color display, the B-mode image can be displayed behind the color elastogram to confirm tissue location. At this time SE can only be done when the tissues are static. A SE elastogram cannot be obtained when the tissue is moving (e.g., a tendon moving through its range of motion). However, an elastogram can be obtained when the MSK tissue is at various stages of its range of motion or in contraction.

Because strain is relative, the exact stiffness of tissues cannot be determined. Therefore, to evaluate the stiffness of a tissue, it is compared to that of another tissue. For example, the stiffness of an abnormal tendon can be compared to that of a normal tendon or any normal tissue. Dividing the strain value of the tissue of interest by that of a normal tissue (one which has stable strain such as fat or relaxed muscle) calculates the strain ratio of the tissue of interest. The strain ratio can be used as a semi-quantitative measurement of tissue elasticity.

To perform SE in the MSK system, the transducer should be held perpendicular to the area of interest so that the strain is applied uniformly to the tissues. The transducer should be aligned to the orientation of the tissues; that is, it should be parallel to the tendons or muscle bundles. Because most MSK tissues are anisotropic, elastography results will vary if the transducer is angled and not parallel to the normal anatomy of the tissue. Obtaining a short cine loop is helpful so that the best image can be identified on review. Applying pressure with the transducer will increase the stiffness of the tissues and leads to inaccurate results. The elastogram should be obtained with minimal transducer pressure.[13] A steady hand and soft touch are needed to obtain accurate elastograms.

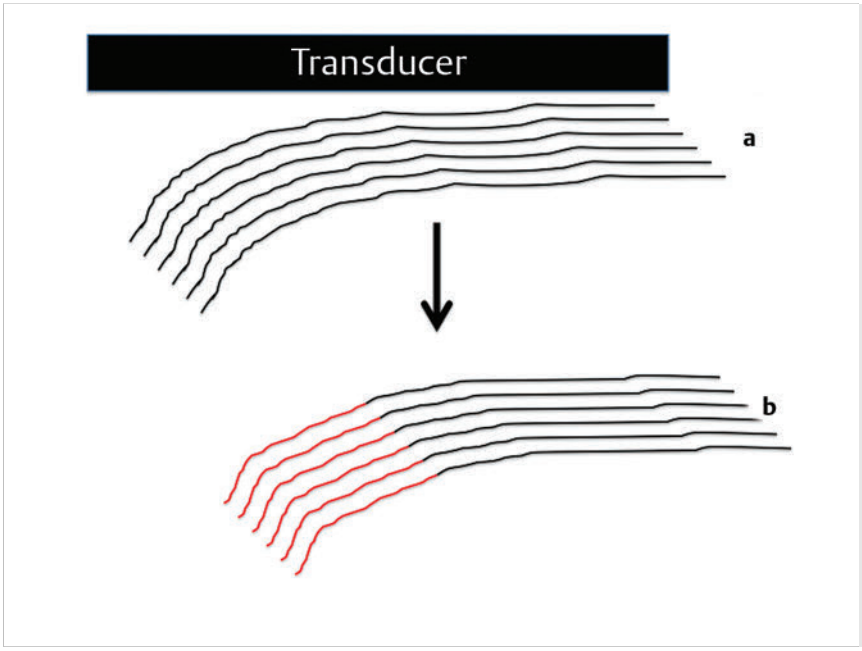

Fig. 10.1 Schematic demonstrating the effect of the transducer not being parallel to the fibers of a tendon or muscle. (**a**) The transducer is placed on a tendon with the parallel fibers depicted. (**b**) In the resulting ultrasound image, fibers that are parallel to the transducer are visualized (black lines). However, where the tendon is not perpendicular to the transducer, the tendon fibers are not visualized (red lines).

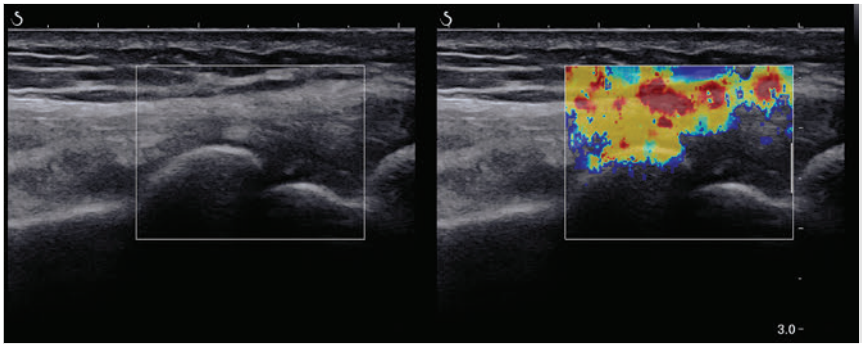

Fig. 10.2 When the transducer is not parallel to a tendon or muscle fibers, inadequate images are obtained. Not only is the B-mode image degraded, but the elastogram is inaccurate. In this case, the tendon shows normal stiffness where parallel to the transducer, but, where the tendon curves, the B-mode image is degraded with the tendon appearing hypoechoic and the two-dimensional shear wave imaging unable to calculate a stiffness value (no color-coding).

It is helpful to have several tissues in the FOV to allow for an appropriate dynamic range of stiffnesses for scaling of results. If a strain ratio is desired, both the tissue of interest and the reference tissue should be included in the FOV. Try not to include bone in the elastographic FOV because due its marked stiffness, it will affect the scaling of the elastographic image.

Since most MSK applications involve scanning of superficial tissue, the use of a high-frequency linear transducer is preferred. When the tissue of interest is very superficial (just a few millimeters below the skin), the use of ample coupling gel or a standoff pad is recommended to increase the distance between the transducer and tissue of interest.[14]

10.2.2 Tips and Tricks

1. Align the transducer with the normal anatomical features of the MSK tissue.
2. Maintain the tissue or area of interest in the FOV during the acquisition.
3. Be aware of the state of the MSK tissue. The elasticity changes with the degree of muscle contraction and of stress on the tendon.
4. Do not apply precompression.
5. Minimize motion while scanning (of both the patient and sonologist.)

10.2.3 Artifacts and Pitfalls

For most MSK elastography applications, the transducer must be aligned with the normal anatomical structure of the tissue of interest. ▶ Fig. 10.2 demonstrates the difference in results if the transducer is not aligned properly with the tissue. As the SE image is calculated based on the changes in the B-mode signal with the addition of stress, bad B-mode images will lead to poor or inaccurate elastograms.

Ideally it would be useful to obtain the change in stiffness of the tissue during its range of motion. However, this cannot be done dynamically with SE, but one can evaluate the tissue of interest at various points in its range of motion.

10.2.4 Interpretation of Results

A detailed discussion of how to interpret results is provided in the Section 10.4, Applications. In general, SE compares the stiffness of the tissue of interest to either the normal form of that tissue or to another tissue that has relatively uniform stiffness across patients. The strain ratio calculated can be used as a semiquantitative method to assess stiffness. For tendons and muscles, many pathologic states are softer than the normal tissue. For masses, malignant lesions are usually stiffer than the normal tissue. The use of color or power Doppler can also add additional information, demonstrating hyperemia and healing of the tissue.

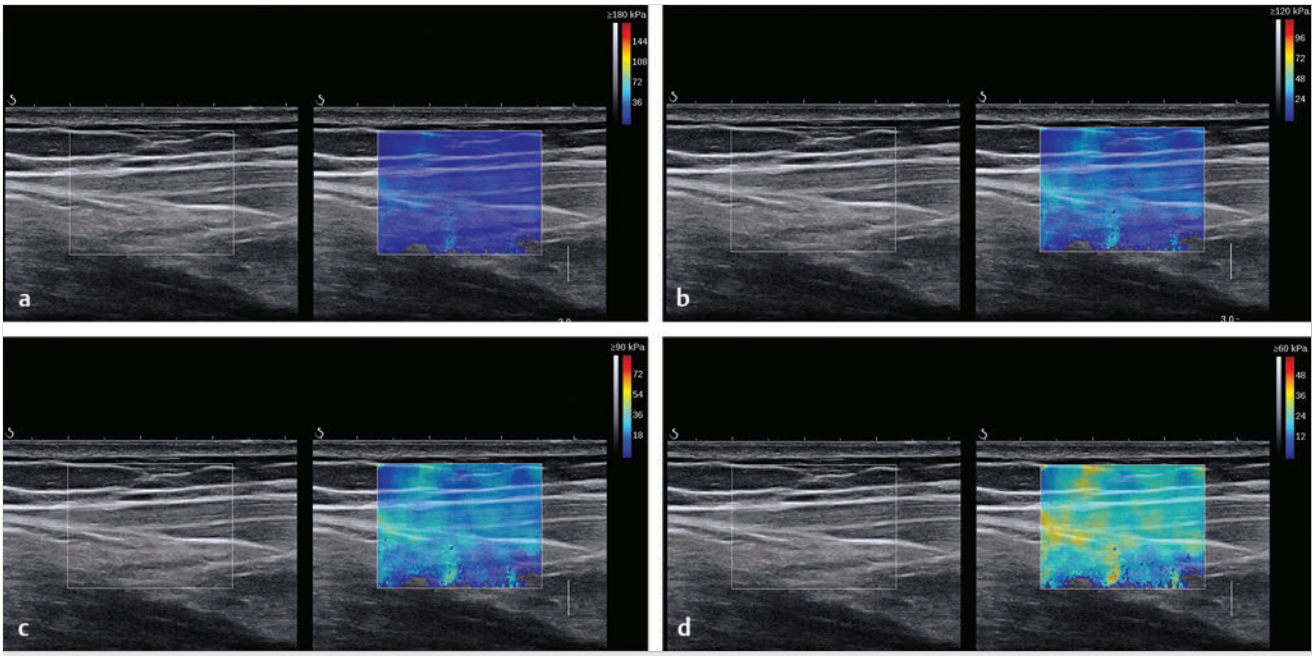

Fig. 10.3 The tissues in the musculoskeletal system have a wide range of stiffnesses from very soft fat to very stiff tendons. To adequately visualize the tissues of interest, the color scale on two-dimensional shear wave imaging can be adjusted to identify stiffness changes in the tissues. In this series of images the stiffness scale is adjusted from 180 kPa (**a**), to 120 kPa (**b**), to 90 kPa, (**c**) to 60 kPa (**d**). Note that with the decreasing stiffness range, more variability can be identified in the stiffness of the tissues.

10.3 Shear Wave Imaging

10.3.1 Techniques

In shear wave elastography (SWE), a low-frequency strong push pulse, called an acoustic radiation force impulse (ARFI), designed to generate shear waves is applied to the tissue. B-mode ultrasound is then used to monitor the tissue displacement caused by the shear wave as it passes through the tissue, and with this the velocity of the shear wave can then be calculated. The shear wave speed increases in stiffer tissues and is slower in softer tissues. Therefore, SWE provides a quantitative measurement of the tissue stiffness. That stiffness can be expressed as shear wave speed in meters per second (m/s) or can be converted to Young's modulus in kilopascals (kPa) by making some assumptions regarding the tissue.[12]

There are two types of SWE, point shear wave elastography (p-SWE) and two-dimensional shear wave elastography (2D-SWE). In p-SWE, a small ROI is placed on the tissue of interest and when activated the stiffness value in that small ROI is obtained. With 2D-SWE, a large FOV is placed over the area of interest and when activated the shear wave speeds for each pixel are calculated and displayed as a color-coded map. A small ROI can then be placed to obtain the stiffness value of a certain location. 2D-SWE can be performed either as a single shot (one image) or in real-time (with continuous updating of the elastographic measurements). However, when using real-time 2D-SWE, the transducer must remain in one location for several seconds to get a stable and accurate measurement.

Tendons are very stiff and their shear wave velocities are quite high. The appropriate default settings must be selected so that the system can monitor the fast shear wave speeds. The stiff tissue also attenuates the shear waves as they travel. Therefore, closer ARFI pulses are needed to measure tendons accurately.

As with SE, applying precompression with the transducer will increase the stiffness of all the tissues. The examination should be obtained with minimal pressure applied by the transducer. Ample coupling gel is often very helpful.

10.3.2 Tips and Tricks

1. When using real-time 2D-SWE, the transducer must remain in one location fo several seconds to allow the image to stabilize for accurate stiffness measurements.
2. Adjust the maximum stiffness scale to be appropriate for the tissue of interest (▶ Fig. 10.3).
3. Do not apply precompression.
4. Watch for motion (of both the patient and the sonologist).

10.3.3 Artifacts and Pitfalls

1. If the proper preset is not selected, the number and spacing of ARFI pulses may not be sufficient to get accurate measurements (▶ Fig. 10.4). With very stiff tissues, the shear wave may dissipate before the next ARFI pulse and give an alternating pattern of stiff followed by soft.
2. The ARFI pulse is similar to other ultrasound pulses and can be reflected or refracted. Having appropriate alignment with the tissue is needed to obtain an accurate elastogram.
3. In the near field, the ARFI pulse can be very strong and have reverberations that can lead to a region of high stiffness just under the transducer. This is called the bang artifact (▶ Fig. 10.5). This can also occur when there is too much precompression applied.

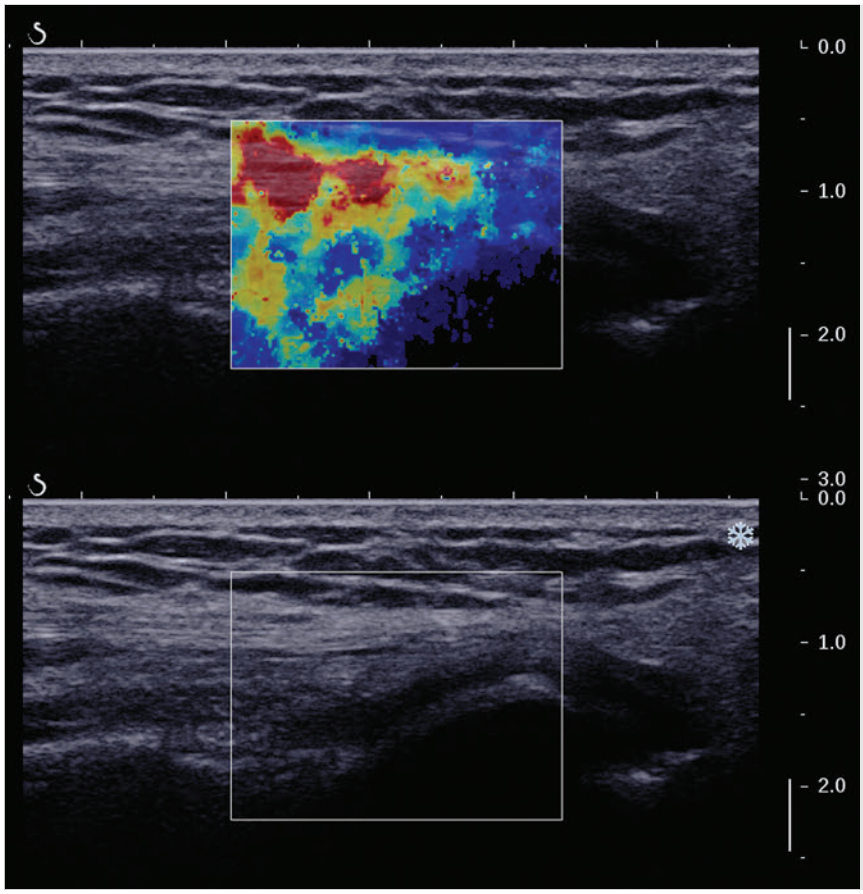

Fig. 10.4 To perform two-dimensional shear wave imaging, multiple acoustic radiation force impulse (ARFI) pulses are used and the shear wave speeds at each ARFI pulse are measured over several millimeters. If the ARFI pulses are too widely spaced for the tissue being interrogated, the shear waves may be attenuated between the ARFI pulses and therefore the speed reading may be inaccurate or there may be no reading at all and so no color-coding of the elastogram may be seen in this area. Also the B-mode tracing pulses must be appropriately placed to accurately measure the expected shear wave velocity. This occurs especially when very stiff tissues are being evaluated such as tendon. The appropriate preset must be selected to have the appropriate number and spacing of ARFI pulses as well as spacing of the B-mode tracking pulses. In this example, where a preset for soft tissues was used on a stiff tendon, note the "banding" of the color-coding (*arrows*). This is where the ARFI push pulses were too widely spaced and the low stiffness values between pulses are due to attenuation. This can be corrected by choosing the appropriate preset.

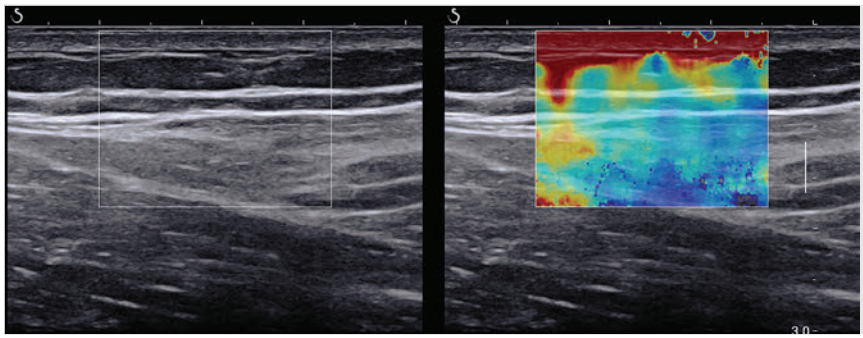

Fig. 10.5 If too much precompression is applied or there is poor coupling between the transducer and the skin, an area of high stiffness in the near field is seen, the bang artifact. Applying less precompression and using ample coupling gel can eliminate this artifact.

10.3.4 Interpretation of Results

With SWE, a quantitative measure of stiffness is obtained. That value can be used to determine if a tissue is normal or abnormal. The stiffness ratio of the tissue of interest to normal tissues can also be used as in SE. In general for tumors, a cutoff value can be obtained to distinguish benign from malignant lesions. Cutoff values and comparison to normal tissues can also be used to determine injury and monitor healing.

10.4 Applications

10.4.1 Tendons

In most tendons, their tension has a reproducible and difficult-to-control effect on imaging. For example, when the patella tendon is contracted, it is uniformly stiff. However, when relaxed, even a normal tendon may demonstrate soft spots and more relatively slack points. Controlling the tendon tension is important in obtaining consistent results. Soft regions in tendons correspond to edema, tendinitis, and/or neovascularization.

Achilles Tendinopathy

Most work with elastography on tendons has been done on the Achilles tendon. Achilles tendinopathy usually occurs 3 to 5 cm from the insertion. The second most common location is at the insertion. Less commonly it occurs at the myotendinous junction of the gastrocnemius.[15,16] Achilles tendinopathy is believed to begin with microtears leading to a degenerative cascade.[15,16] Tendinopathy is a degenerative process with collagen fiber separation, increased cellularity, neovascularization, and fatty

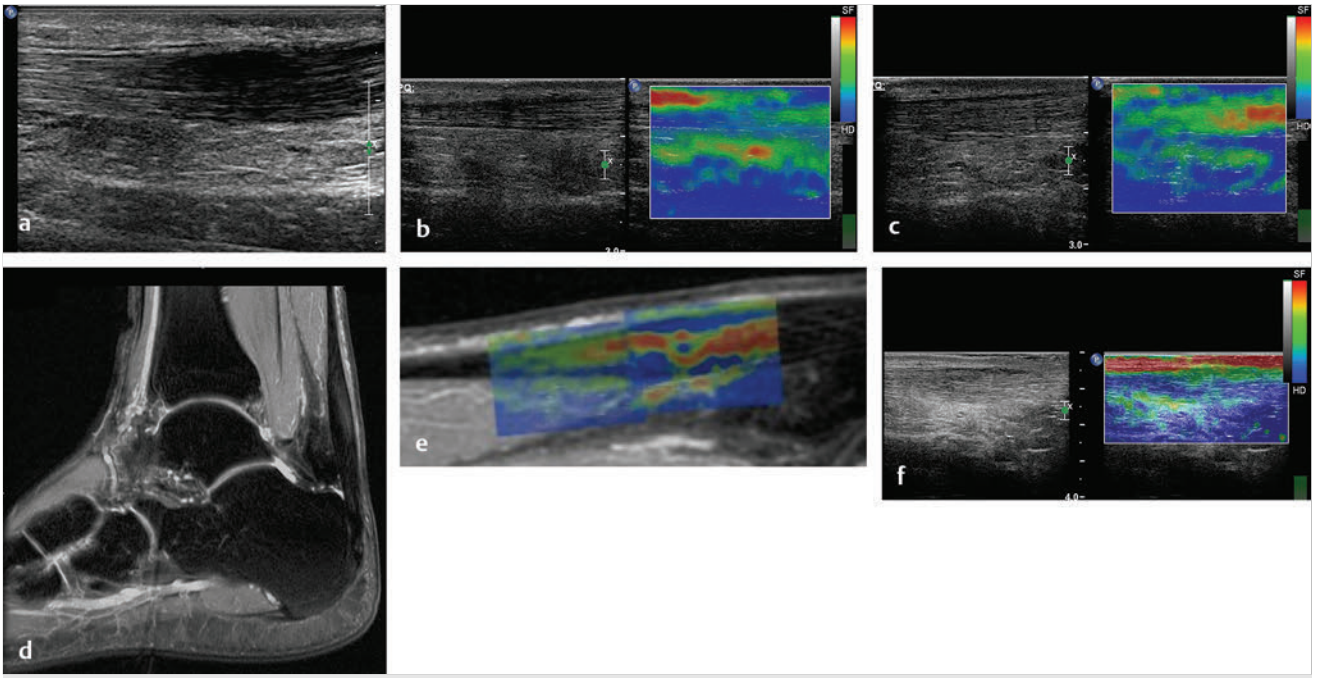

Fig. 10.6 (**a**) The B-mode image of a runner who presents with Achilles tendon pain demonstrates a hypoechoic area consistent with a small tear or tendonosis. (**b**) The SE image just above the hypoechoic area demonstrates the tendon is stiff (blue) but is softer as it nears the hypoechoic area. (**c**) Over the area of hypoechogenicity the tendon becomes very soft (red). (**d**) The corresponding T2-weighted magnetic resonance (MR) image taken at the same time demonstrates an area of increased signal at the site of hypoechogenicity on US. (**e**) Fusion of the strain elastography (SE) image and T2-weighted MR image confirms the areas of abnormality on both modalities are identical. After two months of treatment the patient returned for (**f**) a repeat SE image that shows the tendon has returned to near normal with only a small area of softness (green).

infiltration.[17] This process softens and weakens the tendon and eventually leads to spontaneous tendon rupture.[18,19]

Elastography, both strain and shear wave techniques, can be used to identify the softening of the tendon in tendinopathy. The Achilles tendon is normally very stiff. The tendon stiffness value varies with the degree of extension of the tendon. Aubry et al measured the mean stiffness value of the Achilles tendon as 104 kPa during extension, 464 kPa in the neutral position, and 410 kPa during maximum dorsiflexion in the longitudinal plane.[20] Using 2D-SWE, the Achilles tendon in healthy volunteers in the resting position was 51.5 kPa.[21]

Elastography had a sensitivity and specificity of more than 90% in detecting tendinopathy compared to clinical findings.[22]

The strain elastography of surgically sutured Achilles tendon ruptures has been investigated using a color scale. The Achilles tendon showed a homogeneous stiff structure in healthy volunteers, while in patients with complete tendon rupture 38 months after surgical repair, a stiff elastogram with a heterogeneous pattern was found.[4]

▶ Fig. 10.6 is an example of a patient with Achilles tendonitis using SE. ▶ Fig. 10.6a is the B-mode image. ▶ Fig. 10.6b is just superior to the abnormal area and ▶ Fig. 10.6c is the area of tendinopathy. The tendon is soft (red) at the area of tendinitis and small tears, while it is stiff (blue) in the areas that are normal. The elastographic findings are similar to the magnetic resonance imaging (MRI) findings (▶ Fig. 10.6d). ▶ Fig. 10.6e is the fused MRI and SE images. The abnormal findings are similar on both techniques. This patient was followed during his treatment and SE was able to monitor the healing of the tendon (▶ Fig. 10.6f).

▶ Fig. 10.7a shows a normal Achilles tendon and ▶ Fig. 10.7b an abnormal Achilles tendon on 2D-SWE. Note the stiffness (red) of the tendon in the normal state and the softness (blue) of the tendon in the abnormal state.

Lateral Epicondylitis

Lateral epicondylitis (tennis elbow) includes partial tendon tears, vascular proliferation, fibrosis and mucoid and calcific degeneration.[5] The origin of lateral epicondylitis is the extensor carpi radialis brevis tendon.

The common signs and symptoms of lateral epicondylitis include pain and weakened grip strength, worsening with forearm activity. The symptoms usually develop gradually.[23]

Elastography has been used for the evaluation of lateral epicondylitis.[24] As with other tendons, the normal tendon is homogenously stiff. In lateral epicondylitis there is irregular softening at the origin of the extensor.

▶ Fig. 10.8 demonstrates a case of lateral epicondylitis. The softer (red) area is the tendinitis, while the stiff area (blue) is the normal tendon. The same patient after treatment shows the tendon is now stiff (blue) in the area of prior tendinitis.

Compared with clinical examination in 38 elbows with lateral epicondylitis, conventional B-mode ultrasound (US) had a sensitivity of 95%, a specificity of 89%, and an accuracy of 91%, whereas elastography had a sensitivity of 100%, a specificity of 89%, and an accuracy of 94%.[24]

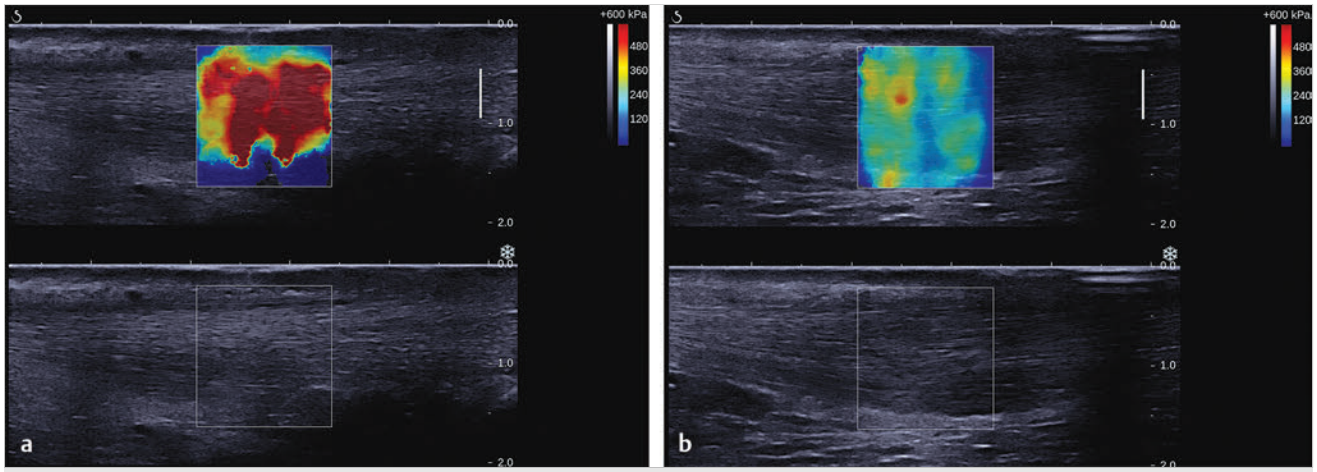

Fig. 10.7 The two-dimensional shear wave elastography images of a (**a**) normal and (**b**) abnormal Achilles tendon are presented. Note that the normal tendon is stiff (red), while the abnormal tendon is soft (blue).

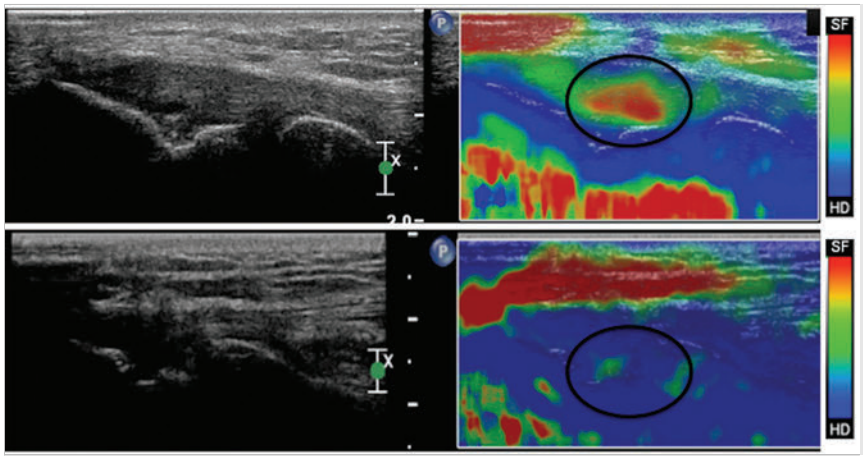

Fig. 10.8 Compression strain image of a 58-year-old male who presented with left elbow pain. On initial evaluation the tendon was soft (red) consistent with lateral epicondylitis. After treatment the patient returned for a follow-up exam that confirmed the tendinitis had resolved with the tendon entirely stiff (blue).

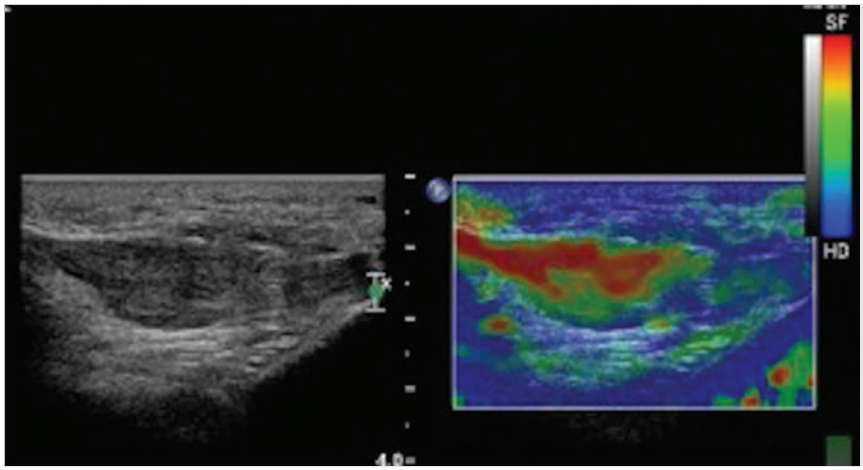

Fig. 10.9 Strain elastography images from a 45-year-old male who hit his knee on a tree skiing, show a large area of softness (red) in the suprapatellar tendon representing tendinitis.

Patellar Tendinopathy

Patellar tendinopathy is characterized by mucoid degeneration of the patellar tendon and includes abnormal collagen, tenocytes, and vascular structure.[25]

B-mode US can depict hypoechogenic regions in a tendon with patellar tendinopathy.[26] However, it has also been reported that asymptomatic athletes had abnormal tendon morphology including hypoechoic regions on B-mode US,[27,28] and that these did not help predict subsequent development of symptoms.[29]

In one study symptomatic tendons appeared significantly softer compared to nonsymptomatic tendons.[30]

▶ Fig. 10.9 is the superior patellar tendon in a patient with recent trauma to the knee. Note that the tendon has very soft areas (red) representing small tears and or tendinopathy.

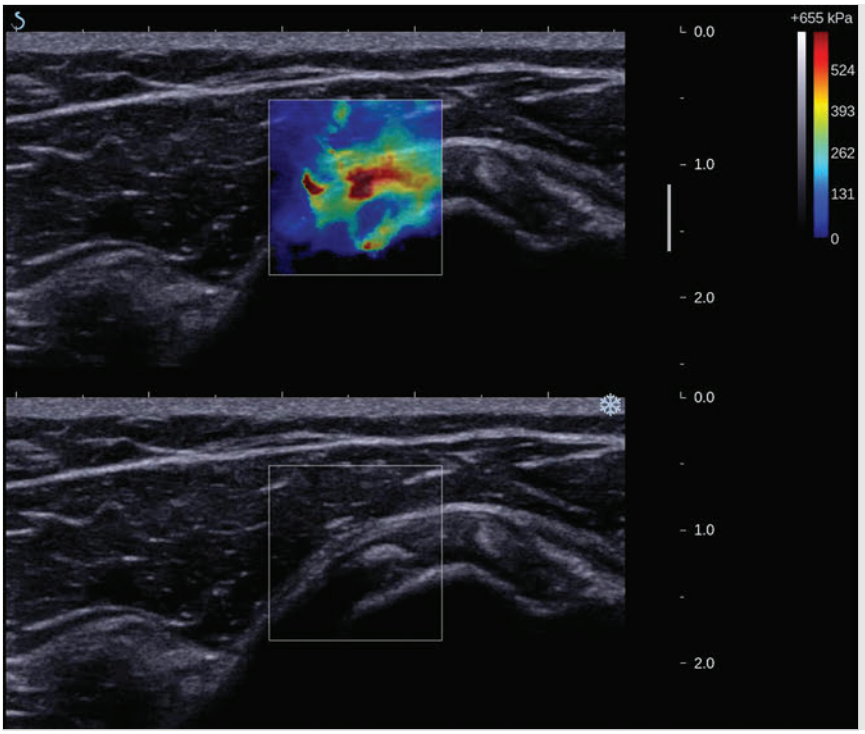

Fig. 10.10 Two-dimensional shear wave elastography images from a 64-year-old male who presents with shoulder pain. On the B-mode images two echogenic foci are noted in the supraspinatus tendon representing calcific tendinitis. On elastography, the calcification is very stiff (color-coded red > 500kPa) and the adjacent tendon is teal, which is normal tendon stiffness. The blue areas are soft and represent tendinitis.

Rotator Cuff Tendinopathy

B-mode US cannot easily differentiate subacromial bursitis from a degenerated and enlarged supraspinatus tendon.[31] However, elastography can improve the differentiation of the soft subacromial bursa from the stiffer rotator cuff tendon.[31]

▶ Fig. 10.10 is the 2D-SWE of a patient with calcific tendinitis of the rotator cuff. Note that the calcification is very stiff on elastography. The tendon itself is relatively soft consistent with tendinosis.

Finger Tendon Tears and Trigger Finger Snapping Symptoms

Buck et al[32] have used strain elastography to identify small tears, such as digital tendon lesions, by evaluating the strips of equine digital flexor tendons with respect to diagnostically relevant quantitative measurements.

In trigger fingers, increased stiffness of the first annular pulley is considered to be the cause of snapping symptoms. The strain ratio of subcutaneous fat to that of the affected first annular pulley in the trigger finger and to that of the adjacent normal finger is 4.2 and 2.4, respectively. Three weeks after corticosteroid injection, the snapping disappeared in all patients and the strain ratio for the affected annular pulley in the trigger finger decreased from 4.2 to 2.5, which is normal.[33]

10.4.2 Plantar Fasciitis

Plantar fasciitis is a common cause of heel pain. The etiology of plantar fasciitis is multifactorial with mechanical overload and degeneration regarded as the main factors.[34] Conventional B-mode US has been used in the diagnostic evaluation of plantar fasciitis and shows increased thickness and loss of echogenicity of the plantar fascia.[35,36,37]

Elastography has demonstrated a significantly softer plantar fascia in older healthy patients (> 50 years old) than in a younger group (18–50 years old). Softer plantar fascia were observed in subjects with plantar fasciitis in healthy subjects.[38] Sconfienza et al[39] found SE can show plantar fasciitis, increases the diagnostic performance of B-mode US, and assists in cases of inconclusive B-mode US findings.

▶ Fig. 10.11 is a 56-year-old who presents with right heel pain. In ▶ Fig. 10.11a the painful right plantar fascia is soft (red), while in the left foot in ▶ Fig. 10.11b, the nonpainful plantar fascia is stiff (blue). After several months of treatment, the right plantar fascia has become normal (stiff, blue) and the patient's pain has resolved (▶ Fig. 10.11c).

10.4.3 Muscle

The evaluation of the mechanical properties and function of muscles can be monitored by elastography.

2D-SWE has been used to determine the stiffness of muscle at various degrees of contraction. The stiffness value of the gastrocnemius muscle is 16.5 kPa at rest and 225.4 kPa during contraction; the soleus is 14.5kPa at rest and 55.0 kPa during contraction; and the tibialis anterior is 40.6 kPa at rest and 268.2 kPa during contracture.[40]

Bouillard et al[41] compared surface electromyography and SWE in evaluating muscle force and found SWE provided a more accurate estimate ($R2 = 0.98$ versus $R2 = 0.95$).

Exercise-induced changes of muscle have been evaluated with elastography. Yanagisawa et al evaluated muscles before and after exercise. Using strain ratios, they determined that muscle stiffness increased during exercise and returned to pre-exercise level 30 minutes after exercise.[42]

Muscle contusions, strains, or tears are softer than normal muscle. Injuries to muscle from trauma or ischemia and/or

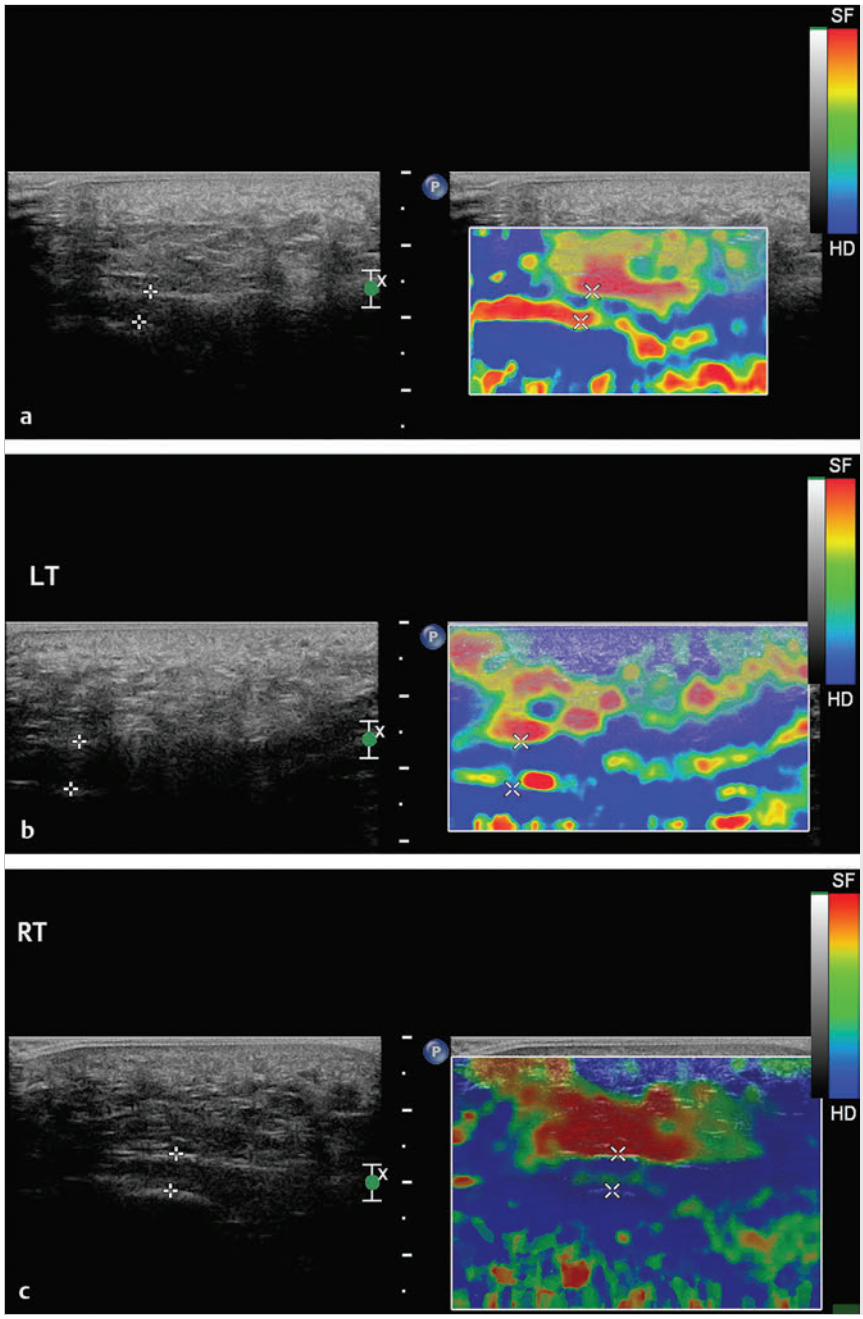

Fig. 10.11 Strain elastography images from a 56-year-old male who presents with right heel pain. In (**a**) the painful right plantar fascia is soft (red) while in (**b**) the nonpainful left plantar fascia is stiff (blue). After several months of treatment, in (**c**) the right plantar fascia has become stiff (blue), which is normal, and the patient's pain has resolved.

neurologic dysfunction can be evaluated by elastography.[7] Elastography may also be able to monitor healing.[43]

Berko et al[44] evaluated the normal range of muscle elasticity in children. They found the resting muscle elasticity in children is significantly lower in the biceps brachii than in the rectus femoris, and in the nondominant biceps brachii than in the dominant biceps brachii. Elasticity significantly increases immediately postexercise in both muscle groups; resting differences between biceps brachii and rectus femoris elasticity, and dominant and nondominant biceps brachii elasticity, do not persist after exercise. The change in muscle elasticity with exercise is higher in younger children.

▶ Fig. 10.12 demonstrates the change in stiffness of a muscle as it contracts. ▶ Fig. 10.12a is the relaxed muscle, while ▶ Fig. 10.12b and ▶ Fig. 10.12c are the muscle at increasing degrees of contraction. Note the increase in stiffness that can be quantified with 2D-SWE.

Images from a 72-year-old female who "pulled her muscle" are presented in ▶ Fig. 10.13. The B-mode image (▶ Fig. 10.13a) shows a hypoechoic area suggesting a muscle tear with hematoma. The strain elastogram confirms a soft area representing the muscle tear and hematoma on SE (▶ Fig. 10.13b) and on 2D-SWE (▶ Fig. 10.13c).

Elastography has been evaluated in pain management. The taut band in myofascial pain syndrome has been shown to be stiffer than the adjacent normal tissue.[45,46] Elastography may be able to identify the areas needed for treatment.

Congenital muscular dystrophy includes a range of genetic disorders characterized by muscle weakness and contractures.[47] A few studies have evaluated elasticity of muscles in

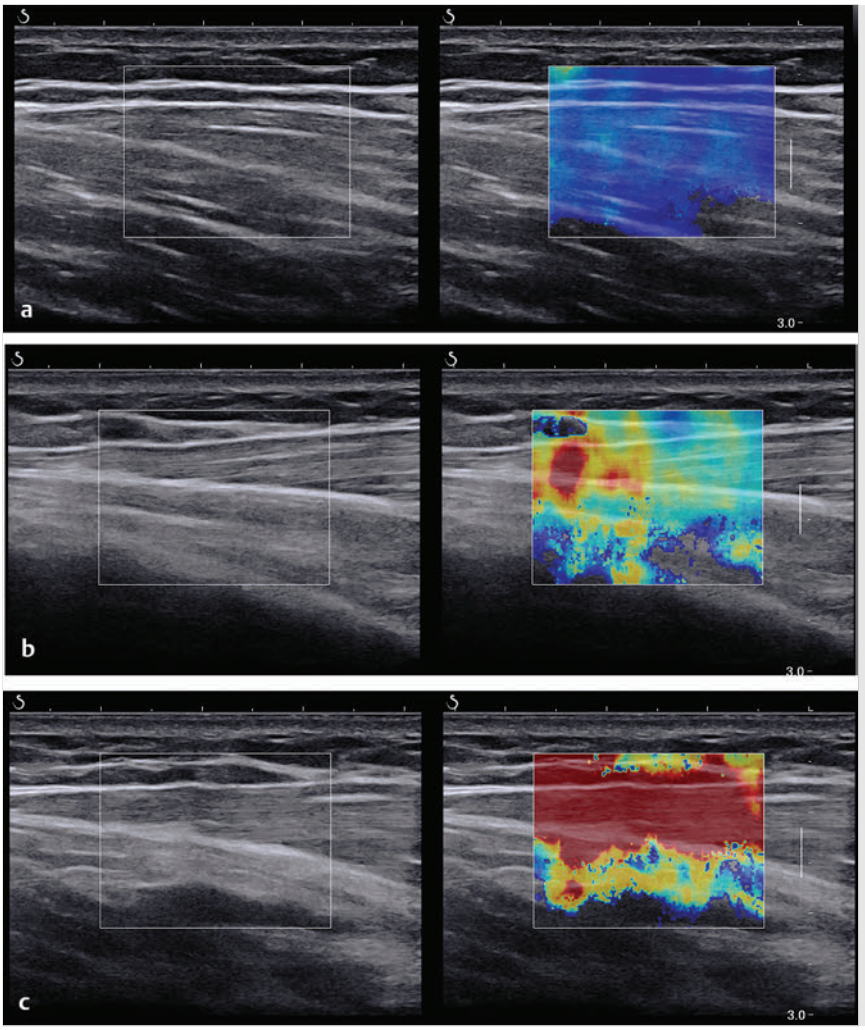

Fig. 10.12 This series of images demonstrates the increasing stiffness of muscle when the muscle is contracted. In (**a**) the muscle is in the resting state, while (**b**) and (**c**) show increasing muscle contraction. Note the marked increase in stiffness with muscle contraction.

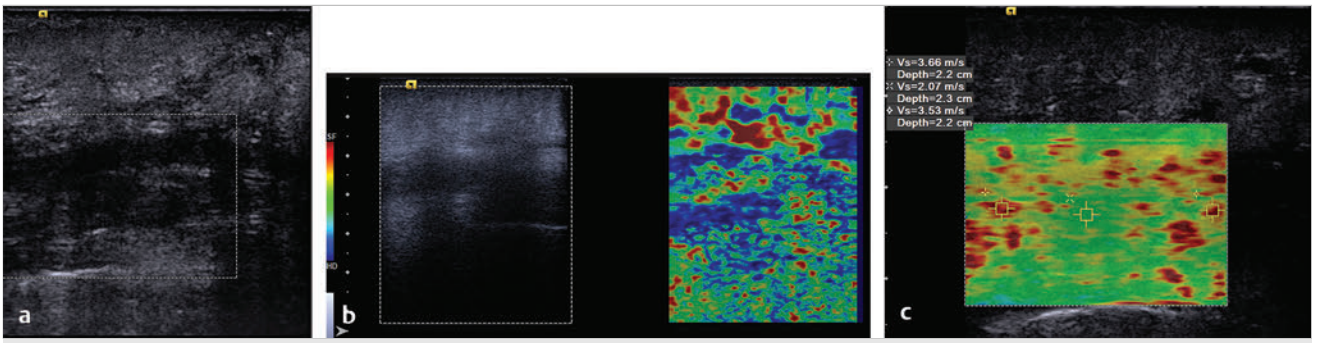

Fig. 10.13 A 72-year-old female injured her upper thigh. (**a**) The B-mode image shows an area of hypoechogenicity with the possibility of some fluid in the muscle consistent with a muscle tear. (**b**) In the SE image the area of the muscle tear is soft (red and green) compared to the normal muscle (blue). (**c**) The 2D-SWE image in the same location demonstrates similar findings with the area of the tear green with a stiffness value of 2.07 m/s while the normal muscle has stiffness values of approximately 3.6 m/s.

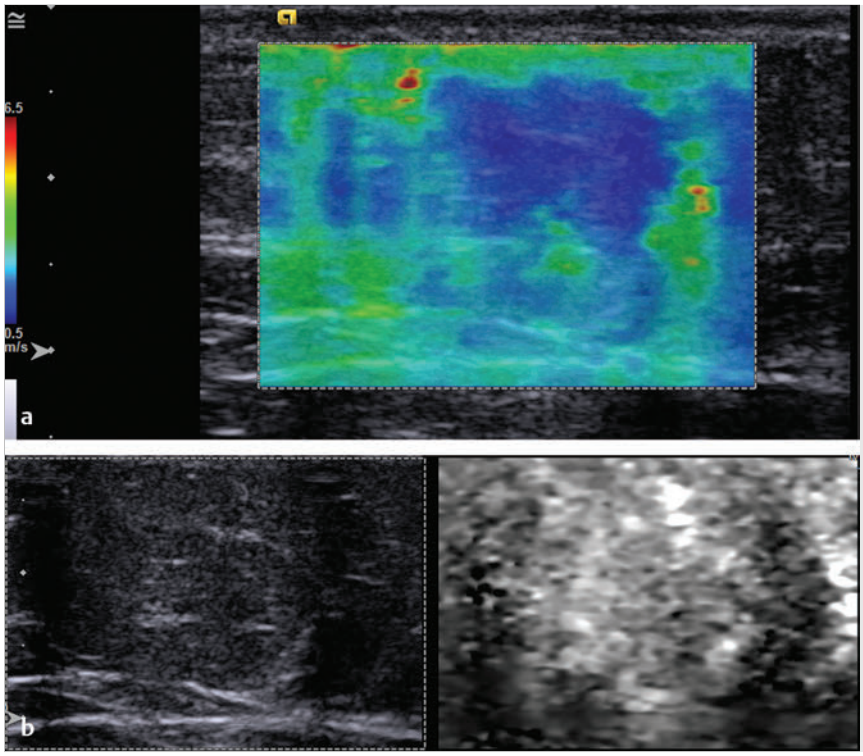

Fig. 10.14 A 28-year-old female presents with a palpable abnormality in the right axilla. (**a**) On 2D-SWE imaging the lesion is very soft (blue) with a stiffness value of 1.2 m/s, less than the surrounding tissues. (**b**) On SE the same lesion is very soft (white). These elastographic finding are diagnostic of this biopsy-proven lipoma.

muscular dystrophy. In qualitative color strain imaging, analysis of congenital Bethlem myopathy demonstrated that hyperechoic areas at the periphery and central part of the affected muscles are stiffer than the normal-appearing areas.[48]

Elastography can depict contracted muscles in patients with cerebral palsy to select the location for botulinum toxin injection. One study identified that the relaxed muscle structures in spastic cerebral palsy appeared soft, while contracted or degenerated muscle fibers appeared stiff on elastography.[49]

Early research suggests elastography might contribute to the understanding of the relationship between muscle function and mechanical properties.

10.4.4 Pressure-Ulcer Detection

Experiments have demonstrated that elastography is a promising technique for pressure-ulcer detection. Strain elastography showed differences between healthy areas and areas early in pressure-ulcer, development, characterized by softer findings close to the skin layer and stiffer findings close to bone.[50]

10.4.5 Rheumatology

Increasingly conventional B-mode ultrasound and color or power Doppler ultrasound are being used to evaluate arthritis.[51] To date there has been little research to determine if elastography can be used in evaluation of arthritis.

10.4.6 Musculoskeletal Tumors

In general, elastography can be used to characterize masses as benign or malignant. Benign lesions are usually softer and have homogeneous stiffness throughout, while malignant lesions are stiffer and have heterogeneous stiffness.[52] Other chapters in this book discuss stiffness in tumors of other organs. There are very few published papers on MSK tumors or tumorlike masses. Pierucci et al have written a review of tumor and tumorlike lesions of the MSK system.[53]

One excellent application is the ability to diagnosis a lipoma with elastography due to the extreme softness of the lipoma. ▶ Fig. 10.14 is an example of an axillary lipoma. Note the extreme softness of the lipoma on both 2D-SWE (▶ Fig. 10.14a) and SE (▶ Fig. 10.14b).

There is little literature on the characterization of soft tissue tumors. ▶ Fig. 10.15 is an example of a squamous cell carcinoma presenting as an upper arm mass. The palpable mass in the upper arm of this patient on ultrasound is a heterogeneous mass that is more hypoechoic centrally and with an area of slight hyperechogenicity surrounding the mass that may be edema (▶ Fig. 10.15a). The mass has some internal blood flow on color Doppler (▶ Fig. 10.15b). SE demonstrates the mass to be stiff including the area of surrounding suspected edema (▶ Fig. 10.15c). The heterogeneity of the mass can be appreciated more using Virtual Touch Imaging (VTi, Siemens Ultrasound, Mountain View, CA) (▶ Fig. 10.15d). In this technique, an ARFI push pulse is used to displace the tissue and the displacement (not shear wave velocity) is measured. Therefore it is a strain technique. On 2D-SWE (▶ Fig. 10.15e), the stiffness of the mass is confirmed to be heterogeneous with the highest stiffness value greater than the scale of 6.5 m/s, while the more normal tissue has a stiffness value of 2.65 m/s. The appearance of the mass on gadolinium-enhanced MRI is shown in ▶ Fig. 10.15f.

10.5 Published Guidelines

The European Federation of Societies of Ultrasound in Medicine and Biology (EFUSMB) clinical guidelines recommend strain

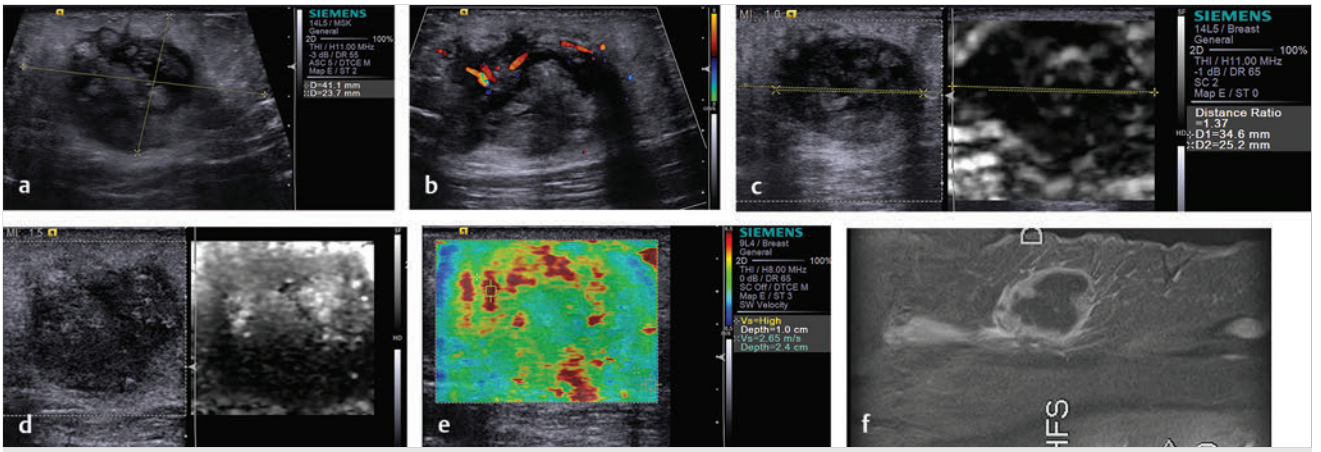

Fig. 10.15 A 38-year-old female presents with a palpable mass in her upper arm. (**a**) On B-mode ultrasound the mass is heterogeneous with a central area that is more hypoechoic and a rim of increased hyperechogenicity. The mass measures 4.1 cm. (**b**) On color Doppler it demonstrates the presence of moderate blood flow in the mass. (**c**) On SE the mass including the peripheral area of hyperechogenicity is very stiff. The lesion has a heterogeneous pattern of stiffness. (**d**) A strain image obtained using ARFI technology (VTI, Siemens Ultrasound, Mountain View, CA) is similar to the SE image. (**e**) The mass on 2D-SWE is heterogeneous in stiffness with a maximum stiffness value of > 6.5 m/s. (**f**)The same mass on T1-weighted gadolinium-enhanced MRI demonstrates enhancement in the periphery of the mass. On surgical pathology, the mass was found to be a squamous cell carcinoma.

elastography as a supplementary tool to conventional ultrasound scanning to increase the diagnostic confidence in diagnosing Achilles tendinopathy. Strain elastography can be used to depict stiffness changes in congenital muscle spasticity.[54]

10.6 Conclusion

Elastography is a relatively new diagnostic imaging modality for musculoskeletal ultrasound. With the unique adaptation of of compression strain and shear wave imaging techniques we can evaluate previously uninvestigated properties of soft tissues. Tissue injury, whether it be chronic degenerative tendon changes or an acute tear in a ligament or tendon, is often associated with a decrease in the tensile properties of the structure and an associated softness. Elastography can provide relative quantitative assessment of these changes by providing sonographic feedback on these properties. This is a new dimension of tissue injury previously unexplored in depth.

Furthermore, the natural healing process is associated with a corresponding increase in tensile strength, tissue consolidation, and density. These qualities of tissue healing are also demonstrated by elastography.

The introductory state of the modality is not without shortcomings. It is very operator dependent. To procure accurate measurements requires a steady hand and a thorough understanding of the relative properties of contractile tissues. The operator must understand the optimal technique to study a tissue whether it be in a contracted state or relaxed.

In addition, overpressure (precompression) has a strong influence on the accuracy of the image achieved. Applying the right compression is clearly an acquired skill.

In the present state of elastography there is useful diagnostic information to be gathered from healthy and injured tissues. However, further developments in the field could make it more operator friendly for musculoskeletal ultrasound. The low cost and availability of ultrasound elastography may allow for serial follow-up studies to monitor treatment response and healing of tendon and muscle injuries. Little work has been done to determine if elastographic results can help in tailoring physical therapy regimens.

References

[1] Klauser AS, Tagliafico A, Allen GM et al. Clinical indications for musculoskeletal ultrasound: a Delphi-based consensus paper of the European Society of Musculoskeletal Radiology. Eur Radiol 2012; 22(5):1140–1148
[2] McNally EG. The development and clinical applications of musculoskeletal ultrasound. Skeletal Radiol 2011; 40(9):1223–1231
[3] Shiina T, Nightingale KR, Palmeri ML et al. WFUMB guidelines and recommendations for clinical use of ultrasound elastography: Part 1: basic principles and terminology. Ultrasound Med Biol 2015; 41(5):1126–1147
[4] Tan S, Kudaş S, Özcan AS et al. Real-time sonoelastography of the Achilles tendon: pattern description in healthy subjects and patients with surgically repaired complete ruptures. Skeletal Radiol 2012; 41(9):1067–1072
[5] Chard MD, Cawston TE, Riley GP, Gresham GA, Hazleman BL. Rotator cuff degeneration and lateral epicondylitis: a comparative histological study. Ann Rheum Dis 1994; 53(1):30–34
[6] Sandrin L, Catheline S, Tanter M, Hennequin X, Fink M. Time-resolved pulsed elastography with ultrafast ultrasonic imaging. Ultrason Imaging 1999; 21 (4):259–272
[7] Huard J, Li Y, Fu FH. Muscle injuries and repair: current trends in research. J Bone Joint Surg Am 2002; 84-A(5):822–832
[8] Gharaibeh B, Chun-Lansinger Y, Hagen T et al. Biological approaches to improve skeletal muscle healing after injury and disease. Birth Defects Res C Embryo Today 2012; 96(1):82–94
[9] Botar Jid C, Vasilescu D, Damian L, Dumitriu D, Ciurea A, Dudea SM. Musculoskeletal sonoelastography. Pictorial essay. Med Ultrasound 2012; 14(3):239–245
[10] Klauser AS, Miyamoto H, Bellmann-Weiler R, Feuchtner GM, Wick MC, Jaschke WR. Sonoelastography: musculoskeletal applications. Radiology 2014; 272(3):622–633
[11] Lalitha P, Reddy MCh, Reddy KJ. Musculoskeletal applications of elastography: a pictorial essay of our initial experience. Korean J Radiol 2011; 12(3):365–375
[12] Barr RG. Sonographic breast elastography: a primer. J Ultrasound Med 2012; 31(5):773–783
[13] Barr RG, Zhang Z. Effects of precompression on elasticity imaging of the breast: development of a clinically useful semiquantitative method of precompression assessment. J Ultrasound Med 2012; 31(6):895–902

[14] Klauser AS, Faschingbauer R, Jaschke WR. Is sonoelastography of value in assessing tendons? Semin Musculoskelet Radiol 2010; 14(3):323–333
[15] van Dijk CN, van Sterkenburg MN, Wiegerinck JI, Karlsson J, Maffulli N. Terminology for Achilles tendon related disorders. Knee Surg Sports Traumatol Arthrosc 2011; 19(5):835–841
[16] Maffulli N, Sharma P, Luscombe KL. Achilles tendinopathy: aetiology and management. J R Soc Med 2004; 97(10):472–476
[17] Aström M, Rausing A. Chronic Achilles tendinopathy. A survey of surgical and histopathologic findings. Clin Orthop Relat Res 1995(316):151–164
[18] Kainberger F, Mittermaier F, Seidl G, Parth E, Weinstabl R. Imaging of tendons—adaptation, degeneration, rupture. Eur J Radiol 1997; 25(3):209–222
[19] Kannus P, Józsa L. Histopathological changes preceding spontaneous rupture of a tendon. A controlled study of 891 patients. J Bone Joint Surg Am 1991; 73 (10):1507–1525
[20] Aubry S, Risson JR, Barbier-Brion B, Tatu L, Vidal C, Kastler B. [Transient elastography of calcaneal tendon: preliminary results and future prospects][in French] J Radiol 2011; 92(5):421–427
[21] Arda K, Ciledag N, Aktas E, Aribas BK, Köse K. Quantitative assessment of normal soft-tissue elasticity using shear-wave ultrasound elastography. AJR Am J Roentgenol 2011; 197(3):532–536
[22] De Zordo T, Chhem R, Smekal V et al. Real-time sonoelastography: findings in patients with symptomatic achilles tendons and comparison to healthy volunteers. Ultraschall Med 2010; 31(4):394–400
[23] Faro F, Wolf JM. Lateral epicondylitis: review and current concepts. J Hand Surg Am 2007; 32(8):1271–1279
[24] De Zordo T, Lill SR, Fink C et al. Real-time sonoelastography of lateral epicondylitis: comparison of findings between patients and healthy volunteers. AJR Am J Roentgenol 2009; 193(1):180–185
[25] Khan KM, Maffulli N, Coleman BD, Cook JL, Taunton JE. Patellar tendinopathy: some aspects of basic science and clinical management. Br J Sports Med 1998; 32(4):346–355
[26] Fritschy D, de Gautard R. Jumper's knee and ultrasonography. Am J Sports Med 1988; 16(6):637–640
[27] Lian O, Holen KJ, Engebretsen L, Bahr R. Relationship between symptoms of jumper's knee and the ultrasound characteristics of the patellar tendon among high level male volleyball players. Scand J Med Sci Sports 1996; 6(5): 291–296
[28] Cook JL, Khan KM, Harcourt PR et al. Victorian Institute of Sport Tendon Study Group. Patellar tendon ultrasonography in asymptomatic active athletes reveals hypoechoic regions: a study of 320 tendons. Clin J Sport Med 1998; 8 (2):73–77
[29] Khan KM, Cook JL, Kiss ZS et al. Patellar tendon ultrasonography and jumper's knee in female basketball players: a longitudinal study. Clin J Sport Med 1997; 7(3):199–206
[30] Rist HJ, Mauch M. [Quantified TDI elastography of the patellar tendon in athletes][in German] Sportverletz Sportschaden 2012; 26(1):27–32
[31] Silvestri E, Garlaschi G, Bartolini B et al. Sonoelastography can help in the localization of soft tissue damage in polymyalgia rheumatica (PMR). Clin Exp Rheumatol 2007; 25(5):796
[32] Buck AR, Verstraete N, Li Y, Schweizer A, Snedeker JG, Buck FM. Detection of small tendon lesions by sonoelastographic visualization of strain profile differences: initial experiences. Skeletal Radiol 2012; 41(9):1073–1079
[33] Miyamoto H, Miura T, Isayama H, Masuzaki R, Koike K, Ohe T. Stiffness of the first annular pulley in normal and trigger fingers. J Hand Surg Am 2011; 36 (9):1486–1491
[34] Wearing SC, Smeathers JE, Urry SR, Hennig EM, Hills AP. The pathomechanics of plantar fasciitis. Sports Med 2006; 36(7):585–611
[35] Gibbon W, Long G. Plantar fasciitis: US evaluation. Radiology 1997; 203(1): 290
[36] Cardinal E, Chhem RK, Beauregard CG, Aubin B, Pelletier M. Plantar fasciitis: sonographic evaluation. Radiology 1996; 201(1):257–259
[37] Gibbon WW. Plantar fasciitis: US imaging. Radiology 1992; 182(1):285
[38] Wu CH, Chang KV, Mio S, Chen WS, Wang TG. Sonoelastography of the plantar fascia. Radiology 2011; 259(2):502–507
[39] Sconfienza LM, Silvestri E, Orlandi D et al. Real-time sonoelastography of the plantar fascia: comparison between patients with plantar fasciitis and healthy control subjects. Radiology 2013; 267(1):195–200
[40] Shinohara M, Sabra K, Gennisson JL, Fink M, Tanter M. Real-time visualization of muscle stiffness distribution with ultrasound shear wave imaging during muscle contraction. Muscle Nerve 2010; 42(3):438–441
[41] Bouillard K, Nordez A, Hug F. Estimation of individual muscle force using elastography. PLoS ONE 2011; 6(12):e29261
[42] Yanagisawa O, Niitsu M, Kurihara T, Fukubayashi T. Evaluation of human muscle hardness after dynamic exercise with ultrasound real-time tissue elastography: a feasibility study. Clin Radiol 2011; 66(9):815–819
[43] Lv F, Tang J, Luo Y et al. Muscle crush injury of extremity: quantitative elastography with supersonic shear imaging. Ultrasound Med Biol 2012; 38(5): 795–802
[44] Berko NS, Fitzgerald EF, Amaral TD, Payares M, Levin TL. Ultrasound elastography in children: establishing the normal range of muscle elasticity. Pediatr Radiol 2014; 44(2):158–163
[45] Shankar H, Reddy S. Two- and three-dimensional ultrasound imaging to facilitate detection and targeting of taut bands in myofascial pain syndrome. Pain Med 2012; 13(7):971–975
[46] Ballyns JJ, Shah JP, Hammond J, Gebreab T, Gerber LH, Sikdar S. Objective sonographic measures for characterizing myofascial trigger points associated with cervical pain. J Ultrasound Med 2011; 30(10):1331–1340
[47] Sparks SE, Escolar DM. Congenital muscular dystrophies. Handb Clin Neurol 2011; 101:47–79
[48] Drakonaki EE, Allen GM. Magnetic resonance imaging, ultrasound and real-time ultrasound elastography of the thigh muscles in congenital muscle dystrophy. Skeletal Radiol 2010; 39(4):391–396
[49] Vasilescu D, Vasilescu D, Dudea S, Botar-Jid C, Sfrângeu S, Cosma D. Sonoelastography contribution in cerebral palsy spasticity treatment assessment, preliminary report: a systematic review of the literature apropos of seven patients. Med Ultrasound 2010; 12(4):306–310
[50] Deprez JF, Brusseau E, Fromageau J, Cloutier G, Basset O. On the potential of ultrasound elastography for pressure ulcer early detection. Med Phys 2011; 38(4):1943–1950
[51] Kang T, Lanni S, Nam J, Emery P, Wakefield RJ. The evolution of ultrasound in rheumatology. Ther Adv Musculoskelet Dis 2012; 4(6):399–411
[52] Krouskop TA, Wheeler TM, Kallel F, Garra BS, Hall T. Elastic moduli of breast and prostate tissues under compression. Ultrason Imaging 1998; 20(4):260–274
[53] Pierucci A, Teixeira P, Zimmermann V et al. Tumours and pseudotumours of the soft tissue in adults: perspectives and current role of sonography. Diagn Interv Imaging 2013; 94(3):238–254
[54] Cosgrove D, Piscaglia F, Bamber J et al. EFSUMB. EFSUMB guidelines and recommendations on the clinical use of ultrasound elastography. Part 2: Clinical applications. Ultraschall Med 2013; 34(3):238–253

11 Elastography of the Salivary Glands, Lymph Nodes, and Testes

Fabrizio Calliada, Vito Cantisani, Chandra Bortolotto, Hector Grazhdani, Emanuele David, Antonio Masciotra, and Andrea Isidori

11.1 Introduction

This chapter evaluates the use of elastography for small parts of the body, specifically the salivary glands, lymph nodes, and testes.

11.2 Salivary Glands

Due to the superficial location of the salivary glands, ultrasound (US), as an easily available, cost-effective, and harmless technique (with no radiation exposure and no need for contrast-agent administration), is the first-line imaging technique of choice for salivary glands diseases. Ultrasound is performed normally by a linear transducer with a frequency of 7 to 15 MHz. The examination should always be conducted with both orthogonal approaches, longitudinal and axial. Among the different imaging techniques available ultrasound examination is considered to have the best diagnostic predictive capability for the detection of both focal and diffuse diseases of the salivary glands.[1] Additionally, magnetic resonance imaging (MRI) or computed tomography (CT) may be required, but only in the presence of pathologic alterations in the deep lobe of the parotid gland or in the inframandibular part of the parotid gland and the submandibular gland, both of which are sometimes not satisfactorily evaluated with ultrasound examination.

Several criteria for distinguishing between benign and malignant lesions are well described in ultrasound examinations of parotid tumors (▶ Fig. 11.1a). Benign tumors usually have been reported to present with regular and sharp margins, a homogeneous hypoechoic structure, and defined vessel distribution, whereas malignancies lack these characteristics and are irregular, heterogeneous, and diffusely perfused (▶ Fig. 11.1b).[2] Unfortunately, features monitored on B-mode and Doppler imaging are inadequate for differentiating benign from malignant salivary gland lesions,[3] since their appearance overlaps extensively within the heterogeneous group of benign and malignant salivary gland lesions. In particular, many benign tumors, above all pleomorphic adenomas, can appear irregularly shaped, with heterogeneous echo structure, and therefore cannot be distinguished from malignancies. For these reasons, even skilled ultrasound operators are not so accurate in differentiating benign from malignant lesions. The introduction of ultrasound contrast agents opened up the possibility of more accurate classification of these lesions. Contrast agents demonstrated some differences in flow kinetics between pleomorphic adenomas and Warthin's tumors;[4] however, results are not unequivocal and contrast-enhanced ultrasound (CEUS) does not appear feasible yet in routine clinical work.

More recently, elastography, an innovative tool for evaluating the stiffness/elasticity characteristics of different tissues and lesions has proven to be useful for differentiating between distinct types of salivary gland lesions (▶ Fig. 11.1c).

A second important clinical scenario is represented by salivary dysfunction as a complication of different possible causes—Sjögren syndrome (SS), radiotherapy, fibrosis, and repeated acute sialadenitis—producing chronic sialadenitis. For all these situations, ultrasound of the major salivary glands is the most attractive imaging option, as it is a noninvasive, inexpensive, and nonirradiating investigation. According to available data, ultrasound yields quite definitive information about the morphological changes of salivary glands. In recent years, also, Doppler imaging and CEUS have been used to evaluate the vascular anatomy of the salivary glands and to analyze the physiological changes in blood flow that occur during salivary stimulation in the diseased glands.

Also in this case, elastography, providing information about the stiffness increase related to fibrotic changes of the glands, could represent an important additional tool, useful to evaluate disease progression and to assess the effect of the therapy.

11.2.1 Focal Lesion Differential Diagnosis

Strain Elastography Imaging

Bhatia et al[5] examined 6 malignant and 59 benign lesions of salivary glands using longitudinal compression and a qualitative 4-point scoring method. They concluded that pleomorphic adenomas were significantly stiffer than Warthin's tumors (▶ Fig. 11.2); however, they thought that strain elastography (SE) might have a limited role in distinguishing benign salivary gland masses from malignant lesions because malignant tumors are prevalently stiff. Dumitriu et al[6] reported preliminary findings using a different qualitative classification whereby the mass was considered malignant if the stiffness in the mass was greater than 50% of the total mass, whereas the mass was considered benign if the stiffness in the mass was less than 50% of the total mass. In another study with 74 salivary gland masses, Dumitriu et al showed that the difference in elastographic score was statistically significant in discriminating benign from malignant tumors, but the overlap between pleomorphic adenomas and malignant tumors and between pleomorphic adenomas and Warthin's tumors limits the role of the technique in clinical practice.[7] Later, the same authors adopted the 4-point scoring method to evaluate 18 malignant and 56 benign salivary gland tumors using both longitudinal and transverse scans. They determined that the differences in the elastographic scores between benign and malignant tumors overall were statistically significant.[7] However, again they pointed out that the differences between malignant tumors and pleomorphic adenomas were not statistically significant. The mean score for pleomorphic adenomas (2.58 ± 0.87) was higher than that for Warthin's tumors (2.15 ± 0.80), but these differences were not statistically significant. Yerli et al[3] examined 36 salivary lesions

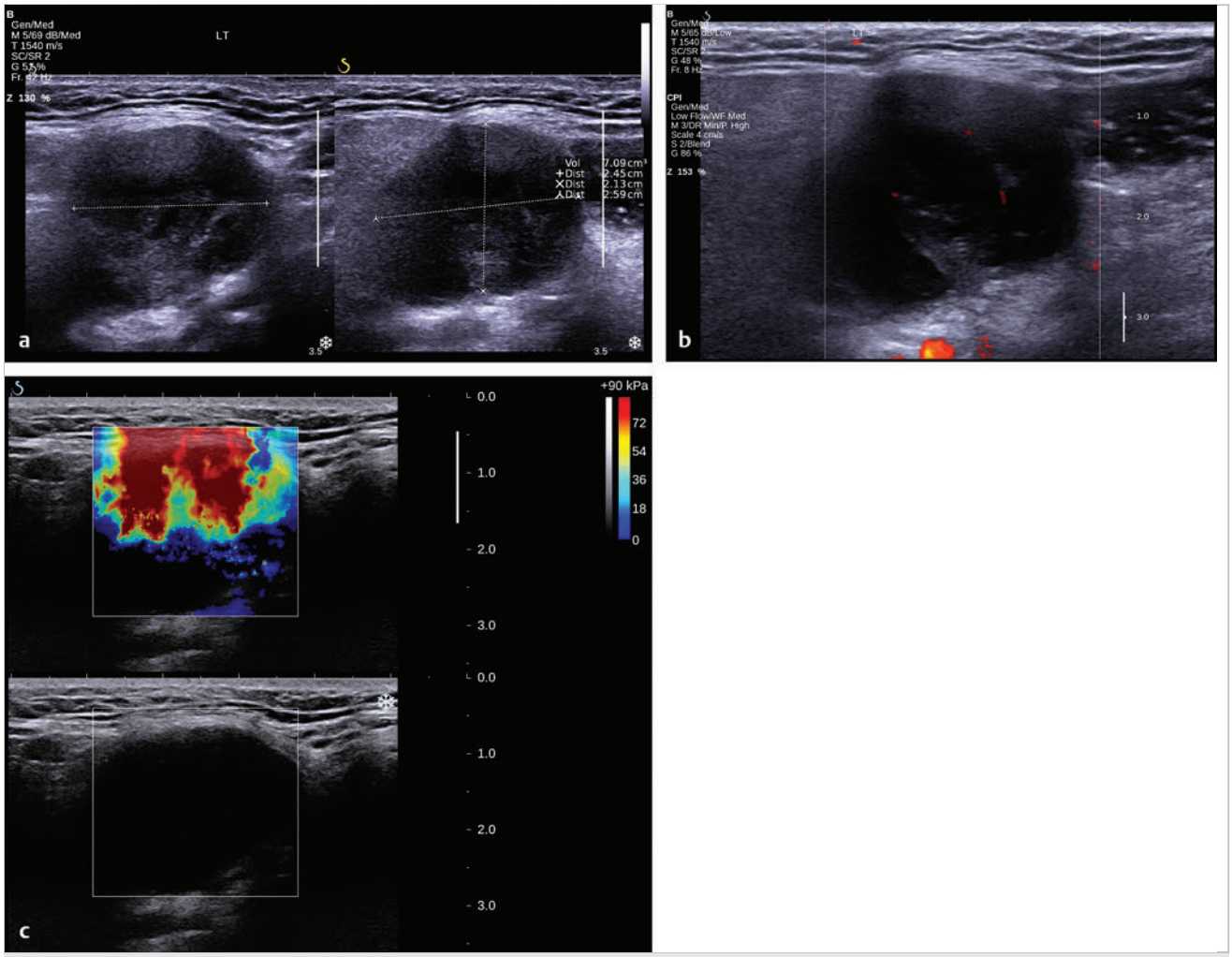

Fig. 11.1 Pleomorphic adenoma of the parotid gland. (**a**) B-mode ultrasound shows a heterogeneous appearance with regular, lobulated margins. (**b**) Power Doppler ultrasound shows little evidence of vascularization. (**c**) Shear wave elastography shows a heterogeneous stiff appearance.

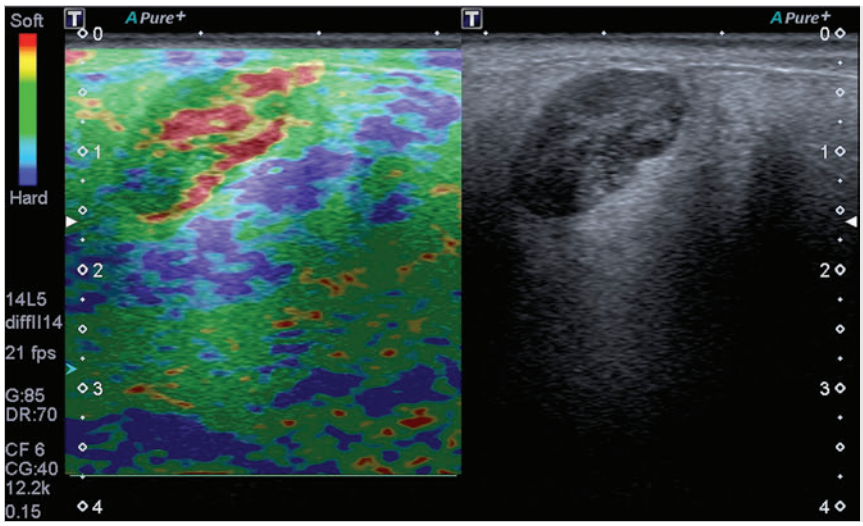

Fig. 11.2 Warthin's tumor at strain elastography. The benign lesion appears mostly soft.

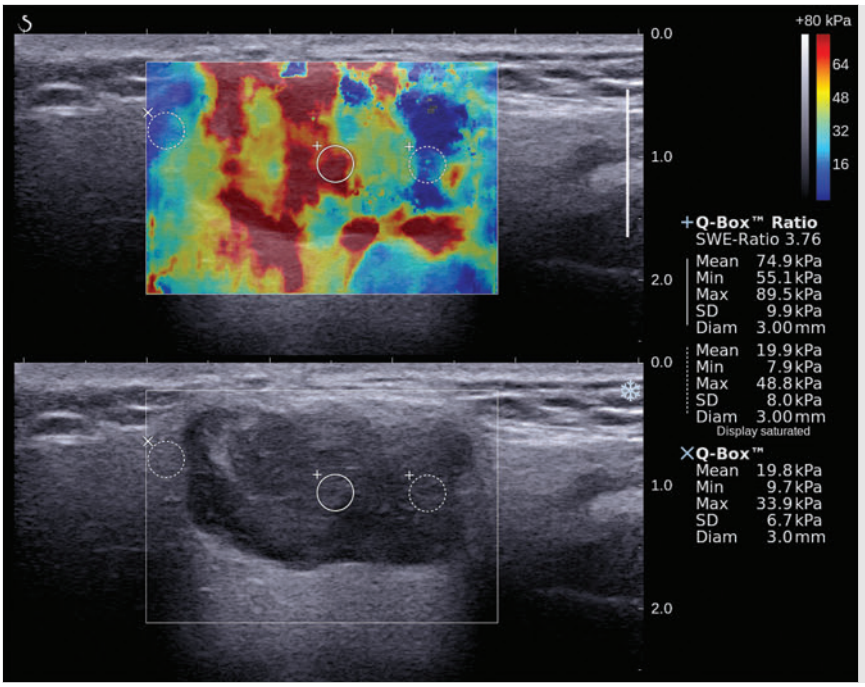

Fig. 11.3 Garland sign is a diagnostic artifact that can be seen as a reticular distribution of stiff tissue within the whole tumor in the elastogram. In such cases quantitative evaluation is less useful than the visual display of a reticular distribution of stiff tissue for lesion characterization.

(28 benign and 8 malignant). They found a score of 3 or 4 in 7 of 11 pleomorphic adenomas, and a score 1 or 2 in 9 of 11 Warthin's tumors. The authors explained the major stiffness of pleomorphic adenomas on a histopathological basis.

Celebi and Mahmutoglu[8] examined 81 salivary lesions (49 benign and 32 malignant) in 75 patients adopting the 4-point scoring method. Elastography correctly diagnosed 30 of 49 benign tumors (sensitivity, 61.2%) and 19 of 32 malignant tumors (specificity, 59.4%). The authors found the diagnostic value of elastography to evaluate pleomorphic adenomas, Warthin's tumors, and high-grade tumors was low, but the diagnostic rates that resulted for low-grade tumors such as mucoepidermoid carcinoma, acinic cell carcinoma, and metastases of basal cell carcinoma were better with elastography.

Mansour et al[9] examined 33 salivary lesions (29 benign and 4 malignant) in 32 patients using B-mode US, color Doppler, strain elastography (SE), and ARFI quantification. The authors did not visualize any significant difference between pleomorphic adenomas and Warthin's tumors at strain elastography (SE) evaluation.

Klintworth et al[2] investigated B-mode and elastographic criteria to differentiate benign from malignant parotid tumors and tried to define elastographic patterns characteristic for pleomorphic adenomas and Warthin's tumors. In the analysis of 57 patients with parotid gland tumors, the authors stated that different patterns were observed for particular histological subtypes of parotid gland tumors. They concluded that elastography can improve the diagnostic performance of ultrasound and can help the differentiation of benign from malignant parotid tumors.

Klintworth et al defined the elastographic *garland sign* pattern. A reticular distribution of stiff tissue within the whole tumor, the garland sign was seen more frequently in malignant parotid tumors (▶ Fig. 11.3). Pleomorphic adenomas showed an elastographic *dense core sign*, a central zone of very stiff tissue with softer tissue in the periphery. Warthin's tumors showed an elastographic *half-half sign*, with a stiff area located in the superficial half of the lesion while the deeper part had a softer appearance. Parotid cysts showed an elastographic *bull's eye sign*, a very soft, elliptic area in the center of a lesion. All the described patterns resulted in statistically significant diagnostic results.

Shear Wave Elastography Imaging

Fewer studies on the evaluation of focal salivary gland lesions with shear wave elastography (SWE) have been published to date. Arda et al[10] reported the normal values of 10.38 ± 3.5 kPa for the parotid glands and 10.92 ± 3.1 kPa for the submandibular glands (▶ Fig. 11.4) in 127 normal subjects. More recently Mantsopoulos et al[11] reported the mean SWE velocities in meters per second in 25 consecutive healthy subject to be 1.854 m/s for parotid glands and 1.932 m/s for the submandibular glands. Bhatia et al[12] in their study of 60 lesions (55 benign and 5 malignant) presented practical aspects and potential pitfalls of the approach in diagnosing focal salivary gland lesions; the authors concluded that the potential role of elastography at this site is unclear and unsuitable for ruling out malignancy (▶ Fig. 11.5). Similarly, Westerland and Howlett[13] in a review paper found the initial results to be disappointing. Wierzbicka et al[14] in their study of 43 patients (33 benign and 10 malignant) found a statistically significant difference between benign and malignant tumor mean elasticity, measured objectively and quantitatively in kilopascals. Moreover, qualitatively malignant tumors visually presented more extensive areas of stiffness. However, the very high standard deviation and range of the results partially confirmed a more skeptical point of view. Olgum et al[15] have tried to suggested that the relative proportions of stromal to cellular components of pleomorphic adenomas have an effect on the stiffness values determined by SWE, noting

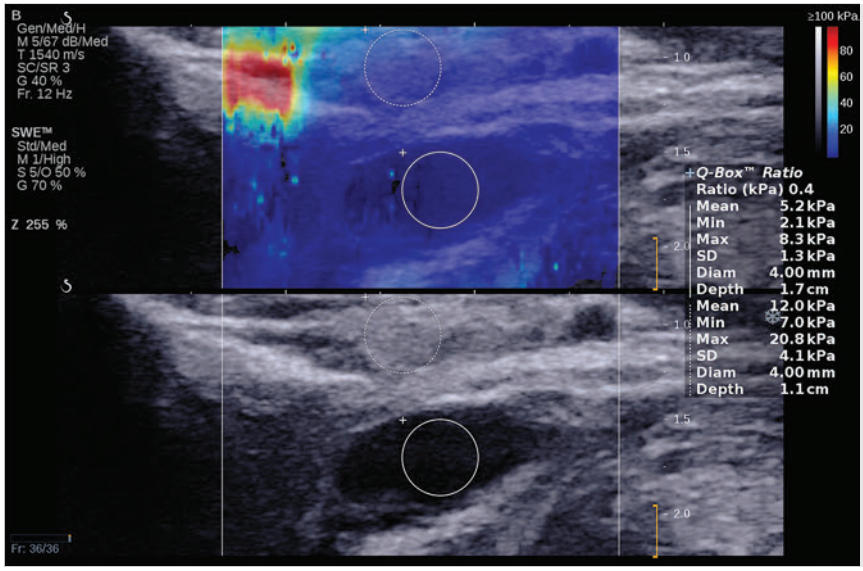

Fig. 11.4 Sublingual gland with a small cyst at shear wave elastography. The quantitative evaluation shows a mean value of 12 kPa, in line with the results of Arda and colleagues[10] (note that the cyst has a lower mean elasticity value).

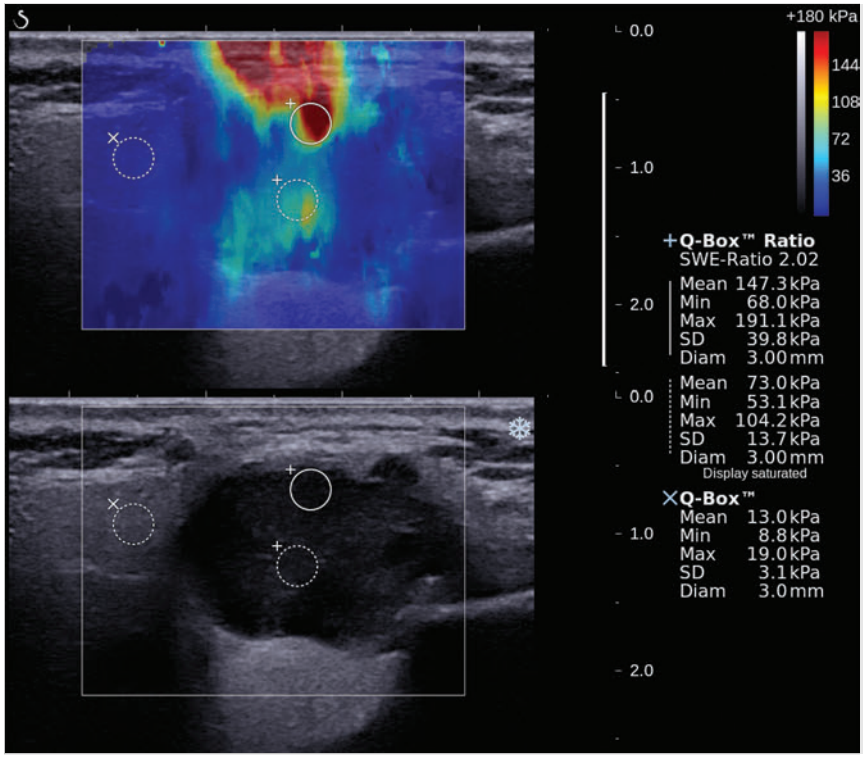

Fig. 11.5 Adenoma with malignant transformation at shear wave elastography quantitative evaluation.

relatively low kilopascal values with a low stromal component of the tumor and, conversely, high kilopascal values with an increased stromal component.

11.2.2 Fibrosis: Salivary Gland Diffuse Pathologies

After having discussed the use of elastography to characterize salivary gland focal lesions, we will focus now on the evaluation of diffuse pathologies. Focal and diffuse pathologies are investigated equally in other organs (e.g., the liver), while in the salivary glands diffuse pathologies are less frequently and more poorly investigated as compared to focal lesions. Elastography is generally applied to chronic diffuse pathologies (▶ Fig. 11.6) since acute ones (e.g., acute inflammation) are easily evaluated combining B-mode and Doppler information.[16] The application of elastography has therefore a limited value for acute diffuse pathologies.

Strain Elastography Imaging

Almost no studies on diffuse pathologies of salivary glands have been performed with SE, the main limitation probably being the fact that, in order to obtain quantitative data, a reference

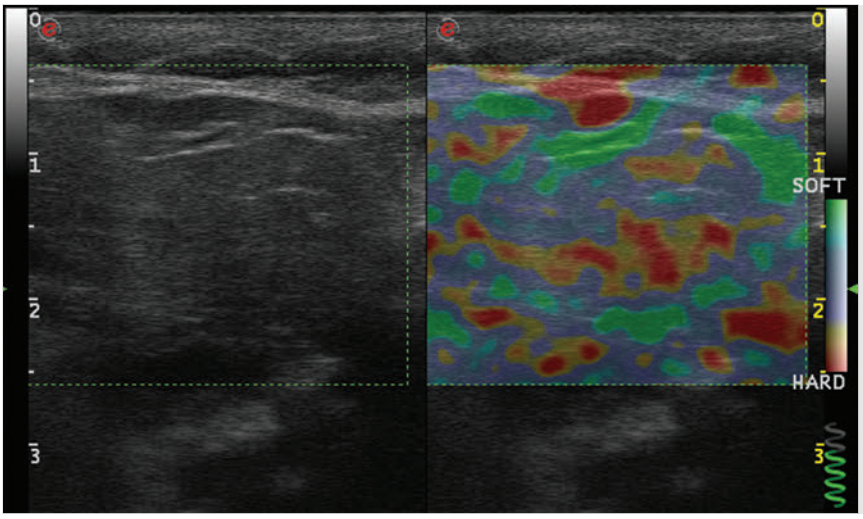

Fig. 11.6 Sjögren sialoadenitis of the parotid gland at strain elastography. The strain evaluation demonstrates an inhomogeneous increase of the stiffness values of the entire gland.

tissue (e.g., normal parenchyma or subcutaneous tissue) is needed. However, in a diffuse pathology of the salivary glands, normal parenchyma is not present and subcutaneous tissues are generally very thin, thus making reference ROI placements almost impossible. In addition, color-coded maps are useless in the follow-up of a chronic diffuse pathology in which only subtle elasticity modifications are expected. The sum of these factors has probably generated the paucity of research concerning the use of strain imaging in diffuse pathologies of the salivary glands.

Badea and colleagues[17] reported a case in which the fractal value difference between healthy and pathologic submandibular glands increases the most when real-time SE is used, while a lower value is reported when using SWE. As a result, the article thus suggests fractal analysis as a tool to quantify color-coded maps of SE imaging in order to obtain quantitative data (the fractal value). The application of fractal analysis to SE requires a thorough process of validation, since the literature reports results from only a single case.

Shear Wave Elastography Imaging

As already stated, almost all the research performed to evaluate the use of elastography for diffuse pathologies of the salivary glands employs SWE to quantitatively assess parenchymal stiffness. There are two main lines of research: the first one is more developed and regards postradiation gland evaluation, while the second one concerns chronic inflammatory diseases (e.g., Sjögren syndrome).

Postradiation changes in salivary glands lead to different degrees of feeding impairment thus heavily influencing the quality of life.

Badea and colleagues[16] evaluated the submandibular glands of 18 patients who had undergone radiation therapy. The results were compared to the values of a control group composed of healthy volunteers. The elasticity mean value in pathologic patients was 2.13 ± 0.52 m/s versus an elasticity mean value of 1.82 ± 0.41 m/s in the control group. This difference is statistically significant ($p < 0.05$) and it demonstrates the capability of SWE to differentiate between a gland subjected to radiotherapy and a normal one. A salivation test (a clinical test to estimate gland functioning) was additionally performed; however, the results do not correlate to the elastographic values.

A similar study was conducted by Kaluzny and colleagues.[18] Fifty-two patients who had undergone radiotherapy for head and neck cancer were evaluated, and the results were compared to a control group composed of healthy volunteers. The parotid mean elasticity value was 41.7 kPa for pathologic glands (versus 26.03 kPa for healthy controls; $p = 0.0018$) and was 37.6 kPa for pathologic submandibular glands (versus 22.4 kPa for healthy controls; $p = 0.0005$). The results were also correlated to the intensity of symptoms, which were evaluated by using a clinical index; however, no statistically significant correlation was found. Measures were repeated several times after radiotherapy but the impact of time on elasticity remains unclear.

The results from these studies are promising since SWE–unlike B-mode sonography–can differentiate between post-radiation glands and nonirradiated ones. However, further studies are needed to fully investigate the correlation between the severity of symptoms and the elasticity value, and to explore variations related to treatments addressed to reduce post-radiation salivary impairment.

The other major line of research in the field of diffuse salivary glands pathologies is chronic inflammatory diseases.

Wierzbicka and colleagues[19] recently published their results on 78 patients with a large number of different chronic inflammatory pathologies ranging from Sjögren syndrome (20 patients) to Stensen's duct stenosis (15 patients). In all subgroups mean elasticity values are significantly higher than mean elasticity values of healthy controls (e.g., 111 kPa for patients with Sjögren syndrome versus 24 kPa for healthy patients). Unlike in postradiotherapy patients, in this study, elasticity correlates with the severity of symptoms.

For patients with sialolithiasis, similar results were obtained by Zengel and colleagues[20] on a smaller but more homogeneous group of 30 patients. The average elasticity value on the afflicted side was 3.20 ± 1.04 m/s with a highly significant difference in comparison to the healthy side of the patient (1.90 ± 0.45 m/s; $p < 1.87451E-17$).

These results suggest that SWE has the potential to become a valuable diagnostic tool for chronic inflammatory diseases of the salivary glands. However, both the authors point out that

more studies are needed to evaluate the temporal evolution of stiffness, and the correlation between elasticity and response to therapy.

Summary

Elastography has shown the ability to improve ultrasound evaluation over B-mode US alone in the detection of diffuse pathologies of the salivary glands. The future steps are to further explore the potential of correlating elasticity value with clinical indexes, functional tests, response to therapy, and evolution of structural changes over time.

11.2.3 Artifacts and Pitfalls

After having discussed the techniques, tips and tricks concerning the study of salivary glands, we will now focus on artifacts and pitfalls. We will not discuss the general types of artifacts that are common to all anatomical structures and which have already been covered in Chapters 1 to 3. We will focus only on artifacts that are specific or particularly relevant to salivary glands. These artifacts can be divided into two major groups: artifacts related to the position of salivary glands and to their surrounding structure, and artifacts related to histological features (both related to the healthy parenchyma and to pathologic nodules).

Artifacts Related to Gland Position and Surrounding Structures

These artifacts can be found both in SE and SWE, although they are more prominent in SE.

SE is greatly affected by mistracking artifacts related to the sliding of the transducer.[2] The sliding is caused by the anatomy of the area, which is slippery and presents only a few plane surfaces suitable to hold the probe firmly. Furthermore, artery pulsation and breathing tend to cause a lateral sliding of the probe while compressing–releasing. This out-of-plane compression–release leads to low-quality elastograms affected by mistracking artifacts.[12,13] On the other hand precompression artifacts can be as negative as mistracking artifacts: in order to hold the probe in the same position, the operator must apply an excessive pressure on the transducer. This pressure compresses the parenchyma and the lesion before the elastography is performed thus modifying the elasticity of tissues. For these reasons compression–release movements on this area must be extremely gentle and, at the same time, very precise in order to avoid both out-of-plane and precompression artifacts. SWE has the advantage of being free from compression–release artifacts.[10]

Nonetheless, other artifacts related to salivary gland position and surrounding structures affect both techniques in the same way. These artifacts are caused by three factors: the proximity to the skin,[5] the proximity to osseous planes such as the ramus of the mandible[12] and the temporal bone,[3] and the presence of convex cutaneous surfaces. All these factors contribute, with different mechanisms, to generate local inhomogeneity of the stress thus hiding the real elasticity of the tissue.

The proximity to the skin, which presents in this area only a small amount of subcutaneous tissue, generates a hard Stripe on the superficial margin of the nodule within the gland (and less frequently on the superficial margin of the gland as well). This linear horizontal artifact can also present a vertical component[12] crossing the nodule and completely (for smaller nodules) or partially hiding their true elasticity. This artifact is caused both by a local stress concentration and by the presence of an interface between tissues showing a different elasticity.[21] It is easy to rule out its artifactual nature since no inhomogeneity can be seen on B-Mode images.

At deeper levels, the bone cortex (e.g., the ramus of the mandible and the temporal bone) can reflect waves thus determining focal inhomogeneity of the stress and harder artifactual areas.[3]

Lastly, the convexity of the cutaneous surface (both related to the anatomical site and/or big-size nodules) can focally concentrate the stress in the central part of the lesion that will therefore appear hard. This artifact can completely alter the interpretation of the elastogram. Bhatia et al also reported such a central hard area in a lesion that proved to be a lipoma.[12] To neutralize this artifact, a practical tip is using a considerable amount of gel in order to artificially smooth the probe-skin interface without losing the acoustic window on the sides of the probe.

Artifacts Related to Histological Feature

The parenchyma of healthy salivary glands is generally stiffer than that of other superficial organs (e.g., breast) thus leading to a quicker reduction of signal intensity in the deeper areas of the glands.[3] This phenomenon does not generate proper artifacts; however, it limits the possibility to discriminate the elasticity of deeper lesions, thus representing a major limitation especially in the study of lesions of the deep lobe of the parotid gland.[7]

Salivary glands lesions (similar to thyroid lesions) often present with cystic components that are more rarely seen in other organs (e.g., the liver). Salivary glands, unlike the thyroid gland, can also show a dilatation of the ducts. All these cystic and pseudocystic aspects of both parenchyma and nodule can lead can lead to inaccurate measurement, with an artificial hardening of the surrounding tissues,[21] related to the inability of elastography to measure the elasticity of the fluid components. These artifacts can be avoided by measuring the elasticity in the solid portion of the lesion most distant from the cystic portion.

On the other hand, some authors suggest exploiting this artifact in order to find hidden cystic portions of salivary gland lesions. These lesions are often very fibrous and thus very hypoechoic on B-mode ultrasound; this makes it extremely hard to identify these small cystic areas.[6] However, their typical color stratification pattern is easy to detect with the aid of elastography,[14] thus revealing hidden cystic areas and giving the operator more information to identify the nature of the lesion.

11.3 Lymph Nodes

Lymph node evaluation in medicine is generally aimed at finding metastases from solid tumors[22] or assessing primary involvement from hematologic diseases. Differential diagnosis between neoplastic nodes and non-neoplastic nodes (both normal and with infective or rheumatologic involvement) is another critical diagnostic challenge.[23]

Before the development of modern imaging, lymph node neoplastic involvement had always been assessed by clinical examination,[24] as neoplastic involvement usually increases lymph node stiffness. Metastatic tissue is generally more highly cellulated and thus more stiff than normal lymph node tissue; however, clinical examination has proven to be highly inaccurate in separating normal from metastatic nodes.[25]

Several modalities have been employed to address lymph node evaluation: US, CT, MRI, and nuclear medicine (fluorodeoxyglucose positron emission tomography [FDG-PET], lymphoscintigraphy).[26] Combined modalities (PET/MR and PET/CT) have been employed as well. The introduction of a novel contrast medium such as ultrasmall particles of iron oxide (USPIO) in contrast medium[27] or of a new generation of US contrast agent with perflbutane microbubble,[28] demonstates that each modality is subject to a constant updates. With all these options available, several criteria have been taken into account: nodal size, shape, site, outline, internal appearance, and behavior after contrast medium administration. However, all these modalities, techniques, and criteria (or combination of them) have been demonstrated to be suboptimal in separating normal from metastatic nodes and for this reason invasive staging approaches are still irreplaceable.[29] If we take into account these considerations, ultrasound is frequently advocated as an important instrument in lymph node evaluation (both for superficial and deep lymph nodes, thanks to endoscopic ultrasound [EUS]).[29] In fact, US shows sensitivity and specificity close to that of other imaging modalities, and it can also be used to guide biopsies and to target the most probable metastatic site inside the lymph node.[30]

As already extensively stated, the principle of elastography is simple and effective and can be exploited in order to identify micrometastatic foci (seen as hard areas) thereby realizing an empowerment of US, enhancing prebiopsy evaluation of lymph nodes and thus directly influencing the choice and final outcome of the patient's treatment.

Elastography can be used to assess superficial and deep lymph nodes with a superficial linear probe and an endoscopic ultrasound probe, respectively.

11.3.1 Superficial Lymph Nodes: Indications and Clinical Applications

Strain Elastography Imaging

Lyshchik et al[31] published one of the first clinical studies to evaluate the diagnostic effectiveness of SE by examining 141 lymph nodes, of which 98 were confirmed benign and 43 were confirmed malignant by histopathology. They classified the nodes according to visualization, brightness compared to the neighboring muscles, and the regularity of the outline. Using a strain ratio cutoff value of > 1.5, SE demonstrated sensitivity, specificity, and accuracy values of 85%, 98%, and 92%, respectively. According to a meta-analysis of nine SE studies that included 50 to 155 cervical or axillary lymph nodes,[32] the pooled sensitivity and specificity values for detecting malignancies were 74% and 90% using an elastographic scale and 88% and 81% using strain ratios, respectively. The 4-point elastographic scale for suspect malignant lymph nodes proposed by Lo et al is simpler and used more widely. In general, metastatic lymph nodes demonstrate higher stiffness (▶ Fig. 11.7) than benign lymph nodes (▶ Fig. 11.8), so elastographic scale scores of 1 and 2 indicate benign lymph nodes, and elastographic scale scores of 3 and 4 indicate malignant lymph nodes.[33]

Rubaltelli et al[34] reported their experience with the elastography of superficial lymph nodes with 53 patients, 28 of whom had malignant forms of lymphadenopathy (metastatic in 21 cases, non-Hodgkin's lymphomas in 7). The remaining 25 had benign disease. Compared with cytological and/or histological diagnosis, elastography displayed a sensitivity of 75%, specificity of 80%, and accuracy of 77% with positive and negative predictive values of 80% and 70%, respectively. Later, a meta-analysis was published by Yin et al[32] that included 9 studies and analyzed 835 lymph nodes. The pooled sensitivity and specificity for the diagnosis of malignant lymph nodes were 0.74 (95% confidence interval [CI]: 0.66–0.81) and 0.90 (95% CI: 0.82–0.94) for elastographic scale score, and 0.88 (95% CI: 0.79–0.93) and 0.81 (95% CI: 0.49–0.95) for strain ratio, respectively. Strain ratio SE was more reliable than qualitative SE, and they

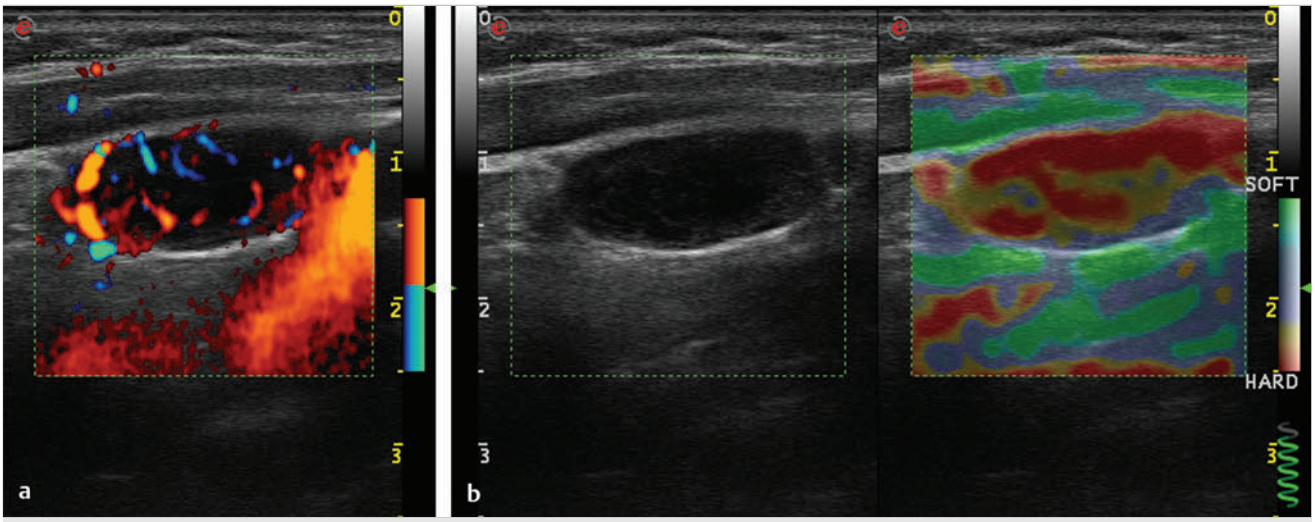

Fig. 11.7 Metastatic lymph node. (**a**) Power Doppler evaluation. (**b**) Strain elastography evaluation. The node appears mostly hard.

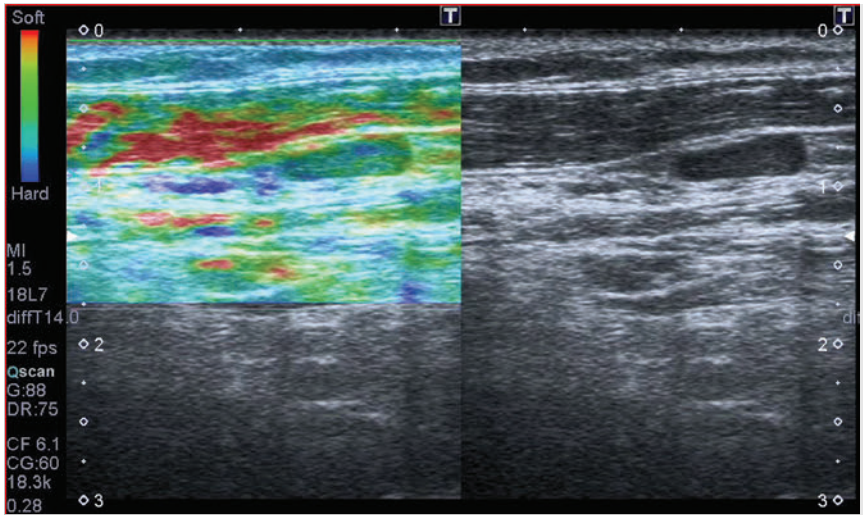

Fig. 11.8 Reactive lymph node at strain elastography. The node appears mostly soft.

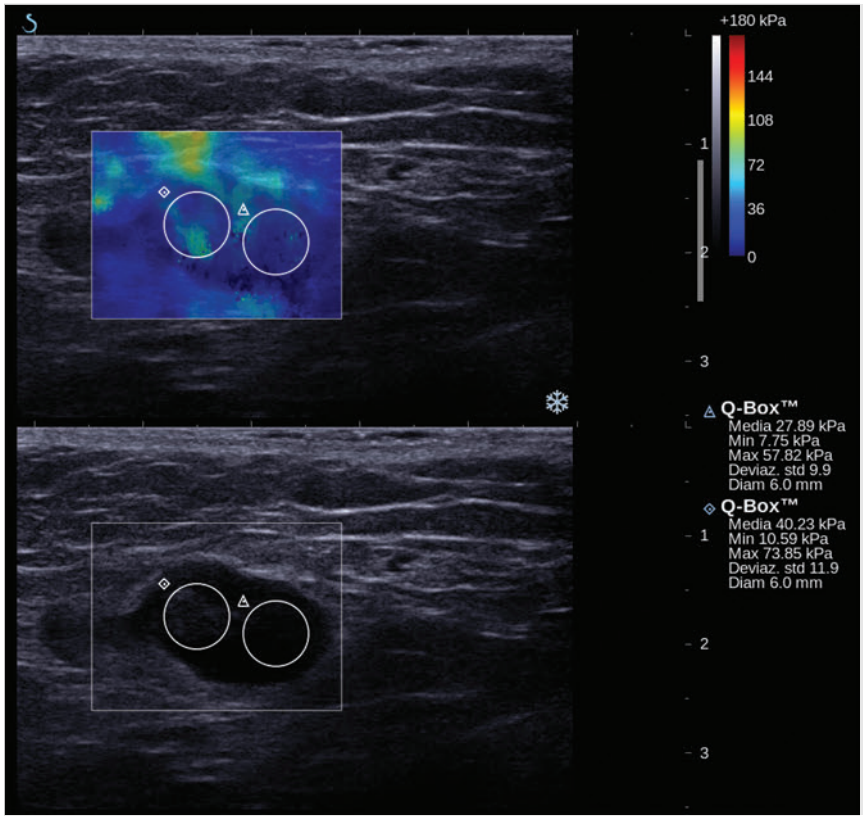

Fig. 11.9 Asymmetrical cortical growth of a lymph node in a breast cancer patient. Note the presence of stiffness foci in the lymph node cortex with relatively high kilopascal values at SWE evaluation.

concluded that strain ratios from SE can potentially help to select suspicious lymph nodes for biopsy.

ARFI and Shear Wave Elastography Imaging

There are relatively few clinical studies that have compared acoustic radiation force impulse shear wave imaging and SWE. Bhatia et al[35] has reported that the median elastic modulus of malignant lymph nodes (▶ Fig. 11.9, ▶ Fig. 11.10) is higher than that of benign lymph nodes (▶ Fig. 11.11). However, discrimination power was low because the optimal cutoff value of 30.2 kPa demonstrated sensitivity, specificity, and accuracy values of 41.9%, 100%, and 61.8%, respectively. Another study has reported that the maximum elastic modulus can be used to differentiate malignant lymph nodes, and that a cutoff value of 19.4 kPa resulted in accuracy, sensitivity, and specificity values of 94%, 91%, and 97%, respectively (▶ Fig. 11.12, ▶ Fig. 11.13, ▶ Fig. 11.14).[36]

Limitations and Pitfalls

The accuracy of SE measurements using freehand compression is very dependent on the compression technique, because excessive compression alters tissue stiffness and nonaxial

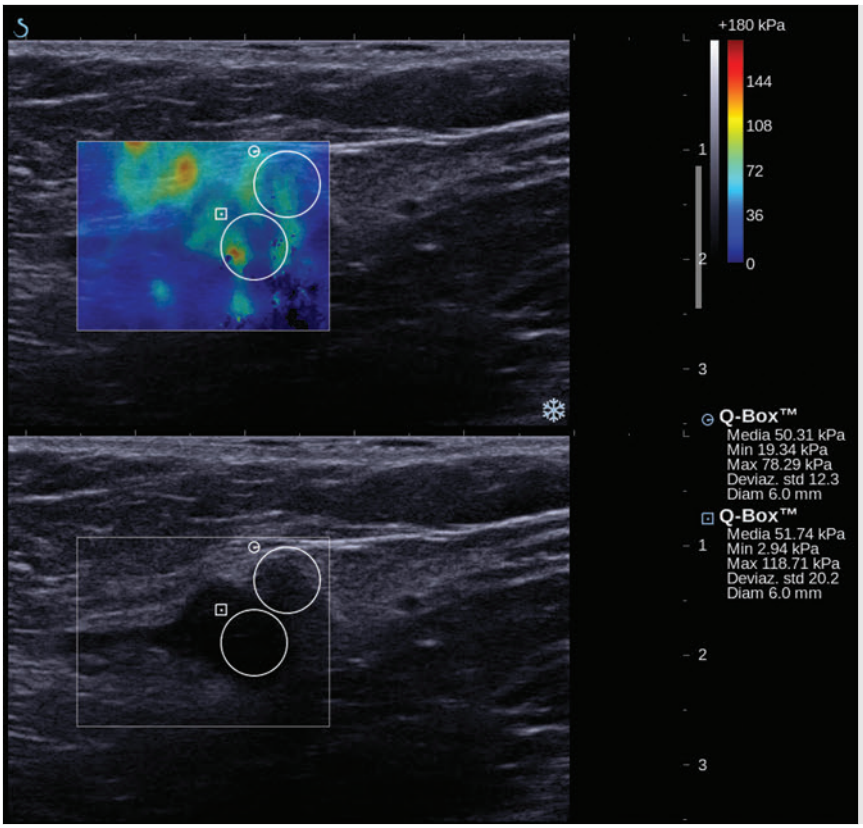

Fig. 11.10 Asymmetrical cortical growth of a lymph node in breast cancer patient from Fig. 11.9. Note the stiffness foci in the lymph node cortex with relatively high kilopascal values at shear wave elastography evaluation.

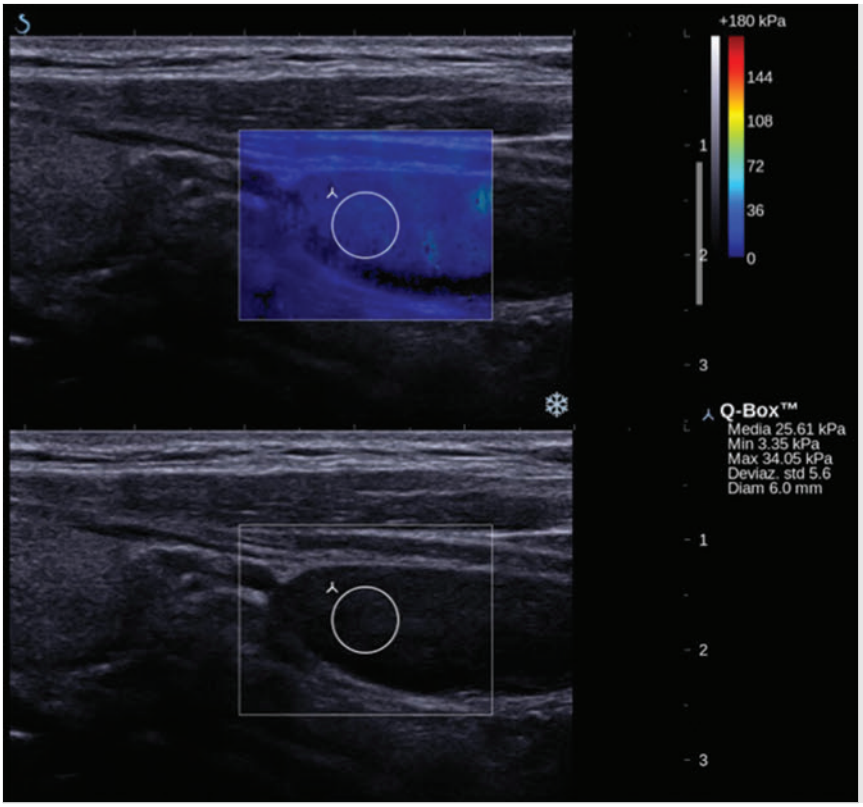

Fig. 11.11 Symmetrical growth of the lymph node cortex in an inflammatory lymph node. Note the homogeneity of stiffness distribution in the lymph node cortex with low kilopascal values at shear wave elastography evaluation.

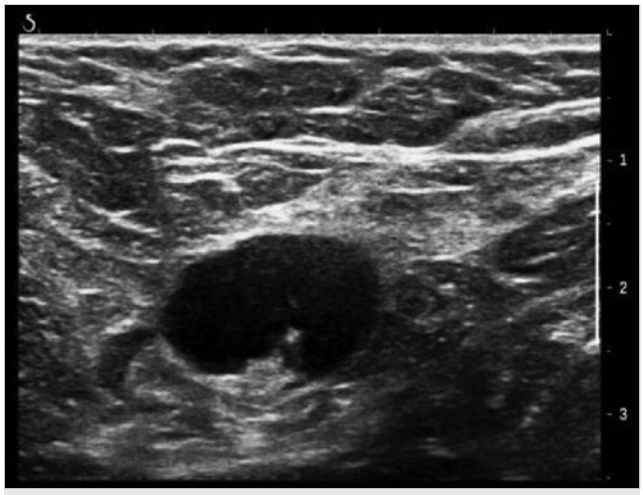

Fig. 11.12 Metastatic lymph node in patient with breast cancer. At B-mode ultrasound, the lymph node presents a thicker and hypoechoic cortex with tiny hilum.

displacement can degrade the accuracy of the software's correlation algorithms. In addition, results characterizing lymph nodes as benign or malignant were somewhat inferior to those obtained characterizing thyroid nodules, and the difference is partly related to technical factors. The thyroid parenchyma can be compressed uniformly, and in general the elastic characteristics of focal lesions in this gland can easily be compared with those of the adjacent normal tissue. In contrast, the elastographic study of lymph nodes is affected by the position of the node (superficial or deep) and its relation to nearby structures such as muscles, superficial bones, or large blood vessels.[34]

Because SWE does not require freehand compression, it may be less operator-dependent than SE. Nevertheless, elastography has several unresolved issues and limitations:

- Elastography can be problematic if there is a focal convex bulge on the skin overlying the ROI because, under these circumstances, it may be impossible to apply a linear transducer without producing focal stress concentrations within the tissue of interest, thereby resulting in spuriously stiff elastograms.[37]
- There are still unresolved issues regarding ROI selection in most studies on strain ratio or SWE. The selection of a representative ROI is subjective sometimes.
- The distance from the transducer, anisotropy, and stretch stress in overlying muscle all induce variations.[38]
- High-quality elastograms are often hard to obtain due to pulsations from nearby great vessels.[38]
- Intranodal necrosis in metastatic lymph nodes might confound the elastographic scale; some investigators have modified their qualitative scoring systems to classify nodes that demonstrate a specific strain pattern (using a 5-point scale), peripheral low strain (shown by high stiffness), or central high strain (shown by low stiffness) (▶ Fig. 11.15).[38]
- Alam et al[39] used a 5-point scale for elastography and reported sensitivity, specificity, and accuracy values of 83%, 100%, and 89%, respectively.

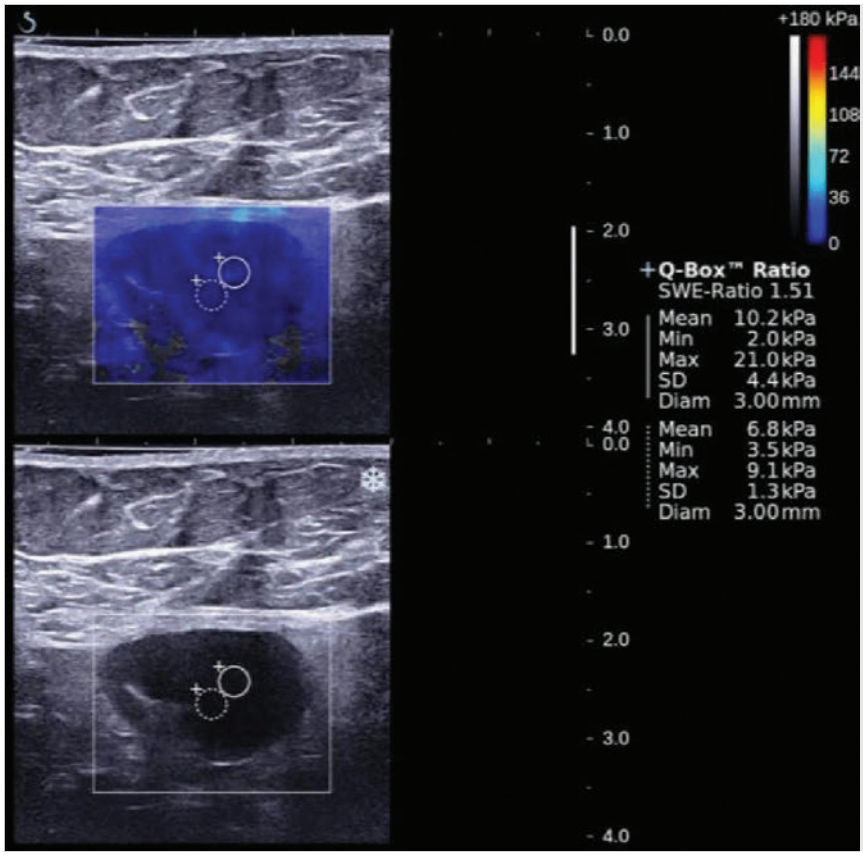

Fig. 11.13 Metastatic lymph node in patient with breast cancer from ▶ Fig. 11.12. At two-dimensional shear wave elastography, the lymph node appears soft.

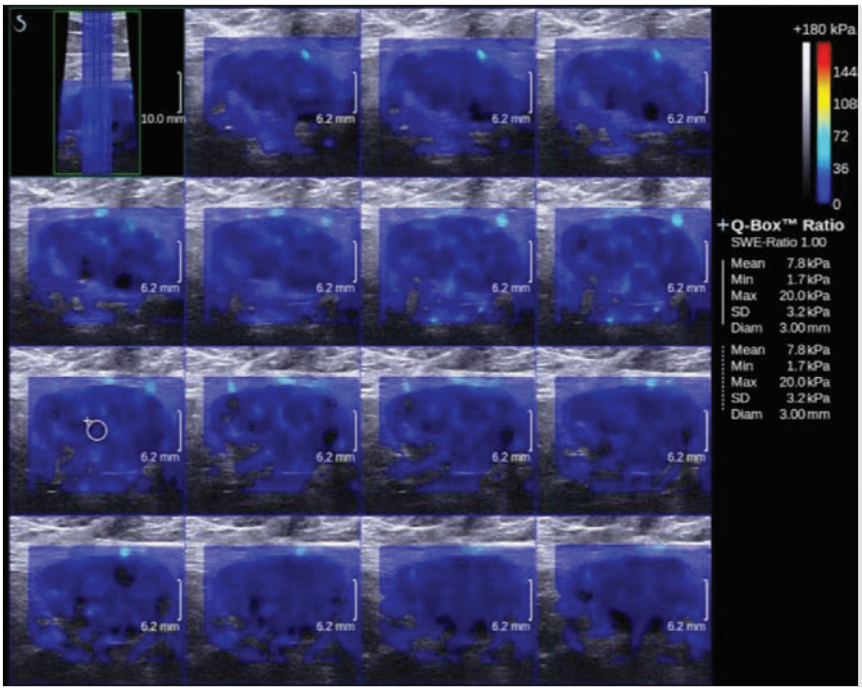

Fig. 11.14 Metastatic lymph node in patient with breast cancer from ▶ Fig. 11.12. Three-dimensional SWE confirms the low stiffness of the lymph node.

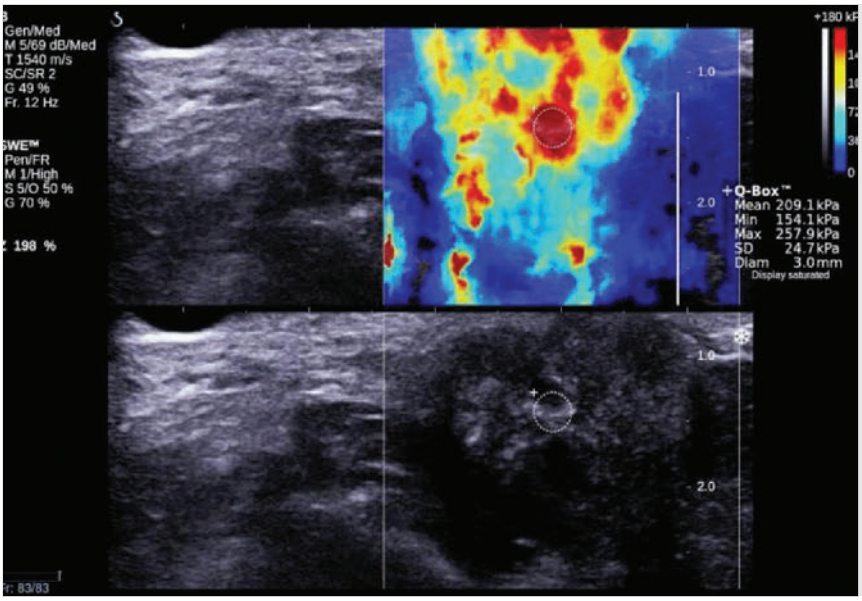

Fig. 11.15 Neuroendocrine tumor (NET) lymph node metastasis. The lymph node appears heterogeneous, with some stiff areas at strain elastography evaluation, as represented at shear wave elastography evaluation with high kPa values.

11.3.2 Deep Lymph Nodes: Indications and Clinical Applications

Deep lymph nodes in the mediastinum or abdomen can be subjected to elastographic studies during endoscopic ultrasound (EUS) examinations. Only SE is currently available, and it can be used with longitudinal and radial echo-endoscopes, the former having the advantage that suspicious regions can be biopsied under direct visualization.[40]

Săftoiu et al[41] proposed a quantitative assessment based on the analysis of histograms, in which the color gradations within the field of view (automatically acquired in all frames of a 10-second recording), were represented as numerical values. In the characterization of abdominal and mediastinal nodes, endoscopic SE performed with this software displayed a sensitivity of 85.4%, specificity of 91.9%, and accuracy of 88.5%[41]

EUS elastography can be recommended to support discrimination of benign and malignant lymph nodes by identifying malignant areas within lymph nodes and targeting these areas for endoscopic ultrasound–guided fine needle aspiration (EUS-FNA). The reliable classification of benign and malignant lymph nodes is important for patient prognosis and selection of appropriate therapy for many cancers, for example, esophageal, stomach, bronchial, and pancreatic carcinoma. The endosonographic B-mode criteria for detecting malignancy have an accuracy of between 50% and 100%.[42]

With an accuracy of > 85% documented in several large studies, EUS-FNA delivers the most reproducible results in the

diagnosis of metastatic lymph node infiltration.[43] However, sensitivity of EUS-FNA depends on the appropriate selection of lymph nodes and focal infiltration within the lymph nodes for biopsy.

EUS elastography has the potential to further improve the accuracy of EUS-FNA by targeting lymph nodes for needle sampling. A recent meta-analysis calculated a pooled sensitivity of 88% and a pooled specificity of 85% for EUS elastography in differentiating between benign and malignant lymph nodes.[44]

However, Larsen et al found that EUS elastography did not perform better than EUS morphology in differentiating between malignant and benign lymph nodes in patients with resectable upper gastrointestinal cancer.[45] These findings conflict with the results of another group, which showed superior accuracy of EUS elastography strain ratios in comparison with conventional EUS criteria in differentiating malignant and benign lymph nodes in the nodal staging of esophageal cancer.[46]

The lymph node architecture using EUS elastography has not been studied in detail.

Limitations and Pitfalls

A number of technical factors specific to EUS elastography may adversely influence elastographic assessment in clinical practice. The small size and penetration depth of EUS transducers limits the applicability of EUS elastography for characterizing large and deep-seated lesions.

If the field of view (FOV) is too small to adequately represent the tissue surrounding the lesion or if there is a size discrepancy between the lesion and the surrounding tissue, assessment of relative stiffness differences between the lesion and surrounding normal tissue may be impaired. Moreover, the reproducibility of EUS elastography may be reduced in several anatomical sites in which the effects of physiological movement are too weak or too strong (heart and/or large arterial vessels) or in which compression with the transducer is difficult (left adrenal gland, spleen, or parts of the liver). Interposition of large vessels, cystic lesions, and dilated ducts between the target lesion and the transducer may impair strain assessments.

The utility of EUS elastography for discrimination of malignant lesions or infiltrations from benign disease may be hampered by tumor necrosis (which is soft) and by fibrosis (which is hard).[42]

11.3.3 Summary

US is commonly used in the differential diagnosis of superficial lymphadenopathy, and B-mode imaging is the most important component of this approach. High-definition images can be obtained with high-frequency transducers, and the scanning plane can be modified in real-time to optimize visualization of the lymph node, even those measuring only a few millimeters in diameter. Additional diagnostic information can be obtained with Doppler studies of node vascularization, but the findings are frequently ambiguous and sometimes even FNA fails to provide a definitive answer. The only choice in these cases is lymphadenectomy and histological examination of the entire node. Precisely for these reasons SE and SWE have great potential as diagnostic aids (in addition to the B-mode and Doppler images) to avoid the radical procedures.

According to the European Federation of Societies for Ultrasound in Medicine and Biology (EFSUMB) guidelines, EUS elastography is recommended as an additional tool for discrimination of benign and malignant lymph nodes and it may be used for identifying the most suspicious lymph node and/or harder lymph node regions for malignant invasion (▶ Fig. 11.16) that should be targeted for EUS-FNA.[40]

11.4 Testis

Conventional US, although very sensitive for the detection of testicular pathology, clearly does not provide histological diagnosis. Besides US, several tools have been adopted to improve the sensitivity and specificity of the preoperative characterization of testicular masses, including MRI and CEUS.[47] The emergence of elastography as an innovative tool for assessing different tissues and lesions for their stiffness/elasticity characteristics provides an additional potentially useful method for differentiating focal testis lesions and diffuse pathologies.

11.4.1 Strain Elastography Imaging

Techniques

Certainly most focal testicular lesions differ in their consistency from the surrounding parenchyma. For this reason, strain elastography (SE) could be helpful in differentiating testicular lesions, thus allowing the clinician to choose between a watchful-waiting follow-up, in the presence of likely benign lesions, and surgical removal for suspected malignant tumors. It is also true that in most cases the testis is readily palpable, allowing a direct examination of large solid masses; the role of elastosonography, therefore, is limited to small-size, nonpalpable incidental intratesticular masses. At SE evaluation, the normal testis shows a medium, homogeneous level of elasticity (▶ Fig. 11.17), and sometimes some linear structures can be seen, related to fluid component (i.e., vessels). Preliminary findings about SE and testicular lesions were reported in 2005,[48] where 15 patients affected by inflammatory and neoplastic diseases were submitted to US and SE examinations. Authors concluded that SE improved the discovery of testicular nodules, and had the ability to distinguish between testicular lesions and inflammatory changes based on the tissue elasticity.

Grasso et al[49] reported their experience in testicular elastography, evaluating 41 patients who presented with scrotal pain, painless enlargement of the scrotum, or testicular nodules. They concluded that SE could be used as a complement to B-mode US assessment in cases of solid lesions smaller than 10 mm, but not alone, because the elastographic pattern shown by benign and malignant lesions was quite similar. In a series of 88 patients[50] the SE findings of 144 testicular lesions were analyzed, considering shape, size, elastographic criteria, and compared to the histological diagnosis or the benign behavior in the follow-up examinations. Authors assigned an elastographic score (from 1 to 5, where a score of 1 indicated even strain for the entire hypoechoic lesion and the highest value 5 corresponded to the absence of strain in the entire hypoechoic lesion and in the surrounding area), according to the distribution and degree of strain as suggested by Itoh et al[51] for breast lesion classification. In this study, nearly 94% of benign lesions showed

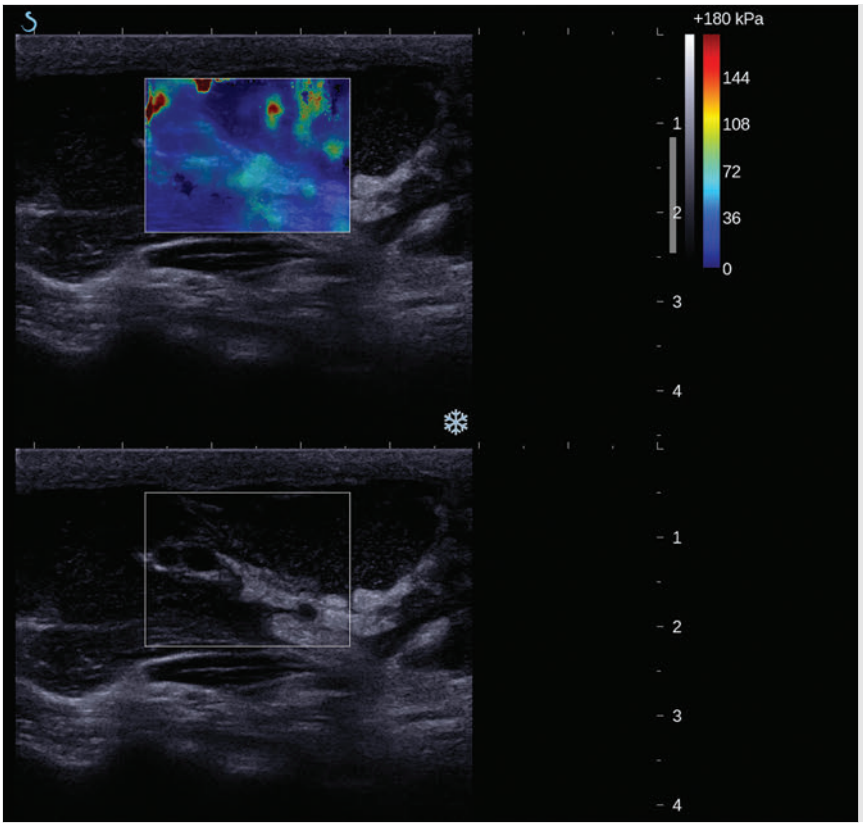

Fig. 11.16 Non-Hodgkin's lymphoma at SWE. Note the enlarged jugular lymph nodes (with low general elasticity values) with very high-stiffness small foci.

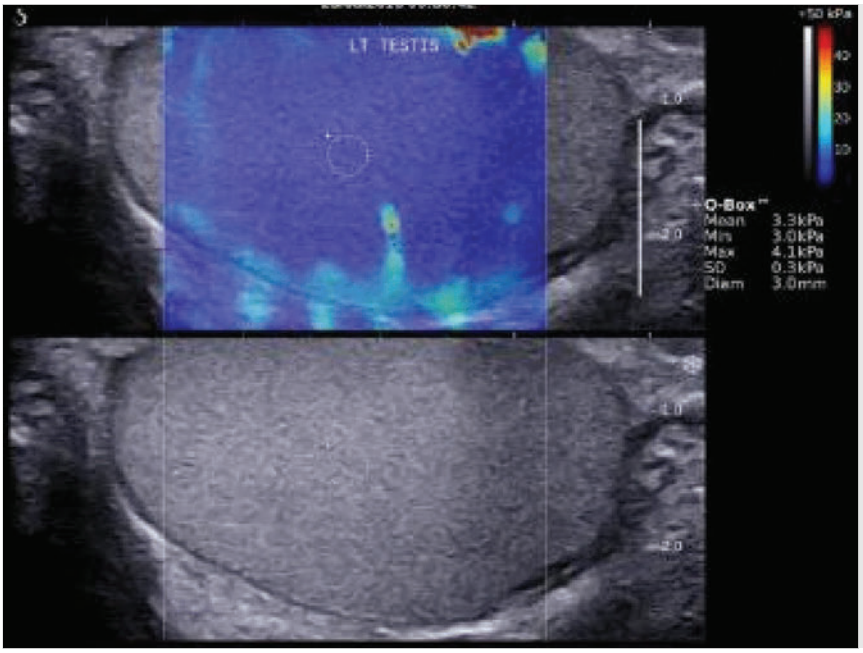

Fig. 11.17 Normal testis as shown at shear wave elastography.

a complete elastic pattern (scores 1 and 2), while malignant nodules exhibited a stiff pattern (scores 4 and 5) in 87.5% of the cases (▶ Fig. 11.18, ▶ Fig. 11.19). The authors concluded that SE could be a useful technique in selected cases, such as small testicular nodules and pseudonodules (in agreement with previous studies), having a good sensitivity and specificity in differentiating malignant from benign lesions. A very recent retrospective study[52] evaluated 50 patients affected by testicular lesions. In 34 out of 50 cases findings from histological examination and in 16 out of 50 cases findings from clinical and US follow-up were used as the reference standard. In this series, SE provided additional information in differentiating between malignant and benign lesions, showing a sensitivity of 100% (all testicular cancers appeared as hard regions, characterized by increased tissue stiffness), a specificity of 81%, and an accuracy of 94% in the diagnosis of testicular tumors. Neoplastic lesions were

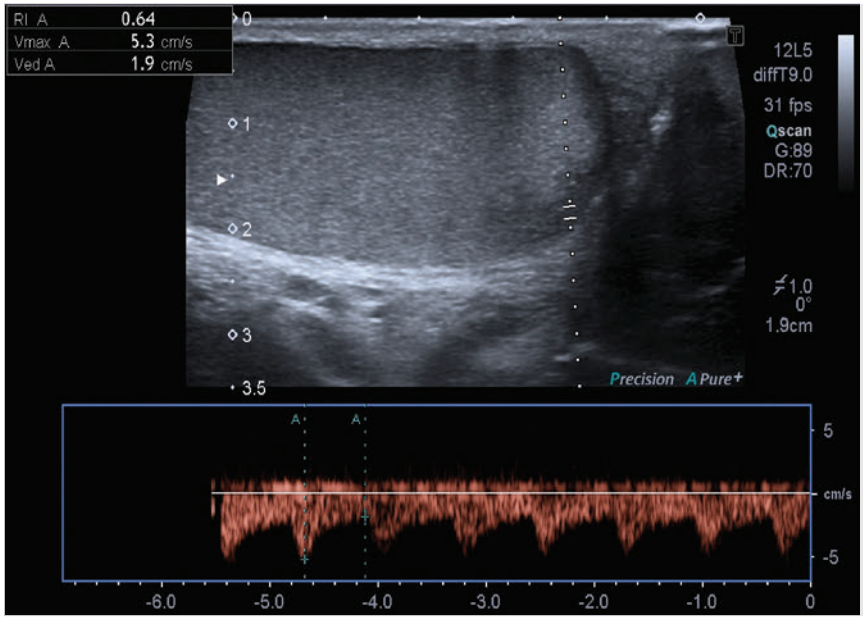

Fig. 11.18 Seminoma of the testis. Color Doppler ultrasound shows a hypoechoic area, with tiny peripheral color flow signal with low resistivity index (RI).

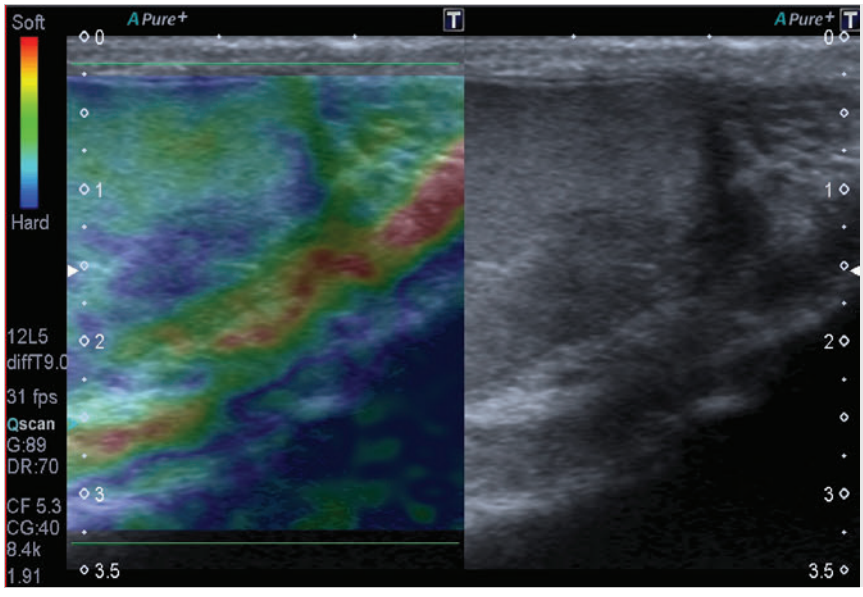

Fig. 11.19 Same case of Fig. 11.18. The testicular lesion at strain elastography appears blue, corresponding to a stiff lesion. Final histological diagnosis was a seminoma.

excluded in the absence of increased tissue stiffness (i.e., orchitis, partial infarction, and cysts, which appeared as soft). Authors concluded that this technique could be complementary to conventional US but could not be a stand-alone imaging modality. Huang et al[53] reviewed the potential of SE beyond conventional B-mode imaging in the characterization of both benign and malignant intratesticular lesions, confirming the existing data for stiff lesions as more likely to be malignant, and soft lesions as suggesting benignity.

On the contrary, application of SE to non-neoplastic cases might offer greater advantages. A number of scrotal diseases are associated with changes in tissue elasticity (atrophy or sclerosis of seminal tubules, inflammation, or traumas). Min Li et al correlated different scores of strain in 1,192 testes showing average or low strain (i.e., scores 3 to 5) in patients with non-obstructive azoospermia, and this rate was significantly higher than the rate in obstructive azoospermic and control testes. SE is a promising imaging method with great potential for the differential diagnosis of azoospermia.[54]

Artifacts and Pitfalls

SE has a number of limitations in improving the diagnostic rate of testicular masses.

On the technical side, involuntary movements, such as those related to tissue perfusion or breathing, can interfere with the generation of a proper elastogram; however, this limitation is minimal with the testis, making it an ideal tissue to be explored by SE.[47] The principal limitation of SE is related to the manual external compression source by which the tissue is deformed to create the strain. As the driving force is not exactly known, SE may only assess the compressibility ratio (strain ratio) of

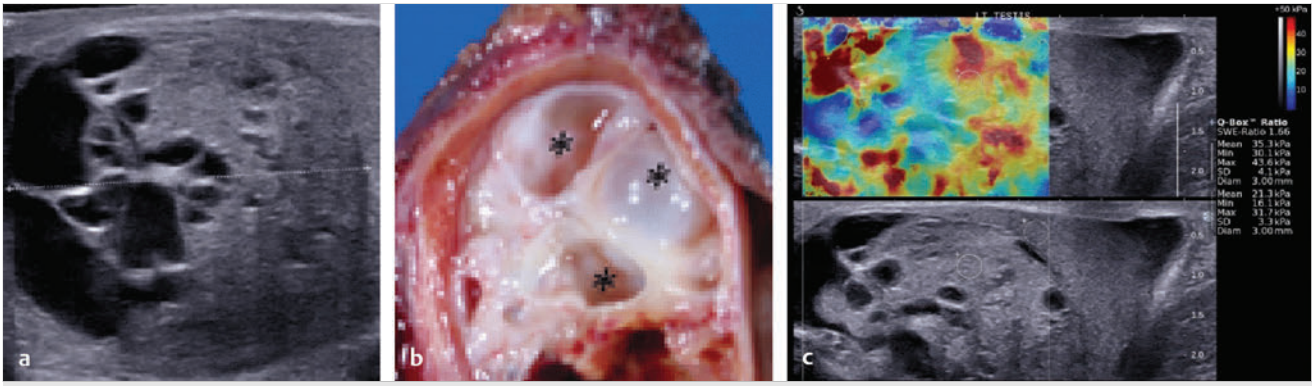

Fig. 11.20 Yolk sac cancer (solid and cystic). Appear as a solid and cystic lesion (**a**) at conventional ultrasound and (**b**) at gross pathology. It presents a heterogeneous appearance (**c**) at SWE.

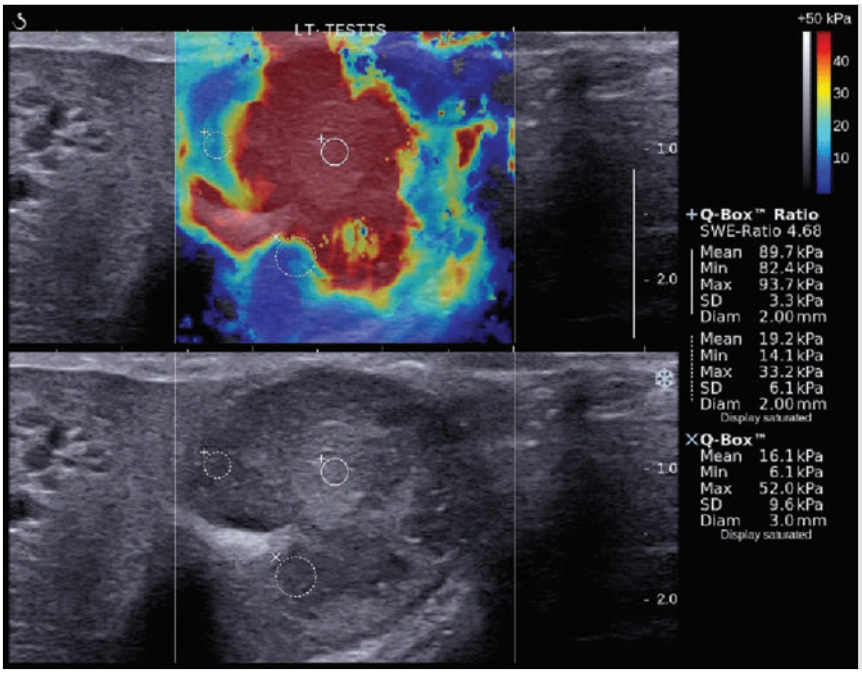

Fig. 11.21 Testicular seminoma. The hypoechoic lesion appears markedly stiff at SWE.

different tissues and consequently the relative elasticity, and not the absolute value of their strain.

An artifact resulting from nonuniform stress distribution is easily recognized by a priori information such as the shape of the tumor. Artifacts due to the nonlinearity of tissue are also observed. The nonlinearity becomes marked when the compression generates strain in excess of several percent.[55]

Pitfalls are mainly related to the characteristics of the lesions: intralesion calcifications are common and may bias the stiffness of the lesion as has been shown for peripheral calcifications. SE should be interpreted with caution in extensive cystic areas since fluid in the cystic areas may cause artifacts (▶ Fig. 11.20).

Interpretation of Results

While most malignant lesions appear stiff (e.g., seminoma), confirming the characteristics already reported in literature, some benign neoplastic lesions (e.g., leydigiomas) and benign or non-neoplastic lesions (e.g., epidermoid cysts) may also appear stiff. The SE pattern is quite similar in the presence of a focal testicular lesion, probably due to the high and tight cellularity typical of neoplasms. For this reason, the series published by Correas showed that the joint use of US and SE had no significant diagnostic improvement over the use of US and Doppler findings.[47]

11.4.2 Shear Wave Elastography Imaging

All the clinical conditions previously discussed may potentially be studied with SWE (▶ Fig. 11.21), but only one case report is present to date in the literature. This report showed the potential utility of SWE for identifying segmental infarction of the testis in the case of a man with acute scrotal pain. Other applications are yet to be explored.

11.4.3 Published Guidelines

There are only a few reports available in the literature regarding the efficacy of elastography for scrotal lesion evaluation, and in European Federation for Societies of Ultrasound in Medicine and Biology (EFSUMB) guidelines,[56] the testis is only mentioned in the final chapter on future perspectives. Elastography is identified as a possible tool to differentiate benign from malignant lesions.

11.4.4 Summary

Elastography is a simple, noninvasive diagnostic examination technique that adds tissue elasticity information to the morphological assessment of conventional US, and should be combined with conventional US for the characterization of testis lesions. Larger systematic clinical studies are required on the characterization of testicular lesions with this newly developed technique, with the purpose of further characterization of non-palpable testicular lesions, especially benign neoplasms, where follow-up or biopsies are now becoming increasingly requested as alternatives to radical surgery. Finally, elastography might offer greater advantages for the characterization of functional and non-neoplastic testicular disorders, applications that today still remain unexplored.

References

[1] Bialek EJ, Jakubowski W, Zajkowski P, Szopinski KT, Osmolski A. US of the major salivary glands: anatomy and spatial relationships, pathologic conditions, and pitfalls. Radiographics 2006; 26(3):745–763

[2] Klintworth N, Mantsopoulos K, Zenk J, Psychogios G, Iro H, Bozzato A. Sonoelastography of parotid gland tumours: initial experience and identification of characteristic patterns. Eur Radiol 2012; 22(5):947–956

[3] Yerli H, Eski E, Korucuk E, Kaskati T, Agildere AM. Sonoelastographic qualitative analysis for management of salivary gland masses. J Ultrasound Med 2012; 31(7):1083–1089

[4] Steinhart H, Zenk J, Sprang K, Bozzato A, Iro H. Contrast-enhanced color Doppler sonography of parotid gland tumors. Eur Arch Otorhinolaryngol 2003; 260(6):344–348

[5] Bhatia KS, Rasalkar DD, Lee YP et al. Evaluation of real-time qualitative sonoelastography of focal lesions in the parotid and submandibular glands: applications and limitations. Eur Radiol 2010; 20(8):1958–1964

[6] Dumitriu D, Dudea SM, Botar-Jid C, Băciuț G. Ultrasonographic and sonoelastographic features of pleomorphic adenomas of the salivary glands. Med Ultrasound 2010; 12(3):175–183

[7] Dumitriu D, Dudea S, Botar-Jid C, Baciut M, Baciut G. Real-time sonoelastography of major salivary gland tumors. AJR Am J Roentgenol 2011; 197(5): W924-W930

[8] Celebi I, Mahmutoglu AS. Early results of real-time qualitative sonoelastography in the evaluation of parotid gland masses: a study with histopathological correlation. Acta Radiol 2013; 54(1):35–41

[9] Mansour N, Stock KF, Chaker A, Bas M, Knopf A. Evaluation of parotid gland lesions with standard ultrasound, color duplex sonography, sonoelastography, and acoustic radiation force impulse imaging - a pilot study. Ultraschall Med 2012; 33(3):283–288

[10] Arda K, Ciledag N, Aktas E, Aribas BK, Köse K. Quantitative assessment of normal soft-tissue elasticity using shear-wave ultrasound elastography. AJR Am J Roentgenol 2011; 197(3):532–536

[11] Mantsopoulos K, Klintworth N, Iro H, Bozzato A. Applicability of shear wave elastography of the major salivary glands: values in healthy patients and effects of gender, smoking and pre-compression. Ultrasound Med Biol 2015; 41(9):2310–2318

[12] Bhatia KS, Cho CC, Tong CS, Lee YY, Yuen EH, Ahuja AT. Shear wave elastography of focal salivary gland lesions: preliminary experience in a routine head and neck US clinic. Eur Radiol 2012; 22(5):957–965

[13] Westerland O, Howlett D. Sonoelastography techniques in the evaluation and diagnosis of parotid neoplasms. Eur Radiol 2012; 22(5):966–969

[14] Wierzbicka M, Kałużny J, Szczepanek-Parulska E et al. Is sonoelastography a helpful method for evaluation of parotid tumors? Eur Arch Otorhinolaryngol 2013; 270(7):2101–2107

[15] Olgun DC, Kantarci F, Taskin U et al. Relative proportions of stromal to cellular components of pleomorphic adenomas: determination with shear wave elastography. J Ultrasound Med 2014; 33(3):503–508

[16] Badea AF, Tamas Szora A, Ciuleanu E et al. ARFI quantitative elastography of the submandibular glands: normal measurements and the diagnosis value of the method in radiation submaxillitis. Med Ultrasound 2013; 15(3):173–179

[17] Badea AF, Lupsor Platon M, Crisan M et al. Fractal analysis of elastographic images for automatic detection of diffuse diseases of salivary glands: preliminary results. Comput Math Methods Med 2013; 2013:347238

[18] Kałużny J, Kopeć T, Szczepanek-Parulska E et al. Shear wave elastography: a new noninvasive tool to assess the intensity of fibrosis of irradiated salivary glands in head and neck cancer patients. Biomed Res Int 2014; 2014:157809

[19] Wierzbicka M, Kałużny J, Ruchała M, Stajgis M, Kopeć T, Szyfter W. Sonoelastography—a useful adjunct for parotid gland ultrasound assessment in patients suffering from chronic inflammation. Med Sci Monit 2014; 20:2311–2317

[20] Zengel P, Schrötzlmair F, Schwarz F et al. Elastography: a new diagnostic tool for evaluation of obstructive diseases of the salivary glands; primary results. Clin Hemorheol Microcirc 2012; 50(1–2):91–99

[21] Bhatia KS, Lee YY, Yuen EH, Ahuja AT. Ultrasound elastography in the head and neck. Part I. Basic principles and practical aspects. Cancer Imaging 2013; 13(2):253–259

[22] Lai G, Rockall AG. Lymph node imaging in gynecologic malignancy. Semin Ultrasound CT MR 2010; 31(5):363–376

[23] Stramare R, Scagliori E, Mannucci M, Beltrame V, Rubaltelli L. The role of contrast-enhanced gray-scale ultrasonography in the differential diagnosis of superficial lymph nodes. Ultrasound Q 2010; 26(1):45–51

[24] Dabirmoghaddam P, Sharifkashany S, Mashali L. Ultrasound-guided fine needle aspiration cytology in the assessment of cervical metastasis in patients undergoing elective neck dissection. Iran J Radiol 2014; 11(3):e7928

[25] Saindane AM. Pitfalls in the staging of cervical lymph node metastasis. Neuroimaging Clin N Am 2013; 23(1):147–166

[26] Riegger C, Koeninger A, Hartung V et al. Comparison of the diagnostic value of FDG-PET/CT and axillary ultrasound for the detection of lymph node metastases in breast cancer patients. Acta Radiol 2012; 53(10):1092–1098

[27] Birkhäuser FD, Studer UE, Froehlich JM et al. Combined ultrasmall superparamagnetic particles of iron oxide-enhanced and diffusion-weighted magnetic resonance imaging facilitates detection of metastases in normal-sized pelvic lymph nodes of patients with bladder and prostate cancer. Eur Urol 2013; 64 (6):953–960

[28] Matsuzawa F, Einama T, Abe H et al. Accurate diagnosis of axillary lymph node metastasis using contrast-enhanced ultrasonography with Sonazoid. Mol Clin Oncol 2015; 3(2):299–302

[29] Rossi CR, Seno A, Vecchiato A et al. The impact of ultrasound scanning in the staging and follow-up of patients with clinical stage I cutaneous melanoma. Eur J Cancer 1997; 33(2):200–203

[30] Sohn YM, Hong IK, Han K. Role of [18F]fluorodeoxyglucose positron emission tomography-computed tomography, sonography, and sonographically guided fine-needle aspiration biopsy in the diagnosis of axillary lymph nodes in patients with breast cancer: comparison of diagnostic performance. J Ultrasound Med 2014; 33(6):1013–1021

[31] Lyshchik A, Higashi T, Asato R et al. Cervical lymph node metastases: diagnosis at sonoelastography—initial experience. Radiology 2007; 243(1):258–267

[32] Ying L, Hou Y, Zheng HM, Lin X, Xie ZL, Hu YP. Real-time elastography for the differentiation of benign and malignant superficial lymph nodes: a meta-analysis. Eur J Radiol 2012; 81(10):2576–2584

[33] Lo WC, Cheng PW, Wang CT, Liao LJ. Real-time ultrasound elastography: an assessment of enlarged cervical lymph nodes. Eur Radiol 2013; 23(9):2351–2357

[34] Rubaltelli L, Stramare R, Tregnaghi A et al. The role of sonoelastography in the differential diagnosis of neck nodules. J Ultrasound 2009; 12(3):93–100

[35] Bhatia KS, Cho CC, Tong CS, Yuen EH, Ahuja AT. Shear wave elasticity imaging of cervical lymph nodes. Ultrasound Med Biol 2012; 38(2):195–201

[36] Choi YJ, Lee JH, Lim HK et al. Quantitative shear wave elastography in the evaluation of metastatic cervical lymph nodes. Ultrasound Med Biol 2013; 39 (6):935–940

[37] Bhatia KS, Lee YY, Yuen EH, Ahuja AT. Ultrasound elastography in the head and neck. Part II. Accuracy for malignancy. Cancer Imaging 2013; 13(2):260–276

[38] Choi YJ, Lee JH, Baek JH. Ultrasound elastography for evaluation of cervical lymph nodes. Ultrasonography 2015; 34(3):157–164

[39] Alam F, Naito K, Horiguchi J, Fukuda H, Tachikake T, Ito K. Accuracy of sonographic elastography in the differential diagnosis of enlarged cervical lymph nodes: comparison with conventional B-mode sonography. AJR Am J Roentgenol 2008; 191(2):604–610
[40] Cosgrove D, Piscaglia F, Bamber J et al; EFSUMB. EFSUMB guidelines and recommendations on the clinical use of ultrasound elastography. Part 2: Clinical applications. Ultraschall Med 2013; 34(3):238–253
[41] Săftoiu A, Vilmann P, Hassan H, Gorunescu F. Analysis of endoscopic ultrasound elastography used for characterisation and differentiation of benign and malignant lymph nodes. Ultraschall Med 2006; 27(6):535–542
[42] Dietrich CF, Săftoiu A, Jenssen C. Real time elastography endoscopic ultrasound (RTE-EUS), a comprehensive review. Eur J Radiol 2014; 83(3):405–414
[43] Jenssen C, Dietrich CF. Endoscopic ultrasound-guided fine-needle aspiration biopsy and trucut biopsy in gastroenterology - an overview. Best Pract Res Clin Gastroenterol 2009; 23(5):743–759
[44] Xu W, Shi J, Zeng X et al. EUS elastography for the differentiation of benign and malignant lymph nodes: a meta-analysis. Gastrointest Endosc 2011; 74 (5):1001–1009, quiz 1115.e1–1115.e4
[45] Larsen MH, Fristrup C, Hansen TP, Hovendal CP, Mortensen MB. Endoscopic ultrasound, endoscopic sonoelastography, and strain ratio evaluation of lymph nodes with histology as gold standard. Endoscopy 2012; 44(8):759–766
[46] Paterson S, Duthie F, Stanley AJ. Endoscopic ultrasound-guided elastography in the nodal staging of oesophageal cancer. World J Gastroenterol 2012; 18 (9):889–895
[47] Correas JM, Drakonakis E, Isidori AM et al. Update on ultrasound elastography: miscellanea: prostate, testicle, musculo-skeletal. Eur J Radiol 2013; 82 (11):1904–1912
[48] Pallwein L, Pallwein E, Schurich M, Fischbach V, Steiner H, Frauscher F. Sonoelastography of the testicles: preliminary results in the diagnosis of different pathological processes. Paper presented at Fourth International Conference on the Ultrasonic Measurement and Imaging of Tissue Elasticity; October 16–19, 2005; Austin, TX
[49] Grasso M, Blanco S, Raber M, Nespoli L. Elasto-sonography of the testis: preliminary experience. Arch Ital Urol Androl 2010; 82(3):160–163
[50] Goddi A, Sacchi A, Magistretti G, Almolla J, Salvadore M. Real-time tissue elastography for testicular lesion assessment. Eur Radiol 2012; 22(4): 721–730
[51] Itoh A, Ueno E, Tohno E et al. Breast disease: clinical application of US elastography for diagnosis. Radiology 2006; 239(2):341–350
[52] Aigner F, De Zordo T, Pallwein-Prettner L et al. Real-time sonoelastography for the evaluation of testicular lesions. Radiology 2012; 263(2):584–589
[53] Huang DY, Sidhu PS. Focal testicular lesions: colour Doppler ultrasound, contrast-enhanced ultrasound and tissue elastography as adjuvants to the diagnosis. Br J Radiol 2012; 85(Spec No 1):S41–S53
[54] Li M, Du J, Wang ZQ, Li FH. The value of sonoelastography scores and the strain ratio in differential diagnosis of azoospermia. J Urol 2012; 188(5): 1861–1866
[55] Shiina T, Nightingale KR, Palmeri ML et al. WFUMB guidelines and recommendations for clinical use of ultrasound elastography: Part 1: basic principles and terminology. Ultrasound Med Biol 2015; 41(5):1126–1147
[56] Bamber J, Cosgrove D, Dietrich CF et al. EFSUMB guidelines and recommendations on the clinical use of ultrasound elastography: part 1: basic principles and technology. Ultraschall Med 2013; 34(2):169–184

12 Magnetic Resonance Elastography

Bogdan Dzyubak

12.1 Introduction

Magnetic resonance elastography, or MRE, is a quantitative dynamic elastography technique that images shear wave propagation with phase-contrast magnetic resonance imaging (MRI) to calculate the underlying stiffness of tissues.[1] The most established application of MRE is for the detection and staging of hepatic fibrosis. Mechanical changes have long been known to occur due to the deposition of connective tissue during the progression of fibrosis, and MRE has been shown to have a very high sensitivity and specificity, 98% and 99% respectively, for fibrosis detection,[2] which far surpasses any nonelastographic technique.[3,4,5,6,7,8,9] Furthermore, MRE is able to characterize the stiffness of the entire organ yielding a sample much greater than that obtained in biopsy (1/50,000th of the liver volume) or ultrasound transient elastography (1/100th). Between its Food and Drug Administration (FDA) approval in 2007 and the summer of 2015, the clinical hepatic MRE product has been implemented at over 450 sites worldwide and continues to be adopted at an increasing rate. Product versions of MRE are available from major MRI manufacturers (GE, Siemens, and Phillips) as an upgrade to standard 1.5-T and 3-T MRI systems and have standardized parameters. This includes the hardware for generating shear waves and delivering them to the patient, the imaging pulse sequence, and the stiffness calculation (inversion) software. Both the widespread use of hepatic MRE and the development of MRE applications for other organs and tumors will be covered in this chapter.

The acoustic waves used in MRE are generated by a dedicated active driver system. Due to the limitation on the use of magnetic components within a strong magnetic field, the active driver is typically located away from the MRI scanner or outside of the scan room, with energy delivered to the patient via a series of tubes or other connectors, and a passive driver coupled to the body. ▶ Fig. 12.1 illustrates the standard driver setups used for abdominal and brain MRE. This setup can deliver compressional sound waves to the body which are mode-converted to shear waves at interfaces between tissues with different acoustic impedances.[10] Because the majority of shear waves are generated in tissues, rather than at the driver surface, they have a shorter effective travel distance and experience less attenuation. Additionally, organs behind structures that attenuate shear waves, such as the skull, the rib cage, and fluid,[11] can be imaged with this approach. The passive driver can come in the form of a plastic "drum" or a soft "pillow." The pillow driver, while generating waves with slightly lower efficiency, tends to have a better connection with the body resulting in better energy transfer. As a result, the waves delivered to the liver still have sufficient amplitude and are more parallel, which leads to lower interference and more accurate stiffness images (elastograms). The pillow driver is also more comfortable for the patient. For custom applications higher shear wave frequencies (> 60 Hz) may be useful. These can be generated more efficiently by custom drivers which will be discussed in Section 12.3 Emerging Applications.

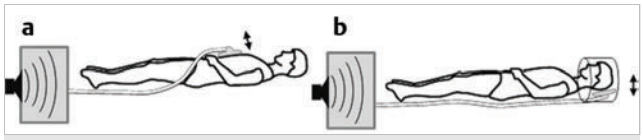

Fig. 12.1 Common setups for commercial acoustic drivers for liver (**a**) and brain (**b**) magnetic resonance elastography.

Either two-dimensional (2D) slices or three-dimensional (3D) volumes can be acquired in MRE, thus allowing whole organs to be characterized. Shear wave propagation information is encoded into the MRI phase images while anatomical information is contained in the magnitude image (▶ Fig. 12.2). The encoded phase is directly proportional to the displacement of tissue at every pixel along the direction of motion encoding (typically done in the through-plane direction for clinical MRE). Multiple phase images, with different offsets between the applied motion and encoding (called phase-offsets), are typically acquired to image the wave propagation over time. High-amplitude motion may lead to a phase-wrapping artifact. Phase images are typically preprocessed using phase unwrapping, directional filtering, frequency filtering or curl processing[12] (to remove longitudinal waves), polynomial fitting, or another method of smoothing.[13] The processed phase images are commonly referred to as *wave images*. From these, the quantitative elastogram which contains stiffness values at every pixel in units of kilopascals (kPa) is calculated. The wave images and elastograms, or stiffness maps, are often displayed in color but may also be in grayscale.

The clinical version of MRE uses a standard inversion, with fixed parameters, to calculate the elastograms. A number of inversions have been developed for the preclinical applications in other organs. Different elasticity parameters may be calculated

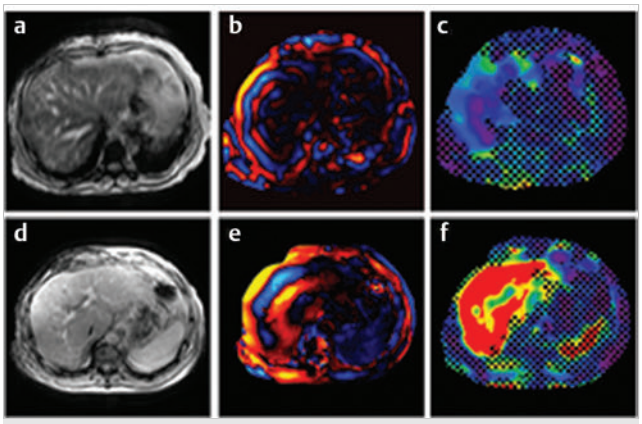

Fig. 12.2 Hepatic magnetic resonance elastography (MRE) of a normal (**a, b, c**) and a fibrotic (**d, e, f**) patient. Pathology cannot be identified on the magnitude image (**a, d**) but is clear on the elastograms (**c, f**). The checkerboard pattern represents a mask based on the standard confidence threshold of 95%. Note that wave attenuation is higher in soft livers, resulting in (**e**) having higher wave amplitude than (**b**).

by the inversions all of which may be loosely referred to as "stiffness" in the literature. Shear modulus, G, is a complex-valued parameter which consists of the storage, G', and loss, G'', moduli, $G = G' + i^*G''$ (sometimes denoted $\mu = \mu_r + i^*\mu_i$). G' describes how energy is stored and released by tissue. It is sometimes reported as "stiffness" in publications. G'' is associated with energy loss in tissue and a delay in stimulus response. A purely elastic material would have $G'' = 0$, no attenuation, and exhibit no delay between applied stress and the response of the tissue. Inversions using shear wave speed (c_s) or wavelength (λ) to calculate stiffness cannot calculate G' and G'', instead calculating an effective shear modulus equal to $\rho^*c_s^2$ or $\rho^*(\lambda^*f)$,[2] where ρ is the tissue density and f is the vibration frequency. Inversions calculating the complex shear modulus may report either its individual parts or its absolute value: $|G| = \sqrt{(G')^2 + (G'')^2}$. This quantity is also called "stiffness" or "shear stiffness" in many publications and is the quantity calculated by the FDA-approved clinical version on MRE. The magnitude of the shear modulus, $|G|$, will always be greater than the storage modulus, with the difference ranging between 10% and 50% for most tissues, depending on the value of G''. Young's modulus, reported in ultrasound, is very nearly equal to $3|G|$. Note that all shear moduli have units of kilopascals (kPa). Clinical hepatic MRE reports the shear modulus, which is directly related to Young's modulus used in ultrasound. The moduli used in other applications are noted in the corresponding sections. Custom inversions may be able to calculate other parameters, usually requiring multifrequency acquisitions,[14,15,16,17] which may have a higher predictive value than stiffness in a particular application. The shear and loss moduli, as well as the shear wave attenuation, tend to increase with frequency, and their values should only be compared at the same, or similar, frequencies.

Note that all MRE stiffness values in this chapter are given as the shear modulus, G, expressed in kilopascals (kPa), which is approximately one-third of Young's modulus, which is reported with the ultrasound techniques and also expressed in kilopascals.

The value of MRE has been investigated for a number of applications other than hepatic fibrosis staging. Feasibility has been demonstrated in organs such as the brain, kidneys, muscle, and lungs, as well as for tumors in the breast, brain, and liver. A number of applications have demonstrated tentative diagnostic value and are areas of active research and may be available for clinical purposes in the future. The FDA-approved hepatic application with well-established parameters and setup will be covered first, followed by the preclinical applications, which may use either the clinical version of MRE or custom drivers and inversions.

12.2 Magnetic Resonance Elastography of Hepatic Fibrosis

The most clinically important and widespread application of MRE is for the detection and staging of hepatic fibrosis. Cirrhosis, with complications in the form of hepatocellular carcinoma and portal hypertension, is among the leading causes of death in many developed countries. Conditions such as hepatitis B and C, nonalcoholic fatty liver disease (NASH), pharmacological toxicity, and biliary obstruction can all lead to inflammation and necrosis of liver parenchyma followed by deposition of a significant amount of extracellular connective tissue resulting in liver fibrosis and, if this process continues, cirrhosis. MRE is able to detect the increase in hepatic stiffness resulting from fibrosis with a remarkable sensitivity of 98% and specificity of 99%.[2] Recent evidence shows that fibrosis can be reversed effectively by removal of etiology of chronic liver disease, especially in the case of chronic viral hepatitis with the use of new antiviral treatment.[18,19] With the emergence of new therapies and the promise for reversibility of liver fibrosis, a noninvasive and reliable method for fibrosis staging is important for both drug trials and individual patient follow-up and dose optimization. The current gold standard, liver biopsy, carries a risk of complications and is prone to error due to its small sample size and poor interobserver agreement.[20,21,22] MRE is able to stage fibrosis noninvasively with high accuracy,[8] which is significantly better than a serum liver function test[3,23] or any other non-elastography method.[6]

Ultrasound transient elastography (FibroScan, Echosens, Paris, France) is another method which is able to diagnose fibrosis based on the change in stiffness. It obtains a quantitative stiffness measurement along a one-dimensional (1D) line using an ultrasound transducer to both excite and sample the shear waves. ARFI-based ultrasound elastography techniques can measure liver stiffness in a small (5 mm x 5 mm) region of interest (point shear wave elastography, [pSWE]) or in a larger field of view of about 20 cm^3 (two-dimensional shear wave elastography [2D-SWE]). Some vendors provide real-time 2D-SWE assessment of liver stiffness. MRE has the advantage of being able to sample the entire organ, reducing sampling error, and has little operator dependence. Its accuracy is better than or equal to that of transient elastography,[23,24,25,26] while the cost of MRE, when done as part of a limited MR exam, is approximately twice as high as that of FibroScan.[26] Contraindications for MRE include those for any MRI study such as patient claustrophobia or metallic implants, though many recent implants, even pacemakers, are made to be MR-safe with limits to the acquisition sequence.[27]

Two hepatic MRE exams of a nonfibrotic and a cirrhotic patient are shown in ▶ Fig. 12.2. The MRI magnitude images, (**a**) and (**d**), show anatomical images. In (**b**) and (**e**), single-phase images are shown, containing a snapshot of wave-propagation information. The wavelengths in the cirrhotic patient, in (**e**), are longer than those in the normal patient. This difference is reflected in the elastograms, (**c**) and (**f**).

The average hepatic stiffness of healthy subjects at 60 Hz is about 2.1 to 2.3 kPa in the Western population[7,28,29] and 2.1 kPa in the Asian population.[30] Sex, age, and body mass index do not appear to affect liver stiffness. The diagnostic threshold for separating healthy liver from stage 1 fibrosis is widely accepted as 2.93 kPa.[2] The diagnostic gray zone around this threshold in which patient history should be considered with most care is approximately ±0.5 kPa and is roughly based on the standard deviation of stiffnesses in normal subjects, which is 0.3 to 0.6 kPa.[2,7] Longitudinal differences in liver stiffness of approximately 20 to 30% (0.6–0.9 kPa for patients with suspected fibrosis) usually represent meaningful changes. Suggested cutoff stiffnesses for higher fibrosis stages can be found in the

literature.[2,23,24] A number of recent studies using data from large populations retrospectively have confirmed the high accuracy of MRE in fibrosis staging. These studies may lead to a refinement of initial staging thresholds, possibly providing separate cutoff values for different etiologies.[3,8,9]

The liver is one of the easiest organs for performing elastography as the inversion assumptions are well satisfied due to its size and relative homogeneity and isotropy. Many approaches to acquisition and inversion can yield good results in hepatic tissue. Furthermore, new MRE methods, such as multifrequency MRE[31] or faster acquisitions approaches,[32] are often tested in the liver. While research papers have significant variation in methodology and parameter settings, the technique used in the FDA-approved clinical MRE is highly standardized. The repeatability of MRE using this methodology is very high, with intraclass correlation coefficients being well above 0.9 for the stiffnesses obtained for repeat acquisitions on the same scanner,[33] cross-vendor comparisons,[34] and the stiffness calculation from the acquired images.[33] The failure rate is also fairly low (about 5.6%) and occurs mainly due to iron overload in the liver or operator error during the MRE driver setup.[35] Iron overload causes a decrease in signal intensity due to its T2* effect limiting the ability to monitor the shear waves. Due to the high accuracy, noninvasiveness, and high reproducibility of MRE, a number of clinics are using it in place of biopsy as the primary method of fibrosis detection.

The most common indication for an hepatic MRE exam is the presence of known risk factors for fibrosis, such as fatty liver disease, viral hepatitis, or another chronic liver disease. Follow-up of patients with known fibrosis is another common indication. MRE acquisition takes less than a minute, with the elastograms subsequently calculated on the scanner automatically in less than 3 minutes. The data is then transferred to a workstation for region of interest (ROI) drawing performed by technicians or radiologists with special training. MRE can be performed anytime during a liver MRI study or as a single acquisition for the purpose of evaluation of hepatic fibrosis. The liver stiffness is not affected by the presence of gadolinium contrast agents and therefore can be performed before or after a contrast injection.[36] Typically, MRE is performed as part of a full or limited abdominal MRI protocol. The combination of MRE and Dixon sequence, enabling fat and iron quantification, is diagnostically beneficial and can be performed in less than 10 minutes.

12.2.1 Acquisition

The standard clinical application uses an acoustic active driver (▶ Fig. 12.1a) to deliver 60 Hz waves to a passive driver placed on the abdominal wall of the patient, typically under a receive-only torso coil array used to boost the signal-to-noise ratio (SNR), and secured with an additional strap. A soft passive driver may also be used. Vibration amplitude is typically set at 50% or less of the active driver's maximum setting[37] to achieve sufficient wave penetration across the liver.

The images are typically acquired on a 1.5T or a 3T scanner, with sequences available from all major manufacturers. Imaging at 3T generally provides a better SNR; however, it can lead to a higher failure rate in the liver as iron-related signal loss is more significant at 3T and increased iron in the liver co-occurs with fibrosis.[38,39]

Typical imaging parameters include: 4 slices, each with 4 phase offsets and a resolution of 1.7 × 3.4 × 10 mm. Signal saturation below and above the slice of interest and first gradient moment nulling are used to remove blood-flow artifacts. Each slice (all phase offsets) is acquired during a 14 second breath-hold performed at end expiration for reproducibility and tolerability. The superior and inferior slices should be at least 1 cm into the liver to avoid through-plane wave propagation artifacts. The full image acquisition is performed in less than 1 minute and has no operator dependence. A 3D-MRE acquisition, with motion encoding in all three directions, and corresponding inversions have been developed for the liver.[31,40] However, the acquisition typically requires multiple breath-holds, which can create inconsistencies between slices and time offsets, and the time requirements are approximately 10 to 15 times greater than for the 2D sequence. For this reason, 2D hepatic MRE, which is effective as long as elastograms are screened for artifacts,[41] remains the standard.

12.2.2 Processing and Quality Control

The processing of clinical liver MRE images is referred to as the multimodel direct inversion (MMDI) algorithm. In a preprocessing step, phase unwrapping and directional filtering are performed and waves with spatial frequencies below 2 cycles per field of view (FOV) and above 128 cycles per FOV are filtered from the image. A processing window of 11 × 11 pixels is used to calculate the elastogram as well as the confidence map for masking out regions with low wave quality. All clinical MRE, as well as research MRE using this implementation, are reported from elastograms masked at 95% confidence to remove regions with low wave quality. To exclude areas with partial-volume or wave-propagation artifacts, magnitude, phase, and elasticity images are reviewed manually to select a ROI for the stiffness measurement which includes all parenchyma while avoiding:

- Nonhepatic tissue such as blood vessels, hepatic fissures, kidneys, gallbladder, intestines, tumors, etc.
- Voxels within 5 pixels of the liver boundaries (half the size of the processing kernel) and their partial-volume.
- Areas where waves are not planar or concentric. While directional filtering is able to handle some wave interference, prominent "swirling" or standing-wave patterns can cause a biased stiffness estimate.

An ideal exam should have more than 50 cm^3 of artifact-free hepatic tissue available (2000 pixels using the standard resolution) to avoid sampling error and concerns about latent artifacts. The wave-analysis step in the ROI selection process is especially subjective and so the ROI selection should be performed only by trained readers. While the reproducibility of the stiffness measurement from elastograms is good, with intraclass correlations above 0.9 measured in multiple studies,[30,42,43] the interreader variability is the largest limitation to MRE reproducibility.[33] An automated method for selecting ROIs has also been developed and validated,[42] although it is mainly used in research settings at this time.

12.2.3 Physiological Confounders

Patient-specific parameters should always be considered, as in some cases they can affect stiffness and, potentially, confound the diagnosis or staging of disease. Hepatic MRE should be performed on patients in a fasting state, as food intake has been observed to increase liver stiffness by 5 to 48%, particularly in fibrotic patients. The cause of this is likely increased mesenteric flow and portal pressure in the liver, which is not compensated for as effectively in fibrotic patients due to disrupted homeostatic mechanics.[44] Other acute or chronic obstructions to the flow of bile or blood may also lead to increased hepatic stiffness. Both hepatic and splenic stiffnesses were found to increase with portal hypertension, which can develop in advanced fibrosis.[45] The measurement of the spleen stiffness has been suggested as a way to account for portal hypertension as a confounding variable.[40] It may be possible to calculate tissue pressure directly during an MRE exam by using a multifrequency acquisition and a poroelastic inversion,[46] although this method is not at a stage for routine clinical use at this time. Inflammation of the liver parenchyma, which may occur in patients with active hepatitis C, for example, can also lead to increased hepatic stiffness.[47,48] Hepatic steatosis (deposition of fat in the liver) does not appear to affect stiffness.[2] On the other hand, nonalcoholic steatohepatitis (NASH), which is characterized by inflammation and fibrosis, does affect stiffness and can be distinguished from steatosis alone with high accuracy.[49]

12.3 Emerging Applications

The ability to measure tissue elasticity information is relatively new and its value in various organs and diseases is under active investigation. MRE offers unique advantages in the characterization of several organs. Brain elastography, for example, is currently only feasible with MRE due to strong attenuation of ultrasound signals by the skull. In addition, 3D imaging and motion encoding made possible by MRE allows the complicated wave propagation in heterogeneous organs, like the kidney, or hollow organs, like the heart, to be captured, possibly enabling more accurate stiffness reconstructions. More sophisticated inversions calculating additional elasticity parameters, such as porosity or dispersion information, from multidirectional or multifrequency wave information have also been developed and their clinical value for different applications is being investigated. The following sections will summarize the preferred setups and inversions for use in several organs and the current physiological and pathological findings of those applications.

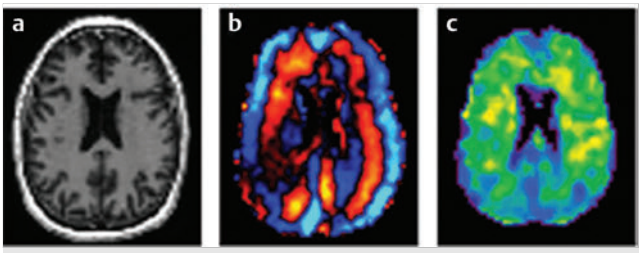

Fig. 12.3 Example of brain magnetic resonance elastography (MRE). (**a**) Anatomical magnitude image; (**b**) shear waves are generated by the skull and propagate inward from all directions (sagittal and coronal motion images not shown); (**c**) elastogram is eroded from cerebral spinal fluid (CSF) by the size of the processing kernel. (Courtesy of Dr. John Houston and Dr. Arvin Arani.)

12.3.1 Brain Magnetic Resonance Elastography

MRE of the brain is an area of active research and significant clinical interest. Changes in the mechanical properties of brain tissue may be a way to detect disease at early stages before anatomical changes take place, or to better characterize distributed damage such as that due to traumatic brain injury. While studies of brain deformation involving tissue stress–strain measurements have been previously performed, the results are highly variable due to the difference in approaches and the fact that the applied stresses may not be well known, and that the measured strain is a relative quantity. A large number of ex vivo mechanical studies of the brain have been performed, but the differences in preparation methods, the type of tissue studied, and animal species studied make results significantly variable.[50,51,52] Due to attenuation within the skull, the only ultrasound elastography application in the brain has been in intraoperative procedures.[53] MRE is thus the only technique at the moment capable of providing absolute quantitative insight into the viscoelastic properties of in vivo normal brain physiology and disease processes noninvasively. A set of MRE images from a brain exam are shown in ▶ Fig. 12.3. The normal brain stiffness has been calculated by several studies and is shown in ▶ Table 12.1.

As can be seen in ▶ Table 12.1, the mean stiffness of the normal brain has been measured in numerous studies and has resulted in fairly similar values. However, due to the studies having used different frequencies and inversions and some studies having limited patient populations, more investigation is needed to understand the range of normal variations and to determine the threshold stiffness for different diseases.

Table 12.1 Normal brain stiffnesses reported by different sources

Subjects	Frequency (Hz)	Stiffness (kPa)	Quantity calculated	Study
45	60	2.6–3.0, depending on region	G'	Arani et al 2015[54]
38	25–62.5	WB: 3.3	$\|G\|$	Streitberger et al 2012[55]
10	60	WB: 2.99, CB: 2.38	$\|G\|$	Murphy et al 2013[56]
8	80	WM: 2.41 + *i*1.21	$G' + iG''$	Zhang et al 2011[57]
5	90	GM: 3.1 + *i*2.5, WM: 2.7 + *i*2.5	$G' + iG''$	Gree et al 2008[58]

Abbreviations: WB, whole brain; WM, white matter; GM, gray matter; CB, cerebellum.

The normal brain stiffness has been observed to change based on age and sex, so patient matching should be done when drawing comparisons. Significant differences in regional brain stiffness based on age and sex have been reported in an older adult population.[54] The cerebrum, as well as the frontal, temporal, occipital, and parietal lobes, were reported to become approximately 10 to 15% softer between the ages of 60 and 90 years. Female occipital and temporal lobes were 10% and 5% stiffer than their male counterparts. Another study,[59] using a greater age range of 20- to 80-years-old, found a linear decrease in the shear modulus of 150 Pa (or 8% stiffness) per decade, with the ratio of storage modulus to loss modulus remaining the same with age and with women having stiffer brains than men.

Diseases such as multiple sclerosis (MS) and Alzheimer's disease (AD) cause axonal degradation secondary to demyelination and plaque buildup, respectively. Investigations were done into whether or not these processes lead to mechanical changes detectable by MRE and have yielded tentatively promising results. One study of AD[60] found a significant difference between the median whole-brain stiffnesses of AD patients (2.2 kPa, range 1.96–2.29; $n = 7$) and gender- and/or age-matched Pittsburgh compound B [PIB]-negative controls (2.37 kPa, range 2.17–2.62; $n = 7$) and PIB-positive cognitively normal controls (2.32 kPa, range 2.18–2.67; $n = 7$), with the two control groups not being significantly different. Similarly, an animal study using an AD mouse model found a 22.5% lower stiffness in diseased mice than the control mice.[61]

Patients with MS were also found to have a reduced brain stiffness (-20%) in a study of 23 patients and 38 controls.[55] The value of alpha, the power law exponent determining the frequency dependence of stiffness, also decreased by 6.1%. The patients were at a moderate-advanced disease stage, however, with brain volume loss in the range of 1.7 to 7.5%. In a mouse model, it was found that demyelination caused a significant reduction in viscoelasticity parameters, with the loss modulus decreasing faster than the storage modulus. The stiffness change was found to be reversible if remyelination occurred.[62]

Normal pressure hydrocephalus (NPH), a condition characterized by dementia and a progressive gait disorder, is another condition where shear and loss moduli of patients have been found to be significantly lower, by about 20%, than those of the normal volunteers.[63] The exponent of the power law material model used in this multifrequency study was also decreased in patients by 9%, causing the stiffness to increase less with vibrational frequency. This parameter was described as a measurement of tissue structure by the authors. Three months following shunt treatment to drain cerebrospinal fluid (CSF), the patient shear moduli and the structure parameter increased and ceased to be significantly different from those of the normal volunteers.

Finally, a study of autoimmune encephalomyelitis (AE) in rats also found that acute necroinflammation (14 days after immunization) leads to a decrease in both storage and loss moduli.[64] The moduli normalized at day 28, corresponding to the clinical recovery stage. Interestingly, this finding is the opposite of the necroinflammation studies in the human liver which found that stiffness increases with inflammation.[65,66] Further studies into the effects of these physiological changes are warranted.

In most diseases (except brain tumors, covered in Section 12.3.2, Tumor Characterization and Treatment Response), the stiffness (including the storage and loss moduli) and sometimes the exponential frequency scaling coefficient have been observed to decrease with respect to the normal value. The results in AD, MS, NPH, and AE are intriguing, though further studies evaluating the diagnostic performance of MRE with respect to existing methods and in the context of different disease stages are needed. The new information provided by elastography may be of value either as a standalone or as an additional biomarker for these diseases.

Acquisition

To deliver waves into the brain past the mechanical shielding of the skull, instead of applying shear waves directly to the skull, brain MRE shakes the skull (▶ Fig. 12.1b) to generate shear waves at internal interfaces through inertial effects. In all brain MRE techniques used in clinical studies, the head itself is rocked either via an acoustic pillow driver[54] or by an electromechanically driven head cradle.[67] In mice studies, an electromechanically driven bite-bar driver has also been used.[64]

As the direction of motion in the brain cannot be guaranteed to be planar, full 3D-MRE acquisitions and inversions are used in the brain. Either single-frequency excitations (in the 60–100 Hz range)[54,68] or multifrequency excitations (with 4 frequencies in the 25 to 62.5 Hz range) have been used.[59,63,67,69] The choice of excitation frequency is a balance between the resolution of the elastogram and wave attenuation. At 100 Hz, approximately 50% of the brain (deep tissue) has been masked out due to having an insufficient SNR in some studies.[52] The use of higher frequencies allows different structures, such as white and gray matter, to be separated without significant partial-volume effects. Thus, lower frequency approaches typically report larger regional or whole-brain stiffnesses. Multifrequency MRE allows additional parameters, such as the power law coefficient for stiffness change with frequency or poroelasticity coefficients, to be calculated. At this time, these additional parameters have not been demonstrated to give a better separation between normal and abnormal tissues than stiffness alone. Other sources of vibration, including physiological cardiac pulsation,[70] motion of the patient table,[71] and patient humming[69] (with frequency recorded by a microphone being used to adjust gradient encoding frequency) have been explored. While the motion amplitude of these approaches is generally sufficient, their reproducibility is not as high as that for a more typical driver system.

The images are typically acquired using 3T scanners, and sometimes higher field strengths. Susceptibility-related signal fall-off, such as that seen in the liver and lung, is not as big a concern in the brain, except in the vicinity of sinuses which contain air. The higher field strength is preferred for better SNR.

Processing and Quality Control

A direct inversion (DI) of the Helmholtz equation is typically used to calculate the stiffness in brain MRE. Additional parameters may be calculated if multiple frequencies are acquired, and curl filtering, enabled by the full 3D vector MRE acquisition,

is almost always used as a preprocessing step to remove longitudinal waves.

Due to the irregular shape of tissue boundaries both within and at the surface of the brain, a small-sized processing kernel is typically used in the brain (3 × 3 × 3 voxels, vs 11x11 for liver) to improve the resolution of the elastogram. This leads to increased variability in the reconstructed stiffness, manifesting as "spike" noise. A median filter can be used to reduce the elastogram noise and has been used to smooth data for display purposes. Reporting median stiffnesses, rather than mean stiffnessses, is another way to reduce the noise.[54] A more traditional smoothing filter (moving average or gaussian smoothing), is not effective at removing the spike noise, however.

There are several approaches to prevent partial-volume effects from different tissues (especially CSF), which are blurred together due to the effective inversion kernel size, from biasing the stiffness of a region. One suggested solution to the trade-off between excluding regions affected by partial-volume effects and keeping as much of the brain tissue as possible was to design all filtering and processing kernels in the spatial, rather than the spatial-frequency, domain, so that the extent of the bias from partial-volume effects is known exactly.[56] The resulting kernels required 3 pixels to be eroded from the masks to avoid partial-volume effects. Additionally, an image classification technique based on a separately acquired and registered registered 3D Inversion Recovery-Spoiled Gradient echo (IR-SPGR) T1 volume[56] with high anatomical quality has been used to calculate fractions of white matter, gray matter, and CSF in each voxel and to remove voxels with > 30% CSF.[72] Another approach, which has been applied to finite-element inversions, but need not be limited to them, was to regularize the stiffness inversion itself based on tissue segmentations.[73] This approach makes it more likely for voxels that were segmented as the same tissue type to have similar stiffnesses in the elastogram. As long as the segmentation, done on a separate high-quality T1-weighted anatomical magnetized-prepared rapid acquisition gradient echo magnetic resonance imaging (MPRAGE MRI) is reliable and the registration of the images is good, this approach has the advantage of being able to handle complex tissue boundaries.

Automated segmentation of anatomical images is used actively to determine whole-brain ROIs or measure regional stiffnesses using a registration-based atlas segmentation.[54] The success of the segmentations is enabled by minimal patient motion of the head during brain MRE scans and fairly consistent relative tissue intensities.

Wave attenuation is high in the brain, as reflected by the loss modulus being an order of magnitude higher than that in the liver, and a metric for excluding low SNR regions is useful. Motion SNR, measured directly from phase images, has been used to mask the brain with a threshold of 5.[56] The shear-strain SNR has been suggested as a more direct way of predicting the bias of noise on the stiffness reconstruction.[74] Its calculation requires motion encoding in all three directions, which is available in brain MRE. A threshold of 4 has been suggested for brain tissue. However, the value of shear-strain SNR changes with wavelength and the value of the threshold may need to be redefined depending on the frequencies used. Nearly all SNR or quality-of-fit measurements change with frequency filtering (smoothing), acquisition resolution, and the size of the processing kernel, so these should be kept constant whenever possible. No manual ROI selection is done in brain MRE to exclude areas with wave interference, though manual segmentation of brain tissue types based on the anatomical images is sometimes done.

Physiological Confounders

As discussed previously, age, sex,[54] and inflammation,[64] are known to affect brain stiffness. Intracranial pressure is also likely to be a factor based in the observed changes in stiffness seen in the liver due to portal hypertension.[44]

12.3.2 Tumor Characterization and Treatment Response

The microenvironment of tumors often contains a significant amount of connective tissue, which is organized differently from normal parenchyma. Tumors in superficial organs, such as the breast and lymph nodes, are commonly screened using palpation as their elastic properties are known to contrast with regular tissues. Increased stiffness of the tumor microenvironment has additionally been observed to contribute to tumor progression and metastasis.[75,76,77] The ability to quantitatively study the elastic properties of tumors noninvasively in vivo is new. This section demonstrates the feasibility of using MRE to measure tumor stiffness in a multitude of organs and examines the known clinical applications and preferred imaging methods for tumor MRE.

The stiffness of a tumor may be of direct clinical interest in some cases. During the resection of meningiomas in the brain, softer tumors can be removed with suctioning, while stiffer tumors require tedious dissections resulting in longer procedures. The stiffnesses of meningiomas in 12 patients were assessed using a standard brain MRE technique.[78] The stiffness measured with MRE was found to correlate significantly with the qualitative rating given by the surgeon at the time of operation and be a better treatment planning predictor than the T1- and T2-weighted anatomical MRI used currently.

The ability to distinguish benign tumors from malignant ones is of paramount importance. In the breast, contrast-enhanced MRI (CE-MRI) has the ability to detect tumors with a 98% sensitivity.[79] However, the technique lacks specificity, leading to many unnecessary biopsies. 3D-MRE performed at 65 Hz found that the shear moduli of cancerous tumors were higher than those of benign tumors (1.3 kPa for fibroadenomas and 1.2 kPa for mastopathy), which were stiffer than normal parenchyma (0.87 kPa).[12] A later study with 39 patients having malignant tumors and 29 having benign tumors found a similar, statistically significant, order of stiffnesses:malignant > benign > normal tissue.[80] Furthermore, using multifrequency data, the study determined that malignant lesions had a high power law coefficient (stiffness increased faster with frequency) and low attenuation, while benign tumors had the opposite relationship. The MRE-derived loss modulus was capable of separating the two groups with high accuracy (area under the receiver operating characteristic curve [AUROC] = 0.91) and when combined with CE-MRE led to a specificity increase from 40% (for CE-MRE alone) to 60%, with the AUROC increasing to 0.96. Similar

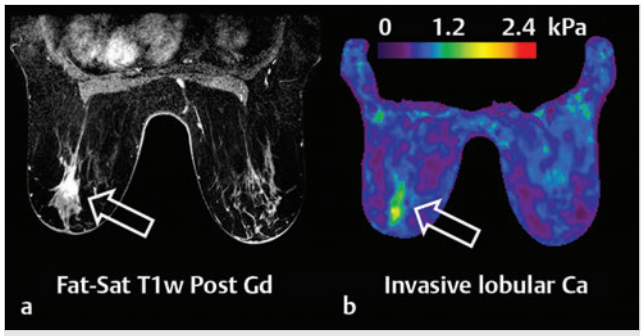

Fig. 12.4 Magnetic resonance elastography (MRE) of ductal carcinoma. (**a**) Contrast-enhanced magnetic resonance imaging (MRI) shows enhancing lesion; (**b**) MRE detects lesion with high contrast from parenchyma. (Courtesy of Dr. Jun Chen.)

results were observed in a later study of 57 patients where the accuracy of MRE alone rivaled that of CE-MRI (AUROC of 0.91 versus 0.93), and their combination resulted in an improvement of the AUROC to 0.96, mainly due to increased specificity.[81] An example of a breast tumor MRE is shown in ▶ Fig. 12.4.

In a study using a standard hepatic MRE setup and a 60 Hz driving frequency,[29] the calculated stiffnesses of malignant tumors (> 7.5 kPa) were significantly higher than the stiffnesses of liver parenchyma with advanced fibrosis, and much higher than the stiffnesses of benign tumors (~ 2.7 kPa), which were in the range of normal parenchyma-mild fibrosis. Another study of 76 patients[82] also found that malignant hepatic tumors were significantly stiffer than benign tumors. The absolute stiffnesses calculated in this study were lower due to the use of a 50 Hz driving frequency and, possibly, the type of inversion being used. Another study of 100 hepatic tumors in 63 patients found that both shear and loss modulus measurements outperformed hepatic CE-MRE-based separation of benign and malignant tumors. The loss modulus was found to be the best predictor of malignancy with an AUROC curve of 0.81.[83]

In a study of xenograft tumors in mouse brains which used 1000 Hz waves delivered via a bite-bar transducer, the stiffnesses of different types of tumors, including human gliomas (n = 8), rat gliomas (n = 7), and metastatic human breast carcinomas (n = 5), were significantly different from each other and from the stiffness of the brains of the control mice (n = 6).[84] In another study using humans (n = 16), malignant tumors tended to have lower stiffness than white matter and benign tumors (significance not evaluated).[85] This observation is different from results in the liver and the breast, where malignant tumors tend to be stiffest. The study speculates that normal neuronal tissue is highly organized resulting in it having a high stiffness, which is lost as the extracellular matrix deteriorates and the tissue is replaced with less-organized tumor tissue.

MRE has also been evaluated as a biomarker for chemotherapy response. In a study of implanted mouse flank tumors,[86] chemotherapy was given to 27 mice, with 8 mice kept as controls, over 4 days. The animals were imaged using shear waves delivered to the tumor via a needle driven by a piezoelectric stack at 800 Hz. The study found a significant difference in stiffness between the chemotherapy group, where tumor stiffness decreased, and the control group, starting on day 3. Tumor volume also decreased in the chemotherapy group but the change was not significant, which indicates that MRE may be able to demonstrate treatment–response effects earlier than volume-based measurements. Another study of mouse xenograft tumors[87] treated with a vascular disrupting agent (4 treated, 6 controls) demonstrated a significant decrease in the shear and loss moduli in the treatment group with respect to controls (the shear modulus being more significant) 24 hours posttreatment. The elasticity changed only in the center of the tumor, with the rim remaining at baseline, which agreed with postmortem pathology demonstrating hemorrhagic necrosis only in the center. The change in the apparent diffusion coefficient (ADC), a more established biomarker of tumor response measured with diffusion-weighted MRI, was not significant at this time point.

Studies characterizing tumor ablation response have also been performed. In a pig study, a 4.5 to 15 W laser was applied for 2 minutes to ablate hepatic tumors through an incision in the abdomen.[88] A custom inertial driver was attached to the applicator and used to deliver 60 Hz waves through it directly to the liver. The stiffness of the tumor increased significantly in response to ablation. The stiffness continued increasing in the minutes after ablation, and during pauses, most likely reflecting physiological response to damage. An interventional MRE setup using a needle driver delivering 100 Hz vibrations to the tumor intraoperatively and calculating stiffness in real-time has also been demonstrated.[89]

In summary, the ability of MRE to separate benign and malignant tumors has been tentatively demonstrated in the brain, liver, and breast. While the difference between all tumors and normal parenchyma were significant in these studies, the value of MRE in tumor screening has not been investigated due to the cost being higher than that of conventional techniques like ultrasound and mammography. Nonetheless, incidental findings are likely to happen as MRE continues to become more widespread. Finally, while studies of treatment response have provided tentatively promising results, validation in human subjects with end-point comparisons to existing response biomarkers is warranted.

Acquisition

3D-MRE is used for all tumor imaging as through-plane wave propagation cannot be avoided. The parameters of the MRI acquisition depend on the organ being imaged and can be found in the individual references.

Standard acoustic drum[29] and pillow drivers[90] have been used to image brain and liver tumors at 50 to 60 Hz. Several breast studies use unilateral[91] or bilateral[80] electromechanical drivers delivering 60 Hz vibrations through plate-shaped passive drivers. An approach that uses a pillow driver to deliver vibrations to the sternum to avoid precompressing the breast, which is a known confounding factor in MRE and ultrasound elastography,[92, 93] has also been demonstrated.[94] Finally, piezoelectric[86,89] and inertial drivers[88,95,96] have been used to deliver high-frequency vibrations to superficial tumors or deep tumors intraoperatively for improved elastogram resolution.

Processing and Quality Control

Tumor detection and contouring is done manually, often using separately acquired and registered anatomical images. The minimum tumor size quantifiable by the shear wave frequency

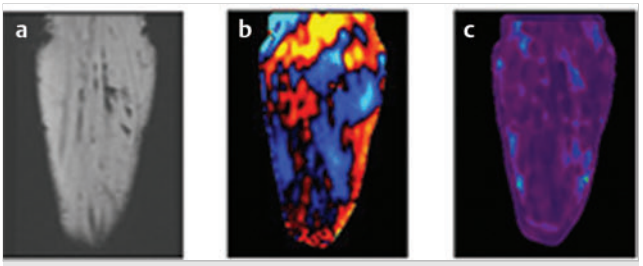

Fig. 12.5 Magnetic resonance elastography of the gastrocnemius muscle. Magnitude (**a**), phase (**b**), and elasticity (**c**) images. Only the axial direction of wave propagation (along the muscle fibers) is shown. (Courtesy of Roger Grimm.)

being used should be considered and regions with partial-volume effects should be excluded based on the size of the composite processing kernel if an absolute stiffness value is desired. Since a variety of frequencies are used in tumors, stiffnesses should only be compared between similar acquisition setups. Quantitative SNR metrics should be used for larger tumors imaged at high frequency as wave attenuation may be an issue.

Multiple inversions calculating different parameters have been applied to tumors based on one or more acoustic wave frequencies. Multiple elasticity parameters should be investigated for each application as some may be more useful than others. Due to the large variety of tumor types present in each tissue, it is likely that information from other modalities, such as diffusion, functional, or perfusion imaging, will be required for accurate characterization of some tumor types.

Physiological Confounders

The scope of physiological parameters that can affect tumor elasticity is not well known. Pressure and prestrain in the tissue and inflammatory activity, which are known to affect the stiffness of hepatic and brain tissue, are likely to affect tumor stiffness as well.

12.3.3 Other Organs

This section describes some studies in organs which are especially challenging to image or simply have not received as much research attention at this time. While the diagnostic stiffness thresholds and diagnostic utility have not been firmly established in these applications, they provide useful insight into additional physiological effects on MRE stiffness and alternative approaches to MRE acquisition.

The elastic properties of the lung are critical for healthy function and both restrictive lung diseases, such as pulmonary fibrosis, and obstructive diseases, such as emphysema, cause changes to the microenvironment which affect elastic properties. MRE of the lung was performed successfully using a short echo-time (short-TE) spin-echo acquisition to deal with the susceptibility-related signal loss.[97] Incidentally, this acquisition has also allowed MRE to be performed in livers with hemochromatosis,[98] a major cause of exam failures. A standard acoustic drum driver was used to deliver vibrations to the chest wall at 50 Hz. MRE images of the lung are shown in ▶ Fig. 12.5. Unlike the density of other tissues, lung density cannot be equated to

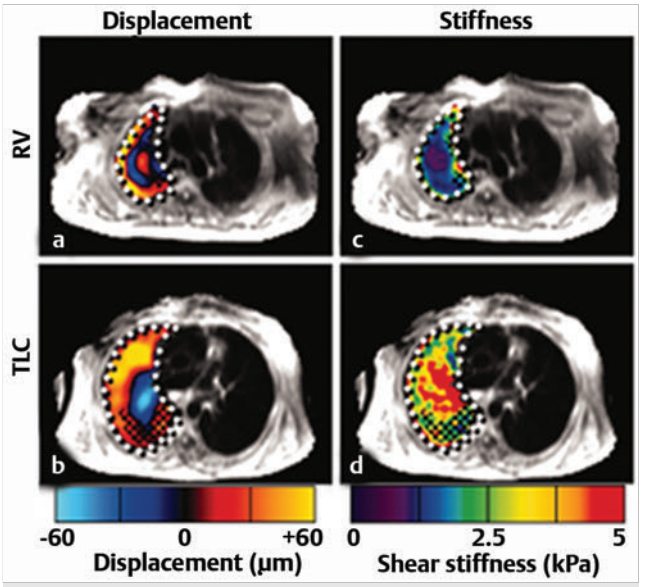

Fig. 12.6 Magnetic resonance elastography of the lungs. Wave images (**a, b**) and elastograms (**c, d**) overlaid on anatomical images are shown for the same patient at full expiration (RV, residual volume) and full inspiration (TLC, total lung capacity). (Adapted with permission from Mariappan YK, Glaser KJ, Levin DL, et al. Estimation of the absolute shear stiffness of human lung parenchyma using (1) H spin echo, echo planar MR elastography. J Magn Reson Imaging. 2014 Nov;40(5):1236.)

that of water and cannot be assumed to be constant, since it changes during the respiratory cycle (0.08-0.5 g/ml). Proton MR images were used to correct for tissue density, and lung stiffnesses were measured to be 0.9 kPa at full expiration, 1.5 kPa at full inspiration, and 1.1 kPa at mid-inspiration,[99] though the measurement SNR was lower than that used in the liver or brain. The ability to distinguish lung disease from normal parenchyma has not been investigated at this time.

The mechanical properties of muscle are known to change significantly during active and passive contraction,[100] as well as due to disease processes, such as spasms or inflammation. Numerous research studies have applied MRE to different muscles in vivo.[101] An example of muscle MRE is shown in ▶ Fig. 12.6. Due to the anisotropy of muscle, 3D-MRE is typically required to calculate whole muscle stiffness, though it may be possible to characterize a fusiform muscle, or a planar portion of a more complex muscle type, by performing 2D-MRE with an oblique slice. In general, higher frequencies (> 100 Hz) are desirable as muscle stiffness, particularly in a contracted state, can be high. Studies have found that the anisotropic characteristics of muscles lead waves to propagate primarily along the fiber directions,[102] with stiffness across the fibers being lower than stiffness along the fibers.[103] Stiffness of muscles was found to increase significantly with applied load by several studies.[102, 104,105] Furthermore, both the relaxed muscle stiffness and the change in stiffness with load have been found to be significantly different in patients with neuromuscular disorders[106,107] and myositis[108] compared to normal subjects. Muscle dimensions and insertion angles vary significantly between individuals, however, and should be taken into account for population studies.[109] Also, the experimental setup needs to account for both active and passive components of muscle stiffness. Additional

studies with tightly controlled variables are needed to evaluate the utility of MRE for the diagnosis of muscular disease.

Studies of the kidneys have been performed in patients and animals. An acute induced arterial stenosis resulted in lower renal blood flow and lower stiffness. In chronic stenosis, reduced flow (-60%) confounded the diagnosis of pathology-confirmed fibrosis, making the kidneys have normal stiffness.[110] While this can be confounding, either renal flow or fibrosis can be studied with MRE if the other condition can be excluded based on other information. A study using multifrequency MRE (30–60 Hz)[111] found a statistically significant difference in the stiffnesses of various kidney regions, with the medulla being stiffer than the cortex which was stiffer than the hilus. As the cortex is only 6 mm thick, frequencies above 200 Hz, which are technically challenging to deliver, are required to fully separate the regions.[112] Kidney studies are done with setups similar to liver MRE, but the driver is placed on the posterior body wall.

Cardiac MRE has been a historically challenging endeavor as the cardiac wall is thin and stiff, requiring high-frequency waves (> 200 Hz) for accurate stiffness quantification. One proposed approach is to compare wave amplitudes inside and outside of the heart at low driving frequencies (around 20 Hz) to calculate relative stiffness differences between the heart and other tissue, or between different phases of the cardiac cycle. Imaging the heart across the cardiac cycle, a study[113] found a 2.5 times increase in wave amplitude in diastole with respect to systole which corresponded to a 37 times higher stiffness in systole, based on the model. Patients with echocardiographically proven relaxation abnormalities were found to have lower wave amplitudes (corresponding to higher stiffnesses) and lower ratios of left ventricular amplitudes to chest wall amplitudes than normal subjects.[114] A significantly reduced shear wave amplitude was also found in patients with diastolic dysfunction.[115] Direct inversions of the shear wave displacements have also been performed using higher shear wave frequencies (160 Hz). A much smaller increase in systolic stiffness with respect to diastolic stiffness was found by studies using direct inversion (1.3 times increase[116] and 2.5 times increase[117]) than the previously described study comparing wave amplitudes. Ventricular pressure was also shown to correlate with cardiac stiffness using different methods.[118,119] Setups for delivering shear waves at > 200 Hz and inversions modeling thin-shell wave propagations are currently being investigated.

12.3.4 Tips and Tricks

Although the failure rate for the standard hepatic MRE technique is only 5%, it may be higher in novel applications or at new sites. Several modes of failure can be easily identified at the scanner, allowing the exam to be reacquired. Noisy phase images with visible waves can result from having a low magnitude signal (▶ Fig. 12.7a), often caused by iron overload or other susceptibility artifacts. Higher motion amplitude and motion-encoding gradients, thicker imaging slices, or using a different pulse sequence (gradient recalled echo (GRE) versus spin-echo echo planar imaging [SE EPI], for example) can be used to boost the signal. Alternatively, a different field-strength scanner (1.5T instead of 3T) may be preferable. Although SNR tends to be better at higher field strengths, susceptibility-related signal loss is also more significant. Lack of motion or low amplitude motion

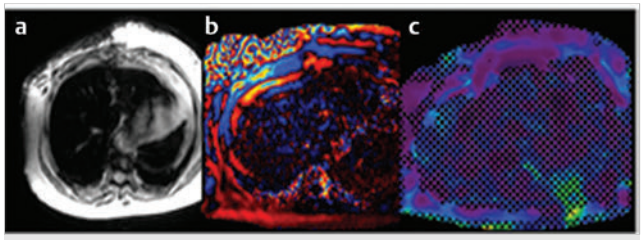

Fig. 12.7 Identifying failed magnetic resonance elastography examinations (hepatic examples). (**a**) Low-magnitude signal (possible iron overload); (**b**) low wave amplitude (driver issue likely); (**c**) liver region in elastogram masked out (low-magnitude signal or low wave amplitude).

can be detected by noting flat phase images (▶ Fig. 12.7b). This is usually caused by poor driver coupling to the body, a loose tube-driver connection or because the active driver was accidentally turned off. Securing the driver, checking all connections, increasing motion amplitude, and shifting the driver to a different location on the body are all possible ways of increasing the amplitude of motion delivered to the tissue.

If a confidence map reflecting wave quality is available, such as those provided by the multiple model direction inversion (MMDI) technique, the fraction of the organ being masked out based on the standard threshold should be checked (▶ Fig. 12.7c). A driver may also become loose during the course of the exam causing the wave amplitude to decrease or disappear in slices or phase offsets acquired later in the exam. If the phase images do not appear to propagate in a continuous manner, the driver should be readjusted and the exam performed again.

Patient motion, as well as respiratory motion, cardiac motion, and flow artifacts, all manifest as standard MRI "ghosting," where tissue aliases to a different location in the image. If these artifacts fall outside of the organ of interest, they can be ignored; otherwise, a new acquisition may need to be performed, possibly with a different slice prescription. Some facilities may be equipped with a strain gauge that can be used to monitor breath-hold quality, such as providing feedback to the patient via an indicator (possibly a mirror) in particularly challenging cases.

Out-of-plane wave propagation can sometimes occur if the driver is located at the superior or inferior part of the liver. This possibility should be considered if a systematic stiffness increase is seen as slices become more distant from the driver location. The driver should be repositioned at the center of the liver, or, at a minimum, only the slice(s) closest to the driver should be analyzed. If interference from reflected waves is a problem, it may be beneficial to reduce the amplitude so that the reflected-waves, amplitude becomes much smaller.

The size and material of the driver, as well as the dimensions of the connective tubing give rise to resonant frequencies in the system causing motion to be higher at some mechanical wave amplitudes than others. As long as the amplitude is sufficient, variations in the tube lengths and driver sizes do not affect the stiffness calculation. However, it may be advantageous to try a passive driver with different dimensions or use a different tube length if the amplitude delivered to the patient is insufficient. In proof-of-concept research applications, it may be more practical to change the driving frequency by a small amount (several hertz) to be on resonance.

12.4 Conclusion

MRE has a wide range of applications with some, such as hepatic fibrosis staging, having well-established clinical utility. MRE is replacing biopsy as the method of choice for fibrosis detection at a number of institutions due to its highly reproducible results, lower sampling error, and the potential to be included in a standard abdominal MRI exam to provide comprehensive information at little added cost. Brain MRE is an emerging application with tentative utility demonstrated for characterization of degenerative diseases (e.g., Alzheimer's disease, multiple sclerosis, and normal pressure hydrocephalus) as well as tumor resection planning. MRE was also shown to significantly improve specificity of malignant tumor detection when used in combination with contrast-enhanced MRI, while also having high standalone accuracy. The ability to characterize the early treatment response of tumors is also a compelling initial result, but one that requires more investigation.

Several applications, like lung MRE, are novel and their clinical efficacy remains to be explored. Stiffness can be directly related to a disease process in some cases, such as fibrosis, and may be the best diagnostic parameter. In other instances, such as breast tumors, elasticity measurements may provide additional information, which is most useful when combined with information from other diagnostic methods. Factors such as blood (or CSF) pressure and inflammation should be considered when performing MRE exams as their effect on tissue stiffness can be confounding or, if used correctly, diagnostically valuable. The ability of MRE to image practically any organ, including the brain, the lungs, and individual muscles, makes it an extremely powerful tool. Furthermore, vector motion encoding and volume-based acquisitions allow inversions of complex wavefronts occurring in small or thin organs to be performed, and spatial variations in stiffness of larger organs to be evaluated. Numerous inversions calculating different parameters, as well as acquisitions at different shear wave frequencies, have been proposed for newer applications. A comparative investigation of which techniques yield the greatest diagnostic value, followed by a standardization of these applications, is currently a topic of paramount importance. The elasticity values provided by MRE, either on their own or in combination with functional, diffusional, anatomical, or spectroscopic data obtainable from MRI concurrently, are valuable biomarkers with many potential applications in the study of physiology and the diagnosis of diseases.

References

[1] Muthupillai R, Lomas DJ, Rossman PJ, Greenleaf JF, Manduca A, Ehman RL. Magnetic resonance elastography by direct visualization of propagating acoustic strain waves. Science 1995; 269(5232):1854–1857

[2] Yin M, Talwalkar JA, Glaser KJ et al. Assessment of hepatic fibrosis with magnetic resonance elastography. Clin Gastroenterol Hepatol 2007; 5(10):1207–1213.e2

[3] Ichikawa S, Motosugi U, Morisaka H et al. Validity and reliability of magnetic resonance elastography for staging hepatic fibrosis in patients with chronic hepatitis B. Magn Reson Med Sci 2015; 14(3):211–221

[4] Tang A, Cloutier G, Szeverenyi NM, Sirlin CB. Ultrasound elastography and MR elastography for assessing liver fibrosis: Part 2, diagnostic performance, confounders, and future directions. AJR Am J Roentgenol 2015; 205(1): 33–40

[5] Cui J, Ang B, Haufe W et al. Comparative diagnostic accuracy of magnetic resonance elastography vs. eight clinical prediction rules for non-invasive diagnosis of advanced fibrosis in biopsy-proven non-alcoholic fatty liver disease: a prospective study. Aliment Pharmacol Ther 2015; 41(12):1271–1280

[6] Venkatesh SK, Yin M, Takahashi N, Glockner JF, Talwalkar JA, Ehman RL. Non-invasive detection of liver fibrosis: MR imaging features vs. MR elastography. Abdom Imaging 2015; 40(4):766–775[Epub ahead of print]

[7] Batheja M, Vargas H, Silva AM et al. Magnetic resonance elastography (MRE) in assessing hepatic fibrosis: performance in a cohort of patients with histological data. Abdom Imaging 2015; 40(4):760–765

[8] Singh S, Venkatesh SK, Wang Z et al. Diagnostic performance of magnetic resonance elastography in staging liver fibrosis: a systematic review and meta-analysis of individual participant data. Clin Gastroenterol Hepatol 2015; 13(3):440–451.e6

[9] Su LN, Guo SL, Li BX, Yang P. Diagnostic value of magnetic resonance elastography for detecting and staging of hepatic fibrosis: a meta-analysis. Clin Radiol 2014; 69(12):e545–e552

[10] Mariappan YK, Rossman PJ, Manduca A, Romano A, Ehman RL. High frequency mode conversion technique for stiff lesion detection in magnetic resonance elastography. Paper presented at 15th Annual Meeting of the International Society for Magnetic Resonance in Medicine; May 6–12, 2006; Seattle, WA

[11] Venkatesh SK, Yin M, Ehman RL. Magnetic resonance elastography of liver: technique, analysis, and clinical applications. J Magn Reson Imaging 2013; 37(3):544–555

[12] Sinkus R, Tanter M, Xydeas T, Catheline S, Bercoff J, Fink M. Viscoelastic shear properties of in vivo breast lesions measured by MR elastography. Magn Reson Imaging 2005; 23(2):159–165

[13] Manduca A, Oliphant TE, Dresner MA et al. Magnetic resonance elastography: non-invasive mapping of tissue elasticity. Med Image Anal 2001; 5(4): 237–254

[14] Klatt D, Hamhaber U, Asbach P, Braun J, Sack I. Noninvasive assessment of the rheological behavior of human organs using multifrequency MR elastography: a study of brain and liver viscoelasticity. Phys Med Biol 2007; 52(24): 7281–7294

[15] Holm S, Sinkus R. A unifying fractional wave equation for compressional and shear waves. J Acoust Soc Am 2010; 127(1):542–559

[16] Riek K, Klatt D, Nuzha H et al. Wide-range dynamic magnetic resonance elastography. J Biomech 2011; 44(7):1380–1386

[17] Clayton EH, Garbow JR, Bayly PV. Frequency-dependent viscoelastic parameters of mouse brain tissue estimated by MR elastography. Phys Med Biol 2011; 56(8):2391–2406

[18] Fowell AJ, Iredale JP. Emerging therapies for liver fibrosis. Dig Dis 2006; 24 (1–2):174–183

[19] Friedman SL, Bansal MB. Reversal of hepatic fibrosis — fact or fantasy? Hepatology 2006; 43(2) Suppl 1:S82–S88

[20] Thampanitchawong P, Piratvisuth T. Liver biopsy:complications and risk factors. World J Gastroenterol 1999; 5(4):301–304

[21] Ratziu V, Charlotte F, Heurtier A et al; LIDO Study Group. Sampling variability of liver biopsy in nonalcoholic fatty liver disease. Gastroenterology 2005; 128(7):1898–1906

[22] Regev A, Berho M, Jeffers LJ et al. Sampling error and intraobserver variation in liver biopsy in patients with chronic HCV infection. Am J Gastroenterol 2002; 97(10):2614–2618

[23] Huwart L, Sempoux C, Vicaut E et al. Magnetic resonance elastography for the noninvasive staging of liver fibrosis. Gastroenterology 2008; 135(1):32–40

[24] Ichikawa S, Motosugi U, Morisaka H et al. Comparison of the diagnostic accuracies of magnetic resonance elastography and transient elastography for hepatic fibrosis. Magn Reson Imaging 2015; 33(1):26–30

[25] Bensamoun S, Wang L, Robert L, Charleux F, Latrive JP, Ho Ba Tho MC. Measurement of the liver stiffness with two imaging techniques: magnetic resonance elastography and fibroscan. J Magn Reson Imaging 2008; 28(5):1287–1292

[26] Xanthakos SA, Podberesky DJ, Serai SD et al. Use of magnetic resonance elastography to assess hepatic fibrosis in children with chronic liver disease. J Pediatr 2014; 164(1):186–188

[27] Nordbeck P, Ertl G, Ritter O. Magnetic resonance imaging safety in pacemaker and implantable cardioverter defibrillator patients: how far have we come? Eur Heart J 2015; 36(24):1505–1511[E-pub ahead of print]

[28] Lee DH, Lee JM, Han JK, Choi BI. MR elastography of healthy liver parenchyma: normal value and reliability of the liver stiffness value measurement. J Magn Reson Imaging 2013; 38(5):1215–1223

[29] Venkatesh SK, Yin M, Glockner JF et al. MR elastography of liver tumors: preliminary results. AJR Am J Roentgenol 2008; 190(6):1534–1540

[30] Venkatesh SK, Wang G, Teo LLS, Ang BWL. Magnetic resonance elastography of liver in healthy Asians: normal liver stiffness quantification and reproducibility assessment. J Magn Reson Imaging 2014; 39(1):1–8
[31] Hirsch S, Guo J, Reiter R et al. MR elastography of the liver and the spleen using a piezoelectric driver, single-shot wave-field acquisition, and multifrequency dual parameter reconstruction. Magn Reson Med 2014; 71(1):267–277
[32] Garteiser P, Sahebjavaher RS, Ter Beek LC et al. Rapid acquisition of multifrequency, multislice and multidirectional MR elastography data with a fractionally encoded gradient echo sequence. NMR Biomed 2013; 26(10):1326–1335
[33] Lee Yj, Lee JM, Lee JE et al. MR elastography for noninvasive assessment of hepatic fibrosis: reproducibility of the examination and reproducibility and repeatability of the liver stiffness value measurement. J Magn Reson Imaging 2014; 39(2):326–331
[34] Serai SD, Yin M, Wang H, Ehman RL, Podberesky DJ. Cross-vendor validation of liver magnetic resonance elastography. Abdom Imaging 2015; 40(4):789–794
[35] Yin M, Talwalkar JA, Glaser KJ, Ehman RL. MR elastography of the liver: observations from a review of 1,377 exams. Paper presented at 19th Annual Meeting of the International Society for Magnetic Resonance in Medicine; May 7–13, 2011; Montreal, Canada
[36] Hallinan JT, Alsaif HS, Wee A, Venkatesh SK. Magnetic resonance elastography of liver: influence of intravenous gadolinium administration on measured liver stiffness. Abdom Imaging 2015; 40(4):783–788
[37] Venkatesh SK, Ehman RL. Magnetic resonance elastography of liver. Magn Reson Imaging Clin N Am 2014; 22(3):433–446
[38] Pietrangelo A, Caleffi A, Corradini E. Non-HFE hepatic iron overload. Semin Liver Dis 2011; 31(3):302–318
[39] Grady L. Random walks for image segmentation. IEEE Trans Pattern Anal Mach Intell 2006; 28(11):1768–1783
[40] Nedredal GI, Yin M, McKenzie T et al. Portal hypertension correlates with splenic stiffness as measured with MR elastography. J Magn Reson Imaging 2011; 34(1):79–87
[41] Yin M, Glaser KJ, Talwalkar JA, Manduca A, Ehman RL. Validity of a 2-D wave field model in MR elastography of the liver. Paper presented at 17th Annual Meeting of the International Society for Magnetic Resonance in Medicine; April 18–24, 2009; Honolulu, HI
[42] Dzyubak B, Glaser K, Yin M et al. Automated liver stiffness measurements with magnetic resonance elastography. J Magn Reson Imaging 2013; 38(2): 371–379
[43] Shire NJ, Yin M, Chen J et al. Test-retest repeatability of MR elastography for noninvasive liver fibrosis assessment in hepatitis C. J Magn Reson Imaging 2011; 34(4):947–955
[44] Yin M, Talwalkar JA, Venkatesh SK, Ehman RL. MR elastography of dynamic postprandial hepatic stiffness augmentation in chronic liver disease. Paper presented at 17th Annual Meeting of the International Society for Magnetic Resonance in Medicine; April 18–24, 2009; Honolulu, HI
[45] Yin M, Kolipaka A, Woodrum DA et al. Hepatic and splenic stiffness augmentation assessed with MR elastography in an in vivo porcine portal hypertension model. J Magn Reson Imaging 2013; 38(4):809–815
[46] Hirsch S, Guo J, Reiter R et al. Towards compression-sensitive magnetic resonance elastography of the liver: sensitivity of harmonic volumetric strain to portal hypertension. J Magn Reson Imaging 2014; 39(2):298–306
[47] Ichikawa S, Motosugi U, Nakazawa T et al. Hepatitis activity should be considered a confounder of liver stiffness measured with MR elastography. J Magn Reson Imaging 2015; 41(5):1203–1208
[48] Shi Y, Guo Q, Xia F et al. MR elastography for the assessment of hepatic fibrosis in patients with chronic hepatitis B infection: does histologic necroinflammation influence the measurement of hepatic stiffness? Radiology 2014; 273(1):88–98
[49] Chen J, Talwalkar JA, Yin M, Glaser KJ, Sanderson SO, Ehman RL. Early detection of nonalcoholic steatohepatitis in patients with nonalcoholic fatty liver disease by using MR elastography. Radiology 2011; 259(3):749–756
[50] Cheng S, Clarke EC, Bilston LE. Rheological properties of the tissues of the central nervous system: a review. Med Eng Phys 2008; 30(10):1318–1337
[51] Chatelin S, Constantinesco A, Willinger R. Fifty years of brain tissue mechanical testing: from in vitro to in vivo investigations. Biorheology 2010; 47(5–6):255–276
[52] Kruse SA, Rose GH, Glaser KJ et al. Magnetic resonance elastography of the brain. Neuroimage 2008; 39(1):231–237
[53] Scholz M, Lorenz A, Pesavento A et al. Current status of intraoperative real-time vibrography in neurosurgery. Ultraschall Med 2007; 28(5):493–497
[54] Arani A, Murphy MC, Glaser KJ et al. Measuring the effects of aging and sex on regional brain stiffness with MR elastography in healthy older adults. Neuroimage 2015; 111:59–64
[55] Streitberger KJ, Sack I, Krefting D et al. Brain viscoelasticity alteration in chronic-progressive multiple sclerosis. PLoS ONE 2012; 7(1):e29888
[56] Murphy MC, Huston J III, Jack CR Jr et al. Measuring the characteristic topography of brain stiffness with magnetic resonance elastography. Paper presented at the 21st Annual Meeting of the International Society for Magnetic Resonance in Medicine; April 20–26, 2013; Salt Lake City, UT
[57] Zhang J, Green MA, Sinkus R, Bilston LE. Viscoelastic properties of human cerebellum using magnetic resonance elastography. J Biomech 2011; 44(10): 1909–1913
[58] Green MA, Bilston LE, Sinkus R. In vivo brain viscoelastic properties measured by magnetic resonance elastography. NMR Biomed 2008; 21(7):755–764
[59] Sack I, Beierbach B, Wuerfel J et al. The impact of aging and gender on brain viscoelasticity. Neuroimage 2009; 46(3):652–657
[60] Murphy MC, Huston J III, Jack CR Jr et al. Decreased brain stiffness in Alzheimer's disease determined by magnetic resonance elastography. Paper presented at 19th Annual Meeting of the International Society for Magnetic Resonance in Medicine; May 7–13, 2011; Montreal, Canada
[61] Murphy MC, Curran GL, Glaser KJ et al. Magnetic resonance elastography of the brain in a mouse model of Alzheimer's disease: initial results. Magn Reson Imaging 2012; 30(4):535–539
[62] Schregel K, Wuerfel E, Garteiser P et al. Demyelination reduces brain parenchymal stiffness quantified in vivo by magnetic resonance elastography. Proc Natl Acad Sci U S A 2012; 109(17):6650–6655
[63] Freimann FB, Streitberger KJ, Klatt D et al. Alteration of brain viscoelasticity after shunt treatment in normal pressure hydrocephalus. Neuroradiology 2012; 54(3):189–196
[64] Riek K, Millward JM, Hamann I et al. Magnetic resonance elastography reveals altered brain viscoelasticity in experimental autoimmune encephalomyelitis. Neuroimage Clin 2012; 1(1):81–90
[65] Shi Y, Guo Q, Xia F, Dzyubak B, Glaser KJ, Ehman RL. MR elastography for the assessment of hepatic fibrosis in patients with chronic hepatitis B: does histological necroinflammation influence the masurement of liver stiffness. Paper presented at the 23rd Annual Meeting of the International Society for Magnetic Resonance in Medicine; May 10–16, 2014; Milan, Italy
[66] Ichikawa S, Motosugi U, Ichikawa T et al. Magnetic resonance elastography for staging liver fibrosis in chronic hepatitis C. Magn Reson Med Sci 2012; 11 (4):291–297
[67] Streitberger K-J, Wiener E, Hoffmann J et al. In vivo viscoelastic properties of the brain in normal pressure hydrocephalus. NMR Biomed 2011; 24(4):385–392
[68] Murphy MC, Curran GL, Glaser KJ et al. MR elastography of the brain in a mouse model of Alzheimer's disease. Paper presented at the 18th Annual Meeting of the International Society for Magnetic Resonance in Medicine; May 1–7, 2010; Stockholm, Sweden
[69] Rossman PJ, Rose GH, Riederer SJ, Ehman RL. A local gradient feedback system for use in MR elastography. Paper presented at the 6th Annual Meeting of the International Society for Magnetic Resonance in Medicine, April 18–24, 1998; Sydney, Australia
[70] Soellinger M, Rutz AK, Kozerke S, Boesiger P. 3D cine displacement-encoded MRI of pulsatile brain motion. Magn Reson Med 2009; 61(1):153–162
[71] Gallichan D, Robson MD, Bartsch A, Miller KL. TREMR: Table-resonance elastography with MR. Magn Reson Med 2009; 62(3):815–821
[72] Jack CR, Lowe VJ, Senjem ML et al. 11C PiB and structural MRI provide complementary information in imaging of Alzheimer's disease and amnestic mild cognitive impairment. Brain 2008; 131(3):665–680
[73] McGarry M, Johnson CL, Sutton BP et al. Including spatial information in nonlinear inversion MR elastography using soft prior regularization. IEEE Trans Med Imaging 2013; 32(10):1901–1909
[74] McGarry MDJ, Van Houten EEW, Perriñez PR, Pattison AJ, Weaver JB, Paulsen KD. An octahedral shear strain-based measure of SNR for 3D MR elastography. Phys Med Biol 2011; 56(13):N153–N164
[75] Paszek MJ, Zahir N, Johnson KR et al. Tensional homeostasis and the malignant phenotype. Cancer Cell 2005; 8(3):241–254
[76] Cox TR, Bird D, Baker AM et al. LOX-mediated collagen crosslinking is responsible for fibrosis-enhanced metastasis. Cancer Res 2013; 73(6):1721–1732
[77] Baker AM, Bird D, Lang G, Cox TR, Erler JT. Lysyl oxidase enzymatic function increases stiffness to drive colorectal cancer progression through FAK. Oncogene 2013; 32(14):1863–1868

[78] Murphy MC, Huston J III, Glaser KJ et al. Preoperative assessment on meningioma stiffness by MR elastography. Paper presented at 20th Annual Meeting of the International Society for Magnetic Resonance in Medicine, May 5–11, 2012; Melbourne, Australia
[79] Heywang-Köbrunner SH, Viehweg P, Heinig A, Küchler C. Contrast-enhanced MRI of the breast: accuracy, value, controversies, solutions. Eur J Radiol 1997; 24(2):94–108
[80] Sinkus R, Siegmann K, Xydeas T, Tanter M, Claussen C, Fink M. MR elastography of breast lesions: understanding the solid/liquid duality can improve the specificity of contrast-enhanced MR mammography. Magn Reson Med 2007; 58(6):1135–1144
[81] Siegmann KC, Xydeas T, Sinkus R, Kraemer B, Vogel U, Claussen CD. Diagnostic value of MR elastography in addition to contrast-enhanced MR imaging of the breast-initial clinical results. Eur Radiol 2010; 20(2):318–325
[82] Doblas S, Garteinser P, Haddad N et al. Magnetic resonance elastography measurements of viscosity: a novel biomarker for human hepatic tumor malignancy? Proc of 19th Ann Meet of ISMRM. 2011:389.
[83] Daire J, Sinkus R, Wagner M, Haddad N, Vilgrain V, Beers B. Is shear viscosity a sign for malignancy in liver tumours? Proc of 18th Ann Meet of ISMRM. 2010:4658.
[84] Jamin Y, Boult JK, Li J et al. Exploring the biomechanical properties of brain malignancies and their pathologic determinants in vivo with magnetic resonance elastography. Cancer Res 2015; 75(7):1216–1224
[85] Simon M, Guo J, Papazoglou S et al. Non-invasive characterization of intracranial tumors by magnetic resonance elastography. New J Phys 2013; 15:1–15
[86] Pepin KM, Chen J, Glaser KJ et al. MR elastography derived shear stiffness—a new imaging biomarker for the assessment of early tumor response to chemotherapy. Magn Reson Med 2014; 71(5):1834–1840
[87] Li J, Jamin Y, Boult JKR et al. Tumour biomechanical response to the vascular disrupting agent ZD6126 in vivo assessed by magnetic resonance elastography. Br J Cancer 2014; 110(7):1727–1732
[88] Chen J, Woodrum DA, Glaser KJ, Murphy MC, Gorny K, Ehman R. Assessment of in vivo laser ablation using MR elastography with an inertial driver. Magn Reson Med 2014; 72(1):59–67
[89] Corbin N, Vappou J, Breton E et al. Interventional MR elastography for MRI-guided percutaneous procedures. Magn Reson Med 2016; 75(3):1110–1118
[90] Murphy MC, Huston J III, Glaser KJ et al. Preoperative assessment of meningioma stiffness using magnetic resonance elastography. J Neurosurg 2013; 118(3):643–648
[91] McKnight AL, Kugel JL, Rossman PJ, Manduca A, Hartmann LC, Ehman RL. MR elastography of breast cancer: preliminary results. AJR Am J Roentgenol 2002; 178(6):1411–1417
[92] Krouskop TA, Wheeler TM, Kallel F, Garra BS, Hall T. Elastic moduli of breast and prostate tissues under compression. Ultrason Imaging 1998; 20(4):260–274
[93] Barr RG, Zhang Z. Effects of precompression on elasticity imaging of the breast: development of a clinically useful semiquantitative method of precompression assessment. J Ultrasound Med 2012; 31(6):895–902
[94] Chen J, Brandt K, Ghosh K et al. Noncompressive MR elastography of breasts. Paper presented at 21st Annual Meeting of the International Society for Magnetic Resonance in Medicine; April 20–26, 2013; Salt Lake City, UT
[95] Arani A, Plewes D, Chopra R. Transurethral prostate magnetic resonance elastography: prospective imaging requirements. Magn Reson Med 2011; 65(2):340–349
[96] Arani A, Da Rosa M, Ramsay E, Plewes DB, Haider MA, Chopra R. Incorporating endorectal MR elastography into multi-parametric MRI for prostate cancer imaging: initial feasibility in volunteers. J Magn Reson Imaging 2013; 38(5):1251–1260
[97] Mariappan YK, Glaser KJ, Hubmayr RD, Manduca A, Ehman RL, McGee KP. MR elastography of human lung parenchyma: technical development, theoretical modeling and in vivo validation. J Magn Reson Imaging 2011; 33(6):1351–1361
[98] Dzyubak B, Mariappan Y, Glaser J, Venkatesh S, Ehman R. Evaluation of spin-echo based sequences for MR Elastography of liver with iron overload. Proc of 23th Ann Meet ISMRM. 2015:1908.
[99] Mariappan YK, Glaser KJ, Levin DL et al. Estimation of the absolute shear stiffness of human lung parenchyma using (1) H spin echo, echo planar MR elastography. J Magn Reson Imaging 2014; 40(5):1230–1237
[100] Jenkyn TR, Ehman RL, An KN. Noninvasive muscle tension measurement using the novel technique of magnetic resonance elastography (MRE). J Biomech 2003; 36(12):1917–1921
[101] Ringleb SI, Bensamoun SF, Chen Q, Manduca A, An KN, Ehman RL. Applications of magnetic resonance elastography to healthy and pathologic skeletal muscle. J Magn Reson Imaging 2007; 25(2):301–309
[102] Bensamoun SF, Ringleb SI, Littrell L et al. Determination of thigh muscle stiffness using magnetic resonance elastography. J Magn Reson Imaging 2006; 23(2):242–247
[103] Papazoglou S, Rump J, Braun J, Sack I. Shear wave group velocity inversion in MR elastography of human skeletal muscle. Magn Reson Med 2006; 56(3):489–497
[104] Dresner MA, Rose GH, Rossman PJ, Muthupillai R, Manduca A, Ehman RL. Magnetic resonance elastography of skeletal muscle. J Magn Reson Imaging 2001; 13(2):269–276
[105] Klatt D, Papazoglou S, Braun J, Sack I. Viscoelasticity-based MR elastography of skeletal muscle. Phys Med Biol 2010; 55(21):6445–6459
[106] Basford JR, Jenkyn TR, An KN, Ehman RL, Heers G, Kaufman KR. Evaluation of healthy and diseased muscle with magnetic resonance elastography. Arch Phys Med Rehabil 2002; 83(11):1530–1536
[107] Ringleb S, Kaufman K, Basford J, et al. Magnetic resonance elastography: a noninvasive method to differentiate between healthy and pathologic muscle stiffness. Paper presented at the 30th Annual Meeting of American Society of Biomechics; Sept. 6–9, 2006; Blacksburg, VA
[108] McCullough MB, Domire ZJ, Reed AM et al. Evaluation of muscles affected by myositis using magnetic resonance elastography. Muscle Nerve 2011; 43(4):585–590
[109] Hobbie RJ, Wikswo JP. Intermediate physics for medicine and biology. 1st ed. New York, NY: John Wiley & Sons, 1988:6–12
[110] Warner L, Yin M, Glaser KJ et al. Noninvasive in vivo assessment of renal tissue elasticity during graded renal ischemia using MR elastography. Invest Radiol 2011; 46(8):509–514
[111] Streitberger KJ, Guo J, Tzschätzsch H et al. High-resolution mechanical imaging of the kidney. J Biomech 2014; 47(3):639–644
[112] Lee CU, Glockner JF, Glaser KJ et al. MR elastography in renal transplant patients and correlation with renal allograft biopsy: a feasibility study. Acad Radiol 2012; 19(7):834–841
[113] Sack I, Rump J, Elgeti T, Samani A, Braun J. MR elastography of the human heart: noninvasive assessment of myocardial elasticity changes by shear wave amplitude variations. Magn Reson Med 2009; 61(3):668–677
[114] Elgeti T, Beling M, Hamm B, Braun J, Sack I. Cardiac magnetic resonance elastography: toward the diagnosis of abnormal myocardial relaxation. Invest Radiol 2010; 45(12):782–787
[115] Elgeti T, Knebel F, Hättasch R, Hamm B, Braun J, Sack I. Shear-wave amplitudes measured with cardiac MR elastography for diagnosis of diastolic dysfunction. Radiology 2014; 271(3):681–687
[116] Kolipaka A, Araoz PA, MCGee KP, Manduca A, Ehman RL. In vivo cardiac MR elastography in a single breath hold. Paper presented at the 18th Annual Meeting of the International Society for Magnetic Resonance in Medicine; May 1–7, 2010; Stockholm, Sweden
[117] Robert B, Sinkus R, Gennisson JL, Fink M. Application of DENSE-MR-elastography to the human heart. Magn Reson Med 2009; 62(5):1155–1163
[118] Kolipaka A, Araoz PA, McGee KP, Manduca A, Ehman RL. Magnetic resonance elastography as a method for the assessment of effective myocardial stiffness throughout the cardiac cycle. Magn Reson Med 2010; 64(3):862–870
[119] Elgeti T, Rump J, Hamhaber U et al. Cardiac magnetic resonance elastography. Initial results. Invest Radiol 2008; 43(11):762–772

13 Future Applications for Elastography

David O. Cosgrove

13.1 Introduction

New applications of elastography may be grouped into those contingent on technology advances and those related to as-yet-undeveloped clinical applications; the two are interlinked. Because comparisons between pre- and postdistortion images are the essence of strain elastography, any imaging technique can be used for this approach, including magnetic resonance (MR) (see Chapter 12) and optical techniques, notably optical coherence tomography (OCT) and optoacoustic methods. For shear wave elastography, new ways to create the acoustic radiation force impulses and to measure the shear wave speed are being explored.

13.2 Ultrasound Methods

One application that requires a slow compression is poroelastography, in which the flow of interstitial fluid under compression, which occurs over several seconds, is measured. The clinical analogy is the demonstration of pitting edema, for example, over the ankle, shown by sustained gentle finger compression and then palpation of the resulting pitting of the skin. The problem has been modeled mathematically.[1,2] An ultrasound application has been described in transplant kidneys, where steady probe compression and relaxation was applied in 3 second cycles and speckle tracking was used to assess the resulting distortion.[3] Significant differences were obtained in the relaxation times compared to the Banff scores indicating differences in edema.

New ways to displace the tissues under examination include sending several acoustic radiation force impulses (ARFIs) from different parts of the array simultaneously. Known as *comb push elastography* it allows higher frame rates than achievable with a single push pulse. The overlap of several shear waves leads to interference patterns that may reveal new tissue properties.[4]

The shear waves produced by conventional ARFI push pulses are currently assumed to travel at a single speed, which is used to assess tissue stiffness. But this is a simplification. Actually shear waves occupy a range of frequencies from around 50 to 500 Hz. Those of higher frequencies travel faster than those of lower frequencies (unlike compressional audible sound and ultrasound waves, in which all frequencies travel at the same speed). This phenomenon, known as dispersion, seems to result from properties of the viscous component of the tissue. Understanding how each manufacturer's shear wave system deals with this dispersion could lead to improvements in the spread of reading due to improved consistency across systems.[5] Estimation of the dispersion has been shown in ex vivo animal and human studies to allow diagnosis of the amount of fat in the liver and could provide information on the degree of steatosis, which is a major clinical problem.[6]

The concept of harnessing the shear waves that are generated throughout our bodies by native cardiovascular movements is the subject of active research.[7] The challenge is to detect these low amplitude shear waves from noise and to decipher the complex interference patterns produced when they overlap. It could open the way to a wider range of shear wave speed estimations.

13.3 Optical Methods

Optical coherence tomography (OCT) is powerful technique for imaging superficial structures such as the skin and the eye using laser light at visible wavelengths and a phase-sensitive technique to produce tomograms with submicron resolution. It has become a standard technique for examining the retina and subretinal layers in ophthalmology and can be adapted as a strain elastographic method by comparing OCT scans taken before and after a small distorting force is applied; for example to the cornea by a puff of air (as used to measure intraocular pressure in glaucoma).[8] An important potential application is in keratoconus, in which the cornea softens and projects anteriorly. Sufferers experience progressive changes to their refraction, and may be offered laser treatment, which has the disastrous effect of further weakening the cornea.[9]

Optical coherence elastography has been developed to assess the mechanical properties of the skin in tumors and in burns.[10, 11] Using a probe with a transparent membrane to contact the skin and apply a distorting force (which could be manual, in a handheld device, or automatic, using a piezoelectric crystal), phantom and clinical studies have been performed. The use of a 1 mm thick Elastosil transparent stress sensor plate between the probe and the skin to measure the applied stress allows quantitative estimates of the skin's elasticity. The trial images have strikingly high strain contrast at submillimeter resolution. If similar stress sensors could be incorporated into ultrasound transducers, quantitative strain ultrasound elastography might become possible.

13.4 Optoacoustic Methods

When a coherent light beam traverses or is back-scattered from a material that is vibrated mechanically, the movement of the material disturbs the light beam and changes the laser speckle pattern. A camera looking at the laser detects a reduction in the laser speckle contrast. This effect can be harnessed to sense the arrival of a shear wave, forming an alternative detection system to ultrasound with the advantage of better sensitivity than ultrasound offers.

The approach has been developed into an experimental shear wave system in which one or more ARFI pulses are directed into a test object and the time-of-flight of the shear wave is measured optically with great accuracy.[12] In the experimental system, the camera watches for the transient reduction in laser speckle contrast while an ARFI pulse is sent into the material some distance to one side; repositioning the ARFI pulse can be used to measure the shear wave speed. Both theoretical models and simulation have been developed for the system. Like all optical systems, it is depth limited and, even using the longer wavelengths of infrared light, only 20 to 30 mm of penetration

can be achieved, so clinical use would be limited to structures close to the probes such as small parts and endoscopic applications.

13.5 New Clinical Applications

There are several clinical applications that are being explored but are not yet in clinical use. The literature regarding the most promising of these are summarized below.

13.5.1 Obstetrics and Gynecology

One of the most compelling possible clinical uses is assessment of the softening of the uterine cervix before delivery in late pregnancy (▶ Fig. 13.1). In the normal process, as well as in cervical shortening, there is a reduction in the cervix's stiffness that allows cervical dilatation to permit passage of the fetal head along the birth canal. These changes are conventionally assessed by a combination of transvaginal ultrasound and manual palpation; these form the basis for the Bishop's score that is used in obstetric decision-making. If this ripening occurs early, premature delivery is more likely, with devastating consequences for the neonate.

Attempts to use strain elastography have not proved very successful, probably because of the complex structure of the cervix, with intertwined layers of fibrous tissue and smooth muscle, and the difficulty of applying the necessary force uniformly.[13] The shear wave approach seems more promising, though this may necessitate the development of special small transducers that can be applied directly to the posterior surface of the cervix via the posterior fornix.[14]

Another obstetrical application that is promising is in ectopic gestations, where suspicious adnexal masses that proved to be ectopic showed increased stiffness on strain elastography (termed the *blue eye sign*).[15] This was reliable regardless of the β-HCG (beta-human chorionic gonadotropin) level or the conventional ultrasound features.

The stiffness of predominantly cystic ovarian masses has been studied in a small group of patients (26) using transvaginal strain elastography and a subjective scoring system.[16] Most lesions showed the mixed pattern suggestive of simple cysts, but 3 of the masses contained stiffer regions and these corresponded to carcinomas, as confirmed on histology. The method could be a useful adjunct to conventional transvaginal assessment when the diagnosis of ovarian cancer is entertained.

Polycystic ovaries (PCO) were found to be stiffer than normal ovaries on strain elastography in a study of 48 patients compared with an equal number of healthy volunteers,[16] and the interobserver correlations were excellent. Measurement of ovarian stiffness merits further investigation as a means to improve the diagnosis of PCO in conjunction with ovarian appearance and volume.

A pilot study of over 200 women (some normal and others with a variety of uterine pathologies) using transvaginal strain elastography demonstrated that the normal myometrium had a uniform, stiff appearance that was distinct from the serosa, which presented a laminar pattern.[17] Leiomyomas (56 cases, confirmed on histology or MR) were also found to be uniformly stiff but somewhat stiffer than normal myometrium (▶ Fig. 13.2). Adenomyomatosis (11 cases, confirmed on MR) were softer than myometrium with an irregular pattern and margins. Some artifacts that are important to recognize were highlighted in the study, as was the need for practice in order to obtain repeatable results.

In a case report of a women with a leiomyosarcoma compared with another with a simple leiomyoma (fibroid), the malignancy was found to be stiffer on strain and shear wave elastography, both performed using an ARFI method.[18] The leiomyosarcoma also showed more heterogeneity of stiffness through the lesion. Larger studies are needed.

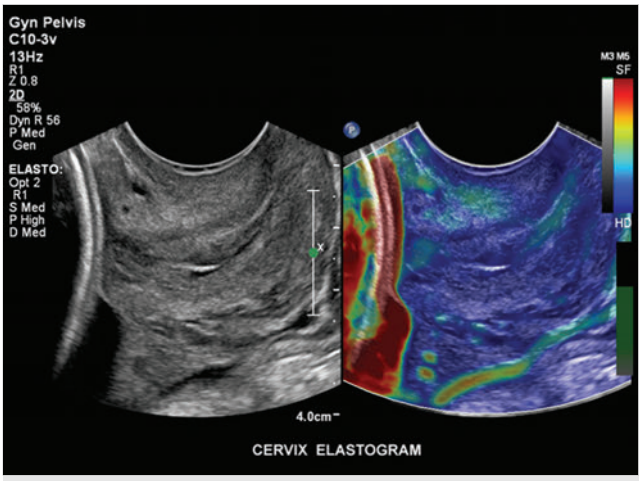

Fig. 13.1 Uterine cervix. Part of the stiff (red coding) fetal head can be discerned on the left of this strain elastogram taken with a transvaginal probe. The endocervix is slightly stiffer than the muscular portion, indicating that ripening has not progressed. (Courtesy of Dr. John MacQuarry, Philips Medical Systems, Bothel, Washington.)

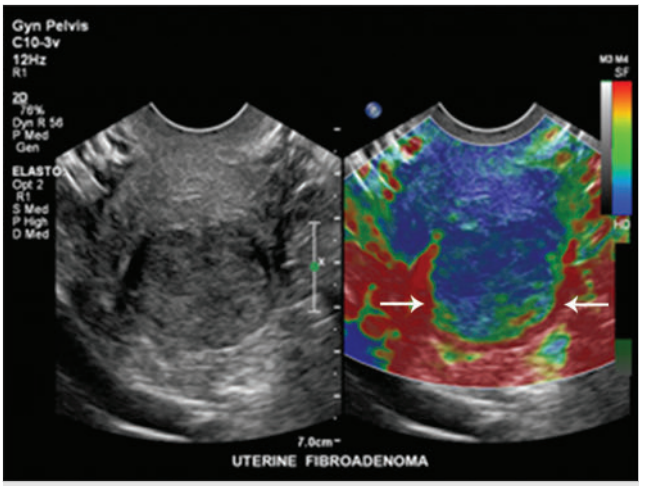

Fig. 13.2 Uterus with fibroid. In this transvaginal strain elastogram of the uterus, the myometrium has a uniform, rather stiff appearance while the fundal fibroid (*arrowheads*) is stiffer and somewhat heterogeneous. (Courtesy of Dr. John MacQuarry, Philips Medical Systems, Bothel, WA.)

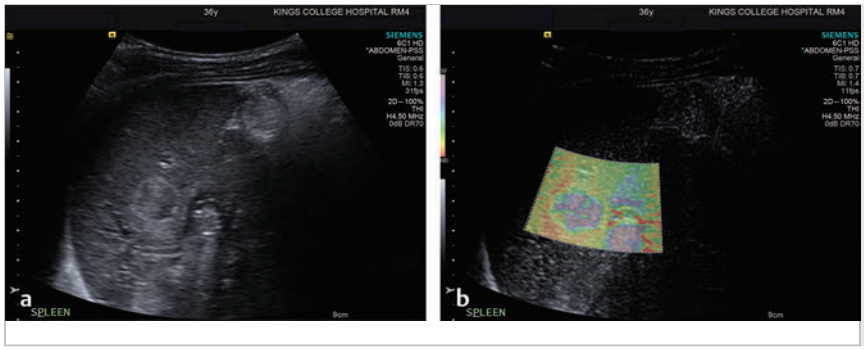

Fig. 13.3 Splenic abscess. A 36-year-old male recently arrived from the Middle East presented with fever and left upper quadrant pain. The B-mode scan (**a**) showed a well-defined, solid-appearing heterogeneous splenic mass. On ARFI strain elastography, it was found to be of mixed medium-to-soft stiffness (green-to-mauve) in comparison to the surrounding spleen, which was also somewhat heterogeneous. It proved to be a bacterial abscess, caught in the preliquefactive phase. (Courtesy of Prof. Paul Sidhu, King's College Hospital, London, UK.)

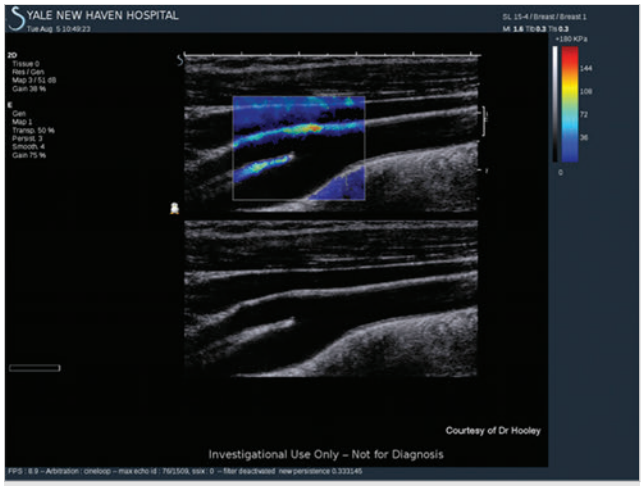

Fig. 13.4 Carotid plaque. This small atheromatous plaque is stiffer than the surrounding artery on shear wave elastography, suggesting it is stable.

13.5.2 Spleen

The spleen's mechanical properties are affected by the hemodynamic changes that occur in portal hypertension, and this has been proposed as an alternative to assessing the liver itself, especially where the liver is difficult to evaluate because it is badly damaged and heterogeneous (▶ Fig. 13.3). In a study of 123 patients with varying degrees of liver fibrosis and cirrhosis (mainly attributable to hepatitis C), using the SuperSonic imaging (SSI) shear wave elastography system (Aixplorer, SuperSonic Imagine), spleen stiffness was higher than liver stiffness at all grades.[19] A cutoff value between mild and severe liver fibrosis of 23 kPa (cf., 11 kPa for normal liver) is recommended. A high body mass index (BMI) and small spleen size were associated with failed spleen measurements, which were more common than failed liver measurements.

Patients with biliary atresia were studied following a Kasai procedure using an ARFI approach (Virtual Touch quantification [VTq], Siemens) and spleen stiffness was found to correlate with the development of portal hypertension and to predict the need for liver transplantation using a threshold of 2.55 m/s.[20] Combining liver and spleen stiffness values improved the predictive value.

Transient strain elastography (TSE, FibroScan, Echosens) and shear wave elastography (SSI, Aixplorer, SuperSonic Imagine) were compared in a well-run prospective study of 79 patients with a variety of diffuse liver diseases of advanced degree.[21] A striking finding was the high failure rate of TSE (58% compared with 3% for SSI SWE), mainly attributable to ascites, which is a recognized limitation of the mechanical push used by the FibroScan. However, while the liver measurements were useful at predicting portal hypertension in these cirrhotic patients, spleen stiffness was less useful, though the combination was strongest.

13.5.3 Neuroectoderm

The brain might seem an unlikely choice of organ for ultrasound elastography, but mapping the increased stiffness of brain tumors to guide brain surgery is of great interest to surgeons, and so intraoperative methods have been developed.[22] Meningiomas are stiffer than gliomas.

Another organ whose mechanical properties can be studied with ultrasound (as well as with OCT) is the eye. In a study of 14 eyes blinded by glaucoma, strain elastography was used to assess the stiffness of the optic nerve and of the retrobulbar fat.[23] Vibration was applied via the closed eyelids and strain maps developed, from which nerve-to-fat ratios were calculated. Suggested applications include tumors, inflammation, and autoimmune changes, such as occur in Graves' syndrome exophthalmos. While strain elastography is likely safe in the eye, the push pulses used in ARFI elastography are above the upper limit of the Food and Drug Administration (FDA) recommendations for acoustic power in the eye, so such studies may be unwise, though it has been used experimentally in keratoconus, where it was able to monitor improvements in corneal stiffness after cross-linking therapy.[24]

13.5.4 Vascular System

The compliance of arterial and venous walls is an important topic in hypertension and in selecting vessels for grafting and dialysis arteriovenous fistula formation, and it can be measured using ultrasound elastography.[25] Thus far it has remained a research tool, but simpler implementations could lead to wider clinical use.

Shear wave elastography has been used for evaluating plaque in the carotid arteries, and here, as in many musculoskeletal applications, it is softer tissue that is pathologic. Soft plaque, thanks to its abundant lipid content, is more vulnerable to rupture and thus is associated with a higher risk of stroke, both using experimental and commercial imaging systems (▶ Fig. 13.4).[26,27] That such small structures can be assessed qualitatively for stiffness using ultrasound is a tribute to the sophistication of the technology.

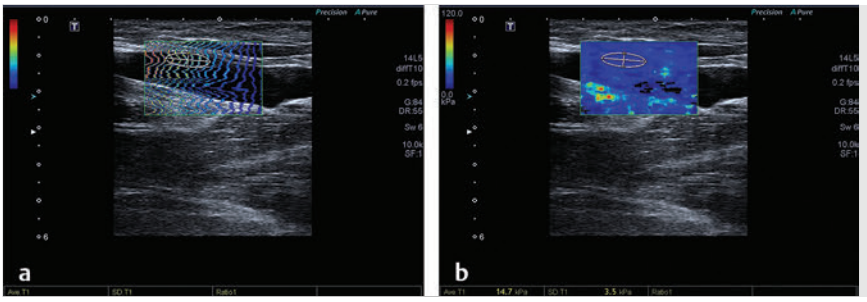

Fig. 13.5 Thrombus. Following insertion of a PICC, this patient experienced a sense of fullness in the left arm. B-mode ultrasound showed a dilated subclavian vein and there were no signals within it on Doppler. Shear wave elastography showed stiff tissue, indicating that the thrombus had undergone organization. (**a**) shows the propagation of the shear wave, which can be used as a quality indicator. The stiffness is shown in (**b**) as averaging 14.7 kPa.

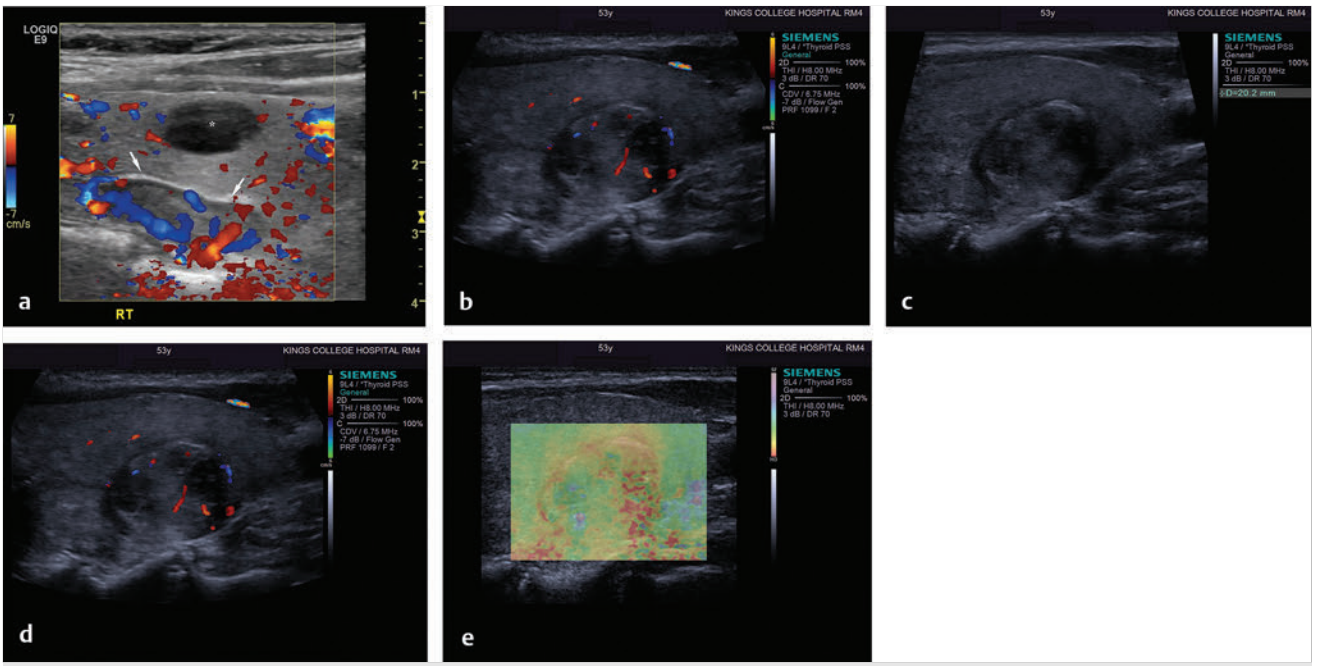

Fig. 13.6 Parathyroid gland. An encapsulated, hypervascular nodule (*arrows* in **a**) lying deep to the lower pole of the right lobe of the thyroid is seen in this patient with hypercalcemia; on strain elastography (**b**), it had intermediate signals, perhaps slightly less stiff than the adjacent thyroid. Its capsule shows as a stiff (blue) region, in keeping with its fibrous nature. There is also an incidental thyroid cyst (*asterisk* in **a**), which showed the typical blue-green-red artifact given by fluid. The 15 mm nodule indenting the posterior surface of the right lobe of the thyroid gland in (**c**) had a heterogeneous texture and was moderately vascular on Doppler (**d**). On strain elastography (**e**), it had a mixed pattern, with extensive stiff regions (coded in red), which is unexpected for a simple parathyroid adenoma. It proved to a parathyroid carcinoma on biopsy and subsequent excision. ([a, b] Courtesy of Dr. Chris Harvey, Hammersmith Hospital, Imperial College, London. [c, d, e] Courtesy of Prof. Paul Sidhu, King's College Hospital, London, UK.)

The stiffness of a venous thrombus changes as it develops: initially, the thrombus is very soft but if fibrosis occurs as it matures, the thrombus stiffens and measurements of this could be useful to estimate the age of a thrombus[28] (▶ Fig. 13.5). Either strain or shear wave approaches could be used.

13.5.5 Miscellaneous

The thyroid has been studied extensively with elastography, in an attempt to reduce the high and unnecessary biopsy rate for thyroid nodules (see Chapter 8), but its use in parathyroid nodules is less well explored.[29] However, this could be a useful application because these nodules are typically softer than those of the thyroid. Elastography might confirm the diagnosis in difficult cases, for example, for intrathyroidal parathyroid nodules (▶ Fig. 13.6). It may also be able to alert clinicians to the presence of rare parathyroid carcinoma.

Salivary glands (parotid and submandibular) have been studied in Sjögren's syndrone;[30] normal glands could be completely separated from those with chronic inflammation, and the strain scores correlated well with the B-mode scores, though whether elastography offered any advantage was not made clear.

Bladder wall stiffness is a factor in the unstable bladder that is a cause of stress incontinence; attempts to measure it using elastography show promise (▶ Fig. 13.7).[31]

The development of pressure sores can be predicted by the development of stiffer regions in the deeper layers of ischemic subcutaneous tissue before surface damage is visible.[32]

Somewhat related is the potential for stiffness estimates in the nasal turbinates, the inferior ones of which are accessible to ultrasound.[33] Nasal edema did not affect the results in healthy volunteers. The clinical interest here is in providing a quantitative assessment of the results of surgery.

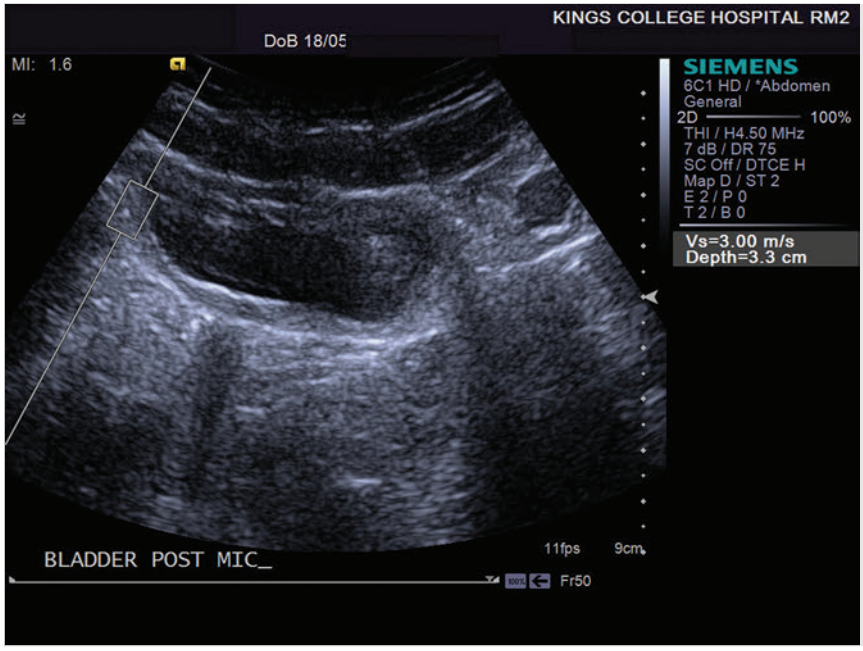

Fig. 13.7 Bladder wall. In this patient with an overactive bladder, the postmicturition wall shows an ARFI shear wave speed of 3 m/s, consistent with an increase in stiffness that could signify increased muscle tone or to fibrosis.

Monitoring the effects of interstitial therapy is a potential role for shear wave elastography, especially in the liver using thermal techniques such as high-intensity focused ultrasound (HIFU). Coagulated tissue is stiffer than normal, and the higher shear wave speed this produces can be demonstrated with SWE. This could form a practical alternative to contrast-enhanced ultrasound for monitoring interstitial ablations.[34]

13.6 Conclusion

New techniques and applications for elastography are promising and could have a major clinical impact.

References

[1] Righetti R, Srinivasan S, Kumar AT, Ophir J, Krouskop TA. Assessing image quality in effective Poisson's ratio elastography and poroelastography: I. Phys Med Biol 2007; 52(5):1303–1320

[2] Righetti R, Ophir J, Kumar AT, Krouskop TA. Assessing image quality in effective Poisson's ratio elastography and poroelastography: II. Phys Med Biol 2007; 52(5):1321–1333

[3] Gao J, Hentel K, Kazam J, Min R. Ultrasound strain relaxation time ratio: a quantitative marker for the assessment of cortical inflammation/edema in renal allografts. Ultraschall Med 2015; 41:112

[4] Song P, Zhao H, Manduca A, Urban MW, Greenleaf JF, Chen S. Comb-push ultrasound shear elastography (CUSE): a novel method for two-dimensional shear elasticity imaging of soft tissues. IEEE Trans Med Imaging 2012; 31(9): 1821–1832

[5] http://qibawiki.rsna.org/index.php?title=Ultrasound_SWS_Biomarker_Ctte. 2015. Accessed 13 May 2015, 2015.

[6] Barry CT, Mills B, Hah Z et al. Shear wave dispersion measures liver steatosis. Ultrasound Med Biol 2012; 38(2):175–182

[7] Brum J, Catheline S, Benech N, Negreira C. Quantitative shear elasticity imaging from a complex elastic wavefield in soft solids with application to passive elastography. IEEE Trans Ultrason Ferroelectr Freq Control 2015; 62(4):673–685

[8] Schmitt J. OCT elastography: imaging microscopic deformation and strain of tissue. Opt Express 1998; 3(6):199–211

[9] Ford MR, Dupps WJ Jr, Rollins AM, Roy AS, Hu Z. Method for optical coherence elastography of the cornea. J Biomed Opt 2011; 16(1):016005

[10] Wang RK, Sampson DD, Boppart SA, Kennedy BF. Special section guest editorial: optical elastography and measurement of tissue biomechanics. J Biomed Opt 2013; 18(12):121501

[11] Es'haghian S, Kennedy KM, Gong P, Sampson DD, McLaughlin RA, Kennedy BF. Optical palpation in vivo: imaging human skin lesions using mechanical contrast. J Biomed Opt 2015; 20(1):16013

[12] Cheng Y, Li S, Eckersley RJ, Elson DS, Tang MX. Detecting tissue optical and mechanical properties with an ultrasound modulated optical imaging system in reflection detection geometry. Biomed Opt Express 2015; 6(1):63–71

[13] Myers KM, Feltovich H, Mazza E et al. The mechanical role of the cervix in pregnancy. J Biomech 2015; 48(9):1511–1523

[14] Feltovich H, Hall TJ, Berghella V. Beyond cervical length: emerging technologies for assessing the pregnant cervix. Am J Obstet Gynecol 2012; 207(5):345–354

[15] Gazhonova VCS, Zubarev A. Real-time sonoelastography improved early detection of ectopic pregnancy. Paper presented at the European Congress of Radiology (ECR); March 4–8, 2010; Vienna, Austria

[16] Ciledag N, Arda K, Aktas E, Aribas BK. A pilot study on real-time transvaginal ultrasonographic elastography of cystic ovarian lesions. Indian J Med Res 2013; 137(6):1089–1092

[17] Stoelinga B, Hehenkamp WJ, Brölmann HA, Huirne JA. Real-time elastography for assessment of uterine disorders. Ultrasound Obstet Gynecol 2014; 43(2): 218–226

[18] Furukawa S, Soeda S, Watanabe T, Nishiyama H, Fujimori K. The measurement of stiffness of uterine smooth muscle tumor by elastography. Springerplus 2014; 3:294

[19] Grgurevic I, Puljiz Z, Brnic D et al. Liver and spleen stiffness and their ratio assessed by real-time two dimensional–shear wave elastography in patients with liver fibrosis and cirrhosis due to chronic viral hepatitis. Eur Radiol 2015; 25(11):3214–3221

[20] Uchida H, Sakamoto S, Kobayashi M et al. The degree of spleen stiffness measured on acoustic radiation force impulse elastography predicts the severity of portal hypertension in patients with biliary atresia after portoenterostomy. J Pediatr Surg 2015; 50(4):559–564

[21] Elkrief L, Rautou PE, Ronot M et al. Prospective comparison of spleen and liver stiffness by using shear-wave and transient elastography for detection of portal hypertension in cirrhosis. Radiology 2015; 275(2):589–598

[22] Chauvet D, Imbault M, Capelle L et al. In vivo measurement of brain tumor elasticity using intraoperative shear wave elastography. Ultraschall Med 2015 April 15[Epub ahead of print]

[23] Vural M, Acar D, Toprak U et al. The evaluation of the retrobulbar orbital fat tissue and optic nerve with strain ratio elastography. Med Ultrasound 2015; 17(1):45–48

[24] Urs R, Lloyd HO, Silverman RH. Acoustic radiation force for noninvasive evaluation of corneal biomechanical changes induced by cross-linking therapy. J Ultrasound Med 2014; 33(8):1417–1426

[25] Biswas R, Patel P, Park DW et al. Venous elastography: validation of a novel high-resolution ultrasound method for measuring vein compliance using finite element analysis. Semin Dial 2010; 23(1):105–109
[26] Ribbers H, Lopata RG, Holewijn S, Pasterkamp G, Blankensteijn JD, de Korte CL. Noninvasive two-dimensional strain imaging of arteries: validation in phantoms and preliminary experience in carotid arteries in vivo. Ultrasound Med Biol 2007; 33(4):530–540
[27] Ramnarine KV, Garrard JW, Kanber B, Nduwayo S, Hartshorne TC, Robinson TG. Shear wave elastography imaging of carotid plaques: feasible, reproducible and of clinical potential. Cardiovasc Ultrasound 2014; 12:49
[28] Wang C, Wang L, Zhang Y, Chen M. A novel approach for assessing the progression of deep venous thrombosis by area of venous thrombus in ultrasonic elastography. Clin Appl Thromb Hemost 2014; 20(3):311–317
[29] Ünlütürk U, Erdoğan MF, Demir O, Culha C, Güllü S, Başkal N. The role of ultrasound elastography in preoperative localization of parathyroid lesions: a new assisting method to preoperative parathyroid ultrasonography. Clin Endocrinol (Oxf) 2012; 76(4):492–498
[30] Iagnocco A, Iorgoveanu V, Priori R. Involvement of salivary glands in primary Sjögren's syndrome: elastographic assessment and correlations with ultrasonographic findings. Ann Rheum Dis 2014; 73(2):474–475
[31] Ying H, Da L, Luo J et al. Quantitative assessment of bladder neck compliance by using transvaginal real-time elastography of women. Ultrasound Med Biol 2013; 39(10):1727–1734
[32] Deprez JF, Brusseau E, Fromageau J, Cloutier G, Basset O. On the potential of ultrasound elastography for pressure ulcer early detection. Med Phys 2011; 38(4):1943–1950
[33] Kısmalı E, Göde S, Turhal G, Öztürk K, Raşit M. A new insight for evaluation of the inferior turbinate with ultrasound elastography. J Ultrasound Med 2015; 34(5):777–782
[34] Hoyt KPK, Rubens DJ. Sonoelastographic shear velocity imaging: experiments on tissue phantom and prostate. IEEE Ultrason Symp. 2006:1686–1689.

Index

Note: Page numbers set **bold** or *italic* indicate headings or figures, respectively.

T

U

V

W

Y